Fourier Transform Spectroscopy of Selected Transient Species

by

Gang Li

A thesis
presented to the University of Waterloo
in fulfillment of the
thesis requirement for the degree of
Doctor of Philosophy
in
Chemistry

Waterloo, Ontario, Canada, 2003

I hereby declare that I am the sole author of this thesis. This is a true copy of the thesis, including any required final revisions, as accepted by my examiners.

I understand that my thesis may be made electronically available to the public.

Acknowledgements

First of all, I would like to express my thanks to Dr. Peter F. Bernath, my Ph.D. Supervisor, Professor of Chemistry and Physics of the University of Waterloo, for his providing me with the opportunity and financial support to work in his Laboratory, and for guiding me to walk around in the beautiful spectroscopic world. His encouragement, patience and tolerance are indispensable to my successful completion of the Ph.D. studies and research. One thing that my eight-year old son Tony still does not understand is why Dr. Bernath teaches me and also pays me. He believes that I definitely should pay Dr. Bernath for what I have learned.

I also would like to express my thanks to the members of my Ph.D. Supervisory Committee, Dr. Robert J. Le Roy, Dr. John W. Hepburn and Dr. Frederick R. W. McCourt of the University of Waterloo and Dr. John D. Goddard of the University of Guelph for their active support during various stages of my graduate studies. Dr. Le Roy served as much more than a member of the Supervisory Committee. Apart from his valuable advice and many ready answers to my questions, I really feel lucky to have Dr. Le Roy around because his group develops software tools. Dr. Le Roy's DSParFit has been one of the major tools I have used in the research. Complementing the roles of Dr. Bernath, Dr. Le Roy, and the Committee in my Ph.D. education, Dr. Tsuyoshi Hirao, a Post Doctoral Fellow working in the Laboratory during most of my Ph.D. studies, served as a ready "handbook" of both theories and experiments.

I would also express my thanks to the graduating Ph.D. students from the Bernath Laboratory when I just started my Ph.D. studies, Dr. Pina Colarusso, Dr. Keqing Zhang, Dr. Zulfikar Morbi and Dr. Chunfeng Zhao, for their practical advice; and Treana Parekunnel and the new friends working in the Laboratory: Sean McLeod, Dr. Chris Boone, Ray Nassar, Keith Tereszchuk, Iouli Gordon, Andrew Janca, Dr. Dominique Appadoo, Alireza Shayesteh, Dr. Kaley Walker, and other friends.

Last, but never the least, many thanks go to Wei Yang, a long time friend of mine, Bujin Guo, and Charlie Shu Zhang, and their families for their sincere support in various aspects during my early life at Waterloo.

****

In the final version of my thesis, I would re-express my thanks to my Supervisor and my Supervisory Committee, and thank Dr. Kentarou Kawaguchi of Okayama University, Dr. James D. D. Martin, Dr. Kam Tong Leung, and Dr. Mark D. Pritzker of the University of Waterloo, for their wonderful questions and comments durng my Oral Defense. Definitely, no fellow graduate students should forget to express our thanks to Cathy Van Esch, the Graduate Secretary.

Abstract

The procedures and results of experimental and/or theoretical studies of four transient molecules, GeO, WO, BeH, and MgH are reported in the thesis. Two of them, GeO and WO, are diatomic molecules composed of heavy atoms, and the other two are diatomic molecules with hydrogen as one of their component atoms.

The GeO species was generated using a high temperature furnace. The rovibrational spectrum of five isotopomers were detected in emission using a Bruker IFS 120 HR Fourier transform spectrometer. Combined-isotopomer Dunham-type molecular constants have been derived for GeO using the DSParFit computer program. Analysis shows that the Born-Oppenheimer approximation is valid, as expected, for a molecule composed of heavy atoms.

The WO molecule was generated using a microwave discharge cell, and the spectra of electronic transitions of various systems were detected in emission using both the Bruker IFS 120 HR Fourier transform spectrometer at Waterloo and the McMath Pierce One-Meter Fourier transform spectrometer at the National Solar Observatory in Arizona. The ground electronic state has been confirmed to be $X^3\Sigma^-$ based on the analysis of seven 0-0 bands.

BeH and MgH are typical molecules with small reduced masses, and the effects of Born-Oppenheimer breakdown were expected. Both of these molecules have rotational perturbations in their excited electronic states. A "new" method of data processing was used, i.e., treatment of the electronic data as if they were from fluorescence series. Thus the harmful influence of the perturbed upper electronic states on the ground electronic state molecular constants is eliminated. By using the DSParFit computer program, accurate sets of combined-isotopomer Dunham-type molecular constants have been derived for the ground electronic states of the two molecules, and Born-Oppenheimer breakdown correction terms have been obtained.

Chapter 1 introduces the concepts of ro-vibrational and electronic emission spectroscopy, the principles of Fourier transform spectroscopy, the experimental means for generating transient species, and the spectroscopic models.

Chapter 2 presents the experiments and analysis for the ro-vibrational studies of the GeO isotopomers.

Chapter 3 describes the results of experiments and rotational analysis of the electronic systems of the WO molecule.

Chapter 4 presents the method of treatment and derivation of accurate molecular constants for the ground electronic state of the BeH isotopomers.

Chapter 5 presents, in a similar manner to that of Chapter 4, the derivation of molecular constants for the ground electronic state of the MgH isotopomers.

For my son, my wife and my parents

Table of Contents

List of Tables

List of Illustrations

Chapter 1

Introduction

The energy levels of a molecule are quantized as governed by the Schrödinger equation in quantum chemistry, whereas molecular spectroscopy involves the detection and interpretation of transitions between the energy levels. The real test of any quantum mechanical theory lies in the ability to reproduce observed experimental data.

This Chapter presents the theoretical and experimental foundations for the spectroscopic studies and theoretical analysis of transient chemical species. Section 1.1 presents the principles of rotational, vibrational and electronic spectroscopy, and the techniques of emission spectroscopy and Fourier transform spectroscopy. Section 1.2 summarizes the experimental techniques used for the generation and detection of the chemical species in a laboratory environment, i.e., the high temperature cells and discharge plasma cells. Section 1.3 presents an overview of the theoretical models and software tools used in the processing of the spectroscopic data of diatomic molecules. This Chapter is concluded by pointing out the importance of both theoretical and experimental foundations in successful spectroscopic research.

1.1 Fourier Transform Emission Spectroscopy

Molecular spectroscopy may be defined as the study of the interaction of electromagnetic waves and molecules. The rotational, vibrational, and electronic energies in a molecule are all quantized. It is the undulating interconnected electric and magnetic fields interacting with molecules that give rise to spectra. Although the dual electric-magnetic character of electromagnetic radiation is of great importance, it is the oscillating electric field which is more often involved than the magnetic field in interaction with molecules.

1.1.1 Rotational, Vibrational and Electronic Spectroscopy

Generally, the vibrational transitions of a molecule are in the infrared (IR) region[1] of electromagnetic radiation, which is between the visible and the microwave, or 10–13,000 cm^{-1} (0.75 μm–1.0 mm).

The pure rotational transitions generally occur in the microwave or millimetre wave region, while the electronic transitions occur in the visible or ultraviolet region of the electromagnetic spectrum.

1.1.1.1 Rotational and Vibrational Spectroscopy

For gas phase molecules, rotational transitions accompanying the vibrational transitions are usually observed in high resolution spectroscopic experiments using a high resolution spectroscopic instrument, such as a Fourier transform spectrometer (FTS). By analysis of the observed ro-vibrational spectra, relevant physical information about the molecules can be extracted from the line positions, line widths, and line intensities[1]. From the line positions, it is possible to determine the energy level pattern of the molecules. Also, more direct physical information, such as the force constants, bond lengths and moments of inertia, may be calculated from the systematic trends in line positions.

The vibrational transitions are detected in the infrared region of the electromagnetic spectrum. The relative intensity depends on the square of the transition dipole moment. The strength of vibrational transitions is usually about two orders of magnitude weaker than those of the pure rotation and electronic transitions, in consideration of the fact that the strength of the vibrational transitions depends on the change of the electric dipole; the strength of the pure rotational transitions depends on the magnitude of the permanent dipole; and in electronic transitions, the electronic state

[1]Near-IR, 4,000–13,000 cm^{-1} (0.75–2.5 μm), the overtone region; Mid-IR, 400–4,000 cm^{-1} (2.5–25 μm), the fundamental region; Far-IR, 10–400 cm^{-1} (25 μm–1 mm).

changes, so the dipole change is also large. Also, the rates of emission are much smaller for vibrational transitions than for electronic transitions. Nevertheless the rates of infrared emission are adequate to provide an acceptable signal to noise ratio (S/N), even for transient molecules [2, 3]. The advantages of the Fourier transform spectrometers as listed in Section 1.1.3.4 make such systems a successful tool in the infrared experiments.

1.1.1.2 Diode Laser Spectrometer vs. Fourier Transform Spectrometer

There are two kinds of instruments that are widely used in high resolution infrared spectroscopy: diode laser spectrometers and Fourier transform spectrometers.

The laser source of a diode laser spectrometer provides both the high intensity necessary for high sensitivity, and the narrow linewidth needed for high resolution. There are two reasons that limit the applications of a diode laser spectrometer. One is that its tunable range is narrow, and the other is that it has no inherent means of calibration.

Fourier transform emission spectroscopy for the study of high temperature transient species has been much explored in Bernath's lab [2]. Emission spectra of high temperature molecules yield increased sensitivity over absorption spectra and cover a wider spectral region than those of a diode laser spectrometer.

1.1.1.3 Electronic Spectroscopy

Electronic transitions generally occur in the visible or ultraviolet range of the electromagnetic spectrum. The spectroscopic data for electronic transitions give information about energy levels of the electronic states involved, in addition to information on the related vibrational and rotational energy levels of the electronic states[4].

Whereas the advantages of Fourier transform spectrometers are in infrared experiments, as listed in Section 1.1.1.1 and Section 1.1.3.4, they can also be used for the detection of electronic transitions of gas phase molecules at high resolution. However, the hardware configuration needs to be made suitable for the frequency range by changing beamsplitters, detectors, filters, windows, etc. It may also be necessary to change the method for generating the species of interest.

1.1.2 Emission Spectroscopy

The electronic emission spectra of gas phase molecules provide more information about the molecules than do the absorption spectra. The molecules are normally found in the lowest few vibrational levels of the ground electronic state, based on

the Boltzmann distribution. Most absorption spectra show only the 0-0, 1-0, 2-0, 3-0, ... progression series. However, emission transitions may come from many vibrational levels of the excited electronic state involved into many excited vibrational levels of the ground electronic state.

For a molecule with many isotopomers, emission spectra can be much more complicated. Using an absorption spectrum as a guide for the assignment of the emission spectra can be very helpful.

Similarly, the infrared rovibrational emission spectra provide more information about the molecule than the absorption counterpart. Many different bands may be observed.

Although emission spectroscopy is common in the visible and ultraviolet region, the technique has been neglected in the infrared and far infrared regions until recently [2]. In addition, infrared emission spectroscopy has the following properties, compared with infrared absorption spectroscopy [2].

(1) Sensitivity

Emission spectroscopy is more sensitive than absorption spectroscopy, because emission spectra can have zero background. For an absorption spectrum, the noise arises mainly from shot-noise[2] from the background continuum. In emission spectra, the background continuum is absent. Although the emission signal is relatively low, the signal-to-noise ratio is improved [2].

Since transient molecules[3] and radical species[4] have low concentrations because of their great reactivity, it is advantageous to use emission spectroscopy to study them. For transient molecules, emission spectroscopy is a technique that improves the performance of the spectrometer experimental system [2].

The improvement in sensitivity obtained by working in emission rather than in absorption with high temperature molecules, ions, and free radicals is typically a factor of 10 in the mid-infrared region. At the same time, the instrument of choice is the high resolution Fourier transform spectrometer [2] considering the advantages of the FTS as described in Section 1.1.3.4.

[2]The shot-noise is due to the fluctuating nature of radiation, which is composed of photons arriving randomly in time.

[3]Transient species refers to a short-lived reaction intermediate. It can be defined only in relation to a time scale fixed by the experimental conditions and the limitations of the technique employed in the detection of the intermediate. A successful experimental method produces sufficient concentration of the transient species for spectroscopic observation.

[4]An atom or group of atoms that is highly chemically reactive because it has at least one unpaired electron.

The rate of spontaneous emission between two states is determined by the *Einstein A factor*. Although emission spectroscopy is not as favorable in the infrared region as in the visible, infrared experiments are possible, and a number of high temperature molecules have been recorded in emission in the near infrared [2].

(2) Temperature

Emission spectroscopy requires that the sample be at a different temperature (higher or lower) than the spectrometer [2, 3, 5].

In emission spectroscopy, a sample is generally heated to a temperature greater than the temperature of the detector. It is possible to obtain emission spectra of a sample by either heating or cooling it with respect to the detector [5]. Higher temperatures are more favorable, since the emitted power increases strongly with temperature.

In an emission experiment, the radiation detected is essentially a relative flux of radiation as a result of the temperature difference between the sample and the detector. A large temperature difference is desirable, since it will increase the flux of radiation and hence the signal to noise ratio of the emission spectra.

(3) Blackbody Radiation

Infrared emission spectroscopy is plagued by thermal blackbody emission from the spectrometer itself, as well as from the high temperature cell or discharge cell used to excite the sample [2]. For infrared emission spectroscopy, in addition to the potential interference from the infrared emission from the support material, it is also possible to observe undesired stray light emitting from the walls of the spectrometer or from any of the spectrometer optical components. This stray light can also interfere with the infrared emission measurement, causing a base line distortion in the emission spectra [5].

The blackbody radiation is a continuum that provides nothing but noise. It cannot be avoided, but its effects can be minimized by limiting the field of view with a cold aperture, by preventing the spectrometer from looking directly at hot objects, and by limiting the spectral range of the detectors with cold filters.

1.1.3 Fourier Transform Spectroscopy

The majority of the experiments reported in this thesis have been carried out using the Bruker IFS 120 HR Fourier transform spectrometer. The Bruker spectrometer offers

high resolution and excellent sensitivity. Its modular construction allows the system to be easily configured for specialized applications. The specially designed permanently aligned interferometer provides high sensitivity and stability. The computer-controlled selection of optical components makes the experimental setup and spectral range change fast and easy. The spectrometer has a resolution of better than 0.002 cm^{-1}, and a spectral range from 5 cm^{-1} in the far-IR to above 50,000 cm^{-1} in the UV (with wavelength from 200 nm to 2 mm). The high vacuum optics bench can be evacuated to less than 0.02 Torr for distortion-free baselines. The instrument is equipped with two liquid helium cooled bolometers, liquid nitrogen cooled MCT and InSb detectors, a Si diode detector, a DTGS detector, and other detectors.

1.1.3.1 Working Principle

The schematic illustration of the optics of the Bruker IFS 120 HR high resolution Fourier transform spectrometer (FTS) is shown in Fig. 1.1. The core part of the Fourier transform spectrometer is a Michelson interferometer, as shown in Fig. 1.2. The Michelson interferometer is a device that divides a beam of radiation into two paths, and then recombines the two beams after a path difference has been introduced. A condition is thereby created under which interference between the beams can occur. The *interferogram*, i.e., the intensity variation of the beam as a function of optical path difference (also called optical retardation), emerging from the interferometer can be measured by using a detector. The principle of a high resolution Fourier transform spectrometer, and its signal flow and signal processing steps are as follows [6, 7, 8, 9, 10, 11].

(1) Emission Source

An experimental emission source can be thought of as a source of radiation with a characteristic intensity distribution as a function of frequency (wavenumber). In the spectroscopic experiments, the emission source is the cell containing transient molecules that are emitting electromagnetic radiation. The transient species are excited using various means, such as high temperature furnace, microwave discharge, radio frequency discharge, DC or AC electric discharges, or a combination of the methods mentioned above. When the chemical species makes transitions from the excited states to lower states, the emission of radiation occurs.

(2) Interferogram

The Michelson interferometer optics (fixed mirror, moving mirror, beamsplitter, etc.) as shown in Fig. 1.2 generates an optical path difference for the input

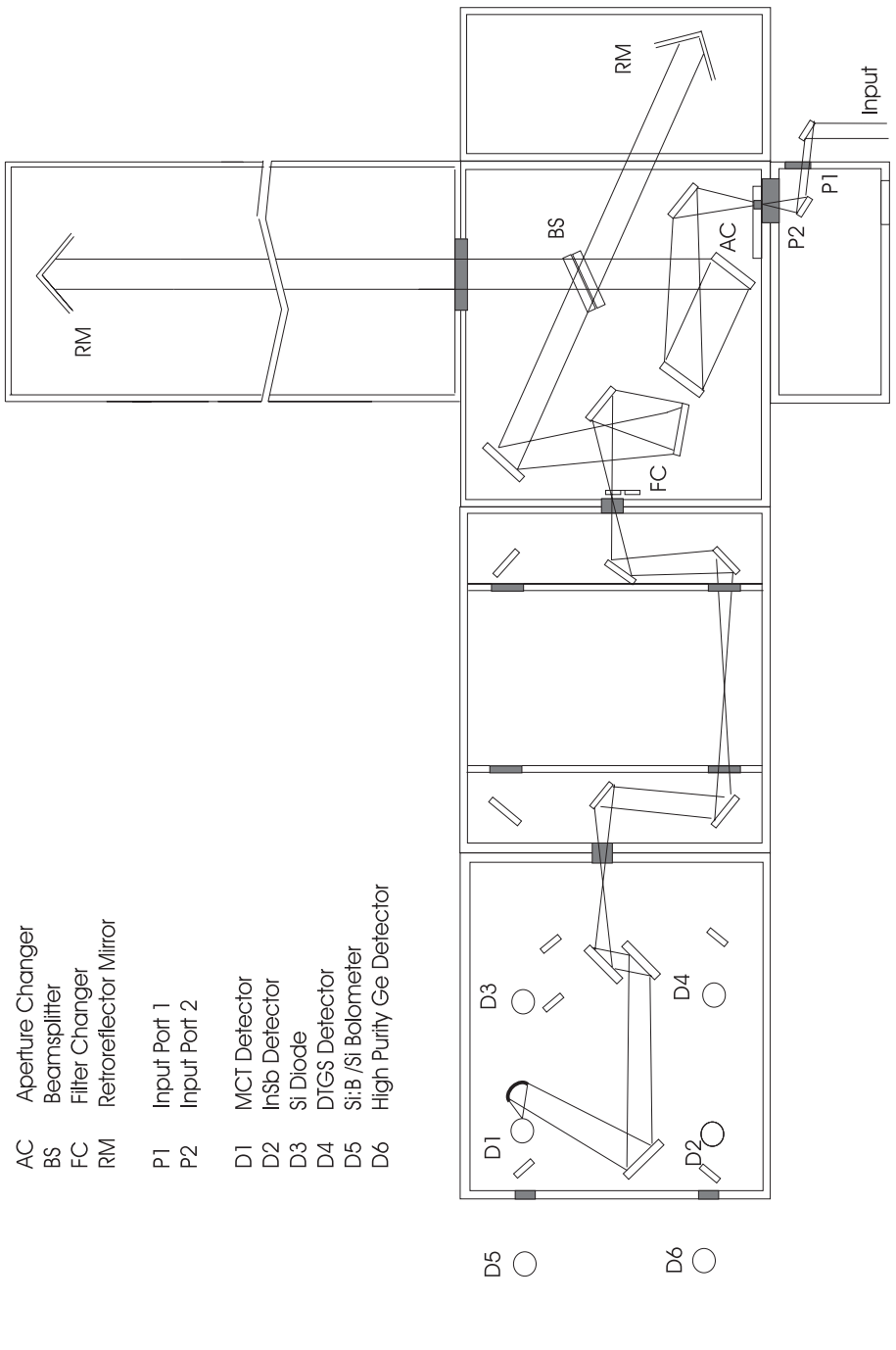

Figure 1.1: Schematic Illustration of the Optics of Bruker IFS 120 HR Fourier Transform Spectrometer

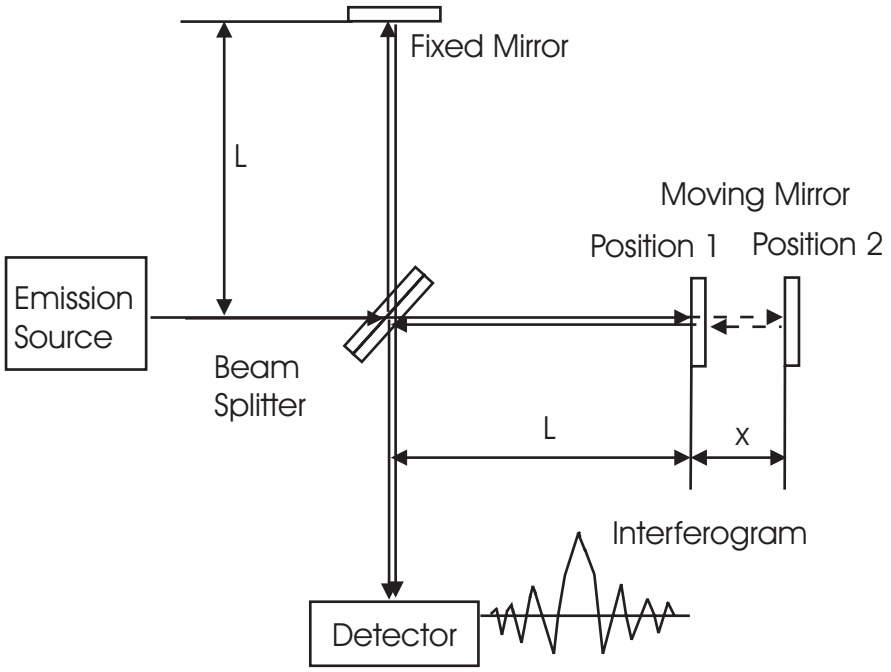

Figure 1.2: A Schematic Illustration of the Michelson Interferometer

Table 1.1: Beamsplitters

Beamsplitter	Range (cm^{-1})
Mylar film	0-1,000
KBr	350 - 6,000
KCl	750 - 6,000
CaF_2	1,000-7,000
Quartz	4,000 - 30,000

signal, and produces interferograms as measured with the detectors. The materials and the working frequency range of the beamsplitters[5] for the spectroscopic experiments are shown in Table 1.1.

The Michelson interferometer in the FTS converts the source emission (intensity vs. frequency) into an interferogram (intensity vs. optical path difference). The interferometer divides the radiation, introduces an optical path difference, and generates the interferogram. The spectral information in the source is preserved in the interferogram.

[5]In fact, the materials listed here are the beamsplitter substrates. The beamsplitters need to have coatings on the substrates. For example, Ge/KBr represents a germanium coating on a KBr substrate.

The interferograms are different for different type of sources. The relations between the interferograms and different types of sources, e.g., monochromatic sources, polychromatic sources, and continuous sources, obey different mathematical rules.

- Monochromatic Source

$$I(x) = S(\overline{\nu})cos(2\pi\overline{\nu}x) \tag{1.1}$$

where
x - the optical path difference;
$\overline{\nu}$ - the wavenumber of the monochromatic source;
$S(\overline{\nu})$ - the intensity of the emission source at wavenumber $\overline{\nu}$.

The interferogram of a helium-neon laser is a monochromatic example.

- Polychromatic Source

$$I(x) = \sum_i S(\overline{\nu_i})cos(2\pi\overline{\nu_i}x) \tag{1.2}$$

where
x - the optical path difference;
$\overline{\nu_i}$ - the wavenumbers of the polychromatic source;
$S(\overline{\nu_i})$ - the intensity of the emission source at wavenumber $\overline{\nu_i}$.

In high resolution spectroscopy, gas phase emission sources are polychromatic because the emission line positions are resolved.

- Continuous Source (Continuum)

$$I(x) = \int_{-\infty}^{+\infty} S(\overline{\nu})cos(2\pi\overline{\nu}x)d\overline{\nu} \tag{1.3}$$

where
x - the optical path difference;
$\overline{\nu}$ - the wavenumber of the continuous source;
$S(\overline{\nu})$ - the intensity of the emission source at the wavenumber $\overline{\nu}$.

For example, emission from a hot radiating solid object, or emission sources as in low resolution spectroscopy, for which the transitions are not resolved.

The effect of measuring the signal over a limited retardation (optical path difference) is to cause the spectra to have a finite resolution. The maximum

retardation of the interferogram determines the maximum resolution. Approximately, $\Delta\overline{\nu} = (\Delta_{max})^{-1}$, where $\Delta\overline{\nu}$ is the resolution. Δ_{max} is the maximum retardation.

(3) Spectrum

The spectrum is recovered using Fourier transform software (including apodization, phase correction, zero filling, etc.). The interferogram is a cosine Fourier transform of the source spectrum. The final spectrum output from the Fourier transform spectrometer is the inverse cosine Fourier transform of the interferogram.

1.1.3.2 Detectors

The detectors used in Fourier transform spectrometers can be classified as *thermal detectors* or *photon detectors* according to their working principles [12].

(1) Thermal Detector

Thermal detectors exhibit a change in some measurable electrical property that accompanies a change in temperature of the sensitive element, caused by absorption of radiation by the sensitive element. For example, the silicon bolometer, and the DTGS (deuterated triglycine sulfate) detector.

(2) Photon Detector

Photon detectors are also called *quantum detectors*. This category of detectors is based on the creation of charge carriers (electron-hole pairs) in a semiconductor material due to absorbed electromagnetic radiation, followed by subsequent collection and amplification of the charges created. Photon detectors are more sensitive, and have fast response times. They usually operate below or at liquid nitrogen temperatures. Photon detectors include MCT (mercury cadmium telluride), InSb (indium antimonide), Si:B (boron doped silicon), and Si diode detectors.

Most infrared detectors are to be cooled either with liquid helium and/or liquid nitrogen. One reason for cooling the detector to such low temperatures is to minimize the blackbody radiation emitted from its surroundings. Blackbody radiation interferes with the signal obtained by the detector and is a major factor for a low signal-to-noise ratio. The working temperatures and ranges of working frequencies of the detectors are shown in Table 1.2 and Table 1.3.

Table 1.2: Detectors and Working Temperatures

Working temperature	Detector
Room temperature	Si photo diode, DTGS, PMT
Liquid nitrogen (77 K)	MCT, InSb
Liquid helium (4 K)	Si bolometer, Si:B

Table 1.3: Detectors and Range of Working Wavenumber

Detector	Working Wavenumber Range (cm^{-1})
Si Bolometer	0–400
Si:B Detector	350 – 2,000
MCT	800–2,400
InSb	1,850–6,000
Si photo diode	9,000 – 45,000 (220 – 1,100 nm)
PMT	13,000–25,000 (visible region)

According to their positions in the Bruker 120 IFS HR high resolution Fourier transform spectrometer, the detectors are also classified as *internal detectors* or *external detectors*.

(1) Internal Detectors

The MCT, InSb and Si photo diode detectors are built-in detectors for the spectrometer. The MCT and InSb detectors must be cooled with liquid nitrogen, while the Si photodiode operates at room temperature.

(2) External Detectors

In low wavenumber experiments, the external detector pack needs to be used. The Si:B detector and the Si bolometer are in the same detector package. Liquid helium cooling is necessary for them to operate properly. The outer part of the detector assembly needs to be cooled with liquid nitrogen, and the inner part with liquid helium.

1.1.3.3 Further Discussions

The interferogram and the spectrum are a Fourier transform pair. For a monochromatic line, the interferogram is a cosine function; for two monochromatic lines, the interferogram shows a beat pattern; for a Lorentzian shaped single line, it is a sinusoidal interferogram with an exponentially damped envelope; and for a broad band

spectrum of a polychromatic source, the result is a general interferogram [6], which is characterized by its high centerburst and two decaying side wings. When the emission source has a broader range, the interferogram wings decay faster, because more frequency components in the source give more chance of cancellation. In any case, the interferogram is the cosine Fourier transform of the source function.

The computer software in the Fourier transform spectrometer converts the interferogram into a spectrum. The Fourier transform conversion also includes such necessary mathematical manipulations as apodization, phase correction, zero filling, etc.

(1) Interferogram Sampling

The sampling of the interferogram is triggered by the zero crossings of the interferogram (interference fringes) of the built-in helium-neon laser in the Fourier transform spectrometer.

An FTS can be configured to collect either double-sided or single-sided interferograms [13]. This means both low-resolution measurements, with their improved signal-to-noise ratios, and high-resolution measurements are readily accommodated. Every point on an interferogram contains information about all frequencies present in the spectrum. Because this frequency information is dependent on the distance that the mirror has moved from the interferogram centerburst (the point of zero path difference), sampling on either side of the centerburst provides the same frequency information. At lower resolutions, collecting equal amounts of data before and after the centerburst, i.e., a double-sided data collection, samples each frequency element twice and thus yields a superior signal-to-noise ratio. The signal-to-noise ratio of a double-sided data collection is equal to $\sqrt{2}$ times that of a single-sided data collection, because the number of measurements is doubled. Also, less time is required to collect one double-sided interferogram than is required to collect two single-sided interferograms.

High-resolution measurements require more retardation, that is, greater mirror travel. But mechanical restrictions allow only a relatively small portion of the interferogram to be sampled before the interferogram centerburst. To circumvent this limitation, a single-sided interferogram can be collected to achieve the desired resolution.

(2) Filtering

It could be inferred that the higher the frequency of the components present in the interferogram signal, the higher the sampling rate should be. If the sampling

rate is not high enough to sample the signal correctly then a phenomenon called *aliasing* occurs. Aliasing is the replication of the original spectrum with respect to the folding wavenumber, and the Nyquist frequency (wavenumber) is the folding wavenumber. The only solution to the aliasing problem is to ensure that the sampling rate is high enough to avoid any spectral overlap, or to use an anti-aliasing filter.

The filtering solution is more practical. Because only a certain wavenumber range of the spectrum is to be detected, it is better to filter the interferogram to fulfill the *Nyquist sampling theorem*. The filtering eliminates the aliasing (the frequency folding). Without filtering, its mirror image would apear on the wavenumber axis. Wavenumber components higher than half of the sampling frequency need to be filtered out either electronically or optically to ensure that the spectrum is recovered correctly.

(3) Apodization

The process of apodization is the removal of the sidelobes of the lines in a spectrum by multiplying the interferogram with a suitable function prior to the Fourier transformation. A suitable function must cause the intensity of the interferogram to fall smoothly to zero at both ends [14].

Because it is impossible to collect an interferogram to infinite optical path difference, i.e., the interferogram has to be truncated, so some error arises in the resulting spectrum. This is equivalent to multiplying the ideal interferogram by a boxcar function, so the spectrum recovered is broadened with sidelobes. A practical interferogram always has a finite retardation. The product of an ideal interferogram (collected to infinite optical path difference) and a boxcar function is equivalent to the convolution of the true spectrum with a sinc function (with sidelobes). Apodization functions are used to correct the spectral line shape, i.e., to suppress the sidelobes. The apodization is realized by multiplying the interferogram by a decaying function, i.e., the apodization function [15].

When the interferogram is multiplied by an apodization function, the transform of the interferogram, i.e., the spectrum, is technically free from sidelobes. The apodization function not only controls the instrument line shape caused by the trucation of the interferogram, but also smooths out the amplitude of high spatial frequencies in the interferogram. Any function that has a value of unity at zero path difference and decreases with increasing retardation will serve as an apodization function.

Table 1.4: Coefficients of Norton-Beer Function

	C_0	C_1	C_2	C_3	C_4
Weak	0.384093	-0.087577	0.703484	0	0
Medium	0.152442	-0.136176	0.983734	0	0
Strong	0.045335	0	0.554883	0	0.399782

The drawback of using the apodization function is the worsening of the spectral resolution, because the extremes of the interferogram wings are reduced by the apodization function. Therefore, it is necessary to make a compromise between the reduction in spectral distortion (the sidelobes) and the worsening of the resolution [12].

The specific function depends on the experiment being performed. If either high resolution or good quantitative accuracy is required, a function such as the Norton-Beer weak function shown in Eqn. (1.4) can be used. Strong apodization can be applied for spectra containing both weak and intense lines, especially when their width is of the same order as the instrument resolution [6]. The coefficients of the Norton-Beer function listed in Table 1.4 are the empirical parameters for

$$A(x) = \sum_{i=0}^{4} C_i[1 - (x/L)^2]^i \tag{1.4}$$

where
L - the range of the optical path difference of the interferogram;
C_i - the coefficients as shown in Table 1.4.

(4) Phase Correction

The non-zero phase phenomenon comes from the fact that the input of the sampled interferogram to the Fourier transform software is not a mirror image about zero retardation (zero optical path difference). It comes from the mismatching of sampling point and zero retardation, and optical properties, such as the change of the beamsplitter refractive index with wavenumber, etc. The filtering process can also bring about phase errors. In other words, the phase error is caused by optical, electrical or sampling effects, e.g., phase lag caused by electronic filters to remove high frequency noise; even when the interferogram

is symmetrical about zero optical path difference, the first data point could actually be sampled before the zero retardation point.

The result of the Fourier transform of an arbitrary function is a complex function, which has both a real and an imaginary part. The symmetric component of the interferogram contributes to the real cosine part; and the asymmetric components of the interferogram brings about the imaginary sine part. In Fourier transform spectroscopy, an ideal interferometer produces a symmetric interferogram about the zero path difference, and only the cosine part is present in the transformed result. However, the imperfection of a real world interferometer always brings about a non-zero imaginary part in the transformed results, which means that the real component is distorted [15]. It is therefore necessary to correct the data for such phase distortion.

The phase angle can be computed from a region of the interferogram measured symmetrically on either side of the zero retardation point, or the *centerburst*. The short double-sided portion of the interferogram can be used to calculate the phase spectrum, by means of the *Mertz algorithm* [12].

(5) Zero Filling

Zero filling is a technique used to bring extra data points to the sampled interferogram data. According to the *Nyquist theorem*, the spectral information can be entirely recovered as long as the sampling frequency is at least double the highest frequency component in the interferogram. Such a sampling frequency is called the *Nyquist frequency*. Therefore, it is not necessary to sample too many data points from the interferogram. It is necessary to have sufficient data points to achieve the desired resolution and smooth spectral line shape. However, acquiring more data points takes more time.

The requirement for more data points can be realized by addition of a block of zero data points to the acquired data and then Fourier transformation of the data with this block of zeros included [16]. This process is called *zero filling*. Usually, data are sampled in blocks of 2^N points.

Another advantage of zero filling is that the extra data points help to smooth out the spectral line shape [15]. Using extra zeros in the interferogram helps to interpolate the spectra. Usually a factor of 8 (8 times extra zeros) is used for zero filling.

For a signal with a frequency that aways lies half way between the sampling

points, the picket-fence effect[6] occurs. The zero filling and interpolation techniques solve this problem.

(6) Fourier Transfrom

This is the final and major step in the realization of the spectrum recovery. The fast Fourier transform algorithms available make this step easier.

The quality of the detected spectrum is affected by many factors, such as the intensity of the signal source, the efficiency of the beam splitter (reflectance and transmittance) and other optics, and performance of the electronics (detectors, amplifiers), etc.

1.1.3.4 Advantages of Fourier Transform Spectrometers

Compared with dispersive spectrometers using slits or dispersive elements, a Fourier transform spectrometer (FTS) has some unique advantages.

(1) Throughput Advantage (Jacquinot Advantage)

The circular aperture of an FTS has a larger area than that of a slit. The beam splitter is used instead of a dispersive element (e.g., a diffraction grating). Therefore, the signal intensity is high, and more energy gets to the detector than is possible with a dispersive spectrometer. This additional energy on the detector increases the spectrum's potential signal-to-noise ratio.

(2) Multiplex Advantage (Fellget Advantage)

Signals of all frequencies enter the FTS and arrive at the detector at the same time and with the same signal-to-noise ratio. The measurement is faster. The time saved can be used to do more scans to reduce the detector-limited noise (The signal to noise ratio is increased by a factor of $\sqrt{N}$ after taking N measurements).

An FTS does not separate light into individual frequencies before measurement. This means each point in the interferogram contains information from each wavelength in the input light. In other words, if 1,000 data points along the interferogram are collected, each wavelength in the input light is sampled

[6]This effect is produced by the inability of the discrete Fourier transform (DFT) to observe the spectrum as a continuous function, since computation of the spectrum is limited to integer multiples of the fundamental frequency. Observation of the spectrum with the DFT is analogous to looking at it through a sort of "picket-fence", since we can observe the exact behavior only at discrete points. The major peak of a particular component could lie between two of the discrete transform lines, and the peak of this component might not be detected without some addition processing.

1,000 times. By contrast, a dispersive spectrophotometer that measures 1,000 individual points across a spectrum samples each wavelength only once.

The throughput advantage and the multiplex advantage allow high resolving power[7][6]. Together the throughput and multiplex advantages allow an FTS to obtain a high-quality infrared spectrum in a fraction of the time needed to get the same spectrum on a dispersive instrument.

(3) Precision Advantage (Connes Advantage)

The zero crossings of interference fringes of the internal helium-neon laser are used to control the scanner movement and the signal sampling. Therefore, the FTS has a built-in wavenumber calibration standard of high precision. In reality, however, if the reference laser is even slightly misaligned, a small wavenumber shift will be introduced. Calibration of FTS spectra against other standards of higher accuracy is necessary.

(4) Computation and Software Advantage

The high resolution spectrum is obtained through powerful signal processing techniques, such as apodization, phase correction, zero filling, and Fourier transformation.

In addition, the FTS has the advantage of spectral resolution. To increase the resolution of a dispersive spectrometer, the slit through which light must pass needs to be narrowed, thereby decreasing energy throughput. As the resolution increases, the advantage of an FTS over a dispersive instrument increases [13]. Also, the resolution is constant for the whole spectral range for a FTS.

[7]The optical resolving power is defined as $\lambda/\Delta\lambda_{min}$ for a signal of a certain wavelength.

1.2 Generation of Transient Species

Transient chemical species exist only under special experimental conditions. In the experiments reported in this thesis, a high temperature cell or microwave discharge cell with low internal gas pressure is used for the generation of such species. Generally, the high temperature furnace is used to obtain rovibrationally excited species, and the microwave plasma cell is used to generate electronically excited species. The high temperature cell can also be used together with other excitation methods, e.g., DC or AC discharge electrodes, to generate electronically excited species. In all cases, vacuum pumping is necessary to bring the pressure of the gas mixture to a suitably low value in order to provide a condition for the reaction to occur in order for transient species to form, and at the same time to prevent interfering species from building up in the cell. Normally the background pressure inside the cells is kept at around 10^{-2} to 10^{-3} Torr, and the working pressure in the cells is about 1 Torr.

1.2.1 High Temperature Cell

1.2.1.1 Configuration

The experimental setup of the high temperature cell used for the generation and excitation of transient chemical species is shown in Fig. 1.3.

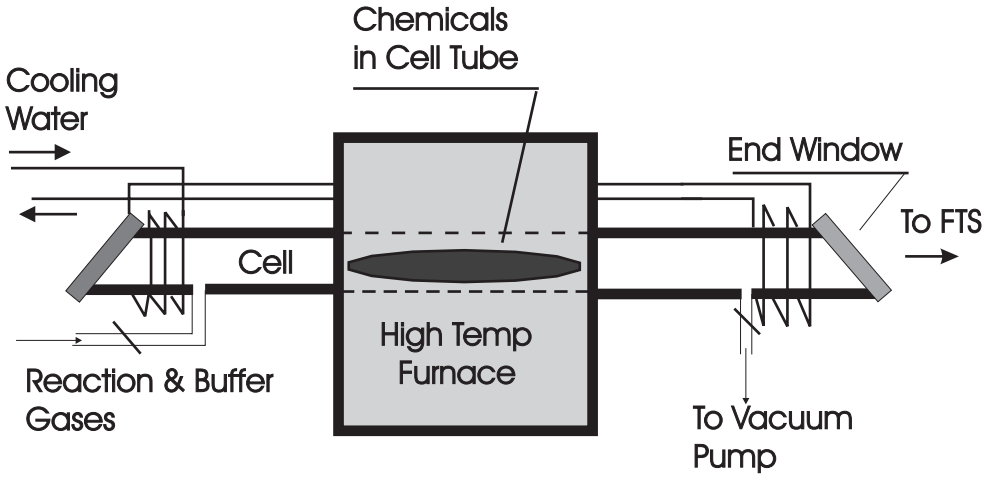

Figure 1.3: High Temperature Cell and High Temperature Furnace

At elevated temperatures (usually 800-1,500 °C), the solid chemicals in the cell begin to vaporize. There is in the cell a mixture of the vapour of the solid chemicals (usually in powder form), reaction gases and a buffer gas. Argon is usually used as the buffer gas in the high temperature cell in experiments involving the observation

of ro-vibrational spectra. The collisions of the heavy argon atoms with the sample gases provide them with thermal excitation energy. The presence and bombardment of the argon atoms also helps to prevent the formation of deposits in the water cooled ends of the cell. Argon should be used to protect the tubes, valves, and windows, especially for FTS experiments using corrosive gases or highly depositing substances. For experiments involving low vapor pressure substances, argon may not be necessary because there will be little deposit. Helium is an alternative buffer gas, and neither argon nor helium participate in reactions.

Water cooling is used to bring down the temperature of the end windows to protect them from harm due to the high temperature in the middle part of the cell. Generally, for infrared spectroscopic experiments, KRS-5 (thallium bromoiodide) windows are used; KRS-5 can not endure temperatures greater than 300 °C, as shown in Table 1.6.

Nitrogen gas is used to purge the cell-spectrometer interface to remove the influence of interfering species (H_2O, CO_2, etc.) in the air. Nitrogen contributes no interference to the infrared spectrum[3].

There is an interesting anecdote about the high temperature furnace experiments. When the mullite cell was heated up without chemicals in it, a very good diatomic molecular spectrum appeared at about 850 °C. It was identified as the SiO molecule, which came from the mullite cell itself! A literature search showed that the Fourier transform infrared spectrum of SiO was published by researchers from the same Laboratory [17] a few years before and was discovered in a similar manner.

1.2.1.2 Cells and Windows

There are three types of commonly used tube cells for experiments using the high temperature furnace, i.e., alumina, mullite, and quartz.

Alumina or aluminum oxide (Al_2O_3) is one of the most refractory ceramic oxides. It has a melting point of 2,015 °C. Alumina is a hard, zero porosity ceramic material for high temperature applications. Its vacuum properties are excellent, with low outgassing and high temperature stability. An alumina ceramic cell is more expensive than a mullite cell. Because alumina is less resistant to thermal shock, a longer time must be allowed for its heating up and cooling down, e.g., 60 minutes for every 500 °C.

Mullite is a good, low-cost refractory material, with a nominal composition of $3Al_2O_3.2SiO_2$. Mullite has a melting point of 1,800 °C. It has good thermal shock and stress resistance, and good thermal strength. Mullite has a low coefficient of thermal expansion, and it is resistant to many corrosive environments. A mullite cell is less expensive than an alumina cell. It is suitable for lower working temperatures.

Table 1.5: Materials and Properties of Cells

Material	Melting Point °C	Working Temperature °C
Alumina	2,015	< 1,500
Mullite	1,800	< 1,300
Quartz	1,610	< 1,000

Table 1.6: End Window Materials

Material	Transmission Range (cm^{-1})	Melting Point (°C)
KRS-5	250 – 16,000 (0.6 – 40 μm)	414.5
CaF_2	1,000 – 76,000 (0.13 – 10 μm)	1,360
Crystal Quartz	3,000 – 25,000 (0.4 – 3 μm)	1,467

Because mullite is more resistant to thermal shock, it takes less time to heat it up or to let it cool down.

Quartz is pure crystalline silicon dioxide SiO_2.[8] Quartz melts at approximately 1,610 °C. The temperature properties of the three tube cells are summarized in Table 1.5.

There are three types of commonly used end windows for the cells, KRS-5, calcium fluoride, and quartz. KRS-5 (thallium bromoiodide) is used as infrared windows where transmission in the 0.6 - 40 μm range is desired. The melting point of KRS-5 is 414 °C, and it is only slightly soluble in water, but can be dissolved in alcohol, nitric acid, and aqua regia. KRS-5 is considered toxic, and hence protective gloves are needed when handling it.

Calcium fluoride (CaF_2) is used for optical windows in the 0.15 - 9 μm range. The polished surfaces are stable and will last several years under normal conditions. Due to its low refractive index, calcium fluoride can be used without anti-reflection coating. It has a melting temperature of 1,350-1,402 °C.

The three types of commonly used windows [18] are listed in Table 1.6.

1.2.1.3 Working Principle

At relatively low temperatures, chemical substances exist in the solid state. Heating through its melting point, sufficient energy is delivered to the system to overcome the potentials binding the molecules in the lattice, and the system passes into the liquid

[8]The impure variety of silicon dioxide SiO_2 is the more commonly known glass.

state. Further addition of heat increases the thermal motion of the molecules in the liquid, and the more energetic ones escape into the vapour phase.

For most of the chemical substances used in the spectroscopic experiments carried out by the author, sufficient sublimation occurs at a temperature lower than the boiling point, and sufficient vapour pressure is obtained below the melting point.

The collision of the gas phase molecules or atoms among themselves or with buffer gases, e.g., argon, excites them, and reaction can take place. This may result in the formation of the new unstable transient species.

The high temperature cell not only heats up the reagents to make the reaction occur, but also acts as a source of blackbody radiation to excite the new species. The radiation from the high temperature cell raises the newly formed species to excited vibrational or rotational states. As in any gas mixture, the collisions among the molecules or atoms promote energy exchange to contribute to the reaction and excitation. Emission spectra are observed when the spontaneous transitions to lower ro-vibrational energy levels occur.

When a high temperature cell is operated in combination with other more energetic excitation means such as DC, AC, or RF discharges, more energy is brought to the species and electronic emission spectra may be observed.

1.2.2 Microwave Discharge Cell

1.2.2.1 Configuration

The configuration of the microwave discharge cell for the generation of transient chemical species is shown in Fig. 1.4. The solid chemicals usually in the powder form are placed in the quartz cell. The microwave head is mounted across the cell. An electric heating tape can also be wound around the portion of the cell that carries the chemicals when heating is necessary. The reaction gases and buffer gas are let in from one end and the vacuum pump is connected to the other end. The spectroscopic radiation from the plasma in the cell is collected with a lens and sent to the FTS.

The main advantage of the microwave-cell is that the cell can be operated with electrodes external to the discharge tube. However, the build-up of deposits inside the cell does change the power coupling into the discharge cell[3].

1.2.2.2 Working Principle

At room temperature or at an elevated temperature for some of the solid chemicals, sublimation occurs and sufficient vapour pressure is obtained below the melting point.

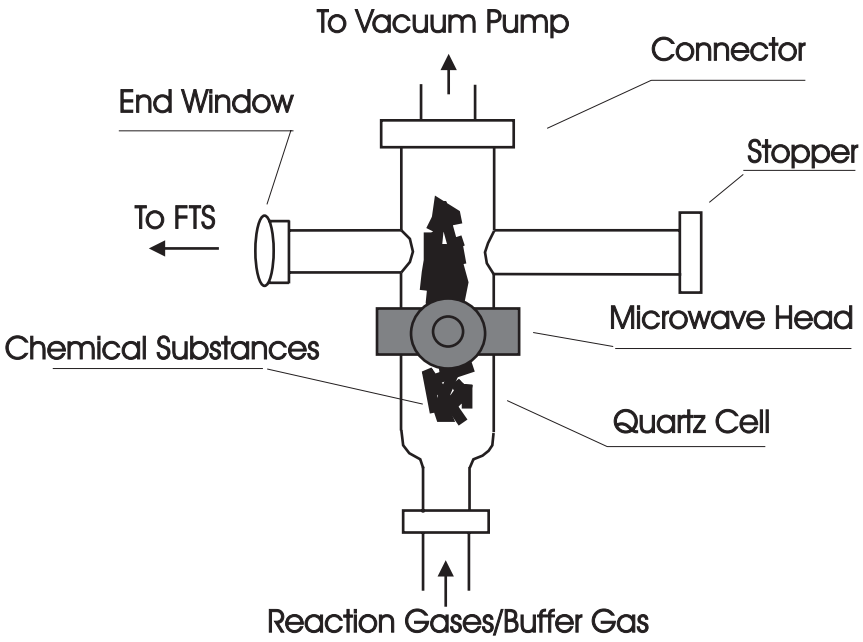

Figure 1.4: Illustration of Microwave Discharge Cell

Having enough vapour pressure is an important factor for a successful spectroscopic experiment.

The gas phase mixture in the microwave discharge cell is composed of a buffer gas (e.g., usually helium, because argon has too many atomic lines from its electronic transitions), reaction gases, and vapour from the solid chemical powder. A plasma in the gaseous mixture is maintained in the microwave discharge cell after the discharge is started.

The plasma state is considered to be the "fourth state of matter". By definition, a plasma is assumed to be electrically neutral and to consist of an equal density of positive ions and negative electrons [19]. It is characterised by a collection of charged particles (ions and electrons) of low density[20, 21]. Microwave energy is transferred to the gas mixture by electrons colliding with gas neutrals and other particles, e.g., ions [21].

The plasma consists of an equal number of mobile light electrons and heavy static ions. Because the difference in mass and hence in mobility between the electrons and ions is large, it is assumed that the ions provide a static charged medium, and that only the electrons are mobile. If the electrons were completely free to move in the medium without any hindrance, there would be no transfer of energy from the electrons to the surrounding heavy ions and gas molecules. The plasma would be "loss-less". However, there are actually elastic and inelastic collisions between the electrons and the other particles in the plasma, and this causes the electrons to lose

some energy [19].

The very high frequencies of microwave radiation involved[3] mean that when microwave fields are applied across a reaction gas mixture, electrons move only short distances before the direction of the field changes. Microwave techniques have made it possible to study interactions between electrons, atoms, and ions without the disturbance of electrode phenomena [22].

The energy transferred to the gas phase reactants in the quartz cell may make the reaction take place. Also, the new species may be formed and pumped to excited states by the the kinetic energy of electrons making it possible for emission spectra to be observed.

1.2.3 Other Excitation Methods

The formation of plasmas using electrical discharges [3] is also commonly used in experiments of electronic emission spectroscopy. Electrical pumping of a gas phase reactant mixture to its excited states is achieved by allowing a current (either CW, RF or pulsed) to pass through the gas mixture [23, 24, 25].

It is the electrons that are responsible for the phenomena occurring in a gas discharge. They acquire energy from the applied electric field and lose or exchange energy through three processes: (1) inelastic collisions with the atoms or molecules of the gas mixture, which raises the atoms or molecules to their excited states, or ionizes them, (2) elastic collisions with atoms or molecules, and (3) electron-electron collisions.

1.3 Spectroscopic Data Processing

The goal of spectroscopic experiments and analyses is to determine numerical values for one or more quantities for the molecule under study, i.e., the set of molecular constants, by measuring and analyzing the spectra of a molecule. Other properties of the molecule can be derived from the molecular constants thus obtained. The molecular constants can not be measured directly. The raw spectroscopic data must be analyzed mathematically or numerically in order to derive the molecular constants. This involves the data reduction process. Because of the experimental errors inherent in any experiment, it is necessary to process the spectroscopic data statistically, which makes the data processing more complicated.

The theory of molecular spectroscopy [4, 26, 27] provides the equations or mathematical models, which are mostly expressed as differences of energy levels, for the processing of the spectroscopic data. The general models work equally well for microwave (pure rotational) data, infrared (ro-vibrational) data and electronic transition data (rotational and vibrational transitions between energy levels of different electronic states). The number of microwave data is usually small, with only information on lower vibrational levels and lower rotational levels (usually one or two vibrational levels of the ground electronic state), but they are usually of the highest accuracy. FT-IR data give us information about a few vibrational levels of the ground electronic state with a continuous coverage of a large frequency range, and with medium accuracy. Electronic transition data from spectrographs give us information about ro-vibrational levels of the electronic states concerned, but with lower accuracy. FTS electronic data have higher accuracy than those from spectrographs. Other sources of spectroscopic data include infrared data from infrared diode laser experiments, which usually have an accuracy comparable to the FTS data, but the number of lines is usually small.

If available, microwave, infrared, and electronic data from different sources should be used together with the newly measured set of experimental data in the overall fitting to derive the most reliable set of molecular constants.

1.3.1 Spectroscopic Models and Software

For diatomic molecules, there are several models that can be used to analyze spectroscopic data. The ro-vibrational energy levels for the simplest electronic state, the $^1\Sigma$ state, may be described by band constants, i.e., G_v, B_v, D_v, $\cdots$, etc., generalized Dunham expansions, near-dissociation expansions, or the individual term values $T(v, J, p)$, i.e., as a function of vibrational and rotational quantum numbers and par-

ity, for each isotopomer. For more complicated electronic states, other terms need to be added to the equations, such as the Λ-doubling constants, etc.

The band constant model and the Dunham constant model are most commonly used. Under the Born-Oppenheimer approximation, both models are derived from the eigenvalues of the Schrödinger equation with a particular form of the potential energy assumed. In a diatomic molecule, the potential energy depends on the distance between the two atoms. In order to solve the Schrödinger equation for the vibrating rotor model to predict the vibration-rotation spectra of diatomic molecules, and to derive the eigenvalues or energies, several empirical forms of $V(r)$ have been proposed [26]. The different forms of potentials give different models for the energy expression. Using the Morse potential, the Schrödinger equation can be solved analytically, the energy levels are expressed as the band constants[9] [26]. Using the Dunham potential, which is a Taylor series expansion about the equilibrium distance r_e, with the first-order semiclassic WKB theory[10] and with some changes in notation, the energy levels can be expressed in the Dunham constants [26].

For the spectroscopic data measured in the experiments reported in this thesis, two software tools have been used. The LSQFIT-D[11] is a PC-based small and flexible software tool. It does least-squares fits of the data and can be used for both band-constant fits and Dunham-constant fits. Also, LSQFIT-D can be used to generate and predict line positions using either band constants or Dunham molecular constants. It is very useful in an initial check of the experimental spectroscopic data to make sure that the quantum number assignments are correct and that the lines picked belong to the same branch or series.

DSParFit [28] is a powerful Unix-based comprehensive software tool that performs least-squares fits of diatomic molecular data consisting of microwave, infrared, or electronic vibrational bands, fluorescence series, etc. DSParFit represents the levels of each electronic state by any of the four models of molecular constants mentioned above, or some combination of them. In addition, by using generalized Dunham expansions, not only can a set of mass-reduced Dunham constants for all the isotopomers be obtained from the least-squares fit, but also the Born-Oppenheimer breakdown correction terms, if any, can be determined. This is very useful in checking the validity of the Born-Oppenheimer approximation for a specific diatomic molecule.

[9] In fact, there are only contributions from the vibrational term value, one anharmonicity term, the rotational constant term, one centrifugal distortion term, and one vibration-rotation term.

[10] Sometimes the WKB approximation is also referred to as the JWKB approximation.

[11] Bernath Laboratory, Dept. of Chemistry, University of Waterloo.

1.3.1.1 Band Constant Model

For a $^1\Sigma$ electronic state of a diatomic molecule, the energy of a ro-vibrational level modelled in terms of band constants $G(v), B_v, D_v, H_v, L_v$, etc., is given by Eqn. (1.5).

$$\begin{aligned} E(v,J) &= G(v) + F_v(J) \\ &= G(v) + B_v J(J+1) - D_v[J(J+1)]^2 + H_v[J(J+1)]^3 \\ &+ L_v[J(J+1)]^4 + \cdots \\ &= \sum_m K_m(v)[J(J+1)]^m, \end{aligned} \tag{1.5}$$

in which $G(v)$ represents the vibrational term values, $F_v(J)$ gives the rotational energy levels for a given vibrational level, while v and J are the usual vibrational and rotational quantum numbers. The constants B_v, D_v, H_v, L_v, etc., are all dependent on the vibrational levels, i.e., they have different values for different vibrational levels, which represents implicitly the vibration-rotation interactions.

Eqn. (1.5) is the band-constant equation for ro-vibrational levels of the ground electronic state. For general ro-vibrational levels of electronic states, $G(v)$ is replaced by $T_e + G(v)$, where T_e is the electronic term value of the electronic state under study.

After fitting the measured and other available spectroscopic data, including microwave, infrared (vibrational-rotational) and electronic data using the proper program, the constants for the appropriate ro-vibrational levels are determined. The number of available (valid) constants is determined by the number and type of data available.

1.3.1.2 Dunham Constant Model

With the Dunham potential expression, by using the JWKB first order semiclassical quantization condition [26], the eigenvalues of the Schrödinger equation can be expressed in terms of Dunham constants [26], i.e., the energy levels are given by Eqn. (1.6),

$$E(v,J) = \sum_{l,m} Y_{lm}(v+1/2)^l[J(J+1)]^m \tag{1.6}$$

where Y_{lm} are the Dunham constants, and v and J are the usual vibrational and rotational quantum numbers.

The Dunham constants Y_{lm} have their correspondences with the band constant counterparts. For data sets with more vibrational levels, more Y_{lm} with different l values can be obtained, and for data sets with high J values, more Y_{lm} with different m values can be obtained.

1.3.1.3 Combined-Isotopomer Dunham-Type Analysis and Born-Oppenheimer Breakdown Correction

The regular Dunham constants for different isotopomers of the same molecular species are different, because the reduced masses are different. In general, the isotopomer dependence of the Dunham constants is $Y_{lm} \propto \mu^{-(l+2m)/2}$, where μ is the reduced mass of the isotopomer. Defining a set of mass-reduced constants as $U_{lm} = \mu^{(l+2m)/2} Y_{lm}$, the spectroscopic data from different isotopomers of the same molecule may be fit together using Eqn. (1.7),

$$E(v, J) = \sum_{l,m} \mu^{-(l+2m)/2} U_{lm} (v + 1/2)^l [J(J+1)]^m \tag{1.7}$$

The mass-reduced Dunham constant model, Eqn. (1.7), allows us to combine the Dunham constants of different isotopic forms of a molecule, which makes the set of molecular constants more compact. From the mass-reduced Dunham constants, the ones for the individual isotopomers can be easily calculated by using the mass-scaling factors. There are two approximations for the mass scaling to be valid, i.e., different isotopomers experience exactly the same effective internuclear potential energy function, and the first order JWKB approximation or Bohr-Sommerfeld quantization condition is exact [29, 26].

For molecules composed of two heavy atoms such as GeO and SiO, the Born-Oppenheimer approximation may be valid so that Eqn. (1.7) may work. However, for a diatomic molecule composed of at least one light atom, such as MgH and BeH, the Born-Oppenheimer approximation may break down. Therefore, some small correction terms must be added to Eqn. (1.7), otherwise the data for different isotopomers will not "come together" in the global fitting [17].

With the Born-Oppenheimer breakdown correction terms included, Eqn. (1.7) becomes Eqn. (1.8) [30].

$$\begin{aligned} E(v, J) \;=\; & \sum_{l,m} \mu^{-(l/2+m)} U_{lm} \left\{ 1 + \frac{m_e}{M_A} \Delta^A_{lm} + \frac{m_e}{M_B} \Delta^B_{lm} \right\} \\ \times \; & (v + 1/2)^l \, [J(J+1)]^m \end{aligned} \tag{1.8}$$

where
U_{lm} - the mass-reduced Dunham constants;
Δ_{lm} - the empirical Ross-Eng-Kildal parameters that correct for breakdown in the Born-Oppenheimer approximation on the centers of the atom A and B [31, 32, 33];
μ - the reduced mass;
M_A and M_B - the masses of the two atoms;
m_e - the electron mass.

Eqn. (1.8) is based on the assumption that the principal effect of the nonadiabatic corrections to the Born-Oppenheimer approximation is the replacement of the nuclear reduced mass in the effective radial Schrödinger equation by the atomic reduced mass, and the first order adiabatic correction terms depend separately on the inverse masses of the two component atoms M_A and M_B [31].

Le Roy [29] listed nine disadvantages of Eqn. (1.8), such as the unobvious meaning of U_{lm} because of the various units and magnitudes, the parameters Δ^A_{lm} and Δ^B_{lm} alone do not indicate the magnitude of the corrections, other drawbacks of the multiplicative parameters, and especially, the parameters $\Delta^A_{l,m}$ and $\Delta^B_{l,m}$ depend on the available number of data of minor isotopomers, etc. In consideration of the difficulties to be encountered when using Eqn. (1.8), Le Roy proposed a revised formulation that is based on two key requirements. The first is that the atomic mass-dependent correction terms should be additive, rather than multiplicative, and the second is that the properties of a selected dominant isotopomer should be used as the reference point for the corrections.

In Le Roy's formulation, the observed transitions for isotopomer-α of species A-B formed from atoms of mass M^α_A and M^α_B are expressed as differences between level energies written as

$$\begin{aligned} E^\alpha(v,J) &= \sum_{l,m}\left\{ Y^1_{l,m} + \frac{\Delta M^\alpha_A}{M^\alpha_A}\,\delta^A_{l,m} + \frac{\Delta M^\alpha_B}{M^\alpha_B}\,\delta^B_{l,m}\right\} \\ &\times \left(\frac{\mu_1}{\mu_\alpha}\right)^{m+l/2}(v+1/2)^l\,[J(J+1)]^m \end{aligned} \tag{1.9}$$

or in a detailed form,

$$E^\alpha(v,J) = \sum_{(l,m)\neq(0,0)} Y^1_{l,m}\left(\frac{\mu_1}{\mu_\alpha}\right)^{m+l/2}(v+1/2)^l\,[J(J+1)]^m \tag{1.10}$$

$$+ \quad \sum_{(l,m)\geq(0,0)} \left\{ \frac{\Delta M_A^\alpha}{M_A^\alpha}\, \delta_{l,m}^A + \frac{\Delta M_B^\alpha}{M_B^\alpha}\, \delta_{l,m}^B \right\}$$
$$\times \quad \left(\frac{\mu_1}{\mu_\alpha}\right)^{m+l/2} (v+1/2)^l \left[J(J+1)\right]^m$$

where $\Delta M_{A,B}^\alpha = M_{A,B}^\alpha - M_{A,B}^1$ and
$\delta_{l,m}^A$ and $\delta_{l,m}^B$ are the Born-Oppenheimer and JWKB breakdown correction terms due to atoms A and B respectively in the diatomic molecule A-B,
μ_1 and μ_α are the reduced masses of the dominant isotopomer and of isotopomers-α.

The condition $\alpha = 1$ identifies a selected reference species, in general chosen to be the most abundant isotopomer. This expression is equivalent to the familiar Ross-Eng-Kildal-Bunker-Watson[31, 34, 33] expansion, except that the Born-Oppenheimer and JWKB breakdown terms are included as additive rather than multiplicative corrections, and the reference species (isotopomer $\alpha = 1$) is a real physical molecule.

The conventional Dunham constants for other ($\alpha \neq 1$) isotopomers are then generated as

$$Y_{l,m}^\alpha \;=\; \left\{ Y_{l,m}^1 + \frac{\Delta M_A^\alpha}{M_A^\alpha}\, \delta_{l,m}^A + \frac{\Delta M_B^\alpha}{M_B^\alpha}\, \delta_{l,m}^B \right\} \left(\frac{\mu_1}{\mu_\alpha}\right)^{m+l/2} \tag{1.11}$$

Other advantages of this expansion are discussed elsewhere[29]. In addition, all the equations are coded in DSParFit [28, 35] and readily available for application. When the Born-Oppenheimer breakdown constants become important, it is necessary to include $\delta_{l,m}^A$ and $\delta_{l,m}^B$ in the combined global fitting of the isotopomers.

1.3.2 Spectroscopic Data Analysis

Generally, the spectroscopic study of a molecular species in the laboratory involves such steps as generating the species of interest chemically or physically, recording the spectra, measuring the line positions (frequencies or wavenumbers) of the spectra, assigning proper quantum numbers to the lines, and fitting the line positions to some equations or mathematical models to derive the molecular constants.

Mathematical models, spectroscopic data and their uncertainties, and other statistical concepts are very important for the analysis of the data. Extensive experience and judgement are necessary in the optimization of the fitted molecular constants.

The mathematical models are generally expressed as polynomials with the vibrational and rotational quantum numbers as independent variables. Therefore, spectroscopic data reduction usually involves multi-parameter least-squares fitting to determine the molecular constants.

1.3.2.1 Uncertainty or Errors in the Data

All experimental measurements have an inherent uncertainty or error [36, 37, 38, 39]. The reliability of data can be expressed using a few concepts. *Accuracy* is the agreement of the experimental measurement with the true value, accepted value, or predicted value of the quantity; *precision* is the agreement of the measurements with one another; and *uncertainty* is a measure of the confidence in the value of an observable, usually described in probablistic terms.

In spectroscopic data reduction, *uncertainty* often refers to the absolute error in a measurement. It is related to the resolution and signal to noise ratio of the spectra. And the term *error* refers to the difference between the observable and the predicted value, i.e., the absolute error.

The line position *uncertainty* σ_n is estimated using an empirical formula [26], as shown in Eqn. (1.12),

$$\sigma_n = \frac{FWHM}{S/N} \tag{1.12}$$

where FWHM is the full width of a spectral line at its half maximum, and S/N is the signal to noise ratio of the spectrum.

The spectroscopic data from the Bruker IFS 120 HR Fourier transform spectrometer has typically a 0.002 cm^{-1} accuracy (or uncertainty). A typical uncertainty for microwave data is 0.000001 cm^{-1}, and 0.05 cm^{-1} is typical for old electronic data recorded using a spectrograph. Usually, it is necessary to calibrate the experimental data to a standard, and to calibrate data from different sources to the same wavenumber scale. Even though Fourier transform spectrometers use the interference fringes of a built-in He-Ne laser to control the sampling of the interferogram and movement of the scanner, the possible misalignment of the laser optics causes slight wavenumber shifts, so the FTS experimental data still need to be calibrated against suitable standards. The spectroscopic data from the Bruker IFS 120 HR FTS reported in the chapters to follow are calibrated either to the standard CO lines or to argon atomic lines, or other standards.

1.3.2.2 Dimensionless Standard Error, Variance, and Confidence Limit

In the process of the derivation of the molecular constants, one common way of representing the quality of a model fit to an experimental data set, and the ability of a given set of parameters to reproduce those data accurately is the *dimensionless standard error* $\overline{\sigma}_f$, or DSE for short [28, 35], defined as

$$\overline{\sigma}_f = \left\{ \frac{1}{N-M} \sum_{i=1}^{N} \left[\frac{y_{calc}(i) - y_{obs}(i)}{u(i)} \right]^2 \right\}^{1/2} \tag{1.13}$$

In this expression, each of the N experimental data $y_{obs}(i)$ has an uncertainty of $u(i)$, $y_{calc}(i)$ is the predicted value from the respective spectroscopic model, and M is the number of parameters in the mathematical model. The weighting with $u(i)$ allows data with very different magnitudes and very different absolute uncertainties (such as microwave data and FTS electronic data) to be combined and treated in an appropriately balanced manner. The quantity $\overline{\sigma}_f$ is the square root of the conventional *reduced chi-squared* (χ^2) formula, or formula of *chi-squared* per degree of freedom[12][39, 40].

Another similar concept often used in analysis of spectroscopic data is the *final variance* as defined in Eqn. (1.14).

$$var = \frac{1}{N-M} \sum_{i=1}^{N} \left[\frac{y_{obs}(i) - y_{calc}(i)}{u(i)} \right]^2 \tag{1.14}$$

The *variance* is the standard deviation squared, which is equivalent to $\overline{\sigma}_f^2$ here.

If the experimental uncertainties are estimated correctly, a value of $\overline{\sigma}_f \sim 1$ means that on average, the predictions of the model differ from the input data by less than the associated experimental uncertainties. Normally a fit with $\overline{\sigma}_f \sim 1$ is acceptable, for example, $\overline{\sigma}_f \sim 1.200$ indicates a good fit. Generally, sets of spectroscopic data from measurements of similar spectrometers under similar experimental conditions should have similar values for the uncertainties.

The quality of the fitting of an individual datum is represented by the root mean square residual (RMSR) of the average dimensionless residuals [28] shown as Eqn. (1.15),

$$RMSR = \left\{ \frac{N-M}{N} \right\}^{1/2} \overline{\sigma}_f \tag{1.15}$$

Other related important concepts are the *confidence limit* and *confidence level*. The confidence limit is an interval, and the confidence level is a percentage for the estimated value to fall within the interval. They are the quantities indicating the reliability of the derived molecular constants.

[12]The *chi-squared* formula is commonly used in testing the agreement between two sets of data quantitatively, usually the observed and the predicated values. For good agreement, the *chi-squared* formula has a result of about $N - M$, and the *reduced chi-squared* formula gives a result of about 1.0.

1.3.2.3 Residuals, Bad Data Points, Fitting Needs

It is possible to spoil the final results by entering a few numbers incorrectly, or by failing to recognize bad data points or outliers, "Garbage in, garbage out" as said by Taylor [39]. Examination of the fitting residuals can reveal the presence of bad data points.

The *dimensionless residual* of a spectroscopic datum is defined as

$$r(i) = \frac{y_{obs}(i) - y_{calc}(i)}{u(i)} \tag{1.16}$$

where $y_{obs}(i)$ are the measured values; $y_{calc}(i)$ are the the predicated values, and $u(i)$ are the uncertainty of the measured data $y_{obs}(i)$. Normally a good set of data should have residuals with absolute values less than 2.0, i.e., $y_{obs}(i)$ and $y_{calc}(i)$ differ by twice the $u(i)$ at the most[13].

Extensive experience and good judgement are necessary in the optimizing process of the derivation of molecular constants. Residuals of the data in the fitting file often provide very useful information.

If the residuals of some isolated data are all very large, say, $r(i) > 10$, then they may be bad data points coming from a wrong measurement or a typographic error. If the assignment is correct, such data should be removed from the data set by giving them very large uncertainty values, for example, 100 times the regular uncertainty values. It is necessary to remove the few data with the largest residuals first, then redo the fitting and repeat the data removal process until all the residuals have acceptable values.

If a group of data at high J all show large residuals and the assignment is correct, then more molecular parameters, e.g., more centrifugal distortion constants in the band constant model, are needed in the fitting.

1.3.2.4 Optimization of Molecular Constants

Normally if the quantum numbers (mostly rotational quantum numbers in vibration bands) are assigned correctly for the measured spectroscopic data, with the bad data points removed, when a proper set of molecular constants is used in the data fitting, the DSE or the variance should be close to 1.0.

It is necessary to check the validity of the individual molecular constants, starting

[13]If the distribution of the random noise is assumed to be Gaussian, the experimental data should be allowed to have a larger residual, such as 3, corresponding to 3σ. In practice, there are also other interferences in the measured line positions, such as blending of lines. Therefore, it is safe to have a data set with stricter requirement of residuals, such as 2.

from the most significant ones (vibrational term values, rotational constants, lower order centrifugal distortion constants, etc., in that order). If a resulting constant has a larger uncertainty than its value, then this constant and the ones of higher order are generally invalid, and some or all of the higher order constants should be removed. The removal of higher order constants should start from the highest order ones and fitting is repeated until a valid set of molecular constants are obtained. The final DSE should not change much, generally less than 0.1 during this optimization process, otherwise something else may be wrong.

Take, for example, the ro-vibrational levels in the ground electronic state. The vibrational spacings decrease gradually with the increase of the vibrational quantum number v, because of the anharmonicity, and the vibration-rotation interaction. The spacings between rotational levels of a vibrational level also decrease gradually with the increase of the rotational quantum number J. Therefore, for a good fitting result, the band constants should have a regular pattern, i.e., from lower order to higher order molecular constants, the results should be in decreasing order of magnitudes and have reasonable sign patterns. For some special cases, a higher order constant may be larger than a lower order one. Sometimes this is acceptable in consideration of the fact that the constants are the coefficients of a polynomial representing the molecular energy levels.

If looking across the vibrational levels, the band constants for different vibrational levels, such as the rotational constants B, centrifugal distortion constants D, etc., for the vibrational levels should change gradually in a regular pattern with the increase of v.

The physical meanings of Dunham constants are not as straight forward as those of the band constants. However, Dunham constants have correspondences with band constants. They can be mapped to their corresponding band constants in order to find the physically meaningful patterns of magnitudes and signs.

1.3.2.5 Rounding and Reporting of Molecular Parameters

All the molecular parameters from the least-squares fit have uncertainties that come from the propagation of the uncertainties of the raw spectroscopic data through the spectroscopic models. The uncertainties of the parameters are the confidence limits of the related confidence level (e.g., 95 % confidence level).

There are several ways of rounding the fitted parameters with respect to their uncertainties [29, 41]. The simplest and most common approach is to round off all parameters at the first, second, or third digit of their uncertainties. Le Roy [41] pointed out that because of correlations between the parameters, spectral line fre-

quencies (wavenumbers) generated from the resulting constants might differ from the observed spectroscopic data by orders of magnitude more than the residual discrepancies associated with the original fit. It is obvious that it is not a good choice to perform the parameter rounding in this way.

An alternative method to the uncertainty-based method for the parameter rounding is to round off the parameters at the first significant digit of the parameter sensitivity $S(P_j)$. The total parameter sensitivities yielded by a proper least-squares fitting have two sources, i) the actual sensitivity of the predicated data $y_{calc}(i)$ to the value of the given parameter P_j, i.e., $\partial y_{calc}(i)/\partial P_j$, and ii) the interparameter correlation, i.e., the change in the value of one parameter is compensated for by a correlated change in one or more other parameters. The sensitivities are typically 2 to 5 orders of magnitude smaller than the associated overall parameter uncertainties, and clearly provide a more selective and systematic basis to perform rounding. The drawback of this method is that it is still necessary to report a large number of significant digits [41].

The best way available is to use the algorithm of sequential rounding and refitting [41]. The essential idea is to round off first the parameter with the largest relative uncertainty to the first significant digit of its *uncertainty* $U(P_j)$, and repeat the fitting to the remaining parameters while holding the rounded value(s) fixed, allowing the inter-parameter correlation to compensate for the effect of the parameter rounding. This process is repeated until there is only one free parameter left. Rounding of this final parameter should use the first digit of the *sensitivity*, rather than the *uncertainty*.[14] This approach can lead to significant reduction in the number of significant digits which must be reported, with essentially no loss in the quality of the representation of the original data set. The algorithm of sequential rounding and refitting has been implemented in the software package DSParFit [28, 35], and can be invoked using a switch in the control file input.

[14] In fact, when there is only one parameter left, there is no large difference between the uncertainty and the sensitivity.

1.4 Conclusion

Understanding the principles behind the experimental apparatus is crucial for experimental success. Because the outcomes of experiments are affected by many factors, it is necessary to have a thorough understanding of the experimental system for trouble shooting and improvement during the experimental process.

Experiments are an important step in the spectroscopic study of transient molecular species. However, the analysis and processing of the spectroscopic data are also important. The latter process requires more background knowledge, and is generally even more time consuming, and involves significant mathematical and computational efforts.

After the spectra of a chemical species have been recorded successfully, data measurement and data analysis become the next important step. Only with thorough understanding of the spectroscopic models and various statistical concepts and with good judgment, can the researcher arrive at the most reliable set of molecular constants or parameters.

Bibliography

[1] M. Mueller. *Fundamentals of Quantum Chemistry: Molecular Spectroscopy and Modern Electronic Structure Computations*. Kluwer Academic/Plemum Publishers, New York, 2001.

[2] P. F. Bernath. Infrared Fourier Transform Emission Spectroscopy. *Chemical Society Review*, 25:111–115, 1996.

[3] P. F. Bernath. Infrared Emission Spectroscopy. *Annu. Rep. Prog. Chem., Sect. C*, 96:177–225, 2000.

[4] S. Svanberg. *Atomic and Molecular Spectroscopy: Basic Aspects and Practical Applications*. Springer, New York, 2001.

[5] F. M. Mirabella. *Modern Techniques in Applied Molecular Spectroscopy*. John Wiley & Sons, Inc., New York, 1998.

[6] P. R. Griffiths and J. A. De Haseth. *Fourier Transform Infrared Spectrometry*. Wiley, New York, 1986.

[7] H.A. Willis. *Laboratory Methods in Vibrational Spectroscopy*, chapter 6, pages 121–143. Wiley Chichester, 1988.

[8] A. P. Thorne. *Spectrophysics*. Chapman and Hall, London, 2nd edition, 1988.

[9] J. W. Brault. *Fourier Transform Spectroscopy*. National Solar Observatory, Tucson, Arizona 85726.

[10] B. P. Lathi. *Communication Systems*. John Wiley & Sons, Inc., New York, 1968.

[11] S. P. Davis, M. C. Abrams, and J. W. Brault. *Fourier Transform Spectrometry*. Academic Press, New York, 2001.

[12] A. A. Christy, Y. Ozaki, and V. G. Gregoriou. Modern Fourier Transform Infared Spectroscopy. In D. Barceló, editor, *Comprehensive Analytical Chemistry*, volume XXXV, Amsterdam, 2001. Elsevier.

[13] H. N. Hsieh. FTIR Instrumentation. *http://web.njit.edu/ hsieh/ene669/FTIR.html*, 2002.

[14] B. Stuart. Modern Infared Spectroscopy. In D. J. Ando, editor, *Analytical Chemistry by Open Learning*, Chichester, 1996. John Wiley & Sons.

[15] S. F. Johnston. *Fourier Transform Infrared: A Constantly Evolving Technology*. Ellis Horwood, New York, 1991.

[16] P. R. Griffiths. *Transform Techniques in Chemistry*. Plenum Press, New York, 1978.

[17] J. M. Campbell, D. Klapstein, M. Dulick, and P. F. Bernath. Infrared absorption and emission spectra of SiO. *The Astrophysical Journal. Supplement Series*, 101:237–254, 1995.

[18] K. Matthews. Optics: A simple guide. Technical report, Crystran Ltd., 2001. `http://www.crystran.co.uk/optics.htm`.

[19] A. J. Baden Fuller. *An Introduction to Microwave Theory and Techniques*. Pergamon Press, New York, 2nd edition, 1979.

[20] G. V. Marr. *Plasma Spectroscopy*. Elsevier Publishing Company, New York, 1968.

[21] M. Capitelli and C. Gorse. *Plasma Technology: Fundamentals and Applications*. Plenum Press, New York, 1992.

[22] A. D. MacDonald. *Microwave Breakdown in Gases*. John Wiley & Sons, Inc., New York, 1966.

[23] A. von Engel. *Electric Plasmas : Their Nature and Uses*. Taylor & Francis, London, 1983.

[24] O. Svelto. *Principles of Lasers*. Plenum Press, New York, 4th edition, 1998.

[25] A. M. Howatson. *An Introduction to Gas Discharges*. Pergamon Press, New York, 1965.

[26] P. F. Bernath. *Spectra of Atoms and Molecules*. Oxford University Press, New York, 1995.

[27] P. F. Bernath. Electronic Spectroscopy of Diatomic Molecules. In Stephen Wilson, editor, *Handbook of Molecular Physics and Quantum Chemistry*, volume 3 of *Molecules in the Physicochemical Environment: Spectroscopy, Dynamics, and Bulk Properties*, chapter 16. John Wiley & Sons, Ltd, 2002.

[28] R. J. Le Roy. *DSParFit 2.0: A Computer Program for Fitting Multi-Isotopomer Diatomic Molecule Spectra*. Dept. of Chemistry, University of Waterloo, Waterloo, Ont. N2L 3G1, Canada, 2001.

[29] R. J. Le Roy. Improved parameterization for combined isotopomer analysis of diatomic spectra and its application to HF and DF. *Journal of Molecular Spectroscopy*, 194(2):189–196, 1999.

[30] J. M. Campbell, D. Klapstein, M. Dulick, and P. F. Bernath. Infrared absorption and emission spectra of SiO. *The Astrophysical Journal Supplementary Series*, 101:237–254, 1995.

[31] A. H. M. Ross, R. S. Eng, and H. Kildal. Heterodyne measurements of $^{12}C^{18}O$, $^{13}C^{16}O$, and $^{13}C^{18}O$ laser frequencies: Mass dependence of Dunham coefficients. *Optics Communications*, 12:433–438, 1974.

[32] J. K. G. Watson. The isotope dependence of the equilibrium rotational constants in $^1\Sigma$ states of diatomic molecules. *Journal of Molecular Spectroscopy*, 45:99–113, 1973.

[33] J. K. G. Watson. The isotope dependence of diatomic Dunham coefficients. *Journal of Molecular Spectroscopy*, 80:411–421, 1980.

[34] P. R. Bunker. The nuclear mass dependence of the Dunham coefficients and the breakdown of the Born-Oppenheimer approximation. *Journal of Molecular Spectroscopy*, 68:367–371, 1977.

[35] R. J. Le Roy. Computer Programs Distributed by Robert J. Le Roy. Technical report, Dept. of Chemistry, University of Waterloo, 2003. `http://scienide.uwaterloo.ca/~leroy/`.

[36] J. R. Barrante. *Applied Mathematics for Physical Chemistry*. Prentice Hall, Upper Saddle River, N.J., 1998.

[37] R. G. Mortimer. *Mathematics for Physical Chemistry*. Macmillan, New York, 1981.

[38] H. W. Salzberg. *Physical Chemistry Laboratory: Principles and Experiments*. Macmillan, New York, 1978.

[39] J. R. Taylor. *An Introduction to Error Analysis : The Study of Uncertainties in Physical Measurements*. Mill Valley, California, 1982.

[40] G. M. Clarke and D. Cooke. *A Basic Course in Statistics*. Arnold, New York, 4th edition, 1998.

[41] R. J. Le Roy. Uncertainty, sensitivity, convergence, and rounding in performing and reporting least-squares fits. *Journal of Molecular Spectroscopy*, 191(2):223–231, 1998.

Chapter 2

Fourier Transform Infrared Emission Spectroscopy of GeO

The infrared spectra of the isotopomers of germanium monoxide have been generated using the high temperature furnace and detected using the Bruker IFS 120 HR high resolution Fourier transform spectrometer. Combined-isotopomer analysis has been carried out using the computer program DSParFit for the newly measured spectral lines plus data available from the literature.

In this Chapter, Section 2.1 summarizes the previous work done by other researchers on the GeO molecule using other techniques, and points out the importance of the Fourier transform infrared technique and the method of the combined-isotopomer analysis in the study of GeO. Section 2.2 presents the principle of the experimental setup and details of the experimental procedures. Section 2.3 describes the details of the spectral line measurement and assignment process and the software tools used. Section 2.4 presents the results of the combined-isotopomer analysis of the newly measured FT-IR lines of the GeO species together with data available from the literature. This is the application of the theory of combined-isotopomer Dunham-type analysis described in Chapter 1. Section 2.5 concludes this Chapter with a summary of the findings such as the advantages of the experimental and analytical procedures, and the results of spectral analysis of the GeO species. The line positions of the infrared transitions of the GeO species are tabulated in Appendix A.

It should be pointed out that the current Chapter is part of a co-authored publication [1] in which the name E. G. Lee was used instead of the current name, Gang Li, of the author.

2.1 Background

As one of the important oxides of group IVa elements, germanium monoxide (GeO) has been studied extensively, both theoretically[2, 3, 4, 5] and in a variety of experiments, including microwave spectroscopy[6, 7], chemiluminescence studies of low-lying electronic states[8, 9, 10], photoelectron spectroscopy[11], electronic absorption [12, 13, 14] and emission[15] spectroscopy, and in matrix isolation[16, 17] and gas phase infrared spectroscopy[18].

Summaries of early spectroscopic work were reported by Capelle and Brom[10], Huber and Herzberg[19] and Żyrnicki[15]. However, the only existing results in the infrared region consist of matrix isolation measurements[16, 17] which give approximate vibrational spacings, and a set of accurate gas phase diode laser measurements involving levels $v = 0-6$ [18]. While the latter are of very high quality, they consist of only a modest number of lines spanning a limited range of vibrational and rotational energies.

Fourier transform infrared emission spectroscopy is a useful means of studying the vibration-rotation spectra of unstable species such as GeO[20]. The high sensitivity and continuous coverage of a wide wavenumber range are major factors in making this technique useful[20, 21].

The GeO species reported in this Chapter was generated using the high temperature cell described in Section 1.2.1. The high resolution infrared spectra were recorded in emission using the Bruker IFS 120 HR Fourier transform spectrometer. The newly measured FT-IR spectroscopic data for all five isotopomers are combined with earlier microwave[6, 7] and diode laser measurements[18], and treated simultaneously in a Dunham-type analysis with isotopomer mass scaling which allows for the presence of atomic mass dependent Born-Oppenheimer breakdown terms.

2.2 Fourier Transform Infrared Experiment

This section presents the details of the experimental setup and the experimental procedures for the Fourier transform infrared investigation of the GeO molecule.

The high temperature infrared spectra of the GeO species were detected without great difficulty. Germanium has a melting point of 938.3 °C and a boiling point of 2,820 °C [22]. It is expected that at around the highest working temperature of the high temperature cell (1,500 °C), there is enough vapor pressure in the cell to make the expected reactions possible. The GeO molecule was one of three possible chemical species to be detected in the experiment. The other two were GeH_x ($x = 1, 2$).

Usually, it takes a few days to prepare for an infrared spectroscopic experiment in which the high temperature furnace cell is used. The preparation typically includes pre-pumping and pre-cooling of the Si:B detector, and transferring liquid helium and liquid nitrogen, setting up of the detectors, beamsplitter, filters, etc., for the Fourier transform spectrometer; and the evacuation of the high temperature cell with the chemical powder to be used to remove water vapor and residual air, etc. The heating up of the alumina ceramic cell from room temperature to 1,500 °C, its maximum working temperature, takes a few hours. In order to make effective use of resources, two routes for the experiments were planned. The first was to detect GeH_x ($x = 1$, 2) species, and the second was to detect GeO.

With the germanium powder in the cell, after overnight vacuum pumping, the heating up of the high temperature cell was started. Beginning at 500 °C, hydrogen gas was let into the cell every 50 °C or 100 °C as the temperature was increased. Up to 1,500 °C, the maximum working temperature of the cell, there appeared no evidence for the GeH_x species. At about 1,500 °C, oxygen gas was let into the high temperature cell, and an intense infrared spectrum of GeO was recorded.

2.2.1 Experimental Setup

The high resolution infrared emission spectra of GeO were obtained in emission with the experimental setup shown in Fig. 2.1. The main components of the system are a Bruker IFS 120 HR high resolution Fourier transform spectrometer, a commercial CM Rapid Temp furnace, a 1.2 meter long alumina ceramic tube cell with water-cooled end windows, gas lines, a vacuum pump, and pressure gauges. This is a typical application of the high temperature cell described in Section 1.2.1 in the generation of transient chemical species. In order to obtain the most intense signal possible, appropriate cell windows, beamsplitter, and detector must be chosen for the wavenumber region in question. The infrared spectra of the germanium oxide

molecule are expected to appear in the range of 500 - 1500 cm^{-1} [18]. Therefore, a KRS-5 (thallium bromoiodide) end window (working wavenumber range 250-16,000 cm^{-1}), a KBr beamsplitter (working wavenumber range 350-6,000 cm^{-1}) and a liquid helium cooled boron-doped Si (Si:B) detector (working wavenumber range 350-2,000 cm^{-1}) were used.

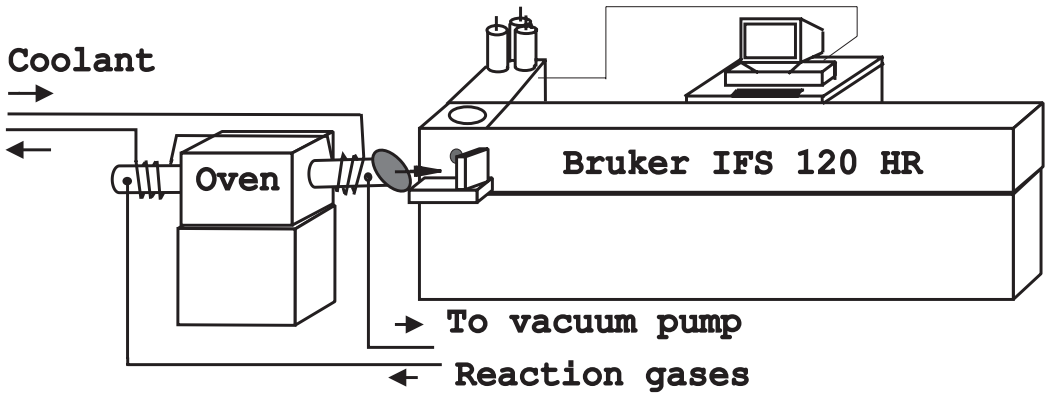

Figure 2.1: Experimental Setup for Fourier Transform Infrared Study of GeO

2.2.2 Experimental Procedures

Five grams of germanium powder (Aldrich) containing the five naturally occurring stable isotopes was placed in the cell. With the cell sealed, overnight pumping was carried out at a temperature of about 200° C to remove impurities (especially water vapour) from the cell. Germanium has a melting point of 934.3° C. The concentraton of the GeO species in the cell is expected to increase, and intense emission is expected to occur above this temperature. More ro-vibrational transitions are expected at higher temperatures. With the furnace at its maximum working temperature of 1,500° C, 18 torr of argon buffer gas and 2 torr of oxygen gas were let into the cell. The valves connected to the cell from the input and output gas lines were kept nearly closed (but not closed) to maintain a high concentration of GeO molecules, while minimizing the concentration of interfering species.

In order to obtain a survey spectrum in a relatively short time (a few minutes), the spectrometer was first set to a resolution of 0.05 cm^{-1} and 10 scans were co-added. A high intensity spectrum consisting of clear P and R branches with sets of evenly spaced lines in the region 800 - 1,100 cm^{-1} appeared, and was identified as being due to GeO by comparisons with the line positions reported in the diode laser experiment of Thompson *et al.*[18]. A higher resolution spectrum was then recorded by setting the spectrometer resolution to 0.006 cm^{-1} and increasing the number of scans to 30. It

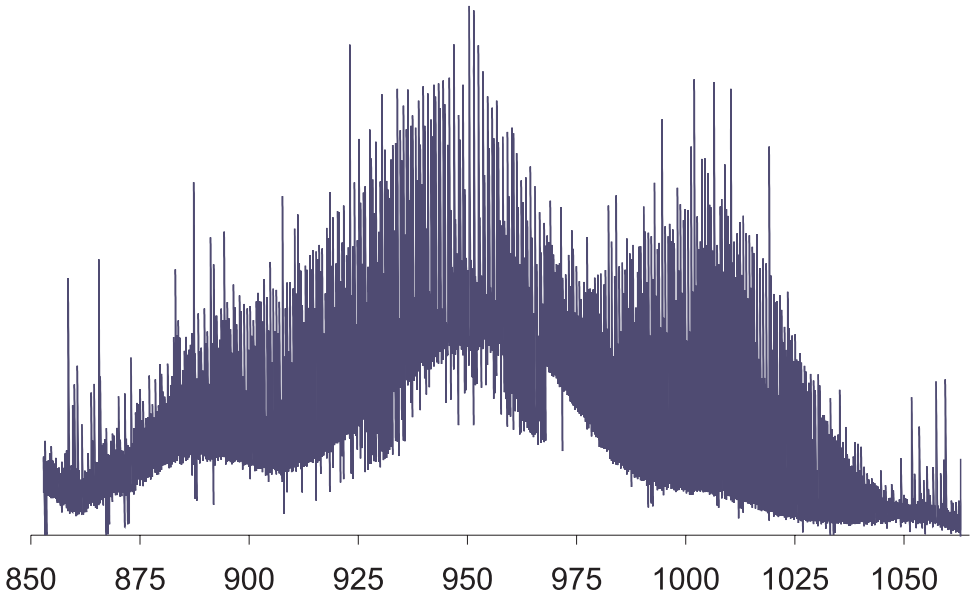

Figure 2.2: High Temperature Fourier Transform Infrared Spectra of Ground State GeO. The absorption lines are due to H_2O and GeH_4. The baseline of the spectrum is not flat because of the underlying continuum.

took about an hour to complete the recording and the Fourier transform computation. Another spectrum was recorded in the same way and the two were added together to reduce the noise and obtain the final spectrum, which is shown in Fig. 2.2.

Theoretically, for random noise, the signal to noise ratio increases as the square root of the number of measurements co-added, i.e., there is a $\sqrt{N}$ trend. However, in reality, the experimental conditions may change at least slightly from one scan of the moving mirror to another, such as the detector coolant liquid helium escaping with time, the concentrations of the GeO molecule and interference species in the cell may not be constant, and the performance of the whole experimental system may fluctuate. Therefore, the spectra were not taken as a large chunk for a large number of co-additions. Instead, 30 scans were co-added for each spectral recording, and then the two of such a spectrum was added together. If one of the spectra had a problem, the other could be still be useful.

2.3 Measurement and Assignment of Spectral Lines

The five naturally occurring stable isotopes of germanium have abundances 35.9% of ^{74}Ge, 27.7% of ^{72}Ge, 21.2% of ^{70}Ge, 7.7% of ^{73}Ge, and 7.4% of ^{76}Ge respectively[1][23] Although there are three naturally occurring oxygen isotopes, ^{16}O is overwhelmingly dominant (99.8% abundance)[23], and is the only one observed here. Therefore, only five isotopomers of the GeO species were observed in this work.

The ro-vibrational line positions in the spectrum were measured using J. Brault's computer program PC/DECOMP[2]. The program PC/DECOMP determines the center of a spectral line by fitting its profile to a Voigt line shape function, which is a convolution of Gaussian and Lorentzian functions[24].

A Loomis-Wood program[3] and a plot of the spectrum were used to help in the identification of the lines belonging to a given band. The plot was made using ATLAS, a function of the PC/DECOMP software. The spectra of GeO are plotted in a well dispersed manner so that the spectral lines belonging to the same vibrational band are easily identified by the feature of even spacings between the lines. The approximate numerical line positions can be read from the plot, which is helpful for the initial identification and grouping of data points using the Loomis-Wood program.

The Loomis-Wood program plots the line positions that appear to belong to the same band in a regular curve pattern. The intensities of the spectral lines are represented with different colors. When some of the data that belong to the same band are picked, the program updates the curve pattern and makes the identification of other lines of the same band easier. After one whole series of spectral lines have been picked, the spectral data can be saved in an ASCII file. The Loomis-Wood program also assigns a serial number for each line picked. The numbers are usually not the correct rotational quantum numbers for the lines. However, they do help in making rotational quantum number assignments. The numbering is made according to the even spacings of the lines. For spectral lines with even spacing, the serial numbers are continuous; for any missing line in the series, the numbering integer also jumps by one.

The diode laser data[18] served as a guide for identifying and assigning the major bands of the five isotopomers. Hot bands were identified and assigned using predictions made from the molecular constants derived from the least squares fitting of the

[1]The 2nd edition (1993) of the handbook "Quantities Units and Symbols in Physical Chemistry" [23] has a wrong mass for ^{72}Ge, which should be 71.9920789 instead of 71.9220789. This error was discovered when DSParFit was used to fit the data of all five isotopomers together. The data for ^{72}GeO appeared incompatible with the rest.

[2]J. Brault, program PC/DECOMP, version 2.60 (1993)

[3]C.N. Jarman, program Loomis-Wood, version 2.0 (1993)

fundamental bands and any hot bands already identified for each isotopomer.

The PC-based program LSQFIT-D[4] was used to fit the assigned data of each isotopomer to band constants to check the correctness of the quantum number assignments. The predictions of the weaker bands were also generated by using the LSQFIT-D program with fixed values of the molecular constants derived so far. The spreadsheet tool MS-Excel was used very often in the matching of the rotational quantum numbers and the spectroscopic data for the input file for LSQFIT-D.

A total of 1,228 P and R lines were assigned in the first seven $\Delta v = -1$ sequence bands of the ^{74}GeO isotopomer, 1,223 lines in the 1–0 to 8–7 bands of ^{72}GeO, 1,029 in the 1–0 to 7–6 bands of ^{70}GeO, 789 lines in the 1–0 to 6–5 bands of ^{73}GeO, and 848 lines in the 1–0 to 6–5 bands of ^{76}GeO. Some spectral lines were obscured by absorption due to residual impurities, such as water vapour and GeH_4, in the high temperature cell, and many other lines are blended; this is illustrated by the segment of the GeO spectrum shown in Fig. 2.3. For the unblended FT-IR data used in the present analysis, the line position uncertainties were estimated to be ca. 0.002 cm^{-1}.

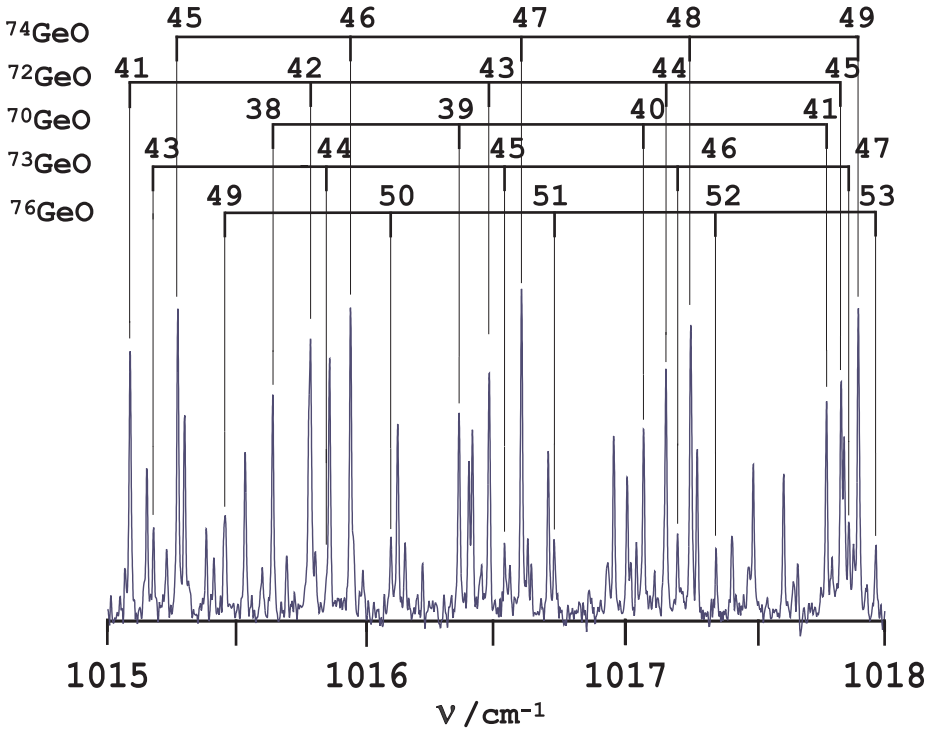

Figure 2.3: Expanded View of a Portion of the Fourier Transform Infrared Spectra of GeO

After all the measurable spectral lines of the bands of the GeO spectrum were picked and assigned, the line positions were calibrated using the diode laser data [18].

[4]Bernath's Group, Dept. of Chemistry, University of Waterloo.

Table 2.1: Overview of the GeO($X\,^1\Sigma^+$) Data Used in the Combined-Isotopomer Analysis.

Isotopomer	FT-IR Data			Diode Laser Data			Microwave Data		
(Abundance)	v_{max}	J_{max}	# lines	v_{max}	J_{max}	#lines	v_{max}	J_{max}	#lines
^{70}Ge^{16}O(21.2%)	7	100	1029	5	82	19	1	1	2
^{72}Ge^{16}O(27.7%)	8	103	1223	6	80	27	1	1	2
^{73}Ge^{16}O(7.7%)	6	90	789	4	80	15	0	1	1
^{74}Ge^{16}O(35.9%)	8	110	1228	6	79	25	2	1	5
^{76}Ge^{16}O(7.4%)	7	91	848	5	78	12	1	1	2

Data from the diode laser experiments of Thompson *et al.*[18] (with an average uncertainty 0.00055 cm^{-1}) were taken as the calibration standard. Some 90 matching ro-vibrational transitions from the measured FT-IR spectrum and the diode laser experiment were fitted to the expression $\nu_{DL}(i) = A \times \nu_{FT}(i) + B$, where $\nu_{DL}(i)$ are the diode laser data and $\nu_{FT}(i)$ the measured FT-IR transition frequencies, to determine the calibration factor $A = 1.000001869$. The intercept B in the linear equation was not determined, and only the slope A is meaningful in the formula above. Up to now the data processing has been done only for individual isotopomers. After calibration, the individual data files of the isotopomers were combined into one large single file, in accordance with the required channel-4 format [25] of the program DSPartFit [26], and the combined-isotopomer analysis was carried out.

An overview of the extent and range of the three types of data used in the analysis reported in this Chapter is given in Table 2.1.

2.4 Combined-Isotopomer Dunham-Type Analysis

In the program DSPartFit [25, 26, 27], following Section 1.3.2.2, the quality of fit of the spectral line positions to a spectroscopic model is indicated by the value of the dimensionless standard error $\overline{\sigma}_f$,

$$\overline{\sigma}_f \quad = \quad \left\{ \frac{1}{N-M} \sum_{i=1}^{N} \left[\frac{y_{calc}(i) - y_{obs}(i)}{u(i)} \right]^2 \right\}^{1/2} , \tag{2.1}$$

in which each of the N experimental data $y_{obs}(i)$ has an uncertainty $u(i)$, and $y_{calc}(i)$ is the value of datum–i predicted by the M–parameter model being fitted. All parameter uncertainties quoted here are 95% confidence limit uncertainties.

The first stage of the combined-isotopomer Dunham-type analysis consists of fitting to separate band constants and then Dunham expansions for each of the five individual isotopomers. Generally, the band-constant fit has fewer constraints (i.e., larger degree of freedom of parameter selection) than the Dunham-constant fit because it usually results in more constants than the Dunham fit. In other words, a data set with a good band-constant fit may not have a good Dunham-constant fit, and a data set with a good Dunham-constant fit mostly has a good band-constant fit. The combined-isotopomer Dunham-type fit has the most constraints, because all the isotopomers are to be fit together. Also, in a band-constant fit, the energies of different vibrational levels are treated separately, whereas in a Dunham-constant fit, the energies of different vibrational levels are fit together. Therefore, it is a good practice to start with the band-constant fit for a data set. After making sure that the data sets behave properly in a band-constant fit, a Dunham-constant fit can be started. The combined-isotopomer Dunham-type fit is the final step of the data analysis.

In all cases of the individual isotopomer fits, the residual discrepancies were comparable to the experimental uncertainties ($\overline{\sigma}_f \sim 1$), and the internal consistency of the fits showed that there were no mis-assignments or anomalies in these data sets. However, the total number of independent Dunham parameters required to represent the data for the five isotopomers ($5 \times 11 = 55$) was rather large. In order to simplify the representation of these data sets and to search for physically interesting information about Born-Oppenheimer breakdown effects, all of the 5,117 FT-IR lines, the 98 diode laser measurements[18], and the 12 microwave data[6, 7] for the five isotopomers were simultaneously fit to a combined-isotopomer Dunham-type expression for the energy levels. Following Section 1.3.1.3, observed transitions for isotopomer-α

of the species GeO formed from atoms of mass M^{α}_{Ge} and M_O (the atomic mass of ^{16}O) are expressed as differences between energy levels written as

$$\begin{aligned} E^{\alpha}(v,J) \;=\; & \sum_{(l,m)\neq(0,0)} Y^1_{l,m} \left(\frac{\mu_1}{\mu_\alpha}\right)^{m+l/2} (v+1/2)^l \left[J(J+1)\right]^m \\ + \; & \sum_{(l,m)\geq(0,0)} \left\{ \frac{\Delta M^{\alpha}_{Ge}}{M^{\alpha}_{Ge}}\, \delta^{Ge}_{l,m} \right\} \left(\frac{\mu_1}{\mu_\alpha}\right)^{m+l/2} (v+1/2)^l \left[J(J+1)\right]^m \end{aligned} \tag{2.2}$$

where $\Delta M^{\alpha}_{Ge} = M^{\alpha}_{Ge} - M^1_{Ge}$, and $\alpha = 1$ identifies the selected reference species, the most abundant isotopomer ^{74}Ge^{16}O (35.9%).

The conventional Dunham constants for other ($\alpha \neq 1$) isotopomers are then generated as

$$Y^{\alpha}_{l,m} \;=\; \left\{ Y^1_{l,m} \,+\, \frac{\Delta M^{\alpha}_{Ge}}{M^{\alpha}_{Ge}}\, \delta^{Ge}_{l,m} \right\} \left(\frac{\mu_1}{\mu_\alpha}\right)^{m+l/2} \tag{2.3}$$

The complete data set was fit to Eqn. (2.2) using the program DSParFit [25, 27, 26], which simplifies the resulting parameters by applying the sequential rounding and refitting procedure described in Section 1.3. This yielded the molecular constants given in the first column of Table 2.2. A search for significant Born-Oppenheimer breakdown effects showed that their inclusion could at best reduce the dimensionless standard error $\overline{\sigma}_f$ by only ca. 1%, and the resulting parameter value(s) had large relative uncertainties (e.g., $\delta^{\rm Ge}_{1,0} = -8.(\pm 2.)\times 10^{-3}$). The final fits reported below were therefore performed without including such correction terms. In this case Eqn. (2.3) collapses to the simple first-order semiclassical relationship $Y^{\alpha}_{l,m} = Y^1_{l,m}(\mu_1/\mu_\alpha)^{m+l/2}$ used to determine the molecular constants for the "minority" isotopomers reported below.

For the user's convenience, those constants for the minority isotopomers, rounded at the first digit of the parameter sensitivity[28], are shown in the last four columns of Table 2.2. The results in the last row of this table show that the rounded constants generated from the ^{74}Ge^{16}O parameters determined from the combined-isotopomer analysis reproduce the input data for the individual minority isotopomers with no significant loss of precision.

A list of all the FT-IR lines measured in this experiment (after the calibration) and their residuals from the fitting using DSParFit are given as Tables A.1 to A.5 in Appendix A.

Table 2.2: Parameters for $X\,^1\Sigma^+$ state GeO obtained by fitting all FT-IR, diode laser and microwave data to Eqn. (2.2); The numbers in parentheses are the 95% confidence limit uncertainties in the last significant digits shown.

	Constant	All-Isotopomer Fit ^{74}Ge^{16}O	Generated from ^{74}Ge^{16}O Constants and Eqn(2.3) ^{70}Ge^{16}O	^{72}Ge^{16}O	^{73}Ge^{16}O	^{76}Ge^{16}O
	$Y_{1,0}$	986.49295 (33)	991.49568	988.92877	987.69269	984.17858
	$Y_{2,0}$	−4.47014 (15)	−4.515593	−4.492242	−4.481019	−4.44919
10^3	$Y_{3,0}$	4.65 (3)	4.7211	4.6845	4.667	4.6173
10^3	$Y_{4,0}$	−0.010 (2)	−0.0102	−0.0101	−0.01005	−0.00991
	$Y_{0,1}$	0.4856978 (4)	0.49063646	0.4880993	0.48687989	0.48342152
10^4	$Y_{1,1}$	−30.7832 (9)	−31.2539	−31.01179	−30.89565	−30.56705
10^4	$Y_{2,1}$	0.0126 (2)	0.012858	0.012725	0.012661	0.012482
10^4	$Y_{3,1}$	−0.00009 (2)	−0.0000923	−0.0000911	−0.0000905	−0.0000889
10^8	$Y_{0,2}$	−47.10 (2)	−48.063	−47.567	−47.33	−46.66
10^8	$Y_{1,2}$	−0.0617 (7)	−0.06328	−0.06247	−0.06208	−0.06098
10^{14}	$Y_{0,3}$	−7. (1)	−7.2	−7.1	−7.1	−6.9
No. of Data		5227	1050	1252	805	862
No. Parameters		11	0	0	0	0
$\overline{\sigma}_f$		0.806	0.789	0.732	0.867	1.017

2.5 Conclusion

The high temperature cell method is effective for the generation of high temperature species, such as GeO with precursors whose melting points are below 1,500°C (the maximum working temperature of the furnace). Thermal radiation from the high temperature cell not only sublimates or melts the solid chemicals to create the vapour pressure necessary to facilitate the reaction, but also promotes the newly generated species to excited ro-vibrational states. It is a very effective means for generating transient species for experimental studies using infrared emission spectroscopy. Very often, several hot bands can be detected in the ro-vibrational spectra generated this way.

Combined-isotopomer Dunham-type analysis produces many fewer molecular constants used to describe the isotopomers than does representing the isotopomers individually. In addition, the global fitting of data for all the isotopomers allows the exploration of the Born-Oppenheimer breakdown effect. As expected, for the GeO species as an example of a diatomic molecule composed of two heavy atoms, such breakdown effect is, at best, marginally observable.

Bibliography

[1] E. G. Lee (Gang Li), J. Y. Seto, T. Hirao, P. F. Bernath, and R. J. LeRoy. FTIR Emission Spectra, Molecular Constants and Potential Curve of Ground State GeO. *Journal of Molecular Spectroscopy*, 194:197–202, 1999.

[2] V. Kellő and A. J. Sadlej. Quasirelativistic studies of molecular electric properties: Dipole moments of the group IVa oxides and sulfides. *Journal of Chemical Physics*, 98(2):1345–1351, 1993.

[3] J. Leszczynski and J. S. Kwiatkowski. Molecular structures and vibrational IR spectra of GeX and XGeY species (X, Y = O, S, Se) by *ab initio* Hartree-Fock and Post-Hartree-Fock study. *Journal of Chemical Physics*, 97:12189–12192, 1993.

[4] Z. Barandiarán and L. Seijo. Quasirelativistic *ab initio* model potential calculations on the group IV hydrides (XH_2, XH_4; X=Si, Ge, Sn, Pb) and oxides (XO; X = Ge, Sn, Pb). *Journal of Chemical Physics*, 101(5):4049–4054, 1994.

[5] F. L. Sefyani, J. Schamps, and D. Duflot. Theoretical study of the radiative properties of the $A^1\Pi - X^1\Sigma^+$ system of the GeO molecule. *Journal of Quantitative Spectroscopy and Radiative Transfer*, 54(6):1027–1034, 1995.

[6] T. Tőrring. Das mikrowellenrotationsspektrum des GeO. *Zeitschrift fur Naturforschung*, A21:287–289, 1966.

[7] R. Honerjäger and R. Tischer. g_J Faktor der Molekeln GeO und SiS und Anisotropie ihrer Magnetisierbarkeit. *Zeitschrift fur Naturforschung*, A28:1374–1375, 1973.

[8] G. H. Leroy, E. Wilson, and S. G. Hadley. Reaction of atomic silicon and germanium with nitrous oxide to produce electronically excited silicon monoxide and germanium monoxide. *Chemical Physics Letters*, 27(3):439–441, 1974.

[9] G. Hager, R. Harris, and S. G. Hadley. The $a^3\Sigma^+ - X^1\Sigma^+$ and $b^3\Pi - X^1\Sigma^+$ band system, of SiO and the $a^3\Sigma^+ - X^1\Sigma^+$ band system of GeO observed in chemiluminescence. *Journal of Chemical Physics*, 63(7):2810–2820, 1975.

[10] G. A. Capelle and J. M. Brom, Jr. Reactions of germanium vapor with oxidizers: Photon yields and a new GeO band system. *Journal of Chemical Physics*, 63(12):5168–5176, 1975.

[11] E. A. Colbourn, J. M. Dyke, A Fackerell, A. Morris, and I. R. Trickle. Vacuum ultraviolet photoelectron spectrum of the GeO ($X^1\Sigma^+$) molecule. *Journal of the Chemical Society: Faraday Transactions II*, 74:2278–2285, 1978.

[12] A. Lagerqvist and I. Renhorn. The low-lying electronic states of GeO. *Physica Scripta*, 25:241–256, 1982.

[13] O Appelbald, S. Fredin, and A. Lagerqvist. On the $E^1\Sigma^+ - X^1\Sigma^+$ system of GeO in the vacuum ultraviolet region. *Physica Scripta*, 25:933–938, 1982.

[14] O. Appelbald, S. Fredin, A. Lagerqvist, and F. Alberti. The spectra of $^{74}Ge^{16}O$ and $^{74}Ge^{18}O$ in the vacuum ultraviolet region. *Physica Scripta*, 28:160–170, 1982.

[15] W. Żyrnicki. High resolution studies of the $A^1\Pi - X^1\Sigma^+$ band system of GeO. *Journal of Molecular Spectroscopy*, 89:557–560, 1981.

[16] J. S. Ogden and M. J. Ricks. Matrix isolation studies of group IV oxides. II. Infrared spectra and structures of GeO, Ge_2O_2, Ge_3O_3 and Ge_4O_4. *Journal of Chemical Physics*, 78:352–357, 1970.

[17] A. Bos, J. S. Ogden, and L. Orgee. Matrix isolation infrared study of the reaction between germanium vapor and molecular oxygen. The characterization and mechanism of formation of molecular germanium dioxide and ozone. *Journal of Physical Chemistry*, 78(17):1763–1769, 1974.

[18] G. A. Thompson, A. G. Maki, and A. Weber. The infrared spectra of GeO. *Journal of Molecular Spectroscopy*, 116:136–142, 1986.

[19] K. P. Huber and G. Herzberg. *Constants of Diatomic Molecules. Molecular Spectra and Molecular Structure IV.* Van Nostrand Reinhold Company, Toronto, 1979.

[20] P. F. Bernath. Infrared Fourier transform emission spectroscopy. *Chemical Society Reviews*, 25:111–115, 1996.

[21] P. F. Bernath. Infrared Emission Spectroscopy. *Annu. Rep. Prog. Chem., Sect. C*, 96:177–225, 2000.

[22] Mark Winter. WebElement Printable Table. Technical report, The University of Sheffield and WebElements Ltd, UK, 2003. `http://www.webelements.com/webelements/elements/text/Ge/heat.html`.

[23] I. Mills, T. Cvitaš, K. Homann, N. Kallay, and K. Kuchitsu. *Quantities, Units and Symbols in Physical Chemistry*. Boston, International Union of Pure and Applied Chemistry, 2nd edition, 1993.

[24] P. F. Bernath. *Spectra of Atoms and Molecules*. Oxford University Press, New York, 1995.

[25] R. J. Le Roy. Computer Programs Distributed by Robert J. Le Roy. Technical report, Dept. of Chemistry, University of Waterloo, 2003. `http://scienide.uwaterloo.ca/~leroy/`.

[26] R. J. Le Roy. *DspartFit 2.0: A Computer Program for Fitting Multi-Isotopomer Diatomic Molecule Spectra*. Dept. of Chemistry, University of Waterloo, Waterloo, Ont. N2L 3G1, Canada, April 2001.

[27] R. J. Le Roy. Improved parameterization for combined isotopomer analysis of diatomic spectra and its application to HF and DF. *Journal of Molecular Spectroscopy*, 194(2):189–196, 1999.

[28] R. J. Le Roy. Uncertainty, sensitivity, convergence, and rounding in performing and reporting least-squares fits. *Journal of Molecular Spectroscopy*, 191(2):223–231, 1998.

Chapter 3

Fourier Transform Emission Spectroscopy of WO

Considering the importance of tungsten and its compounds as high temperature materials, the number of publications of spectroscopic studies of tungsten monoxide is relatively small. One reason might be due to the complicated spectroscopy of the WO molecule, because the partially filled *d*-electron shell usually leads to a complicated electronic structure with a large number of low-lying energy states. Another reason might be the difficulty in generating the species in a laboratory environment because of the high melting points of precursors. In the limited number of papers discussing the ground electronic state of WO, very different conclusions were given. WO was suggested to have a $^3\Sigma^-$ ground state from an absorption spectroscopic study in neon and argon matrices [1], and from an absorption spectroscopic study in gas phase [2]. However, a later *ab initio* calculation [3] predicted the ground state to be $^5\Pi$.

In the spectroscopic investigations reported in this Chapter, the electronic spectra of tungsten monoxide were detected in emission using two high resolution Fourier transform spectrometers. The WO species was generated in the gas phase using microwave discharge cells, and the spectra were generated using vaporized WCl_6 and helium buffer gas without added O_2. In addition to new and high accuracy spectroscopic information (line positions, and molecular constants for the bands) obtained for this molecule, analysis of the bands of several systems confirms that the ground electronic state of tungsten monoxide is $^3\Sigma^-$.

In this Chapter, Section 3.1 summarizes the historical background of the spectroscopic studies of the tungsten monoxide molecule. Section 3.2 describes the details of the experimental procedures and the observations from the experiments, while Section 3.3 presents the theoretical basis for the spectroscopic analysis, and Section 3.4 describes the details of the analysis of the electronic emission spectra of tungsten

monoxide. Finally, Section 3.5 concludes this Chapter by identifying and discussing the nature of the ground electronic state of the tungsten monoxide molecule.

The current Chapter is part of a co-authored publication [4].

3.1 Background

The results of the high resolution Fourier transform spectroscopy of the gas phase WO species reported in this Chapter provide more experimental information about this molecule. The results of the rotational analysis of the gas phase spectra are helpful in the clarification of some confusion about the ground electronic state of WO. In the experimental study of the WO species reported in this Chapter, the first spectrum of tungsten monoxide was detected in emission using a Bruker IFS 120 high resolution Fourier transform spectrometer at Waterloo, and another spectrum was recorded using the one-meter Fourier transform spectrometer of the US National Solar Observatory.[1] The rotational analysis reported in this Chapter is based on the latter spectra, which were recorded in the range of 9,000 - 34,500 cm^{-1}, and detected with a spectral resolution of 0.03 cm^{-1}. It took 1 hour 20 minutes to complete the recording. Results of the rotational analysis of the bands of various electronic systems show that the ground electronic state is $^3\Sigma^-$, which confirmed the low temperature matrix studies[1] and the earlier gas phase studies [2]. The prediction for the ground electronic state, $^5\Pi$, made by the *ab initio* calculations [3] is incorrect.

This Section summarizes the literature on previous investigations of the WO molecule in terms of contributions to the understanding of the spectroscopic properties of the molecule, the techniques used in the investigations, and the results.

3.1.1 Summary

The early low-resolution gas phase spectrum of WO was detected in emission in the 1950s using a DC discharge between pure tungsten electrodes [5], in which several bands of two electronic systems were detected in the near infrared, visible, and ultraviolet regions. Two years later, four new systems in the infrared region were reported [6]. Limited by the techniques available then (low-dispersion spectrographs), only band heads of transitions between low vibrational levels of the electronic states were reported in these two early papers [5, 6], and only tentative vibrational analyses were made to derive the Deslandres tables.

The ground electronic state of WO was first identified to be of $^3\Sigma^-$ symmetry in the 1960s when the electronic absorption spectra of $W^{16}O$ and $W^{18}O$ trapped in low temperature matrices of neon and argon were obtained [1]. Numerous strong absorptions clearly due to WO were observed in the visible region. The bands were assigned to seven distinct electronic transitions of WO. Some of them due to the systems previously observed in the gas phase [5, 6]. The $W^{18}O$ spectrum appeared to be rather

[1] US National Solar Observatory, Kitt Peak, Tucson, Arizona, USA. http://www.nso.edu.

regular, so its vibrational structure could be analyzed, but many perturbations were observed in the $W^{16}O$ spectrum. The vibrational levels of the excited states of $W^{16}O$ appeared to interact strongly. Based on comparison with the neighboring oxides in the periodic table, the value $\Delta G''_{1/2} = 1054.9$ cm^{-1} of the gas spectra [5, 6] was confirmed by the matrix spectra, and the ground state configuration of WO was proposed to be a $\sigma^2\delta^2$ configuration, yielding a $^3\Sigma^-$ ground electronic state. As pointed out by Weltner and McLeod [1], results of rotational analyses of gas phase spectra of WO were needed to determine whether these predictions were correct.

The infrared absorption of the diatomic WO in matrices was re-examined in the early 1980s using krypton and argon matrices [7]. The sputtering technique was used to produce the species instead of vaporization of the solid oxide or by passing oxygen into a heated tungsten cell [1]. The results for $W^{16}O$ were in accordance with previous measurements and the $W^{18}O$ peak observed provided firm support for the assignments. Vibrational constants (ω_e and $\omega_e x_e$) of $W^{16}O$ in both argon and krypton matrices were derived from the measured frequencies of $W^{16}O$ and $W^{18}O$ [7].

The breakthrough in the gas phase studies of WO (only the $^{186}W^{16}O$ isotopomer actually) was made in the early 1980s [2], when the first rotational analysis was made. The WO molecule was generated in the gas phase by photolysis of $W(CO)_6$ in the presence of oxygen, and numerous bands attributed to ten separate systems were recorded in absorption. The wavenumbers of the lines of the WO spectrum with natural isotopic abundance were recorded with an accuracy of 0.1 cm^{-1}. Another spectrum was recorded with tungsten hexacarbonyl 97% enriched with ^{186}W and 73% enriched with ^{18}O to facilitate band identification (from the ratio of $W^{16}O$ and $W^{18}O$ band intensities, and isotopic vibrational frequency shifts), with an accuracy of better than 0.5 cm^{-1}.

In the gas phase spectra, the symbols, using letters from A to G, used by Weltner *et al.* [1] were retained to designate the band systems. Among the sixty bands of $W^{16}O$ observed, only the *D*-*X* (8 bands) and *H*-*X* (5 bands) systems are easily distinguishable. The bands with $v'' \geq 1$ are very weak. Only fourteen rather strong and well-developed bands assigned to the *D*-*X*, *E*-*X*, *F*-*X*, *H*-*X*, etc., were selected for the rotational analysis. The results of the analysis confirmed the identification of several WO bands suggested on the basis of the vibrational structure analysis [1, 7], and have shown that the transitions investigated have the same lower electronic state. Based on the analysis of the possible electron configuration, it was suggested that the WO molecule probably has a $^3\Sigma^-$ ground state with the configuration of $\cdots\delta^2\sigma^2$ with a coupling characteristic of the angular momenta close to Hund's case (c), and the transitions considered are associated with the $X_1 0^+$ state, one of the spin components

of the $^3\Sigma^-$ state. The splitting of the $X_1 0^+$ and $X_2 1$ components was identified as being about 71 cm^{-1}, a number that seemed unreasonably low for a heavy molecule like WO [2]. The transitions to the second component $X_2 1$ state of the $^3\Sigma^-$ state, were not observed in the matrix spectra [1, 7]. Based on the observation of many similar electronic states in a narrow energy range, all with nearly equal rotational and vibrational constants, the assumption of a Hund's case (c) coupling for the WO molecule was confirmed. The perturbations in the vibrational and rotational structure also indicate the presence of a great number of interacting states as is common for Hund's case (c). Unfortunately most of the observed perturbations could not be analyzed due to the amount of overlap between different bands [2].

In a computational study of the low-lying electronic states of WO in the mid-1980s [3], the ground electronic state of WO was identified as $^5\Pi$. In the investigation of the bonding nature of the first, second, and third row transition metal oxides, CrO, MoO, and WO, the differences in the bonding and the ordering of the low-lying states when moving down the column from CrO, through MoO to WO were considered. The low-lying states, $^5\Pi$, $^5\Sigma^+$, $^7\Pi$, and $^7\Sigma^+$ were investigated for each of CrO, MoO and WO. Both self-consistent field (SCF), and multiconfiguration self-consistent field (MCSCF) calculations were performed. It was concluded that for all three systems, the ground state is $^5\Pi$, but the ordering of the higher states is different for WO than for CrO and MoO: $^5\Sigma^+$ is the second excited state in CrO and MoO, while it is the fourth excited state in WO [3].

3.1.2 Contributions in Chronological Order

The key contributions to the studies of WO are summarized in chronological order as follows.

1. 1952, Gatterer *et al.* [5]. The emission spectrum was generated by using arc discharge between tungsten electrodes; a few bandheads of two electronic systems were recognized.

2. 1954, Vittalachar *et al.* [6]. A few bandheads of four more electronic systems were reported.

3. 1965, Weltner *et al.* [1]. By using low temperature argon and neon matrices, vibrational bands of seven electronic transitions were detected in absorption, the ground electronic state was identified as $^3\Sigma^-$.

4. 1979, Efremov *et al.* [8]. By using intracavity laser spectroscopic technique, and a flash photolysis cell with $W(CO)_6$ placed in the cavity of a Nd^{3+}-glass

laser, an absorption band was detected at 12911 cm^{-1}; although details were not given, it was concluded that for this molecule, Hund's case (c) is valid and the ground state is of the 0^+ type (a component of the $^3\Sigma^-$ state).

5. 1981, Green *et al.* [7]. Vibrational constants were determined from infrared spectra of matrix-isolated WO species.

6. 1981, Samoilova *et al.* [2]. An absorption spectrum of gaseous $^{186}W^{16}O$ was recorded in the near UV region, and a rotational analysis was performed; the ground electronic state was identified as $^3\Sigma^-$.

7. 1985, Nelin and Bauschlicher [3]. This is an *ab initio* investigation of the low-lying electronic states; the ground electronic state was identified as $^5\Pi$.

8. 1997, Kuzyakov *et al.* [9]. The *A*-*X* and *B*-*X* transitions were detected by using the laser intracavity spectroscopic technique; the bands were rotationally analyzed.

9. 1998, Kraus *et al.* [10]. By using a conventional laser vaporization source and cavity ring-down technique, the quartets associated with the four major isotopes of tungsten were observed; strong interstate perturbations between vibrational levels of different electronic states, also reported in the matrix experiments [1], were also observed in the gas phase molecules generated this way.

10. 1998, Bare *et al.* [11]. Laser-ablated tungsten atoms were reacted with dioxygen, and the products were isolated in solid argon matrices; the infrared spectrum of WO were recorded using a Fourier transform spectrometer.

11. 1998, Lorenz *et al.* [12]. The fluorecence spectra and vibrational relaxation behaviour of WO in solid neon were studied; the solid neon matrices containing WO molecule were generated by laser vaporization tungsten in the presence of a small amount of oxygen; both the oxygen and the tungsten isotopic structures were resolved; the fluorescence spectra were reported as a complementary contribution to the absorption studies.

12. 1999, Lorenz *et al.* [13]. Matrix samples were prepared through reactions of tungsten atoms from laser vaporization of solid tungsten with trace oxygen in the neon carrier gas; the infrared and visible absorption spectra were recorded using a Fourier transform spectrometer; Both the oxygen and tungsten isotopic structures were observed.

3.1.3 Techniques Used and Results

Previous investigations of the WO molecule can also be classified according to the techniques used, as follows.

3.1.3.1 Gas phase electronic emission and absorption spectroscopy

In 1952, Gatterer *et al.* [5] reported the earliest gas phase electronic emission spectra detected, obtained by employing an electric discharge between tungsten electrodes, and employing a low-dispersion spectrograph. In 1954, Vittalachar *et al.* [6] reported a few bandheads of four additional electronic systems. Only bandheads were identified, so that the rotational structure could not be analyzed. Gas phase visible emission studies in the 1950s yielded a vibrational frequency ($\Delta G_{1/2}$) of about 1055 cm^{-1} for the lower state, presumably the ground state. The electronic systems have 0-0 bands located at 20799.9, 22417.8[5] and 12911.0, 14160.8, 16073.3, and 21226.9 cm^{-1} [6].

In 1981, Samoilova *et al.* [2] reported gas phase electronic absorption spectrum of WO. The spectrum was obtained by flash photolysis of a mixture of $W(CO)_6$ vapor with either $^{16}O_2$ or a mixture of $^{16}O_2$ with argon. Many transition bands, assigned to 10 systems, were recorded. An analysis of the rotational structure of 14 bands of $^{186}W^{16}O$ was carried out. Molecular constants were obtained for the ground state $X0^+$.

3.1.3.2 Spectroscopy in solid matrices

The WO molecule was also studied using the techniques of electronic absorption, vibrational relaxation and fluorescence, and laser-induced fluorescence in low temperature neon, argon, and/or krypton matrices.

In 1965, Weltner *et al.* [1] reported electronic absorption spectra of WO in low-temperature neon and argon matrices. The bands observed in the argon matrices were similar to those observed in the neon matrices, but with broader, and shifted, bands. The $W^{18}O$ spectrum has a regular vibrational structure. In the $W^{16}O$ spectrum, the structure is regular only in one single progression assigned to the D-X transition. The upper states of the remaining transitions perturb one another. Strong perturbations were observed arising from interactions among the A, B, and C states. The high-lying E and F states were also observed to interact. Some bands of the A to G electronic systems were detected in the ultraviolet and visible. Two infrared bands appeared at 1047 and 1064 cm^{-1} in neon and 1050 and 1062 cm^{-1} in argon. The infrared absorption bands were not observed, but seven visible bands were observed

and assigned the $^1\Sigma^-$ symmetry[2] for the ground electronic state.

In 1981, Green *et al.* [7] investigated WO infrared spectra in krypton and argon matrices. The vibrational constants ω_e and $\omega_e x_e$ of $W^{16}O$, in both argon and krypton matrices were derived from the measured frequencies of $W^{16}O$ and $W^{18}O$. The constants are $\omega_e = 1055.98 \pm 1.0$, $\omega_e x_e = 2.93 \pm 0.5$ cm^{-1} for $^{184}W^{16}O$/Kr, and $\omega_e = 1057.51 \pm 1.0$, $\omega_e x_e = 3.33 \pm 0.5$ cm^{-1} for $^{184}W^{16}O$/Ar.

In 1998, Bare *et al.* [11] carried out an argon matrix-isolated spectroscopic investigation of the oxides formed by direct reaction of dioxygen and laser-ablated tungsten atoms. Infrared bands of WO were observed at 1054.5 and 1051.1 cm^{-1} for $W^{16}O$ and at 999.3 and 996.2 cm^{-1} for $W^{18}O$. The argon matrix bands observed are in excellent agreement (0.2 cm^{-1} difference) with the sputtering matrix work [7] and the gas-phase WO ground state fundamental value of 1053.7 cm^{-1} [5]. The argon matrix sites cause blue and red-shifts of the WO fundamental by only 0.7 and 2.6 cm^{-1}, respectively, from the gas-phase values.

Also in 1998, Lorenz *et al.* [12] reported vibrational relaxation and fluorescence spectra of WO in solid neon. The WO spectra were examined with absorption and fluorescence techniques. Extensive vibrationally unrelaxed emission from several electronic states was observed, and quite intense ground state vibrational fluorescence was detected in the spectral range 500 - 30,000 cm^{-1}, with a typical resolution of 0.5 cm^{-1} for visible and 0.06 cm^{-1} for infrared. Fluorescence series from the A, B, D, and E states were observed. The visible bands of WO exhibit interstate interactions as observed by Weltner [1], so that only the $W^{18}O$ spectrum can be reasonably fitted (to give $\omega_e = 1064.65$ cm^{-1}, $\omega_e x_e = 4.046$ cm^{-1}).

In 1999, Lorenz *et al.* [13] reported laser-induced fluorescence in a solid neon matrix. Absorption and fluorescence spectra of WO were investigated in the spectral range from the infrared to the ultraviolet. Several new states were identified in the near infrared range. Infrared absorption of the diatomic WO was clearly observed, even though it could not be clearly identified in the previous matrix investigation [1]. The measured neon matrix frequencies of 1056.98 and 1001.77 cm^{-1} for $^{186}W^{16}O$ and $^{186}W^{18}O$, respectively, are in excellent agreement with the values deduced from the electronic absorption data [2], *viz.*, 1056.7 and 1002.1 cm^{-1}, respectively. In the visible region, the spectral data overlapped those of the matrix [1] and the gas phase data [2]. The observations are essentially in agreement. As numerous very low-lying electronic states are expected for WO, transitions in the near infrared region below 12000 cm^{-1} were also studied. A most prominent group of five vibrational progressions, clearly

[2]The symmetry of the ground state WO should be $^3\Sigma^-$. The $^1\Sigma^-$ symmetry here could be a typographic error in the original paper.

due to WO, appears close to 7500 cm^{-1}. Two additional pairs of transitions appear at higher energies.

Fluorescence spectra of WO, studied in the range 12,000 to 25,000 cm^{-1}, provide valuable information complementary to absorption studies. Various transitions from the A, B, C, D and E states to the X state were observed. The ground state molecular constants are $\omega_e = 1064.469$ cm^{-1} and $\omega_e x_e = 3.9982$ cm^{-1}. Emission from low-lying electronic states in the infrared, and extensive ground state vibrational emission, in addition to fluorescence from several visible electronic states, were observed, due to the usually slow relaxation of WO,

3.1.3.3 Intracavity laser and cavity ringdown laser spectroscopy

In 1997, Efremov *et al.*[8] investigated WO spectra using the intracavity laser technique. High sensitivity absorption spectra were recorded in the spectral range 9,398-9,466 cm^{-1}, with 0.05 cm^{-1} accuracy, by using WO 97%-enriched ^{186}W. Spectra were reported most likely the 1-4 band of a system, with the 0-0 band located at 12,911 cm^{-1} [6].

Also in 1997, Kuzyyakov *et al.* [9] applied the intracavity laser technique to study the WO molecule. Electronic absorption spectra in the range 12,500 - 18,181 cm^{-1} (550-800 nm) were recorded. Analysis of the 0-0 and 1-0 bands of the A-X and B-X systems was carried out for the first time. There have not been analyzed in the gas phase spectra [2]. The rotational constants for the A and B states were presented.

In 1998, Kraus *et al.* [10] used the cavity ringdown laser technique to record a series of bands in the region of 21,000-24,000 cm^{-1}. Only the 0-0 band of the F-X system was reported. It was observed that the P branch shows quartets caused by the four major isotopes of tungsten. Because the vibrational frequency ω_e for the ground electronic state is larger than that of the F state, the zero point energy of the ground state will also be larger, so one would expect the heavier isotopic species to be shifted to the blue. However, the observations showed the opposite, with the lines of the heavier isotopic species being red-shifted.

3.2 Experiments

The microwave discharge cell shown in Fig. 3.1, and discussed in Section 1.2.2, was used in the experiments to generate the WO species. The WO spectra were first detected using the Bruker IFS 120 high resolution Fourier transform spectrometer at Waterloo. The WO spectra used in the final analysis were detected by using the McMath-Pierce one-meter Fourier transform spectrometer of the National Solar Observatory[3] at Kitt Peak, Arizona, USA.

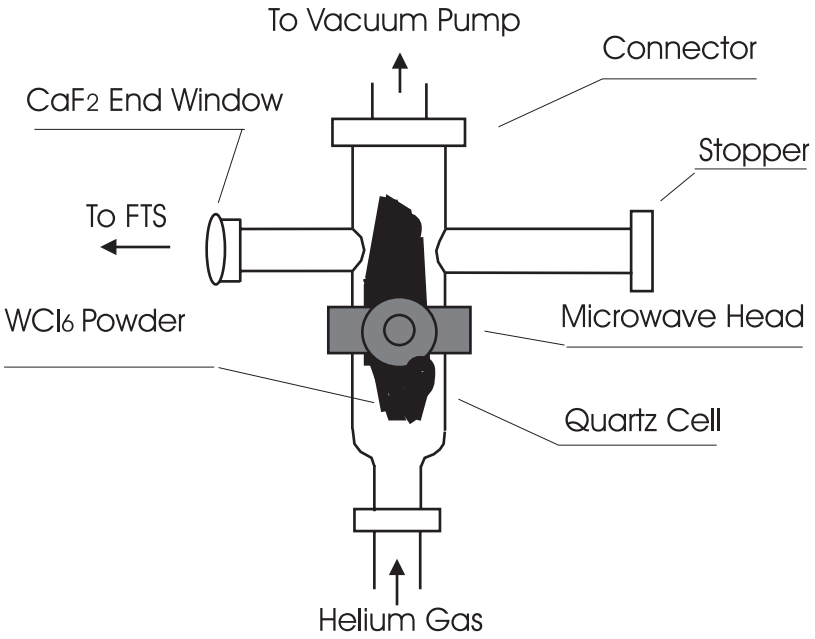

Figure 3.1: Microwave Discharge Cell for the Generation of WO

The original goal of the experiments was to detect the electronic transitions of WCl using WCl_6 as the precursor in a microwave discharge cell, with helium gas as the buffer. After some WCl_6 powder was placed in the quartz cell, pumping was performed for an hour or so to remove air trapped in the cell and the sample powder. Then about 3 Torr of helium buffer gas was let into the cell and the microwave discharge was started. The Bruker spectrometer was set to 0.5 cm^{-1} resolution in order to detect a survey spectrum in the range 19,000 - 21,000 cm^{-1}, the region of possible WCl spectra. A spectrum with clear band heads was obvious, even though the helium and tungsten atomic lines were more intense. The spectrum was not due to WCl, but something else.

What was it? Experience suggested that the spectrum might be due to a nitride or oxide because of nitrogen and oxygen impurities in the cell, even though efforts were

[3]http://nsokp.nso.edu/mp/fts/

taken to make the cell and tubing air-tight (with a leakage of ca. 1-2 mTorr/s). A literature search was carried out for WN and WO. Surprisingly, the Fourier transform spectrum of WN [14] was detected when researchers were trying to detect WO! The current spectrum detected was due precisely to WO. Where did the oxygen come from? The air? Air was tested in the experiment, but even a tiny amount of air extinguished the spectrum. A tiny amount of pure oxygen also killed the spectral signal. The source of the oxygen in the generated WO species is suspected to be water vapor absorbed onto the WCl_6 powder from the air. The powder changes color very quickly from dark brown to deep dark brown immediately upon its exposure to air while being transferred from the sample bottle into the cell. Limited by laboratory conditions, systematic experiments to discover the source of oxygen were not carried out. Without added oxygen, the spectral signal of WO is quite good. With some air or oxygen added into the cell, the spectrum disappears.

The following sub-sections present the details of the experiments at the University of Waterloo.

3.2.1 Initial Experiments on WO

After the spectrum was identified as that of WO, a series of systematic experiments were carried out.

The Bruker IFS 120 high resolution Fourier transform spectrometer at the University of Waterloo was used in the initial experiments. A quartz microwave discharge cell, as shown in Fig. 3.1, with a heating tape wrapped around the part of the tube holding the sample was used for the generation of the expected WO species.

The heating tape was powered with a Staco Energy Products's Type 3PN2210 variable voltage transformer. The temperature of the tape was controlled by adjusting the output voltage of the variable transformer, which can be changed between 0-110% of the 120 VAC input. The maximum output voltage brings the heating tape to about 300-400 °C. Settings between 0-110% give the temperatures between room temperature and the maximum temperature.

With some WCl_6 powder (enough to last for some time in the experiment, but not too, much so as not to cover more than half the cell cross-section) in the cell, and after pumping for about two hours to remove gas phase interferences, 3 Torr of helium buffer gas was let into the cell, and the microwave discharge was started. With the heating tape power off, a diatomic spectrum was detected. Checking the frequencies against reference showed that the initial spectrum was the WO spectrum. Then, a systematic set of experiments were carried out to investigate the WO species.

The preparation of each experiment took from several hours to a few days. Espe-

cially, once the WCl_6 sample was consumed, another experimental cycle needed to be started, including the introduction of a fresh sample to the cell, pumping the cell for several hours to remove gas phase impurities, etc. Due to the length of time needed in the preparation and detection of the WO spectra, the experiments were carried out in several individual parts, with different experimental goals, such as testing for the best experimental conditions and detection of different regions of the spectra, and so forth.

3.2.2 Detection of the $D(0,0)$ Band and Optimizing the Experimental Conditions

The experimental system was set up for the detection of the $D(0,0)$ band at 20,800 cm^{-1}. A quartz beamsplitter as seen in Table 1.1 and a PMT detector (effective for the visible region) as seen in Table 1.3 were employed for this experiment.

3.2.2.1 Pressure of helium buffer

With some fresh WCl_6 powder in the microwave discharge cell, and after pumping for 4-5 hours to remove the residual gaseous impurities, at a background cell pressure of 0.068 Torr, 3 Torr of helium buffer was let into the discharge cell. At a resolution of 0.1 cm^{-1}, the microwave discharge successfully generated the WO species, and the $D(0,0)$ band of WO, located at 20,800 cm^{-1}, was detected. Once the $D(0,0)$ band was detected, the experimental conditions were optimized to improve the spectral intensity and the signal-to-noise ratio.

With more helium added to bring the cell pressure to 10 Torr, the signal intensity of the spectrum was seen to increase to a value above that obtained using 3 Torr of helium. The pressure readings of the cell were the total pressures in the microwave discharge cell, including the vapor pressure from the WCl_6 and the pressure of the helium buffer gas. However, the vapor pressure of WCl_6 contributes only a small portion of the total pressure. Because of the light mass of the helium atoms, the linewidth of the spectrum detected did not change much because the pressure broadening by the helium gas is small. With further increase in the amount of helium, the intensity of the spectrum was seen to drop. The best condition was therefore to use 10 Torr helium as the buffer gas.

3.2.2.2 Roles of oxygen, cell temperature, and other conditions

Three more sets of experiments have been performed. The first set probed the use of small amounts of O_2 with different buffer gases, e.g., 3 Torr of argon or 10 Torr

of helium were tested separately. The second set was to explore the role of O_2 and temperature in the generation of the WO species; in this set of experiments, a pressure of 10 Torr of helium was used with a combination of heating voltages, with or without O_2. The third set of experiments tested other experimental conditions.

In the first set of experiments, which was conducted with a background pressure of 0.05 Torr, obtained after a fresh WCl_6 sample had been placed in the cell and the background pumping had been completed, a small amount of O_2 was added. The spectral intensity decreased drastically when even as little as 0.02 Torr of O_2 was added, and the signal to noise ratio became much worse. It was concluded that the addition of O_2 gas did not help in the detection of the WO spectrum generated using WCl_6. After the O_2 input had been terminated, the signal intensity remained low, even when the sample was heated up to 30% of the maximum heating voltage.

In the second set of experiments, fresh samples of WCl_6 was used. With the cell pressure maintained at 10 Torr using the helium buffer gas, with or without O_2, the results from different heating temperatures were compared. Heating conditions of 10%, 40%, 60% and 80% of the maximum value were tested.

The last set of experiments included keeping both the upstream and downstream valves of the cell nearly closed, while maintaining the cell pressure at about 10 Torr, with helium as the buffer gas. This was to build up the concentration of the WO species in the cell, while at the same time removing interfering species. Also, in order to investigate the conditions that would provide the best signal-to-noise ratio, a sample of WCl_6 was left in the open air in the fume hood for 8 hours. The results were not obviously better. However, the used sample from the experiments was put in a sealed vial for about 2 weeks during the Christmas Holidays in 1999. After the Holidays, this used sample in the sealed vial was used in the experiments, and a good spectrum was detected.

3.2.2.3 Optimized conditions

The following conclusions were made:

1) The WO spectrum can be detected by using WCl_6 powder in a microwave discharge cell with helium or argon buffer gas. However the use of argon buffer gas generates more atomic lines than does the helium buffer gas. 2) The best WO spectrum was recorded when the discharge plasma showed a bright yellowish color: any experimental conditions that generated such a color gave a good spectrum of WO. 3) The intensity of the WO spectrum generated using helium was better than that using argon: the best spectrum was achieved using 10 Torr of helium. 4) When even a small amount of O_2 was added, as little as 0.02 Torr, the intensity of the WO

spectrum decreased drastically. 5) Heating the sample did not help in the generation of the WO species.

3.2.3 Detection and Advantages of High Resolution Spectra

The spectra of WO species were detected segment by segment from 13,900 to 26,000 cm^{-1} in 6 parts. The best experimental conditions, as described in Section 3.2.2, were used.

The bandhead positions helped to identify the molecule. A good way to do co-addition using the Bruker 120 IFS high resolution spectrometer is to set the number of co-additions to a larger number. The spectrometer can be stopped at any number of co-additions when the operator decides that the number of co-additions have been enough.

The experiments were repeated using the McMath-Pierce one-meter Fourier transform spectrometer of the National Solar Observatory at Kitt Peak, Tucson, Arizona. The WO spectra employed in the final analysis are those detected at Kitt Peak, which have a resolution of 0.03 cm^{-1} and cover the range 9,000 - 34,500 cm^{-1} in two parts.

The McMath-Pierce one-meter spectrometer[4] has a folded Michelson interferometer housed in a vacuum vessel. It is the instrument of choice when very highly accurate line positions, broad spectral coverage, a stable instrumental profile, etc., are required. It has the following features:

1. maximum path difference of 1 meter;
2. minimum resolution element of 0.005 cm^{-1}.[5]
3. spectral range of 550 cm^{-1} to 45,000 cm^{-1} (2,200 Å to 18 μm);
4. typical wavenumber accuracy of 10^{-3} to 10^{-4} cm^{-1}.

The WO spectra reported in this Chapter have the following advantages over those published previously.

1. Gas phase molecules: higher resolution than previous spectra for rotational analysis.
2. High accuracy: easy spectroscopic calibration using helium atomic lines.

[4] http://nsokp.nso.edu/mp/fts/

[5] The resolution of a Fourier transform spectrometer is determined by the maximum optical path difference. For the McMath-Pierce one-meter Spectrometer, the maximum optical path difference is 1 meter, so the resolution should not be so high. However, the specially designed optical folding mechanisms in the system help to achieve the high resolution.

3. Emission spectra: more information about the molecule and better signal-to-noise ratio.

4. Wide spectral coverage: made available by using different detectors and beam splitters.

5. High resolution: splittings due to the tungsten isotopes (^{182}W, ^{183}W, ^{184}W, and ^{186}W) are resolved for some bands.

3.3 Theoretical Basis

This section presents the theoretical basis for the analysis of the spectra of WO, such as the molecular orbitals and angular momenta, the coupling cases of angular momenta and the term symbols, the properties of Λ-doubling of the states, and the emission spectra.

3.3.1 Molecular Orbitals, Hund's Cases and Term Symbols

3.3.1.1 Molecular Orbitals and Angular Momentum

Molecular orbitals can be formed as linear combinations of atomic orbitals. However, the quantum numbers of the electrons in a diatomic molecule are not the same as those in the atoms [15, 16]. There are four quantum numbers for an electron in an atom, i.e., the principal quantum number n, the angular quantum number l, the magnetic quantum number m_l and the spin quantum number m_s. In a diatomic molecule, the electrons experience the Coulomb electric field of both the nuclei, which has a rotational symmetry with respect to the internuclear axis (molecular axis). Therefore, the angular quantum number l is no longer a good quantum number. The projection of the angular momentum $\mathbf{l}$ along the molecular axis is $l_z = m_l\hbar$, where $m_l = l, l-1, \cdots -l$. The energy of these states are the same for l_z along $+z$ and $-z$ directions, and the quantum number is the same as that of the magnetic quantum number. The double degeneracy can be lifted by perturbations, e.g., molecular rotation. For this reason, a new quantization condition is introduced, $\lambda = |m_l|$, where $m_l = l, l-1, \cdots, -l$. The orbital wavefunctions of electronic states with $\lambda = 0, 1, 2, \cdots$ are called $\sigma, \pi, \delta, \cdots$, corresponding to the $s, p, d \cdots$ electronic orbitals in an atom.

The orbital and spin motions of the electrons create magnetic moment, which interact with one another and contribute to the coupling between the motions of the electrons. The orbital angular momenta of all electrons in the molecule are coupled to give a resultant $\mathbf{L}$, and all the electron spin momenta in the molecule are coupled to give a resultant $\mathbf{S}$.

3.3.1.2 Hund's Cases and Term Symbols

If there is no highly charged nucleus in the molecule, the spin-orbit coupling between $\mathbf{L}$ and $\mathbf{S}$ is weak and the internuclear electrostatic field uncouples them. The orbital angular momentum $\mathbf{L}$ and spin $\mathbf{S}$ are coupled to the internuclear axis individually. In this case, the total electronic orbital angular momentum $\mathbf{L}$ is strongly coupled to the internuclear electrostatic field. Its magnitude of $\mathbf{L}$ is thus not defined; only the axial

component $\Lambda\hbar$, i.e., the projection of $\mathbf{L}$ along the intermolecular axis is defined, where $\Lambda = 0, 1, 2, \cdots$. The projection quantum number Λ is a good quantum number, while L is not. In a molecule, there is a two-fold degeneracy in the axial projection of the angular momentum L_z, i.e., the electronic states with $\Lambda > 0$ are doubly degenerate.

The coupling of the total electronic spin angular momentum $\mathbf{S}$ to the internuclear axis is not due to the internal electrostatic field, but is caused by the magnetic field generated from the orbital motion of the electrons. The projection of $\mathbf{S}$ on the molecular axis is $\Sigma\hbar$, where $\Sigma = S, S-1, \cdots, -S$. The magnitude of the total electronic spin angular mpmentum S is a good quantum number. The multiplicity $2S+1$ represents the number of spin components. The spin-orbit interaction splits the components of a multiplet. The splittings between adjacent spin components are constant for Hund's case (a), but not for Hund's case (c).

The electronic states of a diatomic molecule are represented by term symbols ${}^{2S+1}\Lambda$, with $2S+1$ representing the term multiplicity. The symbols are Σ for $\Lambda = 0$, Π for $\Lambda = 1$, Δ for $\Lambda = 2$, Φ for $\Lambda = 3$, etc. The spin components are represented by ${}^{2S+1}\Lambda_\Omega$, where $\Omega = |\Lambda + \Sigma|$, and Σ is the projection of the total electronic spin $\mathbf{S}$ along the molecular axis as shown in Fig. 3.2 [15, 16]. Notice that for a diatomic molecule, only the internuclear axial components are important. The axial projection of the total angular momentum is the sum of the axial projection of the electronic orbital angular momentum $\Lambda\hbar$ and the axial projection of the electronic spin $\Sigma\hbar$.

For a Σ state, there is no orbital angular momentum, and therefore, no internal magnetic field to couple $\mathbf{S}$ to the internuclear axis. For this reason, when spin-spin coupling is neglected, the quantum number Σ is not defined. The Σ state, whatever its multiplicity, has only one spin component. This is no longer true when spin-spin coupling is included.

In heteronuclear diatomic molecules such as WO, the quantum numbers Λ, S and Ω are not quite sufficient. The symmetry properties of the electronic wavefunction Ψ_e need also to be specified. The symmetry property concerns the symmetry of Ψ_e with respect to reflection across any σ_v plane containing the internuclear axis: if Ψ_e is symmetric to (unchanged by) the reflection, the state is labelled '+', while if it is antisymmetric to (changed in sign by) the reflection, the state is labelled by '–'.

Like all assumed coupling of angular momenta, as shown in Fig. 3.2, Hund's case (a) represents a commonly used approximation when the vectors $\mathbf{L}$ and $\mathbf{S}$ are strongly coupled to the intermolecular axis and weakly coupled together. Another extreme coupling approximation is Hund's case (c). In Hund's case (c), the spin-orbit coupling is so large that the coupling between the vectors $\mathbf{L}$ and $\mathbf{S}$ can not uncoupled by the axial electrostatic field. In this case, Ω is a good quantum number and Λ is

no longer a good quantum number. However, the $\Sigma, \Pi, \Delta, \cdots$ labels for the electronic states of Hund's case (a) are retained for Hund's case (c). Hund's case (c) is to be found in molecules with at least one highly charged nucleus.

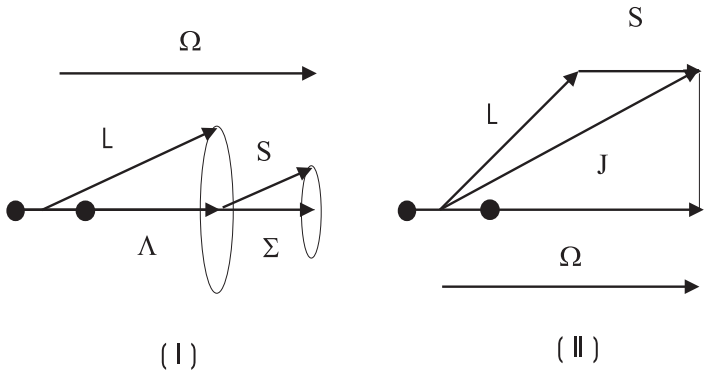

Figure 3.2: (I) Hund's Case (a) and (II) Hund's Case (c) Coupling of the Total Electronic Orbital and Spin Angular Momenta in Diatomic Molecules.

For the WO molecule, which contains the highly charged W nucleus, the spin-orbit coupling between **L** and **S** is strong, and the result is Hund's case (c) rather than the usual Hund's case (a).

3.3.2 Properties of Emission Spectra and Λ-Doubling

In contrast to the selection rules for pure rotational spectra (molecules possessing a permanent electric dipole moment) and ro-vibrational spectra (a change of electric dipole moment during vibration), electronic spectra are possible for all molecules since changes in the electron distribution in a molecule are always accompanied by an electric dipole change. For this reason, a great many spectral lines are to be expected in an electronic transition [17], especially, when rotational fine structure is observed in high resolution spectroscopy.

Electronic emission spectra are more complicated than electronic absorption spectra, because in absorption the majority of the molecules are usually in the ground vibrational state and the result is mainly the $v'' = 0$ progression. In electronic emission spectra, the numbers of v' and v'' levels involved can be large, so there can be many bands from various combinations of v' and v''. Because the molecules in the upper state may not be in thermal equilibrium, and hence not in a Boltzmann distribution, the intensity pattern may be irregular. In addition to the roles of the the electric dipole selection rule, which is $\Delta J = J' - J'' = 0, \pm 1$ (except for $J' = J'' = 0$), and the parity selection rule, which requires that the initial and the final states for the transition have different total parities, in determining the rotational fine structure,

the spectral lines in a vibrational progression are not all observed to be of the same intensity.

Some of the bands of the WO spectra are found to have Λ-type doubling (or Ω-doubling) patterns because of the Λ-doubling of energy in one or both of the vibrational levels of the two electronic states involved. Λ-type doubling arises because all states with $\Lambda > 0$ are doubly degenerate: this can be thought of classically as being caused by the same energy being associated with clockwise or counter-clockwise motion of the electrons about the internuclear axis. The degeneracy may be split due to the interaction between the orbital motions and the overall rotation of the molecule [15, 16].

The lines of each band with Λ-doubling for $\Omega = 1$ are fit to the energy level expression shown in Eqn. (3.1).

$$\begin{aligned} E_v &= T_v + F_v(J) \\ &= T_v + B_v J(J+1) - D_v[J(J+1)]^2 + H_v[J(J+1)]^3 + \cdots \\ &\quad \pm 1/2\{q_v J(J+1) + q_{Dv}[J(J+1)]^2 + q_{Hv}[J(J+1)]^3 + \cdots\} \end{aligned} \tag{3.1}$$

in which the q's are Λ-doubling constants, and + and – correspond to e and f parities, respectively.

The energy levels without Λ-type doubling are fit to Eqn. (3.2), the usual band constant model.

$$\begin{aligned} E_v &= T_v + F_v(J) \\ &= T_v + B_v J(J+1) - D_v[J(J+1)]^2 + H_v[J(J+1)]^3 + \cdots \end{aligned} \tag{3.2}$$

The spectra and other information on some of the WO bands are shown in Fig. 3.3 to Fig. 3.10. These bands are plotted with the line positions and intensities measured using PC/GENCOMP.[6] Therefore, there is no random baseline noise in the figures. However, there are still spectral lines from other sources (tungsten and helium atomic lines, or lines from other bands) in these plots of the "raw" spectra. The most intense helium atomic lines have been removed.

[6]PC/GENCOMP is a spectral line measurement program similar to PC/DECOMP, but able to handle spectra with a larger spectral range.

3.4 Analysis of WO Spectra

The analysis of the WO spectra starts from the 0-0 bands of the seven electronic transitions, i.e., A-X, B-X, C-X, C'-X, D-X, D'-X and F-X, because the 0-0 bands are usually of higher intensity. The electronic absorption spectra reported by Samoilova *et al.* [2] were used as references because the absorption spectra give mainly 0-0 bands. Only the details of the analysis of the 0-0 bands and other bands of the D-X, D'-X, and F-X transitions are reported in this Chapter, as bands of the other electronic systems were analyzed by a colleague.[7] The work reported in this Chapter is a part of a co-authored publication [4]. The final conclusions drawn from both the results of analyses made in this Chapter and the results of analyses by other colleagues are reported herein.

Because results of detailed rotational analyses of high resolution spectra of the WO molecule were not available prior to the co-authored work [4], the symmetries of the excited electronic states are unknown, and even the symmetry of the ground electronic state was unclear [1, 3, 2, 8]. The bands are labeled with vibrational quantum numbers corresponding to the upper to lower states. They could be either vibrational transitions between spin components of electronic states or between different electronic states. Because of the intrinsic complexity of the spectra, and because of the low-lying states with high multiplicities possible for WO (typical of transition metal-containing molecules with an open d-shells), further experiments and analyses need to be combined with theoretical results from *ab initio* calculations in order to identify the symmetries of the excited electronic states.

3.4.1 $D(0,0)$ Band

No isotopic splittings have been observed in the $D(0,0)$ band detected here. As shown in Fig. 3.3, the $D(0,0)$ band is red-degraded and has an R head. In the $D(v'=0)$–$X(v''=0)$ transition, the Q branch is composed of stronger lines; and the P and R lines overlap after the returning R branch passes the band origin. The existence of an R head shows that $B' < B''$, i.e., the upper electronic state has a longer effective bond length.

The result of fitting the identified frequencies of the line positions of the P, Q, and R branches to energy levels expressed via Eqns. (3.1) and (3.2) leads to the set of constants given in Table 3.1. The rotational constants $B'' = 0.415266(35)$ cm^{-1} and $B' = 0.388629(34)$ cm^{-1} have been obtained[8] for the $X(v''=0)$ and the $D(v'=0)$

[7] Dr. Ram S. Ram, Dept. of Chemistry, University of Arizona, Tucson AZ 85721, USA.

[8] A better set of molecular constants could be obtained by using the Unix-based software DSParFit

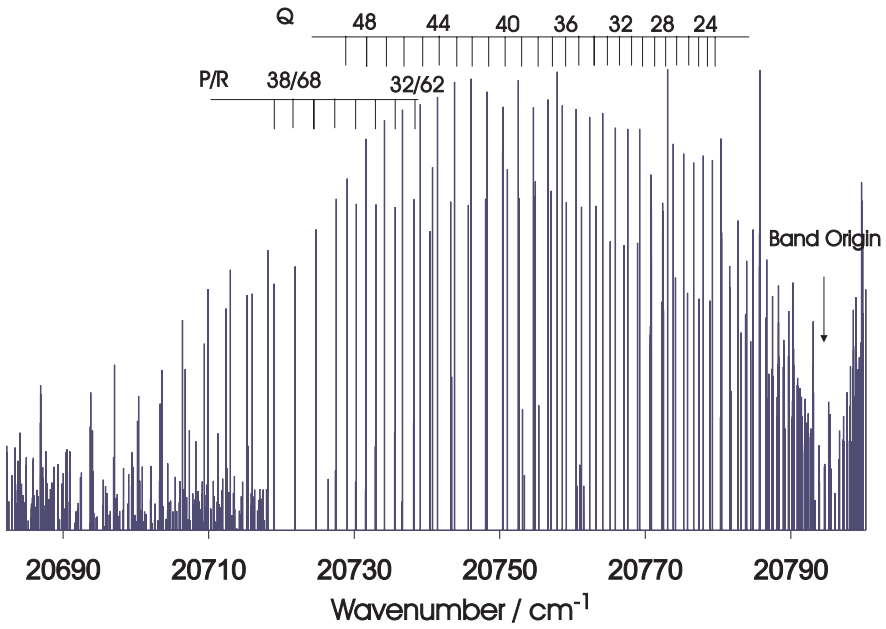

Figure 3.3: The $D(0,0)$ band, with a band head located at 20799.87 cm^{-1}. The Q branch is composed of stronger lines, and the P and R lines overlap after the returning R branch passes through the band origin.

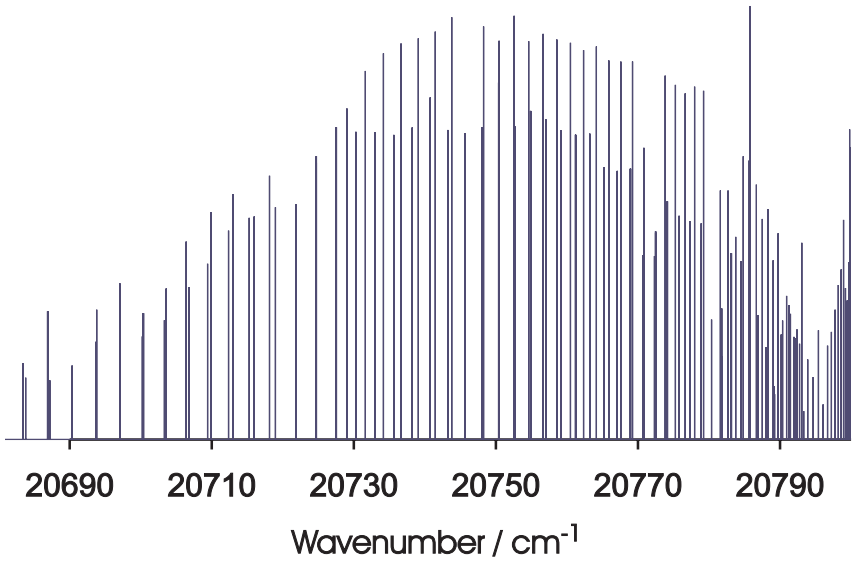

Figure 3.4: The $D(0,0)$ band with noise and interference removed.

Table 3.1: Molecular Constants of the $D(0,0)$ Band

	(cm^{-1})		
	Molecular Constant		Uncertainty
Upper State			
T'	2.07938669	D+04	$1.5D-03$
B'	3.88629	D−01	$3.4D-05$
D'	1.739	D−07	$6.5D-09$
q'	−2.807	D−04	$1.0D-06$
Lower State			
T''	0.0	D+00	
B''	4.15265	D−01	$3.5D-05$
D''	1.853	D−07	$6.8D-09$

Final Variance = 1.136

levels, respectively.

The spectrum containing only spectral lines from the $D(0,0)$ band is shown in Fig. 3.4. Some lines have been removed for reasons such as blending with helium atomic lines or other strong interference.

The Fortrat parabola for the $D(0,0)$ band is shown in Fig. 3.5.

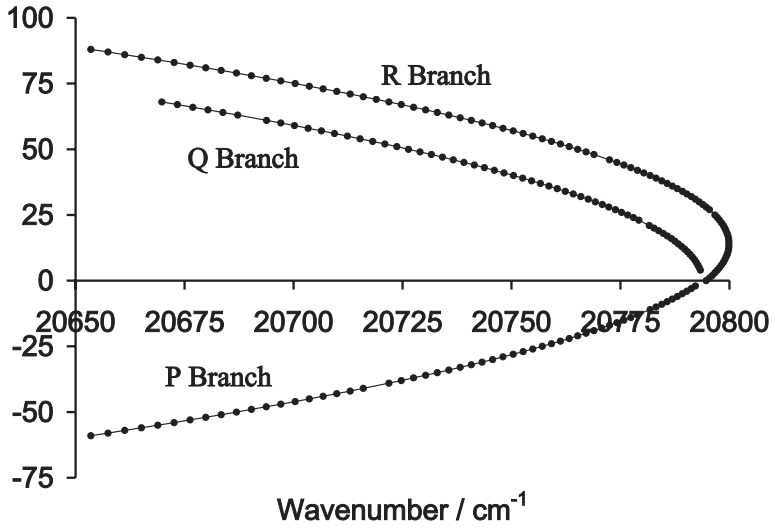

Figure 3.5: The Fortrat parabola of the $D(0,0)$ band. The y-coordinate is m, and the x-coordinate is *wavenumber*.

with sequential rounding and refitting. However, the PC program LSQFIT-D is convenient in the initial data analysis and the results are adequate at this level of analysis. The contents of the tables of the molecular parameters and the uncertainties are the raw outputs of the computer program.

The $D(0,0)$ band was also observed in the neon matrix [1] at 20797 cm^{-1} and in the gas phase absorption spectrum [2] at 20799.8 cm^{-1}. In the fluorescence spectrum in solid neon [12], a fairly strong progression from $v' = 0$ of the D state at 20789.3 cm^{-1} was also observed. The above literature results are in good agreement with the band head wavenumber 20799.87 cm^{-1} obtained in this work.

It may be concluded from the fitting results given in Table 3.1 that the upper state, i.e., the D state, has Λ-doubling of the energy levels, and that the lower state does not have Λ-doubling.

3.4.2 $D'(0,0)$ Band

Fig. 3.6 shows the "raw" spectrum of the $D'(0,0)$ band of the WO spectra, with a band head located at 21,227.48 cm^{-1}. In the $D'(v' = 0)$–$X(v'' = 0)$ transition, no isotopic splittings have been observed. There are a pair of P branches and a pair of R branches in the spectrum of the $D'(0,0)$ band.

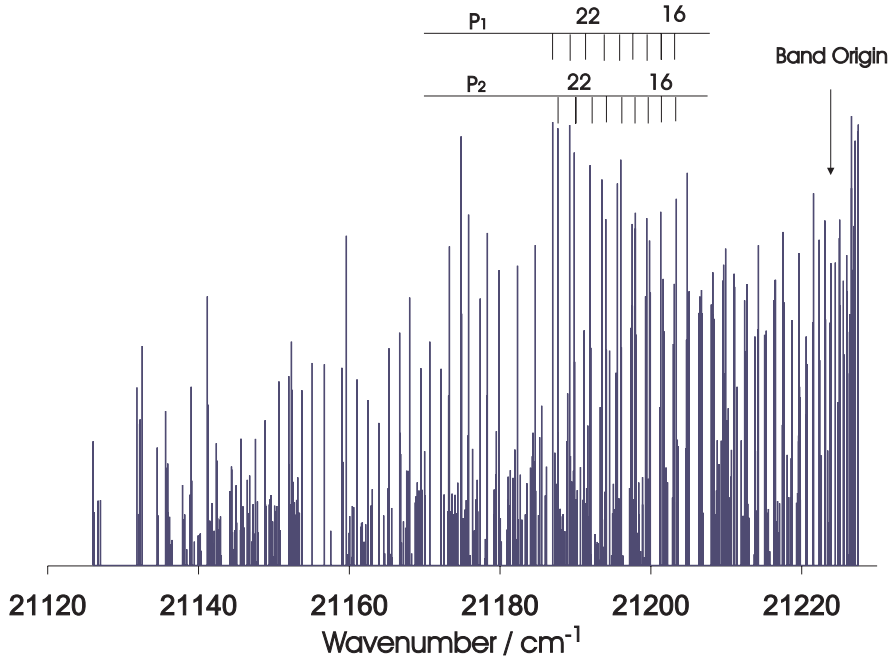

Figure 3.6: The $D'(0,0)$ band, with a band head at 21227.48 cm^{-1}. The doublings are obvious for the P branch. The assignment for the R branch is not shown.

The doublings of the P branch and R branch are due to Λ-doubling in the electronic states associated with the transitions. The fit of the line positions to energy levels as expressed in Eqn. (3.1) leads to the molecular constants given in Table 3.2. The rotational constants for the lower and upper states are $B'' = 0.415984(28)$ cm^{-1} and $B' = 0.384684(27)$ cm^{-1}, respectively. The spectral lines of the $D'(0,0)$ band,

Table 3.2: Molecular Constants of the $D'(0,0)$ Band

	(cm^{-1})		
	Molecular Constant		Uncertainty
Upper State			
T'	2.12222904	D+04	$1.4D-03$
B'	3.84684	D−01	$2.7D-05$
D'	1.751	D−07	$9.6D-09$
q'	1.690	D−03	$8.9D-05$
q'_D	−3.33	D−07	$7.7D-08$
q'_H	7.6	D−11	$2.2D-11$
Lower State			
T''	0.0	D+00	
B''	4.15984	D−01	$2.8D-05$
D''	1.28	D−07	$1.0D-08$
q''	3.59	D−04	$8.8D-05$
q''_D	−3.64	D−07	$7.9D-08$
q''_H	8.3	D−11	$2.4D-11$

Final Variance = 0.947

with noise and interference removed, are shown in Fig. 3.7. The Fortrat parabola of the $D'(0,0)$ transition is shown in Fig. 3.8. The $D'(0,0)$ band head was observed at 21227.7 cm^{-1} in the gas phase absorption spectrum [2], but the wavenumbers of the line positions of the $D'(0,0)$ band were not reported.

It may be concluded from the fitting results given in Table 3.2 that both the upper state, i.e. the D' state, and the lower state have Λ-doubling of the energy levels.

3.4.3 $F(0,0)$ Band

In the $F(0,0)$ band shown in Fig. 3.9, the band head is located at about 23,405.90 cm^{-1}. The spectrum shows clear isotopic splittings in the P branch. Some bands of the WO spectra display quartets caused by the four major isotopes of tungsten, i.e., 26.3% ^{182}W (181.948202(3)), 14.28% ^{183}W (182.950220(3)), 30.7% ^{184}W (183.950928(3)), and 28.6% ^{186}W (185.954357(4)) [18]. While other 0-0 bands of the electronic transitions of WO are not observed, because the isotopic shifts in both the lower and upper electronic states are the same, so they cancel with respect to the spectra observed, the perturbations in the electronic state F make the $F(0,0)$ isotopic splittings observable.

In the $F(0,0)$ band, only the spectra of the three major isotopomers, i.e., ^{182}WO, ^{184}WO and ^{186}WO can be reliably measured and identified. They are referred to as

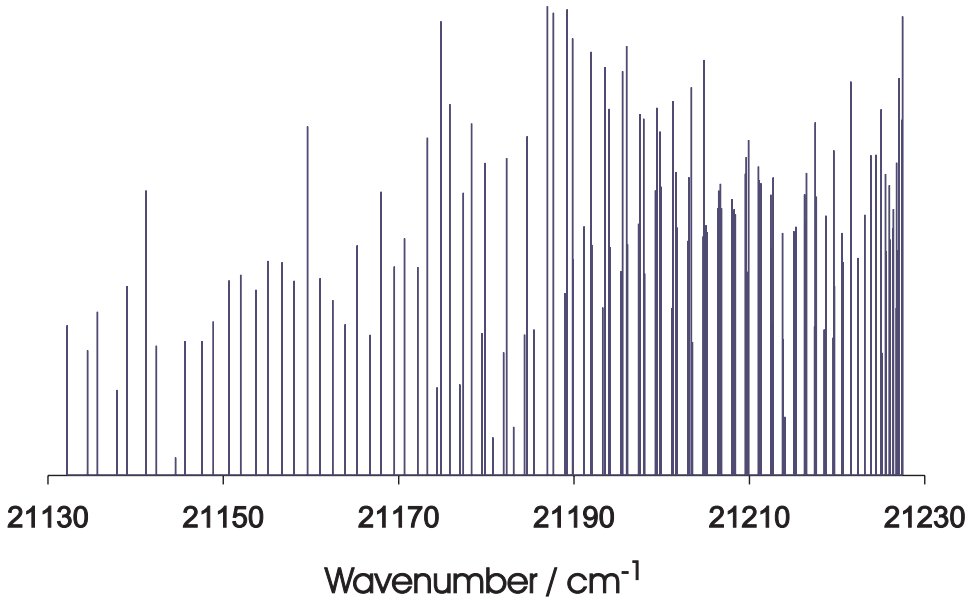

Figure 3.7: The $D'(0,0)$ band, with noise and interference removed.

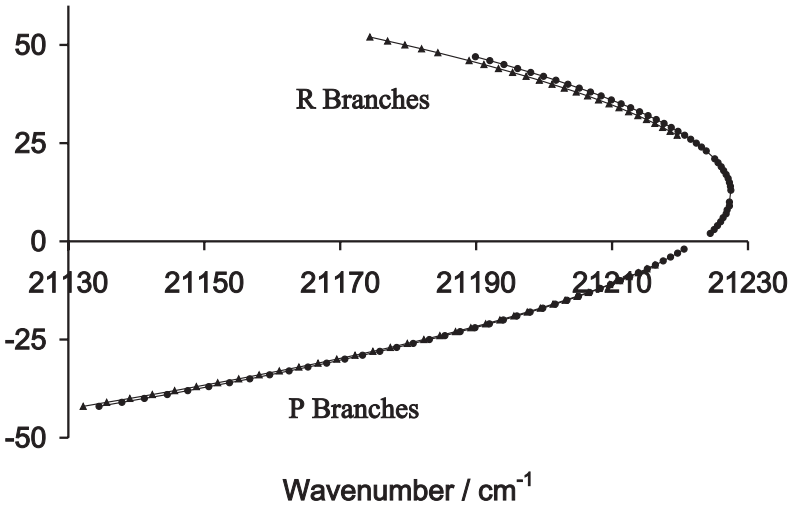

Figure 3.8: The Fortrat parabolae of the $D'(0,0)$ band. The y-coordinate is m, and the x-coordinate is *wavenumber*.

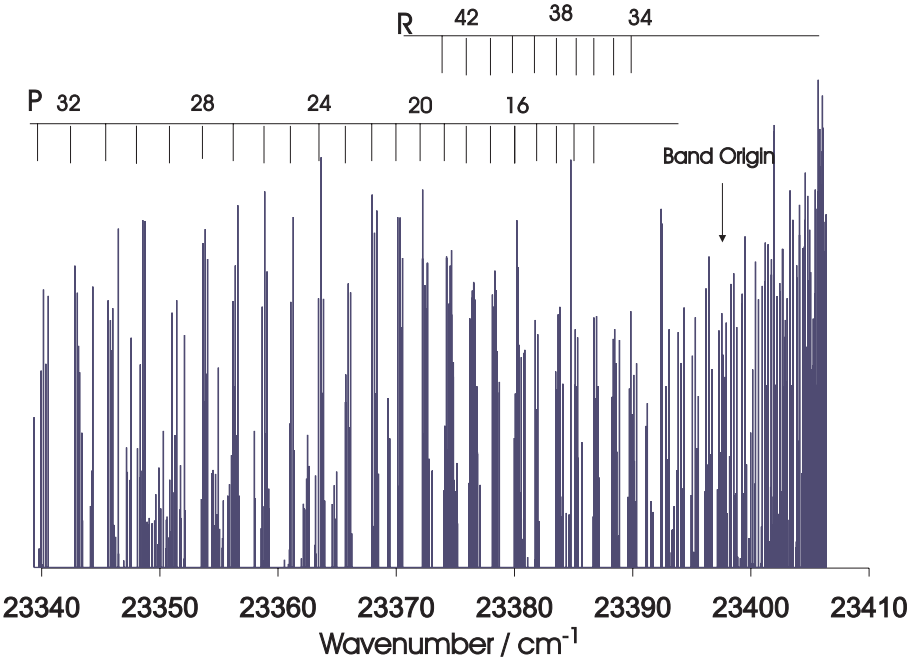

Figure 3.9: The $F(0,0)$ band, with band head located at 23405.90 cm^{-1}. Isotopic splittings are observed.

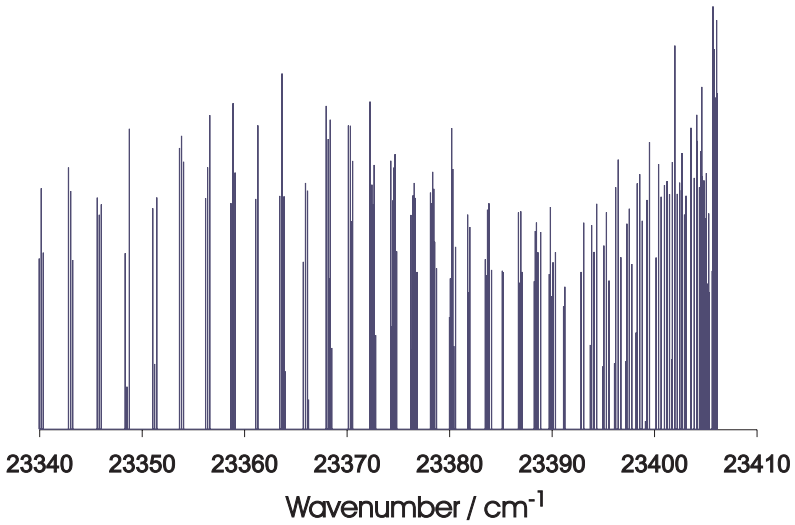

Figure 3.10: The $F(0,0)$ band of WO spectra, with noise and interference removed. Isotopic splittings are observed in both the P and R branches.

Series I, II, and III for ^{186}WO, ^{184}WO, and ^{182}WO, respectively. The fitting results are shown in Tables (3.3) to (3.5).

For Series I (^{186}WO, 28.6%), $B'' = 0.415068(10)$ cm^{-1}, $B' = 0.383233(95)$ cm^{-1}.

For Series II (^{184}WO, 30.7%), $B'' = 0.415544(26)$ cm^{-1}, $B' = 0.383837(24)$ cm^{-1}.

For Series III (^{182}WO, 26.3%), $B'' = 0.415795(54)$ cm^{-1}, $B' = 0.384094(47)$ cm^{-1}.

It may therefore be concluded from the fitting results given in Table 3.3 that neither the upper state, i.e. the F state nor the lower state have Λ-doubling.

The upper energy levels of the E and F systems appear to be perturbing each other in neon matrices [1]. In a spectroscopic study using the cavity ringdown laser technique [10], the 0-0 band of the F-X system was also reported, and it was observed that the P branch shows isotopomer quartets caused by the four major isotopes of tungsten. Because the vibrational frequency ω_e for the ground electronic state is larger than that of the F state, the zero-point energy of the ground state will also be larger, and one would expect the heavier isotopic species to be shifted to the blue. However, the observations show the opposite, with the lines of the heavier isotopic species red-shifted [10].

As shown in Fig. 3.11, isotopic splittings are observed for the rovibrational transitions in the $F(0,0)$ band of the WO spectra. The red-shift pattern of the lines of heavier isotopomers can be identified from the groups of lines with arrows, although the intensities are somewhat contaminated by spectral lines from other sources. From low wavenumber to high wavenumber, i.e., from the left to the right, the isotopomers are ^{186}WO, ^{184}WO, ^{183}WO, and ^{182}WO, which can be identified from their relative intensity corresponding to the natural abundances, i.e., 28.6% ^{186}W, 30.7% ^{184}W, 14.28% ^{183}W, and 26.3% ^{182}W. The observations of the red-shift properties of the heavier isotopomers in this work are consistent with observations of the $F(0,0)$ band of WO from the cavity absorption technique [10].

3.4.4 Results of Analysis

Analyses of the 0-0 bands and some other bands of the A-X, B-X, C-X, C'-X systems and the new $\Omega = 1$ system, i.e., the B'-X system, and the $[11.0]0^+$-X system have been performed by a colleague.[9]. The rotational constants for the two spin components of the lower electronic state were found to be $B'' = 0.4155285(73)$ cm^{-1} and $B'' = 0.416247(19)$ cm^{-1}, respectively. The results of all the analyses from this Chapter, i.e., the F-X, D'-X, and D-X systems, and those of Dr. Ram are summarized in Table 3.6 for the lower states. Only the molecular constants of the major isotopomer,

[9]Dr. Ram S. Ram, Dept. of Chemistry, University of Arizona, Tucson, AZ 85721, USA.

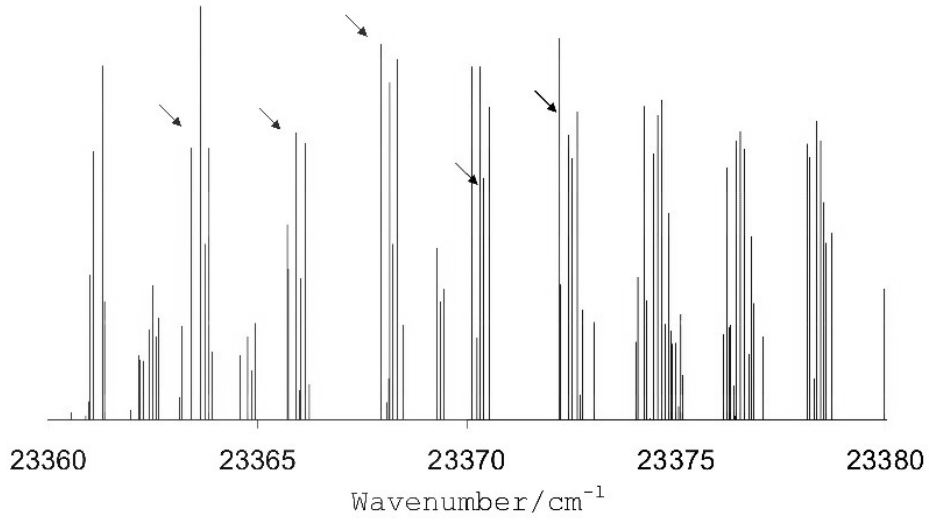

Figure 3.11: A portion of the $F(0,0)$ Band of the WO spectrum. Isotopic splittings are observed for the transitions. The red-shift pattern of the lines of the heavier isotopomers can be identified from the groups with arrows, although the intensities are somewhat contaminated by lines from other sources.

Table 3.3: Molecular Constants of Series I (^{186}WO) of the $F(0,0)$ Band

	(cm^{-1})		
	Molecular Constant		Uncertainty
Upper State			
E'	2.34008900	D+04	$3.5D-03$
B'	3.83233	D−01	$9.5D-05$
D'	2.02	D−07	$5.5D-08$
Lower State			
E''	0.0	D+00	
B''	4.1507	D−01	$1.0D-04$
D''	3.16	D−07	$6.1D-08$

Final Variance = 0.879

Table 3.4: Molecular Constants of Series II (^{184}WO) of the $F(0,0)$ Band

	(cm^{-1})		
	Molecular Constant		Uncertainty
Upper State			
E'	2.34010970	D+04	$1.7D-03$
B'	3.83837	D−01	$2.4D-05$
D'	3.36	D−07	$1.5D-08$
Lower State			
E''	0.0	D+00	
B''	4.15544	D−01	$2.6D-05$
D''	2.56	D−07	$1.8D-08$
H''	−1.17	D−11	$2.6D-12$

Final Variance = 0.357

Table 3.5: Molecular Constants of Series III (^{182}WO) for the $F(0,0)$ Band

	(cm^{-1})		
	Molecular Constant		Uncertainty
Upper State			
E'	2.34013110	D+04	$5.1D-03$
B'	3.84093	D−01	$4.7D-05$
D'	2.48	D−07	$2.8D-08$
Lower State			
E''	0.0	D+00	
B''	4.15795	D−01	$5.4D-05$
D''	1.85	D−07	$3.7D-08$

Final Variance = 0.943

Table 3.6: Rotational Constants for the Lower Electronic States (cm^{-1})

		(cm^{-1})
Bands	B″ for Group I	B″ for Group II
$F(^{184}WO)$	0.415544(26)	.
D'	.	0.415984(28)
D	0.415266(35)	.
C'	.	0.416247(19)
$C, B, A, [11.0]0^+$	0.4155285(73)	.
Average	0.4154462	0.416116

i.e., ^{184}WO, are considered for the bands with isotopic splittings, such as the $F(0,0)$ band. In Table 3.6, the $[11.0]0^+$ state is a new upper state identified with $\Omega = 0^+$ symmetry.

For some electronic systems, additional bands other than the 0-0 band have been analyzed. The result of a global analysis of the $C(0,0)$, $C(0,1)$, $C(0,2)$, $C(1,2)$, $C(1,3)$ bands, $D(0,0)$, $D(0,1)$, $D(1,0)$ bands, $F(0,0)$ band, $D'(0,0)$ band, and the new B'(0,0) band, etc., is shown in Table 3.7 at Page 87.

3.5 Conclusion

Based on the results of rotational analyses of the strong bands out of the total of *ca.* 35 analyzable bands of various electronic systems, two groups of transitions with different lower states can be identified. The energy diagram for the states is shown in Fig. 3.12. The first group consists of seven transitions, six of which have a common lower state. None of these lines show any doubling, and the common lower state behaves like a $^1\Sigma^+$ or an $\Omega = 0^+$ state. This state is labeled as the $X0^+$ state. The transitions with this common lower state have their origins near 10965 cm^{-1} ([11.0]0^+-$X0^+$), 17165 cm^{-1} ($A1$-$X0^+$), 17241 cm^{-1} ($B1$-$X0^+$), 19182 cm^{-1} ($C1$-$X0^+$), 20793 cm^{-1} ($D1$-$X0^+$) and 23401 cm^{-1} ($F0^+$-$X0^+$). These transitions were also observed in the relaxed laser-induced fluorescence measurements of Lorenz *et al.* [12, 13] and in the matrix isolation absorption experiment of Weltner *et al.* [1] (except for the transition at 10965 cm^{-1}), and in the gas phase absorption spectra [2]. These facts suggest that the common lower state for these transitions is a spin component of the ground state of WO.

The other group, including three states, $C'1$, $D'1$, and a new 0^+ state, i.e., $B'0^+$, contains transitions connected to an $\Omega = 1$ lower state. The 0-0 bands of all three states show significant Λ-doubling in the lower electronic state, or more precisely, Ω-doubling for Hund's case (c). The 0-0 bands of these transitions have their origins near 19440 cm^{-1}, 19783 cm^{-1} ($C'1$-$X1$), and 21222 cm^{-1} ($D'1$-$X1$). None of these transitions were observed in the laser-induced fluorescence experiments of Lorenz *et al.* [12, 13], or in the matrix isolated absorption experiment of Weltner *et al.* [1]. In the gas phase electronic absorption spectra of Samoilova *et al.* [2], details of such a state were not reported. The transition with a 0-0 band near 19440 cm^{-1} has been observed for the first time, and the upper state has been labelled as the $B'0^+$ state in Table 3.7. Because none of the bands in the second group were observed in the matrix absorption experiment [1], and the observed D'-X bands with $X1$ as the lower state are very weak in the gas absorption spectra [2], it appears that the lower state is well above the $\Omega = 0^+$ ground state, because in the absorption spectra, the majority of the transitions occur from the lowest energy level of the ground state. The rotational constants of the lowest $\Omega = 0^+$ and $\Omega = 1$ states are similar in magnitude as shown in Table 3.6, which suggests that they are the spin components of the same Hund's case (a) state identified as an $X^3\Sigma^-$ state.

The two lowest states have been assigned as the $\Omega = 0^+$ and $\Omega = 1$ spin components of the $X^3\Sigma^-$ ground electronic state of WO, with the $\Omega = 0^+$ spin component being lower in energy. The rotational constants are B_0'' ($\Omega = 0^+$) = 0.4154462 cm^{-1}, and B_0'' ($\Omega = 1$) = 0.416116 cm^{-1}, respectively, as shown in Table 3.6.

The spin-splitting between the two spin components of $X^3\Sigma^-$ could be determined if some transitions from the excited states of the first group ($F0^+$, $D1$, $C1$, $B1$, and $A1$, etc.) to the lower state ($X1$) are detected, or transitions from the upper states of the second group ($D'1$, $C'1$, and $B'0^+$) to the lower state of the first group ($X0^+$) are detected in the future. At the same time, the spin splitting can also be estimated by using the Λ-doubling constant q and the rotational constant [4].

The spectroscopic data and their residuals from a global fit related to work in this Chapter are listed in Appendix B. The molecular constants of the bands analyzed in this work are reported in Table 3.7.

It is worthwhile pointing out that *ab initio* calculations [4] performed by a colleague[10] have also confirmed that the ground state of WO is $X^3\Sigma^-$. These calculations were performed on the low-lying electronic states of the WO molecule in the triplet, quintet, and septet manifolds in order to decide the ground state symmetry, because the singlet energies are known to be much higher in energy. The program MOLPRO was used for these *ab initio* calculations [4]. The molecular orbitals used in these calculations were first optimized by state-averaged full-valence complete active space self-consistent field (CASSCF) calculations. Then the calculations were performed at the contracted multireference configuration interaction (CMCRI) level of theory with explicit correlation of all valence electrons.

At the levels of the CASSCF calculations, the $^3\Sigma^-$ state is predicted to be the lowest triplet arising from the valence electron configuration $1\sigma^2 2\sigma^2 1\pi^4 3\sigma^2 1\delta^2$: a similar CASSCF investigation of the quintet manifold reveals a single low-lying state of $^5\Pi$ symmetry arising from the configuration $1\sigma^2 2\sigma^2 1\pi^4 3\sigma^1 1\delta^2 2\pi^1$. The $1^5\Pi$ state is located 11,500 cm^{-1} above the lowest $^3\Sigma^-$ state. The conclusion of the preliminary CASSCF investigations is that the ground state of WO should have the $^3\Sigma^-$ symmetry, and the $^5\Pi$ symmetry as predicted in the previous *ab initio* work [3], in which the authors did not consider the possible triplet ground electronic state in their calculations[11]. The CASSCF results have been confirmed by more extensive CMRCI calculations.

[10] Jacky Liévin, Université Libre de Bruxelles, Laboratoire de Chimie Physique Moléculaire, Brussels, Belgium.

[11] Private communication.

Table 3.7: Molecular Constants of ^{184}WO Bands (cm^{-1})

STATE	T_v	B_v	$D_v(\times10^7)$	$H_v(\times10^{12})$	$q_v(\times10^5)$	$q_{Dv}(\times10^8)$	$q_{Hv}(\times10^{11})$
Relative to X0$^+$(v = 0)							
F0$^+$(v = 0)	23401.1058(26)	0.383829(13)	3.146(49)	.	.	.	.
D1 (v = 1)	21772.9803(32)	0.388364(20)	7.49(15)	77.4(33)	−283.32(22)	94.9(23)	15.24(56)
D1 (v = 0)	20793.8722(23)	0.388926(16)	2.674(88)	5.2(15)	−20.718(49)	−0.74(35)	0.154(62)
C1 (v = 1)	20109.7050(18)	0.388349(16)	11.45(12)	−8.3(41)	131.54(65)	172.18(14)	2.49(70)
C1 (v = 0)	19182.46113(91)	0.391446(15)	2.587(91)	−1.77(21)	−8.77(48)	−6.30(78)	3.89(31)
X0$^+$ (v = 3)	3148.5487(21)	0.409494(17)	2.77(11)	3.4(25)	.	.	.
X0$^+$ (v = 2)	2107.0882(15)	0.411534(16)	2.91(16)	7.5(24)	.	.	.
X0$^+$ (v = 1)	1057.5680(21)	0.413555(16)	2.819(92)	4.7(16)	.	.	.
X0$^+$ (v = 0)	0.0	0.415581(15)	2.893(87)	6.6(15)	.	.	.
Relative to X1 (v = 0)							
D′1 (v = 0)	21222.2990(17)	0.384843(23)	1.97(15)	−26.9(30)	−117.93(51)	−0.84(26)	.
B′0$^+$	19439.6206(16)	0.385424(23)	1.94(15)	−25.3(28)	.	.	.
X1 (v = 1)	1059.9266(18)	0.414161(24)	1.73(15)	−27.0(30)	17.65(15)	−0.896(68)	.
X1 (v = 0)	0.0	0.416163(23)	1.62(15)	−27.8(28)	17.65(15)	−0.896(68)	.

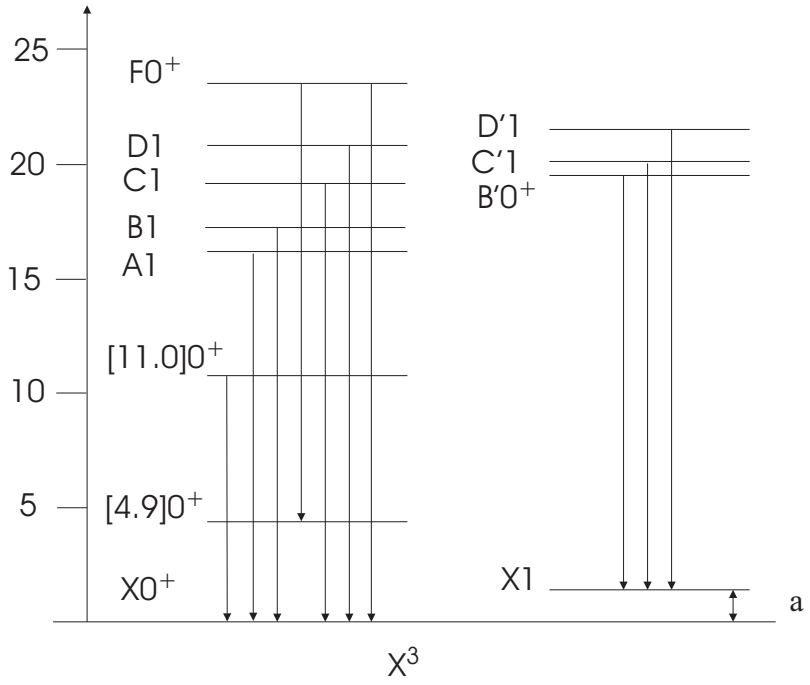

Figure 3.12: The Energy Level Diagram for WO ($cm^{-1} \times 10^3$). The constant a is the spin splitting between the two spin components of the ground state $X^3\Sigma^-$.

Bibliography

[1] W. Weltner Jr. and D. McLeod, Jr. Spectroscopy of tungsten oxide molecules in neon and argon matrices at 4 K and 20 K. *Journal of Molecular Spectroscopy*, 17:276–299, 1965.

[2] A. N. Samoilova, Yu. M. Efremov, and L. V. Gurvich. Electronic spectrum of the $^{186}W^{16}O$ molecule. *Journal of Molecular Spectroscopy*, 86:1–15, 1981.

[3] C. J. Nelin and C. W. Bauschlicher, Jr. On the low-lying states of WO: A comparison with CrO and MoO. *Chemical Physics Letters*, 118(2):221–225, 1985.

[4] R. S. Ram, J. Liévin, G. Li, T. Hirao, and P. F. Bernath. The $X^3\Sigma^-$ ground state of WO. *Chemical Physics Letters*, 343:437–445, 2001.

[5] A. Gatterer and S. G. Krishnamurty. Two band systems of tungsten oxide. *Nature*, 4300:543–543, 1952.

[6] V. Vittalachar and S. G. Krishnamurty. Band spectrum of tungsten oxide. *Current Science (India)*, 23:357–358, 1954.

[7] D. W. Green and K. M. Ervin. Infrared spectra of matrix-isolated tungsten oxides. *Journal of Molecular Spectroscopy*, 89:145–158, 1981.

[8] Yu. M Efremov, L. V. Gurvich, A. N. Savchenko, and E. A. Sviridenkov. The electronic spectra following flash photolysis of metal hexacarbonyls observed by an intracavity Nd^{3+}-glass laser spectroscopic technique. *Chemical Physics Letters*, 1:179–182, 1979.

[9] Yu. Ya. Kuzyakov, E. N. Moskvitina, and E. N. Filippova. Intracavity electronic absorption spectra of MoO and WO molecules in the visible region. *Spectroscopy Letters*, 30(6):1057–1066, 1997.

[10] D. Kraus, R. J. Saykally, and V. E. Bondybey. Cavity ringdown laser absorption spectra of tungsten oxide. *Chemical Physics Letters*, 295:285–288, 1998.

[11] W. D. Bare, P. F. Souter, and L. Andrews. Reactions of laser-ablated molybdenum and tungsten atoms with dioxygen. Resolved infrared spectra of natural molybdenum and tungsten isotopic oxides in argon matrices. *Journal of Chemical Physics*, 102:8279–8286, 1998.

[12] M. Lorenz, J. Agreiter, N. Caspary, and V. E. Bondybey. Relaxation and vibrational fluorescence of WO in solid neon. *Chemical Physics Letters*, 291:291–299, 1998.

[13] M. Lorenz and V. E. Bondybey. Isotopically resolved spectra of tungsten oxides in solid neon. *Chemical Physics*, 241:127–138, 1999.

[14] R. S. Ram and P. F. Bernath. High resolution Fourier transform emission spectroscopy of the $A^4\Pi$ - $X^4\Sigma^-$ system of WN. *J. Opt. Soc. Am. B.*, 11:225–230, 1994.

[15] J. M. Hollas. *Modern Spectroscopy.* John Wiley & Sons, New York, 3rd edition, 1996.

[16] J. M. Hollas. *High Resolution Spectroscopy.* John Wiley & Sons, New York, 2nd edition, 1998.

[17] C. N. Banwell. *Fundamentals of Molecular Spectroscopy.* McGraw-Hill Book Company (UK) Limited, London, 3rd edition, 1983.

[18] I. Mills, T. Cvitaš, K. Homann, N. Kallay, and K. Kuchitsu. *Quantities, Units and Symbols in Physical Chemistry.* Blackwell Scientific Publications, International Union of Pure and Applied Chemistry, 1988.

Chapter 4

Accurate Molecular Constants for the Ground Electronic State of BeH

The BeH molecule is one of the molecules with the lightest mass and simplest structure. With only four electrons, it has been used extensively as a test case for new approaches to theoretical calculations. As with other species, *ab initio* calculations progress hand-in-hand with experimental studies. However, there are many fewer experimental publications than theoretical papers [1, 2, 3, 4, 5, 6, 7, 8, 9, 10, 11, 12][1] in the case of BeH.

Because of strong rotational perturbations between the excited electronic states of $A^2\Pi$ and $C^2\Sigma^+$ [13, 14, 15],[2] molecular constants of the $A^2\Pi$, $C^2\Sigma^+$ and $X^2\Sigma^+$states derived using conventional methods are not very accurate because many data have to be deweighted. This Chapter reports an accurate set of molecular constants for the ground electronic state $X^2\Sigma^+$ obtained by using a special spectroscopic data treatment method, i.e., treating the data of electronic transitions as if they were from "fluorescence series". With this procedure, the resulting molecular constants are accurate because all experimental data with correct assignments are used in the fitting, whereas in the conventional way, the perturbed data have to be rejected.

For a light molecule like BeH, the combined-isotopomer analysis also provides Born-Oppenheimer breakdown correction terms, which are expected to be large because of the small masses of the constituent atoms of the molecule.

Section 4.1 introduces the available experimental studies on the BeH isotopomers from the literature and private correspondence, and the theoretical basis for the

[1] Just to cite a few.

[2] The energy levels are so close that perturbations occur.

derivation of accurate molecular constants. Section 4.2 summarizes the data sources of electronic transitions for the BeH isotopomers, BeH, BeD, and BeT, available for the theoretical analysis, i.e., the old electronic data obtained using spectrographs, and modern electronic data from Fourier transform spectrometers. Section 4.3 describes the method of treatment of the data for the electronic transitions. Section 4.4 presents the details of combined-isotopomer Dunham-type analysis, as applied to the data for the BeH isotopomers. Section 4.5 closes the Chapter with discussions and conclusions.

4.1 Background

The spectroscopic data published in the literature, together with the techniques used in the experiments, are summarized in this Section. The theoretical basis for the theoretical analysis to be carried out is also presented.

4.1.1 Experimental Studies of BeH Isotopomers

Before the systematic experimental studies of the three isotopomers BeH, BeD and BeT by Colin *et al.* [13, 16, 17, 18] in the 1970s and 1980s, only a limited amount of experimental data for BeH and BeD was published by early researchers in the late 1920s and early 1930s. An electronic band system due to the transition of the first excited state to the ground electronic state $A^2\Pi - X^2\Sigma^+$ was observed in emission and analysed for the BeH isotopomer [19, 20, 21]. Similarly, data from the $A^2\Pi - X^2\Sigma^+$ transitions were obtained for the deuterated molecule [22]. In addition, some data for the $B^2\Pi - X^2\Sigma^+$ band system were observed in emission for BeH [23]. The spectra mentioned above were generated using a DC arc between beryllium electrodes in a hydrogen or deuterium atmosphere, and recorded using grating spectrographs and photographic plates.

By using a King furnace[3] containing metallic beryllium heated to 1,800° C in an atmosphere of hydrogen gas, Colin *et al.* [16] obtained high resolution[4] $A^2\Pi - X^2\Sigma^+$ absorption bands of BeH and BeD, and improved vibrational and rotational constants were derived. Some bands of the $A^2\Pi - X^2\Sigma^+$ transition of BeT were also obtained in emission from a sealed beryllium hollow cathode continuous discharge, and analysed [17].

By using an apparatus similar to that used in the earlier $A^2\Pi - X^2\Sigma^+$ experiment [16], Colin *et al.*. [18] obtained the absorption spectra of BeH and BeD in the ultraviolet. A number of new band systems were detected and rotationally analysed, e.g., bands of the $B'^2\Pi - X^2\Sigma^+$, $E^2\Sigma^+ - X^2\Sigma^+$, $F^2\Sigma^+ - X^2\Sigma^+$, and $G^2\Pi - X^2\Sigma^+$ transitions.

In addition, Colin *et al.* [13] observed the $C^2\Sigma^+ - X^2\Sigma^+$ transition of BeH and BeD in a beryllium hollow cathode discharge similar to that used for observing BeT in hydrogen or deuterium gas mixed with argon [17].

Rotational perturbations between the $C^2\Sigma^+$ and $A^2\Pi$ states were observed [13]. Some new bands of the $A^2\Pi - X^2\Sigma^+$ system were also observed simultaneously. These

[3] A King furnace is a graphite tube furnace.

[4] Using a 10 meter vacuum grating spectrograph and photographic plates with a reciprocal dispersion (Å of wavelength for each mm of photographic plate) of 0.3 to 1.5 Å/mm, and an absolute error of ± 0.05 cm^{-1}.

unpublished data on the $A^2\Pi - X^2\Sigma^+$ transition proved very useful in the linking of all the ground state vibrational levels[14] in the data analysis of this Chapter.

In late 1990s, Fourier transform emission spectra of $A^2\Pi - X^2\Sigma^+$ transitions of BeH [14] and BeD [15] were reported. The BeH spectrum was generated using a beryllium hollow cathode discharge lamp, and detected in the 18,000 - 22,500 cm^{-1} spectral region at an instrumental resolution of 0.1 cm^{-1} with an absolute accuracy of ± 0.003 cm^{-1}. A higher resolution spectrum was not recorded because of the large Doppler broadening of the BeH lines. A combined study of cool and hot spectra was carried out [14]. The cool spectrum provides better resolved lines, and the hot spectrum extends the assignments to higher N values. The Fourier transform emission spectra of BeD were generated and recorded in a similar way.

4.1.2 Theoretical Basis

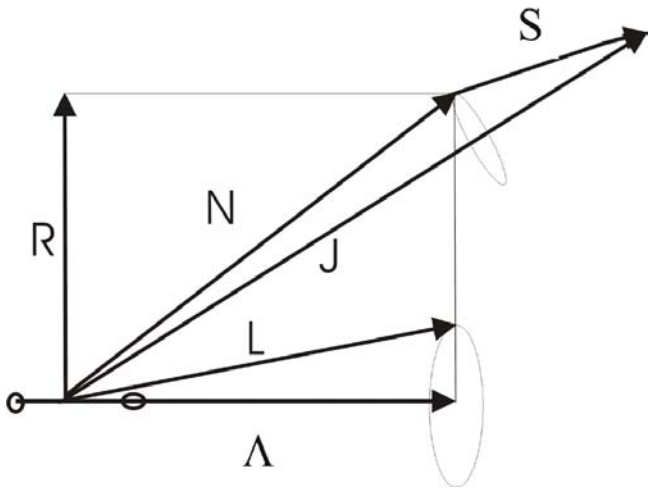

Figure 4.1: Vector Coupling Diagram for Hund's Case (b). **R** - overall rotational angular momentum; $\Lambda\hbar$ - the axial component of the electronic orbital angular momentum; **N** - the resultant of adding **R** and $\Lambda\hbar$; **J** - the total angular momentum, due to the coupling of **N** and **S**.

The coupling of the total orbital angular momentum and spin to the intermolecular axis for the electronic states of a diatomic molecule can assume one of the Hund's cases or lie between two Hund's cases, according to the number of electrons in the component atoms. Hund's case (b) generally applies to Σ states ($\Lambda = 0$) with $S \neq 0$, provided that spin-spin coupling is not large [24]. The **S** vector cannot be coupled to the intermolecular axis by itself. It needs to have the magnetic field associated with the orbiting electrons to couple to the axis. For Σ states ($\Lambda = 0$), there is no axial

component of the orbital angular momentum, and hence no magnetic field and no coupling [24]. For $\Lambda \neq 0$, the **S** vector is coupled to the intermolecular axis by the magnetic field due to the orbiting electrons. However, for light molecules with few electrons, such as BeH and MgH, the coupling of the vector **S** to the intermolecular axis may be very weak [24]. For both the $^2\Sigma^+$ and $^2\Pi$ states of the BeH molecule, Hund's case (b), as shown in Fig. 4.1, is an appropriate approximation.

Fig. 4.1 shows the resulting vector diagram for $\Lambda \neq 0$. The resultant of **R** and $\Lambda\hbar$ is **N**, and the coupling of **N** and **S** produces the total angular momentum of **J** [24]. For Hund's case (b), L is not a good quantum number, but Λ, S, N and J are all good quantum numbers. The values that J can take are determined by N and S, and are given by [24].

$$J = N + S, N + S - 1, \cdots, |N - S| \tag{4.1}$$

where J can have integer or half-odd-integer values.

For the doublet electronic states $A^2\Pi$ and $X^2\Sigma^+$ of the BeH isotopomers, $S = 1/2$. Thus, the possible values for J are $J = N + 1/2$ and $J = N$ - 1/2. Each rotational level has $(2S + 1)$ components when $N \geq S$, the result of spin-rotation interaction, and for the BeH molecule, $(2S + 1) = 2$.

In a $^2\Sigma$ state, the rotational term values $F_1(N)$ and $F_2(N)$ corresponding to the J having values $N + 1/2$ and $N - 1/2$, respectively, are given by [24]

$$\begin{aligned} F_1(N) &= B_v N(N+1) + \frac{1}{2}\gamma N \\ F_2(N) &= B_v N(N+1) - \frac{1}{2}\gamma(N+1) \end{aligned} \tag{4.2}$$

where γ is the spin-rotation coupling constant, which is usually very small. The coupling of spin **S** with the nuclear end-over-end rotation **R** (spin-rotation coupling) may contain small contributions due to direct magnetic coupling, and also to coupling through the orbital motion of the electrons [24].

In the $A^2\Pi - X^2\Sigma^+$ transition of the BeH molecule, the rotational fine structure of the spectra is determined by the properties of the $A^2\Pi$ and $X^2\Sigma^+$ states. Fig. 4.2 shows the rotational energy level diagram of the $A^2\Pi - X^2\Sigma^+$ transition [25]. The upper state is the $A^2\Pi$ state; the lower state is the $X^2\Sigma^+$ state. In the $X^2\Sigma^+$ state, there are two spin components, corresponding to $J'' = N'' + 1/2$ and $J'' = N'' - 1/2$. In the $A^2\Pi$ state, there are also two spin components corresponding to $J' = N' + 1/2$ and $J' = N' - 1/2$. However, because $\Lambda \neq 0$ for the Π state, there are Λ-type

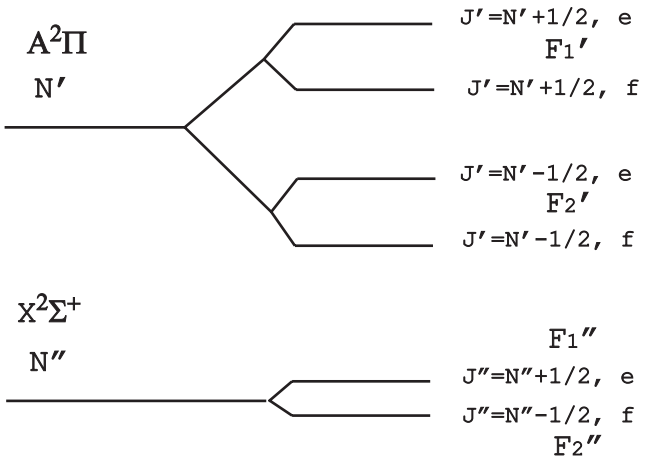

Figure 4.2: Rotational Energy Level Diagram of an $A^2\Pi - X^2\Sigma^+$ Transition.

doublings in each of the spin components. The spin splittings are observed because of the spin-rotation interaction, but the Λ-type doublings are observed also because of the end-over-end molecular rotation.

For the $X^2\Sigma^+$ ground electronic state of the BeH molecule, the approximate energy level formula is $F_1(e) = F_2(f) = BN(N+1)$, with $N = J - 1/2$ for the e levels and $N = J + 1/2$ for the f levels, when the spin splitting in Eqn. (4.2) is neglected (i.e., without consideration of spin-rotation interaction). Although the energy levels $F_1(N)$ and $F_2(N)$ corresponding to the two J values for each N are degenerate in the non-rotating molecule, inclusion of the spin-rotation interaction term splits the levels by the amount $\gamma(N + 1/2)$ [24, 25], as shown in Eqn. (4.2). For the $X^2\Sigma^+$ ground state of BeH, the spin splitting is very small[5], so that the spin splitting between the two spin components can be neglected: in this case, the $X^2\Sigma^+$ ground electronic state can be treated as an $X^1\Sigma^+$ state.

Because the number of electrons in the BeH molecule is small, the spin-orbit coupling constant A is nearly zero, so that Hund's case (b) coupling applies to the $A^2\Pi$ electronic state. The rotational energy levels for a Hund's case(b) $^2\Pi$ state have a fourfold degeneracy[6] for each N, i.e., F_{1e}, F_{1f}, F_{2e}, F_{2f}. The F_1 and F_2 labels are defined so that $N = J - 1/2$ for F_1 levels and $N = J + 1/2$ for F_2 levels.

In a $\Pi - \Sigma$ transition, the lines of the Q branch are stronger than those of the P and R branches, and terminate on rotational levels of the opposite parity ($e - f$ or

[5]This is obvious in consideration of the fact that, the spin-rotation couplings are rarely observed directly even in very high resolution spectroscopy, e.g., the far infrared and millimeter wave spectroscopy of MgH as described in Chapter 5.

[6]In general, the rotational energy levels for Hund's case (b) $^{2S+1}\Lambda$ states are given by $BN(N+1)$ and there are $2(2S+1)$ degenerate levels for $\Lambda \neq 0$, i.e., Λ-type doubling, and $2S+1$ degenerate levels for $\Lambda = 0$ [25]

$f - e$); the P and R branch lines terminate on rotational levels of the same parity ($e - e$ or $f - f$)[25].

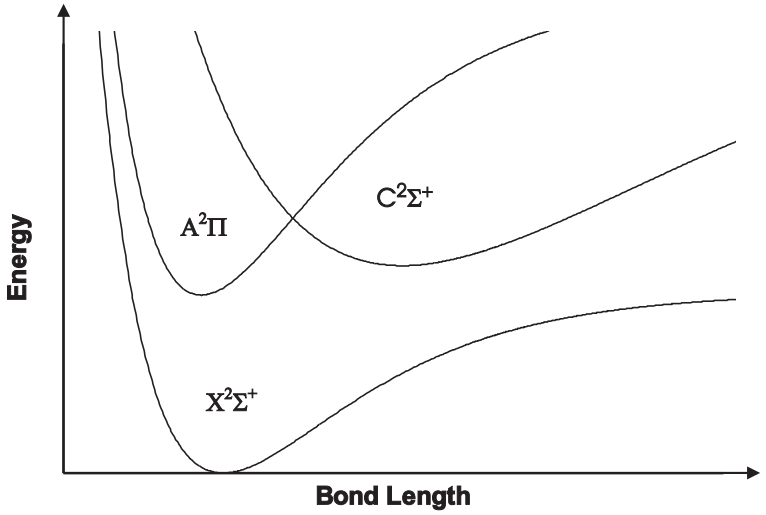

Figure 4.3: Qualitative Potential Curves of the Electronic States of BeH

4.2 Spectroscopic Data Sources of BeH Isotopomers

The data used in this Chapter are those detected in or after the 1970s. The spectrographic data published before the 1970s were all improved by more recent experiments. Because the data sets from the $B^2\Pi - X^2\Sigma^+$, $B'^2\Pi - X^2\Sigma^+$, $G^2\Pi - X^2\Sigma^+$, $E^2\Sigma^+ - X^2\Sigma^+$, and $F^2\Sigma^+ - X^2\Sigma^+$ transitions are very small, only data from the $A^2\Pi - X^2\Sigma^+$ bands and $C^2\Sigma^+ - X^2\Sigma^+$ bands for the BeH isotopomers are considered.

Table 4.1: Vibrational Bands of the $A^2\Pi - X^2\Sigma^+$ System of BeH

		v'						
		0	1	2	3	4	5	6
	0	X[a,b]						
	1	X[c]	X[a,b]					
	2		X[c]	X[a,b]				
	3			X[c]	X[a,b]			
v''	4				X[c]	X[a,b]		
	5					X[c]	X[a,b]	
	6						X[c]	X[b]
	7							X[c]

Note: X - transition observed.
Source: a - Old electronic data, Horne and Colin [16].
b - Fourier transform data, Bernath *et al.* [14].
c - Unpublished data, Colin *et al.* [13, 14].

4.2.1 Electronic Spectroscopy with a Spectrograph

The high resolution BeH and BeD absorption spectra obtained by Colin *et al.* [16] contain $A^2\Pi - X^2\Sigma^+$ bands of the $\Delta v = 0$ sequence, i.e., the 0-0, 1-1, 2-2, 3-3, 4-4 and 5-5 bands for BeH, as shown in Table 4.1, and the 0-0, 1-1, and 2-2 bands for BeD, as shown in Table 4.3. The 0-0, 1-1, 2-2 and 3-3 bands of the $A^2\Pi - X^2\Sigma^+$ transition of BeT, as shown in Table 4.5, were obtained in emission from a sealed beryllium hollow cathode discharge [17].

Colin *et al.* [13] also observed the $C^2\Sigma^+ - X^2\Sigma^+$ transitions of BeH and BeD in a beryllium arc in hydrogen or deuterium gas mixed with argon. The electronic data of the 0-6, 0-7, 0-8, 0-9, 1-9, 1-10, and 2-9 bands of the $C^2\Sigma^+ - X^2\Sigma^+$ system of BeH,

and the 0-8, 0-9, 0-10, 0-11, and 0-12 bands of the $C^2\Sigma^+ - X^2\Sigma^+$ system of BeD are available, as shown in Tables 4.2 and 4.4.

Table 4.2: Vibrational Bands of the $C^2\Sigma^+ - X^2\Sigma^+$ System of BeH

		v'						
		0	1	2	3	4	5	6
	6	X[a]						
	7	X						
v''	8	X						
	9	X	X	X				
	10		X					

Note: X - transition observed.
a - Incorrect identification [14].
Source: All data in this table are old electronic data from Colin *et al.* [13].

4.2.2 Fourier Transform Spectroscopic Data

The data of Fourier transform spectra of the 0-0, 1-1, 2-2, 3-3, 4-4, 5-5, and 6-6 bands of the $A^2\Pi - X^2\Sigma^+$ transition of BeH, i.e., the $\Delta v = 0$ sequence, was detected at an instrumental resolution of 0.1 cm^{-1}, with an absolute accuracy of ± 0.003 cm^{-1} [14]. The Fourier transform BeD spectra of the 0-0, 1-1, 2-2, 3-3, 4-4, 5-5, and 6-6 vibrational bands of the $A^2\Pi - X^2\Sigma^+$ transition [15] were generated and recorded in a similar manner, and the $\Delta v = 0$ sequence of the $A^2\Pi - X^2\Sigma^+$ system was reported for BeD [15]. The Fourier transform data shown in Tables 4.1 and 4.3 are of higher accuracy than the spectrographic data.

4.2.3 Summary of Spectroscopic Data Set

4.2.3.1 BeH Data

The bands available from the $A^2\Pi - X^2\Sigma^+$ and $C^2\Sigma^+ - X^2\Sigma^+$ transitions for BeH are shown in Tables 4.1 and 4.2, respectively. The BeH spectroscopic data for the $A^2\Pi - X^2\Sigma^+$ and $C^2\Sigma^+ - X^2\Sigma^+$ bands published by Colin *et al.* [16] are for low vibrational levels (v'' = 0-5) and high vibrational levels (v'' = 7-10) only, the v'' = 6 band was not identified correctly. If the levels were all linked together and

Table 4.3: Vibrational Bands of the $A^2\Pi - X^2\Sigma^+$ System of BeD

		v'						
		0	1	2	3	4	5	6
	0	X[a,b]						
	1	X[c]	X[a,b]					
	2		X[c]	X[a,b]				
v''	3			X[c]	X[b]			
	4				X[c]	X[b]		
	5					X[c]	X[b]	
	6						X[c]	X[b]

Note: X - transition observed.
Source: a - Old electronic data, Horne and Colin [16].
b - Fourier transform data,
Bernath *et al.* [15].
c - Unpublished old electronic data,
Colin *et al.* [13, 15].

the $v'' = 6$ gap were filled, then the experimental data would be more useful [14], and a global fitting could be carried out. An attempt was made, using a Fourier transform spectrometer and hollow cathode discharge, to fill the $v'' = 6$ gap, but it was unsuccessful [14]. The Fourier transform data detected have longer diagonal sequences, i.e., from 0-0 to 6-6 [14]. In order to fill the $v'' = 6$ gap, the unpublished $A^2\Pi - X^2\Sigma^+$ data of Colin *et al.* from the same arc spectra used for the $C^2\Sigma^+ - X^2\Sigma^+$ analysis [13] were employed, and the 0-1 to 6-7 bands of the $\Delta v = -1$ sequence were identified [14]. Thus the $v'' = 0$-10 levels in the $X^2\Sigma^+$ state and $v' = 0$-6 levels in the $A^2\Pi$ state are linked together on the same energy scale [14].

4.2.3.2 BeD Data

The $A^2\Pi - X^2\Sigma^+$ and $C^2\Sigma^+ - X^2\Sigma^+$ electronic data for BeD are shown in Tables 4.3 and 4.4. The 0-0, 1-1, and 2-2 bands of the $A^2\Pi - X^2\Sigma^+$ system are available from spectrographic data [16]. The Fourier transform experiment detected the $\Delta v = 0$ sequence from 0-0 to 6-6 [15], extended from the 2-2 band of the spectrograph data to the 6-6 band. As in the treatment of the BeH isotopomer, the unpublished data of the $\Delta v = -1$ sequence from 0-1 to 5-6 of the $A^2\Pi - X^2\Sigma^+$ system detected in the spectrograph experiment for the $C^2\Sigma^+ - X^2\Sigma^+$ transition [13, 15] were used to link together the data set from $v'' = 0$ to $v'' = 6$ levels. However, there are not enough

Table 4.4: Vibrational Bands of the $C^2\Sigma^+ - X^2\Sigma^+$ System of BeD

		v'						
		0	1	2	3	4	5	6
	8	X						
	9	X						
v''	10	X						
	11	X						
	12	X						

Note: X - transition observed.
Source: All data in this table are old electronic data from Greef and Colin [13].

spectroscopic data for BeD to bridge directly the gap between $v'' = 6$ and $v'' = 8$.

4.2.3.3 BeT Data

The 0-0, 1-1, 2-2 and 3-3 bands of the $A^2\Pi - X^2\Sigma^+$ electronic transition for BeT are shown in Table 4.5. The four bands of the $A^2\Pi - X^2\Sigma^+$ transition of BeT were detected using a spectrograph and obtained in emission from a sealed beryllium hollow cathode [17]. Some of the BeT data have an accuracy of 0.07 cm^{-1}, and some have an accuracy of 0.02 cm^{-1}.

Table 4.5: Vibrational Bands of the $A^2\Pi - X^2\Sigma^+$ System of BeT

	v'						
	0	1	2	3	4	5	6
0	X						
1		X					
2			X				
3				X			

Note: X - transition observed.
Source: All data in this table are old electronic data from Greef and Colin [17].

4.3 Treatment of Electronic Transition Data

The new method of treatment of electronic data involves two steps. The first is to convert the rotational quantum numbers from N to J. The second is to convert the vibrational bands into "fluorescence series".

4.3.1 Quantum Number Conversion

In order to use the singlet data processing program DSParFit [26, 27, 28], the doublet spectroscopic data for the BeH isotopomers need to be converted into the singlet format. The $X^2\Sigma^+$ ground electronic state of BeH can be considered to be equivalent to an $X^1\Sigma^+$, as the spin splitting is so small that it can be neglected ($\gamma \approx 0$).

For the $X^2\Sigma^+$ ground electronic state, the rotational quantum number used in energy level expressions is N, as in Eqn. (4.2). For a ground state $X^1\Sigma^+$, the rotational quantum number used in the energy level expressions is J, as in Eqns. (1.5) to (1.10). As discussed in Section 4.1.2, the relationship between the two quantum numbers is $J = N\pm$ 1/2, in which $J = N$ + 1/2 for the e parity (or $p = +1$), and $J = N$ - 1/2 for the f parity or ($p = -1$). Because N is integer and J is half-odd integer, the quantum numbers J are all rounded up to the next integer in computer programs:[7] the practical rule for the conversion of quantum numbers here is $J = N$ for an f parity (p = -1) level, and $J = N + 1$ for an e parity ($p = +1$) level.

For the treatment of the doublet spectroscopic data pairs, another way is to average the doublet data of spin splitting pairs, and then convert the rotational quantum number N to J in a manner similar to that used for the $X^2\Sigma^+$ state. However, the term values for each (v',J',p') will be "artificial" because of averaging out the two spin components. The method used in this Chapter is to convert the rotational quantum number from N to J, but to retain the original doublet data format so that the original data are kept along with the corresponding parity p'. Consequently, the term values of the "fluorescence series" are those with the doublet splittings, i.e., the true (v',J',p') term values.

4.3.2 Converting Vibrational Bands to "Fluorescence Series"

The "fluorescence series" method of treating the data from electronic bands with perturbations in the upper states provides an accurate set of molecular constants for the ground electronic state.

[7] Computer programs such as LSQFIT-D and DSParFit use integer quantum numbers instead of half-odd-integers.

Spectroscopic data for the bands of electronic transitions are re-organized in such a way that all rovibronic transitions originating from each unique set of v', J' and p' are grouped together. The groups of such data, or the pseudo "fluorescence series" allow calculations similar to combination differences to be made for the ground electronic state. The perturbations in the upper electronic states can do no harm to the molecular constants obtained in this way for the ground electronic state. At the same time, the fitting also generates a term value for each group with a unique set of v', J' and p', which can be further explored for rotational deperturbation analysis for the perturbed electronic states.

Sometimes there is only one datum in a group formed this way. Combination differences can not be formed for such a group. In the analysis reported in this Chapter, such a "group" is deleted from the data file to increase the computational efficiency.

4.4 Combined Isotopomer Dunham-Type Analysis

Combined-isotopomer Dunham-type analysis is especially advantageous in the study of the isotopomers of such a light molecule as BeH. This method not only reduces the number of parameters required to represent the molecule, but also provides the Born-Oppenheimer breakdown correction terms that are important for light molecules.

4.4.1 Light Molecules and the Born-Oppenheimer Approximation

The refined analysis of the spectra of the isotopomers of light molecules provides measurable quantities which represent the degree of validity of the Born-Oppenheimer approximation. The Born-Oppenheimer approximation assumes that the motion of the electrons in the molecule occurs in the electrostatic field of fixed nuclei of infinite mass. A consequence of this approximation is the invariance of the pure electronic energy of a given state to isotopic substitution. Within this approximation, the potential energy curve of each electronic state of a molecule is therefore the same for all isotopic species.

For light hydrides, it is possible by using high resolution spectra to determine the different values of the electronic term values T_e of a given state for different isotopomers. Electronic isotopic shifts ΔT_e are a direct consequence of the breakdown of the Born-Oppenheimer approximation.

4.4.2 Combined-Isotopomer Dunham-Type Analysis

In all of the fits reported herein, the observed transition energies were weighted by the inverse square of their uncertainties, and the quality of fit is indicated by the value of the dimensionless standard error (DSE)

$$\overline{\sigma}_f \quad = \quad \left\{ \frac{1}{N-M} \sum_{i=1}^{N} \left[\frac{y_{calc}(i) - y_{obs}(i)}{u(i)} \right]^2 \right\}^{1/2} \tag{4.3}$$

in which each of the N experimental data $y_{obs}(i)$ has an uncertainty of $u(i)$, and $y_{calc}(i)$ is the value of datum–i predicted by the M–parameter model being fit. All parameter uncertainties quoted here are 95% confidence-limit uncertainties.

In order to obtained an accurate set of parameters for the $X^2\Sigma^+$ ground electronic state and to explore the Born-Oppenheimer breakdown terms, the data set of electronic transitions measured with a spectrograph [16, 17, 13], and Fourier transform

electronic spectroscopic data [14, 15] are reorganised as "fluorescence" series following Section 4.3.

In the conventional way of describing molecules, each isotopomer needs an individual set of molecular constants. The combined-isotopomer fitting uses one set of parameters to describe all of the isotopomers, which greatly reduces the number of parameters required.

In order to simplify the representation of these data sets and to search for physically interesting information about Born-Oppenheimer breakdown effects, all of the line positions of the transitions of the old electronic spectra (detected using techniques of spectrograph and electric arc) and Fourier transform spectra of the three isotopomers (BeH, BeD, and BeT) were fit simultaneously to a combined-isotopomer Dunham-type expression for the energy levels. Following Section 1.3.1.3, observed transitions for isotopomer–α of species BeH formed from atoms of mass M_{Be} and M_H^α (i.e., hydrogen, deuterium, or tritium) were expressed as differences between energy levels written as

$$\begin{aligned} E^\alpha(v,J) &= \sum_{(l,m)\neq(0,0)} Y_{l,m}^1 \left(\frac{\mu_1}{\mu_\alpha}\right)^{m+l/2} (v+1/2)^l \left[J(J+1)\right]^m \\ &+ \sum_{(l,m)\geq(0,0)} \left\{ \frac{\Delta M_H^\alpha}{M_H^\alpha}\, \delta_{l,m}^H \right\} \\ &\times \left(\frac{\mu_1}{\mu_\alpha}\right)^{m+l/2} (v+1/2)^l \left[J(J+1)\right]^m \end{aligned} \tag{4.4}$$

in which

$$\Delta M_H^\alpha = M_H^\alpha - M_H^1.$$

The condition $\alpha = 1$ for M_H^α, i.e., M_H^1 identifies the selected reference species, the most abundant isotopomer, BeH. The conventional Dunham constants for other ($\alpha \neq 1$) isotopomers are then generated from

$$Y_{l,m}^\alpha = \left\{ Y_{l,m}^1 + \frac{\Delta M_H^\alpha}{M_H^\alpha}\, \delta_{l,m}^H \right\} \left(\frac{\mu_1}{\mu_\alpha}\right)^{m+l/2} \tag{4.5}$$

The transition bands of spectroscopic data used in the analysis are summarized in Tables 4.1 to 4.5. A total of 5,012 spectroscopic data (transitions) were fit to Eqn. (4.4) using the program "DSParFit" [26, 27, 29] with a final dimensionless standard error $\overline{\sigma}_f = 1.209$. The program DSParFit simplifies the resulting parameters by

applying a sequential rounding and refitting procedure [30]. This yields the molecular constants given in the first column of Table 4.7. The numbers in parentheses are the 95% confidence limit uncertainties in the last significant digits shown.

A search for significant Born-Oppenheimer breakdown effects showed that their inclusion could reduce the dimensionless standard error $\overline{\sigma}_f$ drastically. In other words, the data can not be fit to the equation without inclusion of the Born-Oppenheimer breakdown correction terms for the hydrogen atom. The δ_{lm} constants for the hydrogen atom are also included in Table 4.7.

For the user's convenience, the constants for the minority isotopomers, rounded at the first digit of the parameter sensitivity, are shown in the last two columns of Table 4.7. The results in the last row of this table show that the rounded constants generated from the BeH parameters determined from the combined-isotopomer analysis reproduce the input data for the individual minority isotopomers with no significant loss of precision.

The total root mean square residual (RMSR) values of the isotopomers in Table 4.7 are calculated using Eqn. (4.6).

$$RMSR \;=\; \left\{\frac{1}{\sum n_i}\;\sum n_i (RMSR)_i\right\}^{1/2} \tag{4.6}$$

where n_i is the number of data in "fluorescence series" i; $(RMSR)_i$ is the root mean square residual of each of the data in fluorescence series i. The summation is performed with respect to the total number of fluorescence series.

4.4.3 Molecular Constants of BeH Isotopomers

The global fitting of 5,012 electronic transition data gives a dimensionless standard error $\overline{\sigma}_f = 1.209$. The parameters are listed in Table 4.7. The twenty-nine $Y_{l,m}$s for the major isotopomer BeH and nine Born-Oppenheimer breakdown correction terms, the $\delta_{l,m}$ are the result of the global fitting. The $Y_{l,m}$ for the minor isotopomers BeD and BeT have been calculated from the $Y_{l,m}$ of the major isotopomer BeH, together with the $\delta_{l,m}$. The $RMSR$ values in Table 4.7 are the root-meam-square residuals for each individual isotopomer obtained from the global fitting of all the isotopomers.

Following Eqn. (4.6), the output data of the "channel-6" output (the summary of the statistics of each "fluorescence series") of the DSParFit [27, 28] program have been processed using MS-Excel. The $RMSR$ values have been calculated for each of the individual isotopomers, and the steps and intermediate results are listed in Table 4.6.

The energy origins of the fluorescence series, as organized from the electronic transitions of the isotopomers, are listed in Appendix C, and can be used in deperturbation analysis of the excited electronic states.

Table 4.6: The RMSR Values for BeH, BeD and BeT

	BeH	BeD	BeT	Total
Σn_i	2317	2276	419	5012
$\Sigma n_i (RMSR_i)^2$	2611.186	1738.431	272.994	4622.611
$(RMSR)^2 = \Sigma n_i (RMSR)^2 / \Sigma n_i$	1.127	0.7638	0.6515	0.9223
RMSR	1.062	0.874	0.807	0.9604

Table 4.7: Dunham constants and Born-Oppenheimer breakdown correction terms from a total of 5,012 Data: $\overline{\sigma}_f = 1.209$ (95% confidence limit uncertainties) for $X\,^2\Sigma^+$ state of BeH and parameter values calculated for BeD and BeT

		All-Isotopomer Fit	Generated from BeH Constants and Eqn. (4.5)	
	Constant	BeH	BeD	BeT
	$Y_{1,0}$	2059.5861(2800)	1528.8165533	1305.0006677
	$Y_{2,0}$	−34.5362(2900)	−19.0449475	−13.8805992
	$Y_{3,0}$	−1.87725(14000)	−0.76508271	−0.47529306
	$Y_{4,0}$	0.55554(3600)	0.1684399359	0.089387386
10^3	$Y_{5,0}$	−96.9750(49)	−21.81835253	−9.8823656
10^3	$Y_{6,0}$	7.831(330)	1.307410064	0.505427163
10^3	$Y_{7,0}$	−0.269(9)	−0.0333257025	−0.0109959779
	$Y_{0,1}$	10.321514(590)	5.68920292	4.14585733
	$Y_{1,1}$	−0.312125(1100)	−0.127739739	−0.0794661381
10^3	$Y_{2,1}$	−0.9696(8700)	−0.2745932	−0.142297
10^3	$Y_{3,1}$	2.2126(3400)	0.49781167	0.225477929
10^6	$Y_{4,1}$	−976.7(650)	−163.063135	−63.0380168
10^6	$Y_{5,1}$	130.16(590)	16.1251801	5.32058174
10^6	$Y_{6,1}$	−6.39(20)	−0.58743568	−0.165433197
10^3	$Y_{0,2}$	−1.039769(1500)	−0.316233905	−0.167990658
10^6	$Y_{1,2}$	36.087(2000)	8.149545	3.695814
10^6	$Y_{2,2}$	−14.108(840)	−2.3553749	−0.9105563
10^6	$Y_{3,2}$	1.36(20)	0.16848682	0.055593048
10^9	$Y_{4,2}$	200.5(270)	18.432059	5.1908225
10^9	$Y_{5,2}$	−32.6(14)	−2.2238705	−0.53453929
10^9	$Y_{0,3}$	107.883(1700)	18.114837	7.0162564
10^9	$Y_{1,3}$	−22.94(220)	−2.8419763	−0.93772392
10^9	$Y_{2,3}$	10.233(540)	0.94072447	0.26492612
10^9	$Y_{3,3}$	−1.364(34)	−0.09304783	−0.022365386
10^{12}	$Y_{0,4}$	−13.58(91)	−1.24841574	−0.35157791
10^{12}	$Y_{1,4}$	5.27(110)	0.359503	0.08641172
10^{12}	$Y_{2,4}$	−1.81(15)	−0.09162266	−0.018796666
10^{15}	$Y_{0,5}$	0.80(17)	0.0404962	0.008307919
10^{15}	$Y_{1,5}$	−0.63(18)	−0.0236645	−0.00414365
	$\delta_{H;1,0}$	1.3575(1300)		
	$\delta_{H;2,0}$	−0.102(37)		
10^3	$\delta_{H;3,0}$	9.6(24)		
10^3	$\delta_{H;0,1}$	21.091(680)		
10^3	$\delta_{H;1,1}$	−1.008(280)		
10^3	$\delta_{H;2,1}$	0.128(31)		
10^6	$\delta_{H;0,2}$	−6.44(100)		
10^6	$\delta_{H;1,2}$	0.27(22)		
10^9	$\delta_{H;0,3}$	1.24(47)		
# of Data		5012	2276	419
# of Parameters		29 + 9	0	0
# of TermValues		765	812	237
RMSR		1.062	0.874	0.807

4.5 Discussions and Conclusions

4.5.1 "Fluorescence Series" Method of Data Treatment

A high resolution spectroscopic investigation of a molecule leads to an improved quality of spectroscopic data, and hence improved electronic, vibrational and rotational constants for the electronic states involved. However, the perturbations between the $A^2\Pi$ and $C^2\Sigma^+$ electronic states of the BeH molecule prevent one from arriving at an accurate result using conventional methods of data analysis. The pseudo "fluorescence series" method of data treatment completely eliminates the harmful influence of perturbations in the upper states $A^2\Pi$ and $C^2\Sigma^+$ on the molecular constants of the $X^2\Sigma^+$ ground electronic state of the BeH molecule.

4.5.2 Combined-Isotopomer Fitting

The combined-isotopomer analysis takes into account the data of all isotopomers simultaneously. Not only is the number of resulting parameters much smaller, i.e., instead of a set of parameters for each isotopomer, all the isotopomers can be represented with the parameters of the major isotopomer and the Born-Oppenheimer breakdown correction terms, but also the Born-Oppenheimer breakdown effect can be investigated simultaneously.

Generally speaking, the major isotopomer has the largest data set and covers a larger range of rotational and vibrational levels, and the minor isotopomers have smaller data sets. In the case of the minor isotopomers BeD and BeT, the data are either not completely connected or not connected at all with respect to rotational and vibrational levels. Using the combined-isotopomer analysis program DSParFit [27], only a completely connected data set for the major isotopomer is required. The parameters for the minor isotopomers can be generated using Eqn. (4.5), as long as data set of a modest size is available for each of the minor isotopomers for the derivation of the Born-Oppenheimer breakdown correction terms.

4.5.3 Empirical Rules for Molecular Constant Optimization

The data set for each isotopomer should individually fit properly before the combined isotopomer fitting is carried out. For the major isotopomer BeH, because the data set is connected in terms of both the vibrational levels and the rotational levels, both the band-constant fitting and the more restrictive Dunham-constant fitting can be performed. For the unconnected data sets of the minor isotopomers BeD and BeT, an individual Dunham fitting is not possible. In such cases, band-constant fitting for

the isolated bands should be done before the combined isotopomer global fitting. The individual isotopomer fitting is an effective way to find measurements or assignments errors in the spectroscopic data at an early stage.

4.5.3.1 Data fitting and troubleshooting

To find errors in the process of data fitting, it is a good practice to start with a small group of data with some common properties and to increase the size of the data set gradually. For example, start with a group of data for low vibrational levels, and add in data for higher vibrational levels gradually; or alternatively, start with a group of data with low J values and bring in more data by increasing the maximum J gradually. The DSParFit program [27] has a convenient way of specifying such data groups by controlling the maximum v and maximum J values. Using the method of gradually increasing the data set as described above, not only measurement, assignment, or other errors in the data set can be found, but bugs in the computer program (if any) can also be located.

For a data-fitting result, if the residuals of a few isolated data are large, then remove (deweight) these data; if the residuals of a series of data show a systematic trend or a pattern, e.g., the residuals increase or decrease with J systematically, then the number of parameters used for the fitting needs to be adjusted, such as by adding or deleting a higher-order centrifugal constant.

The fitting of the BeH isotopomer started with the $A^2\Pi - X^2\Sigma^+$ data set. After making sure that there was no problems with the $A^2\Pi - X^2\Sigma^+$ data set, the $C^2\Sigma^+ - X^2\Sigma^+$ data set was added in.

4.5.3.2 Data fitting steps

A good way of spectroscopic data fitting is to start with the band constants E, B, D, H, ..., because the band constants are restricted to only individual vibrational levels of the upper and lower electronic states involved. The number of resulting band constants is often larger than that of the corresponding Dunham constants, so a band-constant fit is more relaxed than that of the Dunham-constant fit. A data set that has a good band-constant fit may not have a good Dunham-constant fit; a data set with a good Dunham-constant fit most often has a good band-constant fit.

After obtaining a successful band-constant fit, Dunham-constant fitting can be carried out for the particular isotopomer. The data set needs to be connected properly with respect to both the v and the J quantum numbers to make the Dunham-constant fit successful.

The last step is to carry out the global combined-isotopomer fitting. The global fitting starts with the optimization of the Dunham constants of the major isotopomer (the one with the highest equivalent vibrational quantum number and completely connected data set, and usually with the largest data set), e.g., the BeH isotopomer in this Chapter. Then, the second largest data set is included in the fitting, in this case, the data of the BeD isotopomer. When the two isotopomers are made to fit together, in principle, the Y_{lm} need to be fixed and only the δ_{lm}s are varied to get the best fit. Then the next largest isotopomer is brought in, e.g., the BeT isotopomer here. The δ_{lm} may need to be adjusted slightly, but the Y_{lm}s should be kept more or less the same (they may not be exactly the same in the end, because of the overall optimization process for the parameters).

In this Chapter, the "fluorescence series" converted from the 0-0, 1-1, and 2-2 bands of the BeT isotopomer were fit to band constants for the ground electronic state before the data set was combined with those of the BeH and BeD isotopomers for the global fitting. Because the three BeT bands are not connected with respect to the vibrational levels, a single isotopomer Dunham-constant fit cannot be performed.

4.5.3.3 Criteria for optimizing molecular constants

In a diatomic molecule, both the vibrational and rotational energy levels of an electronic state have regular patterns. Therefore, a set of physically meaningful molecular constants used to describe the rovibrational levels should follow the "rule of patterns". The corresponding values for the band constants G_v, B_v, D_v, and H_v etc., of the vibrational levels of the ground electronic state, should have a similar pattern of plus or minus signs. The vibrational term values G_v and rotational constants B_v represent, respectively, the vibrational term values of the energy levels, and the equivalent bond lengths of the vibrational levels. The pattern of the values of G_v, from G_0 to G_1, to $G_2 \cdots$, G_n, etc., the absolute values should increase gradually, but the differences between G_{n+1} and G_n should decrease monotonically. The absolute values for the rotational constants B_v and the centrifugal distortion constants, D_v, for the ground electronic state should also change smoothly. Higher order constants, e.g., H or L, may not follow the pattern but the lower level ones definitely should follow a regular pattern to be physically meaningful.

This "rule of patterns" also applies to Dunham constants because they have their equivalent counterparts in the band constants. The physical meanings of the Dunham constants are not as straightforward as those of the band constants. Sometimes it is necessary to map them to their corresponding band constants. For example, for $m = 0$, Y_{lm} represent the vibrational term values; for a given value of l, Y_{lm} represent the

rotational levels of the vibrational level, etc.

The optimizing criteria are generally: 1) the uncertainty of a parameter should not be larger than the parameter itself, otherwise the highest order constant should be removed; if the uncertainty of the highest order constant is larger than the highest order constant itself, remove the highest order constant; 2) generally, a higher order constant should be smaller than the lower order ones, e.g., $D_v > H_v > L_v$. 3) the vibrational term values G_v for an electronic state should change monotonically with the increase of the vibrational quantum number v. 4) the rotational constants B_v, which are related to the bond length of the molecule, should change monotonically with the vibrational energy levels in an electronic state. 5) according to definition, the rotational constants B_v have positive values, and the centrifugal constants D_v have a negative sign.

Whether a set of molecular parameters is optimal or not depends on the ability of the set of parameters to reproduce the experimental data. The qualitative criterion is whether the set of parameters is physically meaningful, and the quantitative criterion is the dimensionless standard error (DSE) as described in Section 1.3.2.2. The DSE is based on the reduced *chi*-squared test formula, which is an effective statistical tool in comparing two sets of data, and in this case, the predicated values made using the set of molecular parameters, and the experimental data. A DSE value of $\overline{\sigma}_f \sim 1$ indicates that the molecular parameters reproduce the experimental data very well. For two set of molecular parameters, if one gives $\overline{\sigma} = 1.001$, and the other one gives $\overline{\sigma} = 1.003$, the two set of parameters should be considered statistically equivalent, and both sets of parameters can be considered as the best sets, as long as the parameters are also physically meaningful, such as following the "rule of patterns". Although the set of molecular parameters are not unique in the sense of statistics, all the best sets of molecular parameters for the same vibrational or electronic state of the same molecule should be physically or statistically equivalent. Because the molecular parameters, especially the lower order ones, have clear physical meanings. For example, the vibrational terms values represent the vibrational frequencies; the rotational constants represent the bond lengths, etc.

4.5.3.4 Uncertainty and higher order vs. lower order constants

For a lower order constant, e.g., G_v, B_v, or D_v, the uncertainty needs to be much smaller than the constant itself; for the highest order molecular constant, the uncertainty needs to be smaller than the constant itself, and at the same time needs to be close in absolute value to the constant itself, but not too small. If the uncertainty of the highest order parameter is too small (e.g., one or two orders of magnitude

smaller) compared with the parameter, then another higher order parameter may be necessary in the fitting.

Generally, a higher order molecular constant should be smaller than a lower order molecular constant, e.g., in the band constants, G_v, B_v, D_v, H_v, etc., H_v should be smaller than D_v.

Bibliography

[1] C. Henriet and G. Verhaegen. Accurate calculation of the excited states of the molecule BeH. *Physica Scripta*, 33:299–309, 1985.

[2] F. B. C. Machado, O. Roberto-Neto, and F. R. Ornellas. On the assigment of transitions involving some $^2\Pi$ Rydberg states of the BeH molecule. *Chemical Physics Letters*, 284:293–299, 1998.

[3] F. B. C. Machado, O. Roberto-Neto, and F. R. Ornellas. Radiative transition probabilities and lifetimes for the band systems $A^2\Pi$–$X^2\Sigma^+$ and $C^2\Sigma^+$–$X^2\Sigma^+$ of the BeH molecule. *Chemical Physics Letters*, 305:156–162, 1999.

[4] J. Guan, M. E. Casida, and D. R. Salahub. Time-dependent density-functional theory investigation of excitation spectra of open-shell molecules. *Journal of Molecular Structure*, 527:229–244, 2000.

[5] H. Meisner and J. Paldus. Direct iterative solution of the generalized Bloch equation. II. A general formalism for many-electron systems. III Application of H_2 cluster models. IV. Application to H_2, LiH, BeH, and CH_2. *Journal of Chemical Physics*, 113:2594–2611, 2612–2621, 2622–2637, 2000.

[6] P. G. Szalay and J. Gauss. Spin-restricted open-shell coupled-cluster theory for excited states. *Journal of Chemical Physics*, 112:4027–4036, 2000.

[7] I. D. Petsalakis, D. Papadopoulos, G. Theodorakopoulos, and R. J. Buenker. Theoretical calculations on the linewidths of rovibrational levels of the 3d Rydberg states of BeH and BeD. *Journal of Physics B: Atomic, Molecular and Optical Physics*, 32:3225–3237, 2000.

[8] M. C. Bacchus-Montabonel. A theoretical treatment of the LiH and BeH formation through radiative association. *Journal of Molecular Structure: THEOCHEM*, 463:91–97, 1999.

[9] P. L. Fast, M. L. Sanchez, J. C. Corchado, and D. G. Truhlar. The Gaussian-2 method with proper dissociation, improved accuracy, and less cost. *Journal of Chemical Physics*, 110:11679–11681, 1999.

[10] S. Hirata and M. Head-Gordon. Time-dependent density functional theory for radicals: An improved description of excited states with substantial double excitation character. *Chemical Physics Letters*, 302:375–382, 1999.

[11] T. Nakajima and H. Nakatsuji. Second-order perturbative approximation to the SAC/SAC-CI method. *Chemical Physics Letters*, 300:1–8, 1999.

[12] T. Nakajima and H. Nakatsuji. The energy gradient method for the ground, excited, ionized, and electron attached states calculated by SAC (symmetry-adapted cluster) /SAC-CI (configuration interaction) method. *Chemical Physics*, 242:177–193, 1999.

[13] R. Colin, C. Dreze, and M. Steinhauer. Rotational analysis and deperturbation of the $C^2\Sigma^+$–$X^2\Sigma^+$ band systems of BeH and BeD. *Canadian Journal of Physics*, 61(4):641–655, 1983.

[14] C. Focsa, S. Firth, P. F. Bernath, and R. Colin. Fourier transform emission spectroscopy of the $A^2\Pi$–$X^2\Sigma^+$ system of BeH. *Journal of Chemical Physics*, 109(14):5795–5802, Oct. 1998.

[15] C. Focsa, P. F. Bernath, R. Mitzner, and R. Colin. Fourier transform emission spectroscopy of the $A^2\Pi$–$X^2\Sigma^+$ system of BeD. *Journal of Molecular Spectroscopy*, 192:348–358, 1998.

[16] R. Horne and R. Colin. The $A^2\Pi$–$X^2\Sigma^+$ band system of BeH and BeD in absorption. *Bull. Soc. Chim. Belges*, 81:93–107, 1972.

[17] D. De Greef and R. Colin. The electronic isotope shift in the $A^2\Pi$–$X^2\Sigma^+$ bands of BeH, BeD and BeT. *Journal of Molecular Spectroscopy*, 53:455–465, 1974.

[18] R. Colin and D. De Greef. The absorption spectrum of the BeH and BeD molecules in the vacuum ultraviolet. *Canadian Journal of Physics*, 53(19):2142–2169, 1975.

[19] W. W. Watson. Beryllium hydride band spectra. *Physical Review*, 32:600–606, 1928.

[20] W. W. Watson and A. E. Parker. Evidence of a Be isotope of mass 8 and fine structure measurements in the BeH bands. *Physical Review*, 32:167–175, 1931.

[21] E. Olsson. *Zeitschrift fur Physik*, 73:732, 1932.

[22] P. G. Koontz. Beryllium deuteride spectra. *Physical Review*, 48:707–713, 1935.

[23] W. W. Watson and R. F. Humphreys. Ultraviolet spectra of BeH and BeH^+. *Physical Review*, 52:318–322, 1937.

[24] J. M. Hollas. *High Resolution Spectroscopy*. John Wiley & Sons, New York, 2nd edition, 1998.

[25] P. F. Bernath. *Spectra of Atoms and Molecules*. Oxford University Press, New York, 1995.

[26] R. J. Le Roy. DSParFit and DSPotFit: General purpose parameter and potential fitting programs for diatomic data analysis. In *International Symposium on Molecular Spectroscopy 56th Meeting*, Columbus, Ohio 43210 USA, Jun. 2001. The Ohio State University.

[27] R. J. Le Roy. Computer programs distributed by Robert J. Le Roy. Technical report, University of Waterloo, 2001. `http://leroy.uwaterloo.ca`.

[28] R. J. Le Roy. *DSParFit 2.0: A Computer Program for Fitting Multi-Isotopomer Diatomic Molecule Spectra*. Dept. of Chemistry, University of Waterloo, Waterloo, Ontario N2L 3G1, Canada, Apr. 2001.

[29] R. J. Le Roy. Improved parameterisation for combined isotopomer analysis of diatomic spectra and its application to HF and DF. *Journal of Molecular Spectroscopy*, 194:189–196, 1999.

[30] R. J. Le Roy. Uncertainty, sensitivity, convergence, and rounding in performing and reporting least-squares fits. *Journal of Molecular Spectroscopy*, 191:223–231, 1998.

Chapter 5

Accurate Molecular Constants for the Ground Electronic State of MgH

An accurate set of molecular constants for the $X^2\Sigma^+$ ground electronic state of the MgH and MgD isotopomers are derived from spectroscopic data available from new laboratory experiments of a colleague[1] and data from the literature.

The result of combined-isotopomer Dunham-type analysis provides not only a compact set of molecular constants for the isotopomers, but also Born-Oppenheimer Approximation breakdown correction terms.

In this Chapter, Section 5.1 introduces the background and method of analysis for the MgH molecule. Section 5.2 summarizes the sources of spectroscopic data used in the global analysis, including data sources from various experiments. Section 5.3 describes the details of steps taken in the spectroscopic data analysis, and Section 5.4 presents the theoretical basis for the combined-isotopomer Dunham-type global analysis. As the last part, Section 5.5 closes this Chapter by presenting the conclusions drawn about the MgH molecule and the method of analysis. The resulting energy origins from the global fitting of the "fluorescence series" as organized from the electronic transitions of the MgH isotopomers are listed in Appendix D.

[1]Dr. Ram S. Ram, Dept. of Chemistry, University of Arizona, Tucson AZ 85721, USA.

5.1 Background

Because of their importance in astrophysics and their interest in chemical physics, MgH and MgD have been studied for over more than a century. The $A^2\Pi - X^2\Sigma^+$ green system was observed in solar disk and sunspot spectra long ago. A comprehensive summary of results of earlier research up to the 1970s can be found in Huber and Herzberg [1]. After the 1970s, the studies of MgH and MgD regained new momentum both experimentally and theoretically. More advanced experiments and theoretical calculations have contributed much to the understanding of the properties of MgH and MgD, and their isotopomers due to magnesium.

A unique approach discussed earlier in this thesis has been employed for the data reduction, i.e., treating the perturbed data of electronic transitions as if they were from fluorescence series. Therefore, all data available for the transitions can be used in the global analysis, whereas about 30-40% of the total amount of data would have been rejected had the conventional data fitting method been used, because of perturbations in the excited electronic states. The conventional method performs fitting of the rotationally-resolved electronic transitions to ro-vibrational energy expressions of the upper and lower electronic states as represented by either band constants or Dunham constants.

A more accurate set of molecular parameters for the ground electronic state of the MgH isotopomers can be obtained through the application of a better method of data processing in the comprehensive analysis. In addition, the combined-isotopomer global fitting of the MgH data allows investigation of Born-Oppenheimer breakdown effect in the MgH molecule, another typical molecule containing the light hydrogen atom, similar to BeH in the last Chapter.

In this Chapter, all high resolution spectroscopic data of electronic transitions of MgH and MgD have been re-arranged and treated as "fluorescence series" into the ro-vibrational levels of the ground electronic state. The resulting data set consists of a total of 4700 transitions for a total of six isotopomers of MgH and MgD.

5.2 Spectroscopic Data Sources of MgH and MgD

Numerous spectroscopic data are available for MgH and MgD and their isotopomers. The data have been collected by using different methods in many laboratories, including electronic spectroscopy (spectrograph and an electric arc source) [2, 3, 4, 5, 6, 7, 8, 9], Fourier transform spectroscopy [10, 11], infrared diode laser spectroscopy [12], far infrared [13, 14], and millimeter wave spectroscopy [15], and so forth. Data have also been collected from extraterrestrial sources, i.e., the sunspot umbral spectra [11]. In parallel with the experimental studies, some theoretical calculations have been done [16, 17, 18, 19, 20, 21, 22].

The minor isotopes of magnesium, ^{25}Mg and ^{26}Mg, each has a natural abundance about one-eighth that of ^{24}Mg, i.e., ^{24}Mg :^{25}Mg :^{26}Mg = 78.7% : 10.1% : 11.2%. The intensities of spectral lines from the minor isotopomers are hence weaker than those of the ^{24}Mg-containing isotopomers, and as a result, the minor isotopomers are expected to have smaller data sets.

The $B'\ ^2\Sigma^+$ electronic state has a larger equilibrium bond length than that does the $X^2\Sigma^+$ state, as shown in Fig. 5.1 [4]. Therefore, diagonal Franck-Condon factors are small, and transitions between ro-vibrational levels in the $B'\ ^2\Sigma^+$ and $X^2\Sigma^+$ electronic states happen only for small v' to larger v'' or vice versa. Because certain ro-vibrational energy levels of the $B\ '^2\Sigma^+$ state cross the ro-vibrational energy levels of the $A^2\Pi$ state, as is also shown in Fig. 5.1, numerous rotational perturbations occur between the two electronic states.

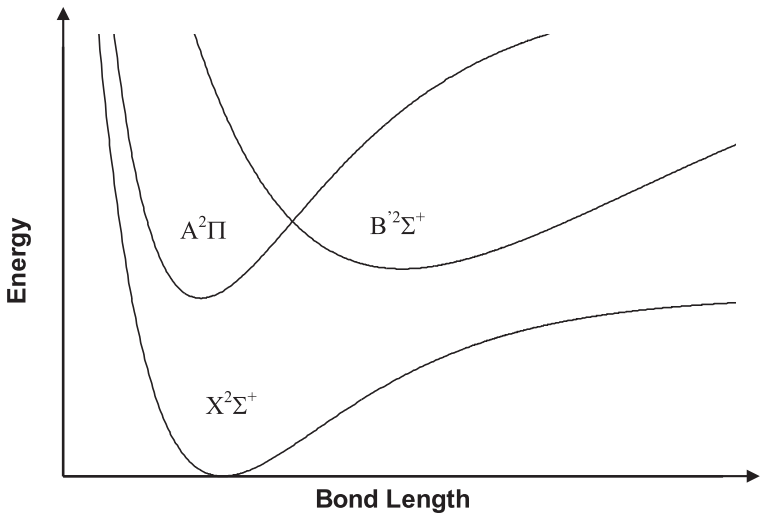

Figure 5.1: Qualitative Potential Curves for the Electronic States of MgH

The spectroscopic data of the MgH isotopomers available from various sources

are summarized in Table 5.1. The data of the $C^2\Pi - X^2\Sigma^+$ transitions in Table 5.1, i.e., the $C^2\Pi - X^2\Sigma^+$ 0-0 and 1-1 bands [3] of ^{24}MgH, and the $C^2\Pi - X^2\Sigma^+$ 0-0, 1-0 and 1-1 bands [3] of ^{24}MgD are not included in the global analysis of this Chapter, because there are only a few data from these transitions, and they are all low resolution electronic data. The spectroscopic data of the isotopomers used in the global analysis are shown in Table 5.2 at Page 130.

5.2.1 Electronic Spectroscopy

Modern investigation of the electronic transitions of the MgH molecule started in the 1970s. Between 1970 and 1980, Balfour and co-workers [2, 3, 4, 5, 6, 7, 8, 9] used an electric arc to generate the MgH and MgD species and a spectrograph to record the electronic spectra, including the $A^2\Pi - X^2\Sigma^+$ system of ^{24}MgH, ^{25}MgH, ^{26}MgH [2], the $A^2\Pi - X^2\Sigma^+$ system of MgD [5], the $B'\ ^2\Sigma^+ - X^2\Sigma^+$ transition of MgH [4, 6], the $B'\ ^2\Sigma^+ - X^2\Sigma^+$ system of MgD [6], and the $C^2\Pi - X^2\Sigma^+$ transitions of MgH and MgD[3].

5.2.2 Fourier Transform Spectroscopy

Fourier transform spectroscopy offers a higher resolution and accuracy for spectral measurements of gas phase molecules. The Fourier transform electronic spectra of MgH were generated using a hollow cathode lamp with a magnesium rod and hydrogen gas[10]. Both the $A^2\Pi - X^2\Sigma^+$ system and the $B'\ ^2\Sigma^+ - X^2\Sigma^+$ system of MgH were reported: the $A^2\Pi - X^2\Sigma^+$ system [10] was reported in 1985, while the $B'\ ^2\Sigma^+ - X^2\Sigma^+$ system was reported only recently[23].

5.2.3 Infrared Diode Laser Spectroscopy

In 1988, Lemoine *et al.* [12] reported the v = 1-0, and 2-1 transition bands of the $X^2\Sigma^+$ ground electronic state of ^{24}MgH and ^{24}MgD, detected using infrared diode laser spectroscopy. Other spectroscopic data of ^{25}MgH, ^{26}MgH, ^{25}MgD, and ^{26}MgD were also available [24]. In the experiments, the tunable infrared diode laser radiation was first passed through a mode selection monochromator and was then divided to provide (i) a beam making a single pass of the absorption and reference gas cells, and (ii) a beam for synchronous relative calibration before the detection with a HgCdTe detector. The absolute accuracy of the line positions from the infrared diode laser spectroscopy [12, 24] is typically better than $\pm$ 0.002 cm^{-1}.

5.2.4 Far Infrared and Millimetre Wave Spectroscopy

The far infrared and millimeter wave spectroscopic data are of the highest resolution in the data set of the MgH molecule used in the global analysis in this Chapter, and some of the spin component doublets, due to spin splittings of the ground electronic state, were detected in these experiments. The corresponding doublet data pairs are averaged to produce the values for the global fitting because the ground state spin splittings were not resolved in most of the lines in the full data set. When only one line is available in the pair, it is dropped. The doublet spectroscopic data due to spin splittings are processed as singlets in the analysis here, i.e., the data used in the global fittings are $P(J) = [P_1(N) + P_2(N)]/2$, and $R(J) = [R_1(N) + R_2(N)]/2$.

The defined nine digit speed of light c = 299,792,458 m/s[25] is used to convert the spectroscopic data from the far infrared and millimetre wave spectroscopy in MHz units to cm^{-1} in order to obtain unit consistency.

5.2.5 Data Set of the Major and Minor Isotopomers

The ^{24}MgH isotopomer is the major isotopomer of the MgH molecule. The vibrational bands of the ^{24}MgH data set are summarized in Fig. 5.2 at Page 131.

The ^{24}MgH data set includes new high resolution Fourier transform spectra of the 0-3, 0-4, 1-3, 1-4 and 1-5 bands of the $B'\ ^2\Sigma^+ - X^2\Sigma^+$ transition[23], together with spectral lines from high resolution Fourier transform spectra from a sunspot coupling the $B'\ ^2\Sigma^+$ state levels $v' = 0, 1$ to the $X^2\Sigma^+$ state levels v''= 3-8, and older lower resolution $B'\ ^2\Sigma^+ - X^2\Sigma^+$ electronic bands involving the v'' = 0-9 levels of the $X^2\Sigma^+$ state, v' = 0-10 levels of the $B'\ ^2\Sigma^+$ state, infrared data of 2-1 and 1-0 rovibrational transitions of the ground electronic state, and some millimeter wave data. The above data set yields a high accuracy description of the ground electronic state for the v''= 0-2 and v'' = 3-9 levels. The v'' = 2-3 transition gap in the high resolution data was bridged using data from the high resolution Fourier transform data of the 1-2 and 1-3 bands of the $A^2\Pi - X^2\Sigma^+$ system.

The data sets of minor isotopomers have a smaller number of transitions than does that of the major isotopomer ^{24}MgH, as shown in Tables 5.1 and 5.2.

5.3 Treatment of Data of Electronic Transitions

As defined in Section 1.3, the conventional data processing approach would fit spectroscopic data to either

a) the band constants G_v, B_v, D_v, H_v, etc., for each vibrational level of the upper and lower electronic states, or

b) the Dunham expansion $\{Y_{lm}\}$ constants for each electronic state.

However, extensive perturbations in the excited electronic states of the MgH molecule make the fitting poor because (most of) the perturbed data cannot be used in the fit. In the case of the MgH and MgD isotopomers, the $B'\ ^2\Sigma^+$ state and the $A^2\Pi$ state perturb each other to such an extent that even after 30-40% of the data from high resolution electronic spectroscopy have been rejected, the fit is still poor. The molecular constants derived using the conventional approach cannot be accurate, because only a small portion of the available data are used in the fitting. In order to arrive at an accurate set of molecular parameters, a different method needs to be adopted for the data processing.

As with the treatment of the BeH isotopomers described in the last Chapter, the approach adopted in this Chapter is to rearrange the data to treat rovibronic transitions from each distinct level (v', J', p') of the upper electronic state(s) as "fluorescence series" into the ro-vibrational levels of the ground electronic state. This completely decouples the determination of the ro-vibrational energy levels of the $X^2\Sigma^+$ ground electronic state from the perturbed ro-vibrational energies of the $A^2\Pi$ and $B'\ ^2\Sigma^+$ excited electronic states. This approach is very similar to forming ground state combination differences using all data for electronic transitions. For rotational combination differences, the resulting data for the ground electronic state are like pseudo pure rotational data, but with the rotational quantum number change $\Delta J = \pm 2$ instead of the usual $\Delta J = \pm 1$ for pure rotational transitions. In addition, the term values ("fluorescence origins") calculated for the ro-vibrational levels of the upper electronic state can be used for a perturbation analysis.

Before the combined-isotopomer global fitting was performed, the individual isotopomers were fit separately. After the band constants were fit for each isotopomer and the quantum number assignments were checked, separate Dunham-constant fits were performed for the two major isotopomers ^{24}MgH and ^{24}MgD, i.e., both types of fits were performed on ^{24}MgH and ^{24}MgD because their data sets are large and the energy levels are all connected. For the minor isotopomers (i.e., ^{25}MgH, ^{26}MgH, ^{25}MgD and ^{26}MgD), only band-constant fits are possible for the vibrational levels, and the band-constant fittings were used to check the quantum number assignments.

After separately fitting each isotopomer, the combined isotopomer fitting was performed. The Dunham constants for the isotopomer with the largest v'' (^{24}MgH, $v''_{max} = 9$) representing the lower electronic state were kept more or less fixed, and only Born-Oppenheimer breakdown correction terms were added and adjusted in the global fit to get the best fit (determined constants, meaningful pattern, and reasonable $\overline{\sigma}_f$). According to Eqn.(1.7), $E(v, J) = \sum_{l,m} \mu^{-(l+2m)/2} U_{lm}(v + 1/2)^l [J(J + 1)]^m$, the vibrational term values with a first-order approximation, i.e., for $l = 1$, and $m = 0$, are $E(v) = \mu^{-1/2} U_{lm}(v + 1/2)$.

For the isotopomers ^{24}MgH and ^{24}MgD, which have the largest data sets, to have equivalent maximium vibrational energies, the ratio of the maximium vibrational quantum numbers should be inversely proportional to the square root of the ratio of their reduced masses. We have $v_{2max} = (v_{1max} + 1/2)(\mu_2/\mu_1)^{1/2} - 1/2 \doteq (9 + 1/2)(2)^{1/2} - 1/2 \doteq 13$. Therefore, the ^{24}MgD ($v''_{max} = 13$) isotopomer has an equivalent v''_{max} to that of ^{24}MgH as far as the ratio of their reduced masses is concerned. The ^{24}MgH isotopomer is used as the reference isotopomer in the combined isotopomer global fitting because it has a larger data set. The spectral data of ^{24}MgH transitions used in the global fits are indicated in Fig. 5.2.

5.4 Combined Isotopomer Dunham-Type Analysis

In the conventional way of describing molecules, each isotopomer needs a separate set of molecular constants. The combined-isotopomer fitting uses one set of parameters to describe all the isotopomers, which greatly reduces the number of parameters required.

As described in Section 1.3.2.2, the observed transition energies were weighted by the inverse squares of their uncertainties, and the quality of fit is indicated by the value of dimensionless standard error

$$\overline{\sigma}_f \;=\; \left\{ \frac{1}{N-M} \sum_{i=1}^{N} \left[\frac{y_{calc}(i) - y_{obs}(i)}{u(i)} \right]^2 \right\}^{1/2}, \tag{5.1}$$

in which each of the N experimental data $y_{obs}(i)$ has an uncertainty of $u(i)$, and $y_{calc}(i)$ is the value of datum–i predicted by the M–parameter model being fitted. All parameter uncertainties quoted here are 95% confidence limit uncertainties.

In order to simplify the representation of these data sets and to search for physically interesting information about Born-Oppenheimer breakdown effects, all of the lines for the transitions of the old electronic spectra (generated using electric arc and recorded using a spectrograph) [2, 3, 4, 5, 6, 7, 8, 9], Fourier transform spectra[2] [10, 11], new sunspot spectra,[3] infrared diode laser [12], far infrared [13, 14], and millimeter wave spectra [15] for the six isotopomers of ^{24}MgH, ^{24}MgD, ^{25}MgH, ^{25}MgD, ^{26}MgH, ^{26}MgD were simultaneously fit to a combined-isotopomer Dunham-type expression for the energy levels. Following Section 1.3.1.3, the observed transitions for isotopomer–α of the MgH species formed from atoms of mass M^{α}_{Mg} (i.e., masses of ^{24}Mg, ^{25}Mg, or ^{26}Mg) and M^{α}_{H} (i.e., masses of H or D) were expressed as differences between energy levels written as

$$\begin{aligned} E^{\alpha}(v,J) \;=\;& \sum_{(l,m)\neq(0,0)} Y^{1}_{l,m} \left(\frac{\mu_1}{\mu_\alpha} \right)^{m+l/2} (v+1/2)^l \left[J(J+1) \right]^m \\ +\;& \sum_{(l,m)\geq(0,0)} \left\{ \frac{\Delta M^{\alpha}_{Mg}}{M^{\alpha}_{Mg}} \, \delta^{Mg}_{l,m} + \frac{\Delta M^{\alpha}_{H}}{M^{\alpha}_{H}} \, \delta^{H}_{l,m} \right\} \\ \times\;& \left(\frac{\mu_1}{\mu_\alpha} \right)^{m+l/2} (v+1/2)^l \left[J(J+1) \right]^m, \end{aligned} \tag{5.2}$$

[2] McMath-Pierce One-Meter Fourier transform spectrometer of the National Solar Observatory, at Kitt Peak, Arizona, USA. http://nsokp.nso.edu/mp/fts/

[3] Detected using the same Fourier transform spectrometer at Kitt Peak.

with

$$\Delta M^{\alpha}_{Mg,H} = M^{\alpha}_{Mg,H} - M^{1}_{^{24}Mg,H}$$

and

$$\Delta M^{\alpha}_{Mg,D} = M^{\alpha}_{Mg,D} - M^{1}_{^{24}Mg,H}$$

The condition $\alpha = 1$ for $M^{\alpha}_{Mg,H}$ identifies a selected reference species, in this case, the most abundant isotopomer, ^{24}MgH. The conventional Dunham constants for other ($\alpha \neq 1$) isotopomers are then generated as

$$Y^{\alpha}_{l,m} = \left\{ Y^{1}_{l,m} + \frac{\Delta M^{\alpha}_{Mg}}{M^{\alpha}_{Mg}} \delta^{Mg}_{l,m} + \frac{\Delta M^{\alpha}_{H}}{M^{\alpha}_{H}} \delta^{H}_{l,m} \right\} \left(\frac{\mu_1}{\mu_\alpha} \right)^{m+l/2} . \tag{5.3}$$

The data set used in the global fitting includes FTS, infrared, millimeter wave and old electronic data, as shown in Table 5.3. A total of 4,700 data were fit to Eqn. (5.2) using program "DSParFit" [26, 27, 28] with a final $\overline{\sigma}_f = 1.205$. The program simplifies the resulting parameters by applying the sequential rounding and refitting procedure [29]. This yields the molecular constants given in the first column of Table 5.4. The numbers in parentheses are the 95% confidence limit uncertainties in the last significant digits shown.

A search for significant Born-Oppenheimer breakdown effects showed that their inclusion could reduce the dimensionless standard error $\overline{\sigma}_f$ drastically. The δ_{lm} for the hydrogen atom is also included in Table 5.4. No statistically significant Born-Oppenheimer breakdown constants δ_{lm} for the magnesium atom could be determined.

For the user's convenience, those constants for the minority isotopomers, rounded at the first digit of the parameter sensitivity[29], are shown in the last two columns of Tables 5.4 and 5.5. The results in the last row of this table show that the rounded constants generated from the ^{24}MgH parameters determined from the combined-isotopomer analysis reproduce the input data for the individual minority isotopomers with no significant loss of precision.

The root mean square residual ($RMSR$) values of the isotopomers are calculated using Eqn.(5.4).

$$RMSR = \left\{ \frac{1}{\sum n_i} \sum n_i (RMSR)_i \right\}^{1/2} \tag{5.4}$$

where n_i is the number of data in "fluorescence series" organized from electronic transitions or ro-vibrational transitions detected using infrared or millimeter wave

spectroscopy, and the index of the data group i; $(RMSR)_i$ is the root mean square residual of each of the data in the "fluorescence series" or transitions (infrared, millimeter wave) i. The summation is performed with respect to the total number of "fluorescence series" and the infrared and millimeter wave transitions.

5.5 Discussions and Conclusions

5.5.1 "Fluorescence Series" Method and Combined-Isotopomer Fitting

A fit of the data set for all six isotopomers of the MgH molecule to the empirical Dunham-type expansions, which include hydrogenic Born-Oppenheimer breakdown correction terms, requires 38 Dunham expansion parameters and 6 Born-Oppenheimer breakdown correction terms, plus the 713 "fluorescence series" origins. The combined-isotopomer fitting greatly reduces the number of parameters required to describe the MgH molecule. The parameter fit computer program used for the analyses is DSParFit[26, 27, 28].

The "fluorescence series" method of treatment of perturbed electronic spectroscopic data is very effective in decoupling the treatment of the ground electronic state from the perturbations in the excited electronic states. All the data of the electronic transitions with perturbations can be used in the global fitting. Therefore, the parameters obtained for the ground electronic state are more accurate than those derived using conventional methods. The perturbation analysis of the excited electronic states can then be carried out using the "fluorescence origins" calculated from the global fitting.

For molecules that contain a light atom like the hydrogen isotopes in the MgH molecule, the Born-Oppenheimer breakdown correction terms for the light atom are so important that they cannot be ignored, and only by including the δ_{lm} in the global analysis can a successful fit be obtained. The Born-Oppenheimer breakdown correction terms for the heavier magnesium atom cannot be determined.

5.5.2 Comparison of the Results of BeH, MgH, and GeO: Born-Oppenheimer Approximation Breakdown Correction Terms

As shown in Table 5.6, it is obvious that the Born-Oppenheimer breakdown correction terms due to the hydrogen isotopes in the MgH molecule and the BeH molecule are comparable in magnitude. The corresponding terms have the same pattern of signs, so the net effect of changes of the potential functions and high order semiclassical corrections with respect to the vibrational and rotational quantum numbers have similar trends. However, the absolute values of corresponding correction terms for the hydrogen isotopes in the BeH molecule are always larger than those in the MgH

molecule. This may be resulted from the increased importance of high order semiclassical corrections with decreased reduced masses.

Both beryllium and magnesium belong to Group IIa in the periodic table, and both BeH and MgH have $X^2\Sigma^+$ ground electronic states. The bonding in the BeH and MgH molecules should be similar, so the potential curves should also be similar.

The starting point in the theory of the Born-Oppenheimer separation is the "clamped nuclei" approximation, based on the fact that the masses of the nuclei and electrons in a diatomic molecule are very different. The size of Born-Oppenheimer breakdown correction terms depend on the masses of the atoms. The correction terms due to the magnesium isotopes cannot be determined because the magnesium isotopes are relatively heavy, so the Born-Oppenheimer approximation is more accurate for such an atom. The lighter beryllium atom has only one stable isotope, so the correction terms associated with beryllium cannot be derived.

In addition, it should be pointed out that there are two contributing factors in the Born-Oppenheimer approximation breakdown correction terms derived through the combined-isotopomer Dunham model as given in Eqn. (1.10). One is the real Born-Oppenheimer breakdown correction part, and the other is the breakdown of the semiclassical JWKB quantization condition used to derive the Dunham formula. Both parts are related to the masses of the component atoms of the diatomic molecule. The DSParFit software cannot determine the two parts separately. However, from the results of the global combined-isotopomer Dunham-type analysis, it can be concluded that the effect due to the overall importance of these terms increases as the masses of the component atoms decrease: light atoms such as the hydrogen isotopes have larger correction terms, while heavy atoms such as the magnesium isotopes and the germanium isotopes have terms which are at best determinable.

Table 5.1: Available Spectroscopic Data for MgH and MgD

Technique	Transition Bands	Accuracy (cm^{-1})
Electronic Spectroscopy	^{24}**MgH** $A^2\Pi - X^2\Sigma^+$, 0-0[2, 3, 7], 0-1 [2, 7] 0-2, 1-0, 1-1, 1-2, 1-3, 2-1, 2-2, 2-3, 2-4, 3-2, 3-5 [7] $B'\ ^2\Sigma^+ - X^2\Sigma^+$, 37 bands ($v'$=0-10, v''=4-6)[6] 13 new bands (v''=5-9) [8] $C^2\Pi - X^2\Sigma^+$, 0-0, 1-1 [3] ^{24}**MgD** $A^2\Pi - X^2\Sigma^+$, 0-0[3], 15 bands [5] $B'\ ^2\Sigma^+ - X^2\Sigma^+$, 16 bands ($v'$=0-2,4-6)[6] 18 new bands (v''=7-13) [8] $C^2\Pi - X^2\Sigma^+$, 0-0, 1-0, 1-1 [3] ^{25}**MgH** $A^2\Pi - X^2\Sigma^+$, 0-0, 0-1 [2] ^{26}**MgH** $A^2\Pi - X^2\Sigma^+$, 0-0, 0-1 [2]	0.05
Fourier Transform Spectroscopy	^{24}**MgH** $A^2\Pi - X^2\Sigma^+$, 0-0, 0-1 [10] $B'\ ^2\Sigma^+ - X^2\Sigma^+$, 0-3, 0-4, 1-3, 1-4, 1-5 [23]	0.001 0.002
Sunspot Umbra	^{24}**MgH** $B'\ ^2\Sigma^+ - X^2\Sigma^+$, 0-3, 0-4, 0-5, 0-6, 0-7, 1-3, 1-4, 1-7, 1-8 [11]	0.002
IR Diode Laser	^{24}**MgH**, ^{24}**MgD** $X^2\Sigma^+$, v=1-0, 2-1 [12] ^{25}**MgH** v=1-0, 2-1[24] ^{25}**MgD** v=2-1 [24] ^{26}**MgH** ^{26}**MgD** v=1-0 [24]	$\pm$0.002
Far Infrared	^{24}**MgH** $X^2\Sigma^+$ ΔF=$\Delta J = 0$, ΔF=$\Delta J = 1$ N = 3-2, 2-1, 1-0 [13, 14]	1 MHz
Millimeter Wave	^{24}**MgH**, ^{24}**MgD**, ^{26}**MgH** $X^2\Sigma^+$ v=0,1 [15]	$\pm$50 kHz

Table 5.2: MgH and MgD Data Used in Global Fitting

Technique	Transition Bands	Accuracy (cm^{-1})
Electronic Spectroscopy	^{24}**MgH** $A^2\Pi - X^2\Sigma^+$, 0-0[2, 3, 7], 0-1 [2, 7] 0-2, 1-0, 1-1, 1-2, 1-3, 2-1, 2-2, 2-3, 2-4, 3-2, 3-5 [7] $B'\ ^2\Sigma^+ - X^2\Sigma^+$, 37 bands ($v'$=0-10, v''=4-6)[6] 13 new bands (v''=5-9) [8] ^{24}**MgD** $A^2\Pi - X^2\Sigma^+$, 0-0[3], 15 bands [5] $B'\ ^2\Sigma^+ - X^2\Sigma^+$, 16 bands ($v'$=0-2,4-6)[6] 18 new bands (v''=7-13) [8] ^{25}**MgH** $A^2\Pi - X^2\Sigma^+$, 0-0, 0-1 [2] ^{26}**MgH** $A^2\Pi - X^2\Sigma^+$, 0-0, 0-1 [2]	0.05
Fourier Transform Spectroscopy	^{24}**MgH** $A^2\Pi - X^2\Sigma^+$, 0-0, 0-1 [10] $B'\ ^2\Sigma^+ - X^2\Sigma^+$, 0-3, 0-4, 1-3, 1-4, 1-5 [23]	0.001 0.002
Sunspot Umbra	^{24}**MgH** $B'\ ^2\Sigma^+ - X^2\Sigma^+$, 0-3, 0-4, 0-5, 0-6, 0-7, 1-3, 1-4, 1-7, 1-8 [11]	0.002
IR Diode Laser	^{24}**MgH**, ^{24}**MgD** $X^2\Sigma^+$, v=1-0, 2-1 [12] ^{25}**MgH** v=1-0, 2-1[24] ^{25}**MgD** v=2-1 [24] ^{26}**MgH**, ^{26}**MgD** v=1-0 [24]	$\pm$0.002
Far Infrared	^{24}**MgH** $X^2\Sigma^+$ ΔF=ΔJ = 0, ΔF=ΔJ = 1 N = 3-2, 2-1, 1-0 [13, 14]	1 MHz
Millimeter Wave	^{24}**MgH**, ^{24}**MgD**, ^{26}**MgH** $X^2\Sigma^+$ v=0,1 [15]	$\pm$50 kHz

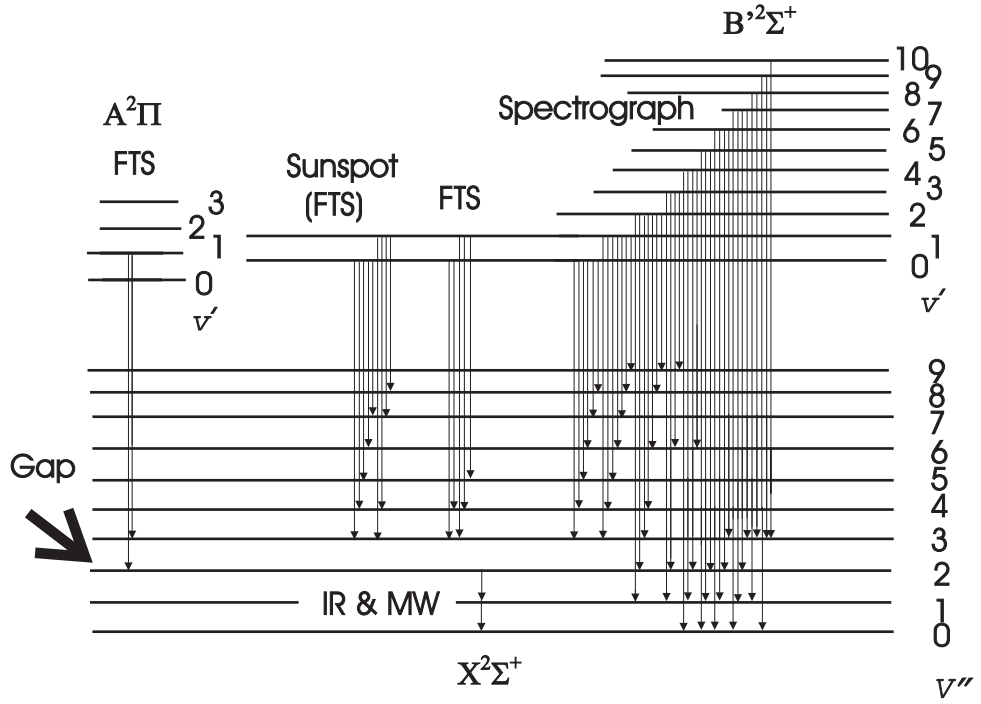

Figure 5.2: Data of ^{24}MgH Transitions Used in the Global Fitting

Table 5.3: The Global Fitting Data Set

Isot.	No. of Series	No. of Fluo.Trans.	No. of MW Trans.	No. of IR Trans.
^{24}MgH	265	1963	7	67
^{25}MgH	58	274	0	7
^{26}MgH	58	354	5	1
^{24}MgD	207	1388	7	42
^{25}MgD	63	289	0	2
^{26}MgD	62	289	0	5
Total	713	4557	19	124

Table 5.4: Dunham Constants for ^{24}MgH, ^{25}MgH and ^{26}MgH
(from a total of 4,700 Data, $\overline{\sigma}_f = 1.205$, 95% confidence limit uncertainties) for $X\,^2\Sigma^+$ state ^{24}MgH and those calculated for ^{25}MgH and ^{26}MgH

		All-Isotopomer Fit	Generated from ^{24}MgH Const. and Eqn.(5.3)	
	Constant	^{24}MgH	^{25}MgH	^{26}MgH
	$Y_{1,0}$	1492.7427(410)	1491.5366904	1490.4270313
	$Y_{2,0}$	−29.78286(5000)	−29.7347554	−29.69052829
	$Y_{3,0}$	−0.3682(280)	−0.3673083	−0.36648911
10^3	$Y_{4,0}$	18.(8)	17.941901	17.888567
10^3	$Y_{5,0}$	−14.4653(13000)	−14.4069607	−14.3534486
10^3	$Y_{6,0}$	1.514(110)	1.50667571	1.49996267
10^6	$Y_{7,0}$	−98.26(340)	−97.705645	−97.197948
	$Y_{0,1}$	5.826488(160)	5.817077186	5.80842494
	$Y_{1,1}$	−0.179807(600)	−0.179371546	−0.178971502
10^3	$Y_{2,1}$	−0.7(8)	−0.6977406	−0.6956665
10^3	$Y_{3,1}$	1.66(49)	1.65330513	1.64716422
10^3	$Y_{4,1}$	−1.72633(18000)	−1.717978514	−1.710324013
10^6	$Y_{5,1}$	558.4(370)	555.249665	552.364485
10^6	$Y_{6,1}$	−90.22166(450000)	−89.6401746	−89.1080447
10^6	$Y_{7,1}$	7.1075(2900)	7.05598638	7.00888173
10^9	$Y_{8,1}$	−225.(8)	−223.188785	−221.533875
10^6	$Y_{0,2}$	−363.5(6)	−362.32671	−361.24968
10^6	$Y_{1,2}$	31.33(190)	31.203644	31.087744
10^6	$Y_{2,2}$	−33.(2)	−32.8403555	−32.6940344
10^6	$Y_{3,2}$	12.4208(10000)	12.35072535	12.28654871
10^6	$Y_{4,2}$	−1.46(31)	−1.45059019	−1.44197907
10^9	$Y_{5,2}$	−160.(50)	−158.840355	−157.779962
10^9	$Y_{6,2}$	44.4006(46000)	44.0431821	43.7166087
10^9	$Y_{7,2}$	−2.475(160)	−2.45309314	−2.43309234
10^9	$Y_{0,3}$	21.6(23)	21.49551	21.39973
10^9	$Y_{1,3}$	−32.9(24)	−32.714387	−32.544398
10^9	$Y_{2,3}$	39.58(210)	39.3249039	39.09146
10^9	$Y_{3,3}$	−17.60912(65000)	−17.4814929	−17.3647892
10^9	$Y_{4,3}$	2.988(87)	2.96394707	2.94196986
10^{12}	$Y_{5,3}$	−173.2(43)	−171.666963	−170.26731
10^{12}	$Y_{0,4}$	12.(6)	11.92266	11.85188
10^{12}	$Y_{1,4}$	−9.4(22)	−9.331871	−9.269573
10^{12}	$Y_{2,4}$	−3.(1)	−2.9758505	−2.953785
10^{15}	$Y_{3,4}$	2685.6(3200)	2661.8291	2640.1264
10^{15}	$Y_{4,4}$	−321.(21)	−317.9017	−315.07517
10^{15}	$Y_{0,5}$	−13.1(45)	−12.994547	−12.898194
10^{15}	$Y_{1,5}$	10.349(2400)	10.257398	10.173767
10^{15}	$Y_{2,5}$	−2.29(31)	−2.2678969	−2.2477325
	$\delta_{H;1,0}$	0.98(1)		
10^3	$\delta_{H;2,0}$	−59.(6)		
10^3	$\delta_{H;3,0}$	7.14(54)		
10^3	$\delta_{H;0,1}$	7.40(6)		
10^3	$\delta_{H;1,1}$	−0.61(7)		
10^3	$\delta_{H;2,1}$	0.097(7)		
No. of Data		2037	281	360
No. of Parameters		38 + 6	0	0
No. of Term Values		270	59	59
RMSR		1.338	0.764	1.123

Table 5.5: Dunham Constants for ^{24}MgD, ^{25}MgD and ^{26}MgD
(Calculated from those of $X\,^2\Sigma^+$ State ^{24}MgH and the Born-Oppenheimer Breakdown Correction Terms)

		Generated from ^{24}MgH Constants and Eqn.(5.3)		
	Constant	^{24}MgD	^{25}MgD	^{26}MgD
	$Y_{1,0}$	1077.334903	1075.66215	1074.121933
	$Y_{2,0}$	−15.5182492	−15.470097	−15.4258261
	$Y_{3,0}$	−0.13693854	−0.13630167	−0.13571701
10^3	$Y_{4,0}$	4.8771476	4.8469275	4.8192262
10^3	$Y_{5,0}$	−2.82777065	−2.80588566	−2.78585467
10^3	$Y_{6,0}$	0.213533472	0.211551887	0.209740882
10^6	$Y_{7,0}$	−9.998623	−9.8904555	−9.7917468
	$Y_{0,1}$	3.03479278	3.025376	3.01671826
	$Y_{1,1}$	−0.067641328	−0.067326742	−0.067037945
10^3	$Y_{2,1}$	−0.1765357	−0.1754419	−0.1744392
10^3	$Y_{3,1}$	0.32450757	0.3219961	0.3196974
10^3	$Y_{4,1}$	−0.243480342	−0.241220852	−0.239155863
10^6	$Y_{5,1}$	56.8209961	56.206293	55.6453434
10^6	$Y_{6,1}$	−6.62365334	−6.54182394	−6.46726167
10^6	$Y_{7,1}$	0.376467073	0.371238844	0.366482035
10^9	$Y_{8,1}$	−8.5983673	−8.4657915	−8.3453497
10^6	$Y_{0,2}$	−98.491285	−97.881008	−97.321597
10^6	$Y_{1,2}$	6.1245916	6.0771915	6.0338069
10^6	$Y_{2,2}$	−4.65429628	−4.61110454	−4.57163085
10^6	$Y_{3,2}$	1.26390084	1.250227659	1.237750145
10^6	$Y_{4,2}$	−0.107186388	−0.105862195	−0.104655601
10^9	$Y_{5,2}$	−8.4748128	−8.3571178	−8.2500353
10^9	$Y_{6,2}$	1.69676742	1.67060542	1.64683794
10^9	$Y_{7,2}$	−0.068238902	−0.067082425	−0.066033365
10^9	$Y_{0,3}$	3.046448	3.018178	2.99234
10^9	$Y_{1,3}$	−3.3477987	−3.3115814	−3.2785312
10^9	$Y_{2,3}$	2.90577893	2.8698806	2.83717033
10^9	$Y_{3,3}$	−0.932712467	−0.919759318	−0.90797413
10^9	$Y_{4,3}$	0.1141863181	0.1124257106	0.1108262447
10^{12}	$Y_{5,3}$	−4.7753445	−4.6944146	−4.6210016
10^{12}	$Y_{0,4}$	0.880984	0.8701002	0.860183
10^{12}	$Y_{1,4}$	−0.4978952	−0.4909807	−0.4846896
10^{12}	$Y_{2,4}$	−0.1146449	−0.11287722	−0.11127133
10^{15}	$Y_{3,4}$	74.045412	72.79053	71.652204
10^{15}	$Y_{4,4}$	−6.3853573	−6.2673953	−6.1605496
10^{15}	$Y_{0,5}$	−0.5006161	−0.4928972	−0.4858848
10^{15}	$Y_{1,5}$	0.28533511	0.2804994	0.27611285
10^{15}	$Y_{2,5}$	−0.04555286	−0.04471133	−0.04394909
No. of Data		1437	291	294
No. of Parameters		0	0	0
No. of Term Values		202	63	60
RMSR		1.120	1.000	1.252

Table 5.6: Comparison of Born-Oppenheimer Breakdown Correction Terms for MgH and BeH

Born-Oppenheimer Breakdown Correction Terms		MgH	BeH
	$\delta_{H;1,0}$	0.98(1)	1.3575(1300)
	$\delta_{H;2,0}$	−0.059(6)	−0.102(37)
10^3	$\delta_{H;3,0}$	7.14(54)	9.6(24)
10^3	$\delta_{H;0,1}$	7.40(6)	21.091(680)
10^3	$\delta_{H;1,1}$	−0.61(7)	−1.008(280)
10^3	$\delta_{H;2,1}$	0.097(7)	0.128(31)
10^6	$\delta_{H;0,2}$	0.0	−6.44(100)
10^6	$\delta_{H;1,2}$	0.0	0.27(22)
10^9	$\delta_{H;0,3}$	0.0	1.24(47)

Bibliography

[1] K.P. Huber and G. Herzberg. *Constants of Diatomic Molecules, Molecular Spectra and Molecular Structure IV*. Van Nostrand Reinhold Company, Toronto, 1979.

[2] W. J. Balfour. The $A^2\Pi - X^2\Sigma^+$ Systems of ^{24}MgH, ^{25}MgH and ^{26}MgH. *The Astrophysical Journal*, 162:1031–1035, 1970.

[3] W. J. Balfour. The electronic spectrum of magnesium hydride and magnesium deuteride. *Journal of Physics B: Atomic and Molecular Physics*, 3:1749–1756, 1970.

[4] W. J. Balfour and H. M. Cartwright. Low-lying electronic states of magnesium hydride. *Chemical Physics Letters*, 32(1):82–85, 1975.

[5] W. J. Balfour and H. M. Cartwright. The ground state and $A^2\Pi$ excited state of magnesium deuteride. *Canadian Journal of Physics*, 53:1477–1482, 1975.

[6] W. J. Balfour and H. M. Cartwright. The $B'\ ^2\Sigma^+ - X^2\Sigma^+$ systems of MgH and MgD. *Canadian Journal of Physics*, 54:1898–1904, 1976.

[7] W. J. Balfour and H. M. Cartwright. The $A^2\Pi - X^2\Sigma^+$ system and dissociation energy of magnesium hydride. *Astronomy and Astrophysics, Supplement Series*, 26:389–397, 1976.

[8] W. J. Balfour and B. Lindgren. High-resolution emission spectra of MgH and MgD in the 600-850 nm wavelength region. *Canadian Journal of Physics*, 56:767–779, 1978.

[9] W. J. Balfour. MgH and MgD in the 230-235 nm region. *Journal of Molecular Spectroscopy*, 79:507–511, 1980.

[10] P. F. Bernath, J. H. Black, and J. W. Brault. The spectrum of magnesium hydride. *The Astrophysical Journal*, 298:375–381, 1985.

[11] L. Wallace, K. Hinkle, G. Li, and P. F. Bernath. The MgH $B'\ ^2\Sigma^+ - X^2\Sigma^+$transition: A new tool for studying magnesium isotopes abundances. *The Astrophysical Journal*, 524:454–461, 1999.

[12] B. Lemoine, C. Demuynck, J. L. Destombes, and P. B. Davies. Infrared diode laser spectra of MgH and MgD ($X^2\Sigma^+$). *Journal of Chemical Physics*, 89(2):673–677, 1988.

[13] K. R. Leopold, L. R. Zink, D. A. Evenson, K. M. Jennings, and M. Mizushima. The far infrared spectrum of magnesium hydride. *Journal of Chemical Physics*, 84(3):1935–1937, 1986.

[14] L. R. Zink, D. A. Jennings, K. M. Evenson, and K. R. Leopold. Laboratory measurements for the astrophysical identification of MgH. *The Astrophysical Journal*, 359:L65–L66, 1990.

[15] L. M. Ziurys, W. L. Barclay, Jr., and M. A. Anderson. The millimeter-wave spectrum of the MgH and MgH radicals. *The Astrophysical Journal*, 402:L21–L24, 1993.

[16] A. C. H. Chan and Ernest R. Davidson. Theoretical study of the MgH molecule. *Journal of Chemical Physics*, 52(8):4108–4121, 1970.

[17] M.L. Sink, A. D. Bandrauk, W. H. Henneker, H. Lefebvre-Brion, and G. Raseev. Theoretical study of the low-lying electronic states of MgH. *Chemical Physics Letters*, 39(3):505–510, 1976.

[18] R. P. Saxon, K. Kirby, and B. Liu. Ab initio configuration interaction study of the low-lying electronic states of MgH. *Journal of Chemical Physics*, 69(12):5301–5309, 1978.

[19] M. L. Sink and A. D. Bandrauk. A theoretical study of the $B'\ ^2\Sigma^+ - X^2\Sigma^+$ band system in MgH and MgD. *Canadian Journal of Physics*, 57:1178–1184, 1979.

[20] B. M. Tripathi and V. P. Gaur. Partition functions and dissociation constants for MgH. *Journal of Quantitative Spectroscopy and Radiactive Transfer*, 22:407–409, 1979.

[21] D. L. Cooper. Spin splitting in the $X^2\Sigma^+$ state of MgH. *Journal of Chemical Physics*, 76(7):3692–3693, 1982.

[22] F. Jenc and B.A. Brandt. The ground state reduced potential curves (RPC) of the metal hydrides CuH and MgH. *Spectrochimica Acta*, 41A(10):1211–1214, 1985.

[23] G. Li, J. Y. Seto, P. F. Bernath, and R. J. Le Roy. Accurate molecular constants, potential curve and Born-Oppenheimer breakdown correction functions for $X^2\Sigma^+$ MgH and MgD. In *International Symposium on Molecular Spectroscopy 56th Meeting*, Columbus, Ohio 43210 USA, June 2001. The Ohio State University.

[24] B. Lemoine, C. Demuynck, J. L. Destombes, and P. B. Davies. Infrared laser spectra of ^{25}MgH, ^{26}MgH, ^{25}MgD and ^{26}MgD. *Private Communication*, 2000.

[25] P. F. Bernath. *Spectra of Atoms and Molecules*. Oxford University Press, New York, 1995.

[26] R. J. Le Roy. Improved parameterisation for combined isotopomer analysis of diatomic spectra and its application to HF and DF. *Journal of Molecular Spectroscopy*, 194:189–196, 1999.

[27] R. J. Le Roy. DSParFit and DSPotFit: General purpose parameter and potential fitting programs for diatomic data analysis. In *International Symposium on Molecular Spectroscopy 56th Meeting*, Columbus, Ohio 43210 USA, June 2001. The Ohio State University.

[28] R. J. Le Roy. Computer programs distributed by Robert J. Le Roy. Technical report, University of Waterloo, 2001. `http://leroy.uwaterloo.ca`.

[29] R. J. Le Roy. Uncertainty, sensitivity, convergence, and rounding in performing and reporting least-squares fits. *Journal of Molecular Spectroscopy*, 191:223–231, 1998.

APPENDIX

Appendix A

Fourier Transform Infrared Data for GeO

The Fourier transform infrared spectroscopic data of the five isotopomers of the ground state GeO are listed in Appendix A

The 1-0 to 7-6 bands of the ^{70}GeO data are listed in Table A.1.
The 1-0 to 8-7 bands of the ^{72}GeO data are listed in Table A.2.
The 1-0 to 6-5 bands of the ^{73}GeO data are listed in Table A.3.
The 1-0 to 8-7 bands of the ^{74}GeO data are listed in Table A.4.
The 1-0 to 7-6 bands of the ^{76}GeO data are listed in Table A.5.

A.1 Fourier Transform Infrared Data for ^{70}GeO

Table A.1: Fourier Transform Infrared Data for ^{70}GeO (cm^{-1})

J'	J''	Obs	Unc	Calc-Obs	(Calc-Obs)/Unc
1,048 ^{70}GeO infrared transitions in 7 bands					
The 1-0 Band, 200 data, $J"_{min} = 0$, $J"_{max} = 100$ $Unc._{Avge} = 2.0D-03$, $Unc._{Max} = 5.0D-03$ $(Err/Unc.)_{Avge} = 8.3D-03$, RMSR = 0.55					
98	99	857.15874	0.20D-02	-0.00232	-1.1577
97	98	858.69448	0.20D-02	-0.00165	-0.82422
96	97	860.22441	0.20D-02	-0.00034	-0.17002
95	96	861.75199	0.20D-02	-0.00188	-0.94021
94	95	863.27013	0.20D-02	0.00082	0.41001
93	94	864.78535	0.20D-02	0.00124	0.6204
92	93	866.297	0.20D-02	0.0	0.00091
91	92	867.79935	0.20D-02	0.00283	1.41629
90	91	869.29976	0.20D-02	0.00236	1.18137
89	90	870.79839	0.20D-02	-0.00157	-0.78405
88	89	872.28304	0.20D-02	0.00321	1.60485
87	88	873.76897	0.20D-02	0.00144	0.71786
86	87	875.25175	0.20D-02	-0.00246	-1.23017
85	86	876.72457	0.20D-02	-0.0017	-0.84955
84	85	878.19104	0.20D-02	0.00011	0.0546
83	84	879.65364	0.20D-02	0.00047	0.23697
82	83	881.11145	0.20D-02	0.00031	0.15741
81	82	882.56529	0.20D-02	-0.00122	-0.60933
80	81	884.01122	0.20D-02	-0.00019	-0.09352
79	80	885.45262	0.20D-02	0.00002	0.00963
78	79	886.8891	0.20D-02	-0.00021	-0.10515
77	78	888.31982	0.20D-02	-0.00007	-0.03311
76	77	889.74491	0.20D-02	0.00032	0.16055
75	76	891.16938	0.20D-02	-0.00406	-2.02955
74	75	892.57939	0.20D-02	0.0006	0.30144
73	74	893.98864	0.20D-02	0.00061	0.30313
72	73	895.39279	0.20D-02	0.00028	0.14034
71	72	896.79252	0.20D-02	-0.00105	-0.52727
70	71	898.18447	0.20D-02	-0.00007	-0.03498
69	70	899.57182	0.20D-02	0.00005	0.0269
68	69	900.95403	0.20D-02	-0.00015	-0.07693
67	68	902.33051	0.20D-02	-0.0001	-0.05179
66	67	903.70224	0.20D-02	-0.00081	-0.40293
65	66	905.06654	0.20D-02	0.00042	0.20922
64	65	906.42698	0.20D-02	-0.00001	-0.00556
63	64	907.78205	0.20D-02	-0.00059	-0.29267
62	63	909.13019	0.20D-02	0.00023	0.11252
61	62	910.4743	0.20D-02	-0.00048	-0.24025
60	61	911.81307	0.20D-02	-0.0014	-0.70138
59	60	913.14368	0.20D-02	0.00028	0.13878
58	59	914.47126	0.20D-02	-0.0006	-0.30008
57	58	915.7918	0.20D-02	-0.00003	-0.01344
56	57	917.107	0.20D-02	0.00029	0.14338
55	56	918.41707	0.20D-02	0.00013	0.06504
54	55	919.72134	0.20D-02	0.00014	0.07107
53	54	921.0202	0.20D-02	-0.00007	-0.03384
52	53	922.31334	0.20D-02	-0.0002	-0.10013
51	52	923.60069	0.20D-02	-0.00019	-0.09321

Table A.1, Fourier Transform Infrared Data for ^{70}GeO (cm^{-1}) (*Cont'd*)

J'	J''	Obs	Unc	Calc-Obs	(Calc-Obs)/Unc
50	51	924.87978	0.20D-02	0.00241	1.20651
49	50	926.15801	0.20D-02	0.0002	0.0986
48	49	927.42851	0.20D-02	0.00003	0.01265
47	48	928.6937	0.20D-02	-0.00052	-0.26172
46	47	929.95206	0.20D-02	0.00004	0.01994
45	46	931.20457	0.20D-02	0.00073	0.3673
44	45	932.45303	0.20D-02	-0.00025	-0.1252
43	44	933.69481	0.20D-02	-0.00029	-0.14292
42	43	934.93044	0.20D-02	0.00007	0.03364
41	42	936.15855	0.20D-02	0.00218	1.089
40	41	937.3853	0.20D-02	-0.00012	-0.06231
39	40	938.60397	0.20D-02	-0.00013	-0.06573
38	39	939.81687	0.20D-02	-0.00015	-0.07683
37	38	941.02433	0.20D-02	-0.00055	-0.27608
36	37	942.22518	0.20D-02	-0.00016	-0.07892
35	36	943.42132	0.20D-02	-0.00088	-0.44096
34	35	944.61028	0.20D-02	-0.00026	-0.12761
33	34	945.79431	0.20D-02	-0.00056	-0.27945
32	33	946.96908	0.20D-02	0.00254	1.268
31	32	948.1426	0.20D-02	0.00101	0.5042
30	31	949.30937	0.20D-02	0.00035	0.1736
29	30	950.47045	0.20D-02	-0.00051	-0.25429
28	29	951.6243	0.20D-02	-0.00005	-0.02512
27	28	952.77301	0.20D-02	-0.00037	-0.18436
26	27	953.91562	0.20D-02	-0.00052	-0.25769
25	26	955.05198	0.20D-02	-0.00035	-0.17556
24	25	956.18281	0.20D-02	-0.0006	-0.29863
23	24	957.30723	0.20D-02	-0.0004	-0.20247
22	23	958.42564	0.20D-02	-0.00018	-0.08768
21	22	959.53838	0.20D-02	-0.00026	-0.12988
20	21	960.64522	0.20D-02	-0.00043	-0.21461
19	20	961.74581	0.20D-02	-0.00037	-0.1826
18	19	962.83995	0.20D-02	0.00013	0.06562
17	18	963.92937	0.20D-02	-0.00068	-0.34066
16	17	965.01244	0.20D-02	-0.00118	-0.592
15	16	966.088	0.20D-02	-0.00022	-0.10909
14	15	967.15821	0.20D-02	0.00002	0.01242
13	14	968.22306	0.20D-02	-0.00045	-0.22314
12	13	969.28082	0.20D-02	0.00009	0.04358
11	12	970.33329	0.20D-02	-0.00019	-0.09306
10	11	971.37885	0.20D-02	0.00035	0.17616
9	10	972.41912	0.20D-02	0.00005	0.02565
8	9	973.45351	0.20D-02	-0.0005	-0.25038
7	8	974.48073	0.20D-02	-0.00003	-0.01254
6	7	975.50227	0.20D-02	-0.00002	-0.01159
5	6	976.51587	0.20D-02	0.00176	0.88175
4	5	977.52699	0.20D-02	-0.00016	-0.07824
3	4	978.53001	0.20D-02	-0.00016	-0.0823
2	3	979.52345	0.20D-02	0.00321	1.60387
1	2	980.51561	0.20D-02	0.00165	0.82444
0	1	981.50389	0.20D-02	-0.00225	-1.12626
1	0	983.44944	0.20D-02	0.00225	1.12529
2	1	984.41159	0.50D-02	0.00574	1.14841
3	2	985.37484	0.20D-02	0.00186	0.93236
4	3	986.33072	0.20D-02	-0.00092	-0.46147
5	4	987.27687	0.20D-02	-0.00026	-0.13136
6	5	988.21917	0.20D-02	-0.00207	-1.03307
7	6	989.1487	0.20D-02	0.00259	1.29262

Table A.1, Fourier Transform Infrared Data for ^{70}GeO (cm^{-1}) (*Cont'd*)

J'	J''	Obs	Unc	Calc-Obs	(Calc-Obs)/Unc
8	7	990.0791	0.20D-02	0.00004	0.01981
9	8	991.00405	0.20D-02	-0.00339	-1.69726
10	9	991.91639	0.20D-02	-0.00057	-0.28446
11	10	992.82652	0.20D-02	-0.00189	-0.94264
12	11	993.72781	0.20D-02	-0.00075	-0.37267
13	12	994.62479	0.20D-02	-0.00168	-0.8404
14	13	995.51275	0.20D-02	0.00001	0.00334
15	14	996.39643	0.20D-02	-0.00043	-0.21743
16	15	997.27292	0.20D-02	-0.00011	-0.0535
17	16	998.14352	0.20D-02	-0.00031	-0.15581
18	17	999.00575	0.20D-02	0.0014	0.69974
19	18	999.86507	0.20D-02	-0.00044	-0.21777
20	19	1000.71589	0.20D-02	-0.00024	-0.11911
21	20	1001.56036	0.20D-02	-0.00017	-0.0857
22	21	1002.39858	0.20D-02	-0.00035	-0.17264
23	22	1003.22855	0.20D-02	0.00124	0.61813
24	23	1004.05444	0.20D-02	0.00037	0.18617
25	24	1004.87303	0.20D-02	0.00028	0.14101
26	25	1005.68718	0.20D-02	-0.00191	-0.95432
27	26	1006.49023	0.20D-02	0.00045	0.2252
28	27	1007.28926	0.20D-02	0.00027	0.13259
29	28	1008.08201	0.20D-02	-0.00021	-0.10715
30	29	1008.86785	0.20D-02	-0.00036	-0.18101
31	30	1009.64683	0.20D-02	-0.00026	-0.12901
32	31	1010.41984	0.20D-02	-0.0008	-0.39767
33	32	1011.18461	0.20D-02	0.00028	0.14149
34	33	1011.94382	0.20D-02	0.00029	0.14343
35	34	1012.69674	0.20D-02	-0.00007	-0.0339
36	35	1013.44177	0.20D-02	0.00081	0.40446
37	36	1014.18221	0.20D-02	-0.00039	-0.19356
38	37	1014.91472	0.20D-02	-0.00035	-0.17302
39	38	1015.64011	0.20D-02	0.00012	0.05949
40	39	1016.35939	0.20D-02	-0.00002	-0.00761
41	40	1017.07156	0.20D-02	0.00024	0.12058
42	41	1017.77742	0.20D-02	0.00007	0.03746
43	42	1018.47701	0.20D-02	-0.00057	-0.28359
44	43	1019.16922	0.20D-02	-0.00058	-0.28768
45	44	1019.85359	0.20D-02	0.00048	0.23856
46	45	1020.53115	0.20D-02	0.00156	0.77898
47	46	1021.2045	0.20D-02	0.00005	0.02694
48	47	1021.86949	0.20D-02	0.0001	0.05228
49	48	1022.52793	0.20D-02	-0.00011	-0.05666
50	49	1023.17905	0.20D-02	0.00016	0.07895
51	50	1023.82343	0.20D-02	0.00032	0.16241
52	51	1024.46159	0.20D-02	-0.00014	-0.07146
53	52	1025.09228	0.20D-02	0.0	0.00065
54	53	1025.71634	0.20D-02	-0.00011	-0.0575
55	54	1026.33201	0.20D-02	0.00127	0.6329
56	55	1026.94304	0.20D-02	0.00038	0.19061
57	56	1027.54684	0.20D-02	-0.00019	-0.0956
58	57	1028.14437	0.20D-02	-0.00142	-0.71248
59	58	1028.73183	0.20D-02	0.00047	0.23471
60	59	1029.31439	0.20D-02	0.00031	0.15422
61	60	1029.88998	0.20D-02	0.00016	0.07976
62	61	1030.45513	0.20D-02	0.00346	1.73006
63	62	1031.02031	0.20D-02	-0.00026	-0.13118
64	63	1031.57417	0.20D-02	0.00033	0.16475
65	64	1032.12174	0.20D-02	0.00019	0.09654

Table A.1, Fourier Transform Infrared Data for ^{70}GeO (cm^{-1}) (*Cont'd*)

J'	J''	Obs	Unc	Calc-Obs	(Calc-Obs)/Unc
66	65	1032.66104	0.20D-02	0.0013	0.64786
67	66	1033.19539	0.20D-02	0.0003	0.15239
68	67	1033.72211	0.20D-02	-0.00011	-0.05621
69	68	1034.24176	0.20D-02	-0.00053	-0.26429
70	69	1034.75332	0.20D-02	0.00006	0.0318
71	70	1035.25722	0.20D-02	0.00123	0.6157
72	71	1035.75642	0.20D-02	-0.00002	-0.00898
73	72	1036.24766	0.20D-02	-0.00043	-0.21362
74	73	1036.72857	0.20D-02	0.00236	1.18039
75	74	1037.20811	0.20D-02	-0.00063	-0.31336
76	75	1037.67635	0.20D-02	0.00053	0.26423
77	76	1038.139	0.20D-02	0.0001	0.05073
78	77	1038.59523	0.20D-02	-0.00109	-0.5448
79	78	1039.04306	0.20D-02	-0.00108	-0.53879
80	79	1039.48285	0.20D-02	-0.00024	-0.11769
81	80	1039.91472	0.20D-02	0.0013	0.65202
82	81	1040.34245	0.20D-02	-0.00025	-0.1256
83	82	1040.76013	0.20D-02	0.00099	0.49694
84	83	1041.17374	0.20D-02	-0.00094	-0.47133
85	84	1041.57688	0.20D-02	0.00031	0.15308
86	85	1041.97487	0.20D-02	-0.00058	-0.29084
87	86	1042.36515	0.20D-02	-0.00106	-0.5306
88	87	1042.74528	0.20D-02	0.0013	0.64776
89	88	1043.12271	0.20D-02	-0.00097	-0.48729
90	89	1043.48965	0.20D-02	-0.00009	-0.0468
91	90	1043.84952	0.20D-02	0.0005	0.25166
92	91	1044.20305	0.20D-02	0.00007	0.03703
93	92	1044.54797	0.20D-02	0.00088	0.43824
94	93	1044.88859	0.20D-02	-0.00141	-0.70731
95	94	1045.21835	0.20D-02	-0.00025	-0.12572
96	95	1045.54067	0.20D-02	0.00093	0.4669
97	96	1045.85817	0.20D-02	-0.00048	-0.24206
98	97	1046.16377	0.20D-02	0.00253	1.26677
99	98	1046.47029	0.20D-02	-0.00281	-1.40425
100	99	1046.76139	0.20D-02	-0.00021	-0.10577
101	100	1047.04421	0.20D-02	0.00318	1.58954
The 2-1 Band, 195 data, $J"_{min} = 0$, $J"_{max} = 98$ Unc.$_{Avge}$ = 2.0D-03, Unc.$_{Max}$ = 3.0D-03 (Err/Unc.)$_{Avge}$ = 1.7D-01, RMSR = 0.55					
96	97	851.86528	0.20D-02	0.00111	0.55425
95	96	853.38411	0.20D-02	0.00152	0.76191
94	95	854.90023	0.20D-02	-0.00053	-0.26675
93	94	856.4091	0.20D-02	-0.00055	-0.27698
92	93	857.91355	0.20D-02	-0.00137	-0.68394
91	92	859.41074	0.20D-02	-0.00014	-0.06783
90	91	860.90386	0.20D-02	-0.00008	-0.03883
89	90	862.39333	0.20D-02	-0.00161	-0.80715
88	89	863.87341	0.20D-02	0.00098	0.49201
87	88	865.35272	0.20D-02	-0.0009	-0.45149
86	87	866.82627	0.20D-02	-0.00232	-1.15799
85	86	868.29106	0.20D-02	-0.00026	-0.12758
84	85	869.7524	0.20D-02	-0.00003	-0.0156
83	84	871.20956	0.20D-02	-0.00094	-0.47218
82	83	872.66071	0.20D-02	-0.00117	-0.58259
81	82	874.10624	0.20D-02	-0.00109	-0.54708
80	81	875.54621	0.20D-02	-0.00079	-0.3959
79	80	876.98177	0.20D-02	-0.00144	-0.71928

Table A.1, Fourier Transform Infrared Data for ^{70}GeO (cm^{-1}) (*Cont'd*)

J'	J''	Obs	Unc	Calc-Obs	(Calc-Obs)/Unc
78	79	878.40927	0.20D-02	0.00062	0.30756
77	78	879.83402	0.20D-02	0.00005	0.02425
76	77	881.25386	0.20D-02	-0.00098	-0.4894
75	76	882.66588	0.20D-02	0.00041	0.20636
74	75	884.07528	0.20D-02	-0.00098	-0.48878
73	74	885.47699	0.20D-02	-0.00008	-0.04015
72	73	886.8754	0.20D-02	-0.00132	-0.65796
71	72	888.26587	0.20D-02	-0.00005	-0.02254
70	71	889.65237	0.20D-02	-0.00025	-0.12419
69	70	891.03273	0.20D-02	0.00024	0.12183
68	69	892.40888	0.20D-02	-0.00053	-0.2649
67	68	893.77852	0.20D-02	-0.00027	-0.13463
66	67	895.14397	0.20D-02	-0.00131	-0.65264
65	66	896.50143	0.20D-02	0.00016	0.08063
64	65	897.85537	0.20D-02	-0.00037	-0.18504
63	64	899.20266	0.20D-02	0.00023	0.11495
62	63	900.5432	0.20D-02	0.00205	1.02526
61	62	901.8828	0.20D-02	-0.00072	-0.35948
60	61	903.21392	0.20D-02	-0.00057	-0.28461
59	60	904.53913	0.20D-02	-0.00007	-0.0355
58	59	905.85934	0.20D-02	-0.00014	-0.07247
57	58	907.17402	0.20D-02	-0.00026	-0.13101
56	57	908.48302	0.20D-02	-0.0003	-0.15143
55	56	909.78608	0.20D-02	-0.00001	-0.00409
54	55	911.08414	0.20D-02	-0.00033	-0.16442
53	54	912.37582	0.20D-02	0.00011	0.05717
52	53	913.66186	0.20D-02	0.00055	0.27528
51	52	914.9462	0.20D-02	-0.00296	-1.48052
50	51	916.21838	0.20D-02	0.00003	0.01437
49	50	917.48794	0.20D-02	-0.00003	-0.01549
48	49	918.74916	0.20D-02	0.00258	1.28953
47	48	920.00998	0.20D-02	-0.00011	-0.05612
46	47	921.26214	0.20D-02	0.00015	0.07722
45	46	922.50934	0.20D-02	-0.00033	-0.166
44	45	923.75006	0.20D-02	-0.00005	-0.02614
43	44	924.98553	0.20D-02	-0.00027	-0.13372
42	43	926.21744	0.20D-02	-0.00267	-1.3342
41	42	927.43906	0.20D-02	-0.00054	-0.26806
40	41	928.65773	0.20D-02	-0.00121	-0.60578
39	40	929.86929	0.20D-02	-0.00057	-0.28281
38	39	931.07607	0.20D-02	-0.00093	-0.46474
37	38	932.27577	0.20D-02	-0.00001	-0.00698
36	37	933.47084	0.20D-02	-0.00028	-0.14012
35	36	934.65993	0.20D-02	-0.00038	-0.1896
34	35	935.84291	0.20D-02	-0.00021	-0.10598
33	34	937.02047	0.20D-02	-0.00047	-0.2348
32	33	938.19149	0.20D-02	-0.00004	-0.02158
31	32	939.35749	0.20D-02	-0.00045	-0.22687
30	31	940.51841	0.20D-02	-0.00167	-0.83617
29	30	941.67098	0.20D-02	-0.00043	-0.21515
28	29	942.81851	0.20D-02	-0.00005	-0.02425
27	28	943.96053	0.20D-02	-0.00007	-0.03415
26	27	945.09755	0.20D-02	-0.001	-0.50033
25	26	946.22731	0.20D-02	-0.00062	-0.30842
24	25	947.35144	0.20D-02	-0.00055	-0.27402
23	24	948.46971	0.20D-02	-0.00058	-0.28771
22	23	949.58211	0.20D-02	-0.0007	-0.3501
21	22	950.68808	0.20D-02	-0.00036	-0.18177

Table A.1, Fourier Transform Infrared Data for ^{70}GeO (cm^{-1}) (*Cont'd*)

J'	J''	Obs	Unc	Calc-Obs	(Calc-Obs)/Unc
20	21	951.7878	0.20D-02	0.00022	0.11159
19	20	952.88263	0.20D-02	-0.0003	-0.15057
18	19	953.97059	0.20D-02	0.00003	0.01604
17	18	955.05198	0.20D-02	0.00091	0.45586
16	17	956.12857	0.20D-02	0.00057	0.28321
15	16	957.19953	0.20D-02	-0.00021	-0.10258
14	15	958.26445	0.20D-02	-0.00099	-0.49716
13	14	959.32106	0.20D-02	0.00046	0.2288
12	13	960.3737	0.20D-02	-0.0002	-0.10033
11	12	961.41979	0.20D-02	-0.00039	-0.19532
10	11	962.45968	0.20D-02	-0.00049	-0.24677
9	10	963.49234	0.20D-02	0.00052	0.25952
8	9	964.52073	0.20D-02	-0.00032	-0.16205
7	8	965.54437	0.20D-02	-0.00255	-1.27724
6	7	966.5564	0.20D-02	0.00069	0.34323
5	6	967.56656	0.20D-02	-0.00037	-0.18637
4	5	968.57054	0.20D-02	-0.00142	-0.71177
3	4	969.56523	0.20D-02	0.00063	0.31633
2	3	970.55649	0.20D-02	-0.00008	-0.0379
1	2	971.54044	0.20D-02	0.00033	0.16487
1	0	974.45474	0.20D-02	0.00171	0.85716
2	1	975.41633	0.20D-02	-0.00047	-0.23493
3	2	976.36996	0.20D-02	-0.00096	-0.47901
4	3	977.31668	0.20D-02	-0.0008	-0.40083
5	4	978.25852	0.20D-02	-0.00206	-1.03121
6	5	979.19132	0.20D-02	-0.00058	-0.2909
7	6	980.11906	0.20D-02	-0.00035	-0.1758
8	7	981.04105	0.20D-02	-0.00069	-0.34677
9	8	981.95615	0.20D-02	-0.00047	-0.23456
10	9	982.86642	0.20D-02	-0.00177	-0.88507
11	10	983.76802	0.20D-02	-0.00076	-0.37915
12	11	984.66425	0.20D-02	-0.00075	-0.37262
13	12	985.55426	0.20D-02	-0.00089	-0.44644
14	13	986.4373	0.20D-02	-0.00046	-0.23141
15	14	987.31372	0.20D-02	0.00019	0.0965
16	15	988.18408	0.20D-02	0.00048	0.24149
17	16	989.04967	0.20D-02	-0.00088	-0.4424
18	17	989.90799	0.20D-02	-0.00142	-0.71107
19	18	990.75678	0.20D-02	0.00112	0.55955
20	19	991.60312	0.20D-02	-0.00035	-0.17646
21	20	992.43948	0.20D-02	0.00168	0.83995
22	21	993.27359	0.20D-02	-0.00051	-0.25709
23	22	994.1006	0.20D-02	-0.00212	-1.05865
24	23	994.91754	0.20D-02	-0.00016	-0.08059
25	24	995.73141	0.20D-02	-0.00166	-0.82892
26	25	996.536	0.20D-02	-0.00041	-0.20462
27	26	997.33477	0.20D-02	0.00011	0.05632
28	27	998.12821	0.30D-02	-0.00058	-0.19472
29	28	998.91408	0.20D-02	-0.00029	-0.14584
30	29	999.69369	0.20D-02	-0.00032	-0.1609
31	30	1000.46656	0.20D-02	-0.00021	-0.10344
32	31	1001.23303	0.20D-02	-0.0003	-0.14909
33	32	1001.99367	0.20D-02	-0.00118	-0.58967
34	33	1002.74543	0.20D-02	0.00019	0.09477
35	34	1003.49285	0.20D-02	-0.00074	-0.36783
36	35	1004.23264	0.20D-02	-0.0007	-0.34752
37	36	1004.9648	0.20D-02	0.00031	0.15412
38	37	1005.69036	0.20D-02	0.00123	0.61553

Table A.1, Fourier Transform Infrared Data for ^{70}GeO (cm^{-1}) (*Cont'd*)

J'	J''	Obs	Unc	Calc-Obs	(Calc-Obs)/Unc
39	38	1006.4115	0.20D-02	-0.00012	-0.05839
40	39	1007.12508	0.20D-02	-0.00061	-0.30423
41	40	1007.83092	0.20D-02	-0.00008	-0.03859
42	41	1008.52775	0.20D-02	0.00274	1.36842
43	42	1009.22356	0.20D-02	-0.00016	-0.07983
44	43	1009.90978	0.20D-02	-0.00023	-0.11496
45	44	1010.58854	0.20D-02	0.0004	0.19788
46	45	1011.26345	0.20D-02	-0.00191	-0.95294
47	46	1011.9276	0.20D-02	-0.00024	-0.11858
48	47	1012.58643	0.20D-02	-0.00005	-0.02571
49	48	1013.23495	0.20D-02	0.00363	1.81551
50	49	1013.88447	0.20D-02	-0.00051	-0.25662
51	50	1014.52296	0.20D-02	-0.00046	-0.22828
52	51	1015.15466	0.20D-02	-0.00047	-0.23567
53	52	1015.78031	0.20D-02	-0.0013	-0.64999
54	53	1016.39746	0.20D-02	-0.00051	-0.25298
55	54	1017.00843	0.20D-02	-0.00042	-0.20984
56	55	1017.6122	0.20D-02	-0.00003	-0.01732
57	56	1018.2106	0.20D-02	-0.00119	-0.59666
58	57	1018.80114	0.20D-02	-0.00142	-0.70912
59	58	1019.38333	0.20D-02	-0.00023	-0.11595
60	59	1019.9587	0.20D-02	0.00083	0.41657
61	60	1020.53115	0.20D-02	-0.00216	-1.07784
62	61	1021.09179	0.20D-02	-0.00031	-0.15547
63	62	1021.64667	0.20D-02	0.0003	0.15239
64	63	1022.19558	0.20D-02	-0.00011	-0.05558
65	64	1022.73748	0.20D-02	-0.00053	-0.26569
66	65	1023.27123	0.20D-02	0.00017	0.08573
67	66	1023.79918	0.20D-02	-0.00037	-0.18266
68	67	1024.31758	0.20D-02	0.0016	0.7978
69	68	1024.83278	0.20D-02	-0.0003	-0.14923
70	69	1025.33903	0.20D-02	-0.00033	-0.16514
71	70	1025.83994	0.20D-02	-0.00211	-1.05629
72	71	1026.33201	0.20D-02	-0.00216	-1.07906
73	72	1026.81624	0.20D-02	-0.00148	-0.73985
74	73	1027.29288	0.20D-02	-0.00034	-0.17006
75	74	1027.76427	0.20D-02	-0.00109	-0.54609
76	75	1028.22759	0.20D-02	-0.00093	-0.46438
77	76	1028.6841	0.20D-02	-0.00112	-0.56134
78	77	1029.13286	0.20D-02	-0.00075	-0.37292
79	78	1029.57565	0.20D-02	-0.00159	-0.79657
80	79	1030.00896	0.20D-02	-0.00016	-0.07825
81	80	1030.4378	0.20D-02	-0.00148	-0.73942
82	81	1030.85796	0.20D-02	-0.00135	-0.67657
83	82	1031.26799	0.20D-02	0.00166	0.82932
84	83	1031.67183	0.20D-02	0.0036	1.80076
85	84	1032.07409	0.20D-02	-0.00015	-0.07328
86	85	1032.46548	0.20D-02	-0.00031	-0.15429
87	86	1032.85036	0.20D-02	-0.00126	-0.62832
88	87	1033.22384	0.20D-02	0.00188	0.94211
89	88	1033.598	0.20D-02	-0.00298	-1.48906
90	89	1033.95699	0.20D-02	-0.00001	-0.00288
91	90	1034.31264	0.20D-02	-0.00104	-0.52191
92	91	1034.66127	0.20D-02	-0.00242	-1.21224
93	92	1034.99797	0.20D-02	0.00075	0.37505
94	93	1035.33047	0.20D-02	0.00073	0.36737
95	94	1035.65764	0.20D-02	-0.00134	-0.67139
96	95	1035.97485	0.20D-02	-0.00088	-0.44235

Table A.1, Fourier Transform Infrared Data for ^{70}GeO (cm^{-1}) (*Cont'd*)

J'	J''	Obs	Unc	Calc-Obs	(Calc-Obs)/Unc
97	96	1036.28548	0.20D-02	-0.00128	-0.63814
98	97	1036.58908	0.20D-02	-0.00208	-1.03939
99	98	1036.87851	0.20D-02	0.00383	1.91626
The 3-2 Band, 171 data, $J"_{min}$ = 2, $J"_{max}$ = 91					
Unc.$_{Avge}$ = 2.0D-03, Unc.$_{Max}$ = 5.0D-03					
(Err/Unc.)$_{Avge}$ = -4.4D-03, RMSR = 0.52					
90	91	852.5322	0.20D-02	0.00016	0.08108
89	90	854.01105	0.20D-02	0.00251	1.25738
88	89	855.49074	0.20D-02	-0.00123	-0.61577
87	88	856.96135	0.20D-02	-0.00116	-0.57854
86	87	858.42535	0.20D-02	0.00026	0.12891
85	86	859.88686	0.20D-02	-0.00111	-0.55369
84	85	861.34099	0.20D-02	-0.00039	-0.19659
83	84	862.79044	0.20D-02	-0.0003	-0.15006
82	83	864.23278	0.20D-02	0.0016	0.8008
81	82	865.67362	0.20D-02	-0.00033	-0.16441
80	81	867.10693	0.20D-02	-0.00006	-0.03088
79	80	868.53515	0.20D-02	-0.00005	-0.02387
78	79	869.95948	0.20D-02	-0.00149	-0.74365
77	78	871.37445	0.20D-02	0.00106	0.52956
76	77	872.78882	0.20D-02	-0.00117	-0.58456
75	76	874.1945	0.20D-02	-0.00009	-0.04634
74	75	875.59708	0.20D-02	-0.0013	-0.65096
73	74	876.99186	0.20D-02	-0.00013	-0.06377
72	73	878.38221	0.20D-02	0.00006	0.02994
71	72	879.76765	0.20D-02	-0.00027	-0.13513
70	71	881.14897	0.20D-02	-0.00191	-0.9543
69	70	882.5219	0.20D-02	-0.00062	-0.30783
68	69	883.89015	0.20D-02	-0.0001	-0.05113
67	68	885.25495	0.20D-02	-0.00161	-0.80444
66	67	886.61066	0.20D-02	0.0005	0.25182
65	66	887.96388	0.20D-02	-0.0004	-0.19759
64	65	889.31138	0.20D-02	-0.00108	-0.53806
63	64	890.6523	0.20D-02	-0.00069	-0.34494
62	63	891.98985	0.20D-02	-0.00245	-1.22359
61	62	893.31963	0.20D-02	-0.00198	-0.98936
60	61	894.64282	0.20D-02	-0.00047	-0.23263
59	60	895.96011	0.20D-02	0.00139	0.69629
58	59	897.2737	0.20D-02	0.00139	0.69691
57	58	898.58383	0.20D-02	-0.00073	-0.36609
56	57	899.88648	0.20D-02	-0.00097	-0.48307
55	56	901.18249	0.20D-02	-0.00016	-0.07945
54	55	902.47368	0.20D-02	-0.00013	-0.06566
53	54	903.75918	0.20D-02	-0.00004	-0.02209
52	53	905.04044	0.20D-02	-0.00135	-0.67417
51	52	906.31287	0.20D-02	0.00054	0.26769
50	51	907.58209	0.20D-02	-0.00001	-0.00693
49	50	908.84373	0.20D-02	0.00134	0.67156
48	49	910.10202	0.20D-02	0.00038	0.18765
47	48	911.35471	0.20D-02	-0.00068	-0.33903
46	47	912.60102	0.20D-02	-0.00104	-0.51897
45	46	913.84055	0.20D-02	-0.00034	-0.16768
44	45	915.07506	0.20D-02	-0.00033	-0.16553
43	44	916.30423	0.20D-02	-0.00072	-0.35804
42	43	917.52692	0.20D-02	-0.00036	-0.18069
41	42	918.7437	0.20D-02	0.00016	0.08109
40	41	919.95614	0.20D-02	-0.00075	-0.37329

Table A.1, Fourier Transform Infrared Data for ^{70}GeO (cm^{-1}) (*Cont'd*)

J'	J''	Obs	Unc	Calc-Obs	(Calc-Obs)/Unc
39	40	921.16132	0.20D-02	-0.00017	-0.08423
38	39	922.36164	0.20D-02	-0.00051	-0.25733
37	38	923.555	0.20D-02	0.00031	0.15699
36	37	924.74361	0.20D-02	0.00008	0.03817
35	36	925.92665	0.20D-02	-0.00041	-0.20437
34	35	927.10267	0.20D-02	0.0003	0.14895
33	34	928.27402	0.20D-02	-0.00016	-0.08242
32	33	929.43914	0.20D-02	-0.00024	-0.11911
31	32	930.59928	0.20D-02	-0.0012	-0.60164
30	31	931.75044	0.20D-02	0.00094	0.46951
29	30	932.89864	0.20D-02	0.00016	0.07865
28	29	934.04121	0.20D-02	-0.00088	-0.43967
27	28	935.17599	0.20D-02	-0.00004	-0.0211
26	27	936.30588	0.20D-02	-0.00023	-0.11625
25	26	937.42992	0.20D-02	-0.0005	-0.25063
24	25	938.54766	0.20D-02	-0.00041	-0.20483
23	24	939.65896	0.20D-02	0.00018	0.09045
22	23	940.76451	0.20D-02	0.00055	0.27463
21	22	941.86511	0.20D-02	-0.00011	-0.05284
20	21	942.95887	0.20D-02	0.00009	0.04731
19	20	944.04761	0.20D-02	-0.00068	-0.34047
18	19	945.12907	0.20D-02	-0.00017	-0.08685
17	18	946.20509	0.20D-02	-0.00026	-0.12753
16	17	947.27436	0.20D-02	0.00038	0.19193
15	16	948.33623	0.20D-02	0.00238	1.19087
14	15	949.39655	0.20D-02	-0.00012	-0.06148
13	14	950.44858	0.20D-02	-0.00039	-0.19574
12	13	951.49262	0.20D-02	0.00124	0.62245
11	12	952.53404	0.20D-02	-0.00059	-0.29269
10	11	953.56755	0.20D-02	-0.0006	-0.30177
9	10	954.59487	0.20D-02	-0.00054	-0.27054
8	9	955.61312	0.20D-02	0.00248	1.24029
7	8	956.63018	0.20D-02	0.00055	0.275
6	7	957.64046	0.20D-02	-0.00074	-0.37214
5	6	958.64265	0.20D-02	-0.0001	-0.05186
3	4	960.62938	0.20D-02	0.00033	0.16304
2	3	961.61299	0.20D-02	0.00101	0.5061
1	2	962.5893	0.20D-02	0.0028	1.39862
3	2	967.38695	0.20D-02	0.00221	1.10511
4	3	968.33131	0.20D-02	-0.0015	-0.75239
6	5	970.18998	0.20D-02	0.00226	1.12839
7	6	971.11477	0.20D-02	-0.00076	-0.38
8	7	972.03014	0.20D-02	-0.00068	-0.34203
9	8	972.93856	0.20D-02	0.00001	0.00644
10	9	973.8404	0.20D-02	0.00095	0.47456
11	10	974.73686	0.20D-02	0.00091	0.45647
12	11	975.62686	0.20D-02	0.00097	0.48633
13	12	976.51187	0.20D-02	-0.00034	-0.17182
14	13	977.3886	0.20D-02	0.00022	0.11123
15	14	978.25852	0.20D-02	0.0012	0.59947
16	15	979.12441	0.20D-02	-0.00021	-0.10288
17	16	979.98292	0.20D-02	-0.00065	-0.3268
18	17	980.83105	0.20D-02	0.00284	1.42179
19	18	981.67989	0.20D-02	-0.00082	-0.40802
20	19	982.51821	0.20D-02	-0.0004	-0.20212
21	20	983.3504	0.20D-02	-0.00034	-0.17157
22	21	984.1745	0.20D-02	0.00133	0.6628
23	22	984.99463	0.20D-02	0.00047	0.23491

Table A.1, Fourier Transform Infrared Data for ^{70}GeO (cm^{-1}) (*Cont'd*)

J'	J''	Obs	Unc	Calc-Obs	(Calc-Obs)/Unc
24	23	985.80869	0.20D-02	-0.00082	-0.41109
25	24	986.61609	0.20D-02	-0.00197	-0.98623
26	25	987.41429	0.20D-02	-0.00044	-0.22151
27	26	988.20812	0.20D-02	-0.0011	-0.5479
28	27	988.99354	0.20D-02	0.00011	0.05364
29	28	989.77316	0.20D-02	0.00054	0.272
30	29	990.54765	0.20D-02	-0.00047	-0.23374
31	30	991.3138	0.20D-02	0.00027	0.1353
32	31	992.07405	0.20D-02	0.00031	0.15319
33	32	992.82652	0.20D-02	0.00152	0.75883
34	33	993.57465	0.20D-02	0.00043	0.21616
35	34	994.31582	0.20D-02	-0.00033	-0.16586
36	35	995.04923	0.20D-02	0.00001	0.00674
37	36	995.7763	0.20D-02	0.00004	0.01779
38	37	996.49704	0.20D-02	-0.00029	-0.14369
39	38	997.21103	0.20D-02	-0.00055	-0.27391
40	39	997.91818	0.20D-02	-0.00066	-0.32886
41	40	998.61757	0.20D-02	0.00027	0.13529
42	41	999.30972	0.20D-02	0.00171	0.85744
43	42	999.99884	0.20D-02	-0.00055	-0.27356
44	43	1000.67807	0.20D-02	0.00033	0.16632
45	44	1001.34976	0.20D-02	0.00199	0.99527
46	45	1002.01788	0.20D-02	0.00045	0.22315
47	46	1002.67914	0.20D-02	-0.00102	-0.51171
48	47	1003.33138	0.20D-02	-0.00027	-0.13548
49	48	1003.97751	0.20D-02	-0.00021	-0.10434
50	49	1004.61804	0.20D-02	-0.00138	-0.68998
51	50	1005.2488	0.20D-02	0.00038	0.19241
52	51	1005.87557	0.20D-02	-0.00071	-0.35389
53	52	1006.49023	0.20D-02	0.00345	1.72491
54	53	1007.1055	0.20D-02	0.00013	0.06258
55	54	1007.71111	0.20D-02	-0.00042	-0.21211
56	55	1008.30877	0.20D-02	0.00008	0.03911
57	56	1008.89866	0.20D-02	0.00145	0.72597
58	57	1009.486	0.20D-02	-0.00156	-0.77828
59	58	1010.06215	0.20D-02	-0.00031	-0.15492
60	59	1010.63291	0.20D-02	-0.00062	-0.31022
61	60	1011.19512	0.20D-02	0.00066	0.32953
62	61	1011.75141	0.20D-02	0.00089	0.44303
63	62	1012.30061	0.20D-02	0.00122	0.60897
64	63	1012.84286	0.20D-02	0.0015	0.75105
65	64	1013.38048	0.20D-02	-0.00059	-0.29707
66	65	1013.90954	0.20D-02	-0.00115	-0.57672
67	66	1014.43048	0.20D-02	-0.00062	-0.30924
68	67	1014.94419	0.20D-02	0.00009	0.04401
69	68	1015.45116	0.20D-02	0.00047	0.23667
70	69	1015.94799	0.50D-02	0.00392	0.78495
71	70	1016.44425	0.20D-02	0.00086	0.42974
72	71	1016.93253	0.20D-02	-0.00133	-0.66262
73	72	1017.4128	0.20D-02	-0.00261	-1.30611
74	73	1017.88198	0.20D-02	0.00007	0.03335
75	74	1018.34745	0.20D-02	-0.00068	-0.34164
76	75	1018.80114	0.20D-02	0.0032	1.59799
77	76	1019.25528	0.20D-02	-0.00054	-0.26921
78	77	1019.69807	0.20D-02	-0.00009	-0.04468
79	78	1020.13618	0.20D-02	-0.00216	-1.07988
80	79	1020.56236	0.20D-02	0.0005	0.24923
81	80	1020.98341	0.20D-02	0.00107	0.53517

Table A.1, Fourier Transform Infrared Data for ^{70}GeO (cm^{-1}) (*Cont'd*)

J'	J''	Obs	Unc	Calc-Obs	(Calc-Obs)/Unc
82	81	1021.40021	0.20D-02	-0.00134	-0.66805
83	82	1021.80482	0.20D-02	0.00121	0.60309
85	84	1022.59802	0.20D-02	0.00054	0.26787
86	85	1022.98369	0.20D-02	0.00022	0.10798
The 4-3 Band, 157 data, $J"_{min}$ = 3, $J"_{max}$ = 84					
Unc.$_{Avge}$ = 2.1D-03, Unc.$_{Max}$ = 5.0D-03					
(Err/Unc.)$_{Avge}$ = -8.5D-02, RMSR = 0.66					
83	84	854.39926	0.20D-02	-0.00079	-0.39444
82	83	855.83701	0.20D-02	-0.00099	-0.49538
81	82	857.26924	0.20D-02	-0.00099	-0.49427
80	81	858.69448	0.20D-02	0.00068	0.33852
79	80	860.11465	0.20D-02	0.00209	1.04278
78	79	861.53024	0.20D-02	0.00272	1.35829
77	78	862.94776	0.20D-02	-0.00394	-1.97028
76	77	864.34831	0.20D-02	0.00101	0.50674
75	76	865.74646	0.20D-02	0.00298	1.48916
74	75	867.14584	0.20D-02	-0.00168	-0.83836
73	74	868.53515	0.20D-02	-0.00166	-0.83111
72	73	869.91835	0.20D-02	-0.00094	-0.46941
71	72	871.29593	0.20D-02	-0.00003	-0.01352
70	71	872.66943	0.20D-02	-0.00047	-0.23384
69	70	874.03592	0.20D-02	0.00066	0.32935
68	69	875.39956	0.20D-02	-0.00081	-0.40423
67	68	876.75514	0.20D-02	0.00031	0.15499
66	67	878.1073	0.20D-02	-0.00063	-0.31323
65	66	879.45378	0.20D-02	-0.00137	-0.68428
64	65	880.79366	0.20D-02	-0.001	-0.49852
63	64	882.12747	0.20D-02	-0.00007	-0.0363
62	63	883.4577	0.20D-02	-0.00109	-0.54298
61	62	884.77952	0.20D-02	0.00078	0.39113
60	61	886.09879	0.20D-02	-0.00033	-0.16447
59	60	887.41197	0.20D-02	-0.00091	-0.45509
58	59	888.71875	0.20D-02	-0.00065	-0.32606
57	58	890.0168	0.20D-02	0.00276	1.38216
56	57	891.31537	0.20D-02	0.00009	0.04413
55	56	892.60228	0.20D-02	0.00347	1.73454
55	56	892.60228	0.20D-02	0.00347	1.73454
54	55	893.89104	0.20D-02	-0.0006	-0.30206
53	54	895.17009	0.20D-02	-0.00058	-0.29109
52	53	896.44353	0.20D-02	-0.00057	-0.28293
51	52	897.71119	0.20D-02	-0.00042	-0.2081
50	51	898.97364	0.20D-02	-0.0007	-0.35199
49	50	900.23069	0.20D-02	-0.00125	-0.62498
48	49	901.48294	0.20D-02	-0.00267	-1.33264
47	48	902.72598	0.20D-02	-0.00054	-0.2703
46	47	903.96565	0.20D-02	-0.00075	-0.37349
45	46	905.19902	0.20D-02	-0.00036	-0.17766
44	45	906.42698	0.20D-02	-0.00027	-0.13329
43	44	907.64952	0.20D-02	-0.00047	-0.23587
42	43	908.86537	0.20D-02	0.00027	0.13414
41	42	910.07612	0.20D-02	0.00036	0.18127
40	41	911.2799	0.20D-02	0.00167	0.83494
39	40	912.48129	0.20D-02	-0.00039	-0.19526
38	39	913.67366	0.20D-02	0.00078	0.39005
37	38	914.86184	0.20D-02	0.00035	0.17547
36	37	916.04374	0.20D-02	0.0004	0.2004
35	36	917.22119	0.20D-02	-0.00091	-0.45567

Table A.1, Fourier Transform Infrared Data for ^{70}GeO (cm^{-1}) (*Cont'd*)

J'	J''	Obs	Unc	Calc-Obs	(Calc-Obs)/Unc
34	35	918.39037	0.20D-02	0.00023	0.11672
33	34	919.55476	0.20D-02	0.00032	0.16207
32	33	920.71471	0.20D-02	-0.00099	-0.49528
31	32	921.86583	0.20D-02	0.00067	0.33417
30	31	923.01331	0.20D-02	0.00011	0.05491
29	30	924.15408	0.20D-02	0.00037	0.18632
28	29	925.29051	0.20D-02	-0.00091	-0.45724
27	28	926.41918	0.20D-02	-0.00034	-0.17125
26	27	927.54101	0.20D-02	0.00116	0.57865
25	26	928.65773	0.20D-02	0.00185	0.92686
24	25	929.77141	0.20D-02	-0.00035	-0.17718
23	24	930.876	0.20D-02	0.00058	0.29082
22	23	931.97598	0.20D-02	0.00017	0.0853
21	22	933.06876	0.20D-02	0.00099	0.49567
20	21	934.15594	0.20D-02	0.00144	0.72125
19	20	935.23976	0.20D-02	-0.00075	-0.37365
18	19	936.31686	0.20D-02	-0.00222	-1.10958
17	18	937.38512	0.20D-02	-0.00086	-0.43223
16	17	938.44851	0.20D-02	-0.00066	-0.33229
15	16	939.5059	0.20D-02	-0.00049	-0.24535
14	15	940.55834	0.20D-02	-0.00142	-0.7122
13	14	941.60157	0.20D-02	0.00079	0.39652
12	13	942.64025	0.20D-02	0.00149	0.74518
11	12	943.67672	0.20D-02	-0.00168	-0.84196
10	11	944.70358	0.20D-02	-0.00133	-0.66563
9	10	945.72475	0.20D-02	-0.0014	-0.70157
8	9	946.73994	0.20D-02	-0.00161	-0.80541
7	8	947.74882	0.20D-02	-0.00164	-0.81787
6	7	948.74662	0.20D-02	0.00328	1.6402
5	6	949.74642	0.20D-02	0.00006	0.02813
4	5	950.73744	0.20D-02	-0.00056	-0.27979
3	4	951.72015	0.20D-02	0.00096	0.48058
2	3	952.70058	0.20D-02	-0.00142	-0.71142
8	7	963.04588	0.20D-02	0.00029	0.14608
9	8	963.94781	0.20D-02	0.00129	0.64275
10	9	964.84651	0.20D-02	-0.00083	-0.41362
11	10	965.73667	0.20D-02	-0.00074	-0.36891
12	11	966.61781	0.20D-02	0.002	1.00106
13	12	967.49619	0.20D-02	0.00113	0.56534
14	13	968.36767	0.20D-02	0.00078	0.38801
15	14	969.23284	0.20D-02	0.00034	0.16824
16	15	970.09132	0.20D-02	0.00018	0.09009
17	16	970.94409	0.20D-02	-0.00068	-0.34237
18	17	971.78873	0.20D-02	0.00016	0.07993
19	18	972.62931	0.20D-02	-0.00139	-0.69388
20	19	973.46216	0.20D-02	-0.00166	-0.82986
21	20	974.28613	0.20D-02	0.00048	0.24116
22	21	975.1029	0.20D-02	0.00335	1.6731
23	22	975.92107	0.20D-02	-0.00168	-0.8399
24	23	976.72581	0.20D-02	0.00023	0.11614
25	24	977.52699	0.20D-02	-0.00082	-0.40977
26	25	978.31962	0.20D-02	0.00015	0.07638
27	26	979.10825	0.20D-02	-0.00141	-0.70636
28	27	979.88738	0.20D-02	-0.00003	-0.01409
29	28	980.66278	0.20D-02	-0.00148	-0.73779
30	29	981.42918	0.20D-02	-0.0005	-0.24843
31	30	982.19038	0.20D-02	-0.00089	-0.44709
32	31	982.94487	0.20D-02	-0.00119	-0.59482

Table A.1, Fourier Transform Infrared Data for ^{70}GeO (cm^{-1}) (*Cont'd*)

J'	J''	Obs	Unc	Calc-Obs	(Calc-Obs)/Unc
33	32	983.68992	0.20D-02	0.00134	0.67234
34	33	984.43483	0.20D-02	-0.0026	-1.30167
35	34	985.16469	0.20D-02	0.00186	0.93208
36	35	985.89518	0.20D-02	-0.00094	-0.47243
37	36	986.61436	0.20D-02	0.0009	0.4486
38	37	987.33028	0.20D-02	-0.00066	-0.3308
39	38	988.0376	0.20D-02	-0.00031	-0.1568
40	39	988.73897	0.20D-02	-0.00071	-0.35549
41	40	989.43562	0.20D-02	-0.0031	-1.54806
42	41	990.12065	0.20D-02	-0.00058	-0.29047
43	42	990.79981	0.20D-02	0.00107	0.53599
44	43	991.47108	0.50D-02	0.00387	0.77409
45	44	992.14212	0.20D-02	0.00014	0.07112
46	45	992.80394	0.20D-02	-0.00113	-0.56251
47	46	993.45694	0.20D-02	-0.00036	-0.18191
48	47	994.1006	0.20D-02	0.00294	1.47186
49	48	994.74481	0.20D-02	-0.0011	-0.55246
50	49	995.37714	0.20D-02	-0.00009	-0.04604
51	50	996.003	0.20D-02	0.00056	0.27994
52	51	996.62272	0.20D-02	0.00051	0.25418
53	52	997.23667	0.20D-02	-0.00063	-0.31445
54	53	997.84321	0.20D-02	-0.00121	-0.60727
55	54	998.4417	0.20D-02	-0.00064	-0.32044
56	55	999.03174	0.20D-02	0.00149	0.74475
57	56	999.61697	0.20D-02	0.00152	0.76204
58	57	1000.19745	0.20D-02	-0.00061	-0.30464
59	58	1000.76893	0.20D-02	-0.00067	-0.33692
60	59	1001.33538	0.20D-02	-0.00265	-1.32593
61	60	1001.89155	0.20D-02	-0.00131	-0.65347
62	61	1002.44266	0.20D-02	-0.00187	-0.93484
63	62	1002.98456	0.20D-02	-0.0002	-0.10186
64	63	1003.52132	0.20D-02	-0.00038	-0.19085
65	64	1004.0525	0.20D-02	-0.002	-0.99815
66	65	1004.57407	0.20D-02	-0.00102	-0.51009
67	66	1005.08776	0.20D-02	0.0008	0.40197
68	67	1005.59733	0.20D-02	-0.0003	-0.14782
69	68	1006.09725	0.20D-02	0.0012	0.59816
70	69	1006.58682	0.50D-02	0.00597	1.19361
71	70	1007.08	0.20D-02	0.00005	0.02342
72	71	1007.55933	0.20D-02	0.00088	0.43991
73	72	1008.03366	0.20D-02	-0.0004	-0.1979
74	73	1008.50102	0.20D-02	-0.00181	-0.90643
75	74	1008.95655	0.20D-02	0.00146	0.72791
76	75	1009.41147	0.20D-02	-0.00181	-0.90634
77	76	1009.85352	0.20D-02	0.00063	0.3149
78	77	1010.294	0.20D-02	-0.00253	-1.26585
79	78	1010.72219	0.20D-02	-0.00059	-0.29454
80	79	1011.1474	0.20D-02	-0.00287	-1.43264
81	80	1011.55925	0.20D-02	0.00101	0.50336
82	81	1011.96814	0.20D-02	0.00061	0.30747
The 5-4 Band, 133 data, $J"_{min} = 0$, $J"_{max} = 72$					
Unc.$_{Avge}$ = 2.6D-03, Unc.$_{Max}$ = 1.0D-02					
(Err/Unc.)$_{Avge}$ = -1.4D-01, RMSR = 0.87					
61	62	876.26146	0.50D-02	0.00835	1.66917
60	61	877.58307	0.20D-02	-0.00166	-0.82925
59	60	878.88773	0.20D-02	-0.00026	-0.1286
58	59	880.18091	0.50D-02	0.00708	1.41575

Table A.1, Fourier Transform Infrared Data for ^{70}GeO (cm^{-1}) (*Cont'd*)

J'	J''	Obs	Unc	Calc-Obs	(Calc-Obs)/Unc
57	58	881.47968	0.50D-02	0.00325	0.64974
56	57	882.77381	0.20D-02	-0.00152	-0.7591
55	56	884.05762	0.20D-02	-0.00155	-0.77641
54	55	885.33428	0.20D-02	-0.00004	-0.01798
53	54	886.61066	0.20D-02	-0.00384	-1.91924
52	53	887.87492	0.20D-02	-0.00115	-0.57558
51	52	889.13813	0.20D-02	-0.00305	-1.52252
50	51	890.38743	0.50D-02	0.00333	0.66583
49	50	891.64038	0.20D-02	0.00041	0.20519
48	49	892.88565	0.20D-02	-0.0005	-0.25106
47	48	894.12521	0.20D-02	-0.00138	-0.68968
46	47	895.35854	0.20D-02	-0.00171	-0.85612
45	46	896.58345	0.20D-02	0.00069	0.34412
44	45	897.80374	0.20D-02	0.00199	0.99557
43	44	899.02038	0.20D-02	0.00123	0.61275
42	43	900.23069	0.20D-02	0.00106	0.53021
41	42	901.43807	0.20D-02	-0.00192	-0.95765
40	41	902.63451	0.20D-02	0.00031	0.15377
39	40	903.8265	0.20D-02	0.00121	0.60389
38	39	905.01158	0.20D-02	0.00324	1.62217
37	38	906.19755	0.20D-02	-0.00139	-0.69685
36	37	907.37274	0.20D-02	-0.00104	-0.51872
35	36	908.53972	0.20D-02	0.00171	0.856
34	35	909.70636	0.20D-02	-0.00102	-0.50818
33	34	910.86578	0.20D-02	-0.00235	-1.17691
32	33	912.00823	0.50D-02	0.00744	1.48774
31	32	913.16263	0.20D-02	-0.00056	-0.28007
30	31	914.29638	0.50D-02	0.00622	1.24374
29	30	915.43667	0.20D-02	0.00058	0.29201
28	29	916.56445	0.20D-02	0.00157	0.78725
27	28	917.68816	0.20D-02	0.00075	0.37458
26	27	918.80599	0.20D-02	-0.00011	-0.05659
25	26	919.91532	0.20D-02	0.00161	0.80302
24	25	921.0202	0.20D-02	0.00185	0.92286
23	24	922.1213	0.20D-02	-0.00008	-0.03765
22	23	923.21457	0.20D-02	-0.00011	-0.05424
21	22	924.30808	0.50D-02	-0.00635	-1.27097
20	21	925.38519	0.20D-02	-0.00218	-1.08792
19	20	926.45848	0.20D-02	-0.00016	-0.08136
18	19	927.52605	0.20D-02	0.00157	0.78659
17	18	928.59044	0.20D-02	0.00049	0.24529
16	17	929.64874	0.20D-02	-0.00053	-0.26596
15	16	930.7024	0.20D-02	-0.00295	-1.47281
14	15	931.74503	0.20D-02	-0.00037	-0.18591
13	14	932.78322	0.20D-02	0.00059	0.29395
12	13	933.81108	0.50D-02	0.00582	1.16447
11	12	934.84395	0.20D-02	-0.00004	-0.01998
10	11	935.86432	0.20D-02	0.00051	0.25476
9	10	936.87965	0.20D-02	0.0	-0.00032
8	9	937.88833	0.20D-02	0.00003	0.01405
7	8	938.89213	0.20D-02	-0.00119	-0.59287
6	7	939.88977	0.20D-02	-0.00236	-1.18181
5	6	940.87932	0.20D-02	-0.00161	-0.80348
4	5	941.86815	0.50D-02	-0.00629	-1.25747
3	4	942.83973	0.20D-02	0.00011	0.05678
2	3	943.81132	0.20D-02	0.00032	0.16222
1	2	944.76588	0.10D-01	0.01138	1.13836
0	1	945.73668	0.20D-02	-0.00001	-0.00523

Table A.1, Fourier Transform Infrared Data for ^{70}GeO (cm^{-1}) (*Cont'd*)

J'	J''	Obs	Unc	Calc-Obs	(Calc-Obs)/Unc
1	0	947.64242	0.50D-02	-0.00559	-1.11894
2	1	948.57436	0.20D-02	0.00319	1.59592
3	2	949.51143	0.20D-02	0.0006	0.29938
5	4	951.36285	0.20D-02	-0.00065	-0.32663
6	5	952.28048	0.20D-02	-0.00263	-1.31271
7	6	953.18946	0.20D-02	-0.00224	-1.12199
8	7	954.09474	0.50D-02	-0.00447	-0.89413
9	8	954.9868	0.20D-02	0.0002	0.10142
10	9	955.87859	0.20D-02	-0.00118	-0.58758
11	10	956.76375	0.20D-02	-0.00228	-1.13829
12	11	957.64046	0.20D-02	-0.00128	-0.64151
13	12	958.51005	0.20D-02	0.00046	0.23178
14	13	959.37353	0.20D-02	0.00194	0.97076
15	14	960.23381	0.20D-02	0.00023	0.11448
17	16	961.93423	0.20D-02	-0.00227	-1.13255
18	17	962.76936	0.20D-02	0.00193	0.9649
19	18	963.60331	0.20D-02	0.00087	0.43331
20	19	964.43122	0.20D-02	-0.00061	-0.30317
21	20	965.25102	0.20D-02	-0.00043	-0.21558
22	21	966.06403	0.20D-02	0.00007	0.0352
23	22	966.86927	0.20D-02	0.00185	0.92314
24	23	967.67004	0.20D-02	0.00159	0.79726
25	24	968.46542	0.20D-02	0.00022	0.11158
26	25	969.25497	0.20D-02	-0.00184	-0.91986
27	26	970.03579	0.20D-02	-0.00171	-0.85316
28	27	970.80869	0.20D-02	-0.0002	-0.09924
29	28	971.57829	0.20D-02	-0.00194	-0.96923
30	29	972.33868	0.20D-02	-0.00105	-0.52406
31	30	973.09324	0.20D-02	-0.00091	-0.45481
32	31	973.8404	0.20D-02	0.00003	0.01746
33	32	974.58402	0.20D-02	-0.00209	-1.0433
34	33	975.31734	0.20D-02	-0.00053	-0.26317
35	34	976.04525	0.20D-02	-0.00019	-0.09316
36	35	976.76437	0.20D-02	0.00231	1.15555
37	36	977.47865	0.20D-02	0.00298	1.49195
38	37	978.1903	0.20D-02	-0.00038	-0.1901
39	38	978.89074	0.20D-02	0.00079	0.3933
40	39	979.58055	0.50D-02	0.00589	1.17841
41	40	980.27476	0.20D-02	-0.00011	-0.05306
42	41	980.95587	0.20D-02	0.00028	0.13993
43	42	981.63094	0.20D-02	-0.00002	-0.01117
44	43	982.30008	0.20D-02	-0.00112	-0.56244
45	44	982.96037	0.20D-02	-0.00014	-0.0701
46	45	983.61499	0.20D-02	-0.00025	-0.12537
47	46	984.26689	0.20D-02	-0.00442	-2.20933
48	47	984.90599	0.20D-02	-0.00258	-1.28821
49	48	985.55431	0.10D-01	-0.01676	-1.67564
50	49	986.16643	0.20D-02	-0.00155	-0.77549
51	50	986.78561	0.20D-02	-0.00023	-0.11635
52	51	987.39931	0.20D-02	-0.00026	-0.13193
53	52	988.00669	0.20D-02	-0.00084	-0.41854
54	53	988.60541	0.20D-02	0.00039	0.19267
55	54	989.20638	0.50D-02	-0.00752	-1.50384
56	55	989.78844	0.20D-02	-0.0034	-1.70161
57	56	990.36394	0.20D-02	0.00037	0.18538
58	57	990.93819	0.20D-02	-0.00152	-0.75991
59	58	991.50864	0.50D-02	-0.00654	-1.30749
60	59	992.06177	0.20D-02	-0.00117	-0.58743

Table A.1, Fourier Transform Infrared Data for ^{70}GeO (cm^{-1}) (*Cont'd*)

J'	J''	Obs	Unc	Calc-Obs	(Calc-Obs)/Unc
61	60	992.61261	0.20D-02	-0.00046	-0.23226
62	61	993.1491	0.50D-02	0.00762	1.52418
63	62	993.69155	0.50D-02	0.00277	0.55374
64	63	994.2254	0.20D-02	-0.00047	-0.23688
65	64	994.74481	0.50D-02	0.00372	0.74417
66	65	995.26983	0.20D-02	-0.00471	-2.35508
67	66	995.77665	0.20D-02	-0.00197	-0.98472
68	67	996.28048	0.20D-02	-0.00328	-1.6399
69	68	996.76826	0.50D-02	0.00441	0.88118
70	69	997.25785	0.50D-02	0.00322	0.64302
71	70	997.7422	0.20D-02	0.00018	0.09244
72	71	998.21585	0.20D-02	0.00077	0.38623
73	72	998.68972	0.50D-02	-0.00597	-1.19499
The 6-5 Band, 109 data, $J"_{min} = 9$, $J"_{max} = 70$					
Unc.$_{Avge}$ = 3.2D-03, Unc.$_{Max}$ = 1.0D-02					
(Err/Unc.)$_{Avge}$ = -5.4D-01, RMSR = 1.17					
69	70	857.15509	0.50D-02	-0.00791	-1.58197
68	69	858.49556	0.50D-02	0.00062	0.12375
67	68	859.83916	0.50D-02	0.00057	0.11487
66	67	861.1779	0.20D-02	-0.00008	-0.0419
65	66	862.51063	0.20D-02	-0.00021	-0.1032
64	65	863.8382	0.20D-02	-0.00065	-0.32709
62	63	866.47685	0.20D-02	-0.00155	-0.77409
61	62	867.77881	0.50D-02	0.00709	1.4188
60	61	869.09053	0.20D-02	0.00045	0.22401
59	60	870.38981	0.20D-02	0.00071	0.35647
58	59	871.69559	0.50D-02	-0.01108	-2.21637
57	58	872.97606	0.20D-02	-0.00313	-1.56365
56	57	874.25797	0.20D-02	-0.00218	-1.0921
55	56	875.53464	0.20D-02	-0.00157	-0.7867
54	55	876.80926	0.20D-02	-0.00452	-2.25787
53	54	878.0704	0.20D-02	0.00042	0.20899
52	53	879.34416	0.10D-01	-0.01288	-1.28833
51	52	880.58492	0.20D-02	0.0012	0.5999
50	51	881.83242	0.50D-02	0.0029	0.57924
49	50	883.07791	0.20D-02	0.00095	0.47745
48	49	884.31428	0.50D-02	0.00248	0.49504
47	48	885.55041	0.20D-02	-0.00142	-0.712
46	47	886.78024	0.20D-02	-0.00471	-2.35678
45	46	887.99874	0.20D-02	-0.00236	-1.18226
44	45	889.21472	0.20D-02	-0.0032	-1.59885
43	44	890.42233	0.20D-02	-0.00137	-0.68716
42	43	891.62193	0.50D-02	0.00274	0.54896
41	42	892.82237	0.20D-02	0.00028	0.13925
40	41	894.01842	0.20D-02	-0.00354	-1.77204
39	40	895.20291	0.20D-02	-0.00156	-0.78205
38	39	896.38245	0.20D-02	-0.00039	-0.19628
37	38	897.55601	0.20D-02	0.00097	0.48471
36	37	898.7261	0.20D-02	0.00001	0.00539
35	36	899.88648	0.50D-02	0.00296	0.59209
34	35	901.06276	0.10D-01	-0.0158	-1.58027
33	34	902.20194	0.20D-02	-0.00328	-1.63987
31	32	904.48412	0.20D-02	0.00041	0.20489
30	31	905.61787	0.20D-02	0.00081	0.40705
29	30	906.75245	0.50D-02	-0.00548	-1.09602
28	29	907.87381	0.20D-02	-0.00442	-2.21205
27	28	908.98175	0.50D-02	0.00415	0.8302

Table A.1, Fourier Transform Infrared Data for ^{70}GeO (cm^{-1}) (*Cont'd*)

J'	J''	Obs	Unc	Calc-Obs	(Calc-Obs)/Unc
26	27	910.1002	0.20D-02	-0.00369	-1.84303
25	26	911.20608	0.20D-02	-0.00487	-2.4332
24	25	912.30064	0.20D-02	-0.00064	-0.32073
23	24	913.38829	0.50D-02	0.00455	0.90954
22	23	914.47126	0.50D-02	0.00847	1.69394
21	22	915.5597	0.20D-02	0.00096	0.48158
20	21	916.63681	0.20D-02	-0.00118	-0.5915
19	20	917.70638	0.20D-02	-0.00176	-0.8801
18	19	918.76862	0.20D-02	-0.00101	-0.50488
17	18	919.82559	0.20D-02	-0.00099	-0.49652
16	17	920.87321	0.20D-02	0.00236	1.17935
15	16	921.90365	0.10D-01	0.01686	1.6864
14	15	922.9597	0.20D-02	-0.00028	-0.13927
13	14	923.99784	0.50D-02	-0.00555	-1.11005
11	12	926.04093	0.20D-02	-0.00112	-0.55852
10	9	946.941	0.20D-02	-0.00472	-2.36036
11	10	947.81851	0.20D-02	-0.00435	-2.17479
12	11	948.68199	0.50D-02	0.0037	0.74019
14	13	950.41128	0.20D-02	-0.00162	-0.80875
16	15	952.10962	0.20D-02	-0.00154	-0.77038
17	16	952.94216	0.50D-02	0.00552	1.10375
18	17	953.79051	0.50D-02	-0.00965	-1.93072
19	18	954.60624	0.20D-02	0.00136	0.68014
20	19	955.42831	0.20D-02	-0.0004	-0.20066
21	20	956.24441	0.20D-02	-0.00266	-1.33025
22	21	957.04759	0.20D-02	0.00153	0.76542
24	23	958.64293	0.20D-02	0.00148	0.73855
25	24	959.43217	0.20D-02	0.00013	0.06404
26	25	960.21587	0.20D-02	-0.0022	-1.09916
27	26	960.99367	0.50D-02	-0.00514	-1.02886
28	27	961.75532	0.20D-02	0.00151	0.75414
29	28	962.51985	0.20D-02	-0.00127	-0.63637
32	31	964.77309	0.50D-02	-0.00871	-1.74168
33	32	965.50273	0.20D-02	-0.00293	-1.46733
34	33	966.22785	0.20D-02	0.00075	0.37739
35	34	966.95349	0.20D-02	-0.00271	-1.35601
36	35	967.67004	0.20D-02	-0.00373	-1.86371
37	36	968.37966	0.20D-02	-0.00446	-2.23172
38	37	969.07821	0.20D-02	-0.00079	-0.39619
39	38	969.77067	0.50D-02	0.00229	0.4587
40	39	970.4682	0.50D-02	-0.00638	-1.2756
41	40	971.14394	0.20D-02	0.00005	0.02541
42	41	971.81949	0.20D-02	-0.00005	-0.02611
43	42	972.48851	0.20D-02	-0.00035	-0.17481
44	43	973.15368	0.20D-02	-0.00353	-1.76675
45	44	973.80786	0.20D-02	-0.00248	-1.23815
46	45	974.45344	0.20D-02	0.00042	0.20977
47	46	975.10185	0.50D-02	-0.00629	-1.25763
48	47	975.72917	0.50D-02	0.00131	0.26164
49	48	976.36996	0.50D-02	-0.01136	-2.27279
50	49	976.97956	0.20D-02	0.00035	0.1765
51	50	977.59264	0.50D-02	0.00176	0.35136
52	51	978.20383	0.20D-02	-0.00179	-0.89265
53	52	978.80582	0.20D-02	-0.00298	-1.48776
54	53	979.40399	0.50D-02	-0.00721	-1.44129
55	54	979.98292	0.50D-02	0.00093	0.18587
56	55	980.56613	0.20D-02	-0.0021	-1.05031
57	56	981.13602	0.50D-02	0.00129	0.25824

Table A.1, Fourier Transform Infrared Data for ^{70}GeO (cm^{-1}) (*Cont'd*)

J'	J''	Obs	Unc	Calc-Obs	(Calc-Obs)/Unc
58	57	981.69782	0.50D-02	0.00586	1.1724
59	58	982.26341	0.20D-02	-0.00027	-0.13528
60	59	982.81619	0.20D-02	-0.00054	-0.26965
61	60	983.3686	0.50D-02	-0.00739	-1.47733
62	61	983.89828	0.50D-02	0.00153	0.30694
63	62	984.43483	0.20D-02	-0.00339	-1.694
65	64	985.49039	0.10D-01	-0.01667	-1.66661
66	65	985.99743	0.10D-01	-0.01308	-1.30768
67	66	986.49725	0.50D-02	-0.00929	-1.85849
68	67	986.98876	0.20D-02	-0.00424	-2.11779
The 7-6 Band, 64 data, $J"_{min} = 14$, $J"_{max} = 64$					
Unc.$_{Avge}$ = 4.3D-03, Unc.$_{Max}$ = 1.0D-02					
(Err/Unc.)$_{Avge}$ = -6.7D-01, RMSR = 1.43					
54	55	868.31278	0.50D-02	-0.0111	-2.22044
53	54	869.56968	0.50D-02	-0.0084	-1.68036
52	53	870.8196	0.20D-02	-0.00434	-2.17056
51	52	872.06499	0.20D-02	-0.00137	-0.68545
50	51	873.30476	0.50D-02	0.00159	0.31757
49	50	874.5494	0.20D-02	-0.00597	-2.98289
48	49	875.77044	0.10D-01	0.00444	0.44372
47	48	876.99231	0.10D-01	0.00834	0.8336
45	46	879.43937	0.20D-02	-0.00422	-2.11164
44	45	880.64407	0.20D-02	-0.0002	-0.10157
43	44	881.84795	0.20D-02	-0.00108	-0.54067
42	43	883.04819	0.20D-02	-0.00404	-2.01934
41	42	884.2273	0.10D-01	0.0084	0.84037
40	41	885.43233	0.50D-02	-0.01082	-2.16307
37	38	888.94532	0.20D-02	-0.00092	-0.46028
36	37	890.10095	0.50D-02	0.00618	1.23691
35	36	891.26633	0.20D-02	-0.00225	-1.12353
34	35	892.42443	0.50D-02	-0.00922	-1.84328
33	34	893.55886	0.50D-02	0.00167	0.33303
32	33	894.69762	0.50D-02	0.00239	0.47733
31	32	895.8385	0.20D-02	-0.00485	-2.42657
30	31	896.96376	0.20D-02	-0.00232	-1.15769
29	30	898.08636	0.20D-02	-0.00299	-1.49564
28	29	899.203	0.20D-02	-0.00358	-1.79102
26	27	901.42545	0.50D-02	-0.0116	-2.32061
25	26	902.50589	0.50D-02	0.00632	1.26487
24	25	903.60732	0.10D-01	-0.00267	-0.2668
23	24	904.70538	0.10D-01	-0.01422	-1.42216
22	23	905.7714	0.20D-02	0.00032	0.16128
21	22	906.84806	0.20D-02	-0.00173	-0.86348
20	21	907.91932	0.20D-02	-0.00433	-2.16571
17	18	911.08414	0.20D-02	0.00088	0.44103
16	17	912.13894	0.50D-02	-0.00925	-1.84914
15	16	913.16578	0.50D-02	0.00257	0.51497
14	15	914.20227	0.20D-02	-0.0013	-0.64886
15	14	942.30197	0.10D-01	0.01503	1.50326
16	15	943.15924	0.20D-02	-0.00238	-1.1905
19	18	945.6372	0.20D-02	0.00076	0.37812
22	21	948.06382	0.20D-02	-0.00275	-1.37496
23	22	948.85433	0.20D-02	0.00151	0.75295
24	23	949.63823	0.50D-02	0.00588	1.17647
27	26	951.96791	0.50D-02	0.00199	0.39709
29	28	953.49016	0.20D-02	-0.00242	-1.20836
32	31	955.71664	0.20D-02	-0.00136	-0.6789

Table A.1, Fourier Transform Infrared Data for ^{70}GeO (cm^{-1}) (*Cont'd*)

J'	J''	Obs	Unc	Calc-Obs	(Calc-Obs)/Unc
33	32	956.44586	0.20D-02	-0.00125	-0.62409
35	34	957.8904	0.50D-02	-0.00697	-1.39435
37	36	959.30603	0.50D-02	-0.01032	-2.06474
40	39	961.3509	0.10D-01	0.01326	1.32597
42	41	962.71561	0.20D-02	-0.00595	-2.9734
45	44	964.67519	0.50D-02	0.00229	0.45881
48	47	966.58099	0.50D-02	0.00351	0.70145
49	48	967.19794	0.10D-01	0.00865	0.86521
51	50	968.42881	0.50D-02	0.00154	0.30754
52	51	969.03542	0.20D-02	-0.00344	-1.71817
53	52	969.62523	0.50D-02	0.00155	0.309
55	54	970.7967	0.20D-02	-0.00093	-0.46307
56	55	971.37875	0.50D-02	-0.00878	-1.75675
57	56	971.94856	0.50D-02	-0.01131	-2.26121
58	57	972.48828	0.10D-01	0.00935	0.93543
60	59	973.6047	0.20D-02	-0.00708	-3.53866
61	60	974.13744	0.20D-02	-0.00023	-0.11729
62	61	974.66794	0.50D-02	0.00189	0.37806
64	63	975.7224	0.50D-02	-0.00824	-1.64881
65	64	976.22523	0.50D-02	0.0006	0.12024

A.2 Fourier Transform Infrared Data for ^{72}GeO

Table A.2: Fourier Transform Infrared Data for ^{72}GeO (cm^{-1})

J'	J''	Obs	Unc	Calc-Obs	(Calc-Obs)/Unc
1,250 ^{72}GeO infrared transitions in 8 bands					
The 1-0 Band, 204 data, $J"_{min}$ = 0, $J"_{max}$ = 103 $Unc._{Avge}$ = 2.0D-03, $Unc._{Max}$ = 2.0D-03 (Err/Unc.)$_{Avge}$ = -1.7D-02, RMSR = 0.49					
99	100	853.81934	0.20D-02	0.00051	0.25717
98	99	855.35207	0.20D-02	0.00008	0.04095
97	98	856.88059	0.20D-02	-0.00127	-0.63564
96	97	858.40193	0.20D-02	-0.00059	-0.29281
95	96	859.91724	0.20D-02	0.00099	0.49444
94	95	861.43212	0.20D-02	-0.00218	-1.08906
93	94	862.93572	0.20D-02	0.00076	0.38158
92	93	864.44001	0.20D-02	-0.00216	-1.07876
91	92	865.93255	0.20D-02	0.00147	0.7348
90	91	867.42425	0.20D-02	0.00073	0.36711
89	90	868.91212	0.20D-02	-0.00138	-0.69195
88	89	870.38981	0.20D-02	0.00146	0.73247
87	88	871.86724	0.20D-02	-0.00067	-0.33473
86	87	873.33775	0.20D-02	-0.00113	-0.56379
85	86	874.80187	0.20D-02	-0.00044	-0.21978
84	85	876.26146	0.20D-02	-0.0005	-0.24791
83	84	877.71478	0.20D-02	0.00044	0.22166
82	83	879.16427	0.20D-02	-0.00007	-0.0363
81	82	880.60811	0.20D-02	-0.00022	-0.11187
80	81	882.04654	0.20D-02	-0.00028	-0.14023
79	80	883.47961	0.20D-02	-0.00029	-0.14668
78	79	884.90699	0.20D-02	0.00006	0.02865
77	78	886.32989	0.20D-02	-0.00044	-0.2194
76	77	887.7468	0.20D-02	-0.0003	-0.15113
75	76	889.15841	0.20D-02	-0.00022	-0.11166
74	75	890.56571	0.20D-02	-0.0012	-0.60129
73	74	891.96544	0.20D-02	0.00002	0.00983
72	73	893.36089	0.20D-02	0.00012	0.06145
71	72	894.75096	0.20D-02	0.00021	0.10332
70	71	896.13608	0.20D-02	-0.00017	-0.0848
69	70	897.51564	0.20D-02	-0.0004	-0.19814
68	69	898.88906	0.20D-02	0.00008	0.03808
67	68	900.25767	0.20D-02	-0.00008	-0.04148
66	67	901.62047	0.20D-02	0.00013	0.063
65	66	902.97849	0.20D-02	-0.00036	-0.17883
64	65	904.32962	0.20D-02	0.00058	0.28785
63	64	905.67648	0.20D-02	0.0003	0.14771
62	63	907.01624	0.20D-02	0.00163	0.81547
61	62	908.35438	0.20D-02	-0.00093	-0.46417
60	61	909.68338	0.20D-02	0.00014	0.06849
59	60	911.00797	0.20D-02	0.00009	0.04316
58	59	912.32643	0.20D-02	0.00064	0.31957
57	58	913.64037	0.20D-02	0.00015	0.07732
56	57	914.94616	0.20D-02	0.00226	1.13117
55	56	916.24969	0.20D-02	0.00106	0.53071
54	55	917.54736	0.20D-02	0.00014	0.07069
53	54	918.83907	0.20D-02	-0.0004	-0.19926
52	53	920.12402	0.20D-02	0.00021	0.1055

Table A.2, Fourier Transform Infrared Data for ^{72}GeO (cm^{-1}) (*Cont'd*)

J'	J''	Obs	Unc	Calc-Obs	(Calc-Obs)/Unc
51	52	921.40398	0.20D-02	0.0002	0.09963
50	51	922.67854	0.20D-02	-0.00003	-0.01724
49	50	923.94682	0.20D-02	0.00039	0.19454
48	49	925.21255	0.20D-02	-0.00229	-1.14536
47	48	926.46678	0.20D-02	0.00088	0.43759
46	47	927.71914	0.20D-02	0.00025	0.12311
45	46	928.9655	0.20D-02	-0.00005	-0.02424
44	45	930.20555	0.20D-02	0.00027	0.13509
43	44	931.44046	0.20D-02	0.00003	0.0158
42	43	932.66963	0.20D-02	-0.00018	-0.08756
41	42	933.89271	0.20D-02	0.0	-0.00036
40	41	935.11039	0.20D-02	-0.00017	-0.08312
39	40	936.32161	0.20D-02	0.00039	0.19379
38	39	937.52856	0.20D-02	-0.00054	-0.27002
37	38	938.72824	0.20D-02	0.00004	0.01991
36	37	939.92295	0.20D-02	-0.00017	-0.08676
35	36	941.11134	0.20D-02	0.00014	0.06946
34	35	942.29456	0.20D-02	-0.00017	-0.08688
33	34	943.47146	0.20D-02	0.00003	0.01375
32	33	944.64273	0.20D-02	0.00005	0.02588
31	32	945.80801	0.20D-02	0.00023	0.11403
30	31	946.96908	0.20D-02	-0.00122	-0.61229
29	30	948.12124	0.20D-02	0.00038	0.19148
28	29	949.27041	0.20D-02	-0.00088	-0.44025
27	28	950.41075	0.20D-02	0.00082	0.4121
26	27	951.54431	0.20D-02	0.00342	1.70798
25	26	952.67737	0.20D-02	0.00061	0.30681
24	25	953.80239	0.20D-02	-0.00005	-0.02683
23	24	954.92094	0.20D-02	-0.00017	-0.08346
22	23	956.03358	0.20D-02	-0.00029	-0.14375
21	22	957.13981	0.20D-02	0.00005	0.02683
20	21	958.24061	0.20D-02	-0.00012	-0.06223
19	20	959.33576	0.20D-02	-0.00061	-0.30659
18	19	960.42367	0.20D-02	0.00018	0.08828
17	18	961.50629	0.20D-02	0.00026	0.1317
16	17	962.58348	0.20D-02	-0.00021	-0.1068
15	16	963.65463	0.20D-02	-0.00066	-0.32787
14	15	964.71917	0.20D-02	-0.0005	-0.25209
13	14	965.77706	0.20D-02	0.00028	0.13998
12	13	966.83027	0.20D-02	-0.0003	-0.15238
11	12	967.87695	0.20D-02	-0.00041	-0.20472
10	11	968.91725	0.20D-02	-0.0002	-0.09762
9	10	969.95154	0.20D-02	-0.00004	-0.02177
8	9	970.97898	0.20D-02	0.00087	0.43716
7	8	971.9997	0.20D-02	0.00243	1.21361
6	7	973.01865	0.20D-02	-0.00037	-0.18312
5	6	974.02599	0.20D-02	0.00233	1.16631
4	5	975.03504	0.20D-02	-0.00281	-1.40371
3	4	976.03008	0.20D-02	-0.00008	-0.03897
2	3	977.02164	0.20D-02	-0.00001	-0.00508
1	2	978.00652	0.20D-02	0.00056	0.2823
0	1	978.98752	0.20D-02	-0.00116	-0.57757
1	0	980.92455	0.20D-02	0.00181	0.90313
2	1	981.88698	0.20D-02	0.00007	0.03726
3	2	982.8414	0.20D-02	0.00012	0.06128
4	3	983.79196	0.20D-02	-0.0022	-1.10055
5	4	984.7315	0.20D-02	0.00025	0.12604
6	5	985.66556	0.20D-02	0.00193	0.96534

Table A.2, Fourier Transform Infrared Data for ^{72}GeO (cm^{-1}) (*Cont'd*)

J'	J''	Obs	Unc	Calc-Obs	(Calc-Obs)/Unc
7	6	986.5981	0.20D-02	-0.00114	-0.56845
8	7	987.52122	0.20D-02	-0.00105	-0.52616
9	8	988.43593	0.20D-02	0.00114	0.57156
10	9	989.34915	0.20D-02	-0.00147	-0.73614
11	10	990.25098	0.20D-02	0.00099	0.49497
12	11	991.15033	0.20D-02	-0.00039	-0.19592
13	12	992.04182	0.20D-02	-0.00025	-0.12456
14	13	992.92721	0.20D-02	-0.00034	-0.17185
15	14	993.80467	0.20D-02	0.00112	0.56147
16	15	994.67845	0.20D-02	-0.0001	-0.05051
17	16	995.54454	0.20D-02	-0.00002	-0.00853
18	17	996.40473	0.20D-02	-0.00043	-0.21349
19	18	997.25778	0.20D-02	-0.0001	-0.05123
20	19	998.10396	0.20D-02	0.00068	0.34239
21	20	998.9453	0.20D-02	-0.00013	-0.06345
22	21	999.77952	0.20D-02	-0.00026	-0.12972
23	22	1000.60685	0.20D-02	0.00005	0.02284
24	23	1001.42816	0.20D-02	-0.00009	-0.04705
25	24	1002.24312	0.20D-02	-0.00036	-0.1795
26	25	1003.0504	0.20D-02	0.00057	0.28358
27	26	1003.85276	0.20D-02	-0.00008	-0.03771
28	27	1004.64786	0.20D-02	0.00002	0.0097
29	28	1005.43286	0.20D-02	0.00369	1.84588
30	29	1006.21862	0.20D-02	0.00007	0.03389
31	30	1006.9943	0.20D-02	-0.00002	-0.01122
32	31	1007.76334	0.20D-02	-0.00003	-0.01641
33	32	1008.52775	0.20D-02	-0.00198	-0.99164
34	33	1009.27838	0.20D-02	0.00327	1.63662
35	34	1010.03094	0.20D-02	-0.00001	-0.00311
36	35	1010.77345	0.20D-02	0.00016	0.07918
37	36	1011.50935	0.20D-02	0.00031	0.15648
38	37	1012.24002	0.20D-02	-0.00093	-0.4662
39	38	1012.96184	0.20D-02	0.00003	0.01462
40	39	1013.67778	0.20D-02	0.00021	0.10741
41	40	1014.38729	0.20D-02	0.00017	0.08715
42	41	1015.09007	0.20D-02	0.00017	0.0873
43	42	1015.78393	0.20D-02	0.0024	1.20179
44	43	1016.47559	0.20D-02	0.00013	0.06409
45	44	1017.15784	0.20D-02	0.00055	0.27412
46	45	1017.83411	0.20D-02	0.00022	0.11031
47	46	1018.50374	0.20D-02	-0.00021	-0.10393
48	47	1019.16922	0.20D-02	-0.00323	-1.61368
49	48	1019.82147	0.20D-02	0.00021	0.10445
50	49	1020.47042	0.20D-02	0.00017	0.08435
51	50	1021.11076	0.20D-02	0.00195	0.97491
52	51	1021.74804	0.20D-02	-0.00001	-0.0055
53	52	1022.37653	0.20D-02	0.00001	0.00298
54	53	1022.99793	0.20D-02	0.00029	0.14372
55	54	1023.61281	0.20D-02	0.00025	0.12555
56	55	1024.22068	0.20D-02	0.00037	0.18731
57	56	1024.82189	0.20D-02	0.00031	0.15284
58	57	1025.41637	0.20D-02	0.00008	0.04095
59	58	1026.00376	0.20D-02	0.00006	0.02995
60	59	1026.58402	0.20D-02	0.00027	0.13465
61	60	1027.15755	0.20D-02	0.0003	0.14834
62	61	1027.72537	0.20D-02	-0.00089	-0.44519
63	62	1028.28441	0.20D-02	-0.00023	-0.11718
64	63	1028.83682	0.20D-02	0.0001	0.05115

Table A.2, Fourier Transform Infrared Data for ^{72}GeO (cm^{-1}) (*Cont'd*)

J'	J''	Obs	Unc	Calc-Obs	(Calc-Obs)/Unc
65	64	1029.38408	0.20D-02	-0.00137	-0.68644
66	65	1029.92126	0.20D-02	0.00026	0.12878
67	66	1030.45569	0.20D-02	-0.00234	-1.16944
68	67	1030.9784	0.20D-02	-0.00022	-0.11237
69	68	1031.49624	0.20D-02	-0.00025	-0.12629
70	69	1032.00677	0.20D-02	0.00001	0.00251
71	70	1032.51066	0.20D-02	-0.00013	-0.06727
72	71	1033.00747	0.20D-02	-0.00024	-0.12194
73	72	1033.49678	0.20D-02	0.00008	0.04219
74	73	1033.97983	0.20D-02	-0.0004	-0.20121
75	74	1034.45545	0.20D-02	-0.00055	-0.27298
76	75	1034.92263	0.20D-02	0.00065	0.32455
77	76	1035.38387	0.20D-02	0.00067	0.33551
78	77	1035.83903	0.20D-02	-0.00034	-0.17146
79	78	1036.28548	0.20D-02	0.0002	0.10227
80	79	1036.72801	0.20D-02	-0.00248	-1.23969
81	80	1037.15767	0.20D-02	0.00054	0.27178
82	81	1037.58497	0.20D-02	-0.00125	-0.62572
83	82	1038.00127	0.20D-02	0.00076	0.38188
84	83	1038.41373	0.20D-02	-0.00058	-0.29183
85	84	1038.81841	0.20D-02	-0.00137	-0.68328
86	85	1039.21403	0.20D-02	-0.00032	-0.15841
87	86	1039.60442	0.20D-02	-0.00128	-0.63967
88	87	1039.98584	0.20D-02	-0.00053	-0.26303
89	88	1040.36079	0.20D-02	-0.00057	-0.28444
90	89	1040.7287	0.20D-02	-0.00084	-0.42139
91	90	1041.08769	0.20D-02	0.0005	0.25012
92	91	1041.44284	0.20D-02	-0.00162	-0.81088
93	92	1041.78743	0.20D-02	-0.0005	-0.25193
94	93	1042.12685	0.20D-02	-0.00155	-0.77402
95	94	1042.45453	0.20D-02	0.0018	0.9018
96	95	1042.78051	0.20D-02	-0.0005	-0.252
97	96	1043.09597	0.20D-02	0.00034	0.16853
98	97	1043.40539	0.20D-02	-0.00017	-0.08266
99	98	1043.70679	0.20D-02	-0.00005	-0.02315
100	99	1044.00164	0.20D-02	-0.00079	-0.39351
101	100	1044.28591	0.20D-02	0.00163	0.81368
102	101	1044.56719	0.20D-02	-0.0004	-0.2022
103	102	1044.83971	0.20D-02	-0.00113	-0.56374
104	103	1045.1042	0.20D-02	-0.00128	-0.64157
The 2-1 Band, 191 data, $J"_{min} = 1$, $J"_{max} = 97$					
Unc.$_{Avge}$ = 2.0D-03, Unc.$_{Max}$ = 2.0D-03					
(Err/Unc.)$_{Avge}$ = -8.9D-02, RMSR = 0.48					
94	95	853.10021	0.20D-02	-0.00001	-0.00329
93	94	854.6005	0.20D-02	-0.00047	-0.2363
92	93	856.09433	0.20D-02	0.00034	0.16787
91	92	857.58444	0.20D-02	-0.00032	-0.1609
90	91	859.06983	0.20D-02	-0.00145	-0.72276
89	90	860.54812	0.20D-02	-0.00069	-0.34285
88	89	862.02301	0.20D-02	-0.00174	-0.87127
87	88	863.48977	0.20D-02	0.0001	0.05172
86	87	864.95332	0.20D-02	-0.00007	-0.03393
85	86	866.41102	0.20D-02	0.00035	0.17656
84	85	867.8651	0.20D-02	-0.00086	-0.43198
83	84	869.31134	0.20D-02	0.00049	0.24527
82	83	870.75215	0.20D-02	0.00201	1.00314
81	82	872.19118	0.20D-02	0.0	0.00143

Table A.2, Fourier Transform Infrared Data for ^{72}GeO (cm^{-1}) (*Cont'd*)

J'	J''	Obs	Unc	Calc-Obs	(Calc-Obs)/Unc
80	81	873.62415	0.20D-02	-0.00124	-0.62004
79	80	875.05179	0.20D-02	-0.00245	-1.22648
78	79	876.46979	0.20D-02	0.00064	0.32197
77	78	877.88533	0.20D-02	0.00087	0.435
76	77	879.29643	0.20D-02	0.00019	0.0975
75	76	880.7015	0.20D-02	0.00021	0.10419
74	75	882.1023	0.20D-02	-0.00088	-0.44015
73	74	883.49764	0.20D-02	-0.00188	-0.9408
72	73	884.8844	0.20D-02	0.00031	0.15715
71	72	886.26859	0.20D-02	-0.0003	-0.15167
70	71	887.646	0.20D-02	0.00045	0.22251
69	70	889.01915	0.20D-02	0.00004	0.01947
68	69	890.38732	0.20D-02	-0.00081	-0.40602
67	68	891.74832	0.20D-02	0.00008	0.04068
66	67	893.10485	0.20D-02	-0.00001	-0.00559
65	66	894.45593	0.20D-02	-0.00011	-0.05517
64	65	895.80145	0.20D-02	-0.00012	-0.05832
63	64	897.14212	0.20D-02	-0.00074	-0.3704
62	63	898.47629	0.20D-02	-0.00036	-0.18154
61	62	899.80492	0.20D-02	0.00006	0.02781
60	61	901.1285	0.20D-02	0.00001	0.00739
59	60	902.44719	0.20D-02	-0.00065	-0.3231
58	59	903.75918	0.20D-02	-0.00015	-0.07393
57	58	905.06654	0.20D-02	-0.00056	-0.28053
56	57	906.36761	0.20D-02	-0.00024	-0.11812
55	56	907.66273	0.20D-02	0.00049	0.24291
54	55	908.9541	0.20D-02	-0.00063	-0.31278
53	54	910.23837	0.20D-02	-0.00022	-0.11053
52	53	911.5176	0.20D-02	-0.00037	-0.1857
51	52	912.79064	0.20D-02	0.00007	0.03636
50	51	914.05854	0.20D-02	0.00003	0.01528
49	50	915.32079	0.20D-02	0.00001	0.00574
48	49	916.57835	0.20D-02	-0.00096	-0.47774
47	48	917.82768	0.20D-02	0.00067	0.33455
46	47	919.07283	0.20D-02	0.0008	0.40219
45	46	920.31335	0.20D-02	-0.0001	-0.05028
44	45	921.54716	0.20D-02	0.00002	0.01185
43	44	922.77516	0.20D-02	0.00027	0.1331
42	43	923.99784	0.20D-02	0.00014	0.06813
41	42	925.21255	0.20D-02	0.00225	1.1264
40	41	926.42393	0.20D-02	0.00198	0.98754
39	40	927.63146	0.20D-02	-0.00019	-0.09383
38	39	928.83114	0.20D-02	-0.00024	-0.11826
37	38	930.02499	0.20D-02	-0.00022	-0.11109
36	37	931.21023	0.20D-02	0.00263	1.31717
35	36	932.39531	0.20D-02	-0.00013	-0.06393
34	35	933.57181	0.20D-02	-0.0001	-0.04986
33	34	934.7424	0.20D-02	0.00005	0.0239
32	33	935.90773	0.20D-02	-0.00037	-0.18312
31	32	937.06699	0.20D-02	-0.00053	-0.26641
30	31	938.21976	0.20D-02	-0.00004	-0.02141
29	30	939.36732	0.20D-02	-0.00018	-0.08873
28	29	940.51081	0.20D-02	-0.00211	-1.05377
27	28	941.64416	0.20D-02	0.00024	0.11791
26	27	942.77484	0.20D-02	-0.00063	-0.31421
25	26	943.90056	0.20D-02	-0.00242	-1.21066
24	25	945.01496	0.20D-02	0.00122	0.60803
23	24	946.12837	0.20D-02	-0.00008	-0.03868

Table A.2, Fourier Transform Infrared Data for ^{72}GeO (cm^{-1}) (*Cont'd*)

J'	J''	Obs	Unc	Calc-Obs	(Calc-Obs)/Unc
22	23	947.2347	0.20D-02	-0.00021	-0.10635
21	22	948.33623	0.20D-02	-0.00148	-0.74046
20	21	949.4291	0.20D-02	-0.00003	-0.01669
19	20	950.51792	0.20D-02	-0.00048	-0.24051
18	19	951.60187	0.20D-02	-0.00204	-1.01752
17	18	952.67737	0.20D-02	-0.00112	-0.55838
16	17	953.7466	0.20D-02	0.00008	0.04148
15	16	954.81102	0.20D-02	0.00009	0.04633
14	15	955.86959	0.20D-02	-0.00005	-0.0244
13	14	956.9213	0.20D-02	0.00064	0.31868
12	13	957.96861	0.20D-02	-0.00031	-0.15499
11	12	959.00946	0.20D-02	-0.00084	-0.42114
10	11	960.04467	0.20D-02	-0.00179	-0.8953
9	10	961.0701	0.20D-02	0.00098	0.49185
8	9	962.09318	0.20D-02	0.00002	0.00966
7	8	963.10904	0.20D-02	0.00018	0.09247
6	7	964.11922	0.20D-02	-0.00007	-0.03537
5	6	965.12204	0.20D-02	0.00092	0.46046
4	5	966.12045	0.20D-02	0.00021	0.10429
3	4	967.11238	0.20D-02	-0.00017	-0.0845
2	3	968.10052	0.20D-02	-0.0029	-1.45172
1	2	969.07821	0.20D-02	-0.00135	-0.67295
2	1	972.93166	0.20D-02	0.00039	0.19726
3	2	973.87956	0.20D-02	0.00078	0.38998
4	3	974.82411	0.20D-02	-0.00171	-0.85565
5	4	975.76139	0.20D-02	-0.00317	-1.58549
6	5	976.68849	0.20D-02	-0.00069	-0.34519
7	6	977.61229	0.20D-02	-0.00118	-0.59061
8	7	978.53001	0.20D-02	-0.00186	-0.93244
9	8	979.43901	0.20D-02	-0.00011	-0.05649
10	9	980.34316	0.20D-02	0.00019	0.09644
11	10	981.24194	0.20D-02	-0.00044	-0.21939
12	11	982.13358	0.20D-02	-0.00024	-0.11988
13	12	983.0197	0.20D-02	-0.00086	-0.4308
14	13	983.89828	0.20D-02	-0.00029	-0.14291
15	14	984.77183	0.20D-02	-0.00103	-0.51709
16	15	985.63752	0.20D-02	-0.00029	-0.14423
17	16	986.49725	0.20D-02	0.00004	0.01993
18	17	987.35092	0.20D-02	0.00005	0.0245
19	18	988.19802	0.20D-02	0.00022	0.10866
20	19	989.03918	0.20D-02	-0.00009	-0.04355
21	20	989.87448	0.20D-02	-0.00096	-0.47795
22	21	990.69834	0.20D-02	0.00318	1.58961
23	22	991.52298	0.20D-02	0.00009	0.04316
24	23	992.33832	0.20D-02	-0.00017	-0.08311
25	24	993.14711	0.20D-02	-0.00033	-0.16515
26	25	993.94828	0.20D-02	0.00063	0.31613
27	26	994.74481	0.20D-02	-0.00026	-0.13021
28	27	995.53353	0.20D-02	0.00015	0.07497
29	28	996.31623	0.20D-02	0.00006	0.03061
30	29	997.09245	0.20D-02	-0.00008	-0.03917
31	30	997.86199	0.20D-02	-0.00007	-0.03528
32	31	998.62277	0.20D-02	0.00213	1.06627
33	32	999.38143	0.20D-02	-0.00011	-0.0555
34	33	1000.13127	0.20D-02	-0.00011	-0.05647
35	34	1000.8742	0.20D-02	0.0002	0.10187
36	35	1001.61098	0.20D-02	0.00007	0.03444
37	36	1002.34102	0.20D-02	0.00006	0.02972

Table A.2, Fourier Transform Infrared Data for ^{72}GeO (cm^{-1}) (*Cont'd*)

J'	J''	Obs	Unc	Calc-Obs	(Calc-Obs)/Unc
38	37	1003.06466	0.20D-02	-0.00017	-0.0838
39	38	1003.78115	0.20D-02	0.00011	0.05385
40	39	1004.49013	0.20D-02	0.00124	0.62115
41	40	1005.19516	0.20D-02	-0.00034	-0.16844
42	41	1005.89201	0.20D-02	-0.00041	-0.20497
43	42	1006.58167	0.20D-02	0.00002	0.01
44	43	1007.26516	0.20D-02	-0.00008	-0.04008
45	44	1007.94152	0.20D-02	0.00024	0.11969
46	45	1008.6118	0.20D-02	-0.00007	-0.03724
47	46	1009.27838	0.20D-02	-0.00343	-1.71699
48	47	1009.93137	0.20D-02	0.00005	0.02386
49	48	1010.58254	0.20D-02	-0.00141	-0.7048
50	49	1011.22471	0.20D-02	-0.00064	-0.3196
51	50	1011.86053	0.20D-02	-0.0003	-0.15165
52	51	1012.48959	0.20D-02	0.0	-0.00209
53	52	1013.1121	0.20D-02	0.00003	0.01744
54	53	1013.72775	0.20D-02	0.00012	0.06178
55	54	1014.33645	0.20D-02	0.00032	0.15927
56	55	1014.94006	0.20D-02	-0.00124	-0.62124
57	56	1015.53417	0.20D-02	-0.00016	-0.08096
58	57	1016.12258	0.20D-02	-0.00025	-0.12605
59	58	1016.70373	0.20D-02	0.00003	0.01728
60	59	1017.27825	0.20D-02	0.00006	0.02783
61	60	1017.8475	0.20D-02	-0.00156	-0.78062
62	61	1018.40673	0.20D-02	-0.00008	-0.03929
63	62	1018.9607	0.20D-02	-0.00027	-0.13441
64	63	1019.50721	0.20D-02	0.00006	0.02777
65	64	1020.04853	0.20D-02	-0.00138	-0.68899
66	65	1020.57968	0.20D-02	0.00038	0.18905
67	66	1021.10597	0.20D-02	0.00001	0.00561
68	67	1021.62401	0.20D-02	0.0009	0.44942
69	68	1022.13756	0.20D-02	-0.00073	-0.3658
70	69	1022.64211	0.20D-02	-0.00038	-0.19137
71	70	1023.13972	0.20D-02	-0.00013	-0.06357
72	71	1023.63092	0.20D-02	-0.00051	-0.25373
73	72	1024.11431	0.20D-02	-0.00014	-0.06816
74	73	1024.59124	0.20D-02	-0.00037	-0.18322
75	74	1025.06046	0.20D-02	0.00002	0.00978
76	75	1025.5227	0.20D-02	0.00029	0.14446
77	76	1025.97788	0.20D-02	0.00051	0.25447
78	77	1026.42683	0.20D-02	-0.00016	-0.08106
79	78	1026.86778	0.20D-02	0.00003	0.01549
80	79	1027.30257	0.20D-02	-0.00076	-0.38178
81	80	1027.72537	0.20D-02	0.00327	1.63574
82	81	1028.14786	0.20D-02	0.00044	0.22163
83	82	1028.55992	0.20D-02	0.00086	0.42999
84	83	1028.96593	0.20D-02	0.00013	0.06338
85	84	1029.36298	0.20D-02	0.00114	0.57085
86	85	1029.75538	0.20D-02	-0.00042	-0.20902
87	86	1030.1392	0.20D-02	-0.00063	-0.31721
88	87	1030.5154	0.20D-02	-0.00047	-0.23618
89	88	1030.88634	0.20D-02	-0.00232	-1.16191
90	89	1031.24495	0.20D-02	0.00088	0.43962
91	90	1031.60106	0.20D-02	-0.00071	-0.35409
92	91	1031.94855	0.20D-02	-0.00098	-0.48905
93	92	1032.2877	0.20D-02	-0.00022	-0.11127
94	93	1032.62126	0.20D-02	-0.00121	-0.60328
95	94	1032.9462	0.20D-02	-0.00091	-0.45611

Table A.2, Fourier Transform Infrared Data for ^{72}GeO (cm^{-1}) (*Cont'd*)

J'	J''	Obs	Unc	Calc-Obs	(Calc-Obs)/Unc
96	95	1033.2637	0.20D-02	-0.00053	-0.26581
97	96	1033.57374	0.20D-02	-0.00006	-0.02993
98	97	1033.87445	0.20D-02	0.00236	1.18096
The 3-2 Band, 190 data, $J"_{min} = 0$, $J"_{max} = 96$					
Unc.$_{Avge}$ = 2.0D-03, Unc.$_{Max}$ = 5.0D-03					
(Err/Unc.)$_{Avge}$ = -8.4D-02, RMSR = 0.59					
94	95	844.79842	0.20D-02	-0.00128	-0.63944
93	94	846.29119	0.20D-02	-0.00095	-0.47351
92	93	847.77777	0.20D-02	0.00041	0.20273
91	92	849.26061	0.20D-02	0.00033	0.16412
90	91	850.73894	0.20D-02	-0.00044	-0.21942
89	90	852.21134	0.20D-02	-0.00048	-0.23816
88	89	853.67742	0.20D-02	0.00061	0.30286
87	88	855.14018	0.20D-02	-0.00022	-0.11163
86	87	856.59547	0.20D-02	0.00119	0.5933
85	86	858.04949	0.20D-02	-0.00138	-0.68757
84	85	859.49606	0.20D-02	-0.00173	-0.86442
83	84	860.93511	0.20D-02	0.00017	0.08257
82	83	862.37005	0.20D-02	0.0009	0.44821
81	82	863.80156	0.20D-02	-0.00023	-0.11263
80	81	865.22667	0.20D-02	-0.00023	-0.11528
79	80	866.64581	0.20D-02	0.00042	0.21014
78	79	868.0608	0.20D-02	-0.00009	-0.04656
77	78	869.46924	0.20D-02	0.00063	0.31438
76	77	870.87406	0.20D-02	-0.00037	-0.18733
75	76	872.27326	0.20D-02	-0.0011	-0.55181
74	75	873.66574	0.20D-02	-0.00047	-0.23433
73	74	875.05179	0.20D-02	0.00124	0.61985
72	73	876.43568	0.20D-02	-0.00028	-0.1395
71	72	877.81298	0.20D-02	-0.0006	-0.29758
70	71	879.18579	0.20D-02	-0.00182	-0.90974
69	70	880.54997	0.20D-02	0.00019	0.09385
68	69	881.91104	0.20D-02	-0.00012	-0.06216
67	68	883.26626	0.20D-02	-0.00002	-0.00796
66	67	884.61606	0.20D-02	0.00007	0.03613
65	66	885.96043	0.20D-02	0.00015	0.07478
64	65	887.29993	0.20D-02	-0.00037	-0.18719
63	64	888.63442	0.20D-02	-0.00136	-0.68015
62	63	889.96122	0.20D-02	-0.00014	-0.06932
61	62	891.28383	0.20D-02	-0.00021	-0.10513
60	61	892.60228	0.20D-02	-0.00164	-0.81783
59	60	893.91277	0.20D-02	-0.00062	-0.30769
58	59	895.21801	0.20D-02	0.00013	0.06487
57	58	896.52057	0.20D-02	-0.00197	-0.98539
56	57	897.81244	0.20D-02	0.00106	0.53115
55	56	899.10419	0.20D-02	-0.00134	-0.67085
54	55	900.38798	0.20D-02	-0.00135	-0.67674
53	54	901.66532	0.20D-02	-0.00048	-0.24187
52	53	902.93765	0.20D-02	-0.0002	-0.10161
51	52	904.2048	0.20D-02	-0.00034	-0.17131
50	51	905.46597	0.20D-02	-0.00011	-0.05631
49	50	906.72107	0.20D-02	0.00057	0.28292
48	49	907.97216	0.20D-02	-0.00037	-0.1839
47	48	909.21538	0.20D-02	0.00092	0.45778
46	47	910.45536	0.20D-02	-0.00021	-0.10743
45	46	911.68844	0.20D-02	-0.00011	-0.05493
44	45	912.91618	0.20D-02	-0.00033	-0.16514

Table A.2, Fourier Transform Infrared Data for ^{72}GeO (cm^{-1}) (*Cont'd*)

J'	J''	Obs	Unc	Calc-Obs	(Calc-Obs)/Unc
43	44	914.13709	0.20D-02	0.00058	0.29153
42	43	915.35435	0.20D-02	-0.00055	-0.27535
41	42	916.56445	0.20D-02	-0.00023	-0.1162
40	41	917.76865	0.20D-02	0.00028	0.1386
39	40	918.96832	0.20D-02	-0.00042	-0.21146
38	39	920.16172	0.20D-02	-0.00059	-0.29686
37	38	921.34855	0.20D-02	0.00005	0.02704
36	37	922.53054	0.20D-02	-0.00022	-0.11028
35	36	923.70636	0.20D-02	-0.00009	-0.04427
34	35	924.87977	0.20D-02	-0.00334	-1.67042
33	34	926.0419	0.20D-02	-0.00111	-0.5542
32	33	927.19915	0.20D-02	0.0002	0.09895
31	32	928.35243	0.20D-02	-0.00033	-0.16657
30	31	929.49934	0.20D-02	-0.00033	-0.16615
29	30	930.63978	0.20D-02	0.0003	0.1496
28	29	931.77585	0.20D-02	-0.00055	-0.27474
27	28	932.90321	0.20D-02	0.00145	0.72526
26	27	934.02971	0.20D-02	-0.00155	-0.77592
25	26	935.14677	0.20D-02	-0.00101	-0.50382
24	25	936.25756	0.20D-02	-0.00009	-0.04398
23	24	937.36309	0.20D-02	0.00019	0.09311
22	23	938.46263	0.20D-02	0.00053	0.26679
21	22	939.55701	0.20D-02	0.00012	0.06159
20	21	940.6447	0.20D-02	0.00045	0.22685
19	20	941.72745	0.20D-02	-0.00023	-0.11291
18	19	942.80148	0.20D-02	0.00185	0.92669
17	18	943.87387	0.20D-02	-0.0004	-0.19995
16	17	944.93735	0.20D-02	0.00028	0.14158
15	16	945.9962	0.20D-02	-0.00041	-0.20433
14	15	947.0481	0.20D-02	-0.00016	-0.07824
13	14	948.09266	0.20D-02	0.00142	0.70913
12	13	949.13384	0.20D-02	0.00034	0.17227
11	12	950.16758	0.20D-02	0.00068	0.34044
10	11	951.19536	0.20D-02	0.00092	0.45809
9	10	952.21924	0.20D-02	-0.00101	-0.50545
8	9	953.23426	0.20D-02	-0.00015	-0.07586
7	8	954.24413	0.20D-02	-0.00023	-0.11379
6	7	955.24878	0.20D-02	-0.00117	-0.5849
5	6	956.24627	0.20D-02	-0.00107	-0.53483
4	5	957.23431	0.20D-02	0.00236	1.18065
3	4	958.22194	0.20D-02	0.00007	0.03594
2	3	959.20757	0.50D-02	-0.00636	-1.2719
1	2	960.17076	0.50D-02	0.0035	0.69919
1	0	963.04771	0.50D-02	0.00866	1.7317
3	2	964.94476	0.20D-02	0.00203	1.01696
4	3	965.8824	0.20D-02	0.00029	0.14471
5	4	966.81008	0.20D-02	0.00226	1.13064
6	5	967.73512	0.20D-02	0.00063	0.31407
7	6	968.66194	0.50D-02	-0.00904	-1.80832
8	7	969.56523	0.20D-02	-0.00145	-0.72477
9	8	970.4682	0.20D-02	0.00018	0.09138
10	9	971.36765	0.20D-02	-0.00095	-0.47314
11	10	972.25828	0.20D-02	0.00043	0.2159
12	11	973.14529	0.20D-02	-0.00088	-0.44239
13	12	974.02596	0.20D-02	-0.00219	-1.09378
14	13	974.89718	0.20D-02	-0.00038	-0.18906
15	14	975.76139	0.20D-02	0.00209	1.04589
16	15	976.62442	0.20D-02	-0.00061	-0.30477

Table A.2, Fourier Transform Infrared Data for ^{72}GeO (cm^{-1}) (*Cont'd*)

J'	J''	Obs	Unc	Calc-Obs	(Calc-Obs)/Unc
17	16	977.47863	0.20D-02	-0.00087	-0.43688
18	17	978.32437	0.20D-02	0.00095	0.47368
19	18	979.16645	0.20D-02	0.00003	0.01607
20	19	980.00091	0.20D-02	0.00033	0.16445
21	20	980.83105	0.20D-02	-0.00147	-0.73716
22	21	981.65186	0.20D-02	-0.00038	-0.18954
23	22	982.46559	0.20D-02	0.00136	0.68135
24	23	983.27444	0.20D-02	0.00152	0.75961
25	24	984.07772	0.20D-02	0.00078	0.38933
26	25	984.87461	0.20D-02	-0.00005	-0.02542
27	26	985.66556	0.20D-02	-0.00143	-0.71557
28	27	986.44722	0.20D-02	-0.00002	-0.01204
29	28	987.22372	0.20D-02	0.00004	0.01925
30	29	987.9938	0.20D-02	-0.00002	-0.00775
31	30	988.75719	0.20D-02	0.00008	0.04111
32	31	989.51429	0.20D-02	-0.00008	-0.0402
33	32	990.26433	0.20D-02	0.00025	0.12735
34	33	991.0049	0.50D-02	0.00349	0.6971
35	34	991.74533	0.20D-02	0.00027	0.13503
36	35	992.47648	0.20D-02	-0.00026	-0.13178
37	36	993.2001	0.20D-02	0.00013	0.06621
38	37	993.91761	0.20D-02	0.00001	0.00308
39	38	994.6248	0.50D-02	0.00357	0.71308
40	39	995.33299	0.20D-02	-0.00052	-0.26086
41	40	996.02976	0.20D-02	0.00015	0.07629
42	41	996.7209	0.20D-02	-0.00021	-0.10689
43	42	997.40306	0.20D-02	0.00172	0.85856
44	43	998.08239	0.20D-02	-0.00021	-0.1035
45	44	998.75206	0.20D-02	0.00081	0.40588
46	45	999.41739	0.20D-02	-0.00055	-0.27434
47	46	1000.07433	0.20D-02	-0.00025	-0.12525
48	47	1000.72502	0.20D-02	-0.00045	-0.22296
49	48	1001.36923	0.20D-02	-0.00092	-0.45913
50	49	1002.01146	0.50D-02	-0.00618	-1.23556
51	50	1002.63615	0.20D-02	-0.00068	-0.33888
52	51	1003.25927	0.20D-02	-0.00039	-0.19523
53	52	1003.8778	0.20D-02	-0.00233	-1.1641
54	53	1004.48999	0.50D-02	-0.00474	-0.94865
55	54	1005.0974	0.50D-02	-0.00921	-1.84181
56	55	1005.68718	0.20D-02	-0.00289	-1.44291
57	56	1006.27351	0.20D-02	0.00003	0.01648
58	57	1006.85667	0.20D-02	-0.00075	-0.37252
59	58	1007.4309	0.20D-02	0.00053	0.26387
60	59	1008.00071	0.20D-02	-0.00067	-0.33555
61	60	1008.56201	0.20D-02	-0.00026	-0.13201
62	61	1009.11705	0.20D-02	-0.0005	-0.25175
63	62	1009.66488	0.20D-02	-0.00047	-0.23599
64	63	1010.20548	0.20D-02	-0.00015	-0.07598
65	64	1010.73931	0.20D-02	-0.00002	-0.008
66	65	1011.26355	0.20D-02	0.00274	1.37171
67	66	1011.78711	0.20D-02	-0.0008	-0.39815
68	67	1012.30061	0.20D-02	-0.00127	-0.63385
69	68	1012.8056	0.20D-02	-0.00023	-0.11669
70	69	1013.30503	0.20D-02	-0.00066	-0.32798
71	70	1013.79641	0.20D-02	-0.00005	-0.02402
72	71	1014.28106	0.20D-02	0.00024	0.11886
73	72	1014.75979	0.20D-02	-0.00061	-0.30567
74	73	1015.2307	0.20D-02	-0.00071	-0.35346

Table A.2, Fourier Transform Infrared Data for ^{72}GeO (cm^{-1}) (*Cont'd*)

J'	J''	Obs	Unc	Calc-Obs	(Calc-Obs)/Unc
75	74	1015.69422	0.20D-02	-0.00049	-0.24684
76	75	1016.15088	0.20D-02	-0.00051	-0.2567
77	76	1016.60032	0.20D-02	-0.00042	-0.20938
78	77	1017.04377	0.20D-02	-0.00145	-0.72627
79	78	1017.47685	0.20D-02	0.00075	0.37623
80	79	1017.90066	0.50D-02	0.00508	1.0169
81	80	1018.3272	0.20D-02	-0.00047	-0.23566
82	81	1018.74045	0.20D-02	0.00009	0.04663
83	82	1019.14847	0.20D-02	-0.00129	-0.64734
84	83	1019.54672	0.20D-02	-0.0001	-0.04899
85	84	1019.93877	0.20D-02	0.00008	0.04073
86	85	1020.3261	0.20D-02	-0.00224	-1.12063
87	86	1020.70377	0.20D-02	-0.00214	-1.06904
88	87	1021.06924	0.20D-02	0.00292	1.45952
89	88	1021.43586	0.20D-02	-0.00043	-0.21742
90	89	1021.79347	0.20D-02	-0.00205	-1.02587
91	90	1022.13756	0.20D-02	0.00257	1.28318
92	91	1022.48335	0.20D-02	-0.00182	-0.90779
93	92	1022.81663	0.20D-02	-0.001	-0.49981
94	93	1023.13972	0.20D-02	0.00268	1.3411
95	94	1023.46393	0.20D-02	-0.0021	-1.04761
96	95	1023.77048	0.20D-02	0.00344	1.7185
97	96	1024.07709	0.20D-02	0.00154	0.77188
The 4-3 Band, 173 data, $J"_{min} = 1$, $J"_{max} = 90$					
Unc.$_{Avge}$ = 2.2D-03, Unc.$_{Max}$ = 5.0D-03					
(Err/Unc.)$_{Avge}$ = -6.8D-02, RMSR = 0.65					
89	90	843.90148	0.20D-02	-0.00067	-0.33415
88	89	845.3598	0.20D-02	0.0015	0.74853
87	88	846.81507	0.20D-02	0.0015	0.74882
86	87	848.26659	0.20D-02	0.00003	0.0165
85	86	849.71125	0.20D-02	0.00018	0.09138
84	85	851.14944	0.20D-02	0.00156	0.77828
83	84	852.58497	0.20D-02	0.00033	0.16702
82	83	854.01516	0.20D-02	-0.00081	-0.40262
81	82	855.43859	0.20D-02	-0.00047	-0.23577
80	81	856.85627	0.20D-02	0.00032	0.16226
79	80	858.2693	0.20D-02	0.00047	0.23635
78	79	859.6792	0.20D-02	-0.00155	-0.77376
77	78	861.07892	0.20D-02	0.00128	0.64165
76	77	862.47559	0.20D-02	0.00183	0.91746
75	76	863.87119	0.20D-02	-0.00188	-0.94162
74	75	865.25479	0.20D-02	0.00106	0.52917
73	74	866.63737	0.20D-02	-0.00035	-0.17536
72	73	868.01302	0.20D-02	-0.0002	-0.10056
71	72	869.38102	0.20D-02	0.00222	1.10836
70	71	870.75171	0.20D-02	-0.00344	-1.71882
69	70	872.1075	0.20D-02	0.0004	0.19755
68	69	873.46387	0.20D-02	-0.00177	-0.88271
67	68	874.81236	0.20D-02	-0.00147	-0.73494
66	67	876.15407	0.20D-02	0.00018	0.09059
65	66	877.49214	0.20D-02	0.00002	0.00859
64	65	878.82647	0.20D-02	-0.00186	-0.93125
63	64	880.15197	0.20D-02	-0.00038	-0.18922
62	63	881.473	0.20D-02	0.00011	0.05437
61	62	882.789	0.20D-02	0.00013	0.06426
60	61	884.10009	0.20D-02	-0.00044	-0.21998
59	60	885.40424	0.20D-02	0.00042	0.21143

Table A.2, Fourier Transform Infrared Data for ^{72}GeO (cm^{-1}) (*Cont'd*)

J'	J''	Obs	Unc	Calc-Obs	(Calc-Obs)/Unc
58	59	886.7055	0.20D-02	-0.00133	-0.66689
57	58	887.99874	0.20D-02	-0.00061	-0.30533
56	57	889.28681	0.20D-02	-0.00026	-0.12913
55	56	890.5667	0.20D-02	0.00272	1.36131
54	55	891.84772	0.20D-02	-0.00098	-0.48937
53	54	893.11884	0.20D-02	-0.00036	-0.18147
52	53	894.38516	0.20D-02	-0.00053	-0.26547
51	52	895.64559	0.20D-02	-0.0004	-0.20169
50	51	896.90018	0.20D-02	-0.00003	-0.01545
49	50	898.14858	0.20D-02	0.00091	0.4528
48	49	899.39356	0.20D-02	-0.00036	-0.18238
47	48	900.63154	0.20D-02	-0.00027	-0.13628
46	47	901.86327	0.20D-02	0.00043	0.21564
45	46	903.09195	0.20D-02	-0.00148	-0.74203
44	45	904.31144	0.20D-02	0.00012	0.06029
43	44	905.52666	0.20D-02	0.00031	0.15724
42	43	906.73821	0.20D-02	-0.00151	-0.75673
41	42	907.94024	0.20D-02	0.00049	0.24306
40	41	909.13891	0.20D-02	0.00012	0.06106
39	40	910.33155	0.20D-02	0.00006	0.03192
38	39	911.5176	0.20D-02	0.00086	0.43013
37	38	912.69938	0.20D-02	0.00019	0.09524
36	37	913.87545	0.20D-02	-0.00054	-0.26822
35	36	915.04407	0.20D-02	0.00042	0.20927
34	35	916.20797	0.20D-02	0.00031	0.15723
33	34	917.36623	0.20D-02	0.00006	0.03017
32	33	918.51812	0.20D-02	0.00039	0.19265
31	32	919.66578	0.20D-02	-0.00088	-0.44093
30	31	920.80503	0.20D-02	0.00044	0.21901
29	30	921.94061	0.20D-02	-0.00041	-0.20308
28	29	923.0688	0.20D-02	0.0003	0.15227
27	28	924.19262	0.20D-02	-0.00048	-0.24047
26	27	925.30968	0.20D-02	-0.00037	-0.18682
25	26	926.42398	0.20D-02	-0.00338	-1.69234
24	25	927.52605	0.20D-02	-0.00006	-0.02752
23	24	928.62614	0.20D-02	-0.00064	-0.31801
22	23	929.71906	0.20D-02	0.00003	0.01571
21	22	930.8057	0.20D-02	0.00106	0.528
20	21	931.88853	0.20D-02	-0.00004	-0.02164
19	20	932.95969	0.50D-02	0.00458	0.91646
18	19	934.02964	0.50D-02	0.00447	0.89433
17	18	935.10016	0.20D-02	-0.00219	-1.09326
16	17	936.15855	0.20D-02	-0.00269	-1.34669
15	16	937.20823	0.20D-02	-0.00048	-0.24002
14	15	938.25585	0.20D-02	-0.00221	-1.10397
13	14	939.29304	0.20D-02	0.00049	0.24592
12	13	940.32956	0.20D-02	-0.00217	-1.08606
11	12	941.3548	0.20D-02	0.00041	0.20453
10	11	942.37714	0.20D-02	-0.00016	-0.07799
9	10	943.39183	0.20D-02	0.00087	0.43572
8	9	944.40207	0.20D-02	0.00029	0.145
7	8	945.40649	0.20D-02	-0.00056	-0.28082
6	7	946.40384	0.20D-02	-0.00043	-0.21737
5	6	947.39517	0.20D-02	-0.00039	-0.19542
4	5	948.37903	0.20D-02	0.00101	0.50444
2	1	955.10498	0.20D-02	-0.00026	-0.13116
4	3	956.97537	0.50D-02	-0.005	-1.00035
5	4	957.89286	0.20D-02	0.001	0.49801

Table A.2, Fourier Transform Infrared Data for ^{72}GeO (cm^{-1}) (*Cont'd*)

J'	J''	Obs	Unc	Calc-Obs	(Calc-Obs)/Unc
6	5	958.81255	0.20D-02	-0.00145	-0.72334
7	6	959.7235	0.20D-02	-0.0014	-0.70069
8	7	960.62713	0.20D-02	-0.00029	-0.14484
9	8	961.52626	0.20D-02	-0.00096	-0.48156
10	9	962.41869	0.20D-02	-0.00122	-0.61168
11	10	963.30358	0.20D-02	-0.00024	-0.12095
12	11	964.18508	0.20D-02	-0.00218	-1.09029
13	12	965.05633	0.20D-02	-0.00019	-0.09541
14	13	965.9248	0.20D-02	-0.00174	-0.87222
15	14	966.78498	0.20D-02	-0.00136	-0.68154
16	15	967.63756	0.20D-02	0.00026	0.13077
17	16	968.48582	0.20D-02	-0.00016	-0.08115
18	17	969.32806	0.20D-02	-0.00095	-0.47316
19	18	970.16239	0.20D-02	-0.00021	-0.10608
20	19	970.98821	0.20D-02	0.00263	1.31411
21	20	971.81547	0.20D-02	-0.00238	-1.18839
22	21	972.62931	0.20D-02	-0.0004	-0.19952
23	22	973.43772	0.20D-02	0.00057	0.28476
24	23	974.24205	0.20D-02	-0.00083	-0.41635
25	24	975.03504	0.20D-02	0.00264	1.32121
26	25	975.82716	0.20D-02	0.00051	0.25643
27	26	976.61171	0.20D-02	-0.00052	-0.26159
28	27	977.3886	0.20D-02	-0.00041	-0.20375
29	28	978.15851	0.20D-02	0.00018	0.08891
30	29	978.92254	0.20D-02	0.00012	0.06053
31	30	979.67968	0.20D-02	0.00042	0.21007
32	31	980.43357	0.20D-02	-0.00258	-1.28844
33	32	981.17628	0.20D-02	-0.00095	-0.47597
34	33	981.91351	0.20D-02	-0.00041	-0.20354
35	34	982.64461	0.20D-02	-0.00032	-0.16214
36	35	983.3686	0.20D-02	0.00027	0.13726
37	36	984.08236	0.50D-02	0.0045	0.89944
38	37	984.80187	0.20D-02	-0.00365	-1.8242
39	38	985.50353	0.20D-02	-0.00057	-0.28708
40	39	986.20119	0.20D-02	-0.00014	-0.07114
41	40	986.89302	0.20D-02	-0.00053	-0.26743
42	41	987.57705	0.20D-02	0.00022	0.10798
43	42	988.26028	0.50D-02	-0.00492	-0.98439
44	43	988.92665	0.20D-02	0.00011	0.0547
45	44	989.59201	0.20D-02	-0.00055	-0.27618
46	45	990.25098	0.20D-02	-0.00154	-0.76973
47	46	990.90146	0.20D-02	-0.00076	-0.38196
48	47	991.54524	0.20D-02	-0.00003	-0.01404
49	48	992.17897	0.50D-02	0.00401	0.80116
50	49	992.81628	0.20D-02	-0.00229	-1.14726
51	50	993.43817	0.20D-02	0.00004	0.01939
52	51	994.05613	0.20D-02	-0.00049	-0.2434
53	52	994.66745	0.20D-02	-0.00117	-0.5867
54	53	995.27009	0.20D-02	0.00001	0.00324
55	54	995.86678	0.20D-02	0.00031	0.15533
56	55	996.4549	0.20D-02	0.00235	1.17335
57	56	997.04189	0.20D-02	-0.00134	-0.6689
58	57	997.61747	0.20D-02	-0.00048	-0.23758
59	58	998.18613	0.20D-02	0.00044	0.22101
60	59	998.75206	0.20D-02	-0.00281	-1.40431
61	60	999.30972	0.50D-02	-0.00469	-0.93788
62	61	999.85131	0.20D-02	0.00259	1.29352
63	62	1000.39657	0.20D-02	-0.00073	-0.36603

Table A.2, Fourier Transform Infrared Data for ^{72}GeO (cm^{-1}) (*Cont'd*)

J'	J''	Obs	Unc	Calc-Obs	(Calc-Obs)/Unc
64	63	1000.92981	0.20D-02	0.00103	0.5157
65	64	1001.45902	0.20D-02	-0.00013	-0.06271
66	65	1001.98131	0.20D-02	-0.00133	-0.66254
67	66	1002.49326	0.20D-02	0.00084	0.41993
68	67	1003.00086	0.20D-02	0.00037	0.18341
69	68	1003.50122	0.20D-02	0.00014	0.07159
70	69	1003.9952	0.20D-02	-0.00072	-0.36134
71	70	1004.47779	0.20D-02	0.00277	1.38731
72	71	1004.96463	0.50D-02	-0.00502	-1.00332
73	72	1005.43286	0.20D-02	-0.00125	-0.62451
74	73	1005.89194	0.50D-02	0.0046	0.92093
75	74	1006.35501	0.20D-02	-0.00061	-0.30413
76	75	1006.8053	0.20D-02	-0.00013	-0.06526
77	76	1007.24625	0.20D-02	0.00259	1.29256
78	77	1007.68369	0.20D-02	0.0017	0.84844
79	78	1008.11393	0.20D-02	0.00088	0.44
80	79	1008.52774	0.50D-02	0.00936	1.87253
81	80	1008.95289	0.20D-02	-0.00066	-0.32901
82	81	1009.35977	0.20D-02	0.00043	0.21308
83	82	1009.76108	0.20D-02	-0.0001	-0.04984
84	83	1010.15327	0.20D-02	0.0013	0.6513
85	84	1010.54142	0.20D-02	-0.00046	-0.22998
86	85	1010.92053	0.20D-02	-0.0004	-0.19962
87	86	1011.28285	0.50D-02	0.00922	1.84396
88	87	1011.64996	0.50D-02	0.00681	1.36104
89	88	1012.01552	0.20D-02	-0.00132	-0.65752
The 5-4 Band, 153 data, $J"_{min} = 1$, $J"_{max} = 80$					
Unc.$_{Avge}$ = 2.3D-03, Unc.$_{Max}$ = 8.0D-03					
(Err/Unc.)$_{Avge}$ = -8.0D-02, RMSR = 0.81					
76	77	854.1089	0.20D-02	-0.00127	-0.63511
75	76	855.49074	0.20D-02	0.0022	1.09772
74	75	856.8724	0.20D-02	0.0005	0.24828
73	74	858.24858	0.20D-02	-0.00108	-0.53866
72	73	859.61749	0.20D-02	-0.00074	-0.36833
71	72	860.98021	0.20D-02	0.00041	0.20393
70	71	862.33855	0.20D-02	0.00055	0.27293
69	70	863.6922	0.20D-02	-0.00002	-0.01165
68	69	865.03746	0.20D-02	0.0024	1.19986
67	68	866.38297	0.20D-02	-0.00086	-0.42771
66	67	867.72048	0.20D-02	-0.00154	-0.76973
65	66	869.05346	0.20D-02	-0.00313	-1.56648
64	65	870.37355	0.20D-02	0.00272	1.36178
63	64	871.69559	0.20D-02	0.00116	0.57965
62	63	873.01198	0.20D-02	-0.00023	-0.11315
61	62	874.3215	0.20D-02	-0.00022	-0.11188
60	61	875.62777	0.20D-02	-0.00245	-1.22692
59	60	876.92356	0.20D-02	0.00028	0.14134
58	59	878.2188	0.20D-02	-0.00194	-0.97233
57	58	879.5044	0.20D-02	-0.00006	-0.02832
56	57	880.78494	0.20D-02	0.00137	0.68301
55	56	882.06304	0.20D-02	-0.00033	-0.1637
54	55	883.33493	0.20D-02	-0.00137	-0.68375
53	54	884.59827	0.20D-02	0.00057	0.28738
52	53	885.85747	0.20D-02	0.00109	0.54437
51	52	887.10778	0.50D-02	0.00489	0.97875
50	51	888.36161	0.20D-02	-0.00042	-0.21051
49	50	889.60483	0.20D-02	-0.00074	-0.36825

Table A.2, Fourier Transform Infrared Data for ^{72}GeO (cm^{-1}) (*Cont'd*)

J'	J''	Obs	Unc	Calc-Obs	(Calc-Obs)/Unc
48	49	890.84154	0.20D-02	-0.00015	-0.07665
47	48	892.07353	0.20D-02	-0.00049	-0.24616
46	47	893.29839	0.20D-02	0.00066	0.32782
45	46	894.52006	0.20D-02	-0.00066	-0.33015
44	45	895.73285	0.20D-02	0.00124	0.61958
43	44	896.94293	0.20D-02	0.00018	0.09145
42	43	898.1486	0.20D-02	-0.00216	-1.07985
41	42	899.34399	0.20D-02	0.00008	0.04012
40	41	900.53654	0.20D-02	-0.00055	-0.27398
39	40	901.72205	0.20D-02	0.00015	0.07733
38	39	902.90231	0.20D-02	0.00037	0.1836
37	38	904.07829	0.20D-02	-0.00088	-0.44064
36	37	905.24565	0.20D-02	0.00074	0.36912
35	36	906.40996	0.20D-02	-0.00036	-0.17758
34	35	907.5673	0.20D-02	-0.00024	-0.1212
33	34	908.71877	0.20D-02	-0.00005	-0.02732
32	33	909.86335	0.20D-02	0.00123	0.61365
31	32	911.00797	0.20D-02	-0.00334	-1.6689
30	31	912.13964	0.20D-02	-0.00077	-0.38538
29	30	913.26371	0.20D-02	0.00358	1.78863
28	29	914.38936	0.20D-02	0.0005	0.24761
27	28	915.506	0.20D-02	0.00057	0.28602
26	27	916.61804	0.20D-02	-0.00061	-0.30668
25	26	917.72231	0.20D-02	0.00011	0.054
24	25	918.82426	0.20D-02	-0.00275	-1.37257
23	24	919.91532	0.20D-02	-0.0006	-0.30188
22	23	921.00215	0.50D-02	-0.00014	-0.02782
20	21	923.15881	0.20D-02	0.00004	0.01774
19	20	924.22453	0.20D-02	0.00382	1.91155
18	19	925.29051	0.20D-02	0.0014	0.69967
17	18	926.34826	0.20D-02	0.00124	0.62153
16	17	927.39963	0.20D-02	0.00149	0.74644
15	16	928.44617	0.20D-02	0.0006	0.29881
14	15	929.48689	0.20D-02	-0.00048	-0.24192
13	14	930.52267	0.20D-02	-0.00263	-1.31644
12	13	931.54898	0.20D-02	-0.00133	-0.66543
11	12	932.57248	0.20D-02	-0.00325	-1.62445
10	11	933.58944	0.50D-02	-0.00467	-0.93368
9	10	934.59229	0.20D-02	0.00198	0.98972
8	9	935.59953	0.20D-02	-0.00184	-0.91847
7	8	936.59558	0.20D-02	-0.00054	-0.26939
6	7	937.58463	0.20D-02	0.00167	0.83633
5	6	938.57524	0.20D-02	-0.00377	-1.88712
4	5	939.55728	0.50D-02	-0.00675	-1.35052
3	4	940.52442	0.20D-02	-0.00096	-0.47901
2	3	941.49355	0.20D-02	-0.00329	-1.64393
1	2	942.4461	0.50D-02	0.00482	0.96369
0	1	943.4069	0.20D-02	-0.00148	-0.7403
2	1	946.23414	0.20D-02	-0.00225	-1.12719
3	2	947.16516	0.20D-02	-0.00351	-1.75474
4	3	948.08634	0.20D-02	-0.00114	-0.56875
5	4	949.00222	0.20D-02	0.00031	0.15511
7	6	950.81883	0.20D-02	-0.00035	-0.17686
8	7	951.7152	0.20D-02	0.00186	0.93074
9	8	952.60809	0.20D-02	0.00129	0.64304
10	9	953.49316	0.20D-02	0.00225	1.12414
11	10	954.37711	0.20D-02	-0.00196	-0.98169
12	11	955.24878	0.20D-02	-0.00019	-0.09537

Table A.2, Fourier Transform Infrared Data for ^{72}GeO (cm^{-1}) (*Cont'd*)

J'	J''	Obs	Unc	Calc-Obs	(Calc-Obs)/Unc
13	12	956.11874	0.20D-02	-0.00304	-1.51764
14	13	956.97516	0.20D-02	0.00133	0.66562
16	15	958.67869	0.20D-02	0.00034	0.1703
17	16	959.52128	0.20D-02	-0.00052	-0.25994
18	17	960.35747	0.20D-02	-0.00136	-0.67815
19	18	961.1848	0.20D-02	0.00029	0.14483
20	19	962.0079	0.20D-02	-0.00024	-0.12182
21	20	962.82251	0.20D-02	0.0013	0.65095
22	21	963.6335	0.20D-02	0.00004	0.02223
23	22	964.43449	0.20D-02	0.00235	1.1761
24	23	965.23504	0.20D-02	-0.00135	-0.67335
25	24	966.02623	0.20D-02	-0.00213	-1.06705
26	25	966.81008	0.20D-02	-0.00206	-1.03093
27	26	967.58527	0.20D-02	0.00019	0.0941
28	27	968.35577	0.20D-02	0.00063	0.31699
29	28	969.12201	0.20D-02	-0.00117	-0.58311
30	29	969.87917	0.20D-02	-0.0004	-0.20223
31	30	970.62956	0.20D-02	0.0006	0.29865
32	31	971.37866	0.20D-02	-0.00364	-1.82144
33	32	972.11336	0.20D-02	-0.00005	-0.02351
34	33	972.84451	0.20D-02	0.00053	0.26649
35	34	973.57	0.20D-02	0.00019	0.09745
36	35	974.28613	0.20D-02	0.00263	1.31346
37	36	974.99858	0.20D-02	0.00214	1.06838
38	37	975.70604	0.20D-02	0.00002	0.01127
39	38	976.40379	0.20D-02	0.00099	0.49606
40	39	977.09801	0.20D-02	-0.00114	-0.56833
41	40	977.78442	0.20D-02	-0.00212	-1.05795
42	41	978.46427	0.20D-02	-0.0032	-1.59882
43	42	979.12828	0.50D-02	0.00489	0.97715
44	43	979.79935	0.20D-02	-0.00078	-0.38884
45	44	980.45602	0.20D-02	0.00126	0.62983
46	45	981.10945	0.20D-02	-0.00017	-0.08711
47	46	981.75414	0.20D-02	0.00041	0.20416
48	47	982.39524	0.20D-02	-0.00214	-1.07247
49	48	983.02917	0.50D-02	-0.00429	-0.85725
50	49	983.6522	0.20D-02	-0.00229	-1.14391
51	50	984.26689	0.20D-02	0.00128	0.63894
52	51	984.87461	0.50D-02	0.00503	1.00574
53	52	985.48523	0.20D-02	-0.00092	-0.45891
54	53	986.08348	0.80D-02	-0.0013	-0.16299
55	54	986.67325	0.20D-02	-0.00003	-0.01598
56	55	987.26226	0.50D-02	-0.00482	-0.96488
57	56	987.83294	0.20D-02	0.00186	0.92818
58	57	988.40755	0.20D-02	-0.00225	-1.12599
59	58	988.96961	0.20D-02	-0.00068	-0.34102
60	59	989.52442	0.20D-02	0.00125	0.62694
61	60	990.07919	0.20D-02	-0.00367	-1.83343
62	61	990.61723	0.20D-02	0.00123	0.61671
63	62	991.15033	0.50D-02	0.00415	0.83043
64	63	991.68337	0.20D-02	0.0002	0.09839
65	64	992.2063	0.20D-02	-0.0006	-0.29757
66	65	992.72054	0.20D-02	0.00035	0.17681
68	67	993.72796	0.20D-02	0.00236	1.18164
69	68	994.22506	0.20D-02	-0.00051	-0.25552
70	69	994.71132	0.20D-02	0.00044	0.22248
71	70	995.19229	0.20D-02	-0.00033	-0.16566
72	71	995.66278	0.20D-02	0.00234	1.1687

Table A.2, Fourier Transform Infrared Data for ^{72}GeO (cm^{-1}) (*Cont'd*)

J'	J''	Obs	Unc	Calc-Obs	(Calc-Obs)/Unc
73	72	996.12736	0.50D-02	0.00387	0.77369
74	73	996.58932	0.20D-02	0.00096	0.47961
75	74	997.04189	0.20D-02	0.00037	0.18338
76	75	997.48519	0.20D-02	0.00196	0.97927
77	76	997.91802	0.50D-02	0.00693	1.38633
78	77	998.35805	0.20D-02	-0.00242	-1.20831
79	78	998.78092	0.20D-02	-0.00173	-0.86457
80	79	999.19486	0.20D-02	0.00075	0.37564
81	80	999.60596	0.20D-02	-0.00108	-0.53911
The 6-5 Band, 147 data, $J"_{min} = 0$, $J"_{max} = 74$					
Unc.$_{Avge}$ = 2.3D-03, Unc.$_{Max}$ = 5.0D-03					
(Err/Unc.)$_{Avge}$ = 8.3D-02, RMSR = 0.92					
72	73	851.24782	0.20D-02	-0.00087	-0.435
71	72	852.60234	0.20D-02	0.00193	0.96688
70	71	853.95601	0.20D-02	0.00022	0.10823
69	70	855.2993	0.20D-02	0.00348	1.73873
68	69	856.63807	0.50D-02	0.00586	1.17128
67	68	857.97638	0.20D-02	0.00328	1.64128
66	67	859.30783	0.20D-02	0.00216	1.07773
65	66	860.6342	0.20D-02	0.00066	0.33214
64	65	861.95492	0.20D-02	-0.00062	-0.31074
63	64	863.27013	0.20D-02	-0.00185	-0.9262
62	63	864.57579	0.20D-02	0.00101	0.50536
61	62	865.87986	0.20D-02	-0.00002	-0.0113
60	61	867.17618	0.20D-02	0.00121	0.60344
59	60	868.46875	0.20D-02	0.00069	0.34419
58	59	869.7524	0.20D-02	0.00359	1.7957
57	58	871.0385	0.20D-02	-0.00148	-0.74243
56	57	872.31107	0.20D-02	0.00144	0.7195
55	56	873.58252	0.20D-02	-0.00006	-0.02899
54	55	874.84843	0.20D-02	-0.00156	-0.77822
53	54	876.10332	0.20D-02	0.00239	1.1965
52	53	877.35726	0.20D-02	0.00172	0.85967
51	52	878.60571	0.20D-02	0.00095	0.47601
50	51	879.84699	0.20D-02	0.00176	0.88008
49	50	881.08487	0.20D-02	0.00037	0.18647
48	49	882.31657	0.20D-02	-0.00046	-0.23022
47	48	883.54356	0.20D-02	-0.00221	-1.10541
46	47	884.76037	0.20D-02	0.00058	0.29049
45	46	885.97388	0.20D-02	0.00103	0.51704
44	45	887.18299	0.20D-02	0.00022	0.10887
43	44	888.38417	0.20D-02	0.00166	0.83044
42	43	889.58693	0.50D-02	-0.00416	-0.83144
41	42	890.7716	0.20D-02	0.00242	1.21125
40	41	891.96544	0.50D-02	-0.00586	-1.17221
39	40	893.14009	0.20D-02	-0.00068	-0.33926
38	39	894.31582	0.20D-02	-0.0023	-1.15051
37	38	895.47903	0.20D-02	0.00286	1.43032
36	37	896.6429	0.20D-02	0.00163	0.81264
35	36	897.80374	0.20D-02	-0.00235	-1.174
34	35	898.95051	0.20D-02	0.00198	0.98997
33	34	900.09743	0.20D-02	0.00038	0.18894
32	33	901.23792	0.20D-02	-0.00058	-0.2925
31	32	902.3715	0.20D-02	-0.00043	-0.21491
30	31	903.49862	0.20D-02	0.00036	0.18117
29	30	904.61681	0.50D-02	0.00426	0.85209
28	29	905.74096	0.50D-02	-0.00364	-0.72731

Table A.2, Fourier Transform Infrared Data for ^{72}GeO (cm^{-1}) (*Cont'd*)

J'	J''	Obs	Unc	Calc-Obs	(Calc-Obs)/Unc
27	28	906.84803	0.20D-02	-0.0003	-0.14989
26	27	907.9483	0.20D-02	0.00399	1.99484
25	26	909.04937	0.20D-02	0.0016	0.8004
24	25	910.14389	0.20D-02	-0.00012	-0.05886
23	24	911.22732	0.20D-02	0.00336	1.68158
22	23	912.31426	0.20D-02	-0.00256	-1.27891
21	22	913.38829	0.20D-02	-0.00149	-0.7459
20	21	914.45519	0.20D-02	0.00078	0.39001
19	20	915.51755	0.20D-02	0.00166	0.82822
18	19	916.5726	0.20D-02	0.0039	1.94812
17	18	917.62617	0.20D-02	0.00166	0.82917
16	17	918.67265	0.20D-02	0.00055	0.27563
15	16	919.71119	0.20D-02	0.00139	0.69699
14	15	920.75298	0.50D-02	-0.007	-1.401
13	14	921.77171	0.20D-02	0.00165	0.82664
12	13	922.79411	0.20D-02	0.00063	0.31369
11	12	923.81162	0.20D-02	-0.00152	-0.76198
10	11	924.81661	0.20D-02	0.0028	1.39895
9	10	925.82343	0.20D-02	-0.00076	-0.37918
8	9	926.8181	0.20D-02	0.00178	0.88801
7	8	927.81193	0.20D-02	-0.00092	-0.46028
6	7	928.79577	0.20D-02	0.0003	0.15037
5	6	929.77141	0.20D-02	0.00362	1.80922
4	5	930.74876	0.20D-02	-0.00088	-0.4395
3	4	931.7155	0.20D-02	-0.00088	-0.44139
2	3	932.67845	0.20D-02	-0.00322	-1.61223
1	2	933.62235	0.50D-02	0.00734	1.46892
0	1	934.57214	0.50D-02	0.00588	1.17656
1	0	936.4571	0.20D-02	-0.00094	-0.46957
2	1	937.38512	0.20D-02	0.00084	0.41881
3	2	938.31618	0.50D-02	-0.00662	-1.32447
4	3	939.2246	0.20D-02	0.00236	1.17966
5	4	940.13376	0.50D-02	0.00437	0.87421
6	5	941.03671	0.50D-02	0.00636	1.27225
7	6	941.94537	0.20D-02	-0.0036	-1.80081
8	7	942.83917	0.50D-02	-0.00496	-0.99184
9	8	943.72026	0.20D-02	0.00013	0.06348
10	9	944.59966	0.20D-02	0.00064	0.31754
11	10	945.47599	0.20D-02	-0.00209	-1.04316
12	11	946.3448	0.20D-02	-0.00359	-1.7945
13	12	947.20556	0.20D-02	-0.00335	-1.67731
14	13	948.05262	0.50D-02	0.00426	0.85102
15	14	948.90414	0.20D-02	0.00107	0.53421
16	15	949.74642	0.20D-02	0.00078	0.39183
17	16	950.58238	0.20D-02	0.00045	0.22458
18	17	951.41286	0.20D-02	-0.00078	-0.38852
19	18	952.23569	0.20D-02	-0.00074	-0.36827
20	19	953.05113	0.20D-02	0.0003	0.1494
21	20	953.86092	0.20D-02	0.00058	0.28853
22	21	954.66485	0.20D-02	0.0003	0.14831
23	22	955.45891	0.20D-02	0.00347	1.73282
24	23	956.25424	0.20D-02	-0.00109	-0.54398
25	24	957.03796	0.20D-02	-0.00049	-0.24296
26	25	957.81492	0.20D-02	0.00041	0.20493
27	26	958.58608	0.20D-02	0.00063	0.31378
28	27	959.34883	0.20D-02	0.00277	1.38259
29	28	960.11159	0.20D-02	-0.00161	-0.80461
31	30	961.6112	0.50D-02	-0.00399	-0.79839

Table A.2, Fourier Transform Infrared Data for ^{72}GeO (cm^{-1}) (*Cont'd*)

J'	J''	Obs	Unc	Calc-Obs	(Calc-Obs)/Unc
32	31	962.34508	0.20D-02	0.00094	0.46789
33	32	963.07811	0.20D-02	0.00016	0.08178
34	33	963.80351	0.20D-02	0.00046	0.22975
35	34	964.52073	0.20D-02	0.00236	1.18066
36	35	965.23504	0.20D-02	0.00059	0.2936
37	36	965.94111	0.20D-02	0.00046	0.23247
38	37	966.64131	0.20D-02	-0.00041	-0.20376
39	38	967.33422	0.20D-02	-0.00061	-0.30614
40	39	968.02229	0.20D-02	-0.00261	-1.30575
41	40	968.69964	0.20D-02	-0.00054	-0.26864
42	41	969.37217	0.20D-02	-0.0003	-0.15089
43	42	970.03579	0.20D-02	0.00217	1.08645
44	43	970.69721	0.20D-02	0.00016	0.08225
45	44	971.35069	0.20D-02	-0.00059	-0.29465
46	45	971.99957	0.20D-02	-0.00346	-1.73025
47	46	972.62891	0.50D-02	0.00649	1.29772
48	47	973.26807	0.20D-02	-0.00011	-0.05719
49	48	973.89533	0.20D-02	-0.00156	-0.78084
50	49	974.51319	0.20D-02	-0.00037	-0.18278
51	50	975.12462	0.20D-02	0.00049	0.24588
52	51	975.72917	0.20D-02	0.00145	0.72393
53	52	976.32779	0.20D-02	0.00154	0.77013
54	53	976.91902	0.20D-02	0.00223	1.11342
55	54	977.50584	0.20D-02	0.0005	0.24755
56	55	978.08211	0.20D-02	0.00248	1.24138
57	56	978.65239	0.50D-02	0.00362	0.72343
58	57	979.22131	0.20D-02	-0.00074	-0.372
59	58	979.77845	0.20D-02	-0.00019	-0.09654
60	59	980.32968	0.20D-02	-0.00061	-0.30633
61	60	980.87333	0.20D-02	-0.00035	-0.17261
62	61	981.40992	0.20D-02	0.00008	0.03832
63	62	981.94165	0.20D-02	-0.00155	-0.77466
64	63	982.46559	0.20D-02	-0.00233	-1.16296
65	64	982.98163	0.20D-02	-0.00215	-1.07283
66	65	983.48722	0.20D-02	0.00153	0.76451
67	66	983.99304	0.20D-02	-0.00199	-0.99735
68	67	984.4822	0.50D-02	0.00416	0.83216
69	68	984.97823	0.20D-02	-0.00355	-1.77365
70	69	985.45691	0.20D-02	-0.00091	-0.45578
71	70	985.9319	0.20D-02	-0.0016	-0.80235
72	71	986.39891	0.20D-02	-0.00135	-0.6747
73	72	986.86163	0.20D-02	-0.00385	-1.92413
74	73	987.31372	0.20D-02	-0.00276	-1.3821
75	74	987.76035	0.20D-02	-0.0033	-1.6499
The 7-6 Band, 123 data, $J"_{min} = 11$, $J"_{max} = 80$					
Unc.$_{Avge}$ = 3.9D-03, Unc.$_{Max}$ = 1.0D-02					
(Err/Unc.)$_{Avge}$ = 2.2D-01, RMSR = 1.06					
79	80	833.30323	0.50D-02	-0.00525	-1.05031
78	79	834.6896	0.50D-02	-0.00349	-0.69852
77	78	836.06947	0.50D-02	-0.00054	-0.10711
76	77	837.43563	0.10D-01	0.01083	1.08292
75	76	838.812	0.50D-02	0.00665	1.33023
74	75	840.18713	0.20D-02	-0.00162	-0.81016
73	74	841.54474	0.20D-02	0.00228	1.1422
72	73	842.90578	0.20D-02	-0.00259	-1.29272
71	72	844.25953	0.50D-02	-0.00554	-1.10804
70	71	845.60212	0.20D-02	-0.00271	-1.35526

Table A.2, Fourier Transform Infrared Data for ^{72}GeO (cm^{-1}) (*Cont'd*)

J'	J''	Obs	Unc	Calc-Obs	(Calc-Obs)/Unc
69	70	846.95026	0.10D-01	-0.01082	-1.0817
68	69	848.27454	0.20D-02	-0.00045	-0.22513
67	68	849.59731	0.50D-02	0.00601	1.20183
66	67	850.92386	0.20D-02	0.00327	1.6353
65	66	852.24213	0.20D-02	0.00338	1.69178
64	65	853.54093	0.10D-01	0.01754	1.75372
63	64	854.85883	0.50D-02	0.00713	1.4262
62	63	856.17068	0.20D-02	-0.00269	-1.34288
61	62	857.46389	0.20D-02	0.00067	0.33317
60	61	858.75843	0.20D-02	-0.00279	-1.39673
59	60	860.04062	0.20D-02	0.00061	0.30707
58	59	861.32119	0.20D-02	0.00013	0.06423
57	58	862.59741	0.20D-02	-0.00152	-0.76062
56	57	863.87119	0.50D-02	-0.00626	-1.25114
55	56	865.12795	0.20D-02	0.0005	0.25224
54	55	866.38297	0.20D-02	0.00345	1.72414
52	53	868.88443	0.20D-02	0.00123	0.61714
51	52	870.13212	0.50D-02	-0.00519	-1.03706
50	51	871.36086	0.20D-02	0.00175	0.87291
49	50	872.59898	0.50D-02	-0.0063	-1.26065
48	49	873.81685	0.20D-02	0.00029	0.1433
47	48	875.03819	0.20D-02	-0.00221	-1.10265
46	47	876.24205	0.50D-02	0.00714	1.42799
45	46	877.45558	0.20D-02	0.00117	0.58581
44	45	878.65994	0.20D-02	-0.00128	-0.64055
43	44	879.85511	0.20D-02	-0.00021	-0.10459
42	43	881.04389	0.20D-02	0.00159	0.79318
41	42	882.22487	0.50D-02	0.00548	1.09696
40	41	883.40584	0.20D-02	0.0037	1.84756
39	40	884.57835	0.50D-02	0.00466	0.93127
38	39	885.74141	0.50D-02	0.00936	1.87154
37	38	886.91174	0.20D-02	0.00105	0.52397
36	37	888.05864	0.50D-02	0.01043	2.08524
35	36	889.21472	0.50D-02	0.00487	0.97432
34	35	890.364	0.20D-02	0.00035	0.17647
33	34	891.50326	0.20D-02	0.00009	0.04469
32	33	892.63686	0.20D-02	-0.00031	-0.15511
31	32	893.76639	0.20D-02	-0.00244	-1.21845
29	30	896.00369	0.20D-02	-0.00237	-1.18287
28	29	897.11812	0.50D-02	-0.00684	-1.36802
27	28	898.21049	0.50D-02	0.00489	0.97884
26	27	899.31187	0.50D-02	0.00177	0.35321
25	26	900.39472	0.10D-01	0.0113	1.13043
24	25	901.48294	0.10D-01	0.0096	0.95976
23	24	902.58659	0.10D-01	-0.01341	-1.34149
22	23	903.64291	0.20D-02	0.005	2.49773
21	22	904.71606	0.20D-02	0.00067	0.33377
20	21	905.77647	0.20D-02	0.00316	1.58006
19	20	906.84803	0.10D-01	-0.01143	-1.1428
17	18	908.93631	0.50D-02	-0.00359	-0.71822
16	17	909.97485	0.50D-02	-0.00302	-0.60372
15	16	911.00797	0.50D-02	-0.003	-0.60038
14	15	912.03087	0.20D-02	0.00125	0.62397
13	14	913.06165	0.50D-02	-0.00837	-1.67409
12	13	914.06343	0.50D-02	0.00499	0.99831
11	12	915.075	0.20D-02	0.00254	1.27135
10	11	916.08738	0.50D-02	-0.00675	-1.34968
12	11	937.45793	0.20D-02	0.0026	1.30045

Table A.2, Fourier Transform Infrared Data for ^{72}GeO (cm^{-1}) (*Cont'd*)

J'	J''	Obs	Unc	Calc-Obs	(Calc-Obs)/Unc
13	12	938.31627	0.20D-02	-0.00086	-0.43138
14	13	939.15349	0.50D-02	0.01048	2.09662
15	14	939.99881	0.50D-02	0.00739	1.47735
17	16	941.66491	0.50D-02	0.00669	1.33812
18	17	942.49235	0.20D-02	0.00241	1.20361
19	18	943.31252	0.20D-02	-0.00099	-0.49271
20	19	944.11939	0.20D-02	0.00253	1.26538
21	20	944.92905	0.50D-02	-0.00314	-0.62717
22	21	945.72406	0.20D-02	-0.00058	-0.28861
23	22	946.50365	0.10D-01	0.01097	1.09749
24	23	947.29921	0.20D-02	0.00012	0.05926
25	24	948.09348	0.10D-01	-0.0159	-1.58983
26	25	948.85047	0.20D-02	-0.0011	-0.54859
27	26	949.61416	0.50D-02	0.00053	0.10594
30	29	951.8749	0.50D-02	-0.00321	-0.64285
31	30	952.60351	0.50D-02	0.00748	1.49531
32	31	953.34277	0.20D-02	0.00098	0.49158
33	32	954.06998	0.20D-02	-0.00001	-0.00312
35	34	955.50295	0.20D-02	-0.00021	-0.10557
36	35	956.2093	0.20D-02	-0.00005	-0.02548
37	36	956.91092	0.20D-02	-0.00175	-0.87748
38	37	957.60137	0.20D-02	0.0011	0.55233
39	38	958.28807	0.20D-02	0.0011	0.54794
40	39	958.96837	0.20D-02	0.00086	0.42818
42	41	960.30948	0.20D-02	-0.00007	-0.03657
43	42	960.96896	0.20D-02	0.00055	0.27626
44	43	961.62102	0.20D-02	0.00191	0.95437
45	44	962.27032	0.20D-02	-0.00067	-0.33326
46	45	962.91127	0.20D-02	-0.0016	-0.7978
47	46	963.54411	0.20D-02	-0.00113	-0.56538
48	47	964.17014	0.20D-02	-0.00058	-0.29208
49	48	964.77031	0.10D-01	0.01908	1.90817
50	49	965.40625	0.50D-02	-0.00378	-0.75505
51	50	966.00678	0.20D-02	0.00202	1.01119
52	51	966.61974	0.10D-01	-0.0114	-1.13975
53	52	967.19919	0.20D-02	0.0019	0.95134
55	54	968.37107	0.50D-02	-0.0049	-0.97929
56	55	968.93794	0.20D-02	0.00054	0.26978
57	56	969.49893	0.50D-02	0.00502	1.00317
58	57	970.06274	0.20D-02	-0.00018	-0.08988
59	58	970.61335	0.20D-02	0.00096	0.47999
60	59	971.15567	0.20D-02	0.00352	1.76142
61	60	971.69168	0.50D-02	0.0055	1.09924
62	61	972.2283	0.20D-02	-0.00004	-0.02124
63	62	972.75199	0.20D-02	0.00043	0.21714
64	63	973.26807	0.20D-02	0.00159	0.79701
65	64	973.77775	0.20D-02	0.00221	1.10698
66	65	974.28613	0.20D-02	-0.00282	-1.40914
67	66	974.78119	0.50D-02	-0.0015	-0.2991
68	67	975.25427	0.10D-01	0.01483	1.48299
69	68	975.76139	0.10D-01	-0.00988	-0.98751
70	69	976.21338	0.10D-01	0.01355	1.35473
71	70	976.68849	0.50D-02	0.00684	1.36881
72	71	977.15066	0.50D-02	0.00604	1.20851
73	72	977.61229	0.20D-02	-0.00126	-0.62996

The 8-7 Band, 42 data, $J"_{min} = 25$, $J"_{max} = 66$
Unc.$_{Avge}$ = 4.4D-03, Unc.$_{Max}$ = 1.0D-02

Table A.2, Fourier Transform Infrared Data for ^{72}GeO (cm^{-1}) (*Cont'd*)

J'	J''	Obs	Unc	Calc-Obs	(Calc-Obs)/Unc
(Err/Unc.)$_{Avge}$ = 7.9D-02, RMSR = 1.18					
65	66	843.88489	0.20D-02	-0.00283	-1.41516
64	65	845.18345	0.50D-02	0.00507	1.01486
63	64	846.47882	0.10D-01	0.01072	1.07242
61	62	849.07615	0.20D-02	-0.00093	-0.46625
57	58	854.17027	0.10D-01	0.01048	1.04782
56	57	855.45757	0.10D-01	-0.01421	-1.42139
54	55	857.94972	0.20D-02	0.00225	1.12516
53	54	859.20233	0.50D-02	-0.00437	-0.87301
51	52	861.67326	0.20D-02	-0.00002	-0.01241
50	51	862.90444	0.20D-02	-0.00194	-0.97037
46	47	867.77821	0.10D-01	-0.0147	-1.47046
43	44	871.34625	0.20D-02	0.00385	1.92253
42	43	872.52878	0.50D-02	0.00551	1.10268
41	42	873.71956	0.50D-02	-0.00675	-1.35009
40	41	874.88514	0.20D-02	0.0005	0.25124
39	40	876.03616	0.10D-01	0.0166	1.66013
38	39	877.21484	0.20D-02	-0.00068	-0.33754
37	38	878.37216	0.20D-02	-0.00232	-1.15881
36	37	879.52633	0.50D-02	-0.00655	-1.30944
35	36	880.66531	0.20D-02	-0.00132	-0.6625
34	35	881.79966	0.20D-02	0.00276	1.37906
33	34	882.93683	0.20D-02	-0.00175	-0.87448
31	32	885.19022	0.50D-02	-0.00717	-1.43359
28	29	888.5109	0.20D-02	0.00057	0.28277
27	28	889.60529	0.20D-02	0.00398	1.99237
26	25	939.91449	0.50D-02	-0.00458	-0.91566
29	28	942.16161	0.50D-02	0.00662	1.3231
30	29	942.8941	0.10D-01	0.0139	1.39003
31	30	943.65233	0.10D-01	-0.01107	-1.1073
35	34	946.50538	0.20D-02	0.00349	1.7456
36	35	947.20233	0.50D-02	0.00703	1.40527
41	40	950.6092	0.20D-02	0.00349	1.74565
43	42	951.92691	0.20D-02	0.00064	0.31872
46	45	953.85458	0.50D-02	-0.00485	-0.96941
47	46	954.47647	0.20D-02	0.00058	0.29149
49	48	955.69289	0.10D-01	0.01863	1.86263
50	49	956.30795	0.10D-01	0.01068	1.0675
52	51	957.51371	0.20D-02	-0.00117	-0.58261
54	53	958.67913	0.20D-02	0.00019	0.09435
55	54	959.25572	0.20D-02	-0.00322	-1.61249
58	57	960.93267	0.20D-02	-0.00163	-0.81415
59	58	961.47891	0.20D-02	-0.00206	-1.03079

A.3 Fourier Transform Infrared Data for ^{73}GeO

Table A.3: Fourier Transform Infrared Data for ^{73}GeO (cm^{-1})

J'	J''	Obs	Unc	Calc-Obs	(Calc-Obs)/Unc
804 ^{73}GeO infrared transitions in 6 bands					
The 1-0 Band, 103 data, $J"_{min}$ = 1, $J"_{max}$ = 90 Unc.$_{Avge}$ = 2.1D-03, Unc.$_{Max}$ = 5.0D-03 (Err/Unc.)$_{Avge}$ = 1.2D-01, RMSR = 0.70					
83	84	876.78206	0.20D-02	-0.00122	-0.60778
82	83	878.22436	0.20D-02	0.0013	0.64808
81	82	879.65737	0.50D-02	0.00782	1.56426
80	81	881.09926	0.20D-02	0.00019	0.0948
79	80	882.52705	0.20D-02	0.00135	0.67538
78	79	883.94708	0.50D-02	0.00496	0.99286
77	78	885.36483	0.50D-02	0.00554	1.108
76	77	886.7779	0.50D-02	0.00548	1.09547
75	76	888.18924	0.20D-02	0.0018	0.8981
74	75	889.59415	0.20D-02	-0.0008	-0.40199
73	74	890.99128	0.20D-02	-0.00097	-0.48684
72	73	892.38166	0.20D-02	0.00023	0.11345
71	72	893.76639	0.20D-02	0.0017	0.84868
70	71	895.14802	0.50D-02	0.00088	0.17541
69	70	896.52057	0.20D-02	0.00375	1.87284
68	69	897.89389	0.20D-02	0.00042	0.21137
67	68	899.25974	0.20D-02	-0.00085	-0.42605
66	67	900.61789	0.20D-02	0.00014	0.07024
65	66	901.96974	0.20D-02	0.002	1.0001
64	65	903.31855	0.20D-02	0.00144	0.71823
63	64	904.66287	0.20D-02	-0.0001	-0.05063
62	63	905.99971	0.20D-02	0.00037	0.18327
61	62	907.33207	0.20D-02	-0.00016	-0.08033
60	61	908.65715	0.20D-02	0.00109	0.54329
59	60	909.97485	0.20D-02	0.00421	2.1039
58	59	911.2954	0.20D-02	-0.00104	-0.51888
57	58	912.60102	0.20D-02	0.00313	1.56477
56	57	913.90908	0.20D-02	-0.00069	-0.34556
55	56	915.20661	0.20D-02	0.00047	0.23495
54	55	916.49943	0.20D-02	0.00078	0.39092
53	54	917.78723	0.20D-02	0.00055	0.27706
52	53	919.07283	0.20D-02	-0.00306	-1.53197
51	52	920.34581	0.20D-02	0.00035	0.17352
50	51	921.61628	0.20D-02	0.00067	0.33319
49	50	922.88241	0.20D-02	-0.00029	-0.14329
48	49	924.14225	0.20D-02	-0.00056	-0.28122
47	48	925.39454	0.20D-02	0.00107	0.53396
46	47	926.64288	0.20D-02	0.001	0.50199
45	46	927.8875	0.20D-02	-0.001	-0.49754
44	45	929.12257	0.20D-02	0.0009	0.44999
43	44	930.35535	0.20D-02	-0.0006	-0.30078
42	43	931.57982	0.20D-02	0.00052	0.25976
41	42	932.8007	0.20D-02	-0.00047	-0.23377
40	41	934.0156	0.20D-02	-0.00117	-0.58676
39	40	935.22418	0.20D-02	-0.00129	-0.64457
38	39	936.42479	0.20D-02	0.00083	0.41729
37	38	937.62317	0.20D-02	-0.00055	-0.27647
36	37	938.81383	0.20D-02	0.00003	0.01365

Table A.3, Fourier Transform Infrared Data for ^{73}GeO (cm^{-1}) (*Cont'd*)

J'	J''	Obs	Unc	Calc-Obs	(Calc-Obs)/Unc
35	36	939.99881	0.20D-02	0.00053	0.2672
34	35	941.179	0.20D-02	0.00005	0.02384
33	34	942.353	0.20D-02	-0.00003	-0.01692
32	33	943.52058	0.20D-02	0.00051	0.25453
31	32	944.68288	0.20D-02	0.00054	0.26762
30	31	945.84162	0.20D-02	-0.00171	-0.85303
29	30	946.99084	0.20D-02	-0.00026	-0.12786
28	29	948.13501	0.20D-02	0.00041	0.20257
27	28	949.27041	0.50D-02	0.00399	0.79715
26	27	950.41075	0.20D-02	-0.00322	-1.61245
25	26	951.53782	0.20D-02	-0.00305	-1.52394
24	25	952.65624	0.20D-02	-0.0001	-0.05207
23	24	953.76848	0.20D-02	0.00313	1.56264
22	23	954.8791	0.20D-02	0.00207	1.0347
21	22	955.98441	0.20D-02	0.00042	0.20862
20	21	957.08364	0.20D-02	-0.00109	-0.54621
19	20	958.17465	0.20D-02	-0.00032	-0.16023
18	19	959.2586	0.20D-02	0.00156	0.78091
17	18	960.34073	0.20D-02	-0.0007	-0.34821
16	17	961.41964	0.50D-02	-0.0057	-1.13929
15	16	962.48023	0.20D-02	0.00163	0.81533
14	15	963.54206	0.20D-02	0.00172	0.86188
13	14	964.5997	0.20D-02	0.0	0.00089
12	13	965.64967	0.20D-02	-0.00007	-0.03331
11	12	966.69266	0.20D-02	0.00083	0.41379
10	11	967.73156	0.20D-02	-0.00024	-0.11851
9	10	968.76164	0.20D-02	0.00147	0.73428
8	9	969.78981	0.20D-02	-0.00098	-0.48848
7	8	970.80869	0.20D-02	-0.0002	-0.10242
6	7	971.82171	0.20D-02	0.00035	0.17683
5	6	972.82665	0.20D-02	0.00289	1.44365
4	5	973.83311	0.20D-02	-0.00221	-1.10261
3	4	974.82411	0.20D-02	0.00204	1.02247
2	3	975.81698	0.20D-02	-0.0017	-0.85189
0	1	977.77438	0.20D-02	0.00072	0.35869
2	1	980.67103	0.20D-02	-0.00246	-1.23246
3	2	981.62272	0.20D-02	-0.00204	-1.0221
4	3	982.56728	0.20D-02	-0.00069	-0.34595
5	4	983.50611	0.20D-02	0.00016	0.08033
6	5	984.43912	0.20D-02	0.0006	0.30107
7	6	985.36843	0.20D-02	-0.0015	-0.74956
8	7	986.28818	0.20D-02	-0.00029	-0.1472
9	8	987.20307	0.20D-02	-0.00049	-0.24264
10	9	988.11245	0.20D-02	-0.00145	-0.72663
11	10	989.01257	0.20D-02	0.00055	0.27507
12	11	989.90799	0.20D-02	0.00095	0.47675
13	12	990.79981	0.20D-02	-0.00135	-0.67748
14	13	991.68337	0.20D-02	-0.00173	-0.86334
15	14	992.55837	0.20D-02	0.00014	0.06843
16	15	993.42604	0.20D-02	0.00297	1.48698
17	16	994.29235	0.20D-02	0.00081	0.4065
18	17	995.15058	0.20D-02	0.00036	0.18118
19	18	996.0025	0.20D-02	-0.00016	-0.0798
20	19	996.8499	0.20D-02	-0.00255	-1.27727
21	20	997.68555	0.20D-02	0.0004	0.19794
22	21	998.51807	0.20D-02	0.00007	0.03502
23	22	999.34413	0.20D-02	-0.00023	-0.11697
24	23	1000.16224	0.20D-02	0.00097	0.48635

Table A.3, Fourier Transform Infrared Data for ^{73}GeO (cm^{-1}) (*Cont'd*)

J'	J''	Obs	Unc	Calc-Obs	(Calc-Obs)/Unc
25	24	1000.9756	0.20D-02	0.00048	0.23852
26	25	1001.78214	0.20D-02	0.00034	0.16955
27	26	1002.58202	0.20D-02	0.00039	0.19257
28	27	1003.37513	0.20D-02	0.00073	0.36268
29	28	1004.16271	0.20D-02	0.00009	0.04297
30	29	1004.94407	0.20D-02	-0.00084	-0.42146
31	30	1005.7166	0.20D-02	0.00053	0.26748
32	31	1006.48661	0.20D-02	-0.0021	-1.05016
33	32	1007.24625	0.20D-02	-0.00091	-0.45629
34	33	1008.00071	0.20D-02	-0.0011	-0.55086
35	34	1008.74653	0.20D-02	0.00079	0.39467
36	35	1009.486	0.20D-02	0.00244	1.21885
37	36	1010.2234	0.20D-02	-0.00044	-0.21829
38	37	1010.95087	0.20D-02	0.00001	0.00678
39	38	1011.67297	0.20D-02	-0.00078	-0.39243
40	39	1012.3869	0.20D-02	-0.00004	-0.02092
41	40	1013.09539	0.20D-02	-0.0005	-0.25018
42	41	1013.79641	0.20D-02	-0.00013	-0.06672
43	42	1014.49112	0.20D-02	-0.00013	-0.06556
44	43	1015.17984	0.20D-02	-0.00082	-0.40823
45	44	1015.85927	0.20D-02	0.0011	0.54873
46	45	1016.53543	0.20D-02	-0.00042	-0.2097
47	46	1017.20289	0.20D-02	0.00005	0.0249
48	47	1017.86457	0.20D-02	-0.00043	-0.21352
49	48	1018.51905	0.20D-02	-0.00044	-0.22152
50	49	1019.16922	0.20D-02	-0.00289	-1.44419
51	50	1019.80374	0.20D-02	0.00354	1.77189
52	51	1020.4419	0.20D-02	-0.00044	-0.21938
53	52	1021.06923	0.20D-02	-0.00038	-0.18911
54	53	1021.68973	0.20D-02	-0.00029	-0.1439
55	54	1022.3025	0.20D-02	0.00072	0.36112
56	55	1022.90962	0.20D-02	0.00056	0.27932
57	56	1023.50873	0.20D-02	0.00157	0.78456
58	57	1024.10348	0.20D-02	0.00009	0.0457
59	58	1024.69014	0.20D-02	-0.00015	-0.07343
60	59	1025.26839	0.20D-02	0.00114	0.57101
61	60	1025.83994	0.20D-02	0.00225	1.12285
62	61	1026.4092	0.20D-02	-0.00126	-0.6291
63	62	1026.96698	0.20D-02	-0.00019	-0.09604
64	63	1027.51804	0.20D-02	0.00067	0.33584
65	64	1028.06135	0.20D-02	0.00235	1.17533
66	65	1028.60181	0.20D-02	-0.00007	-0.0338
67	66	1029.13286	0.20D-02	-0.00004	-0.01778
68	67	1029.65694	0.20D-02	-0.00001	-0.00284
69	68	1030.17395	0.20D-02	0.00011	0.05476
70	69	1030.68443	0.20D-02	-0.00023	-0.11622
71	70	1031.1857	0.20D-02	0.00162	0.80794
72	71	1031.68051	0.20D-02	0.0029	1.45098
73	72	1032.17115	0.20D-02	0.00132	0.6616
74	73	1032.655	0.20D-02	-0.00051	-0.25649
75	74	1033.12861	0.20D-02	0.00083	0.41541
76	75	1033.598	0.20D-02	-0.00068	-0.33902
77	76	1034.0583	0.20D-02	-0.00018	-0.09108
78	77	1034.51319	0.20D-02	-0.00137	-0.68713
79	78	1034.9579	0.20D-02	0.0005	0.25201
80	79	1035.39558	0.20D-02	0.00229	1.14398
81	80	1035.83015	0.20D-02	0.00006	0.02792
82	81	1036.25544	0.20D-02	-0.00006	-0.02753

Table A.3, Fourier Transform Infrared Data for ^{73}GeO (cm^{-1}) (*Cont'd*)

J'	J''	Obs	Unc	Calc-Obs	(Calc-Obs)/Unc
83	82	1036.67544	0.20D-02	-0.00204	-1.01875
84	83	1037.08334	0.20D-02	0.00091	0.45336
85	84	1037.48872	0.20D-02	-0.00082	-0.40858
86	85	1037.88448	0.20D-02	-0.00012	-0.06049
87	86	1038.27281	0.20D-02	0.00079	0.39621
88	87	1038.65517	0.20D-02	0.00045	0.22561
89	88	1039.03044	0.20D-02	-0.00004	-0.01974
90	89	1039.39498	0.20D-02	0.00295	1.47422
91	90	1039.75449	0.20D-02	0.0037	1.85153
The 2-1 Band, 163 data, $J"_{min} = 0$, $J"_{max} = 82$					
Unc.$_{Avge}$ = 2.0D-03, Unc.$_{Max}$ = 1.0D-02					
(Err/Unc.)$_{Avge}$ = 1.4D-01, RMSR = 0.75					
81	82	871.26887	0.20D-02	-0.00008	-0.03751
80	81	872.69661	0.20D-02	-0.00019	-0.09369
79	80	874.11886	0.20D-02	-0.0001	-0.05037
78	79	875.53464	0.20D-02	0.00116	0.58218
77	78	876.94676	0.20D-02	0.00077	0.38386
76	77	878.35355	0.20D-02	0.00038	0.18945
75	76	879.75498	0.20D-02	0.00002	0.0087
74	75	881.14867	0.20D-02	0.00206	1.0315
73	74	882.54323	0.20D-02	-0.00212	-1.06239
72	73	883.92478	0.20D-02	0.00133	0.66681
71	72	885.30547	0.20D-02	0.00028	0.13895
70	71	886.67821	0.20D-02	0.0018	0.89869
69	70	888.04966	0.20D-02	-0.0008	-0.39913
68	69	889.41295	0.20D-02	-0.00064	-0.31971
67	68	890.7716	0.20D-02	-0.00126	-0.62832
66	67	892.12301	0.20D-02	-0.00005	-0.02527
65	66	893.4703	0.20D-02	-0.00017	-0.0857
64	65	894.81105	0.20D-02	0.0008	0.40009
63	64	896.14844	0.20D-02	-0.00033	-0.16317
62	63	897.4786	0.20D-02	0.00032	0.15925
61	62	898.80403	0.20D-02	0.0002	0.10208
60	61	900.12461	0.20D-02	-0.00055	-0.2749
59	60	901.43807	0.20D-02	0.00032	0.15792
58	59	902.74669	0.20D-02	0.00052	0.26035
57	58	904.05106	0.20D-02	-0.00056	-0.27801
56	57	905.3486	0.20D-02	-0.00033	-0.16735
55	56	906.64032	0.20D-02	0.00016	0.08196
54	55	907.92669	0.20D-02	0.00047	0.2346
53	54	909.20962	0.20D-02	-0.00136	-0.67973
52	53	910.48341	0.20D-02	0.00038	0.18863
51	52	911.75376	0.20D-02	-0.00003	-0.01565
50	51	913.01565	0.20D-02	0.00243	1.21714
49	50	914.27637	0.20D-02	0.00045	0.22656
49	50	914.27637	0.20D-02	0.00045	0.22656
48	49	915.53053	0.20D-02	-0.00059	-0.29265
47	48	916.777	0.20D-02	0.00044	0.21907
46	47	918.02041	0.20D-02	-0.00111	-0.55355
45	46	919.25324	0.20D-02	0.00227	1.13406
44	45	920.48589	0.20D-02	0.00016	0.08153
43	44	921.71172	0.20D-02	-0.00079	-0.39651
42	43	922.93065	0.20D-02	-0.00052	-0.26046
41	42	924.14225	0.20D-02	0.00138	0.68934
40	41	925.35003	0.20D-02	0.00139	0.69738
39	40	926.5535	0.20D-02	0.00001	0.00337
38	39	927.7504	0.20D-02	-0.00054	-0.26822

Table A.3, Fourier Transform Infrared Data for ^{73}GeO (cm^{-1}) (*Cont'd*)

J'	J''	Obs	Unc	Calc-Obs	(Calc-Obs)/Unc
37	38	928.9409	0.20D-02	-0.00041	-0.2027
36	37	930.12549	0.20D-02	-0.00012	-0.06055
35	36	931.30249	0.20D-02	0.002	0.9978
34	35	932.47737	0.20D-02	0.00046	0.2319
33	34	933.64555	0.20D-02	-0.00015	-0.07368
32	33	934.8068	0.20D-02	0.00039	0.1956
31	32	935.9637	0.20D-02	-0.00053	-0.26568
30	31	937.11299	0.20D-02	0.00034	0.17193
29	30	938.25585	0.20D-02	0.00183	0.91306
28	29	939.39646	0.20D-02	-0.00027	-0.13284
27	28	940.52972	0.20D-02	-0.00086	-0.43123
26	27	941.65943	0.20D-02	-0.00377	-1.88268
25	26	942.77486	0.20D-02	0.00174	0.87249
24	25	943.89563	0.20D-02	-0.00396	-1.9814
23	24	945.00527	0.50D-02	-0.00442	-0.88392
22	23	946.10179	0.20D-02	0.00233	1.16677
21	22	947.20556	0.20D-02	-0.00407	-2.03717
20	21	948.29336	0.20D-02	-0.00043	-0.21725
19	20	949.3793	0.20D-02	-0.00087	-0.43392
18	19	950.45222	0.50D-02	0.00578	1.15689
17	18	951.53596	0.20D-02	-0.00435	-2.17435
16	17	952.60351	0.20D-02	-0.00426	-2.12922
15	16	953.66232	0.20D-02	-0.00141	-0.70296
14	15	954.71894	0.20D-02	-0.00235	-1.17613
13	14	955.76627	0.20D-02	0.0	0.00073
12	13	956.81039	0.20D-02	-0.00046	-0.22807
10	11	958.87863	0.20D-02	0.00055	0.27521
9	10	959.90589	0.20D-02	-0.00115	-0.57403
8	9	960.92737	0.20D-02	-0.00311	-1.55625
7	8	961.93671	0.20D-02	0.00099	0.49287
5	6	963.94781	0.20D-02	-0.00148	-0.74236
4	5	964.945	0.20D-02	-0.00351	-1.75304
3	4	965.93687	0.50D-02	-0.00631	-1.26196
2	3	966.91819	0.50D-02	-0.0047	-0.93949
1	2	967.88832	0.20D-02	0.00197	0.98495
0	1	968.87186	0.10D-01	-0.01092	-1.09192
1	0	970.78778	0.20D-02	-0.00402	-2.01119
2	1	971.73958	0.20D-02	-0.00367	-1.8346
3	2	972.67686	0.50D-02	0.005	1.00041
5	4	974.55383	0.20D-02	0.00131	0.65632
6	5	975.48173	0.50D-02	0.00072	0.14381
7	6	976.40379	0.20D-02	-0.00027	-0.13611
8	7	977.31822	0.20D-02	0.00013	0.06359
9	8	978.22637	0.20D-02	0.00054	0.26787
10	9	979.12854	0.20D-02	0.00065	0.32599
11	10	980.0257	0.20D-02	-0.00051	-0.25282
12	11	980.91448	0.20D-02	0.00042	0.21071
13	12	981.79922	0.20D-02	-0.00091	-0.4543
14	13	982.67437	0.20D-02	0.00102	0.51146
15	14	983.54551	0.20D-02	0.00063	0.31714
16	15	984.40962	0.20D-02	0.00093	0.4669
17	16	985.27073	0.20D-02	-0.00212	-1.05999
18	17	986.12065	0.20D-02	-0.00035	-0.1744
19	18	986.96548	0.20D-02	0.00014	0.0679
20	19	987.80651	0.20D-02	-0.00196	-0.97903
21	20	988.63698	0.20D-02	0.0001	0.04901
22	21	989.46441	0.20D-02	-0.00122	-0.60877
23	22	990.28363	0.20D-02	-0.00075	-0.3733

Table A.3, Fourier Transform Infrared Data for ^{73}GeO (cm^{-1}) (*Cont'd*)

J'	J''	Obs	Unc	Calc-Obs	(Calc-Obs)/Unc
24	23	991.09767	0.20D-02	-0.00153	-0.76547
25	24	991.90229	0.20D-02	0.00066	0.32891
26	25	992.70343	0.20D-02	-0.00012	-0.06106
27	26	993.49698	0.20D-02	0.00021	0.10375
28	27	994.28446	0.20D-02	0.00012	0.06235
29	28	995.06483	0.20D-02	0.00066	0.32888
30	29	995.84011	0.20D-02	-0.00023	-0.11253
31	30	996.60741	0.20D-02	0.00035	0.1771
32	31	997.37165	0.20D-02	-0.00254	-1.26807
33	32	998.12733	0.20D-02	-0.0034	-1.69902
34	33	998.8724	0.20D-02	-0.00021	-0.10671
35	34	999.61697	0.20D-02	-0.00309	-1.54709
36	35	1000.34935	0.20D-02	-0.00036	-0.18129
37	36	1001.07771	0.20D-02	-0.0002	-0.09977
38	37	1001.79946	0.20D-02	-0.00003	-0.01388
39	38	1002.51484	0.20D-02	-0.0001	-0.05009
40	39	1003.22247	0.20D-02	0.00096	0.48158
41	40	1003.92576	0.20D-02	-0.00028	-0.14037
42	41	1004.61804	0.20D-02	0.00284	1.41754
43	42	1005.30971	0.20D-02	-0.0001	-0.04971
44	43	1005.99438	0.20D-02	-0.00271	-1.35365
45	44	1006.66622	0.20D-02	0.00083	0.41466
46	45	1007.33539	0.20D-02	0.00034	0.16869
47	46	1008.00071	0.20D-02	-0.00301	-1.50664
48	47	1008.65239	0.20D-02	0.00055	0.27712
49	48	1009.30115	0.20D-02	0.00032	0.15888
50	49	1009.94352	0.20D-02	-0.00029	-0.14294
51	50	1010.58017	0.20D-02	-0.00193	-0.96343
52	51	1011.20529	0.50D-02	0.00119	0.23832
53	52	1011.82872	0.20D-02	-0.00078	-0.39136
54	53	1012.44221	0.20D-02	0.00039	0.19396
55	54	1013.05067	0.20D-02	-0.00022	-0.10935
56	55	1013.65148	0.20D-02	0.0	0.00206
57	56	1014.24549	0.20D-02	0.00021	0.10305
58	57	1014.83243	0.20D-02	0.00062	0.31195
59	58	1015.41288	0.20D-02	0.00068	0.33761
60	59	1015.98842	0.20D-02	-0.00123	-0.61614
61	60	1016.55544	0.20D-02	-0.0015	-0.7505
62	61	1017.11337	0.20D-02	0.00043	0.21334
63	62	1017.66669	0.20D-02	0.00006	0.0292
64	63	1018.2106	0.20D-02	0.00218	1.09084
65	64	1018.75187	0.20D-02	0.00001	0.00707
66	65	1019.28345	0.20D-02	0.0006	0.30165
67	66	1019.80637	0.20D-02	0.00289	1.44334
68	67	1020.3261	0.20D-02	0.00139	0.6959
69	68	1020.83849	0.20D-02	0.00026	0.12807
70	69	1021.34483	0.20D-02	-0.00182	-0.91141
71	70	1021.84103	0.20D-02	-0.00077	-0.38381
72	71	1022.33059	0.20D-02	-0.00009	-0.04542
73	72	1022.81663	0.20D-02	-0.00293	-1.46254
74	73	1023.28884	0.20D-02	0.00103	0.51355
75	74	1023.75889	0.20D-02	0.00008	0.04202
76	75	1024.22068	0.20D-02	0.00033	0.16557
77	76	1024.67622	0.20D-02	-0.00025	-0.12665
78	77	1025.12457	0.20D-02	-0.00073	-0.36597
79	78	1025.56412	0.20D-02	0.00047	0.23627
80	79	1026.0038	0.50D-02	-0.00557	-1.11452
81	80	1026.42655	0.20D-02	-0.00182	-0.90954

Table A.3, Fourier Transform Infrared Data for ^{73}GeO (cm^{-1}) (*Cont'd*)

J'	J''	Obs	Unc	Calc-Obs	(Calc-Obs)/Unc
82	81	1026.84397	0.20D-02	0.00012	0.05917
83	82	1027.25745	0.20D-02	-0.00116	-0.58105
The 3-2 Band, 148 data, $J"_{min} = 0$, $J"_{max} = 78$					
Unc.$_{Avge}$ = 2.5D-03, Unc.$_{Max}$ = 5.0D-03					
(Err/Unc.)$_{Avge}$ = 4.5D-02, RMSR = 0.79					
77	78	868.54862	0.50D-02	0.00287	0.57328
76	77	869.95443	0.20D-02	-0.00312	-1.55772
75	76	871.34674	0.20D-02	-0.00093	-0.46697
74	75	872.73685	0.20D-02	-0.00189	-0.94474
73	74	874.11886	0.20D-02	-0.00009	-0.04625
72	73	875.49749	0.20D-02	-0.00026	-0.13172
71	72	876.86837	0.20D-02	0.00194	0.96863
70	71	878.24003	0.20D-02	-0.00202	-1.01038
69	70	879.60021	0.20D-02	0.00011	0.05592
68	69	880.95718	0.20D-02	0.00006	0.03239
67	68	882.30872	0.20D-02	0.00003	0.01373
66	67	883.65459	0.20D-02	0.00024	0.11969
65	66	884.99455	0.20D-02	0.00093	0.46496
64	65	886.32989	0.20D-02	0.00081	0.40443
63	64	887.66151	0.20D-02	-0.00105	-0.52731
62	63	888.98624	0.20D-02	-0.00149	-0.74549
61	62	890.30394	0.20D-02	-0.00037	-0.1854
60	61	891.62133	0.50D-02	-0.00441	-0.88291
59	60	892.92427	0.20D-02	0.00049	0.24353
58	59	894.2266	0.20D-02	0.00049	0.24677
57	58	895.52584	0.20D-02	-0.00193	-0.96289
56	57	896.815	0.20D-02	0.00022	0.10924
55	56	898.1031	0.20D-02	-0.00212	-1.06221
54	55	899.38227	0.20D-02	-0.00108	-0.5424
53	54	900.65599	0.20D-02	-0.00015	-0.07682
52	53	901.92425	0.20D-02	0.00068	0.33925
51	52	903.1903	0.20D-02	-0.00187	-0.93452
50	51	904.4468	0.20D-02	-0.00046	-0.22844
49	50	905.69828	0.20D-02	0.00037	0.1871
48	49	906.94472	0.20D-02	0.00064	0.32168
47	48	908.18684	0.20D-02	-0.0004	-0.19995
46	47	909.42278	0.20D-02	-0.0009	-0.44823
45	46	910.64789	0.20D-02	0.00379	1.89648
44	45	911.87649	0.20D-02	-0.00066	-0.3312
43	44	913.09473	0.20D-02	-0.00041	-0.20668
42	43	914.30586	0.20D-02	0.00126	0.62971
41	42	915.51755	0.50D-02	-0.00332	-0.66301
40	41	916.71678	0.20D-02	-0.00113	-0.56371
39	40	917.91063	0.20D-02	0.00074	0.37064
38	39	919.10151	0.20D-02	-0.00015	-0.07478
37	38	920.28252	0.20D-02	0.0031	1.54954
36	37	921.46242	0.20D-02	0.00172	0.85817
35	36	922.63899	0.20D-02	-0.00209	-1.04433
34	35	923.80475	0.20D-02	-0.00084	-0.4184
33	34	924.96626	0.20D-02	-0.00112	-0.55951
32	33	926.12091	0.20D-02	-0.00033	-0.16306
31	32	927.26704	0.20D-02	0.00319	1.59539
30	31	928.4127	0.20D-02	0.00138	0.69045
29	30	929.55176	0.20D-02	0.00034	0.1716
28	29	930.68416	0.20D-02	0.00014	0.06836
27	28	931.81059	0.20D-02	0.00006	0.03017
26	27	932.92893	0.20D-02	0.00222	1.1117

Table A.3, Fourier Transform Infrared Data for ^{73}GeO (cm^{-1}) (*Cont'd*)

J'	J''	Obs	Unc	Calc-Obs	(Calc-Obs)/Unc
25	26	934.04121	0.50D-02	0.00459	0.91891
24	25	935.14767	0.50D-02	0.0069	1.38058
23	24	936.25756	0.20D-02	-0.0001	-0.05131
22	23	937.35538	0.20D-02	-0.00093	-0.46648
21	22	938.44851	0.20D-02	-0.00298	-1.48969
20	21	939.53388	0.20D-02	-0.00317	-1.58639
19	20	940.60992	0.20D-02	0.00003	0.01284
18	19	941.68785	0.50D-02	-0.00461	-0.92103
17	18	942.75187	0.20D-02	-0.00128	-0.63817
16	17	943.81103	0.20D-02	0.00095	0.47547
15	16	944.86756	0.20D-02	-0.00015	-0.07724
14	15	945.91771	0.20D-02	-0.00087	-0.43681
13	14	946.96934	0.50D-02	-0.00907	-1.81358
12	13	947.99788	0.20D-02	-0.00018	-0.08915
11	12	949.02989	0.20D-02	-0.00078	-0.38805
10	11	950.05678	0.20D-02	-0.00227	-1.13633
9	10	951.07366	0.20D-02	0.00019	0.0955
8	9	952.08568	0.20D-02	0.00146	0.73181
7	8	953.09409	0.20D-02	0.00028	0.14188
6	7	954.09474	0.20D-02	0.00079	0.39511
5	6	955.08867	0.20D-02	0.00194	0.97085
4	5	956.07738	0.20D-02	0.00221	1.10351
3	4	957.06692	0.50D-02	-0.00447	-0.89307
2	3	958.03132	0.50D-02	0.00788	1.57668
1	2	959.00926	0.20D-02	0.00056	0.28096
0	1	959.97481	0.20D-02	-0.00051	-0.25562
1	0	961.87657	0.50D-02	0.00822	1.64441
2	1	962.82344	0.50D-02	0.00734	1.46711
3	2	963.76477	0.50D-02	0.0058	1.16037
4	3	964.70478	0.20D-02	-0.00061	-0.30526
5	4	965.63016	0.20D-02	0.0014	0.69843
6	5	966.5564	0.50D-02	-0.00367	-0.73346
7	6	967.47129	0.50D-02	-0.00362	-0.72491
8	7	968.37966	0.50D-02	-0.00331	-0.6613
9	8	969.28082	0.20D-02	-0.00203	-1.01726
10	9	970.17376	0.20D-02	0.00119	0.59487
11	10	971.06147	0.20D-02	0.00336	1.68245
12	11	971.94854	0.20D-02	-0.0001	-0.05042
13	12	972.82665	0.20D-02	-0.00092	-0.45942
14	13	973.69669	0.20D-02	0.00002	0.0096
15	14	974.56075	0.20D-02	0.00061	0.30579
16	15	975.41633	0.20D-02	0.00335	1.67348
17	16	976.27003	0.20D-02	0.00161	0.8067
18	17	977.11621	0.20D-02	0.00105	0.52468
19	18	977.95133	0.50D-02	0.00516	1.03263
20	19	978.7872	0.20D-02	0.00214	1.0716
21	20	979.61472	0.20D-02	0.00108	0.53879
22	21	980.43357	0.20D-02	0.00227	1.13739
23	22	981.24194	0.50D-02	0.00753	1.5066
24	23	982.05679	0.20D-02	-0.00011	-0.05484
25	24	982.8548	0.20D-02	0.00264	1.31761
26	25	983.6522	0.20D-02	-0.00046	-0.23204
27	26	984.43483	0.50D-02	0.00474	0.94808
28	27	985.22195	0.20D-02	-0.00102	-0.51153
29	28	985.99743	0.20D-02	-0.00164	-0.81809
30	29	986.75868	0.50D-02	0.00548	1.09582
31	30	987.52122	0.50D-02	0.0048	0.96015
32	31	988.28097	0.20D-02	0.00038	0.1886

Table A.3, Fourier Transform Infrared Data for ^{73}GeO (cm^{-1}) (*Cont'd*)

J'	J''	Obs	Unc	Calc-Obs	(Calc-Obs)/Unc
33	32	989.03429	0.50D-02	-0.00415	-0.83073
34	33	989.77316	0.20D-02	-0.00078	-0.39181
35	34	990.50928	0.20D-02	-0.00122	-0.61237
36	35	991.23911	0.20D-02	-0.00195	-0.9744
37	36	991.95975	0.20D-02	-0.00007	-0.03399
38	37	992.67496	0.20D-02	0.00066	0.32797
39	38	993.38533	0.20D-02	-0.0004	-0.19956
40	39	994.08711	0.20D-02	0.00051	0.2574
41	40	994.78387	0.20D-02	-0.00018	-0.09217
42	41	995.47338	0.20D-02	-0.00028	-0.13928
43	42	996.15055	0.50D-02	0.00531	1.06201
44	43	996.83211	0.20D-02	-0.00016	-0.08028
45	44	997.50223	0.20D-02	-0.00087	-0.43621
46	45	998.1678	0.20D-02	-0.00372	-1.85892
47	46	998.81974	0.20D-02	0.00035	0.17562
48	47	999.46903	0.20D-02	0.00035	0.17629
49	48	1000.11185	0.20D-02	0.00009	0.04711
50	49	1000.74782	0.20D-02	-0.00006	-0.02812
51	50	1001.36923	0.50D-02	0.0076	1.5196
52	51	1001.99367	0.50D-02	0.00546	1.09134
53	52	1002.61493	0.20D-02	-0.00028	-0.14168
54	53	1003.22855	0.50D-02	-0.00516	-1.03289
55	54	1003.82527	0.20D-02	0.00004	0.0206
56	55	1004.42197	0.20D-02	-0.00155	-0.77437
57	56	1005.00838	0.20D-02	0.00032	0.16171
58	57	1005.59733	0.50D-02	-0.00718	-1.43693
59	58	1006.16456	0.20D-02	0.00017	0.08688
60	59	1006.73176	0.20D-02	0.0007	0.34911
61	60	1007.29216	0.20D-02	0.00115	0.57269
62	61	1007.84883	0.20D-02	-0.00157	-0.78358
63	62	1008.39399	0.20D-02	0.00034	0.16909
64	63	1008.93619	0.20D-02	-0.00172	-0.86052
65	64	1009.46705	0.20D-02	0.00063	0.31637
66	65	1009.99332	0.20D-02	0.00064	0.31853
67	66	1010.51359	0.20D-02	-0.00031	-0.1553
68	67	1011.02594	0.20D-02	-0.0003	-0.15137
69	68	1011.52934	0.20D-02	0.00168	0.83907
70	69	1012.03058	0.20D-02	-0.00117	-0.58476

The 4-3 Band, 141 data, $J"_{min} = 5$, $J"_{max} = 83$
Unc.$_{Avge}$ = 3.4D-03, Unc.$_{Max}$ = 1.0D-02
(Err/Unc.)$_{Avge}$ = 3.3D-01, RMSR = 1.06

82	83	853.13672	0.50D-02	-0.0004	-0.0792
81	82	854.57155	0.10D-01	-0.01552	-1.55198
80	81	855.97963	0.50D-02	-0.00917	-1.83446
79	80	857.37801	0.50D-02	0.0016	0.31919
78	79	858.79526	0.10D-01	-0.01179	-1.17855
77	78	860.18272	0.20D-02	-0.00069	-0.34338
76	77	861.57572	0.20D-02	-0.00044	-0.21924
75	76	862.96441	0.20D-02	-0.0012	-0.6005
74	75	864.34831	0.20D-02	-0.00249	-1.24737
73	74	865.72546	0.20D-02	-0.00239	-1.19504
72	73	867.09709	0.20D-02	-0.00212	-1.05882
71	72	868.46875	0.50D-02	-0.00724	-1.44756
70	71	869.82574	0.20D-02	-0.00305	-1.52545
69	70	871.17539	0.50D-02	0.00308	0.61649
68	69	872.52876	0.20D-02	0.0001	0.05083
67	68	873.87543	0.20D-02	-0.00158	-0.79179

Table A.3, Fourier Transform Infrared Data for ^{73}GeO (cm^{-1}) (*Cont'd*)

J'	J''	Obs	Unc	Calc-Obs	(Calc-Obs)/Unc
66	67	875.21363	0.20D-02	-0.0002	-0.10194
65	66	876.54614	0.20D-02	0.00143	0.71512
64	65	877.87685	0.20D-02	-0.00057	-0.28584
63	64	879.19651	0.20D-02	0.00303	1.51481
62	63	880.51585	0.20D-02	0.0015	0.75184
61	62	881.83242	0.20D-02	-0.00273	-1.36499
60	61	883.13709	0.20D-02	-0.00054	-0.27108
59	60	884.43893	0.20D-02	-0.00101	-0.50662
58	59	885.74149	0.50D-02	-0.00769	-1.53879
57	58	887.02503	0.20D-02	-0.00087	-0.43743
56	57	888.30833	0.20D-02	0.00066	0.33167
55	56	889.58693	0.20D-02	0.00137	0.68501
54	55	890.86272	0.20D-02	-0.00066	-0.32774
53	54	892.12301	0.50D-02	0.00728	1.45524
52	53	893.38432	0.50D-02	0.00861	1.72288
51	52	894.64282	0.50D-02	0.00719	1.43767
50	51	895.90222	0.20D-02	-0.00072	-0.3613
49	50	897.14212	0.50D-02	0.00528	1.05615
48	49	898.38535	0.20D-02	0.00234	1.1689
47	48	899.62281	0.20D-02	-0.00045	-0.22614
46	47	900.85286	0.20D-02	-0.00146	-0.73011
45	46	902.07463	0.20D-02	0.00018	0.0916
44	45	903.28836	0.20D-02	0.00421	2.10364
43	44	904.50406	0.20D-02	0.0006	0.30052
42	43	905.71083	0.20D-02	0.00025	0.12688
41	42	906.91502	0.50D-02	-0.00319	-0.63705
40	41	908.09488	0.10D-01	0.012	1.20031
39	40	909.29915	0.50D-02	-0.00292	-0.58445
38	39	910.48341	0.50D-02	-0.00355	-0.71036
37	38	911.65781	0.20D-02	-0.00005	-0.02332
36	37	912.82998	0.20D-02	-0.00004	-0.0188
35	36	913.99553	0.20D-02	0.00083	0.4172
34	35	915.1634	0.50D-02	-0.00637	-1.27428
33	34	916.30423	0.50D-02	0.00769	1.53876
32	33	917.46478	0.50D-02	-0.00374	-0.74813
31	32	918.59669	0.50D-02	0.00768	1.53681
30	31	919.73953	0.20D-02	0.00237	1.18357
29	30	920.87321	0.20D-02	0.0004	0.19878
28	29	921.99907	0.20D-02	0.00042	0.21215
27	28	923.1048	0.10D-01	0.01476	1.47564
26	27	924.22453	0.50D-02	0.00923	1.84656
25	26	925.33525	0.50D-02	0.00686	1.37252
24	25	926.443	0.20D-02	0.00159	0.79729
23	24	927.54101	0.20D-02	0.00019	0.09386
22	23	928.62614	0.50D-02	0.00578	1.15622
21	22	929.71906	0.50D-02	-0.00233	-0.46529
20	21	930.79514	0.20D-02	0.00049	0.2469
19	20	931.8672	0.20D-02	0.00141	0.70551
18	19	932.92896	0.50D-02	0.00669	1.33881
17	18	933.99285	0.20D-02	0.00391	1.95577
16	17	935.05065	0.20D-02	0.00125	0.62623
15	16	936.0966	0.20D-02	0.00448	2.23782
14	15	937.14561	0.20D-02	-0.00134	-0.66999
13	14	938.18237	0.20D-02	-0.0009	-0.44792
12	13	939.2124	0.20D-02	0.00029	0.14354
11	12	940.23918	0.20D-02	-0.0013	-0.65127
10	11	941.26083	0.50D-02	-0.00379	-0.75719
9	10	942.26933	0.20D-02	0.00085	0.42281

Table A.3, Fourier Transform Infrared Data for ^{73}GeO (cm^{-1}) (*Cont'd*)

J'	J''	Obs	Unc	Calc-Obs	(Calc-Obs)/Unc
8	9	943.27807	0.20D-02	-0.00081	-0.40455
7	8	944.27541	0.20D-02	0.00288	1.43934
6	7	945.27097	0.20D-02	0.00229	1.14375
5	6	946.26211	0.20D-02	0.00003	0.01307
4	5	947.23473	0.50D-02	0.01019	2.03868
6	5	957.64381	0.50D-02	0.0065	1.30025
7	6	958.56069	0.50D-02	-0.00158	-0.3156
8	7	959.44466	0.10D-01	0.01701	1.70127
9	8	960.35709	0.20D-02	0.00089	0.44593
10	9	961.24885	0.20D-02	-0.00081	-0.40606
11	10	962.12594	0.50D-02	0.00587	1.17386
12	11	963.01212	0.50D-02	-0.00283	-0.56513
13	12	963.87998	0.20D-02	0.0005	0.25083
14	13	964.73774	0.50D-02	0.00762	1.5239
15	14	965.60088	0.20D-02	0.00304	1.51812
16	15	966.45382	0.20D-02	0.00233	1.16512
17	16	967.29839	0.20D-02	0.00364	1.81993
18	17	968.14174	0.20D-02	-0.00019	-0.09329
19	18	968.97418	0.20D-02	0.00053	0.26467
20	19	969.80236	0.20D-02	-0.00087	-0.43715
21	20	970.62077	0.20D-02	0.0011	0.55049
22	21	971.43558	0.20D-02	0.00028	0.14169
23	22	972.24268	0.20D-02	0.00075	0.37556
24	23	973.03462	0.50D-02	0.00995	1.99049
25	24	973.8404	0.20D-02	-0.00112	-0.56223
26	25	974.62949	0.50D-02	-0.00196	-0.39227
27	26	975.40833	0.20D-02	0.00099	0.49502
28	27	976.18273	0.20D-02	0.00191	0.95384
29	28	976.95318	0.20D-02	0.0003	0.14996
30	29	977.71329	0.20D-02	0.00252	1.2624
31	30	978.46523	0.50D-02	0.00641	1.28209
32	31	979.22131	0.20D-02	-0.00037	-0.18258
33	32	979.96035	0.20D-02	0.00337	1.6832
34	33	980.69924	0.20D-02	0.0007	0.35144
35	34	981.42918	0.20D-02	0.00043	0.21621
36	35	982.15299	0.20D-02	-0.00027	-0.13341
37	36	982.86711	0.20D-02	0.00213	1.06648
38	37	983.58006	0.20D-02	-0.00089	-0.44501
39	38	984.27862	0.20D-02	0.00387	1.93606
40	39	984.97823	0.20D-02	0.00097	0.48368
41	40	985.66556	0.20D-02	0.00371	1.85681
42	41	986.35175	0.20D-02	0.00096	0.47944
43	42	987.03004	0.20D-02	-0.00055	-0.27448
44	43	987.69979	0.20D-02	-0.00017	-0.08595
45	44	988.36587	0.50D-02	-0.00281	-0.56245
46	45	989.01257	0.50D-02	0.00724	1.44761
47	46	989.66839	0.20D-02	0.00147	0.73338
48	47	990.30937	0.20D-02	0.00382	1.91086
49	48	990.94924	0.20D-02	0.00056	0.28036
50	49	991.59572	0.10D-01	-0.01605	-1.60484
51	50	992.20851	0.50D-02	-0.00572	-1.14356
52	51	992.81497	0.20D-02	0.00419	2.09505
53	52	993.42604	0.20D-02	0.0027	1.35162
54	53	994.03138	0.20D-02	0.00016	0.07963
55	54	994.62479	0.20D-02	0.00275	1.37289
56	55	995.21782	0.20D-02	-0.0011	-0.54966
57	56	995.79795	0.20D-02	0.00113	0.56582
58	57	996.3729	0.20D-02	0.00171	0.85306

Table A.3, Fourier Transform Infrared Data for ^{73}GeO (cm^{-1}) (*Cont'd*)

J'	J''	Obs	Unc	Calc-Obs	(Calc-Obs)/Unc
59	58	996.94807	0.50D-02	-0.00479	-0.95763
60	59	997.50223	0.20D-02	0.00287	1.43329
61	60	998.05644	0.20D-02	0.00361	1.80384
62	61	998.61459	0.50D-02	-0.00649	-1.29741
63	62	999.13891	0.10D-01	0.01035	1.03499
64	63	999.6922	0.50D-02	-0.00869	-1.7388
65	64	1000.19745	0.10D-01	0.01338	1.33792
66	65	1000.71589	0.10D-01	0.01533	1.53263
67	66	1001.23303	0.10D-01	0.01163	1.16251
The 5-4 Band, 85 data, $J"_{min} = 11$, $J"_{max} = 71$					
Unc.$_{Avge}$ = 3.3D-03, Unc.$_{Max}$ = 1.0D-02					
(Err/Unc.)$_{Avge}$ = 1.6D-01, RMSR = 0.96					
70	71	861.43212	0.50D-02	0.00167	0.33472
69	70	862.78908	0.50D-02	-0.00602	-1.20402
68	69	864.12518	0.20D-02	0.00176	0.87887
67	68	865.46822	0.20D-02	-0.00279	-1.39672
66	67	866.80129	0.20D-02	-0.00279	-1.39694
65	66	868.12934	0.20D-02	-0.00319	-1.59722
64	65	869.44954	0.20D-02	-0.00118	-0.58779
63	64	870.76813	0.20D-02	-0.00298	-1.48893
62	63	872.07573	0.20D-02	0.00075	0.37413
61	62	873.38049	0.20D-02	0.00185	0.92603
60	61	874.6838	0.20D-02	-0.00107	-0.53357
59	60	875.97591	0.20D-02	0.00174	0.87012
58	59	877.26828	0.20D-02	-0.00122	-0.60827
57	58	878.54649	0.50D-02	0.00448	0.89638
56	57	879.82414	0.50D-02	0.00522	1.04499
55	56	881.10041	0.20D-02	0.00183	0.91592
54	55	882.36861	0.20D-02	0.00096	0.48105
53	54	883.63525	0.50D-02	-0.0039	-0.77904
52	53	884.8844	0.50D-02	0.00318	0.63589
51	52	886.13689	0.20D-02	0.00136	0.67758
50	51	887.37628	0.50D-02	0.00704	1.40828
49	50	888.62159	0.20D-02	0.00122	0.60865
48	49	889.85609	0.20D-02	0.0006	0.30107
47	48	891.08451	0.20D-02	0.00047	0.23259
46	47	892.30607	0.20D-02	0.00156	0.77782
45	46	893.51195	0.10D-01	0.01269	1.26927
44	45	894.73604	0.20D-02	-0.00002	-0.01219
43	44	895.95027	0.50D-02	-0.00854	-1.70727
42	43	897.14188	0.20D-02	-0.00008	-0.0421
41	42	898.33316	0.50D-02	0.00301	0.60228
40	41	899.52396	0.20D-02	0.0009	0.44978
39	40	900.7056	0.20D-02	0.00225	1.12468
38	39	901.8828	0.20D-02	0.00234	1.16998
37	38	903.06418	0.50D-02	-0.00748	-1.4959
36	37	904.22194	0.20D-02	0.00059	0.295
34	35	906.53685	0.20D-02	0.0001	0.05126
33	34	907.68803	0.20D-02	-0.0025	-1.24822
29	30	912.22214	0.20D-02	-0.00018	-0.08933
28	29	913.34125	0.20D-02	0.00031	0.15459
27	28	914.45519	0.20D-02	0.00013	0.06368
26	27	915.5597	0.50D-02	0.00353	0.70697
25	26	916.66496	0.20D-02	0.00034	0.17036
24	25	917.76865	0.50D-02	-0.00714	-1.42726
21	22	921.0202	0.50D-02	-0.00536	-1.07293
20	21	922.08589	0.20D-02	0.00159	0.79321

Table A.3, Fourier Transform Infrared Data for ^{73}GeO (cm^{-1}) (*Cont'd*)

J'	J''	Obs	Unc	Calc-Obs	(Calc-Obs)/Unc
19	20	923.15881	0.50D-02	-0.0046	-0.92015
17	18	925.26724	0.20D-02	0.00262	1.3078
16	17	926.31293	0.50D-02	0.00583	1.16534
12	11	954.08981	0.50D-02	0.00742	1.4849
13	12	954.95674	0.50D-02	0.00558	1.11608
16	15	957.51342	0.50D-02	0.00629	1.25819
17	16	958.35984	0.20D-02	-0.00033	-0.16672
18	17	959.18574	0.50D-02	0.00721	1.44211
21	20	961.65491	0.20D-02	0.00015	0.07745
22	21	962.45968	0.20D-02	0.0033	1.65239
25	24	964.84651	0.20D-02	0.00172	0.86239
26	25	965.63016	0.20D-02	0.00028	0.14113
27	26	966.40473	0.20D-02	0.00147	0.73611
28	27	967.17607	0.20D-02	-0.00059	-0.29365
29	28	967.93672	0.20D-02	0.00156	0.78087
30	29	968.69964	0.50D-02	-0.00505	-1.01047
31	30	969.43421	0.10D-01	0.01018	1.01785
32	31	970.18998	0.20D-02	-0.00231	-1.15387
33	32	970.92331	0.20D-02	0.00112	0.55854
34	33	971.65483	0.20D-02	-0.00018	-0.08944
35	34	972.38571	0.50D-02	-0.0074	-1.47956
36	35	973.09324	0.20D-02	0.00217	1.08427
37	36	973.80682	0.20D-02	-0.00089	-0.44597
38	37	974.51338	0.50D-02	-0.00352	-0.70427
39	38	975.22007	0.10D-01	-0.01288	-1.28816
40	39	975.89823	0.20D-02	-0.00032	-0.16234
41	40	976.58231	0.20D-02	-0.0003	-0.15133
42	41	977.25498	0.50D-02	0.00448	0.89644
43	42	977.92618	0.20D-02	0.00409	2.044
44	43	978.5919	0.20D-02	0.00251	1.25622
45	44	979.25589	0.50D-02	-0.00401	-0.80128
47	46	980.54631	0.20D-02	0.00045	0.22356
48	47	981.17628	0.50D-02	0.00786	1.57103
49	48	981.80169	0.10D-01	0.0131	1.31011
52	51	983.6663	0.20D-02	0.00001	0.00714
53	52	984.26689	0.50D-02	0.00307	0.61393
54	53	984.86888	0.20D-02	-0.00206	-1.02915
55	54	985.45691	0.20D-02	-0.00002	-0.01095
56	55	986.0435	0.20D-02	-0.00335	-1.67673
57	56	986.61436	0.50D-02	0.00222	0.44494
The 6-5 Band, 79 data, $J"_{min} = 21$, $J"_{max} = 80$					
Unc.$_{Avge}$ = 3.5D-03, Unc.$_{Max}$ = 1.0D-02					
(Err/Unc.)$_{Avge}$ = 4.0D-03, RMSR = 1.05					
79	80	840.75384	0.50D-02	-0.00811	-1.62222
78	79	842.13918	0.20D-02	-0.00272	-1.35793
77	78	843.51654	0.50D-02	0.00538	1.07618
76	77	844.90672	0.20D-02	-0.00465	-2.32574
75	76	846.27909	0.20D-02	-0.00218	-1.09167
74	75	847.64241	0.50D-02	0.00401	0.80299
71	72	851.72324	0.20D-02	-0.00027	-0.13731
70	71	853.06816	0.50D-02	0.00294	0.58783
65	66	859.73067	0.20D-02	0.00032	0.16089
64	65	861.03993	0.50D-02	0.0068	1.36063
63	64	862.3664	0.50D-02	-0.00936	-1.87223
62	63	863.66328	0.20D-02	-0.00138	-0.69083
61	62	864.95787	0.50D-02	0.00344	0.68818
60	61	866.25692	0.20D-02	-0.00167	-0.83701

Table A.3, Fourier Transform Infrared Data for ^{73}GeO (cm^{-1}) (*Cont'd*)

J'	J''	Obs	Unc	Calc-Obs	(Calc-Obs)/Unc
59	60	867.55099	0.50D-02	-0.00729	-1.45742
58	59	868.82497	0.50D-02	0.0017	0.34021
57	58	870.10482	0.20D-02	-0.00067	-0.33512
56	57	871.3767	0.20D-02	-0.00059	-0.29582
55	56	872.64454	0.20D-02	-0.00199	-0.99691
54	55	873.89467	0.50D-02	0.00878	1.75653
53	54	875.15784	0.20D-02	0.00099	0.49341
52	53	876.40745	0.20D-02	0.00119	0.59412
51	52	877.65403	0.20D-02	-0.00114	-0.57197
50	51	878.88935	0.20D-02	0.00221	1.10477
49	50	880.12895	0.50D-02	-0.00429	-0.85843
48	49	881.35637	0.50D-02	-0.00422	-0.84392
47	48	882.5688	0.50D-02	0.00524	1.04728
46	47	883.78678	0.20D-02	0.00352	1.76247
45	46	884.99562	0.50D-02	0.00533	1.06505
44	45	886.20655	0.20D-02	-0.00059	-0.29666
41	42	889.79189	0.50D-02	-0.00487	-0.97432
40	41	890.96598	0.20D-02	0.00339	1.69271
38	39	893.31849	0.20D-02	-0.00154	-0.77062
36	37	895.64501	0.50D-02	-0.00334	-0.66762
35	36	896.79629	0.20D-02	-0.00085	-0.42314
34	35	897.94114	0.20D-02	0.00232	1.15886
33	34	899.08434	0.20D-02	0.00137	0.68643
32	33	900.22204	0.20D-02	0.00016	0.07917
31	32	901.35399	0.20D-02	-0.00109	-0.54344
30	31	902.47423	0.20D-02	0.0036	1.7981
29	30	903.59857	0.20D-02	-0.00163	-0.81672
26	27	906.92371	0.50D-02	-0.00436	-0.87175
25	26	908.02313	0.50D-02	-0.00799	-1.5979
24	25	909.10669	0.20D-02	-0.00162	-0.80906
21	22	912.33459	0.50D-02	0.00503	1.00549
20	21	913.40879	0.50D-02	-0.00278	-0.55678
22	21	953.51629	0.20D-02	0.00069	0.34265
24	23	955.10216	0.20D-02	-0.00069	-0.34312
26	25	956.65757	0.20D-02	0.00267	1.33639
27	26	957.4283	0.20D-02	0.00165	0.82647
29	28	958.94945	0.20D-02	0.00052	0.25752
30	29	959.70008	0.20D-02	0.00016	0.08166
32	31	961.18445	0.50D-02	-0.00316	-0.63106
33	32	961.92023	0.50D-02	-0.0082	-1.6392
37	36	964.76696	0.20D-02	0.00254	1.27102
38	37	965.46384	0.20D-02	0.0036	1.7984
40	39	966.83276	0.10D-01	0.01075	1.07534
42	41	968.19657	0.50D-02	-0.00347	-0.6949
43	42	968.85918	0.20D-02	-0.00126	-0.62761
45	44	970.16253	0.50D-02	0.00507	1.01377
46	45	970.80932	0.20D-02	0.0031	1.54968
47	46	971.45027	0.20D-02	0.00029	0.14297
48	47	972.09576	0.10D-01	-0.01378	-1.37836
50	49	973.33084	0.50D-02	-0.00619	-1.23798
52	51	974.53786	0.20D-02	0.00249	1.24637
53	52	975.12507	0.10D-01	0.01299	1.29892
54	53	975.72436	0.50D-02	0.00463	0.92519
55	54	976.31622	0.20D-02	-0.0031	-1.54964
56	55	976.88704	0.50D-02	0.00342	0.68424
57	56	977.46237	0.20D-02	-0.00139	-0.6975
58	57	978.02495	0.20D-02	-0.00029	-0.14506
60	59	979.12774	0.50D-02	0.00375	0.75056

Table A.3, Fourier Transform Infrared Data for ^{73}GeO (cm^{-1}) (*Cont'd*)

J'	J''	Obs	Unc	Calc-Obs	(Calc-Obs)/Unc
62	61	980.20462	0.50D-02	0.00624	1.24816
63	62	980.74322	0.20D-02	-0.00301	-1.50285
64	63	981.26371	0.20D-02	-0.00105	-0.52292
65	64	981.77487	0.50D-02	0.00333	0.66559
66	65	982.28787	0.20D-02	-0.00106	-0.52849
67	66	982.78475	0.50D-02	0.00373	0.7454
71	70	984.72764	0.20D-02	-0.00217	-1.08521

A.4 Fourier Transform Infrared Data for ^{74}GeO

Table A.4: Fourier Transform Infrared Data for ^{74}GeO (cm^{-1})

J'	J''	Obs	Unc	Calc-Obs	(Calc-Obs)/Unc
1,253 ^{74}GeO infrared transitions in 8 bands					
The 1-0 Band, 208 data, $J"_{min} = 0$, $J"_{max} = 110$ $Unc._{Avge}$ = 2.0D-03, $Unc._{Max}$ = 5.0D-03 $(Err/Unc.)_{Avge}$ = 1.7D-02, RMSR = 0.40					
100	101	850.58618	0.20D-02	-0.00060	-0.29931
99	100	852.11427	0.20D-02	-0.00008	-0.03924
98	99	853.63719	0.20D-02	0.00054	0.26817
97	98	855.15701	0.20D-02	-0.00085	-0.42723
96	97	856.66844	0.20D-02	0.00104	0.51961
95	96	858.17773	0.20D-02	-0.00004	-0.02142
94	95	859.68284	0.20D-02	-0.00206	-1.03037
93	94	861.17728	0.20D-02	0.00145	0.72268
92	93	862.67274	0.20D-02	-0.00121	-0.60734
91	92	864.16019	0.20D-02	-0.00101	-0.50551
90	91	865.64133	0.20D-02	0.00033	0.1631
89	90	867.11925	0.20D-02	-0.00029	-0.14656
88	89	868.5913	0.20D-02	-0.00023	-0.11468
87	88	870.05908	0.20D-02	-0.00108	-0.54126
86	87	871.52062	0.20D-02	-0.00091	-0.45649
85	86	872.97606	0.20D-02	0.00014	0.06961
84	85	874.42643	0.20D-02	0.00103	0.51688
83	84	875.8735	0.20D-02	0.0	0.0002
82	83	877.3165	0.20D-02	-0.00222	-1.11055
81	82	878.74949	0.20D-02	0.00031	0.1545
80	81	880.18091	0.20D-02	-0.00085	-0.42479
79	80	881.6057	0.20D-02	-0.00067	-0.3335
78	79	883.02479	0.20D-02	-0.00007	-0.03689
77	78	884.43893	0.20D-02	0.00017	0.08501
76	77	885.84823	0.20D-02	-0.00005	-0.02302
75	76	887.25142	0.20D-02	0.00052	0.25881
74	75	888.65018	0.20D-02	0.00018	0.09044
73	74	890.04317	0.20D-02	0.00027	0.13664
72	73	891.4312	0.20D-02	-0.00002	-0.00777
71	72	892.81313	0.20D-02	0.00042	0.21204
70	71	894.19053	0.20D-02	0.00002	0.01092
69	70	895.56083	0.20D-02	0.00134	0.66858
68	69	896.92806	0.20D-02	0.00034	0.16986
67	68	898.28889	0.20D-02	0.00033	0.16463
66	67	899.64404	0.20D-02	0.00059	0.2926
65	66	900.99387	0.20D-02	0.00074	0.36852
64	65	902.33904	0.20D-02	0.00012	0.06225
63	64	903.67785	0.20D-02	0.00042	0.20854
62	63	905.01158	0.20D-02	0.00033	0.16713
61	62	906.34	0.20D-02	0.0001	0.04784
60	61	907.66273	0.20D-02	0.00008	0.04032
59	60	908.97996	0.20D-02	0.00007	0.03438
58	59	910.29142	0.20D-02	0.00033	0.1648
57	58	911.59749	0.20D-02	0.00047	0.23622
56	57	912.8983	0.20D-02	0.00037	0.18347
55	56	914.19351	0.20D-02	0.00032	0.16123
54	55	915.4838	0.20D-02	-0.00034	-0.17079
53	54	916.76803	0.20D-02	-0.0005	-0.24787

Table A.4, Fourier Transform Infrared Data for ^{74}GeO (cm^{-1}) (*Cont'd*)

J'	J''	Obs	Unc	Calc-Obs	(Calc-Obs)/Unc
52	53	918.04554	0.20D-02	0.00052	0.25969
51	52	919.31866	0.20D-02	0.00034	0.17159
50	51	920.58601	0.20D-02	0.00036	0.17754
49	50	921.84763	0.20D-02	0.0005	0.25226
48	49	923.1035	0.20D-02	0.00081	0.40535
47	48	924.35442	0.20D-02	0.00044	0.22156
46	47	925.59951	0.20D-02	0.00028	0.14054
45	46	926.83862	0.20D-02	0.00046	0.23188
44	45	928.07238	0.20D-02	0.00035	0.17536
43	44	929.3004	0.20D-02	0.00033	0.16556
42	43	930.52267	0.20D-02	0.00038	0.19218
41	42	931.74012	0.20D-02	-0.00042	-0.21023
40	41	932.95091	0.20D-02	-0.00025	-0.12699
39	40	934.15594	0.20D-02	-0.00002	-0.00844
38	39	935.35559	0.20D-02	-0.00012	-0.06004
37	38	936.54993	0.20D-02	-0.00063	-0.31709
36	37	937.7366	0.20D-02	0.00079	0.39497
35	36	938.9196	0.20D-02	0.00014	0.07075
34	35	940.09599	0.20D-02	0.00036	0.17983
33	34	941.26696	0.20D-02	0.00022	0.11181
32	33	942.43195	0.20D-02	0.00029	0.14626
31	32	943.59138	0.20D-02	0.00014	0.06776
30	31	944.74483	0.20D-02	0.00017	0.08592
29	30	945.89271	0.20D-02	-0.00004	-0.01978
28	29	947.03425	0.20D-02	0.00027	0.1353
27	28	948.17065	0.20D-02	-0.00011	-0.05434
26	27	949.30257	0.20D-02	-0.00185	-0.92416
25	26	950.42332	0.20D-02	0.00174	0.87038
24	25	951.54447	0.20D-02	-0.00094	-0.47119
23	24	952.65624	0.20D-02	-0.00012	-0.05936
22	23	953.76372	0.20D-02	-0.00089	-0.4446
21	22	954.86452	0.20D-02	-0.00087	-0.43737
19	20	957.04738	0.20D-02	0.00017	0.08733
18	19	958.13051	0.20D-02	0.00011	0.05382
17	18	959.20757	0.20D-02	0.00017	0.08566
16	17	960.27892	0.20D-02	-0.00001	-0.00259
15	16	961.34418	0.20D-02	-0.00004	-0.02146
14	15	962.40413	0.20D-02	-0.00075	-0.37659
13	14	963.45645	0.20D-02	0.00018	0.09152
12	13	964.50326	0.20D-02	0.00063	0.31732
11	12	965.5444	0.20D-02	0.00075	0.37529
10	11	966.5805	0.20D-02	-0.0001	-0.05018
9	10	967.60985	0.20D-02	-0.00024	-0.11972
8	9	968.63279	0.20D-02	-0.00001	-0.00381
7	8	969.64921	0.20D-02	0.00069	0.34691
6	7	970.66128	0.20D-02	-0.00032	-0.15816
5	6	971.6643	0.20D-02	0.00166	0.83042
4	5	972.66528	0.20D-02	-0.00042	-0.20806
3	4	973.65825	0.20D-02	-0.00058	-0.28916
2	3	974.64537	0.20D-02	-0.001	-0.49846
1	2	975.62686	0.20D-02	-0.0019	-0.95165
1	0	978.53001	0.20D-02	-0.00011	-0.05602
2	1	979.48571	0.20D-02	0.00019	0.09377
3	2	980.43376	0.20D-02	0.00196	0.98144
4	3	981.3796	0.20D-02	-0.00024	-0.11878
5	4	982.31656	0.20D-02	0.00026	0.12753
6	5	983.24999	0.20D-02	-0.00194	-0.97044
7	6	984.1745	0.20D-02	-0.00144	-0.71828

Table A.4, Fourier Transform Infrared Data for ^{74}GeO (cm^{-1}) (*Cont'd*)

J'	J''	Obs	Unc	Calc-Obs	(Calc-Obs)/Unc
8	7	985.09176	0.20D-02	0.00009	0.04325
9	8	986.00372	0.20D-02	0.00067	0.33344
10	9	986.91084	0.20D-02	-0.00017	-0.08344
11	10	987.80974	0.20D-02	0.00096	0.48188
12	11	988.7043	0.20D-02	0.00015	0.07366
13	12	989.59201	0.20D-02	-0.00011	-0.05379
14	13	990.47281	0.20D-02	0.00025	0.12367
15	14	991.3478	0.20D-02	0.0001	0.05039
16	15	992.21664	0.20D-02	-0.00022	-0.10947
17	16	993.07494	0.20D-02	0.00368	1.83828
18	17	993.93461	0.20D-02	-0.00015	-0.07705
19	18	994.78387	0.20D-02	0.00007	0.03374
20	19	995.62731	0.20D-02	-0.00026	-0.13024
21	20	996.46304	0.20D-02	0.00074	0.37024
22	21	997.2941	0.20D-02	0.00002	0.00943
23	22	998.11736	0.20D-02	0.0007	0.35139
24	23	998.93554	0.20D-02	0.00004	0.0204
25	24	999.74765	0.20D-02	-0.00098	-0.48944
26	25	1000.55135	0.20D-02	-0.00003	-0.01398
27	26	1001.34976	0.20D-02	-0.00024	-0.11932
28	27	1002.14121	0.20D-02	0.00005	0.02443
29	28	1002.92619	0.20D-02	0.00033	0.16589
30	29	1003.70559	0.20D-02	-0.00028	-0.14132
31	30	1004.47777	0.20D-02	-0.00018	-0.09209
32	31	1005.24416	0.20D-02	-0.00081	-0.40331
33	32	1006.00199	0.20D-02	0.00061	0.3051
34	33	1006.75637	0.20D-02	-0.00106	-0.52875
35	34	1007.50129	0.20D-02	0.00019	0.0952
36	35	1008.24266	0.20D-02	-0.00157	-0.78448
37	36	1008.97399	0.20D-02	0.00015	0.07578
38	37	1009.70036	0.20D-02	0.00024	0.12103
39	38	1010.41984	0.20D-02	0.00063	0.31482
40	39	1011.1334	0.20D-02	0.00033	0.16568
41	40	1011.84002	0.20D-02	0.00036	0.17864
42	41	1012.54021	0.20D-02	0.00018	0.09223
43	42	1013.23495	0.20D-02	-0.00118	-0.59006
44	43	1013.9198	0.20D-02	0.0007	0.35179
45	44	1014.60024	0.20D-02	0.00032	0.16128
46	45	1015.27363	0.20D-02	0.00031	0.15688
47	46	1015.94057	0.20D-02	0.00007	0.03357
48	47	1016.60032	0.20D-02	0.00031	0.15483
49	48	1017.25368	0.20D-02	0.00023	0.11461
50	49	1017.90066	0.20D-02	-0.0002	-0.09813
51	50	1018.53972	0.20D-02	0.00056	0.28005
52	51	1019.16922	0.50D-02	0.00414	0.82763
53	52	1019.79902	0.20D-02	0.00064	0.32239
54	53	1020.41904	0.20D-02	0.00016	0.0789
55	54	1021.03173	0.20D-02	0.00022	0.10751
56	55	1021.63925	0.20D-02	-0.00136	-0.67787
57	56	1022.23664	0.20D-02	0.00039	0.19614
58	57	1022.82933	0.20D-02	0.00002	0.00943
59	58	1023.41368	0.20D-02	0.00115	0.57537
60	59	1023.99342	0.20D-02	0.00005	0.02283
61	60	1024.5651	0.20D-02	0.00014	0.07066
62	61	1025.12951	0.20D-02	0.00065	0.3227
63	62	1025.68803	0.20D-02	0.00015	0.0728
64	63	1026.23897	0.20D-02	0.00033	0.16479
65	64	1026.78423	0.20D-02	-0.00072	-0.35753

Table A.4, Fourier Transform Infrared Data for ^{74}GeO (cm^{-1}) (*Cont'd*)

J'	J''	Obs	Unc	Calc-Obs	(Calc-Obs)/Unc
66	65	1027.32113	0.20D-02	-0.00032	-0.16033
67	66	1027.85073	0.20D-02	0.00044	0.22019
68	67	1028.37438	0.20D-02	0.00021	0.10281
69	68	1028.89044	0.20D-02	0.0006	0.30133
70	69	1029.40188	0.20D-02	-0.00135	-0.67549
71	70	1029.90277	0.20D-02	0.00027	0.13612
72	71	1030.39874	0.20D-02	-0.00019	-0.09509
73	72	1030.88632	0.20D-02	0.00073	0.36464
74	73	1031.3687	0.20D-02	-0.00017	-0.08595
75	74	1031.843	0.20D-02	-0.00003	-0.01315
76	75	1032.31035	0.20D-02	0.00002	0.01227
77	76	1032.77052	0.20D-02	0.0002	0.09801
78	77	1033.22384	0.20D-02	0.00015	0.07329
79	78	1033.66984	0.20D-02	0.00033	0.16679
80	79	1034.10891	0.20D-02	0.00035	0.17718
81	80	1034.54153	0.20D-02	-0.00028	-0.14184
82	81	1034.96485	0.20D-02	0.00126	0.62886
83	82	1035.38387	0.20D-02	-0.00004	-0.01804
84	83	1035.79322	0.20D-02	0.0012	0.60159
85	84	1036.19837	0.20D-02	-0.00053	-0.26361
86	85	1036.59233	0.20D-02	0.00176	0.88049
87	86	1036.98387	0.20D-02	-0.00072	-0.35851
88	87	1037.36471	0.20D-02	0.00031	0.15351
89	88	1037.73885	0.20D-02	0.00082	0.41014
90	89	1038.10744	0.20D-02	-0.00034	-0.16953
91	90	1038.46647	0.20D-02	0.00082	0.41207
92	91	1038.81897	0.20D-02	0.00127	0.63402
93	92	1039.16584	0.20D-02	0.00008	0.04036
94	93	1039.505	0.20D-02	-0.00067	-0.33634
95	94	1039.83657	0.20D-02	-0.00112	-0.56156
96	95	1040.16068	0.20D-02	-0.00142	-0.70777
97	96	1040.47589	0.20D-02	-0.00011	-0.05595
98	97	1040.78637	0.20D-02	-0.00142	-0.71208
99	98	1041.08769	0.20D-02	-0.0009	-0.44867
100	99	1041.38016	0.20D-02	0.00112	0.55877
101	100	1041.66815	0.20D-02	0.00025	0.12272
102	101	1041.94786	0.20D-02	0.00028	0.13764
103	102	1042.22304	0.20D-02	-0.00256	-1.27899
105	104	1042.74528	0.20D-02	-0.00233	-1.16617
106	105	1042.99312	0.20D-02	-0.00008	-0.03984
107	106	1043.23759	0.20D-02	-0.0019	-0.95133
108	107	1043.47106	0.20D-02	-0.00018	-0.09125
109	108	1043.69804	0.20D-02	0.00056	0.27783
111	110	1044.12973	0.20D-02	0.00184	0.91896
The 2-1 Band, 202 data, $J"_{min} = 1$, $J"_{max} = 108$					
Unc.$_{Avge}$ = 2.0D-03, Unc.$_{Max}$ = 2.0D-03					
(Err/Unc.)$_{Avge}$ = 1.1D-02, RMSR = 0.39					
94	95	851.38955	0.20D-02	0.00081	0.40429
93	94	852.88123	0.20D-02	0.0004	0.19919
92	93	854.3684	0.20D-02	-0.00063	-0.31585
91	92	855.84957	0.20D-02	-0.00082	-0.41091
90	91	857.325	0.20D-02	-0.00043	-0.21603
89	90	858.79466	0.20D-02	0.00057	0.2836
88	89	860.26003	0.20D-02	0.00067	0.33298
87	88	861.7194	0.20D-02	0.00157	0.7869
86	87	863.17626	0.20D-02	-0.00021	-0.10465
85	86	864.62608	0.20D-02	-0.00015	-0.07684

Table A.4, Fourier Transform Infrared Data for ^{74}GeO (cm^{-1}) (*Cont'd*)

J'	J''	Obs	Unc	Calc-Obs	(Calc-Obs)/Unc
84	85	866.07053	0.20D-02	0.00004	0.02023
83	84	867.50899	0.20D-02	0.00099	0.49641
82	83	868.94315	0.20D-02	0.001	0.50158
81	82	870.37355	0.20D-02	-0.00047	-0.23435
80	81	871.79717	0.20D-02	-0.00043	-0.21661
79	80	873.2137	0.20D-02	0.00142	0.70974
78	79	874.62813	0.20D-02	0.00009	0.04444
77	78	876.03628	0.20D-02	-0.00025	-0.12255
76	77	877.43832	0.20D-02	0.00022	0.10856
75	76	878.83601	0.20D-02	-0.00028	-0.14242
74	75	880.22785	0.20D-02	-0.00025	-0.12565
73	74	881.61368	0.20D-02	0.00045	0.22369
72	73	882.99521	0.20D-02	0.0001	0.0504
71	72	884.37104	0.20D-02	0.0001	0.04932
70	71	885.74141	0.20D-02	0.0002	0.10027
69	70	887.10778	0.20D-02	-0.00108	-0.54203
68	69	888.46651	0.20D-02	-0.00012	-0.05769
67	68	889.82046	0.20D-02	0.00024	0.11797
66	67	891.16938	0.20D-02	0.00022	0.10983
66	67	891.16938	0.20D-02	0.00022	0.10983
65	66	892.51304	0.20D-02	0.00004	0.01762
64	65	893.85115	0.20D-02	-0.00003	-0.01389
63	64	895.18396	0.20D-02	-0.00023	-0.11493
62	63	896.51103	0.20D-02	-0.00013	-0.06575
61	62	897.83243	0.20D-02	0.00017	0.08345
60	61	899.14848	0.20D-02	0.00034	0.17232
59	60	900.45942	0.20D-02	0.00015	0.07566
58	59	901.76494	0.20D-02	-0.0001	-0.05176
57	58	903.06418	0.20D-02	0.00041	0.20475
56	57	904.35877	0.20D-02	0.00006	0.02991
55	56	905.6476	0.20D-02	-0.00005	-0.02662
54	55	906.9303	0.20D-02	0.00043	0.21504
53	54	908.20834	0.20D-02	0.00004	0.01942
52	53	909.478	0.20D-02	0.00246	1.23129
51	52	910.74683	0.20D-02	0.00015	0.07534
50	51	912.00823	0.20D-02	-0.00031	-0.1537
49	50	913.26371	0.20D-02	-0.00042	-0.21125
48	49	914.51295	0.20D-02	0.00009	0.04747
47	48	915.757	0.20D-02	0.00019	0.09708
46	47	916.99568	0.20D-02	0.00004	0.02219
45	46	918.22887	0.20D-02	-0.00023	-0.11744
44	45	919.45582	0.20D-02	0.00008	0.03778
43	44	920.67742	0.20D-02	0.00009	0.04256
42	43	921.89362	0.20D-02	-0.00017	-0.08358
41	42	923.1035	0.20D-02	0.00024	0.11905
40	41	924.30812	0.20D-02	0.00021	0.10513
39	40	925.50701	0.20D-02	0.00022	0.10918
38	39	926.70022	0.20D-02	0.0002	0.1009
37	38	927.88751	0.20D-02	0.00039	0.19485
36	37	929.06941	0.20D-02	0.00025	0.12563
35	36	930.24548	0.20D-02	0.0002	0.09784
34	35	931.41615	0.20D-02	-0.00021	-0.10393
33	34	932.57993	0.20D-02	0.00052	0.25988
32	33	933.73916	0.20D-02	0.00004	0.01886
31	32	934.89078	0.20D-02	0.00138	0.68762
30	31	936.03847	0.20D-02	0.00085	0.42563
29	30	937.18075	0.20D-02	-0.00006	-0.03247
28	29	938.31627	0.20D-02	-0.00003	-0.01717

Table A.4, Fourier Transform Infrared Data for ^{74}GeO (cm^{-1}) (*Cont'd*)

J'	J''	Obs	Unc	Calc-Obs	(Calc-Obs)/Unc
27	28	939.44576	0.20D-02	0.00021	0.10606
26	27	940.56977	0.20D-02	0.00009	0.04676
25	26	941.68785	0.20D-02	0.00006	0.02946
24	25	942.80148	0.20D-02	-0.00138	-0.69133
23	24	943.90559	0.20D-02	0.00083	0.41392
22	23	945.00803	0.20D-02	-0.00116	-0.58025
21	22	946.10178	0.20D-02	-0.00036	-0.17943
20	21	947.18973	0.20D-02	0.00034	0.17097
19	20	948.27507	0.20D-02	-0.00226	-1.12961
18	19	949.35001	0.20D-02	-0.00038	-0.19169
17	18	950.41954	0.20D-02	0.00098	0.4892
16	17	951.48662	0.20D-02	-0.00116	-0.58248
15	16	952.54313	0.20D-02	0.00131	0.65274
14	15	953.5971	0.20D-02	0.00035	0.17431
13	14	954.64428	0.20D-02	0.0002	0.10171
12	13	955.68553	0.20D-02	0.00001	0.0043
11	12	956.72038	0.20D-02	0.0002	0.1016
10	11	957.75005	0.20D-02	-0.00043	-0.21702
9	10	958.77255	0.20D-02	0.00008	0.03787
8	9	959.78974	0.20D-02	-0.00014	-0.06934
7	8	960.80029	0.20D-02	0.00025	0.12577
6	7	961.80572	0.20D-02	-0.0003	-0.15242
5	6	962.80439	0.20D-02	-0.00017	-0.08451
4	5	963.79749	0.20D-02	-0.00054	-0.27107
3	4	964.78354	0.20D-02	0.00004	0.02217
2	3	965.76382	0.20D-02	0.0003	0.14968
1	2	966.73777	0.20D-02	0.00078	0.39076
0	1	967.70864	0.20D-02	-0.00179	-0.89523
2	1	970.5751	0.20D-02	-0.00021	-0.10723
3	2	971.51902	0.20D-02	-0.00044	-0.21815
4	3	972.45527	0.20D-02	0.00082	0.41057
5	4	973.38669	0.20D-02	0.00072	0.35811
6	5	974.31261	0.20D-02	-0.00009	-0.04612
7	6	975.23129	0.20D-02	0.00012	0.06213
8	7	976.14423	0.20D-02	-0.00015	-0.07286
9	8	977.05059	0.20D-02	-0.00006	-0.03182
10	9	977.95133	0.20D-02	-0.00062	-0.31047
11	10	978.84417	0.20D-02	0.00046	0.23044
12	11	979.73227	0.20D-02	0.00001	0.00522
13	12	980.61344	0.20D-02	0.00021	0.10302
14	13	981.48887	0.20D-02	-0.00015	-0.07683
15	14	982.35728	0.20D-02	0.00021	0.10486
16	15	983.21996	0.20D-02	-0.00003	-0.01269
17	16	984.07772	0.20D-02	-0.00167	-0.83526
18	17	984.92654	0.20D-02	-0.00072	-0.35866
19	18	985.76931	0.20D-02	-0.00007	-0.03367
20	19	986.60753	0.20D-02	-0.00123	-0.61611
21	20	987.43715	0.20D-02	-0.00016	-0.08174
22	21	988.2603	0.20D-02	0.00098	0.48851
23	22	989.07908	0.20D-02	0.00009	0.04392
24	23	989.89033	0.20D-02	0.00032	0.15859
25	24	990.69826	0.20D-02	-0.00256	-1.27833
26	25	991.49466	0.20D-02	-0.00034	-0.16769
27	26	992.28566	0.20D-02	0.00084	0.41965
28	27	993.07422	0.20D-02	-0.00199	-0.99719
29	28	993.8514	0.20D-02	0.00007	0.03596
30	29	994.62479	0.20D-02	-0.00055	-0.27688
31	30	995.39028	0.20D-02	0.00023	0.11349

Table A.4, Fourier Transform Infrared Data for ^{74}GeO (cm^{-1}) (*Cont'd*)

J'	J''	Obs	Unc	Calc-Obs	(Calc-Obs)/Unc
32	31	996.15055	0.20D-02	-0.00028	-0.13889
33	32	996.90339	0.20D-02	0.00013	0.06507
34	33	997.65027	0.20D-02	-0.00003	-0.01554
35	34	998.39034	0.20D-02	0.00009	0.04334
36	35	999.12368	0.20D-02	0.00037	0.18577
37	36	999.85131	0.20D-02	-0.0002	-0.09914
38	37	1000.57133	0.20D-02	0.00027	0.13261
39	38	1001.28539	0.20D-02	0.0001	0.0502
40	39	1001.99228	0.20D-02	0.0005	0.25202
41	40	1002.69326	0.20D-02	0.00021	0.10307
42	41	1003.38778	0.20D-02	-0.00025	-0.12311
43	42	1004.07504	0.20D-02	-0.00009	-0.04303
44	43	1004.75568	0.20D-02	0.00005	0.0233
45	44	1005.43006	0.20D-02	-0.00022	-0.11062
46	45	1006.09725	0.20D-02	0.00003	0.01418
47	46	1006.75637	0.20D-02	0.00166	0.83117
48	47	1007.41163	0.20D-02	0.00046	0.23032
49	48	1008.05954	0.20D-02	-0.0001	-0.04993
50	49	1008.69992	0.20D-02	0.00016	0.07938
51	50	1009.33398	0.20D-02	-0.00001	-0.00282
52	51	1009.96123	0.20D-02	-0.00011	-0.05311
53	52	1010.58254	0.20D-02	-0.00102	-0.51157
54	53	1011.19512	0.20D-02	0.00002	0.01022
55	54	1011.80186	0.20D-02	0.00012	0.06115
56	55	1012.40241	0.20D-02	-0.00038	-0.18988
57	56	1012.99505	0.20D-02	0.00022	0.11101
58	57	1013.58191	0.20D-02	-0.00021	-0.10731
59	58	1014.16234	0.20D-02	-0.00105	-0.52596
60	59	1014.73383	0.20D-02	0.00022	0.1084
61	60	1015.30015	0.20D-02	-0.00021	-0.10437
62	61	1015.85927	0.20D-02	-0.0003	-0.15094
63	62	1016.41115	0.20D-02	-0.00003	-0.01747
64	63	1016.95667	0.20D-02	-0.0003	-0.15015
65	64	1017.49473	0.20D-02	-0.00001	-0.00516
66	65	1018.02618	0.20D-02	-0.00003	-0.0137
67	66	1018.55004	0.20D-02	0.00062	0.30803
68	67	1019.06844	0.20D-02	-0.00021	-0.10619
69	68	1019.57874	0.20D-02	0.00009	0.04741
70	69	1020.08287	0.20D-02	-0.00039	-0.19739
71	70	1020.57969	0.20D-02	-0.00055	-0.27634
72	71	1021.06923	0.20D-02	-0.00042	-0.21169
73	72	1021.55188	0.20D-02	-0.00041	-0.2042
74	73	1022.02681	0.20D-02	0.00031	0.15486
75	74	1022.49568	0.20D-02	0.00006	0.02921
76	75	1022.95729	0.20D-02	0.00003	0.01256
77	76	1023.41368	0.20D-02	-0.00184	-0.92138
78	77	1023.85882	0.20D-02	0.00047	0.23607
79	78	1024.30034	0.20D-02	-0.00067	-0.33589
80	79	1024.73356	0.20D-02	-0.0006	-0.2996
81	80	1025.15929	0.20D-02	-0.00015	-0.07589
82	81	1025.579	0.20D-02	-0.0008	-0.40111
83	82	1025.99088	0.20D-02	-0.00075	-0.3766
84	83	1026.39517	0.20D-02	-0.00026	-0.12823
85	84	1026.79337	0.20D-02	-0.00083	-0.41338
86	85	1027.18284	0.20D-02	0.00016	0.08208
87	86	1027.56538	0.20D-02	0.0009	0.45175
88	87	1027.94251	0.20D-02	-0.00014	-0.07027
89	88	1028.31194	0.20D-02	-0.00069	-0.3464

Table A.4, Fourier Transform Infrared Data for ^{74}GeO (cm^{-1}) (*Cont'd*)

J'	J''	Obs	Unc	Calc-Obs	(Calc-Obs)/Unc
90	89	1028.67451	0.20D-02	-0.00161	-0.80254
91	90	1029.02701	0.20D-02	0.00032	0.16036
93	92	1029.71478	0.20D-02	-0.00035	-0.17496
94	93	1030.04669	0.20D-02	0.0004	0.1999
95	94	1030.37219	0.20D-02	0.00026	0.132
96	95	1030.68644	0.20D-02	0.00408	2.04084
97	96	1031.00051	0.20D-02	0.00077	0.38395
98	97	1031.30326	0.20D-02	0.00145	0.72531
99	98	1031.60106	0.20D-02	-0.00025	-0.12606
100	99	1031.88806	0.20D-02	0.00149	0.7473
101	100	1032.17115	0.20D-02	-0.00021	-0.10514
102	101	1032.44479	0.20D-02	0.00016	0.0791
103	102	1032.70997	0.20D-02	0.0016	0.79945
104	103	1032.97094	0.20D-02	-0.00015	-0.07663
105	104	1033.22384	0.20D-02	-0.00125	-0.62472
106	105	1033.46752	0.20D-02	-0.00055	-0.27738
107	106	1033.70461	0.20D-02	-0.00071	-0.35523
108	107	1033.92926	0.20D-02	0.00412	2.05966
109	108	1034.15523	0.20D-02	0.00016	0.08018
The 3-2 Band, 194 data, $J"_{min} = 1$, $J"_{max} = 100$					
Unc.$_{Avge}$ = 2.0D-03, Unc.$_{Max}$ = 5.0D-03					
(Err/Unc.)$_{Avge}$ = 5.9D-02, RMSR = 0.52					
99	100	835.62536	0.20D-02	0.00135	0.67491
98	99	837.13364	0.20D-02	0.00319	1.59722
97	98	838.63942	0.20D-02	0.00247	1.23306
96	97	840.14287	0.20D-02	-0.00104	-0.51763
95	96	841.63827	0.20D-02	-0.00159	-0.79493
94	95	843.1265	0.20D-02	-0.00008	-0.03891
93	94	844.60813	0.20D-02	0.0029	1.45035
92	93	846.08671	0.20D-02	0.0038	1.8978
90	91	849.03307	0.20D-02	0.00095	0.47672
89	90	850.4974	0.20D-02	0.00064	0.31798
88	89	851.95631	0.20D-02	0.00056	0.28205
87	88	853.41165	0.20D-02	-0.00111	-0.55624
86	87	854.85894	0.20D-02	0.00006	0.02798
85	86	856.30198	0.20D-02	0.00027	0.13459
84	85	857.74028	0.20D-02	0.00001	0.00348
83	84	859.17137	0.20D-02	0.00174	0.8695
82	83	860.60013	0.20D-02	0.00056	0.27751
81	82	862.02297	0.20D-02	0.00004	0.02243
80	81	863.43932	0.20D-02	0.00077	0.384
79	80	864.85215	0.20D-02	-0.00025	-0.12284
78	79	866.2572	0.20D-02	0.00123	0.61672
77	78	867.66005	0.20D-02	-0.00038	-0.18755
76	77	869.05346	0.20D-02	0.00216	1.07928
75	76	870.44752	0.20D-02	-0.00126	-0.62802
74	75	871.83213	0.20D-02	-0.00055	-0.27461
73	74	873.2137	0.20D-02	-0.00213	-1.06566
72	73	874.58628	0.20D-02	-0.00006	-0.03143
71	72	875.9549	0.20D-02	0.00063	0.31291
70	71	877.3165	0.20D-02	0.00296	1.48222
69	70	878.678	0.20D-02	0.00003	0.01623
68	69	880.03104	0.20D-02	0.00018	0.08967
67	68	881.37938	0.20D-02	-0.00036	-0.17756
66	67	882.72191	0.20D-02	-0.00049	-0.24575
65	66	884.05762	0.20D-02	0.00078	0.38987
64	65	885.39017	0.20D-02	-0.00021	-0.10593

Table A.4, Fourier Transform Infrared Data for ^{74}GeO (cm^{-1}) (*Cont'd*)

J'	J''	Obs	Unc	Calc-Obs	(Calc-Obs)/Unc
63	64	886.7135	0.20D-02	0.00259	1.29659
62	63	888.03671	0.20D-02	0.00006	0.03225
61	62	889.35228	0.20D-02	-0.00028	-0.13932
60	61	890.66164	0.20D-02	0.00012	0.06172
59	60	891.96544	0.20D-02	0.00062	0.31002
58	59	893.26525	0.20D-02	-0.00039	-0.19461
57	58	894.55801	0.20D-02	0.00016	0.07751
56	57	895.8465	0.20D-02	-0.00054	-0.26891
55	56	897.12844	0.20D-02	-0.00019	-0.09415
54	55	898.40507	0.20D-02	-0.00007	-0.03352
53	54	899.67602	0.20D-02	0.0002	0.09769
52	53	900.94181	0.20D-02	0.00007	0.03417
51	52	902.20194	0.20D-02	0.00005	0.02565
50	51	903.4564	0.20D-02	0.00012	0.06172
49	50	904.70524	0.20D-02	0.00023	0.11714
48	49	905.94892	0.20D-02	-0.00009	-0.04347
47	48	907.18661	0.20D-02	-0.00001	-0.00544
46	47	908.419	0.20D-02	-0.00026	-0.12912
45	46	909.64549	0.20D-02	-0.00023	-0.11485
44	45	910.86578	0.20D-02	0.00036	0.18199
43	44	912.08094	0.20D-02	0.00044	0.22105
42	43	913.29094	0.20D-02	0.00003	0.01702
41	42	914.49482	0.20D-02	0.00007	0.0344
40	41	915.69323	0.20D-02	-0.0001	-0.05207
39	40	916.88588	0.20D-02	-0.00021	-0.10289
38	39	918.07211	0.20D-02	0.00042	0.21165
37	38	919.25324	0.20D-02	0.00043	0.2161
36	37	920.4291	0.20D-02	-0.00001	-0.00496
35	36	921.59841	0.20D-02	0.00037	0.18307
34	35	922.76286	0.20D-02	-0.00014	-0.07019
33	34	923.92134	0.20D-02	-0.00042	-0.21026
32	33	925.0731	0.20D-02	0.00024	0.12246
31	32	926.21871	0.20D-02	0.00129	0.64261
30	31	927.36127	0.20D-02	-0.00041	-0.20534
29	30	928.49594	0.20D-02	0.0	-0.00187
28	29	929.62466	0.20D-02	0.00054	0.26765
27	28	930.74876	0.20D-02	-0.00012	-0.06229
26	27	931.86739	0.20D-02	-0.00114	-0.57218
25	26	932.9777	0.20D-02	0.00032	0.15757
24	25	934.08378	0.20D-02	0.00016	0.08136
23	24	935.18405	0.20D-02	-0.00005	-0.02625
22	23	936.27791	0.20D-02	0.00027	0.1343
21	22	937.36619	0.20D-02	0.00028	0.14243
20	21	938.44851	0.20D-02	0.00037	0.1826
19	20	939.52519	0.20D-02	0.00019	0.09437
18	19	940.59631	0.20D-02	-0.00036	-0.17783
17	18	941.66056	0.20D-02	0.00004	0.02047
16	17	942.7194	0.20D-02	-0.00009	-0.04622
15	16	943.77286	0.20D-02	-0.0008	-0.39856
14	15	944.81886	0.20D-02	0.00001	0.00295
13	14	945.8598	0.20D-02	-0.00011	-0.0572
12	13	946.89387	0.20D-02	0.00065	0.32537
11	12	947.92249	0.20D-02	0.00087	0.43502
10	11	948.9465	0.20D-02	-0.00031	-0.15371
9	10	949.96285	0.20D-02	0.00017	0.08353
8	9	950.97385	0.20D-02	-0.00005	-0.02387
7	8	951.97862	0.20D-02	-0.00007	-0.03645
6	7	952.97803	0.20D-02	-0.00079	-0.39493

Table A.4, Fourier Transform Infrared Data for ^{74}GeO (cm^{-1}) (*Cont'd*)

J'	J''	Obs	Unc	Calc-Obs	(Calc-Obs)/Unc
5	6	953.97059	0.20D-02	-0.00072	-0.35987
4	5	954.95674	0.20D-02	-0.00031	-0.15686
3	4	955.93465	0.20D-02	0.00226	1.12842
2	3	956.91083	0.20D-02	0.00045	0.22529
2	1	961.68923	0.20D-02	0.00208	1.04143
4	3	963.56144	0.20D-02	-0.00119	-0.59592
5	4	964.48684	0.20D-02	-0.0014	-0.69987
6	5	965.40625	0.20D-02	-0.00182	-0.90829
7	6	966.31933	0.20D-02	-0.0021	-1.05189
8	7	967.22431	0.20D-02	-0.00052	-0.2614
9	8	968.12334	0.20D-02	0.00077	0.38744
10	9	969.01868	0.20D-02	-0.00048	-0.24108
11	10	969.90636	0.20D-02	-0.00034	-0.16774
12	11	970.78771	0.20D-02	-0.00013	-0.06321
13	12	971.66432	0.20D-02	-0.00145	-0.72333
14	13	972.53131	0.20D-02	0.00055	0.2761
15	14	973.39485	0.20D-02	-0.0003	-0.15061
16	15	974.25103	0.20D-02	-0.00011	-0.05428
17	16	975.10185	0.20D-02	-0.00088	-0.44071
18	17	975.9448	0.20D-02	-0.00012	-0.06065
19	18	976.78159	0.20D-02	0.00046	0.23
20	19	977.61229	0.20D-02	0.00076	0.38046
21	20	978.4378	0.20D-02	-0.00012	-0.06003
22	21	979.25589	0.20D-02	0.00004	0.01764
23	22	980.06711	0.20D-02	0.00067	0.33264
24	23	980.87333	0.20D-02	-0.00011	-0.05589
25	24	981.67228	0.20D-02	-0.00004	-0.01879
26	25	982.46559	0.20D-02	-0.00074	-0.37194
27	26	983.24999	0.20D-02	0.00101	0.5038
28	27	984.02936	0.20D-02	0.00134	0.6676
29	28	984.80622	0.20D-02	-0.00229	-1.14653
30	29	985.57078	0.20D-02	-0.0001	-0.04938
31	30	986.33072	0.20D-02	0.00023	0.11309
32	31	987.08447	0.20D-02	0.00024	0.11991
33	32	987.83094	0.20D-02	0.00103	0.51528
34	33	988.57267	0.20D-02	0.00003	0.01326
35	34	989.30806	0.20D-02	-0.00117	-0.58718
36	35	990.03397	0.20D-02	0.00056	0.27806
37	36	990.75678	0.20D-02	-0.00117	-0.58693
38	37	991.47108	0.20D-02	-0.00097	-0.4832
39	38	992.17892	0.20D-02	-0.00088	-0.44162
40	39	992.87945	0.20D-02	-0.00008	-0.03822
41	40	993.57465	0.20D-02	-0.00056	-0.27899
42	41	994.26235	0.20D-02	-0.00016	-0.07992
43	42	994.9437	0.20D-02	-0.00004	-0.02197
44	43	995.61863	0.20D-02	-0.00015	-0.07624
45	44	996.28658	0.20D-02	0.00006	0.03129
46	45	996.94783	0.20D-02	0.00031	0.15465
47	46	997.60347	0.20D-02	-0.00051	-0.25726
48	47	998.2512	0.20D-02	-0.00011	-0.05547
49	48	998.89285	0.20D-02	-0.00034	-0.17105
50	49	999.52581	0.20D-02	0.0014	0.69995
51	50	1000.15699	0.20D-02	-0.00181	-0.90341
52	51	1000.77552	0.20D-02	0.0009	0.44762
53	52	1001.3906	0.20D-02	0.00029	0.14647
54	53	1001.994	0.50D-02	0.00461	0.92122
55	54	1002.59973	0.20D-02	-0.00019	-0.09422
56	55	1003.19379	0.20D-02	-0.00009	-0.04648

Table A.4, Fourier Transform Infrared Data for ^{74}GeO (cm^{-1}) (*Cont'd*)

J'	J''	Obs	Unc	Calc-Obs	(Calc-Obs)/Unc
57	56	1003.78115	0.20D-02	-0.00011	-0.05486
58	57	1004.36126	0.20D-02	0.00031	0.15453
59	58	1004.93534	0.20D-02	-0.00007	-0.03447
60	59	1005.50246	0.20D-02	-0.00033	-0.16301
61	60	1006.06214	0.20D-02	0.00001	0.00276
62	61	1006.61515	0.20D-02	0.00014	0.07167
63	62	1007.16167	0.20D-02	-0.0001	-0.05246
64	63	1007.70123	0.20D-02	-0.00028	-0.14081
65	64	1008.23579	0.20D-02	-0.00236	-1.17959
66	65	1008.75905	0.20D-02	-0.00004	-0.01999
67	66	1009.27838	0.20D-02	-0.00073	-0.36323
68	67	1009.78903	0.20D-02	0.00033	0.16447
69	68	1010.294	0.20D-02	0.00011	0.05688
70	69	1010.79217	0.20D-02	-0.00026	-0.13224
71	70	1011.28273	0.20D-02	-0.00001	-0.00415
72	71	1011.76708	0.20D-02	-0.00053	-0.26509
73	72	1012.24002	0.20D-02	0.00336	1.67865
74	73	1012.71189	0.20D-02	0.0013	0.65081
75	74	1013.17651	0.20D-02	-0.00053	-0.2649
76	75	1013.63246	0.20D-02	-0.00073	-0.36428
77	76	1014.08047	0.20D-02	-0.00004	-0.01964
78	77	1014.52296	0.20D-02	-0.00088	-0.44178
79	78	1014.95667	0.20D-02	-0.00003	-0.01703
80	79	1015.38403	0.20D-02	0.00008	0.03827
81	80	1015.80494	0.20D-02	-0.00046	-0.23222
82	81	1016.21817	0.20D-02	-0.00044	-0.21934
83	82	1016.6245	0.20D-02	-0.00064	-0.32046
84	83	1017.02217	0.20D-02	0.00068	0.33854
85	84	1017.4128	0.20D-02	0.00188	0.9413
86	85	1017.79848	0.20D-02	0.00087	0.43691
87	86	1018.17778	0.20D-02	-0.00093	-0.46702
88	87	1018.54981	0.20D-02	-0.00266	-1.33139
89	88	1018.91037	0.20D-02	-0.00012	-0.06214
90	89	1019.26719	0.20D-02	-0.00105	-0.52668
91	90	1019.61293	0.20D-02	0.00186	0.92905
92	91	1019.95875	0.20D-02	-0.00255	-1.27591
93	92	1020.28943	0.20D-02	0.00092	0.461
94	93	1020.61669	0.20D-02	0.00055	0.2738
95	94	1020.93478	0.20D-02	0.00206	1.03152
96	95	1021.24715	0.20D-02	0.002	1.00167
97	96	1021.55188	0.20D-02	0.00228	1.13876
99	98	1022.13755	0.50D-02	0.00464	0.92828
100	99	1022.42318	0.20D-02	0.00202	1.00752
The 4-3 Band, 165 data, $J"_{min} = 1$, $J"_{max} = 87$					
Unc.$_{Avge}$ = 2.1D-03, Unc.$_{Max}$ = 5.0D-03					
(Err/Unc.)$_{Avge}$ = -7.9D-03, RMSR = 0.56					
86	87	846.56679	0.20D-02	0.0015	0.75105
85	86	848.0044	0.20D-02	0.00055	0.27349
84	85	849.43614	0.20D-02	0.00026	0.13118
83	84	850.86263	0.20D-02	0.0	-0.00105
82	83	852.28345	0.20D-02	0.00017	0.08673
81	82	853.69864	0.20D-02	0.00075	0.37425
80	81	855.10898	0.20D-02	0.00091	0.45646
79	80	856.51623	0.20D-02	-0.00109	-0.54685
78	79	857.91443	0.20D-02	0.00068	0.33915
77	78	859.30783	0.20D-02	0.00198	0.9893
76	77	860.69975	0.20D-02	-0.00054	-0.2716

Table A.4, Fourier Transform Infrared Data for ^{74}GeO (cm^{-1}) (*Cont'd*)

J'	J''	Obs	Unc	Calc-Obs	(Calc-Obs)/Unc
75	76	862.08321	0.20D-02	0.00009	0.04628
74	75	863.46169	0.20D-02	0.0004	0.19775
73	74	864.83543	0.20D-02	0.00013	0.06261
72	73	866.20492	0.20D-02	-0.00124	-0.61928
71	72	867.56751	0.20D-02	-0.00105	-0.52324
70	71	868.92495	0.20D-02	-0.00106	-0.52936
69	70	870.27818	0.20D-02	-0.00222	-1.10793
68	69	871.62255	0.20D-02	0.0001	0.05079
67	68	872.96409	0.20D-02	-0.00014	-0.06832
66	67	874.30019	0.20D-02	-0.00033	-0.16556
65	66	875.62777	0.20D-02	0.0026	1.29888
64	65	876.95515	0.20D-02	0.0003	0.14967
63	64	878.27464	0.20D-02	0.00046	0.23161
62	63	879.58822	0.20D-02	0.0011	0.54948
61	62	880.89768	0.20D-02	0.00042	0.20792
60	61	882.20215	0.20D-02	-0.00075	-0.37323
59	60	883.49764	0.20D-02	0.0016	0.80065
58	59	884.79131	0.20D-02	0.00029	0.14438
57	58	886.07869	0.20D-02	-0.00021	-0.10738
56	57	887.36016	0.20D-02	-0.00032	-0.1599
55	56	888.63442	0.20D-02	0.00127	0.63649
54	55	889.90609	0.20D-02	-0.00007	-0.03344
53	54	891.16938	0.20D-02	0.00145	0.7249
52	53	892.43019	0.20D-02	-0.00011	-0.05372
51	52	893.68377	0.20D-02	0.00001	0.00529
50	51	894.93353	0.20D-02	-0.00162	-0.8083
49	50	896.17275	0.20D-02	0.00172	0.86013
48	49	897.41123	0.20D-02	0.00022	0.11017
47	48	898.64271	0.20D-02	0.00011	0.0566
46	47	899.86877	0.20D-02	-0.00018	-0.09099
45	46	901.08888	0.20D-02	-0.00015	-0.07291
44	45	902.30212	0.20D-02	0.00114	0.57036
43	44	903.51226	0.20D-02	-0.00012	-0.06147
42	43	904.71606	0.20D-02	-0.0007	-0.34875
41	42	905.91351	0.20D-02	-0.00058	-0.29191
40	41	907.10445	0.20D-02	0.00038	0.18862
39	40	908.29097	0.20D-02	0.00007	0.03253
38	39	909.47175	0.20D-02	-0.0002	-0.10062
37	38	910.64789	0.20D-02	-0.00153	-0.76625
36	37	911.81307	0.20D-02	0.00238	1.19024
35	36	912.97874	0.20D-02	0.00009	0.04341
34	35	914.13709	0.20D-02	-0.00063	-0.31711
33	34	915.28804	0.20D-02	0.0003	0.14816
32	33	916.43596	0.20D-02	-0.0015	-0.75115
31	32	917.57476	0.20D-02	0.00005	0.02449
30	31	918.70889	0.20D-02	0.0005	0.24955
29	30	919.83751	0.20D-02	0.00066	0.32869
28	29	920.96166	0.20D-02	-0.00052	-0.25861
27	28	922.07921	0.20D-02	-0.00091	-0.45284
26	27	923.18953	0.20D-02	0.00012	0.06058
25	26	924.29558	0.20D-02	-0.00043	-0.21393
24	25	925.39454	0.20D-02	0.00027	0.13317
23	24	926.48903	0.20D-02	-0.00043	-0.21356
22	23	927.57785	0.20D-02	-0.00132	-0.65968
21	22	928.65773	0.20D-02	0.00086	0.42925
20	21	929.73445	0.20D-02	0.0003	0.1478
19	20	930.8057	0.20D-02	-0.0007	-0.34961
18	19	931.86739	0.20D-02	0.00195	0.97649

Table A.4, Fourier Transform Infrared Data for ^{74}GeO (cm^{-1}) (*Cont'd*)

J'	J''	Obs	Unc	Calc-Obs	(Calc-Obs)/Unc
17	18	932.92893	0.20D-02	-0.00117	-0.58439
16	17	933.98084	0.20D-02	-0.00059	-0.2929
15	16	935.02636	0.20D-02	0.00043	0.21545
14	15	936.06769	0.20D-02	-0.00032	-0.15985
13	14	937.10146	0.20D-02	0.00052	0.26058
12	13	938.13031	0.20D-02	0.0003	0.15111
11	12	939.15349	0.20D-02	-0.00023	-0.11373
10	11	940.1699	0.20D-02	0.0	0.0004
9	10	941.179	0.20D-02	0.00153	0.76291
8	9	942.18583	0.20D-02	-0.0007	-0.35176
7	8	943.18369	0.20D-02	0.0	0.00069
6	7	944.17474	0.20D-02	0.00147	0.73468
5	6	945.16113	0.20D-02	0.00155	0.77464
4	5	946.14064	0.20D-02	0.00243	1.21488
3	4	947.11942	0.20D-02	-0.00204	-1.02029
2	1	952.83397	0.20D-02	0.00095	0.4747
3	2	953.7636	0.20D-02	0.00275	1.3735
4	3	954.69253	0.20D-02	-0.00093	-0.46341
5	4	955.61312	0.20D-02	-0.00243	-1.21679
6	5	956.5248	0.20D-02	-0.00123	-0.61734
7	6	957.42757	0.20D-02	0.00267	1.33422
8	7	958.33051	0.20D-02	0.00018	0.09214
9	8	959.22768	0.20D-02	-0.00276	-1.37931
10	9	960.11159	0.20D-02	0.00132	0.65918
11	10	960.99367	0.20D-02	0.00098	0.49176
12	11	961.87169	0.20D-02	-0.00156	-0.78224
13	12	962.73959	0.20D-02	-0.00027	-0.13369
14	13	963.60331	0.20D-02	-0.00108	-0.53826
15	14	964.45752	0.20D-02	0.00133	0.66322
16	15	965.30425	0.50D-02	0.0049	0.97998
17	16	966.15272	0.20D-02	0.00042	0.21118
18	17	966.99499	0.50D-02	-0.0042	-0.83959
19	18	967.82204	0.20D-02	0.00006	0.02868
20	19	968.64843	0.20D-02	-0.00138	-0.6916
21	20	969.46583	0.20D-02	-0.0002	-0.10071
22	21	970.27911	0.20D-02	-0.00128	-0.63947
23	22	971.08398	0.20D-02	-0.00033	-0.16379
24	23	971.8824	0.20D-02	0.00066	0.33063
25	24	972.67606	0.20D-02	0.0	-0.00223
26	25	973.46216	0.20D-02	0.00046	0.23182
27	26	974.24205	0.20D-02	0.0007	0.35189
28	27	975.0159	0.20D-02	0.00053	0.26715
29	28	975.78325	0.20D-02	0.0004	0.20166
30	29	976.5437	0.20D-02	0.00071	0.35446
31	30	977.29922	0.20D-02	-0.00055	-0.27526
32	31	978.04693	0.20D-02	-0.0005	-0.24847
33	32	978.78974	0.20D-02	-0.00205	-1.0261
34	33	979.52345	0.20D-02	-0.00103	-0.51402
35	34	980.25051	0.20D-02	0.00011	0.05671
36	35	980.97266	0.20D-02	-0.00038	-0.18976
37	36	981.68868	0.20D-02	-0.0013	-0.64949
38	37	982.39524	0.20D-02	0.00068	0.34166
39	38	983.09619	0.20D-02	0.00169	0.84266
40	39	983.79196	0.20D-02	0.00128	0.63751
41	40	984.4822	0.20D-02	-0.00021	-0.10476
42	41	985.16469	0.20D-02	-0.00056	-0.28017
43	42	985.83955	0.20D-02	0.00009	0.04532
44	43	986.50841	0.20D-02	0.0001	0.0506

Table A.4, Fourier Transform Infrared Data for ^{74}GeO (cm^{-1}) (*Cont'd*)

J'	J''	Obs	Unc	Calc-Obs	(Calc-Obs)/Unc
45	44	987.16981	0.20D-02	0.00092	0.45974
46	45	987.83079	0.50D-02	-0.0045	-0.89936
47	46	988.47498	0.20D-02	0.00019	0.09525
48	47	989.11706	0.20D-02	0.0003	0.14956
49	48	989.75296	0.20D-02	-0.00011	-0.05646
50	49	990.38167	0.20D-02	-0.00005	-0.02399
51	50	991.00489	0.20D-02	-0.00122	-0.60906
52	51	991.61942	0.20D-02	-0.00044	-0.2177
53	52	992.22815	0.20D-02	-0.0006	-0.30111
54	53	992.82663	0.20D-02	0.00273	1.3647
55	54	993.42604	0.20D-02	-0.00165	-0.82642
56	55	994.01253	0.20D-02	0.0001	0.04939
57	56	994.59616	0.20D-02	-0.00209	-1.04399
58	57	995.16924	0.20D-02	-0.00054	-0.2677
59	58	995.73474	0.20D-02	0.00177	0.88715
60	59	996.29783	0.20D-02	-0.00034	-0.17069
61	60	996.8499	0.20D-02	0.00172	0.85772
62	61	997.40306	0.50D-02	-0.00418	-0.83554
63	62	997.93852	0.20D-02	0.00077	0.3834
64	63	998.47287	0.20D-02	-0.00007	-0.03671
65	64	998.99944	0.20D-02	-0.00003	-0.01537
66	65	999.52035	0.20D-02	-0.00124	-0.61882
67	66	1000.03269	0.20D-02	-0.0008	-0.39821
68	67	1000.53994	0.20D-02	-0.0022	-1.09987
69	68	1001.0374	0.20D-02	-0.00076	-0.38
70	69	1001.5288	0.20D-02	-0.00022	-0.10984
71	70	1002.01146	0.20D-02	0.00209	1.04435
72	71	1002.49326	0.20D-02	-0.00173	-0.86369
73	72	1002.96348	0.20D-02	-0.00096	-0.48025
74	73	1003.42849	0.20D-02	-0.00199	-0.9961
76	75	1004.3353	0.20D-02	-0.00192	-0.95837
77	76	1004.77646	0.20D-02	-0.0002	-0.10191
78	77	1005.21192	0.20D-02	0.00015	0.07452
79	78	1005.64108	0.20D-02	-0.00027	-0.1354
80	79	1006.06218	0.20D-02	0.00028	0.14248
81	80	1006.47524	0.20D-02	0.00178	0.89081
82	81	1006.88416	0.20D-02	0.00031	0.15373
83	82	1007.28661	0.20D-02	-0.00182	-0.91012

The 5-4 Band, 171 data, $J"_{min} = 0$, $J"_{max} = 95$
Unc.$_{Avge}$ = 2.4D-03, Unc.$_{Max}$ = 5.0D-03
(Err/Unc.)$_{Avge}$ = -1.6D-02, RMSR = 0.76

76	77	852.36907	0.20D-02	-0.00002	-0.01007
75	76	853.7473	0.20D-02	-0.00067	-0.33558
74	75	855.1171	0.20D-02	0.00179	0.89539
73	74	856.4845	0.20D-02	0.00134	0.66753
72	73	857.8466	0.20D-02	0.00085	0.42574
71	72	859.2007	0.20D-02	0.00304	1.51976
70	71	860.55497	0.20D-02	-0.0003	-0.15069
69	70	861.90076	0.20D-02	-0.00052	-0.26072
68	69	863.24133	0.20D-02	-0.00089	-0.44561
67	68	864.57579	0.20D-02	-0.00052	-0.26061
66	67	865.905	0.20D-02	-0.0003	-0.15095
65	66	867.22713	0.20D-02	0.0016	0.79817
64	65	868.54879	0.20D-02	-0.00145	-0.7236
63	64	869.85919	0.20D-02	0.00136	0.67853
62	63	871.16829	0.20D-02	0.00002	0.00934
61	62	872.47127	0.20D-02	-0.00064	-0.32147

Table A.4, Fourier Transform Infrared Data for ^{74}GeO (cm^{-1}) (*Cont'd*)

J'	J''	Obs	Unc	Calc-Obs	(Calc-Obs)/Unc
60	61	873.76897	0.20D-02	-0.00148	-0.73925
59	60	875.05245	0.50D-02	0.00645	1.29033
58	59	876.34831	0.20D-02	-0.00348	-1.74156
57	58	877.62498	0.20D-02	0.00029	0.14328
56	57	878.90159	0.20D-02	-0.00138	-0.68995
55	56	880.17083	0.20D-02	-0.00117	-0.58651
54	55	881.43504	0.20D-02	-0.00146	-0.7318
53	54	882.69263	0.20D-02	-0.00066	-0.33104
52	53	883.94708	0.20D-02	-0.00226	-1.12966
51	52	885.19256	0.20D-02	-0.00044	-0.21788
50	51	886.43402	0.20D-02	-0.00014	-0.0711
49	50	887.67071	0.20D-02	-0.00066	-0.32969
48	49	888.90022	0.20D-02	0.00042	0.21109
47	48	890.12591	0.20D-02	-0.00027	-0.13411
46	47	891.34529	0.20D-02	-0.00024	-0.12075
45	46	892.5579	0.20D-02	0.00093	0.46586
44	45	893.76639	0.20D-02	0.0006	0.30038
43	44	894.96928	0.20D-02	0.00023	0.11735
42	43	896.1636	0.20D-02	0.00279	1.39648
41	42	897.35837	0.20D-02	-0.00075	-0.37272
40	41	898.54301	0.20D-02	0.00017	0.08445
39	40	899.72287	0.20D-02	0.00019	0.09253
38	39	900.89691	0.20D-02	0.00033	0.16613
37	38	902.06558	0.20D-02	0.00016	0.07982
36	37	903.22803	0.20D-02	0.00049	0.24322
35	36	904.38543	0.20D-02	0.00014	0.07082
34	35	905.53675	0.20D-02	0.00014	0.07227
33	34	906.68246	0.20D-02	0.00001	0.00703
32	33	907.82161	0.20D-02	0.0007	0.34975
31	32	908.9541	0.20D-02	0.00227	1.13494
30	31	910.08202	0.20D-02	0.00263	1.31712
29	30	911.20608	0.20D-02	0.00107	0.53583
28	29	912.32643	0.20D-02	-0.00257	-1.2844
27	28	913.43623	0.20D-02	-0.00148	-0.73907
26	27	914.53921	0.20D-02	0.00061	0.30635
25	26	915.63833	0.20D-02	0.00073	0.36641
24	25	916.73203	0.20D-02	0.00043	0.21551
23	24	917.82016	0.20D-02	-0.00014	-0.07176
22	23	918.90229	0.20D-02	-0.00059	-0.29597
21	22	919.97664	0.20D-02	0.00086	0.43236
20	21	921.04678	0.20D-02	0.00065	0.3227
19	20	922.11198	0.20D-02	-0.00053	-0.26548
18	19	923.16829	0.20D-02	0.00128	0.64228
17	18	924.22453	0.20D-02	-0.00276	-1.37958
16	17	925.26724	0.20D-02	0.0008	0.39844
15	16	926.309	0.20D-02	-0.00064	-0.31932
14	15	927.34305	0.20D-02	-0.00032	-0.15834
13	14	928.3698	0.20D-02	0.00135	0.67576
12	13	929.39177	0.20D-02	0.00181	0.9074
11	12	930.40869	0.50D-02	0.00134	0.26839
10	11	931.41615	0.50D-02	0.00433	0.86636
9	10	932.42413	0.20D-02	0.00079	0.39655
8	9	933.42333	0.20D-02	0.00001	0.00733
7	8	934.41532	0.20D-02	0.00043	0.21267
6	7	935.40145	0.20D-02	0.00064	0.32184
5	6	936.38209	0.20D-02	0.0003	0.14931
4	5	937.36427	0.50D-02	-0.00765	-1.53025
3	4	938.32075	0.50D-02	0.00402	0.80456

Table A.4, Fourier Transform Infrared Data for ^{74}GeO (cm^{-1}) (*Cont'd*)

J'	J''	Obs	Unc	Calc-Obs	(Calc-Obs)/Unc
2	3	939.29365	0.50D-02	-0.0068	-1.36011
1	2	940.24131	0.20D-02	0.00151	0.75367
0	1	941.19765	0.50D-02	-0.00497	-0.99496
1	0	943.07042	0.20D-02	0.0036	1.79766
3	2	944.93664	0.50D-02	-0.00585	-1.17026
4	3	945.84816	0.50D-02	0.00177	0.35313
5	4	946.76064	0.20D-02	0.00224	1.12209
6	5	947.67081	0.20D-02	-0.00116	-0.57858
7	6	948.56857	0.20D-02	0.00165	0.82508
8	7	949.46521	0.20D-02	-0.00064	-0.31762
9	8	950.35569	0.20D-02	-0.00298	-1.48751
10	9	951.23349	0.20D-02	0.00112	0.55969
11	10	952.10538	0.50D-02	0.00488	0.97531
12	11	952.97803	0.20D-02	0.00161	0.80744
13	12	953.84453	0.20D-02	-0.00177	-0.88361
14	13	954.69957	0.20D-02	0.00003	0.01435
15	14	955.54905	0.20D-02	0.0011	0.55053
17	16	957.23431	0.20D-02	-0.002	-1.00066
18	17	958.06315	0.20D-02	0.00075	0.3754
19	18	958.88911	0.20D-02	0.00004	0.02138
20	19	959.70631	0.20D-02	0.00174	0.87156
21	20	960.52068	0.20D-02	-0.00008	-0.03996
22	21	961.33143	0.50D-02	-0.00467	-0.9336
23	22	962.12594	0.20D-02	0.0006	0.29854
24	23	962.91745	0.20D-02	0.00246	1.23184
25	24	963.70763	0.20D-02	-0.00075	-0.37499
26	25	964.48684	0.20D-02	0.00058	0.29222
27	26	965.2607	0.20D-02	0.00084	0.4175
28	27	966.02623	0.20D-02	0.00298	1.49005
29	28	966.78521	0.50D-02	0.00521	1.04156
30	29	967.54479	0.20D-02	0.00037	0.18317
31	30	968.29434	0.20D-02	-0.00093	-0.46308
32	31	969.03549	0.20D-02	-0.00031	-0.15578
33	32	969.77067	0.20D-02	-0.00023	-0.11585
34	33	970.49952	0.20D-02	-0.00034	-0.16923
35	34	971.22068	0.20D-02	0.00073	0.36316
36	35	971.93678	0.20D-02	0.0003	0.15032
37	36	972.64693	0.20D-02	-0.00073	-0.36376
38	37	973.34912	0.20D-02	-0.00036	-0.17996
39	38	974.04508	0.20D-02	-0.00034	-0.16933
40	39	974.73686	0.20D-02	-0.00273	-1.36284
41	40	975.41633	0.20D-02	0.0006	0.29854
42	41	976.09396	0.20D-02	-0.00085	-0.42628
43	42	976.76437	0.20D-02	-0.0017	-0.84829
44	43	977.42417	0.20D-02	0.00142	0.71155
45	44	978.08211	0.20D-02	-0.00025	-0.12285
46	45	978.72992	0.20D-02	0.00155	0.77746
47	46	979.37395	0.20D-02	0.00046	0.23144
48	47	980.00914	0.20D-02	0.00153	0.76303
49	48	980.63993	0.20D-02	0.00029	0.14615
50	49	981.26199	0.20D-02	0.00108	0.53972
51	50	981.87938	0.20D-02	-0.00017	-0.08729
52	51	982.48885	0.20D-02	-0.00025	-0.12606
53	52	983.09485	0.20D-02	-0.00361	-1.80262
54	53	983.68992	0.20D-02	-0.00279	-1.39312
55	54	984.27862	0.20D-02	-0.00237	-1.18368
56	55	984.86019	0.20D-02	-0.0016	-0.80044
57	56	985.43373	0.20D-02	0.0004	0.20048

Table A.4, Fourier Transform Infrared Data for ^{74}GeO (cm^{-1}) (*Cont'd*)

J'	J''	Obs	Unc	Calc-Obs	(Calc-Obs)/Unc
58	57	986.00372	0.20D-02	-0.00085	-0.42703
59	58	986.56539	0.20D-02	-0.00061	-0.30423
60	59	987.12011	0.20D-02	-0.00024	-0.12218
61	60	987.66791	0.20D-02	0.00021	0.1029
62	61	988.20917	0.20D-02	0.00033	0.16477
63	62	988.74113	0.20D-02	0.00288	1.44235
64	63	989.27382	0.20D-02	-0.00217	-1.08558
65	64	989.78844	0.50D-02	0.00395	0.78987
66	65	990.30937	0.20D-02	-0.00315	-1.57304
67	66	990.81312	0.20D-02	0.00002	0.01008
68	67	991.3138	0.20D-02	-0.00067	-0.33729
69	68	991.80678	0.20D-02	-0.00061	-0.3063
70	69	992.28682	0.50D-02	0.00543	1.0867
71	70	992.77328	0.20D-02	-0.0019	-0.94942
72	71	993.2433	0.20D-02	0.00022	0.10893
73	72	993.7076	0.20D-02	0.00106	0.53056
74	73	994.16642	0.20D-02	0.00038	0.18908
75	74	994.62482	0.50D-02	-0.0069	-1.3807
76	75	995.06483	0.20D-02	-0.00283	-1.41321
77	76	995.49996	0.20D-02	-0.00091	-0.45666
78	77	995.93048	0.20D-02	-0.00145	-0.72343
79	78	996.35225	0.20D-02	-0.0003	-0.14986
80	79	996.76773	0.20D-02	0.00006	0.02771
81	80	997.17692	0.20D-02	-0.00039	-0.19703
82	81	997.58529	0.50D-02	-0.00713	-1.42622
83	82	997.97342	0.20D-02	-0.00074	-0.36914
84	83	998.35872	0.20D-02	0.00134	0.67078
85	84	998.74716	0.40D-02	-0.00686	-1.71612
86	85	999.11525	0.20D-02	-0.00188	-0.93944
87	86	999.48046	0.20D-02	-0.00118	-0.59239
88	87	999.83798	0.20D-02	0.00002	0.00752
89	88	1000.18857	0.20D-02	0.00095	0.47406
90	89	1000.54014	0.50D-02	-0.00631	-1.2619
91	90	1000.8742	0.50D-02	-0.00328	-0.656
92	91	1001.1979	0.20D-02	0.00287	1.4373
93	92	1001.52752	0.50D-02	-0.00414	-0.82811
94	93	1001.83078	0.50D-02	0.00794	1.58871
95	94	1002.14133	0.50D-02	0.00546	1.09238
96	95	1002.44266	0.50D-02	0.00491	0.9825

The 6-5 Band, 140 data, $J"_{min} = 3$, $J"_{max} = 80$
Unc.$_{Avge}$ = 2.6D-03, Unc.$_{Max}$ = 5.0D-03
(Err/Unc.)$_{Avge}$ = 1.5D-01, RMSR = 0.92

66	67	857.53843	0.20D-02	-0.00275	-1.37329
65	66	858.85186	0.20D-02	0.0014	0.70129
64	65	860.16844	0.50D-02	-0.00301	-0.6029
63	64	861.46926	0.20D-02	0.00291	1.45586
62	63	862.77273	0.20D-02	0.00076	0.3803
60	61	865.35484	0.50D-02	0.00497	0.99483
59	60	866.64581	0.20D-02	-0.00102	-0.51123
58	59	867.92563	0.20D-02	-0.00134	-0.66923
57	58	869.198	0.20D-02	0.00032	0.15761
56	57	870.46367	0.20D-02	0.00319	1.59403
55	56	871.72889	0.20D-02	0.001	0.49972
54	55	872.98522	0.20D-02	0.00219	1.09441
53	54	874.24094	0.20D-02	-0.00153	-0.76732
52	53	875.48494	0.20D-02	0.00094	0.4693
51	52	876.72457	0.20D-02	0.00223	1.11388

Table A.4, Fourier Transform Infrared Data for ^{74}GeO (cm^{-1}) (*Cont'd*)

J'	J''	Obs	Unc	Calc-Obs	(Calc-Obs)/Unc
50	51	877.9637	0.20D-02	-0.00154	-0.76892
49	50	879.19402	0.20D-02	-0.00206	-1.02945
48	49	880.41868	0.20D-02	-0.00249	-1.24306
47	48	881.6352	0.20D-02	-0.00037	-0.18512
46	47	882.8494	0.20D-02	-0.00153	-0.76594
45	46	884.05762	0.20D-02	-0.00232	-1.161
44	45	885.25495	0.20D-02	0.00216	1.07943
43	44	886.45457	0.20D-02	-0.00127	-0.63514
42	43	887.646	0.20D-02	-0.00216	-1.08
41	42	888.82387	0.50D-02	0.00486	0.97176
40	41	890.01093	0.20D-02	-0.00297	-1.48736
39	40	891.17475	0.50D-02	0.00677	1.35374
38	39	892.349	0.20D-02	0.00039	0.19406
37	38	893.51135	0.20D-02	0.00021	0.10639
36	37	894.66562	0.20D-02	0.00241	1.20594
35	36	895.81815	0.20D-02	0.00063	0.31718
34	35	896.96294	0.20D-02	0.00088	0.43976
33	34	898.1031	0.20D-02	0.00001	0.00314
32	33	899.238	0.20D-02	-0.00136	-0.67805
31	32	900.36379	0.20D-02	0.00063	0.3157
30	31	901.48294	0.20D-02	0.00349	1.74389
29	30	902.60276	0.20D-02	-0.0001	-0.04893
28	29	903.70952	0.20D-02	0.00357	1.7868
27	28	904.81803	0.20D-02	-0.00031	-0.15451
26	27	905.91351	0.20D-02	0.00302	1.51174
25	26	907.01	0.20D-02	-0.00047	-0.23504
24	25	908.0947	0.20D-02	0.00198	0.98972
23	24	909.17711	0.20D-02	0.00087	0.43548
22	23	910.25018	0.20D-02	0.00324	1.62165
21	22	911.32717	0.50D-02	-0.00417	-0.83488
19	20	913.4438	0.20D-02	0.0007	0.34781
18	19	914.49482	0.20D-02	0.00157	0.78553
17	18	915.54313	0.20D-02	-0.00076	-0.37896
16	17	916.57752	0.50D-02	0.00491	0.98147
15	16	917.61437	0.20D-02	0.00219	1.093
14	15	918.64633	0.20D-02	-0.0016	-0.80165
13	14	919.66578	0.20D-02	0.00116	0.5791
12	13	920.67744	0.50D-02	0.00574	1.14793
11	12	921.69566	0.20D-02	-0.00222	-1.11026
10	11	922.69776	0.20D-02	-0.00005	-0.02668
9	10	923.69774	0.20D-02	-0.00176	-0.88006
8	9	924.68682	0.20D-02	0.00141	0.70404
7	8	925.67289	0.20D-02	0.00156	0.77988
6	7	926.65315	0.20D-02	0.00148	0.74193
5	6	927.63146	0.20D-02	-0.00269	-1.3455
4	5	928.59443	0.20D-02	0.00242	1.21195
3	4	929.55221	0.50D-02	0.00665	1.32944
2	3	930.51008	0.50D-02	0.0047	0.93952
4	3	937.03117	0.20D-02	0.00379	1.89264
5	4	937.94635	0.50D-02	-0.00455	-0.90938
6	5	938.83959	0.20D-02	0.00288	1.4377
7	6	939.7274	0.50D-02	0.00954	1.90817
8	7	940.63244	0.50D-02	-0.00724	-1.44846
9	8	941.50982	0.20D-02	-0.00259	-1.2927
10	9	942.37721	0.50D-02	0.00583	1.16602
11	10	943.25184	0.20D-02	0.00076	0.38129
12	11	944.11828	0.20D-02	-0.00237	-1.18481
13	12	944.97085	0.20D-02	0.00211	1.05611

Table A.4, Fourier Transform Infrared Data for ^{74}GeO (cm^{-1}) (*Cont'd*)

J'	J''	Obs	Unc	Calc-Obs	(Calc-Obs)/Unc
14	13	945.82617	0.20D-02	-0.00244	-1.22188
15	14	946.66806	0.20D-02	0.00014	0.07047
16	15	947.49955	0.50D-02	0.00682	1.36494
17	16	948.33623	0.20D-02	0.00201	1.00299
18	17	949.16491	0.20D-02	-0.00114	-0.56852
19	18	949.98354	0.20D-02	-0.00056	-0.27791
20	19	950.79695	0.20D-02	-0.00111	-0.55608
21	20	951.60187	0.20D-02	0.00046	0.23114
22	21	952.40137	0.20D-02	0.00109	0.54288
23	22	953.19537	0.20D-02	0.00083	0.41329
24	23	953.98797	0.50D-02	-0.00443	-0.8854
25	24	954.7636	0.20D-02	0.00088	0.44167
26	25	955.53905	0.20D-02	-0.00003	-0.01717
27	26	956.30722	0.20D-02	-0.00011	-0.05582
28	27	957.06795	0.20D-02	0.00081	0.40472
29	28	957.81805	0.50D-02	0.00591	1.18146
30	29	958.57342	0.20D-02	-0.00073	-0.36502
31	30	959.31413	0.20D-02	0.00082	0.4078
32	31	960.05091	0.20D-02	-0.0002	-0.09878
33	32	960.77535	0.50D-02	0.00464	0.92768
34	33	961.50377	0.20D-02	-0.00103	-0.5141
35	34	962.21809	0.20D-02	0.00088	0.44024
36	35	962.92561	0.20D-02	0.00305	1.52637
37	36	963.6335	0.20D-02	-0.00169	-0.84674
38	37	964.32969	0.20D-02	-0.0013	-0.65008
39	38	965.01238	0.50D-02	0.00602	1.20415
40	39	965.69947	0.20D-02	0.00236	1.1786
41	40	966.3774	0.20D-02	0.00127	0.63361
42	41	967.04892	0.20D-02	-0.00003	-0.01557
43	42	967.70727	0.50D-02	0.00522	1.04399
44	43	968.37107	0.20D-02	-0.00161	-0.80583
45	44	969.01868	0.20D-02	0.0011	0.55108
46	45	969.66394	0.20D-02	-0.00049	-0.24541
47	46	970.30246	0.20D-02	-0.00201	-1.00635
48	47	970.92826	0.20D-02	0.0025	1.25219
49	48	971.55454	0.20D-02	-0.00014	-0.07082
50	49	972.17079	0.20D-02	0.00053	0.26343
51	50	972.78103	0.20D-02	0.00049	0.24396
52	51	973.38669	0.20D-02	-0.0017	-0.85044
53	52	973.98242	0.20D-02	-0.0007	-0.35078
54	53	974.56938	0.20D-02	0.00231	1.15677
55	54	975.15589	0.20D-02	-0.00099	-0.49392
56	55	975.72917	0.20D-02	0.00216	1.08107
57	56	976.30119	0.20D-02	-0.00022	-0.10952
58	57	976.86361	0.20D-02	0.00021	0.10321
59	58	977.42417	0.50D-02	-0.00433	-0.86674
60	59	977.9723	0.20D-02	-0.00327	-1.63592
61	60	978.51884	0.50D-02	-0.00746	-1.49207
62	61	979.04525	0.20D-02	0.00163	0.81417
63	62	979.5748	0.20D-02	0.00071	0.35593
65	64	980.61345	0.20D-02	-0.00132	-0.65815
66	65	981.12031	0.20D-02	-0.00021	-0.10638
67	66	981.6236	0.20D-02	-0.00245	-1.22713
68	67	982.11	0.50D-02	0.00528	1.05538
69	68	982.60361	0.20D-02	-0.00115	-0.57594
70	69	983.08895	0.50D-02	-0.00626	-1.25263
71	70	983.55216	0.50D-02	0.00379	0.75812
72	71	984.02945	0.50D-02	-0.00721	-1.44263

Table A.4, Fourier Transform Infrared Data for ^{74}GeO (cm^{-1}) (*Cont'd*)

J'	J''	Obs	Unc	Calc-Obs	(Calc-Obs)/Unc
73	72	984.48216	0.20D-02	-0.00063	-0.31356
74	73	984.9325	0.20D-02	0.00133	0.66312
75	74	985.37752	0.20D-02	0.00158	0.79206
76	75	985.81491	0.20D-02	0.00244	1.22205
77	76	986.2501	0.20D-02	-0.00154	-0.76829
78	77	986.67302	0.20D-02	-0.0003	-0.1503
79	78	987.08444	0.50D-02	0.00537	1.07387
80	79	987.50149	0.20D-02	-0.00166	-0.82966
81	80	987.90072	0.20D-02	0.00203	1.01522
The 7-6 Band, 118 data, $J"_{min} = 10$, $J"_{max} = 70$					
Unc.$_{Avge}$ = 3.4D-03, Unc.$_{Max}$ = 1.0D-02					
(Err/Unc.)$_{Avge}$ = 1.5D-02, RMSR = 0.99					
69	70	845.22894	0.20D-02	-0.00201	-1.00691
68	69	846.55471	0.20D-02	-0.00052	-0.26119
66	67	849.19089	0.20D-02	0.00171	0.85598
65	66	850.50011	0.20D-02	0.00361	1.80687
64	65	851.80746	0.20D-02	0.00198	0.99233
63	64	853.10882	0.20D-02	0.00093	0.467
62	63	854.40187	0.20D-02	0.00278	1.39069
61	62	855.69381	0.20D-02	0.0003	0.14808
60	61	856.97901	0.20D-02	-0.00089	-0.44614
59	60	858.25354	0.20D-02	0.00314	1.56775
58	59	859.52936	0.20D-02	0.00042	0.20945
57	58	860.79636	0.20D-02	0.00104	0.51869
56	57	862.06699	0.50D-02	-0.00746	-1.49198
55	56	863.31561	0.20D-02	0.00056	0.27835
54	55	864.56675	0.20D-02	0.00056	0.27812
53	54	865.81515	0.20D-02	-0.00223	-1.11586
52	53	867.05264	0.20D-02	0.00036	0.18103
51	52	868.28577	0.20D-02	0.00178	0.88845
50	51	869.51381	0.50D-02	0.00274	0.54841
49	50	870.74027	0.20D-02	-0.00028	-0.14156
48	49	871.95753	0.20D-02	0.00032	0.1603
47	48	873.16994	0.20D-02	0.00019	0.09624
46	47	874.3753	0.20D-02	0.00152	0.76095
45	46	875.57752	0.20D-02	0.0004	0.19894
44	45	876.76775	0.50D-02	0.00564	1.12797
43	44	877.96059	0.20D-02	0.00265	1.32347
42	43	879.14559	0.20D-02	0.00186	0.92916
41	42	880.32483	0.20D-02	0.00119	0.59659
40	41	881.49793	0.20D-02	0.001	0.50037
39	40	882.66588	0.20D-02	0.00029	0.14506
38	39	883.82744	0.20D-02	0.00029	0.14524
37	38	884.98486	0.20D-02	-0.00126	-0.62947
36	37	886.13623	0.20D-02	-0.00245	-1.2246
35	36	887.26674	0.10D-01	0.0115	1.1499
34	35	888.41672	0.20D-02	0.00025	0.12732
33	34	889.54973	0.20D-02	0.00025	0.12337
32	33	890.67129	0.50D-02	0.00594	1.18891
31	32	891.79763	0.20D-02	0.00112	0.55853
30	31	892.91735	0.20D-02	-0.00287	-1.43336
29	30	894.02538	0.20D-02	-0.00094	-0.46882
28	29	895.12559	0.20D-02	0.00302	1.51156
27	28	896.21847	0.50D-02	0.00852	1.70496
25	26	898.40507	0.20D-02	0.00123	0.61315
24	25	899.48599	0.20D-02	0.00121	0.60711
23	24	900.57554	0.10D-01	-0.01327	-1.32713

Table A.4, Fourier Transform Infrared Data for ^{74}GeO (cm^{-1}) (*Cont'd*)

J'	J''	Obs	Unc	Calc-Obs	(Calc-Obs)/Unc
22	23	901.62966	0.20D-02	0.00183	0.91453
21	22	902.69377	0.20D-02	0.00106	0.53191
20	21	903.75918	0.50D-02	-0.00688	-1.37559
19	20	904.81687	0.10D-01	-0.01299	-1.29873
18	19	905.85934	0.10D-01	-0.00978	-0.97754
17	18	906.89476	0.50D-02	-0.00541	-1.08269
16	17	907.92669	0.50D-02	-0.00349	-0.69848
15	16	908.9541	0.20D-02	-0.00298	-1.49178
14	15	909.97485	0.20D-02	-0.00176	-0.87903
13	14	910.99118	0.20D-02	-0.00207	-1.03354
12	13	912.00823	0.50D-02	-0.00906	-1.81237
11	12	913.01565	0.10D-01	-0.01239	-1.23936
10	11	913.99494	0.50D-02	0.00641	1.28131
11	10	934.41532	0.50D-02	0.00614	1.22805
12	11	935.28013	0.20D-02	-0.00144	-0.71956
14	13	936.97318	0.20D-02	0.00117	0.58729
15	14	937.8123	0.20D-02	0.00046	0.23222
16	15	938.64164	0.20D-02	0.00324	1.61879
17	16	939.45244	0.10D-01	0.01825	1.82523
18	17	940.30721	0.10D-01	-0.01703	-1.70333
19	18	941.10187	0.20D-02	0.00146	0.72972
20	19	941.90955	0.20D-02	0.00059	0.29436
21	20	942.70085	0.50D-02	0.00974	1.94856
22	21	943.52099	0.10D-01	-0.01631	-1.63101
23	22	944.29285	0.20D-02	-0.00046	-0.23079
24	23	945.0733	0.20D-02	0.00042	0.2083
25	24	945.8598	0.10D-01	-0.01117	-1.11675
26	25	946.6213	0.50D-02	-0.00417	-0.83309
27	26	947.37826	0.20D-02	0.00095	0.47542
28	27	948.13462	0.20D-02	0.00023	0.11472
29	28	948.88174	0.20D-02	0.0023	1.14936
30	29	949.6256	0.20D-02	0.00117	0.58342
31	30	950.36638	0.20D-02	-0.00335	-1.67414
32	31	951.09222	0.20D-02	0.00058	0.29079
33	32	951.81903	0.20D-02	-0.00296	-1.47769
34	33	952.53357	0.20D-02	-0.00073	-0.36563
35	34	953.2403	0.20D-02	0.00278	1.3911
36	35	953.9449	0.20D-02	0.00189	0.94648
37	36	954.64428	0.20D-02	-0.00032	-0.16049
38	37	955.33405	0.20D-02	0.00053	0.26422
39	38	956.03252	0.10D-01	-0.0139	-1.39008
40	39	956.70011	0.50D-02	-0.00403	-0.80615
41	40	957.372	0.50D-02	-0.00505	-1.01065
42	41	958.03132	0.20D-02	-0.00011	-0.05531
43	42	958.67876	0.50D-02	0.0101	2.01906
44	43	959.33546	0.50D-02	0.00441	0.88246
45	44	959.9844	0.20D-02	-0.00015	-0.07584
46	45	960.62727	0.50D-02	-0.00529	-1.05776
47	46	961.25216	0.20D-02	0.00088	0.43942
48	47	961.8765	0.20D-02	0.00092	0.4596
49	48	962.49788	0.20D-02	-0.00277	-1.38507
50	49	963.10904	0.20D-02	-0.00294	-1.47056
51	50	963.70763	0.20D-02	0.00274	1.37193
52	51	964.3069	0.20D-02	0.00102	0.51137
53	52	964.90358	0.50D-02	-0.00485	-0.96936
54	53	965.47763	0.50D-02	0.00516	1.03261
55	54	966.05863	0.20D-02	0.00147	0.73495
56	55	966.62713	0.20D-02	0.00349	1.74582

Table A.4, Fourier Transform Infrared Data for ^{74}GeO (cm^{-1}) (*Cont'd*)

J'	J''	Obs	Unc	Calc-Obs	(Calc-Obs)/Unc
57	56	967.19406	0.20D-02	0.0003	0.14787
58	57	967.7451	0.50D-02	0.00619	1.23802
59	58	968.30239	0.20D-02	-0.00098	-0.48893
60	59	968.84416	0.20D-02	0.00055	0.27486
61	60	969.37839	0.20D-02	0.00278	1.39017
62	61	969.90831	0.20D-02	0.00247	1.23582
63	62	970.43235	0.20D-02	0.00118	0.59065
64	63	970.94424	0.50D-02	0.00517	1.03333
65	64	971.45321	0.50D-02	0.0052	1.0391
66	65	971.94847	0.10D-01	0.01203	1.20251
67	66	972.45575	0.20D-02	-0.00008	-0.03836
68	67	972.93987	0.50D-02	0.00406	0.81147
69	68	973.42577	0.20D-02	-0.00053	-0.26261
70	69	973.9	0.20D-02	-0.00039	-0.19346
71	70	974.36761	0.20D-02	-0.00059	-0.29517
The 8-7 Band, 30 data, $J"_{min} = 23$, $J"_{max} = 59$ Unc.$_{Avge} = 2.5$D-03, Unc.$_{Max} = 5.0$D-03 (Err/Unc.)$_{Avge} = 7.1$D-01, RMSR = 1.06					
58	59	851.15587	0.50D-02	0.00517	1.03312
56	57	853.6774	0.20D-02	0.00061	0.30628
54	55	856.17142	0.20D-02	0.00159	0.79734
49	50	862.31667	0.50D-02	-0.0028	-0.55933
48	49	863.52229	0.20D-02	0.0031	1.54887
47	48	864.72922	0.20D-02	0.00212	1.05759
45	46	867.11883	0.50D-02	0.00761	1.52131
42	43	870.67304	0.20D-02	0.00396	1.98124
40	41	873.01458	0.20D-02	0.00127	0.63483
39	40	874.17328	0.20D-02	0.0035	1.75189
38	39	875.33237	0.20D-02	-0.00032	-0.15819
37	38	876.47464	0.50D-02	0.00699	1.3977
35	36	878.76332	0.20D-02	0.00036	0.17966
34	35	879.89646	0.20D-02	-0.00033	-0.16321
33	34	881.0202	0.20D-02	0.00267	1.33457
31	32	883.25563	0.20D-02	0.00346	1.73017
28	29	886.56639	0.20D-02	0.0038	1.9015
27	28	887.66207	0.20D-02	0.00025	0.12309
25	26	889.82047	0.50D-02	0.00866	1.73294
22	23	893.03549	0.20D-02	0.00015	0.07375
28	27	939.22642	0.20D-02	0.00083	0.41352
30	29	940.70535	0.20D-02	0.0018	0.90172
31	30	941.43727	0.20D-02	0.00014	0.06932
32	31	942.16157	0.20D-02	-0.00039	-0.19374
33	32	942.87741	0.20D-02	0.00105	0.52666
37	36	945.68347	0.20D-02	-0.00104	-0.52199
41	40	948.37905	0.20D-02	0.00248	1.24053
42	41	949.03916	0.20D-02	0.00067	0.33729
45	44	950.973	0.20D-02	0.00203	1.0139
55	54	956.99305	0.20D-02	-0.00147	-0.73504

A.5 Fourier Transform Infrared Data for ^{76}GeO

Table A.5: Fourier Transform Infrared Data for ^{76}GeO (cm^{-1})

J'	J''	Obs	Unc	Calc-Obs	(Calc-Obs)/Unc
860 ^{76}GeO infrared transitions in 7 bands					
The 1-0 Band, 179 data, $J"_{min}$ = 2, $J"_{max}$ = 91 Unc.$_{Avge}$ = 2.1D-03, Unc.$_{Max}$ = 5.0D-03 (Err/Unc.)$_{Avge}$ = 7.0D-02, RMSR = 0.72					
89	90	865.41518	0.20D-02	-0.00049	-0.24363
88	89	866.87862	0.20D-02	0.00022	0.10881
87	88	868.33578	0.20D-02	0.00204	1.01992
86	87	869.78901	0.20D-02	0.00263	1.31465
85	86	871.23843	0.20D-02	0.00184	0.91795
84	85	872.68725	0.20D-02	-0.00355	-1.77527
83	84	874.11886	0.20D-02	0.00307	1.53493
82	83	875.5557	0.20D-02	-0.00074	-0.37153
81	82	876.98177	0.20D-02	0.00098	0.49028
80	81	878.40921	0.20D-02	-0.0039	-1.94969
79	80	879.82419	0.20D-02	-0.00156	-0.78163
78	79	881.23453	0.20D-02	0.00017	0.08446
77	78	882.64315	0.20D-02	-0.00165	-0.82662
76	77	884.04343	0.20D-02	-0.00041	-0.20488
75	76	885.4402	0.20D-02	-0.00094	-0.47048
74	75	886.83116	0.20D-02	-0.00095	-0.47354
73	74	888.21638	0.20D-02	-0.00053	-0.26419
72	73	889.59415	0.20D-02	0.00202	1.01249
71	72	890.97056	0.20D-02	0.00062	0.31127
70	71	892.33995	0.20D-02	0.00089	0.44705
69	70	893.70676	0.20D-02	-0.0016	-0.80026
68	69	895.06449	0.20D-02	-0.00037	-0.18591
67	68	896.41744	0.20D-02	0.00028	0.14004
66	67	897.766	0.20D-02	-0.00007	-0.03263
65	66	899.10435	0.50D-02	0.00441	0.88237
64	65	900.44735	0.20D-02	-0.00116	-0.57949
63	64	901.77804	0.20D-02	0.00018	0.09096
62	63	903.10421	0.20D-02	0.00061	0.30708
61	62	904.42601	0.20D-02	-0.00001	-0.00631
60	61	905.74096	0.20D-02	0.00077	0.38563
59	60	907.05157	0.20D-02	0.00046	0.22761
58	59	908.35438	0.20D-02	0.00247	1.2345
57	58	909.65634	0.20D-02	-0.00014	-0.06895
56	57	910.94872	0.20D-02	0.00135	0.67699
55	56	912.23847	0.20D-02	-0.00002	-0.00781
54	55	913.5215	0.20D-02	-0.00016	-0.07864
53	54	914.79839	0.20D-02	0.00032	0.15928
52	53	916.06923	0.20D-02	0.00132	0.66073
51	52	917.33576	0.20D-02	0.0011	0.55038
50	51	918.59669	0.20D-02	0.00095	0.47302
49	50	919.85167	0.20D-02	0.00118	0.58843
48	49	921.09978	0.20D-02	0.00271	1.35629
47	48	922.34648	0.20D-02	0.00008	0.04129
46	47	923.58517	0.20D-02	-0.00011	-0.05677
45	46	924.81661	0.20D-02	0.00133	0.66679
44	45	926.0419	0.20D-02	0.00332	1.66167
43	44	927.26704	0.20D-02	-0.00015	-0.07743
42	43	928.48175	0.20D-02	0.00118	0.58923

Table A.5, Fourier Transform Infrared Data for ^{76}GeO (cm^{-1}) (*Cont'd*)

J'	J''	Obs	Unc	Calc-Obs	(Calc-Obs)/Unc
41	42	929.69253	0.20D-02	0.00079	0.39625
40	41	930.89769	0.20D-02	0.00038	0.1884
39	40	932.09768	0.20D-02	-0.00053	-0.26473
38	39	933.28972	0.20D-02	0.00084	0.42162
37	38	934.47692	0.20D-02	0.00138	0.69205
36	37	935.65942	0.20D-02	0.00092	0.46125
35	36	936.83637	0.20D-02	0.00031	0.15384
34	35	938.00696	0.20D-02	0.00034	0.16948
33	34	939.17215	0.20D-02	0.00006	0.0278
32	33	940.32956	0.20D-02	0.00181	0.90343
31	32	941.48463	0.20D-02	0.00015	0.07606
30	31	942.63169	0.20D-02	0.00075	0.37519
29	30	943.77286	0.20D-02	0.00147	0.73554
28	29	944.91019	0.20D-02	0.00026	0.13166
27	28	946.04161	0.20D-02	-0.00083	-0.41684
26	27	947.16501	0.20D-02	0.00029	0.14462
25	26	948.28506	0.20D-02	-0.00105	-0.52437
24	25	949.39655	0.20D-02	0.00035	0.17578
23	24	950.50465	0.20D-02	-0.00068	-0.34038
22	23	951.60187	0.20D-02	0.00331	1.65678
21	22	952.70089	0.20D-02	-0.00035	-0.17329
20	21	953.79051	0.20D-02	-0.00047	-0.23593
19	20	954.87828	0.50D-02	-0.00462	-0.92468
18	19	955.95077	0.20D-02	0.00063	0.31404
17	18	957.02306	0.20D-02	0.00017	0.08578
16	17	958.08711	0.20D-02	0.00205	1.02303
15	16	959.14942	0.20D-02	-0.00026	-0.12964
14	15	960.2038	0.20D-02	-0.00057	-0.28281
13	14	961.24995	0.20D-02	0.00143	0.71307
12	13	962.29481	0.20D-02	-0.00125	-0.62745
11	12	963.3289	0.20D-02	0.00087	0.43501
10	11	964.36121	0.20D-02	-0.0012	-0.59996
9	10	965.38461	0.20D-02	-0.00035	-0.17294
8	9	966.40473	0.20D-02	-0.0022	-1.09945
7	8	967.41569	0.20D-02	-0.00091	-0.45503
6	7	968.424	0.20D-02	-0.00299	-1.49524
5	6	969.42072	0.20D-02	0.00049	0.24444
4	5	970.41367	0.20D-02	0.0017	0.84833
3	4	971.40533	0.20D-02	-0.00185	-0.92407
2	3	972.38571	0.20D-02	-0.00019	-0.09329
1	2	973.36256	0.20D-02	-0.00107	-0.53497
3	2	978.14838	0.20D-02	0.00144	0.71902
4	3	979.09204	0.20D-02	-0.00294	-1.46993
5	4	980.0257	0.20D-02	-0.00347	-1.73565
6	5	980.95073	0.20D-02	-0.00154	-0.76868
7	6	981.87107	0.20D-02	-0.00108	-0.53973
8	7	982.78612	0.20D-02	-0.00153	-0.76443
9	8	983.68992	0.20D-02	0.00307	1.53653
10	9	984.59611	0.20D-02	-0.00093	-0.4625
11	10	985.49039	0.20D-02	0.00077	0.38279
12	11	986.38196	0.20D-02	-0.00107	-0.53322
13	12	987.26236	0.20D-02	0.00204	1.01867
14	13	988.14122	0.20D-02	0.00042	0.20785
15	14	989.01257	0.20D-02	0.00004	0.01853
16	15	989.87448	0.20D-02	0.00282	1.41008
17	16	990.7345	0.20D-02	0.0012	0.60174
18	17	991.58601	0.20D-02	0.0018	0.89778
19	18	992.43354	0.20D-02	0.00005	0.02745

Table A.5, Fourier Transform Infrared Data for ^{76}GeO (cm^{-1}) (*Cont'd*)

J'	J''	Obs	Unc	Calc-Obs	(Calc-Obs)/Unc
20	19	993.27359	0.20D-02	-0.00052	-0.25995
21	20	994.10135	0.50D-02	0.00485	0.9699
22	21	994.93367	0.20D-02	-0.00069	-0.34414
23	22	995.75391	0.20D-02	-0.0005	-0.25247
24	23	996.5674	0.20D-02	0.00006	0.02908
25	24	997.37164	0.20D-02	0.00349	1.74467
26	25	998.17663	0.20D-02	-0.00021	-0.1065
27	26	998.97156	0.20D-02	-0.00027	-0.13521
28	27	999.76115	0.20D-02	-0.0014	-0.70229
29	28	1000.53994	0.20D-02	0.00183	0.9165
30	29	1001.31971	0.20D-02	-0.00235	-1.17451
31	30	1002.08591	0.20D-02	0.00059	0.29314
32	31	1002.84851	0.20D-02	0.00066	0.32961
33	32	1003.60502	0.20D-02	0.00036	0.17806
34	33	1004.35641	0.20D-02	-0.00132	-0.66139
35	34	1005.0974	0.20D-02	0.0009	0.44942
36	35	1005.83511	0.20D-02	-0.00011	-0.05439
37	36	1006.56467	0.20D-02	0.00051	0.25578
38	37	1007.28926	0.20D-02	-0.00043	-0.21644
39	38	1008.00087	0.50D-02	0.00506	1.01162
40	39	1008.71568	0.20D-02	0.0008	0.40083
41	40	1009.42031	0.20D-02	0.00014	0.0725
42	41	1010.11714	0.20D-02	0.00071	0.35412
43	42	1010.80877	0.20D-02	-0.00012	-0.06072
44	43	1011.49258	0.20D-02	0.00026	0.13202
45	44	1012.17065	0.20D-02	-0.00023	-0.11409
46	45	1012.84286	0.20D-02	-0.00149	-0.74402
47	46	1013.50543	0.20D-02	0.00025	0.12577
48	47	1014.16182	0.20D-02	0.00153	0.7643
49	48	1014.81355	0.20D-02	0.00079	0.3951
50	49	1015.45574	0.20D-02	0.00292	1.45817
51	50	1016.09633	0.20D-02	-0.00005	-0.02299
52	51	1016.72739	0.20D-02	-0.00018	-0.08939
53	52	1017.35134	0.20D-02	0.00009	0.04297
54	53	1017.96774	0.20D-02	0.00118	0.58755
55	54	1018.57898	0.20D-02	0.00069	0.34433
56	55	1019.1843	0.20D-02	-0.00063	-0.31325
57	56	1019.78079	0.20D-02	0.00014	0.06877
58	57	1020.37074	0.20D-02	0.00066	0.32932
59	58	1020.95431	0.20D-02	0.00077	0.38735
60	59	1021.53182	0.20D-02	0.00015	0.07677
61	60	1022.10246	0.20D-02	-0.00041	-0.2035
62	61	1022.66387	0.20D-02	0.00144	0.72044
63	62	1023.2235	0.20D-02	-0.00177	-0.88251
64	63	1023.77048	0.20D-02	0.00083	0.41654
65	64	1024.31797	0.50D-02	-0.00394	-0.78742
66	65	1024.85017	0.20D-02	-0.00028	-0.13888
67	66	1025.37825	0.20D-02	0.00061	0.3044
68	67	1025.89985	0.20D-02	0.00108	0.54013
69	68	1026.41346	0.20D-02	0.00263	1.31716
70	69	1026.92668	0.20D-02	-0.00234	-1.17067
71	70	1027.42433	0.20D-02	0.00132	0.66046
72	71	1027.92172	0.20D-02	-0.0017	-0.85064
73	72	1028.40771	0.20D-02	-0.00028	-0.14015
74	73	1028.89044	0.20D-02	-0.00257	-1.28429
75	74	1029.36298	0.20D-02	-0.00165	-0.82425
76	75	1029.82569	0.20D-02	0.00211	1.05374
77	76	1030.2868	0.20D-02	0.00047	0.23344

Table A.5, Fourier Transform Infrared Data for ^{76}GeO (cm^{-1}) (*Cont'd*)

J'	J''	Obs	Unc	Calc-Obs	(Calc-Obs)/Unc
78	77	1030.73861	0.20D-02	0.0011	0.54912
79	78	1031.1857	0.20D-02	-0.00058	-0.29146
80	79	1031.62315	0.20D-02	0.00033	0.16593
81	80	1032.05385	0.20D-02	0.00094	0.47002
82	81	1032.47986	0.20D-02	-0.00083	-0.41545
83	82	1032.89449	0.20D-02	0.0017	0.84873
84	83	1033.30368	0.20D-02	0.00257	1.28525
85	84	1033.70606	0.50D-02	0.00315	0.62933
86	85	1034.10892	0.20D-02	-0.00388	-1.93837
87	86	1034.49474	0.20D-02	-0.00099	-0.49565
88	87	1034.8781	0.20D-02	-0.00279	-1.39585
89	88	1035.25014	0.20D-02	-0.00043	-0.21482
90	89	1035.61942	0.20D-02	-0.00247	-1.2339
91	90	1035.97786	0.20D-02	-0.00086	-0.42896
92	91	1036.33118	0.20D-02	-0.00132	-0.66237
The 2-1 Band, 166 data, $J"_{min} = 0$, $J"_{max} = 83$					
Unc.$_{Avge}$ = 2.1D-03, Unc.$_{Max}$ = 5.0D-03					
(Err/Unc.)$_{Avge}$ = 1.4D-01, RMSR = 0.79					
81	82	868.64375	0.20D-02	0.00017	0.08704
80	81	870.05908	0.20D-02	0.00087	0.4328
79	80	871.46985	0.20D-02	0.00087	0.4346
78	79	872.87624	0.20D-02	0.0	0.00244
77	78	874.27804	0.20D-02	-0.00153	-0.76385
76	77	875.67068	0.20D-02	0.00084	0.42061
75	76	877.06001	0.20D-02	0.00123	0.61572
74	75	878.44507	0.20D-02	0.0006	0.30133
73	74	879.82418	0.20D-02	0.00062	0.31232
72	73	881.19712	0.20D-02	0.00152	0.75856
71	72	882.56529	0.20D-02	0.00185	0.92494
70	71	883.93261	0.20D-02	-0.0023	-1.14878
69	70	885.28805	0.20D-02	0.00009	0.04734
68	69	886.64171	0.20D-02	-0.00107	-0.5369
67	68	887.98817	0.20D-02	-0.00041	-0.20668
66	67	889.3272	0.20D-02	0.00231	1.15285
65	66	890.66315	0.20D-02	0.00272	1.3615
64	65	891.99501	0.20D-02	0.00185	0.92409
63	64	893.32556	0.20D-02	-0.00313	-1.56457
62	63	894.64317	0.20D-02	-0.00058	-0.28967
61	62	895.96008	0.20D-02	-0.00275	-1.37636
60	61	897.26739	0.20D-02	-0.00075	-0.37494
59	60	898.56993	0.20D-02	0.00057	0.28447
58	59	899.86877	0.20D-02	0.00013	0.06656
57	58	901.1607	0.20D-02	0.00114	0.5712
56	57	902.44719	0.20D-02	0.00213	1.06312
55	56	903.73123	0.20D-02	0.00006	0.03209
54	55	905.0116	0.20D-02	-0.00382	-1.91215
53	54	906.27815	0.20D-02	0.0006	0.30022
52	53	907.54388	0.20D-02	0.00034	0.16885
51	52	908.80338	0.20D-02	0.00077	0.38353
50	51	910.05811	0.20D-02	0.00043	0.21404
49	50	911.30697	0.20D-02	0.00041	0.20506
48	49	912.55067	0.20D-02	0.0	0.00127
47	48	913.78767	0.20D-02	0.00071	0.35748
46	47	915.0203	0.20D-02	0.00022	0.10837
45	46	916.24969	0.20D-02	-0.00263	-1.31638
44	45	917.46478	0.20D-02	0.00322	1.608
43	44	918.68061	0.20D-02	0.00272	1.3611

Table A.5, Fourier Transform Infrared Data for ^{76}GeO (cm^{-1}) (*Cont'd*)

J'	J''	Obs	Unc	Calc-Obs	(Calc-Obs)/Unc
42	43	919.89258	0.20D-02	0.00046	0.22764
41	42	921.09981	0.20D-02	-0.00271	-1.35262
40	41	922.29526	0.20D-02	0.00027	0.13487
39	40	923.48719	0.20D-02	0.00112	0.55989
38	39	924.67599	0.20D-02	-0.00058	-0.28795
37	38	925.85585	0.20D-02	0.00099	0.49601
36	37	927.03285	0.20D-02	-0.00027	-0.13359
35	36	928.20197	0.20D-02	0.00066	0.3279
34	35	929.36712	0.20D-02	-0.00015	-0.07489
33	34	930.52267	0.20D-02	0.00292	1.45774
32	33	931.68038	0.20D-02	-0.00191	-0.95471
31	32	932.82479	0.20D-02	0.00082	0.41248
30	31	933.9667	0.20D-02	0.00032	0.15884
29	30	935.10016	0.20D-02	0.00249	1.24406
28	29	936.23283	0.20D-02	-0.00032	-0.16231
27	28	937.35737	0.20D-02	-0.00079	-0.39569
26	27	938.47302	0.20D-02	0.00184	0.91853
25	26	939.58691	0.20D-02	0.00043	0.21491
24	25	940.69393	0.20D-02	0.00007	0.03302
23	24	941.79462	0.20D-02	0.0002	0.10249
22	23	942.88972	0.20D-02	0.0001	0.04776
21	22	943.97852	0.20D-02	0.00044	0.2185
20	21	945.06079	0.20D-02	0.00146	0.72918
19	20	946.14064	0.20D-02	-0.00098	-0.49064
18	19	947.2044	0.50D-02	0.00679	1.35743
17	18	948.27507	0.20D-02	0.00175	0.87631
16	17	949.33602	0.20D-02	0.00053	0.26713
15	16	950.38909	0.20D-02	0.00129	0.64551
14	15	951.43797	0.20D-02	0.0003	0.15103
13	14	952.47958	0.20D-02	0.00065	0.32307
12	13	953.51611	0.20D-02	0.00012	0.06123
11	12	954.54468	0.20D-02	0.0016	0.79994
10	11	955.56916	0.20D-02	0.00121	0.60361
9	10	956.58717	0.20D-02	0.00129	0.64683
8	9	957.60137	0.20D-02	-0.0008	-0.40099
7	8	958.60549	0.20D-02	0.00118	0.58964
6	7	959.6058	0.20D-02	0.00096	0.47808
5	6	960.60553	0.50D-02	-0.0047	-0.94047
4	5	961.59099	0.20D-02	-0.00214	-1.06867
3	4	962.56841	0.20D-02	0.00242	1.21
2	3	963.54397	0.20D-02	0.00278	1.38919
1	2	964.51726	0.20D-02	-0.00066	-0.33158
0	1	965.47929	0.20D-02	0.00107	0.53704
1	0	967.38692	0.20D-02	0.0027	1.35009
2	1	968.33113	0.20D-02	0.00395	1.97323
3	2	969.2808	0.50D-02	-0.00639	-1.27867
4	3	970.20713	0.20D-02	0.00047	0.23475
5	4	971.13035	0.20D-02	0.0043	2.15185
6	5	972.05329	0.20D-02	0.00225	1.12391
7	6	972.97048	0.20D-02	-0.00023	-0.11461
8	7	973.87956	0.20D-02	-0.00078	-0.38943
9	8	974.78119	0.20D-02	-0.00007	-0.03622
10	9	975.67692	0.20D-02	0.00033	0.16439
11	10	976.56681	0.20D-02	0.00036	0.18163
12	11	977.45142	0.20D-02	-0.00056	-0.28016
13	12	978.32437	0.20D-02	0.00394	1.96838
14	13	979.19338	0.50D-02	0.00612	1.2246
15	14	980.06711	0.20D-02	-0.00267	-1.33654

Table A.5, Fourier Transform Infrared Data for ^{76}GeO (cm^{-1}) (*Cont'd*)

J'	J''	Obs	Unc	Calc-Obs	(Calc-Obs)/Unc
16	15	980.92455	0.20D-02	-0.00145	-0.72644
17	16	981.77517	0.20D-02	0.0003	0.15106
18	17	982.62211	0.20D-02	-0.00055	-0.27477
19	18	983.45903	0.20D-02	0.0023	1.15032
20	19	984.2945	0.20D-02	0.00028	0.14063
21	20	985.12247	0.20D-02	-0.00057	-0.28471
22	21	985.94268	0.20D-02	0.0	-0.00137
23	22	986.75868	0.20D-02	-0.00158	-0.79016
24	23	987.56525	0.20D-02	-0.00008	-0.04193
25	24	988.36587	0.20D-02	0.00098	0.48764
26	25	989.15943	0.20D-02	0.00271	1.35273
27	26	989.95179	0.20D-02	-0.00077	-0.38255
28	27	990.7345	0.20D-02	-0.001	-0.49897
29	28	991.50864	0.20D-02	0.00092	0.45768
30	29	992.28055	0.20D-02	-0.00138	-0.68851
31	30	993.04225	0.20D-02	0.0001	0.05171
32	31	993.79711	0.20D-02	0.00195	0.97744
33	32	994.55011	0.20D-02	-0.0008	-0.40218
34	33	995.29218	0.20D-02	0.00088	0.44199
35	34	996.02976	0.20D-02	0.00057	0.28408
36	35	996.76032	0.20D-02	0.00077	0.38325
37	36	997.48488	0.20D-02	0.00045	0.22352
38	37	998.20183	0.20D-02	0.00122	0.60909
39	38	998.91408	0.20D-02	0.00014	0.06896
40	39	999.61697	0.20D-02	0.00186	0.9323
41	40	1000.31636	0.20D-02	0.00053	0.26295
42	41	1001.00839	0.20D-02	-0.00003	-0.01448
43	42	1001.69242	0.20D-02	0.00083	0.41374
44	43	1002.37126	0.20D-02	0.00027	0.13664
45	44	1003.04186	0.20D-02	0.00136	0.67778
46	45	1003.70559	0.20D-02	0.00267	1.33719
47	46	1004.36364	0.20D-02	0.00304	1.5184
48	47	1005.018	0.20D-02	0.00044	0.22043
49	48	1005.66286	0.20D-02	0.00068	0.34178
50	49	1006.30146	0.20D-02	0.00051	0.25747
51	50	1006.93188	0.20D-02	0.00184	0.92097
52	51	1007.55933	0.20D-02	-0.00056	-0.27871
53	52	1008.17715	0.20D-02	-0.00004	-0.0176
54	53	1008.78945	0.20D-02	-0.00071	-0.35675
55	54	1009.39287	0.20D-02	0.00076	0.38232
56	55	1009.99332	0.20D-02	-0.00154	-0.77045
57	56	1010.58254	0.20D-02	0.00063	0.31339
58	57	1011.16785	0.20D-02	-0.00006	-0.03224
59	58	1011.74666	0.20D-02	-0.00104	-0.51841
60	59	1012.31539	0.20D-02	0.00128	0.63881
61	60	1012.88171	0.20D-02	-0.0008	-0.4017
62	61	1013.44177	0.20D-02	-0.00344	-1.72102
63	62	1013.98888	0.20D-02	0.00005	0.02473
64	63	1014.53207	0.20D-02	0.00061	0.30444
65	64	1015.07047	0.20D-02	-0.0009	-0.44804
66	65	1015.59913	0.20D-02	0.00047	0.23618
67	66	1016.12258	0.20D-02	0.00017	0.08593
68	67	1016.63874	0.20D-02	0.00027	0.13507
69	68	1017.15009	0.20D-02	-0.00173	-0.86258
70	69	1017.6505	0.20D-02	0.0003	0.15183
71	70	1018.14916	0.20D-02	-0.00285	-1.4229
72	71	1018.63543	0.20D-02	-0.00055	-0.27296
73	72	1019.11888	0.20D-02	-0.00237	-1.18455

Table A.5, Fourier Transform Infrared Data for ^{76}GeO (cm^{-1}) (*Cont'd*)

J'	J''	Obs	Unc	Calc-Obs	(Calc-Obs)/Unc
74	73	1019.59102	0.20D-02	0.00014	0.07113
75	74	1020.06054	0.20D-02	-0.0017	-0.85165
76	75	1020.51954	0.20D-02	-0.00002	-0.01012
77	76	1020.97295	0.20D-02	0.00025	0.125
78	77	1021.41892	0.20D-02	0.00094	0.47245
79	78	1021.86263	0.20D-02	-0.00313	-1.56403
80	79	1022.29187	0.20D-02	0.00023	0.11431
81	80	1022.71661	0.20D-02	0.00103	0.51668
82	81	1023.13987	0.20D-02	-0.00375	-1.87418
83	82	1023.54477	0.20D-02	0.00275	1.37591
84	83	1023.95551	0.20D-02	-0.00368	-1.83934
The 3-2 Band, 122 data, $J"_{min} = 8$, $J"_{max} = 85$					
Unc.$_{Avge}$ = 2.0D-03, Unc.$_{Max}$ = 5.0D-03					
(Err/Unc.)$_{Avge}$ = 2.4D-01, RMSR = 0.91					
84	85	856.0685	0.20D-02	0.00336	1.67838
82	83	858.91359	0.20D-02	0.0033	1.64863
81	82	860.33133	0.20D-02	0.00026	0.12766
79	80	863.13983	0.20D-02	0.00548	2.73817
77	78	865.93255	0.20D-02	0.00552	2.75941
75	76	868.70915	0.20D-02	0.00062	0.31041
74	75	870.08801	0.20D-02	-0.0003	-0.14888
73	74	871.46286	0.20D-02	-0.00251	-1.25488
72	73	872.82644	0.20D-02	0.00124	0.62232
71	72	874.18846	0.20D-02	0.00124	0.62246
70	71	875.54621	0.20D-02	0.0002	0.10049
69	70	876.89516	0.20D-02	0.00261	1.30619
68	69	878.24003	0.20D-02	0.00376	1.87941
67	68	879.58441	0.20D-02	0.00004	0.01996
66	67	880.92049	0.20D-02	-0.00073	-0.36733
65	66	882.24901	0.20D-02	0.00066	0.33236
64	65	883.57166	0.20D-02	0.00255	1.27384
63	64	884.89071	0.20D-02	0.00263	1.31691
62	63	886.20695	0.20D-02	0.00013	0.06641
61	62	887.51442	0.20D-02	0.00097	0.48705
60	61	888.82387	0.50D-02	-0.00559	-1.11851
59	60	890.11849	0.20D-02	-0.00277	-1.38387
58	59	891.40863	0.20D-02	-0.0009	-0.45092
57	58	892.69549	0.20D-02	-0.00123	-0.61268
56	57	893.97521	0.20D-02	0.00012	0.06063
55	56	895.25066	0.20D-02	0.00026	0.12877
54	55	896.52057	0.20D-02	0.00045	0.22648
53	54	897.78537	0.20D-02	0.00025	0.12351
52	53	899.04537	0.20D-02	-0.00067	-0.33535
51	52	900.30035	0.20D-02	-0.00209	-1.04545
50	51	901.54581	0.20D-02	0.00048	0.23801
49	50	902.79134	0.20D-02	-0.00256	-1.28027
48	49	904.02743	0.20D-02	-0.00172	-0.86058
47	48	905.25578	0.20D-02	0.00129	0.64678
46	47	906.48181	0.20D-02	0.00105	0.52653
44	45	908.91689	0.20D-02	0.00079	0.39695
43	44	910.12611	0.20D-02	0.00057	0.28706
42	43	911.32837	0.20D-02	0.0017	0.84825
41	42	912.5261	0.20D-02	0.00173	0.86531
40	41	913.71847	0.20D-02	0.00148	0.73784
39	40	914.90513	0.20D-02	0.00128	0.64047
38	39	916.08738	0.20D-02	-0.00016	-0.08206
37	38	917.26259	0.20D-02	-0.00024	-0.12014

Table A.5, Fourier Transform Infrared Data for ^{76}GeO (cm^{-1}) (*Cont'd*)

J'	J''	Obs	Unc	Calc-Obs	(Calc-Obs)/Unc
36	37	918.4329	0.20D-02	-0.00109	-0.54409
35	36	919.59514	0.20D-02	0.00043	0.21564
34	35	920.75307	0.20D-02	0.00056	0.27872
31	32	924.19262	0.20D-02	0.00086	0.42936
28	29	927.57785	0.20D-02	0.00375	1.87626
27	28	928.69947	0.20D-02	-0.00003	-0.01307
26	27	929.81171	0.20D-02	-0.00022	-0.11225
25	26	930.91962	0.20D-02	-0.00189	-0.9467
23	24	933.11284	0.20D-02	-0.00008	-0.03812
22	23	934.20084	0.20D-02	0.00071	0.35401
21	22	935.28013	0.20D-02	0.00435	2.17408
20	21	936.35921	0.20D-02	0.00234	1.17158
19	20	937.42992	0.20D-02	0.00284	1.42114
17	18	939.55701	0.20D-02	0.00054	0.26943
16	17	940.60992	0.20D-02	0.00117	0.58713
15	16	941.65965	0.20D-02	-0.00092	-0.46011
14	15	942.70346	0.50D-02	-0.00302	-0.60309
13	14	943.73835	0.20D-02	-0.00212	-1.06132
11	12	945.79333	0.50D-02	-0.00337	-0.67339
10	11	946.80875	0.20D-02	-0.00087	-0.43303
9	10	947.81851	0.20D-02	0.00132	0.65933
8	9	948.82638	0.20D-02	-0.00059	-0.29691
7	8	949.82578	0.20D-02	-0.00002	-0.01227
11	10	967.67004	0.20D-02	0.00042	0.20776
12	11	968.54841	0.20D-02	-0.00032	-0.15793
13	12	969.42072	0.20D-02	-0.00122	-0.61106
14	13	970.28155	0.20D-02	0.00311	1.55259
15	14	971.14346	0.20D-02	0.0001	0.05242
16	15	971.99401	0.20D-02	0.00219	1.09262
17	16	972.84451	0.20D-02	-0.00196	-0.98247
18	17	973.68298	0.20D-02	-0.00038	-0.18871
19	18	974.51319	0.20D-02	0.00317	1.58321
20	19	975.34235	0.20D-02	0.00145	0.72256
21	20	976.16477	0.20D-02	0.00014	0.06854
22	21	976.97759	0.20D-02	0.0021	1.05031
23	22	977.78442	0.20D-02	0.00369	1.84719
24	23	978.5919	0.20D-02	-0.00172	-0.86166
25	24	979.3838	0.20D-02	0.00207	1.03296
27	26	980.95587	0.20D-02	0.00221	1.10443
28	27	981.7327	0.20D-02	0.00188	0.93958
29	28	982.50323	0.20D-02	0.00144	0.71997
30	29	983.26814	0.20D-02	0.00018	0.08971
31	30	984.02795	0.20D-02	-0.00242	-1.21204
32	31	984.77183	0.50D-02	0.00445	0.88954
33	32	985.522	0.20D-02	-0.00144	-0.71848
34	33	986.25578	0.20D-02	0.00259	1.29511
35	34	986.98858	0.20D-02	0.00111	0.55373
36	35	987.71454	0.20D-02	-0.00003	-0.01346
37	36	988.43593	0.20D-02	-0.00311	-1.55746
38	37	989.1487	0.50D-02	-0.00411	-0.82162
39	38	989.84971	0.20D-02	0.00012	0.06077
40	39	990.54765	0.20D-02	0.00087	0.4361
41	40	991.23911	0.20D-02	0.00154	0.77101
42	41	991.9168	0.50D-02	0.00941	1.88182
43	42	992.60524	0.20D-02	-0.00005	-0.0242
44	43	993.27359	0.50D-02	0.00398	0.79553
45	44	993.94833	0.50D-02	-0.00499	-0.99896
46	45	994.60173	0.20D-02	0.00075	0.37621

Table A.5, Fourier Transform Infrared Data for ^{76}GeO (cm^{-1}) (*Cont'd*)

J'	J''	Obs	Unc	Calc-Obs	(Calc-Obs)/Unc
47	46	995.25371	0.20D-02	0.00129	0.64364
48	47	995.90075	0.20D-02	0.00012	0.05892
49	48	996.536	0.50D-02	0.00408	0.81641
52	51	998.41729	0.20D-02	0.00039	0.19337
53	52	999.03174	0.20D-02	-0.00159	-0.79729
54	53	999.63678	0.20D-02	-0.00088	-0.44118
55	54	1000.23417	0.20D-02	0.00075	0.37582
56	55	1000.82776	0.20D-02	-0.00056	-0.27822
57	56	1001.41292	0.20D-02	-0.00019	-0.09319
58	57	1001.99367	0.20D-02	-0.00217	-1.08568
59	58	1002.56356	0.20D-02	-0.00007	-0.03677
60	59	1003.12863	0.20D-02	0.00006	0.03245
62	61	1004.23403	0.50D-02	0.00464	0.92896
63	62	1004.77963	0.20D-02	0.0038	1.90091
64	63	1005.3217	0.20D-02	-0.00035	-0.17473
65	64	1005.85314	0.20D-02	-0.00072	-0.36065
66	65	1006.37641	0.20D-02	0.00021	0.107
67	66	1006.89281	0.20D-02	0.00114	0.57208
69	68	1007.90801	0.20D-02	-0.00007	-0.03518
70	69	1008.40657	0.20D-02	-0.002	-0.99986
71	70	1008.89907	0.50D-02	-0.00478	-0.95673
The 4-3 Band, 143 data, $J"_{min} = 0$, $J"_{max} = 77$					
Unc.$_{Avge}$ = 3.1D-03, Unc.$_{Max}$ = 1.0D-02					
(Err/Unc.)$_{Avge}$ = 3.7D-01, RMSR = 1.05					
76	77	859.00721	0.50D-02	0.00071	0.14116
75	76	860.37447	0.50D-02	0.01017	2.03353
74	75	861.75199	0.20D-02	0.00409	2.046
73	74	863.12207	0.50D-02	0.00017	0.03373
72	73	864.4833	0.50D-02	-0.00019	-0.03853
71	72	865.83475	0.20D-02	0.00391	1.95389
70	71	867.18762	0.20D-02	0.00127	0.63472
69	70	868.53463	0.50D-02	-0.00084	-0.16756
68	69	869.87306	0.50D-02	0.00031	0.06113
67	68	871.19883	0.50D-02	0.00875	1.74988
66	67	872.5285	0.50D-02	0.00793	1.58662
65	66	873.85173	0.50D-02	0.00819	1.63728
64	65	875.18026	0.50D-02	-0.00223	-0.44624
63	64	876.49057	0.20D-02	0.00017	0.08497
62	63	877.80015	0.50D-02	-0.0021	-0.4201
61	62	879.10129	0.20D-02	-0.00134	-0.6715
60	61	880.39499	0.20D-02	0.00144	0.72093
59	60	881.69029	0.50D-02	-0.00282	-0.56323
58	59	882.9732	0.20D-02	-0.00013	-0.06382
57	58	884.25525	0.20D-02	-0.00203	-1.01651
56	57	885.52765	0.20D-02	0.00026	0.12864
55	56	886.79812	0.20D-02	-0.00101	-0.5037
54	55	888.05864	0.20D-02	0.00219	1.09625
53	54	889.31797	0.20D-02	0.00109	0.54328
52	53	890.56571	0.50D-02	0.00606	1.21281
51	52	891.81912	0.20D-02	-0.00014	-0.06767
50	51	893.05605	0.50D-02	0.00461	0.92154
49	50	894.29659	0.20D-02	0.0002	0.1013
48	49	895.52584	0.20D-02	0.00154	0.76939
47	48	896.75316	0.20D-02	-0.00074	-0.37218
46	47	897.97086	0.20D-02	0.00101	0.5063
45	46	899.18551	0.20D-02	0.00024	0.11951
44	45	900.39472	0.20D-02	-0.00069	-0.34281

Table A.5, Fourier Transform Infrared Data for ^{76}GeO (cm^{-1}) (*Cont'd*)

J'	J''	Obs	Unc	Calc-Obs	(Calc-Obs)/Unc
43	44	901.5981	0.20D-02	-0.00137	-0.68608
42	43	902.79134	0.20D-02	0.00246	1.22947
41	42	903.98536	0.20D-02	-0.00011	-0.05655
40	41	905.16857	0.20D-02	0.00249	1.24548
39	40	906.35032	0.20D-02	0.00091	0.45532
38	39	907.5257	0.20D-02	0.00006	0.02754
37	38	908.69333	0.20D-02	0.00127	0.63686
36	37	909.85478	0.20D-02	0.003	1.49781
35	36	911.00797	0.50D-02	0.00729	1.45802
34	35	912.16561	0.20D-02	0.00144	0.71827
33	34	913.3136	0.20D-02	-0.00047	-0.23301
32	33	914.45519	0.20D-02	-0.0017	-0.8491
31	32	915.58708	0.20D-02	0.00104	0.51956
30	31	916.71678	0.20D-02	0.00023	0.11257
29	30	917.84058	0.20D-02	-0.00043	-0.21548
28	29	918.95518	0.20D-02	0.00234	1.17
27	28	920.06984	0.20D-02	-0.00072	-0.36143
26	27	921.17357	0.20D-02	0.00136	0.67981
25	26	922.27481	0.20D-02	0.00014	0.06833
24	25	923.36803	0.20D-02	0.00114	0.56859
23	24	924.45541	0.20D-02	0.00215	1.07524
22	23	925.53851	0.20D-02	0.00162	0.80777
21	22	926.61555	0.20D-02	0.0013	0.65072
20	21	927.68856	0.20D-02	-0.00083	-0.41638
19	20	928.75628	0.50D-02	-0.00353	-0.7056
18	19	929.81171	0.20D-02	0.00018	0.09235
17	18	930.87051	0.50D-02	-0.00536	-1.07112
16	17	931.91486	0.20D-02	-0.00234	-1.16988
15	16	932.95059	0.20D-02	0.00339	1.69547
14	15	933.98084	0.50D-02	0.0087	1.73914
13	14	935.02636	0.50D-02	-0.00721	-1.44133
12	13	936.03847	0.20D-02	0.00436	2.18146
11	12	937.06699	0.50D-02	-0.00643	-1.28533
10	11	938.07364	0.20D-02	-0.00131	-0.65324
9	10	939.07855	0.20D-02	-0.00041	-0.20379
8	9	940.08154	0.50D-02	-0.00358	-0.71624
7	8	941.06254	0.50D-02	0.00924	1.84833
6	7	942.04755	0.10D-01	0.01205	1.20497
5	6	943.03853	0.20D-02	0.00287	1.43603
4	5	944.0179	0.20D-02	-0.00072	-0.36137
3	4	944.97156	0.10D-01	0.01536	1.53645
2	3	945.95308	0.20D-02	-0.00247	-1.23396
1	2	946.89387	0.10D-01	0.01437	1.43693
1	0	949.74642	0.20D-02	-0.00177	-0.88259
3	2	951.60165	0.20D-02	0.00343	1.71648
4	3	952.53357	0.50D-02	-0.00746	-1.49193
5	4	953.43621	0.50D-02	0.00479	0.95769
7	6	955.24878	0.20D-02	0.00354	1.77046
9	8	957.03796	0.20D-02	0.00098	0.48984
10	9	957.9239	0.20D-02	-0.00094	-0.46981
11	10	958.80157	0.20D-02	-0.0008	-0.39822
12	11	959.67426	0.20D-02	-0.00189	-0.94613
13	12	960.5377	0.20D-02	0.00004	0.02073
14	13	961.39181	0.50D-02	0.00505	1.01066
15	14	962.2515	0.20D-02	-0.00177	-0.88412
16	15	963.096	0.20D-02	0.00034	0.16771
17	16	963.92937	0.50D-02	0.00729	1.45855
18	17	964.77309	0.20D-02	-0.00239	-1.19387

Table A.5, Fourier Transform Infrared Data for ^{76}GeO (cm^{-1}) (*Cont'd*)

J'	J''	Obs	Unc	Calc-Obs	(Calc-Obs)/Unc
19	18	965.60088	0.20D-02	-0.00244	-1.21873
20	19	966.41843	0.20D-02	0.00145	0.72596
21	20	967.22385	0.10D-01	0.01114	1.11389
22	21	968.04283	0.20D-02	0.00093	0.46588
23	22	968.84605	0.20D-02	0.00014	0.06957
24	23	969.64921	0.50D-02	-0.00695	-1.39013
25	24	970.43286	0.20D-02	-0.0009	-0.44957
26	25	971.21935	0.50D-02	-0.00406	-0.81163
27	26	971.99957	0.50D-02	-0.00735	-1.46984
28	27	972.76333	0.20D-02	-0.00058	-0.29196
29	28	973.5265	0.20D-02	0.00036	0.17798
30	29	974.28613	0.20D-02	-0.00159	-0.79563
31	30	975.03504	0.20D-02	0.00074	0.37135
32	31	975.78325	0.20D-02	-0.00267	-1.33694
33	32	976.51587	0.20D-02	0.00305	1.52363
34	33	977.25151	0.20D-02	-0.00074	-0.36782
35	34	977.97351	0.20D-02	0.00264	1.31787
36	35	978.6937	0.20D-02	0.00132	0.65971
37	36	979.40399	0.20D-02	0.00339	1.69689
38	37	980.11819	0.50D-02	-0.00496	-0.99262
39	38	980.81367	0.20D-02	-0.00113	-0.56653
40	39	981.50389	0.20D-02	0.00141	0.70602
41	40	982.19038	0.20D-02	0.00114	0.57017
42	41	982.86711	0.50D-02	0.00405	0.80999
43	42	983.54551	0.20D-02	-0.00129	-0.6455
44	43	984.21048	0.20D-02	0.00021	0.10273
45	44	984.86888	0.20D-02	0.00167	0.83377
46	45	985.522	0.20D-02	0.00179	0.89659
47	46	986.16643	0.50D-02	0.00398	0.79608
48	47	986.8105	0.20D-02	-0.00011	-0.05637
49	48	987.43715	0.50D-02	0.00657	1.31434
50	49	988.07047	0.20D-02	-0.00009	-0.04414
51	50	988.69024	0.20D-02	0.00013	0.06264
52	51	989.30806	0.50D-02	-0.0044	-0.87992
53	52	989.90799	0.20D-02	0.00226	1.13245
54	53	990.50928	0.20D-02	0.00086	0.4283
55	54	991.09767	0.50D-02	0.00562	1.12472
56	55	991.68337	0.50D-02	0.00634	1.26873
57	56	992.2542	0.10D-01	0.01518	1.51847
58	57	992.83902	0.20D-02	0.00328	1.64223
59	58	993.40928	0.20D-02	-0.00084	-0.41962
61	60	994.51989	0.20D-02	0.00045	0.22718
62	61	995.06483	0.20D-02	0.00126	0.62861
63	62	995.60715	0.50D-02	-0.00214	-0.42845
64	63	996.13522	0.20D-02	0.00187	0.93684
65	64	996.65982	0.20D-02	0.00251	1.25637
66	65	997.17381	0.50D-02	0.0069	1.38054
67	66	997.68658	0.20D-02	0.00564	2.82053
68	67	998.18613	0.50D-02	0.01073	2.14514
69	68	998.68972	0.20D-02	0.00486	2.43205
70	69	999.18091	0.20D-02	0.00449	2.24691
71	70	999.66953	0.20D-02	-0.00023	-0.11366
The 5-4 Band, 126 data, $J"_{min} = 8$, $J"_{max} = 77$					
Unc.$_{Avge}$ = 3.3D-03, Unc.$_{Max}$ = 1.0D-02					
(Err/Unc.)$_{Avge}$ = 3.3D-01, RMSR = 1.34					
76	77	850.71917	0.10D-01	-0.00382	-0.38196
75	76	852.08103	0.50D-02	0.00456	0.91243

Table A.5, Fourier Transform Infrared Data for ^{76}GeO (cm^{-1}) (*Cont'd*)

J'	J''	Obs	Unc	Calc-Obs	(Calc-Obs)/Unc
74	75	853.44679	0.50D-02	0.00378	0.75641
73	74	854.79606	0.50D-02	0.0142	2.83999
72	73	856.16098	0.20D-02	0.00368	1.83768
71	72	857.51031	0.20D-02	0.00344	1.71906
70	71	858.85682	0.50D-02	0.00072	0.14356
69	70	860.19642	0.50D-02	-0.00043	-0.0852
68	69	861.53024	0.50D-02	-0.00112	-0.22471
67	68	862.85131	0.20D-02	0.00558	2.79235
66	67	864.18072	0.50D-02	-0.00139	-0.27832
65	66	865.49624	0.20D-02	0.00015	0.07362
64	65	866.80793	0.20D-02	0.00014	0.07031
63	64	868.11316	0.20D-02	0.00121	0.60415
62	63	869.41608	0.20D-02	-0.00081	-0.4051
61	62	870.71225	0.20D-02	-0.00148	-0.73774
60	61	872.00073	0.20D-02	0.00012	0.06112
59	60	873.28389	0.20D-02	0.00161	0.80619
58	59	874.55806	0.50D-02	0.00665	1.33091
57	58	875.83754	0.20D-02	0.00095	0.47405
56	57	877.10798	0.50D-02	-0.00119	-0.23748
55	56	878.37007	0.20D-02	-0.00044	-0.22122
54	55	879.62785	0.20D-02	-0.00087	-0.43373
53	54	880.87881	0.20D-02	0.00005	0.0234
52	53	882.12747	0.20D-02	-0.00225	-1.125
51	52	883.37739	0.10D-01	-0.01132	-1.13185
50	51	884.59823	0.20D-02	0.00317	1.58533
49	50	885.82147	0.50D-02	0.00974	1.94739
48	49	887.05161	0.20D-02	0.00385	1.9249
47	48	888.27501	0.20D-02	-0.00085	-0.42572
46	47	889.48701	0.20D-02	0.00028	0.14136
45	46	890.69615	0.20D-02	-0.0013	-0.64928
44	45	891.9016	0.50D-02	-0.00477	-0.95316
43	44	893.10485	0.10D-01	-0.01164	-1.16396
42	43	894.28402	0.20D-02	-0.00004	-0.02034
41	42	895.47015	0.20D-02	-0.00102	-0.50987
40	41	896.6429	0.50D-02	0.00576	1.1525
39	40	897.81391	0.50D-02	0.00864	1.72707
38	39	898.97364	0.10D-01	0.01714	1.71381
36	37	901.30785	0.20D-02	0.0024	1.20024
35	36	902.45974	0.20D-02	0.00174	0.86923
34	35	903.6028	0.50D-02	0.0042	0.84069
33	34	904.7463	0.20D-02	0.00052	0.26222
31	32	907.00843	0.20D-02	0.00089	0.44587
30	31	908.12934	0.20D-02	0.00263	1.31316
29	30	909.25065	0.20D-02	-0.00179	-0.89313
28	29	910.36329	0.20D-02	-0.00329	-1.64342
27	28	911.46489	0.20D-02	0.00048	0.2419
26	27	912.56706	0.20D-02	-0.00209	-1.04269
25	26	913.66186	0.20D-02	-0.00309	-1.54255
24	25	914.74684	0.20D-02	-0.00007	-0.03323
23	24	915.8308	0.20D-02	-0.00184	-0.92007
20	21	919.04058	0.20D-02	-0.00004	-0.01762
19	20	920.0982	0.20D-02	0.00117	0.58594
18	19	921.16131	0.50D-02	-0.00898	-1.79562
17	18	922.2027	0.50D-02	-0.00329	-0.65729
16	17	923.24463	0.50D-02	-0.00401	-0.80277
15	16	924.27621	0.20D-02	-0.0003	-0.15082
14	15	925.30968	0.50D-02	-0.00439	-0.87812
13	14	926.32967	0.20D-02	-0.00092	-0.46096

Table A.5, Fourier Transform Infrared Data for ^{76}GeO (cm^{-1}) (*Cont'd*)

J'	J''	Obs	Unc	Calc-Obs	(Calc-Obs)/Unc
12	13	927.3432	0.20D-02	0.00307	1.5367
11	12	928.35243	0.50D-02	0.00543	1.08684
10	11	929.36661	0.50D-02	-0.00312	-0.6241
9	10	930.36426	0.20D-02	-0.00111	-0.55592
8	9	931.35424	0.20D-02	0.00259	1.29448
7	8	932.34438	0.20D-02	0.00014	0.07046
11	10	949.96285	0.50D-02	-0.00495	-0.99033
12	11	950.82948	0.50D-02	-0.00603	-1.20572
13	12	951.68852	0.50D-02	-0.00574	-1.14833
14	13	952.54313	0.50D-02	-0.00726	-1.45246
15	14	953.38068	0.20D-02	0.00203	1.01402
17	16	955.05908	0.20D-02	-0.00148	-0.74215
18	17	955.88601	0.20D-02	-0.00038	-0.19
19	18	956.71032	0.20D-02	-0.00296	-1.48045
20	19	957.52265	0.20D-02	0.00013	0.06583
21	20	958.32872	0.20D-02	0.00317	1.58301
22	21	959.13576	0.20D-02	-0.0011	-0.54971
23	22	959.93083	0.20D-02	0.00026	0.13188
24	23	960.72114	0.20D-02	0.00004	0.02197
25	24	961.5039	0.20D-02	0.001	0.49979
26	25	962.27024	0.10D-01	0.012	1.19988
27	26	963.04638	0.50D-02	0.00681	1.36205
29	28	964.57028	0.50D-02	0.0056	1.1205
30	29	965.32071	0.50D-02	0.00689	1.37799
31	30	966.07357	0.20D-02	-0.00068	-0.33864
32	31	966.81033	0.20D-02	0.0014	0.69949
33	32	967.54458	0.20D-02	-0.00047	-0.23644
34	33	968.27136	0.20D-02	-0.00134	-0.67244
35	34	968.99211	0.20D-02	-0.00267	-1.33428
36	35	969.70051	0.20D-02	0.00186	0.93202
37	36	970.41309	0.50D-02	-0.00429	-0.85773
38	37	971.11216	0.20D-02	-0.00344	-1.71933
39	38	971.80291	0.20D-02	-0.00081	-0.40389
40	39	972.48851	0.20D-02	0.00043	0.21605
41	40	973.16596	0.20D-02	0.00327	1.63461
42	41	973.8403	0.50D-02	0.00265	0.53029
43	42	974.51319	0.20D-02	-0.00309	-1.54653
44	43	975.17448	0.50D-02	-0.00383	-0.76522
45	44	975.82716	0.20D-02	-0.00255	-1.27488
46	45	976.47505	0.20D-02	-0.0031	-1.54799
47	46	977.11572	0.50D-02	-0.00304	-0.60735
48	47	977.74949	0.20D-02	-0.00272	-1.36206
49	48	978.37861	0.50D-02	-0.00441	-0.88201
50	49	978.99506	0.20D-02	-0.00009	-0.04328
51	50	979.61472	0.50D-02	-0.00565	-1.12917
52	51	980.21344	0.20D-02	0.00305	1.52511
53	52	980.81367	0.20D-02	0.00354	1.76972
54	53	981.40992	0.20D-02	0.0013	0.64979
55	54	981.99786	0.20D-02	0.00066	0.32937
56	55	982.58083	0.20D-02	-0.00176	-0.87762
57	56	983.15714	0.50D-02	-0.00425	-0.85094
58	57	983.71601	0.20D-02	0.00393	1.96413
59	58	984.27744	0.20D-02	0.00278	1.39078
61	60	985.37484	0.20D-02	0.00559	2.79494
62	61	985.90807	0.50D-02	0.01226	2.45211
63	62	986.44722	0.20D-02	0.00619	3.09624
64	63	986.96548	0.10D-01	0.01418	1.41835
65	64	987.48791	0.50D-02	0.01117	2.23423

Table A.5, Fourier Transform Infrared Data for ^{76}GeO (cm^{-1}) (*Cont'd*)

J'	J''	Obs	Unc	Calc-Obs	(Calc-Obs)/Unc
66	65	988.00669	0.20D-02	0.00494	2.47158
67	66	988.50492	0.50D-02	0.0124	2.47946
68	67	989.01183	0.20D-02	0.00429	2.14551
69	68	989.50176	0.20D-02	0.00627	3.13608
71	70	990.46203	0.20D-02	0.0091	4.5484
72	71	990.93793	0.20D-02	0.00436	2.17773
73	72	991.39951	0.20D-02	0.00699	3.49593
74	73	991.86102	0.50D-02	0.00274	0.54867
The 6-5 Band, 71 data, $J"_{min} = 10$, $J"_{max} = 67$					
Unc.$_{Avge} = 4.4$D-03, Unc.$_{Max} = 1.0$D-02					
(Err/Unc.)$_{Avge} = 1.2$D-01, RMSR = 1.17					
66	67	855.84957	0.50D-02	-0.00138	-0.27586
65	66	857.15874	0.50D-02	0.0001	0.01932
61	62	862.33855	0.50D-02	0.00908	1.81517
55	56	869.96023	0.50D-02	0.00802	1.60415
54	55	871.20956	0.50D-02	0.00969	1.93822
53	54	872.46945	0.50D-02	-0.00468	-0.93679
51	52	874.93414	0.50D-02	0.00517	1.03348
50	51	876.16753	0.20D-02	0.00077	0.3863
49	50	877.38961	0.20D-02	0.00216	1.08014
48	49	878.60571	0.50D-02	0.00399	0.7979
47	48	879.82945	0.50D-02	-0.00737	-1.47404
46	47	881.02671	0.20D-02	0.0022	1.1003
45	46	882.22831	0.20D-02	0.00185	0.92552
44	45	883.43217	0.50D-02	-0.00634	-1.26786
43	44	884.61611	0.20D-02	-0.0002	-0.10061
40	41	888.15611	0.20D-02	-0.00361	-1.80669
39	40	889.31797	0.20D-02	0.00213	1.06578
37	38	891.64038	0.20D-02	-0.002	-1.00242
35	36	893.93781	0.20D-02	-0.00384	-1.91883
34	35	895.06947	0.50D-02	0.00377	0.75482
33	34	896.21847	0.10D-01	-0.01164	-1.16431
31	32	898.45909	0.20D-02	-0.00226	-1.12884
28	29	901.80096	0.10D-01	-0.01212	-1.21226
27	28	902.90231	0.10D-01	-0.01432	-1.4321
26	27	903.98536	0.50D-02	-0.00399	-0.79888
22	23	908.29097	0.50D-02	0.00594	1.18891
19	20	911.47558	0.50D-02	-0.00318	-0.63667
18	19	912.5261	0.50D-02	-0.00691	-1.38194
16	17	914.59374	0.20D-02	0.00139	0.69301
15	16	915.62754	0.20D-02	-0.00328	-1.64196
13	14	917.6643	0.20D-02	0.0005	0.24759
12	13	918.67265	0.50D-02	0.00352	0.70442
11	12	919.68092	0.20D-02	0.00069	0.34456
10	11	920.67742	0.50D-02	0.00368	0.73505
9	10	921.67462	0.20D-02	0.0	-0.00041
17	16	946.20509	0.20D-02	0.00002	0.01212
19	18	947.83452	0.10D-01	0.00833	0.83265
20	19	948.65274	0.20D-02	-0.00048	-0.23772
21	20	949.46059	0.50D-02	-0.00522	-1.04428
25	24	952.60351	0.20D-02	0.00091	0.45581
26	25	953.37981	0.20D-02	-0.00403	-2.01456
31	30	957.13981	0.20D-02	-0.00322	-1.6075
33	32	958.59787	0.20D-02	-0.00197	-0.9844
34	33	959.32158	0.50D-02	-0.00572	-1.1438
37	36	961.44219	0.50D-02	-0.00535	-1.07078
38	37	962.12645	0.50D-02	0.00436	0.87269

Table A.5, Fourier Transform Infrared Data for ^{76}GeO (cm^{-1}) (*Cont'd*)

J'	J''	Obs	Unc	Calc-Obs	(Calc-Obs)/Unc
39	38	962.82251	0.50D-02	-0.00424	-0.84889
40	39	963.49547	0.50D-02	0.00371	0.74209
41	40	964.18508	0.10D-01	-0.01153	-1.15337
42	41	964.83921	0.20D-02	0.00214	1.07065
43	42	965.50053	0.20D-02	0.00205	1.02667
44	43	966.15328	0.50D-02	0.00396	0.79211
45	44	966.81001	0.50D-02	-0.00472	-0.94385
46	45	967.4439	0.20D-02	0.00283	1.41619
47	46	968.0809	0.20D-02	0.00065	0.32653
48	47	968.69964	0.10D-01	0.0101	1.01009
49	48	969.32806	0.50D-02	0.00322	0.64476
50	49	969.94595	0.20D-02	0.00022	0.10995
51	50	970.55676	0.20D-02	-0.00237	-1.18656
52	51	971.14394	0.10D-01	0.01199	1.19929
54	53	972.33776	0.20D-02	0.00115	0.57652
55	54	972.91656	0.20D-02	0.00377	1.8865
56	55	973.50377	0.10D-01	-0.00875	-0.87467
58	57	974.62466	0.20D-02	-0.00049	-0.24677
59	58	975.16985	0.50D-02	0.00874	1.74897
60	59	975.72074	0.20D-02	0.0055	2.75243
61	60	976.27057	0.50D-02	-0.00347	-0.69317
62	61	976.78521	0.10D-01	0.01596	1.59605
63	62	977.31705	0.50D-02	0.01136	2.27233
64	63	977.84661	0.20D-02	0.00222	1.10763
65	64	978.34631	0.10D-01	0.01609	1.60891
The 7-6 Band, 41 data, $J"_{min}$ = 21, $J"_{max}$ = 58					
Unc.$_{Avge}$ = 3.3D-03, Unc.$_{Max}$ = 1.0D-02					
(Err/Unc.)$_{Avge}$ = -6.0D-01, RMSR = 1.56					
57	58	859.08204	0.20D-02	0.00498	2.48998
56	57	860.33158	0.50D-02	0.01102	2.20495
55	56	861.59581	0.50D-02	-0.00308	-0.61591
54	55	862.83288	0.20D-02	0.00451	2.2532
53	54	864.07722	0.20D-02	-0.00066	-0.32902
52	53	865.30411	0.50D-02	0.00615	1.22935
51	52	866.53224	0.50D-02	0.0062	1.24003
49	50	868.97529	0.20D-02	0.00297	1.485
47	48	871.39695	0.20D-02	-0.00099	-0.49664
44	45	874.97583	0.50D-02	0.00498	0.99614
43	44	876.16792	0.20D-02	-0.00332	-1.66016
41	42	878.52396	0.50D-02	-0.00858	-1.71697
40	41	879.68457	0.20D-02	-0.00223	-1.11489
39	40	880.84871	0.20D-02	-0.00502	-2.51214
38	39	882.01444	0.10D-01	-0.01506	-1.5059
37	38	883.15013	0.20D-02	-0.0007	-0.35232
34	35	886.57749	0.50D-02	-0.01194	-2.38707
32	33	888.81905	0.20D-02	-0.00454	-2.26764
28	29	893.25644	0.50D-02	-0.01267	-2.53437
23	24	898.6585	0.50D-02	-0.00783	-1.56681
22	23	899.72284	0.50D-02	-0.00819	-1.63891
21	22	900.78521	0.50D-02	-0.01241	-2.482
22	21	941.39059	0.50D-02	0.0054	1.08012
23	22	942.18474	0.20D-02	-0.0043	-2.14924
24	23	942.95884	0.20D-02	-0.00029	-0.14632
25	24	943.73506	0.20D-02	-0.00476	-2.38166
28	27	946.0026	0.50D-02	0.0047	0.93958
29	28	946.76226	0.50D-02	-0.00876	-1.75124
30	29	947.49661	0.20D-02	-0.00332	-1.65773

Table A.5, Fourier Transform Infrared Data for ^{76}GeO (cm^{-1}) (*Cont'd*)

J'	J''	Obs	Unc	Calc-Obs	(Calc-Obs)/Unc
32	31	948.95687	0.20D-02	-0.00329	-1.6432
33	32	949.67854	0.20D-02	-0.00448	-2.24081
34	33	950.39009	0.20D-02	-0.00201	-1.00462
35	34	951.09213	0.50D-02	0.00349	0.69783
39	38	953.86134	0.20D-02	-0.00055	-0.27255
40	39	954.5375	0.20D-02	-0.00171	-0.85745
41	40	955.20727	0.20D-02	-0.00303	-1.51509
43	42	956.52341	0.20D-02	-0.00196	-0.98215
48	47	959.69944	0.20D-02	-0.00036	-0.18035
50	49	960.92475	0.20D-02	-0.00101	-0.50599
51	50	961.52508	0.20D-02	0.00099	0.49516
56	55	964.43572	0.20D-02	0.00161	0.80295

Appendix B

Fourier Transform Electronic Data for WO

The spectroscopic data of WO relative to $X0^+$ are listed in Table B.1.
The spectroscopic data of WO relative to X1 are listed in Table B.2.

B.1 Electronic Data for WO with Respect to X0$^+$

Table B.1: Electronic Data of ^{184}WO Relative to X0$^+$ (v=0)

J'	J''	Obs	Obs-Calc	Unc	(Obs-Calc)/Unc
$C(0,0)$ Band, R Branch (p' = e, p'' = e)					
6	5	19186.43573	0.00337	0.003	1.1
7	6	19186.92407	-0.00081	0.003	-0.3
8	7	19187.37061	0.00162	0.003	0.5
10	9	19188.11498	0.00301	0.003	1.0
12	11	19188.66592	0.00469	0.003	1.6
13	12	19188.85978	-0.00342	0.003	-1.1
14	13	19189.01656	-0.00016	0.003	-0.1
15	14	19189.12908	0.0073	0.003	2.4
16	15	19189.17369	-0.00468	0.003	-1.6
19	18	19189.05358	-0.00364	0.003	-1.2
20	19	19188.91765	-0.00219	0.003	-0.7
21	20	19188.73566	0.00172	0.003	0.6
22	21	19188.48886	-0.01064	90.003	0.0
23	22	19188.23116	0.01464	90.003	0.0
24	23	19187.88571	0.00073	0.003	0.2
25	24	19187.49987	-0.00501	0.003	-1.7
26	25	19187.07612	-0.00006	0.003	0.0
27	26	19186.59656	-0.00232	0.003	-0.8
28	27	19186.06903	-0.00393	0.003	-1.3
29	28	19185.49739	-0.00101	0.003	-0.3
30	29	19184.8716	-0.00359	0.003	-1.2
31	30	19184.20295	-0.00034	0.003	-0.1
32	31	19183.48882	0.00614	0.003	2.0
33	32	19182.71812	0.00477	0.003	1.6
34	33	19181.89169	-0.00358	0.003	-1.2
35	34	19181.03005	0.00165	0.003	0.5
36	35	19180.12172	0.009	0.003	3.0
37	36	19179.15129	0.00309	0.005	0.6
38	37	19178.13322	-0.00158	0.003	-0.5
39	38	19177.07287	0.00039	0.003	0.1
40	39	19175.9658	0.00459	0.003	1.5
41	40	19174.79507	-0.00587	0.003	-2.0
42	41	19173.59395	0.00232	0.003	0.8
43	42	19172.34544	0.0122	90.003	0.0
44	43	19171.04176	0.01606	90.003	0.0
45	44	19169.6666	-0.00238	0.003	-0.8
47	46	19166.8141	0.00638	0.003	2.1
48	47	19165.29914	-0.00393	0.003	-1.3
49	48	19163.74622	-0.00276	0.003	-0.9
50	49	19162.13918	-0.00619	0.003	-2.1
51	50	19160.48489	-0.0073	0.003	-2.4
53	52	19157.03872	0.00199	0.003	0.7
55	54	19153.38025	-0.00166	0.003	-0.6
56	55	19151.48318	0.00368	0.003	1.2
57	56	19149.5285	0.00154	0.003	0.5
58	57	19147.52607	0.0019	0.003	0.6
$C(0,0)$ Band, P Branch (p' = e, p'' = e)					
1	2	19180.73613	-0.01433	0.003	-4.8
2	3	19179.80766	-0.01494	0.003	-5.0
3	4	19178.83738	-0.00903	0.003	-3.0

Table B.1, Electronic Data of ^{184}WO Relative to X0$^+$ (*Cont'd*)

J'	J''	Obs	Obs-Calc	Unc	(Obs-Calc)/Unc
4	5	19177.81506	-0.00684	0.003	-2.3
7	8	19174.46204	0.00361	0.003	1.2
8	9	19173.23679	-0.00388	0.003	-1.3
9	10	19171.98469	0.01009	90.003	0.0
10	11	19170.66419	0.00394	0.003	1.3
11	12	19169.29045	-0.00716	0.003	-2.4
12	13	19167.89021	0.00352	0.003	1.2
13	14	19166.42384	-0.00366	0.003	-1.2
14	15	19164.91868	-0.00136	0.003	-0.5
15	16	19163.36557	0.00125	0.003	0.4
16	17	19161.76344	0.0031	0.003	1.0
17	18	19160.07826	-0.02984	90.003	0.0
18	19	19158.3975	-0.0101	90.003	0.0
19	20	19156.65725	-0.00161	0.003	-0.5
20	21	19154.8631	0.00123	0.003	0.4
21	22	19153.01805	0.00142	0.005	0.3
22	23	19151.12444	0.00131	0.003	0.4
23	24	19149.18016	-0.00123	0.003	-0.4
24	25	19147.19604	0.00464	0.003	1.5
25	26	19145.15593	0.00278	0.003	0.9
28	29	19138.74797	-0.00086	0.003	-0.3
29	30	19136.51675	-0.00076	0.003	-0.3
30	31	19134.24474	0.00684	0.003	2.3
31	32	19131.9125	0.00252	0.003	0.8
32	33	19129.53497	0.00122	0.003	0.4
33	34	19127.11017	0.00098	0.003	0.3
34	35	19124.63388	-0.00239	0.003	-0.8
35	36	19122.11215	-0.00284	0.003	-0.9
36	37	19119.5442	-0.00112	0.003	-0.4
37	38	19116.92739	0.00015	0.003	0.1
38	39	19114.26149	0.00078	0.003	0.3
39	40	19111.5475	0.00179	0.003	0.6
40	41	19108.77884	-0.00337	0.003	-1.1
41	42	19105.97035	0.00018	0.003	0.1
42	43	19103.10883	-0.00072	0.003	-0.2
43	44	19100.20271	0.0024	0.003	0.8
44	45	19097.24521	0.0028	0.003	0.9
45	46	19094.23591	0.00012	0.003	0.0
46	47	19091.17719	-0.00322	0.003	-1.1
47	48	19088.07939	0.00319	0.003	1.1
$C(0,0)$ Band, Q Branch (p' = f, p'' = e)					
1	1	19182.43258	0.01963	90.003	0.0
2	2	19182.32401	0.00742	0.003	2.5
4	4	19181.98734	0.008	0.003	2.7
5	5	19181.75365	0.01518	0.003	5.1
7	7	19181.11664	0.0044	0.003	1.5
8	8	19180.73613	0.00922	0.003	3.1
9	9	19180.29784	0.0044	0.003	1.5
10	10	19179.80766	-0.00419	0.003	-1.4
11	11	19179.28496	0.00281	0.003	0.9
12	12	19178.7057	0.00136	0.003	0.5
13	13	19178.08096	0.00253	0.003	0.8
14	14	19177.40222	-0.00221	0.003	-0.7
15	15	19176.68338	0.00103	0.003	0.3
16	16	19175.90741	-0.00478	0.003	-1.6
17	17	19175.09362	-0.00033	0.003	-0.1
18	18	19174.22718	-0.00046	0.003	-0.2

Table B.1, Electronic Data of ^{184}WO Relative to X0$^+$ (*Cont'd*)

J'	J''	Obs	Obs-Calc	Unc	(Obs-Calc)/Unc
19	19	19173.31542	0.00217	0.003	0.7
20	20	19172.34544	-0.00532	0.003	-1.8
21	21	19171.3403	0.00012	0.005	0.0
22	22	19170.28106	-0.00042	0.003	-0.1
23	23	19169.17317	-0.00147	0.003	-0.5
24	24	19168.02076	0.00114	0.003	0.4
25	25	19166.8141	-0.0023	0.003	-0.8
26	26	19165.56561	0.00069	0.003	0.2
27	27	19164.26485	-0.00029	0.003	-0.1
28	28	19162.9146	-0.00238	0.003	-0.8
29	29	19161.51835	-0.00203	0.003	-0.7
30	30	19160.07826	0.00301	0.003	1.0
31	31	19158.57808	-0.00342	0.003	-1.1
32	32	19157.03872	-0.00028	0.003	-0.1
33	33	19155.44681	-0.00084	0.003	-0.3
34	34	19153.80635	-0.00094	0.003	-0.3
35	35	19152.11946	0.00169	0.003	0.6
36	36	19150.37842	-0.0005	0.003	-0.2
37	37	19148.59215	0.0016	0.003	0.5
38	38	19146.75217	-0.00027	0.003	-0.1
39	39	19144.86225	-0.00211	0.003	-0.7
40	40	19142.92561	-0.00045	0.003	-0.2
42	42	19138.89977	0.0021	0.003	0.7
43	43	19136.80336	-0.00359	0.003	-1.2
45	45	19132.46155	-0.00912	90.003	0.0
46	46	19130.21753	-0.0068	90.003	0.0
47	47	19127.91675	-0.00851	90.003	0.0
48	48	19125.56819	-0.00481	90.003	0.0
49	49	19123.16067	-0.00637	90.003	0.0
$C(0,1)$ Band, R Branch (p' = e, p'' = e)					
24	23	18131.43345	0.00016	0.005	0.0
25	24	18131.14916	-0.00094	0.005	-0.2
26	25	18130.82647	0.00412	0.005	0.8
27	26	18130.44577	-0.00425	0.005	-0.8
28	27	18130.03219	-0.00089	0.005	-0.2
29	28	18129.55787	-0.01365	90.005	0.0
30	29	18129.06024	-0.00508	0.005	-1.0
31	30	18128.50857	-0.00588	0.005	-1.2
32	31	18127.9276	0.00869	0.005	1.7
33	32	18127.28485	0.0062	0.005	1.2
34	33	18126.59662	0.00295	0.005	0.6
35	34	18125.85995	-0.00398	0.005	-0.8
36	35	18125.09043	0.00103	0.005	0.2
37	36	18124.25388	-0.01618	90.005	0.0
38	37	18123.40264	-0.00324	0.005	-0.6
39	38	18122.4767	-0.02013	90.005	0.0
40	39	18121.54359	0.00072	0.005	0.1
41	40	18120.54633	0.00237	0.005	0.5
42	41	18119.49814	-0.00194	0.005	-0.4
43	42	18118.40745	-0.00373	0.005	-0.7
44	43	18117.28948	0.01225	0.005	2.5
45	44	18116.10115	0.00298	0.005	0.6
46	45	18114.86777	-0.0062	0.005	-1.2
47	46	18113.61398	0.0094	0.005	1.9
48	47	18112.29313	0.00318	0.005	0.6
49	48	18110.93216	0.00214	0.005	0.4
50	49	18109.53841	0.01366	90.005	0.0

Table B.1, Electronic Data of ^{184}WO Relative to X0$^+$ (*Cont'd*)

J'	J''	Obs	Obs-Calc	Unc	(Obs-Calc)/Unc
51	50	18108.09194	0.01787	90.005	0.0
53	52	18105.02986	-0.0064	0.005	-1.3
54	53	18103.45186	0.00286	0.005	0.6
55	54	18101.81991	0.00384	0.005	0.8
56	55	18100.14492	0.0075	0.005	1.5
57	56	18098.39823	-0.01472	0.005	-2.9
58	57	18096.64111	-0.00149	0.005	-0.3
59	58	18094.81075	-0.01553	0.005	-3.1
60	59	18092.95907	-0.00483	0.005	-1.0
61	60	18091.0547	-0.00068	0.005	-0.1
62	61	18089.09904	-0.00158	0.005	-0.3
63	62	18087.0884	-0.01113	0.005	-2.2
64	63	18085.06133	0.00933	0.005	1.9
69	68	18074.12695	0.01303	90.005	0.0
70	69	18071.82767	0.04229	90.005	0.0
71	70	18069.44556	0.036	90.005	0.0
72	71	18067.0287	0.04237	90.005	0.0
73	72	18064.55675	0.04121	90.005	0.0
74	73	18062.01735	0.02032	90.005	0.0
75	74	18059.46125	0.0306	90.005	0.0
76	75	18056.83251	0.01627	90.005	0.0
$C(0,1)$ Band, P Branch (p' = e, p'' = e)					
4	5	18120.32157	0.00693	90.005	0.0
5	6	18119.28037	0.01427	90.005	0.0
6	7	18118.15061	-0.02268	0.005	-4.5
7	8	18117.03825	0.00202	0.005	0.4
8	9	18115.84247	-0.01243	0.005	-2.5
9	10	18114.63351	0.00418	0.005	0.8
10	11	18113.35838	-0.00112	0.005	-0.2
11	12	18112.05593	0.01049	90.005	0.0
12	13	18110.68599	-0.00114	0.005	-0.2
13	14	18109.28819	0.0036	0.005	0.7
14	15	18107.83542	-0.00239	0.005	-0.5
15	16	18106.35426	0.00745	0.005	1.5
16	17	18104.81374	0.00217	0.005	0.4
17	18	18103.22846	-0.00365	0.005	-0.7
18	19	18101.60515	-0.00328	0.005	-0.7
19	20	18099.93861	-0.00191	0.005	-0.4
20	21	18098.23309	0.00471	0.005	0.9
21	22	18096.47324	0.00122	0.005	0.2
22	23	18094.67384	0.0024	0.005	0.5
23	24	18092.82948	0.00286	0.005	0.6
24	25	18090.93478	-0.00279	0.005	-0.6
25	26	18088.99908	-0.00521	0.005	-1.0
26	27	18087.02705	0.00029	0.005	0.1
27	28	18084.97803	-0.02696	90.005	0.0
28	29	18082.94002	0.00106	0.005	0.2
29	30	18080.8239	-0.00478	0.005	-1.0
30	31	18078.68206	0.00794	0.005	1.6
31	32	18076.46291	-0.01237	0.005	-2.5
32	33	18074.22866	-0.00349	0.005	-0.7
33	34	18071.94306	-0.00165	0.005	-0.3
34	35	18069.60444	-0.00851	0.005	-1.7
35	36	18067.23978	0.00293	0.005	0.6
36	37	18064.81668	0.00028	0.005	0.1
37	38	18062.33776	-0.01382	0.005	-2.8
38	39	18059.84169	-0.00068	0.005	-0.1

Table B.1, Electronic Data of ^{184}WO Relative to X0$^+$ (*Cont'd*)

J'	J''	Obs	Obs-Calc	Unc	(Obs-Calc)/Unc
39	40	18057.30572	0.01699	0.005	3.4
40	41	18054.68754	-0.00312	0.005	-0.6
41	42	18052.05182	0.00371	0.005	0.7
42	43	18049.35947	-0.0016	0.005	-0.3
43	44	18046.6275	-0.00201	0.005	-0.4
44	45	18043.85492	0.00154	0.005	0.3
45	46	18041.02868	-0.00397	0.005	-0.8
46	47	18038.16528	-0.00201	0.005	-0.4
47	48	18035.26124	0.00399	0.005	0.8
48	49	18032.30366	0.00117	0.005	0.2
49	50	18029.30465	0.00168	0.005	0.3
50	51	18026.26657	0.00794	0.005	1.6
51	52	18023.17562	0.00619	0.005	1.2
52	53	18020.02773	-0.00758	0.005	-1.5
53	54	18016.86489	0.00869	0.005	1.7
54	55	18013.62767	-0.00439	0.005	-0.9
55	56	18010.35267	-0.01014	0.005	-2.0
56	57	18007.04761	-0.00078	0.005	-0.2
57	58	18003.69006	0.00135	0.005	0.3
58	59	18000.28656	0.00284	0.005	0.6
59	60	17996.84228	0.00896	0.005	1.8
60	61	17993.35323	0.01579	0.005	3.2
$C(0,1)$ Band, Q Branch (p' = f, p'' = e)					
4	4	18124.47747	0.02564	90.005	0.0
5	5	18124.25388	0.02268	90.005	0.0
6	6	18123.98124	0.01477	90.005	0.0
7	7	18123.66899	0.01135	90.005	0.0
8	8	18123.30977	0.00507	0.005	1.0
9	9	18122.91349	0.00581	0.005	1.2
10	10	18122.4767	0.01012	0.005	2.0
11	11	18121.98337	0.00197	0.005	0.4
12	12	18121.45497	0.00281	0.005	0.6
13	13	18120.8802	0.00134	0.005	0.3
14	14	18120.26073	-0.00078	0.005	-0.2
15	15	18119.60225	0.00213	0.005	0.4
16	16	18118.89441	-0.00026	0.005	-0.1
17	17	18118.15061	0.00542	0.005	1.1
18	18	18117.35251	0.00086	0.005	0.2
19	19	18116.51408	0.00001	0.005	0.0
20	20	18115.63408	0.00166	0.005	0.3
21	21	18114.7076	0.0009	0.005	0.2
22	22	18113.73746	0.00058	0.005	0.1
23	23	18112.71941	-0.00353	0.005	-0.7
24	24	18111.66352	-0.00133	0.005	-0.3
25	25	18110.56273	0.00016	0.005	0.0
26	26	18109.41357	-0.00249	0.005	-0.5
27	27	18108.2237	-0.00155	0.005	-0.3
28	28	18106.98901	-0.00109	0.005	-0.2
29	29	18105.7081	-0.00241	0.005	-0.5
30	30	18104.38602	-0.0004	0.005	-0.1
31	31	18103.01254	-0.00518	0.005	-1.0
32	32	18101.60515	0.00085	0.005	0.2
33	33	18100.14492	-0.00112	0.005	-0.2
34	34	18098.64185	-0.00096	0.005	-0.2
35	35	18097.09246	-0.00199	0.005	-0.4
36	36	18095.50086	0.00008	0.005	0.0
37	37	18093.86444	0.00281	0.005	0.6

Table B.1, Electronic Data of ^{184}WO Relative to X0$^+$ (*Cont'd*)

J'	J''	Obs	Obs-Calc	Unc	(Obs-Calc)/Unc
38	38	18092.17654	-0.00024	0.005	0.0
39	39	18090.44836	0.00234	0.005	0.5
40	40	18088.67088	0.00179	0.005	0.4
41	41	18086.84445	-0.00127	0.005	-0.3
42	42	18084.97803	0.00241	0.005	0.5
43	43	18083.05676	-0.00171	0.005	-0.3
44	44	18081.09411	0.00017	90.005	0.0
45	45	18079.06807	-0.01357	90.005	0.0
46	46	18077.01089	-0.0103	90.005	0.0
47	47	18074.9024	-0.00974	90.005	0.0
48	48	18072.74058	-0.01347	90.005	0.0
49	49	18070.51936	-0.02705	90.005	0.0
50	50	18068.25594	-0.03276	90.005	0.0
51	51	18065.94968	-0.03068	90.005	0.0
52	52	18063.55561	-0.06518	90.005	0.0
53	53	18061.12832	-0.08102	90.005	0.0
54	54	18058.64409	-0.10125	90.005	0.0
55	55	18056.09932	-0.12875	90.005	0.0
56	56	18053.49455	-0.16221	90.005	0.0
57	57	18050.82671	-0.2039	90.005	0.0
58	58	18048.12254	-0.22621	90.005	0.0
59	59	18045.29297	-0.31731	90.005	0.0
60	60	18042.42052	-0.39373	90.005	0.0
61	61	18039.4888	-0.47085	90.005	0.0
62	62	18036.4783	-0.56711	90.005	0.0
63	63	18033.39051	-0.67992	90.005	0.0
64	64	18030.23586	-0.79766	90.005	0.0
65	65	18026.99668	-0.93677	90.005	0.0
66	66	18023.68413	-1.0848	90.005	0.0
67	67	18020.28555	-1.25304	90.005	0.0
$C(0,2)$ Band, R Branch (p' = e, p'' = e)					
21	20	17083.34859	0.00296	0.003	1.0
22	21	17083.28867	0.00748	0.003	2.5
23	22	17083.17831	0.00201	0.003	0.7
24	23	17083.02736	-0.00359	0.003	-1.2
25	24	17082.83166	-0.01346	0.003	-4.5
26	25	17082.60202	-0.01678	90.003	0.0
27	26	17082.33493	-0.01704	90.003	0.0
28	27	17082.00122	-0.04338	90.003	0.0
29	28	17081.74911	0.05242	90.003	0.0
30	29	17081.34976	0.04156	90.003	0.0
31	30	17080.899	0.01988	90.003	0.0
32	31	17080.42413	0.01471	90.003	0.0
33	32	17079.90479	0.00571	90.003	0.0
34	33	17079.35512	0.00706	0.003	2.4
35	34	17078.75653	0.0002	0.003	0.1
36	35	17078.10638	-0.01748	90.003	0.0
37	36	17077.45554	0.00492	0.003	1.6
38	37	17076.71304	-0.02353	90.003	0.0
39	38	17075.98241	0.00075	0.003	0.2
40	39	17075.1832	-0.00265	0.003	-0.9
41	40	17074.34291	-0.00619	0.003	-2.1
42	41	17073.48209	0.01074	90.003	0.0
$C(0,2)$ Band, P Branch (p' = e, p'' = e)					
5	6	17069.8277	-0.00313	0.003	-1.0
6	7	17068.76484	-0.0015	0.003	-0.5

Table B.1, Electronic Data of ^{184}WO Relative to X0$^+$ (*Cont'd*)

J'	J''	Obs	Obs-Calc	Unc	(Obs-Calc)/Unc
7	8	17067.66325	0.00162	0.003	0.5
8	9	17066.51333	-0.00338	0.003	-1.1
9	10	17065.31736	-0.01423	0.003	-4.7
10	11	17064.10294	-0.00334	0.003	-1.1
11	12	17062.82665	-0.01412	90.003	0.0
12	13	17061.54215	0.00706	0.003	2.4
13	14	17060.19706	0.00784	0.003	2.6
14	15	17058.81422	0.01103	90.003	0.0
15	16	17057.4005	0.02352	90.003	0.0
16	17	17055.90702	-0.00359	0.003	-1.2
17	18	17054.39495	-0.00913	0.003	-3.0
18	19	17052.84792	-0.00948	0.003	-3.2
19	20	17051.27773	0.00718	0.003	2.4
20	21	17049.63902	-0.00454	0.003	-1.5
22	23	17046.25108	-0.01802	90.003	0.0
23	24	17044.5037	-0.01794	90.003	0.0
24	25	17042.70955	-0.02447	90.003	0.0
25	26	17040.8833	-0.02294	90.003	0.0
26	27	17039.00153	-0.03676	90.003	0.0
27	28	17037.12772	-0.00244	90.003	0.0
28	29	17035.17519	-0.00666	90.003	0.0
29	30	17033.20829	0.01494	90.003	0.0
30	31	17031.15361	-0.01103	90.003	0.0
31	32	17029.09478	-0.00092	0.003	-0.3
33	34	17024.84352	0.00641	0.003	2.1
34	35	17022.64265	-0.00476	0.003	-1.6
35	36	17020.40188	-0.01554	90.003	0.0
36	37	17018.14793	0.00084	0.003	0.3
37	38	17015.83628	-0.00014	0.003	0.0
38	39	17013.48774	0.00239	0.003	0.8
39	40	17011.07252	-0.02135	90.003	0.0
40	41	17008.67512	0.01319	90.003	0.0
41	42	17006.18672	-0.00277	0.003	-0.9
42	43	17003.67036	-0.00614	0.003	-2.0
43	44	17001.12599	0.00307	0.003	1.0
$C(0,2)$ Band, Q Branch (p' = f, p'' = e)					
2	2	17075.23837	-0.0143	0.003	-4.8
3	3	17075.12785	-0.00457	0.003	-1.5
4	4	17074.97811	0.00602	0.003	2.0
5	5	17074.77969	0.00801	0.003	2.7
6	6	17074.5331	0.00189	0.003	0.6
7	7	17074.25201	0.00133	0.003	0.4
8	8	17073.93414	0.00404	0.003	1.3
9	9	17073.58105	0.01156	0.003	3.9
10	10	17073.17745	0.00861	0.003	2.9
11	11	17072.72681	-0.00137	0.003	-0.5
12	12	17072.25491	0.00741	0.003	2.5
13	13	17071.73262	0.0058	0.003	1.9
14	14	17071.16174	-0.00441	0.003	-1.5
15	15	17070.56645	0.00096	0.003	0.3
17	17	17069.23761	-0.00662	0.003	-2.2
18	18	17068.52057	-0.00306	0.003	-1.0
19	19	17067.75353	-0.00951	90.003	0.0
20	20	17066.96336	0.0009	0.003	0.3
21	21	17066.11623	-0.00564	0.003	-1.9
22	22	17065.22885	-0.01241	90.003	0.0
23	23	17064.31198	-0.00862	90.003	0.0

Table B.1, Electronic Data of ^{184}WO Relative to X0$^+$ (*Cont'd*)

J'	J''	Obs	Obs-Calc	Unc	(Obs-Calc)/Unc
24	24	17063.34601	-0.01386	90.003	0.0
25	25	17062.34266	-0.01636	90.003	0.0
26	26	17061.28491	-0.0331	90.003	0.0
27	27	17060.19706	-0.03972	90.003	0.0
29	29	17057.99621	0.04281	90.003	0.0
30	30	17056.77658	0.02549	90.003	0.0
31	31	17055.52256	0.01432	90.003	0.0
32	32	17054.23169	0.00696	90.003	0.0
33	33	17052.90521	0.00478	90.003	0.0
34	34	17051.53874	0.00352	0.003	1.2
35	35	17050.12856	-0.00035	0.003	-0.1
36	36	17048.68654	0.0052	0.003	1.7
37	37	17047.19483	0.00251	0.003	0.8
38	38	17045.66189	0.00027	0.003	0.1
39	39	17044.09165	0.00264	0.003	0.9
40	40	17042.47083	-0.00339	0.003	-1.1
41	41	17040.81916	0.00217	0.003	0.7
42	42	17039.11518	-0.00181	0.003	-0.6
43	43	17037.37056	-0.00334	90.003	0.0
44	44	17035.58393	-0.00343	90.003	0.0
45	45	17033.75162	-0.00534	90.003	0.0
46	46	17031.88303	0.00073	90.003	0.0
47	47	17029.94374	-0.01918	90.003	0.0
48	48	17027.96611	-0.03223	90.003	0.0
49	49	17025.97415	-0.01387	90.003	0.0
50	50	17023.90608	-0.02535	90.003	0.0
51	51	17021.77649	-0.05146	90.003	0.0
52	52	17019.62427	-0.05269	90.003	0.0
53	53	17017.39854	-0.07924	90.003	0.0
54	54	17015.14148	-0.08822	90.003	0.0
55	55	17012.8295	-0.10244	90.003	0.0
56	56	17010.43642	-0.14729	90.003	0.0
57	57	17008.01107	-0.17307	90.003	0.0
58	58	17005.50639	-0.22593	90.003	0.0
59	59	17002.96381	-0.26349	90.003	0.0
60	60	17000.35876	-0.30931	90.003	0.0
$C(1,2)$ Band, R Branch (p' = e, p'' = e)					
5	4	18006.06595	0.00973	90.003	0.0
6	5	18006.6087	-0.00016	0.003	-0.1
7	6	18007.12231	0.0059	0.003	2.0
8	7	18007.58419	0.00533	0.003	1.8
9	8	18007.97378	-0.02242	90.003	0.0
10	9	18008.38049	0.01206	90.003	0.0
11	10	18008.69258	-0.00296	0.003	-1.0
12	11	18008.96128	-0.01626	90.003	0.0
13	12	18009.21042	-0.00398	0.003	-1.3
14	13	18009.40471	-0.00142	0.003	-0.5
15	14	18009.55219	-0.00053	0.003	-0.2
16	15	18009.65808	0.00391	0.003	1.3
19	18	18009.70693	0.01935	90.003	0.0
20	19	18009.60797	-0.00042	0.003	-0.1
21	20	18009.47153	-0.0125	90.003	0.0
22	21	18009.30749	-0.00699	0.003	-2.3
23	22	18009.08727	-0.01248	90.003	0.0
24	23	18008.82238	-0.01744	90.003	0.0
25	24	18008.5175	-0.01719	90.003	0.0
26	25	18008.16887	-0.01548	90.003	0.0

Table B.1, Electronic Data of ^{184}WO Relative to X0$^+$ (*Cont'd*)

J'	J''	Obs	Obs-Calc	Unc	(Obs-Calc)/Unc
27	26	18007.76461	-0.02418	90.003	0.0
29	28	18006.92012	0.05814	90.003	0.0
30	29	18006.36443	0.03373	90.003	0.0
31	30	18005.77511	0.02094	90.003	0.0
32	31	18005.14362	0.01125	90.003	0.0
33	32	18004.47511	0.00983	0.003	3.3
34	33	18003.76754	0.01464	0.003	4.9
35	34	18002.99671	0.00151	0.003	0.5
36	35	18002.1909	-0.00128	0.003	-0.4
37	36	18001.34161	-0.0022	0.003	-0.7
38	37	18000.45568	0.00561	0.003	1.9
39	38	17999.51272	0.00176	0.003	0.6
40	39	17998.52839	0.00195	0.003	0.6
41	40	17997.5213	0.0248	90.003	0.0
42	41	17996.43017	0.00907	0.003	3.0
43	42	17995.3017	0.00147	0.003	0.5
44	43	17994.13395	0.0001	0.003	0.0
45	44	17992.90555	-0.01639	90.003	0.0
46	45	17991.66983	0.00536	0.003	1.8
47	46	17990.35067	-0.01073	0.003	-3.6
48	47	17989.01202	-0.00067	0.003	-0.2
49	48	17987.61124	-0.00708	0.003	-2.4
50	49	17986.16412	-0.01411	0.003	-4.7
51	50	17984.71712	0.02474	90.003	0.0
52	51	17983.15916	-0.00157	0.003	-0.5
53	52	17981.58418	0.00094	0.003	0.3
54	53	17979.95555	-0.00429	0.003	-1.4
55	54	17978.28876	-0.00173	0.003	-0.6
56	55	17976.56291	-0.01222	90.003	0.0
57	56	17974.81125	-0.00244	0.003	-0.8
58	57	17973.02015	0.01403	0.003	4.7
59	58	17971.15144	-0.0009	0.003	-0.3
$C(1,2)$ Band, P Branch (p' = e, p'' = e)					
7	8	17994.75244	-0.01894	90.003	0.0
8	9	17993.59836	0.01023	90.003	0.0
9	10	17992.36131	0.00141	0.003	0.5
10	11	17991.09064	0.00395	0.003	1.3
11	12	17989.77527	0.00676	0.003	2.3
12	13	17988.40617	0.00081	0.003	0.3
13	14	17986.99789	0.00063	0.003	0.2
14	15	17985.54399	-0.00021	0.003	-0.1
15	16	17984.04724	0.00104	0.003	0.3
16	17	17982.51516	0.01189	90.003	0.0
17	18	17980.9049	-0.01051	0.003	-3.5
18	19	17979.26381	-0.01881	90.003	0.0
19	20	17977.60265	-0.00228	0.003	-0.8
20	21	17975.87627	-0.00605	0.003	-2.0
21	22	17974.11261	-0.00219	0.003	-0.7
22	23	17972.29503	-0.00736	0.003	-2.5
23	24	17970.43589	-0.0092	90.003	0.0
24	25	17968.52909	-0.0138	90.003	0.0
25	26	17966.57161	-0.0242	90.003	0.0
26	27	17964.56397	-0.03987	90.003	0.0
28	29	17960.52175	0.0365	90.003	0.0
29	30	17958.38025	0.02162	90.003	0.0
30	31	17956.1986	0.01146	90.003	0.0
31	32	17953.97318	0.00243	90.003	0.0

Table B.1, Electronic Data of ^{184}WO Relative to X0$^+$ (*Cont'd*)

J'	J''	Obs	Obs-Calc	Unc	(Obs-Calc)/Unc
32	33	17951.71405	0.00457	0.003	1.5
33	34	17949.40841	0.00509	0.003	1.7
34	35	17947.05598	0.00373	0.003	1.2
35	36	17944.65309	-0.0032	0.003	-1.1
36	37	17942.21732	0.00192	0.003	0.6
37	38	17939.72929	-0.00031	0.003	-0.1
38	39	17937.19641	-0.00245	0.003	-0.8
39	40	17934.62289	-0.00028	0.003	-0.1
40	41	17932.00366	0.00114	0.003	0.4
41	42	17929.3382	0.00132	0.003	0.4
42	43	17926.6242	-0.00205	0.003	-0.7
43	44	17923.87329	0.0027	0.003	0.9
44	45	17921.06711	-0.00278	0.003	-0.9
45	46	17918.22566	0.00154	0.003	0.5
46	47	17915.33637	0.00313	0.003	1.0
47	48	17912.39835	0.00111	0.003	0.4
48	49	17909.40998	-0.00609	0.003	-2.0
49	50	17906.38285	-0.00685	0.003	-2.3
50	51	17903.32078	0.00269	0.003	0.9
51	52	17900.20495	0.00376	0.003	1.3
$C(1,2)$ Band, Q Branch (p' = f, p'' = e)					
2	2	18002.48492	0.0112	0.003	3.7
3	3	18002.34545	0.01497	0.003	5.0
4	4	18002.14303	0.00373	0.003	1.2
5	5	18001.91052	0.01051	0.003	3.5
6	6	18001.61321	0.00079	0.003	0.3
7	7	18001.285	0.00874	0.003	2.9
8	8	18000.86789	-0.02336	90.003	0.0
9	9	18000.45568	-0.00139	0.003	-0.5
10	10	17999.97139	-0.00194	0.003	-0.6
11	11	17999.43058	-0.00905	0.003	-3.0
12	12	17998.84682	-0.00868	0.003	-2.9
13	13	17998.21178	-0.00867	0.003	-2.9
14	14	17997.5213	-0.01262	0.003	-4.2
15	15	17996.78608	-0.00927	0.003	-3.1
16	16	17995.99408	-0.01001	0.003	-3.3
17	17	17995.15453	-0.00494	0.003	-1.6
18	18	17994.25704	-0.00375	0.003	-1.2
19	19	17993.30381	-0.00346	0.003	-1.2
20	20	17992.29505	-0.00306	0.003	-1.0
21	21	17991.23331	0.00085	0.003	0.3
22	22	17990.11455	0.00513	0.003	1.7
23	23	17988.93092	0.00286	0.003	1.0
24	24	17987.68957	0.00219	0.003	0.7
25	25	17986.38889	0.00254	90.003	0.0
26	26	17985.01808	-0.0058	90.003	0.0
27	27	17983.57381	-0.02504	90.003	0.0
29	29	17980.60872	0.05238	90.003	0.0
30	30	17978.96103	0.02468	90.003	0.0
31	31	17977.26324	0.01446	90.003	0.0
32	32	17975.49602	0.00375	0.003	1.3
33	33	17973.66595	0.00057	0.003	0.2
34	34	17971.75768	-0.00894	0.003	-3.0
35	35	17969.78423	-0.01024	0.003	-3.4
36	36	17967.73763	-0.00971	0.003	-3.2
37	37	17965.62877	0.00518	0.003	1.7
38	38	17963.44078	0.01926	0.003	6.4

Table B.1, Electronic Data of ^{184}WO Relative to X0$^+$ (*Cont'd*)

J'	J''	Obs	Obs-Calc	Unc	(Obs-Calc)/Unc
39	39	17961.19701	0.05762	90.003	0.0
40	40	17958.87159	0.09621	90.003	0.0
41	41	17956.48935	0.16172	90.003	0.0
42	42	17954.02878	0.23455	90.003	0.0
43	43	17951.5009	0.32772	90.003	0.0
$C(1,3)$ Band, R Branch (p' = e, p'' = e)					
22	21	16968.79485	0.00096	0.003	0.3
23	22	16968.66299	-0.00546	0.003	-1.8
24	23	16968.50089	-0.00096	0.003	-0.3
25	24	16968.29164	-0.00243	0.003	-0.8
26	25	16968.02962	-0.01548	90.003	0.0
27	26	16967.75499	0.00005	0.003	0.0
28	27	16967.42072	-0.00286	0.003	-1.0
29	28	16967.03448	-0.01653	90.003	0.0
30	29	16966.62814	-0.00907	0.003	-3.0
31	30	16966.18961	0.00742	0.003	2.5
32	31	16965.68235	-0.00358	0.003	-1.2
33	32	16965.1487	0.00028	0.003	0.1
34	33	16964.56831	-0.00135	0.003	-0.5
35	34	16963.9526	0.00296	0.003	1.0
36	35	16963.28657	-0.00178	0.003	-0.6
37	36	16962.59055	0.00477	0.003	1.6
38	37	16961.84286	0.00093	0.003	0.3
40	39	16960.23233	0.00198	0.003	0.7
41	40	16959.36448	0.00187	0.003	0.6
42	41	16958.44475	-0.00881	0.003	-2.9
43	42	16957.50657	0.00337	0.003	1.1
44	43	16956.49401	-0.01751	90.003	0.0
45	44	16955.47996	0.00144	0.003	0.5
46	45	16954.40041	-0.00378	0.003	-1.3
47	46	16953.28588	-0.00266	0.003	-0.9
48	47	16952.13281	0.00126	0.003	0.4
49	48	16950.93784	0.00461	0.003	1.5
50	49	16949.6893	-0.00428	0.003	-1.4
51	50	16948.41954	0.00696	0.003	2.3
53	52	16945.73782	0.01122	0.005	2.2
54	53	16944.32191	0.00031	0.003	0.1
55	54	16942.87739	0.00212	0.003	0.7
56	55	16941.37814	-0.00948	0.003	-3.2
57	56	16939.84442	-0.01421	90.003	0.0
$C(1,3)$ Band, P Branch (p' = e, p'' = e)					
3	4	16957.63879	0.00417	0.003	1.4
4	5	16956.65002	-0.00177	0.003	-0.6
5	6	16955.63395	0.00592	0.003	2.0
6	7	16954.58389	0.02057	90.003	0.0
7	8	16953.45937	0.00168	0.003	0.6
8	9	16952.31512	0.004	0.003	1.3
9	10	16951.13174	0.0081	0.003	2.7
12	13	16947.31544	-0.00026	0.003	-0.1
13	14	16945.96902	0.00445	0.003	1.5
15	16	16943.13774	-0.00189	0.003	-0.6
16	17	16941.67178	0.00597	0.003	2.0
17	18	16940.15963	0.00851	0.003	2.8
18	19	16938.59341	-0.00212	0.003	-0.7
19	20	16936.99464	-0.00443	0.003	-1.5
20	21	16935.36463	0.00291	0.003	1.0

Table B.1, Electronic Data of ^{184}WO Relative to X0$^+$ (*Cont'd*)

J'	J''	Obs	Obs-Calc	Unc	(Obs-Calc)/Unc
21	22	16933.68716	0.00365	0.003	1.2
22	23	16931.97684	0.01242	90.003	0.0
23	24	16930.19311	-0.01136	90.003	0.0
24	25	16928.39991	-0.00373	0.003	-1.2
25	26	16926.55988	-0.00208	0.003	-0.7
26	27	16924.67171	-0.00771	0.003	-2.6
27	28	16922.7535	-0.00252	0.003	-0.8
28	29	16920.79427	0.00251	0.003	0.8
29	30	16918.7852	-0.00145	0.003	-0.5
30	31	16916.74259	0.00189	0.003	0.6
31	32	16914.64647	-0.00742	0.003	-2.5
32	33	16912.5222	-0.00404	0.003	-1.3
33	34	16910.35382	-0.00393	0.003	-1.3
34	35	16908.14477	-0.00365	0.003	-1.2
35	36	16905.90194	0.00368	0.003	1.2
36	37	16903.60515	-0.00211	0.003	-0.7
37	38	16901.26585	-0.00958	0.003	-3.2
38	39	16898.90335	0.00058	0.003	0.2
39	40	16896.48186	-0.00742	0.005	-1.5
40	41	16894.03633	0.00135	0.003	0.5
41	42	16891.54491	0.00505	0.003	1.7
42	43	16889.00589	0.00197	0.003	0.7
43	44	16886.42957	0.0024	0.003	0.8
44	45	16883.81995	0.01034	0.003	3.4
45	46	16881.1483	-0.00296	0.003	-1.0
$C(1,3)$ Band, Q Branch (p' = f, p'' = e)					
2	2	16961.03325	0.00778	0.003	2.6
3	3	16960.89788	0.00341	0.003	1.1
4	4	16960.71522	-0.00438	0.003	-1.5
5	5	16960.50171	0.001	0.003	0.3
6	6	16960.23233	-0.00524	0.003	-1.7
7	7	16959.92975	-0.00021	0.003	-0.1
8	8	16959.57167	-0.0059	0.003	-2.0
9	9	16959.17422	-0.00584	0.003	-1.9
10	10	16958.72557	-0.0115	0.003	-3.8
11	11	16958.23794	-0.01023	0.003	-3.4
12	12	16957.71015	-0.00276	0.003	-0.9
13	13	16957.11785	-0.01294	0.003	-4.3
14	14	16956.49401	-0.00723	0.003	-2.4
15	15	16955.81065	-0.01305	0.003	-4.3
16	16	16955.09084	-0.00667	0.003	-2.2
17	17	16954.31877	-0.00325	0.003	-1.1
18	18	16953.51007	0.01358	0.003	4.5
19	19	16952.62682	0.00665	0.003	2.2
20	20	16951.69368	0.00143	0.003	0.5
21	21	16950.71247	0.0006	0.003	0.2
22	22	16949.6893	0.01117	0.003	3.7
23	23	16948.60534	0.01525	0.003	5.1
24	24	16947.45624	0.00948	0.003	3.2
25	25	16946.26102	0.01392	0.005	2.8
26	26	16945.00472	0.01468	0.003	4.9
27	27	16943.69347	0.01904	0.003	6.3
28	28	16942.30648	0.00737	0.003	2.5
29	29	16940.86827	0.00542	0.003	1.8
30	30	16939.36638	0.00201	0.003	0.7
31	31	16937.79716	-0.00519	0.003	-1.7
32	32	16936.16916	-0.00625	0.003	-2.1

Table B.1, Electronic Data of ^{184}WO Relative to X0$^+$ (*Cont'd*)

J'	J''	Obs	Obs-Calc	Unc	(Obs-Calc)/Unc
33	33	16934.47204	-0.0101	0.003	-3.4
34	34	16932.70953	-0.01153	0.003	-3.8
35	35	16930.87574	-0.0149	0.003	-5.0
36	36	16928.97988	-0.00943	0.003	-3.1
37	37	16927.01158	-0.00386	0.003	-1.3
38	38	16924.98347	0.01612	0.003	5.4
39	39	16922.89522	0.05192	90.003	0.0
40	40	16920.73498	0.09349	90.003	0.0
41	41	16918.51601	0.15591	90.003	0.0
42	42	16916.23124	0.23404	90.003	0.0
43	43	16913.88969	0.33884	90.003	0.0
44	44	16911.49656	0.47753	90.003	0.0
$D(0,0)$ Band, P Branch (p' = e, p'' = e)					
58	59	20653.51688	-0.0376	0.01	-3.8
57	58	20657.43025	-0.04172	0.01	-4.2
56	57	20661.2674	-0.06925	10.01	0.0
55	56	20665.10236	-0.04615	0.01	-4.6
54	55	20668.85791	-0.04963	0.01	-5.0
53	54	20672.59561	-0.01811	0.01	-1.8
52	53	20676.24854	-0.01851	0.01	-1.9
51	52	20679.87122	0.0037	0.01	0.4
50	51	20683.40114	-0.01396	0.01	-1.4
49	50	20686.89861	-0.01118	0.01	-1.1
48	49	20690.34788	-0.00369	0.01	-0.4
47	48	20693.73616	-0.00428	0.01	-0.4
46	47	20697.06878	-0.00758	0.01	-0.8
45	46	20700.37181	0.01247	0.01	1.2
44	45	20703.60321	0.01386	0.01	1.4
43	44	20706.78408	0.01769	0.01	1.8
42	43	20709.90624	0.01581	0.01	1.6
41	42	20712.97925	0.01779	0.01	1.8
40	41	20715.99787	0.01841	0.01	1.8
38	39	20721.87377	0.01745	0.01	1.7
37	38	20724.73436	0.01921	0.01	1.9
36	37	20727.53807	0.01718	0.01	1.7
35	36	20730.28969	0.01616	0.01	1.6
34	35	20732.98932	0.01628	0.01	1.6
33	34	20735.63522	0.0158	0.01	1.6
32	33	20738.22711	0.01447	0.01	1.4
31	32	20740.76577	0.01308	0.01	1.3
30	31	20743.24729	0.00774	0.01	0.8
29	30	20745.67667	0.00345	0.01	0.3
28	29	20748.05531	0.00165	0.01	0.2
27	28	20750.3844	0.00352	0.01	0.4
26	27	20752.65966	0.00482	0.01	0.5
25	26	20754.88108	0.00555	0.01	0.6
24	25	20757.04511	0.00216	0.01	0.2
23	24	20759.1606	0.00353	0.01	0.4
22	23	20761.22154	0.00365	0.01	0.4
21	22	20763.22812	0.00275	0.01	0.3
20	21	20765.18352	0.004	0.01	0.4
19	20	20767.08344	0.00313	0.01	0.3
18	19	20768.93206	0.00433	0.01	0.4
17	18	20770.70321	-0.01857	0.01	-1.9
16	17	20772.48209	0.01967	0.01	2.0
15	16	20774.15453	0.00487	0.01	0.5
14	15	20775.78991	0.00644	0.01	0.6

Table B.1, Electronic Data of ^{184}WO Relative to X0$^+$ (*Cont'd*)

J'	J''	Obs	Obs-Calc	Unc	(Obs-Calc)/Unc
13	14	20777.37358	0.00972	0.01	1.0
12	13	20778.89815	0.00736	0.01	0.7
10	11	20781.78609	0.00182	0.01	0.2
9	10	20783.1619	0.01111	0.01	1.1
8	9	20784.47537	0.01155	0.01	1.2
7	8	20785.69348	-0.02986	0.01	-3.0
6	7	20786.90027	-0.02909	10.01	0.0
5	6	20788.05432	-0.02752	10.01	0.0
4	5	20789.1584	-0.0224	10.01	0.0
3	4	20790.20761	-0.0186	10.01	0.0
2	3	20791.25575	0.03768	10.01	0.0
1	2	20792.1878	0.03143	10.01	0.0
$D(0,0)$ Band, R Branch (p' = e, p'' = e)					
1	0	20794.66262	0.01277	0.01	1.3
2	1	20795.41334	0.0395	10.01	0.0
3	2	20796.06231	0.01807	0.01	1.8
4	3	20796.67951	0.01847	0.01	1.8
5	4	20797.23602	0.01179	0.01	1.2
6	5	20797.7366	0.00278	0.01	0.3
7	6	20798.19486	0.00507	0.01	0.5
8	7	20798.60737	0.01522	0.01	1.5
9	8	20798.93336	-0.00752	0.01	-0.8
10	9	20799.22007	-0.01592	0.01	-1.6
11	10	20799.46803	-0.00944	0.01	-0.9
12	11	20799.66382	-0.00151	0.01	-0.2
13	12	20799.81579	0.01623	0.01	1.6
14	13	20799.87192	-0.00823	0.01	-0.8
15	14	20799.87192	-0.0352	0.01	-3.5
16	15	20799.87192	-0.00853	0.01	-0.9
17	16	20799.80027	0.00011	0.01	0.0
18	17	20799.66382	-0.00241	0.01	-0.2
19	18	20799.46803	-0.01064	0.01	-1.1
20	19	20799.22007	-0.01742	0.01	-1.7
21	20	20798.93336	-0.00932	0.01	-0.9
22	21	20798.60737	0.01312	0.01	1.3
23	22	20798.19486	0.00266	0.01	0.3
24	23	20797.7366	0.00007	0.01	0.0
25	24	20797.23602	0.00876	0.01	0.9
26	25	20796.67951	0.01514	0.01	1.5
28	27	20795.41334	0.03555	10.01	0.0
29	28	20794.66262	0.00851	0.01	0.9
30	29	20793.88988	0.01304	0.01	1.3
31	30	20793.06297	0.01697	10.01	0.0
32	31	20792.18708	0.02551	10.01	0.0
33	32	20791.25575	0.03216	10.01	0.0
34	33	20790.20761	-0.02443	10.01	0.0
35	34	20789.23271	0.04577	10.01	0.0
36	35	20788.05432	-0.03398	10.01	0.0
37	36	20786.90027	-0.03585	10.01	0.0
38	37	20785.69348	-0.03693	10.01	0.0
39	38	20784.47537	0.00418	0.01	0.4
40	39	20783.1619	0.00344	0.01	0.3
41	40	20781.80608	0.01385	0.01	1.4
42	41	20780.36034	-0.01217	0.01	-1.2
43	42	20778.89815	-0.00117	0.01	-0.1
44	43	20777.37358	0.00093	0.01	0.1
45	44	20775.78991	-0.00262	0.01	-0.3

Table B.1, Electronic Data of ^{184}WO Relative to X0$^+$ (*Cont'd*)

J'	J''	Obs	Obs-Calc	Unc	(Obs-Calc)/Unc
46	45	20774.15453	-0.00443	0.01	-0.4
47	46	20772.48609	0.01413	0.01	1.4
49	48	20768.93206	-0.00562	0.01	-0.6
50	49	20767.08344	-0.007	0.01	-0.7
51	50	20765.18352	-0.00628	0.01	-0.6
52	51	20763.22812	-0.00767	0.01	-0.8
53	52	20761.22154	-0.00687	0.01	-0.7
54	53	20759.1606	-0.00708	0.01	-0.7
55	54	20757.04511	-0.00849	0.01	-0.8
56	55	20754.88108	-0.00512	0.01	-0.5
57	56	20752.65966	-0.00581	0.01	-0.6
58	57	20750.3844	-0.00704	0.01	-0.7
59	58	20748.05531	-0.0088	0.01	-0.9
60	59	20745.67667	-0.00684	0.01	-0.7
61	60	20743.24729	-0.00234	0.01	-0.2
62	61	20740.76577	0.00328	0.01	0.3
63	62	20738.22711	0.005	0.01	0.5
64	63	20735.63522	0.00673	0.01	0.7
65	64	20732.98932	0.00767	0.01	0.8
66	65	20730.28969	0.00809	0.01	0.8
67	66	20727.53807	0.00973	0.01	1.0
68	67	20724.7344	0.0125	0.01	1.2
69	68	20721.87367	0.01139	0.01	1.1
70	69	20718.96469	0.0152	0.01	1.5
71	70	20715.99787	0.01433	0.01	1.4
72	71	20712.97925	0.01481	0.01	1.5
73	72	20709.90624	0.01403	0.01	1.4
74	73	20706.78408	0.01724	0.01	1.7
75	74	20703.60321	0.01486	0.01	1.5
76	75	20700.37181	0.01506	0.01	1.5
77	76	20697.06878	-0.00327	0.01	-0.3
78	77	20693.73616	0.00191	0.01	0.2
79	78	20690.34788	0.00453	0.01	0.5
80	79	20686.89861	-0.00077	0.01	-0.1
81	80	20683.40114	-0.00118	0.01	-0.1
82	81	20679.87122	0.01903	0.01	1.9
83	82	20676.24854	-0.00046	0.01	0.0
84	83	20672.59561	0.00287	0.01	0.3
85	84	20668.85791	-0.0255	0.01	-2.6
86	85	20665.10236	-0.01867	0.01	-1.9
87	86	20661.2674	-0.03819	10.01	0.0
88	87	20657.43025	-0.00685	0.01	-0.7
89	88	20653.51688	0.00134	0.01	0.1
$D(0,0)$ Band, Q Branch (p' = f, p'' = e)					
68	68	20669.79582	0.00787	0.01	0.8
67	67	20673.34902	-0.03202	10.01	0.0
66	66	20676.88277	-0.03838	10.01	0.0
65	65	20680.36333	-0.045	10.01	0.0
64	64	20683.80527	-0.03732	10.01	0.0
63	63	20687.20542	-0.01857	10.01	0.0
61	61	20693.79776	-0.0305	10.01	0.0
60	60	20697.06881	0.01762	10.01	0.0
59	59	20700.21429	-0.00705	0.01	-0.7
58	58	20703.33587	-0.00286	0.01	-0.3
57	57	20706.39618	-0.00721	0.01	-0.7
56	56	20709.40854	-0.00677	0.01	-0.7
55	55	20712.37025	-0.00428	0.01	-0.4

Table B.1, Electronic Data of ^{184}WO Relative to X0$^+$ (*Cont'd*)

J'	J''	Obs	Obs-Calc	Unc	(Obs-Calc)/Unc
54	54	20715.27749	-0.00355	0.01	-0.4
53	53	20718.13466	-0.0002	0.01	0.0
52	52	20720.93858	0.00259	0.01	0.3
51	51	20723.68156	-0.00288	0.01	-0.3
50	50	20726.38306	0.00284	0.01	0.3
49	49	20729.02562	0.0023	0.01	0.2
48	48	20731.6172	0.00344	0.01	0.3
47	47	20734.15557	0.00405	0.01	0.4
46	46	20736.64116	0.00456	0.01	0.5
45	45	20739.07395	0.00493	0.01	0.5
44	44	20741.45293	0.00418	0.01	0.4
43	43	20743.78039	0.00458	0.01	0.5
42	42	20746.05453	0.00435	0.01	0.4
41	41	20748.27623	0.00438	0.01	0.4
40	40	20750.44671	0.00589	0.01	0.6
39	39	20752.56196	0.00487	0.01	0.5
38	38	20754.62387	0.00322	0.01	0.3
37	37	20756.63467	0.00319	0.01	0.3
36	36	20758.59229	0.00272	0.01	0.3
35	35	20760.49748	0.00255	0.01	0.3
34	34	20762.34879	0.00126	0.01	0.1
33	33	20764.1473	-0.00007	0.01	0.0
32	32	20765.89416	-0.00027	0.01	0.0
31	31	20767.58878	0.00007	0.01	0.0
30	30	20769.22818	-0.00201	0.01	-0.2
29	29	20770.83187	0.013	0.01	1.3
28	28	20772.32793	-0.0268	0.01	-2.7
27	27	20773.83416	-0.00359	0.01	-0.4
26	26	20775.26274	-0.0052	0.01	-0.5
25	25	20776.64019	-0.00508	0.01	-0.5
24	24	20777.96342	-0.00632	0.01	-0.6
23	23	20779.23309	-0.00824	0.01	-0.8
21	21	20781.58843	-0.0374	10.01	0.0
20	20	20782.68779	-0.05093	10.01	0.0
19	19	20783.76165	-0.03705	10.01	0.0
18	18	20784.81301	0.00727	0.01	0.7
17	17	20785.761	0.00115	0.01	0.1
16	16	20786.67531	0.01431	0.01	1.4
15	15	20787.49186	-0.01734	0.01	-1.7
14	14	20788.28814	-0.01629	0.01	-1.6
13	13	20789.02307	-0.02361	0.01	-2.4
12	12	20789.72166	-0.01429	0.01	-1.4
11	11	20790.35124	-0.02099	0.01	-2.1
10	10	20790.93353	-0.02198	0.01	-2.2
9	9	20791.46313	-0.02265	0.01	-2.3
8	8	20791.95898	-0.00407	0.01	-0.4
7	7	20792.37708	-0.01022	0.01	-1.0
6	6	20792.74696	-0.01156	0.01	-1.2
5	5	20793.06297	-0.01376	0.01	-1.4
4	4	20793.32644	-0.01546	0.01	-1.5
$D(0,1)$ Band, R Branch (p' = e, p'' = e)					
69	68	19673.86546	0.02945	0.05	0.6
67	66	19678.98426	0.04338	0.05	0.9
64	63	19686.17348	-0.06153	0.05	-1.2
63	62	19688.49039	-0.0789	0.05	-1.6
61	60	19692.98991	-0.10193	0.05	-2.0
60	59	19695.20452	-0.07549	0.05	-1.5

Table B.1, Electronic Data of ^{184}WO Relative to X0$^+$ (*Cont'd*)

J'	J''	Obs	Obs-Calc	Unc	(Obs-Calc)/Unc
59	58	19697.36315	-0.05622	0.05	-1.1
58	57	19699.48805	-0.02182	0.05	-0.4
57	56	19701.54452	-0.00694	0.05	-0.1
56	55	19703.5211	-0.02301	0.05	-0.5
55	54	19705.50785	0.02008	0.05	0.4
54	53	19707.3816	-0.00079	0.05	0.0
53	52	19709.23209	0.00415	0.05	0.1
52	51	19711.08018	0.05579	0.05	1.1
51	50	19712.83619	0.0645	0.05	1.3
50	49	19714.59055	0.12074	0.05	2.4
49	48	19716.1473	0.02857	0.05	0.6
47	46	19719.1001	-0.16871	0.05	-3.4
$D(0,1)$ Band, P Branch (p' = e, p'' = e)					
14	15	19718.71433	0.01309	0.05	0.3
16	17	19715.51958	0.00592	0.05	0.1
17	18	19713.85652	0.01073	0.05	0.2
19	20	19710.35638	-0.00559	0.05	-0.1
21	22	19708.55879	1.87802	10.05	0.2
22	23	19704.76042	-0.00577	0.05	-0.1
23	24	19702.81344	0.01114	0.05	0.2
24	25	19700.78034	-0.00878	0.05	-0.2
25	26	19698.72687	0.0002	0.05	0.0
26	27	19696.62002	0.00507	0.05	0.1
27	28	19694.46303	0.00904	0.05	0.2
28	29	19692.25376	0.00997	0.05	0.2
29	30	19690.02021	0.03583	0.05	0.7
30	31	19687.69813	0.02235	0.05	0.4
31	32	19685.33392	0.01593	0.05	0.3
32	33	19682.91678	0.00574	0.05	0.1
33	34	19680.47054	0.0156	0.05	0.3
34	35	19677.96515	0.01543	0.05	0.3
35	36	19675.40315	0.00776	0.05	0.2
$D(0,1)$ Band, Q Branch (p' = f, p'' = e)					
49	49	19676.39885	-0.00385	0.005	-0.8
48	48	19678.79401	-0.00079	0.005	-0.2
47	47	19681.13809	-0.0003	0.005	-0.1
45	45	19685.68776	0.00777	0.005	1.6
44	44	19687.87871	0.00076	0.005	0.2
43	43	19690.02021	-0.00712	0.005	-1.4
42	42	19692.12828	0.00016	0.005	0.0
41	41	19694.19001	0.00971	0.005	1.9
40	40	19696.1846	0.00075	0.005	0.2
39	39	19698.13281	-0.00594	0.005	-1.2
38	38	19700.04729	0.0023	0.005	0.5
37	37	19701.91078	0.00822	0.005	1.6
36	36	19703.70709	-0.00434	0.005	-0.9
35	35	19705.46511	-0.00649	0.005	-1.3
34	34	19707.18582	0.00277	0.005	0.6
33	33	19708.83363	-0.01213	0.005	-2.4
32	32	19710.45288	-0.00685	0.005	-1.4
30	30	19713.54688	0.00552	0.005	1.1
29	29	19715.01072	0.00172	0.005	0.3
28	28	19716.43838	0.01054	0.005	2.1
27	27	19717.83093	0.03306	10.005	0.0
$D(1,0)$ Band, Q Branch (p' = f, p'' = e)					

Table B.1, Electronic Data of ^{184}WO Relative to X0$^+$ (*Cont'd*)

J'	J''	Obs	Obs-Calc	Unc	(Obs-Calc)/Unc
54	54	21691.9005	-0.06123	10.01	0.0
53	53	21694.90002	-0.0317	0.01	-3.2
52	52	21697.84662	-0.00753	0.01	-0.8
51	51	21700.73299	0.00541	0.01	0.5
50	50	21703.56642	0.01572	0.01	1.6
49	49	21706.33965	0.01735	0.01	1.7
48	48	21709.06029	0.01898	0.01	1.9
47	47	21711.72439	0.01764	0.01	1.8
46	46	21714.33639	0.01866	0.01	1.9
45	45	21716.87896	0.00546	0.01	0.5
44	44	21719.37633	0.00298	0.01	0.3
43	43	21721.81266	-0.00404	0.01	-0.4
42	42	21724.19241	-0.01061	0.01	-1.1
41	41	21726.51153	-0.02035	0.01	-2.0
40	40	21728.78081	-0.0221	0.01	-2.2
37	37	21735.24386	-0.02252	0.01	-2.3
36	36	21737.2668	-0.03696	0.01	-3.7
35	35	21739.26426	-0.01816	0.01	-1.8
34	34	21741.18812	-0.01424	0.01	-1.4
33	33	21743.05947	-0.00413	0.01	-0.4
32	32	21744.87158	0.00536	0.01	0.5
31	31	21746.62844	0.01813	0.01	1.8
30	30	21748.32853	0.03251	0.01	3.3
29	29	21749.97199	0.04847	0.01	4.8
28	28	21751.55518	0.06218	10.01	0.0
27	27	21753.08171	0.07703	10.01	0.0
26	26	21754.56193	0.10312	10.01	0.0
25	25	21755.97746	0.12183	10.01	0.0
24	24	21757.33766	0.14222	10.01	0.0
23	23	21758.64131	0.16281	10.01	0.0
22	22	21759.88739	0.18228	10.01	0.0
21	21	21761.07877	0.2032	10.01	0.0
20	20	21762.21048	0.22028	10.01	0.0
19	19	21763.28853	0.23924	10.01	0.0
18	18	21764.3103	0.25714	10.01	0.0
17	17	21765.27424	0.27214	10.01	0.0
16	16	21766.18175	0.28533	10.01	0.0
15	15	21767.0313	0.29488	10.01	0.0
$D(1,0)$ Band, P Branch (p' = e, p'' = e)					
39	40	21695.12829	-0.02094	0.01	-2.1
38	39	21698.20284	-0.00561	0.01	-0.6
37	38	21701.18515	-0.02537	0.01	-2.5
33	34	21712.64533	-0.00234	0.01	-0.2
32	33	21715.35362	-0.01062	0.01	-1.1
31	32	21718.02472	0.00097	0.01	0.1
30	31	21720.62464	-0.00155	0.01	-0.2
29	30	21723.17365	0.00208	0.01	0.2
28	29	21725.65987	-0.00003	0.01	0.0
26	27	21730.46808	0.00269	0.01	0.3
25	26	21732.80804	0.02548	0.01	2.5
23	24	21737.2668	0.0211	0.01	2.1
22	23	21739.39897	0.00729	0.01	0.7
21	22	21741.46629	-0.01429	0.01	-1.4
20	21	21743.52365	0.01125	0.01	1.1
19	20	21745.49184	0.0047	0.01	0.5
18	19	21747.40598	0.0012	0.01	0.1

Table B.1, Electronic Data of ^{184}WO Relative to X0$^+$ (*Cont'd*)

J'	J''	Obs	Obs-Calc	Unc	(Obs-Calc)/Unc
17	18	21749.27164	0.00632	0.01	0.6
16	17	21751.09258	0.02383	0.01	2.4
15	16	21752.7929	-0.02217	0.01	-2.2
14	15	21754.48138	-0.02287	0.01	-2.3
13	14	21756.13054	-0.00576	0.01	-0.6
12	13	21757.69327	-0.01793	0.01	-1.8
11	12	21759.21545	-0.01349	0.01	-1.3
10	11	21760.68201	-0.00751	0.01	-0.8
9	10	21762.08556	-0.00736	0.01	-0.7
8	9	21763.42937	-0.00977	0.01	-1.0
7	8	21764.72624	-0.00192	0.01	-0.2
6	7	21765.9535	-0.00648	0.01	-0.6
5	6	21767.13865	0.00406	0.01	0.4
3	4	21769.31368	0.00155	0.01	0.2
2	3	21770.30839	-0.00667	0.01	-0.7
1	2	21771.26071	-0.00002	0.01	0.0
$D(1,0)$ Band, R Branch (p' = e, p'' = e)					
1	0	21773.75403	-0.00018	0.01	0.0
2	1	21774.47349	0.00266	0.01	0.3
3	2	21775.1337	0.00353	0.01	0.4
4	3	21775.73639	0.00417	0.01	0.4
5	4	21776.28348	0.0065	0.01	0.6
6	5	21776.77151	0.00706	0.01	0.7
7	6	21777.19954	0.00493	0.01	0.5
9	8	21777.87487	-0.00814	0.01	-0.8
10	9	21778.1382	-0.00304	0.01	-0.3
11	10	21778.35491	0.01276	0.01	1.3
12	11	21778.48797	0.00223	0.01	0.2
13	12	21778.58336	0.01136	0.01	1.1
21	20	21777.19954	0.00165	0.01	0.2
22	21	21776.77151	0.00347	0.01	0.3
23	22	21776.28348	0.00265	0.01	0.3
24	23	21775.73639	0.00015	0.01	0.0
25	24	21775.1337	-0.00058	0.01	-0.1
26	25	21774.47349	-0.00143	0.01	-0.1
27	26	21773.75403	-0.00415	0.01	-0.4
28	27	21772.97829	-0.00574	0.01	-0.6
30	29	21771.26071	-0.00277	0.01	-0.3
31	30	21770.30839	-0.00866	0.01	-0.9
34	33	21767.13865	0.00563	0.01	0.6
35	34	21765.9535	-0.0032	0.01	-0.3
36	35	21764.72624	0.00338	0.01	0.3
37	36	21763.42937	-0.00211	0.01	-0.2
38	37	21762.08556	0.00302	0.01	0.3
39	38	21760.68201	0.00601	0.01	0.6
40	39	21759.21545	0.0036	0.01	0.4
41	40	21757.69327	0.00323	0.01	0.3
42	41	21756.13054	0.01999	0.01	2.0
43	42	21754.48138	0.00804	0.01	0.8
44	43	21752.7929	0.01454	0.01	1.5
45	44	21751.02382	-0.00177	0.01	-0.2
46	45	21749.2072	-0.00776	0.01	-0.8
47	46	21747.3388	-0.00763	0.01	-0.8
48	47	21745.41387	-0.00609	0.01	-0.6
49	48	21743.44175	0.00628	0.01	0.6
52	51	21737.14749	0.01415	0.01	1.4
54	53	21732.62654	-0.0141	0.01	-1.4

Table B.1, Electronic Data of ^{184}WO Relative to X0$^+$ (*Cont'd*)

J'	J''	Obs	Obs-Calc	Unc	(Obs-Calc)/Unc
56	55	21727.91622	0.00205	0.01	0.2
57	56	21725.47625	0.0132	0.091	0.1
$F(0,0)$ Band, P Branch (p' = e, p'' = e)					
32	33	23340.15486	0.00389	0.005	0.8
31	32	23343.01871	0.00323	0.005	0.6
30	31	23345.81518	-0.00101	0.005	-0.2
29	30	23348.55681	0.00368	0.005	0.7
28	29	23351.21465	-0.01169	10.005	0.0
27	28	23353.84196	0.00611	0.005	1.2
26	27	23356.3804	-0.00129	0.005	-0.3
25	26	23358.86339	-0.0005	0.005	-0.1
24	25	23361.28677	0.00431	0.005	0.9
23	24	23363.64239	0.00495	0.005	1.0
22	23	23365.93703	0.00819	0.005	1.6
21	22	23368.15973	0.00305	0.005	0.6
20	21	23370.32241	0.00143	0.005	0.3
19	20	23372.42077	-0.00098	0.005	-0.2
18	19	23374.45969	0.00068	0.005	0.1
17	18	23376.43298	0.00023	0.005	0.0
16	17	23378.34506	0.00205	0.005	0.4
15	16	23380.19253	0.00276	0.005	0.6
14	15	23381.97155	-0.0015	0.005	-0.3
13	14	23383.69285	-0.00001	0.005	0.0
11	12	23386.93774	-0.00432	0.005	-0.9
10	11	23388.46957	-0.00189	0.005	-0.4
9	10	23389.9331	-0.0043	0.005	-0.9
$F(0,0)$ Band, R Branch (p' = e, p'' = e)					
10	9	23405.90259	-0.0206	10.005	0.0
11	10	23406.05816	0.00289	0.005	0.6
12	11	23406.12182	-0.00192	0.005	-0.4
13	12	23406.12182	-0.00674	0.005	-1.3
14	13	23406.05816	-0.01157	0.005	-2.3
15	14	23405.94902	0.00179	0.005	0.4
16	15	23405.74193	-0.01911	10.005	0.0
17	16	23405.50995	-0.00118	0.005	-0.2
18	17	23405.20021	0.00271	0.005	0.5
19	18	23404.8174	-0.00272	0.005	-0.5
20	19	23404.37941	0.00046	0.005	0.1
21	20	23403.87516	0.00117	0.005	0.2
22	21	23403.30669	0.00148	0.005	0.3
23	22	23402.67348	0.00091	0.005	0.2
24	23	23401.97998	0.00394	0.005	0.8
25	24	23401.21548	-0.00013	0.005	0.0
26	25	23400.39532	0.0041	0.005	0.8
27	26	23399.50533	0.00247	0.005	0.5
28	27	23398.54728	-0.00319	0.005	-0.6
29	28	23397.53451	0.00049	0.005	0.1
30	29	23396.45224	-0.00124	0.005	-0.2
31	30	23395.30801	-0.00078	0.005	-0.2
32	31	23394.10034	0.00044	0.005	0.1
33	32	23392.83055	0.00377	0.005	0.8
35	34	23390.08584	-0.00174	0.005	-0.3
36	35	23388.61502	-0.00637	0.005	-1.3
37	36	23387.08151	-0.00923	0.005	-1.8
38	37	23385.50954	0.014	10.005	0.0
39	38	23383.83248	-0.00325	0.005	-0.6

Table B.1, Electronic Data of ^{184}WO Relative to X0$^+$ (*Cont'd*)

J'	J''	Obs	Obs-Calc	Unc	(Obs-Calc)/Unc
41	40	23380.31118	-0.0108	0.005	-2.2
42	41	23378.4593	-0.00857	0.005	-1.7
43	42	23376.54314	-0.0057	0.005	-1.1
44	43	23374.5653	0.00052	0.005	0.1
45	44	23372.51831	0.00271	0.005	0.5
46	45	23370.40608	0.00488	0.005	1.0
47	46	23368.23312	0.01165	0.005	2.3

B.2 Electronic Data for WO with Respect to X1

Table B.2: Electronic Data of ^{184}WO Relative to X1 (v=0)

J'	J''	Obs	Obs-Calc	Unc	(Obs-Calc)/Unc
$D'(0,0)$ Band, P Branch (p' = f, p'' = f)					
41	42	21132.17801	0.00932	0.005	1.9
40	41	21135.63723	0.00372	0.005	0.7
39	40	21139.03669	0.00292	0.005	0.6
38	39	21142.35947	-0.00999	0.005	-2.0
37	38	21145.62905	-0.01155	10.005	0.0
36	37	21148.8383	-0.00889	0.005	-1.8
35	36	21151.97944	-0.00982	0.005	-2.0
34	35	21155.07209	0.00527	0.005	1.1
33	34	21158.07646	-0.00342	0.005	-0.7
32	33	21161.02802	-0.00044	0.005	-0.1
31	32	21163.90946	-0.00312	0.005	-0.6
30	31	21166.74172	0.00946	0.005	1.9
29	30	21169.50028	0.01277	10.005	0.0
28	29	21172.1765	-0.00187	0.005	-0.4
27	28	21174.81752	0.01268	10.005	0.0
26	27	21177.37316	0.00621	0.005	1.2
25	26	21179.86529	0.00057	0.005	0.1
24	25	21182.3049	0.00672	0.005	1.3
23	24	21184.66643	-0.00091	0.005	-0.2
22	23	21186.97285	0.00061	0.005	0.1
21	22	21189.21824	0.00536	0.005	1.1
20	21	21191.38881	-0.00048	0.005	-0.1
19	20	21193.50085	-0.00065	0.005	-0.1
18	19	21195.54523	-0.00429	0.005	-0.9
17	18	21197.53018	-0.0032	0.005	-0.6
16	17	21199.4487	-0.0044	0.005	-0.9
15	16	21201.30628	-0.00241	0.005	-0.5
14	15	21203.09749	-0.00268	0.005	-0.5
13	14	21204.82698	-0.00059	0.005	-0.1
12	13	21206.48829	-0.00262	0.005	-0.5
11	12	21208.08691	-0.00328	0.005	-0.7
10	11	21209.63791	0.01248	10.005	0.0
9	10	21211.10401	0.00735	0.005	1.5
8	9	21212.49065	-0.01323	10.005	0.0
7	8	21213.85412	0.00701	0.005	1.4
6	7	21215.12067	-0.00569	0.005	-1.1
5	6	21216.32129	-0.02034	10.005	0.0
$D'(0,0)$ Band, R Branch (p' = f, p'' = f)					
27	26	21220.5219	-0.02247	10.005	0.0
28	27	21219.56974	-0.01085	0.005	-2.2
29	28	21218.53742	-0.01485	10.005	0.0
30	29	21217.43099	-0.02837	10.005	0.0
31	30	21216.28459	-0.01723	10.005	0.0
32	31	21215.06863	-0.01098	0.005	-2.2
33	32	21213.79008	-0.0026	0.005	-0.5
34	33	21212.43465	-0.00633	0.005	-1.3
35	34	21211.02735	0.00288	0.005	0.6
36	35	21209.54512	0.00204	0.005	0.4
37	36	21208.0006	0.00383	0.005	0.8
38	37	21206.38976	0.00427	0.005	0.9
39	38	21204.71416	0.00497	0.005	1.0

Table B.2, Electronic Data of ^{184}WO Relative to X1 (*Cont'd*)

J'	J''	Obs	Obs-Calc	Unc	(Obs-Calc)/Unc
40	39	21202.97351	0.0057	0.005	1.1
41	40	21201.16817	0.00688	0.005	1.4
42	41	21199.29369	0.0041	0.005	0.8
43	42	21197.35306	0.00041	0.005	0.1
44	43	21195.35159	0.00118	0.005	0.2
45	44	21193.27761	-0.0052	0.005	-1.0
46	45	21191.14342	-0.00638	0.005	-1.3
47	46	21188.95165	0.00032	0.005	0.1
49	48	21184.35874	0.00098	0.005	0.2
50	49	21181.96361	0.00106	0.005	0.2
51	50	21179.51122	0.00957	0.005	1.9
52	51	21176.9735	-0.00149	0.005	-0.3
53	52	21174.37251	-0.01003	0.005	-2.0
$D'(0,0)$ Band, P Branch (p' = e, p'' = e)					
41	42	21134.51977	-0.00556	0.005	-1.1
40	41	21137.87882	0.00055	0.005	0.1
39	40	21141.17772	0.00872	0.005	1.7
38	39	21144.55416	0.15659	10.005	0.0
37	38	21147.56358	-0.0005	0.005	-0.1
36	37	21150.66131	-0.00726	0.005	-1.5
35	36	21153.71607	0.00495	0.005	1.0
34	35	21156.69663	0.00485	0.005	1.0
33	34	21159.60946	-0.00115	0.005	-0.2
32	33	21162.47513	0.00746	0.005	1.5
31	32	21165.2645	0.00149	0.005	0.3
30	31	21167.9994	0.00274	0.005	0.5
29	30	21170.66747	-0.00121	0.005	-0.2
28	29	21173.27585	-0.00325	0.005	-0.7
27	28	21175.82431	-0.00366	0.005	-0.7
26	27	21178.3042	-0.01112	0.005	-2.2
25	26	21180.73359	-0.00759	0.005	-1.5
24	25	21183.10435	-0.00123	0.005	-0.2
23	24	21185.41146	0.00291	0.005	0.6
22	23	21187.6546	0.00448	0.005	0.9
21	22	21189.82938	-0.00093	0.005	-0.2
20	21	21191.94314	-0.006	0.005	-1.2
19	20	21194.00259	-0.00404	0.005	-0.8
18	19	21196.00025	-0.00255	0.005	-0.5
17	18	21197.94181	0.00415	0.005	0.8
16	17	21199.81337	0.00215	0.005	0.4
15	16	21201.62247	-0.00104	0.005	-0.2
14	15	21203.37579	0.00126	0.005	0.3
13	14	21205.06311	-0.00118	0.005	-0.2
12	13	21206.69907	0.00628	0.005	1.3
11	12	21208.25579	-0.00425	0.005	-0.9
10	11	21209.76149	-0.00457	0.005	-0.9
9	10	21211.23055	0.01972	10.005	0.0
8	9	21212.60259	0.00822	0.005	1.6
7	8	21213.8671	-0.04957	10.005	0.0
6	7	21215.18744	0.00971	0.005	1.9
5	6	21216.37345	-0.00411	0.005	-0.8
4	5	21217.52071	0.00456	0.005	0.9
3	4	21218.60584	0.01234	0.005	2.5
2	3	21219.62946	0.01986	10.005	0.0
1	2	21220.5853	0.02085	10.005	0.0
$D'(0,0)$ Band, R Branch (p' = e, p'' = e)					

Table B.2, Electronic Data of ^{184}WO Relative to X1 (*Cont'd*)

J'	J''	Obs	Obs-Calc	Unc	(Obs-Calc)/Unc
2	1	21223.77542	0.00422	0.005	0.8
3	2	21224.44895	0.02927	10.005	0.0
4	3	21225.0236	0.01673	10.005	0.0
5	4	21225.51722	-0.01553	10.005	0.0
6	5	21225.96807	-0.02925	10.005	0.0
7	6	21226.34291	-0.05764	10.005	0.0
8	7	21226.78198	0.03955	10.005	0.0
9	8	21226.92233	-0.10064	10.005	0.0
10	9	21227.2647	0.02257	10.005	0.0
11	10	21227.26503	-0.13488	10.005	0.0
14	13	21227.47662	-0.02817	10.005	0.0
15	14	21227.42014	0.00326	0.005	0.7
16	15	21227.26503	-0.00247	0.005	-0.5
17	16	21227.07833	0.02168	10.005	0.0
18	17	21226.77546	-0.00883	0.005	-1.8
19	18	21226.42945	-0.02097	10.005	0.0
20	19	21226.05271	-0.0023	0.005	-0.5
21	20	21225.59234	-0.0057	0.005	-1.1
22	21	21225.0962	0.0167	10.005	0.0
24	23	21223.85224	-0.00533	0.005	-1.1
25	24	21223.1492	-0.00495	0.005	-1.0
26	25	21222.39242	0.00336	0.005	0.7
27	26	21221.5685	0.00623	0.005	1.2
28	27	21220.67213	-0.00163	0.005	-0.3
29	28	21219.71222	-0.01129	0.005	-2.3
30	29	21218.71036	-0.00111	0.005	-0.2
31	30	21217.64033	0.0027	0.005	0.5
32	31	21216.50725	0.00529	0.005	1.1
33	32	21215.306	0.00159	0.005	0.3
34	33	21214.04796	0.00299	0.005	0.6
35	34	21212.72377	0.00017	0.005	0.0
36	35	21211.33515	-0.00512	0.005	-1.0
37	36	21209.90341	0.00848	0.005	1.7
38	37	21208.39317	0.00562	0.005	1.1
39	38	21206.82148	0.00339	0.005	0.7
40	39	21205.16921	-0.0173	10.005	0.0
41	40	21203.4958	0.00302	0.005	0.6
42	41	21201.74194	0.0051	0.005	1.0
43	42	21199.9173	-0.00135	0.005	-0.3
44	43	21198.0377	-0.00046	0.005	-0.1
45	44	21196.09261	-0.00272	0.005	-0.5
46	45	21194.09183	0.00173	0.005	0.3
47	46	21192.01718	-0.00524	0.005	-1.0
48	47	21189.88789	-0.00435	0.005	-0.9
49	48	21187.72097	0.02148	10.005	0.0
$New(0^+,0)$ Band, R Branch (p' = e, p'' = e)					
15	14	19444.68988	-0.01898	10.005	0.0
16	15	19444.54223	-0.01204	0.005	-2.4
17	16	19444.3395	0.00164	0.005	0.3
18	17	19444.04681	-0.0128	0.005	-2.6
19	18	19443.71722	-0.00227	0.005	-0.5
20	19	19443.31572	-0.00177	0.005	-0.4
21	20	19442.85396	0.00039	0.005	0.1
22	21	19442.34854	0.02082	10.005	0.0
23	22	19441.74759	0.00769	0.005	1.5
24	23	19441.08551	-0.00459	0.005	-0.9

Table B.2, Electronic Data of ^{184}WO Relative to X1 (*Cont'd*)

J'	J''	Obs	Obs-Calc	Unc	(Obs-Calc)/Unc
25	24	19440.38626	0.00798	0.005	1.6
40	39	19422.16801	-0.07175	10.005	0.0
41	40	19420.45263	-0.07917	10.005	0.0
42	41	19418.68789	-0.07346	10.005	0.0
43	42	19416.84589	-0.08248	10.005	0.0
44	43	19414.97736	-0.05549	10.005	0.0
45	44	19413.00928	-0.06547	10.005	0.0
46	45	19411.00036	-0.05371	10.005	0.0
47	46	19408.90314	-0.06764	10.005	0.0
48	47	19406.78856	-0.03629	10.005	0.0
49	48	19404.57548	-0.0408	10.005	0.0
50	49	19402.31128	-0.03377	10.005	0.0
52	51	19397.57655	-0.038	10.005	0.0
53	52	19395.15145	-0.00381	0.005	-0.8
54	53	19392.62042	-0.01285	0.005	-2.6
55	54	19390.04085	-0.00773	0.005	-1.5
56	55	19387.4045	0.00332	0.005	0.7
57	56	19384.7029	0.01183	10.005	0.0
58	57	19381.90211	-0.01616	10.005	0.0
59	58	19379.11206	0.0293	10.005	0.0
60	59	19376.23276	0.04818	10.005	0.0
61	60	19373.27823	0.0545	10.005	0.0
$New(0^+,0)$ Band, P Branch (p' = e, p'' = e)					
7	8	19431.25959	0.02383	0.005	4.8
8	9	19429.91092	0.00052	0.005	0.1
9	10	19428.53067	0.00726	0.005	1.5
10	11	19427.05503	-0.01978	90.005	0.0
11	12	19425.55228	-0.01229	90.005	0.0
12	13	19424.00531	0.01261	0.005	2.5
13	14	19422.34625	-0.01294	0.005	-2.6
14	15	19420.6563	-0.00773	0.005	-1.5
15	16	19418.91042	0.00321	10.005	0.0
16	17	19417.10596	0.01722	0.005	3.4
17	18	19415.21535	0.00675	0.005	1.4
18	19	19413.27759	0.01082	0.005	2.2
19	20	19411.25981	-0.00346	0.005	-0.7
20	21	19409.19121	-0.00685	0.005	-1.4
21	22	19407.06266	-0.0085	0.005	-1.7
22	23	19404.88182	-0.00073	0.005	-0.1
23	24	19402.64031	0.00809	0.005	1.6
24	25	19400.31484	-0.00532	0.005	-1.1
25	26	19397.95695	0.01058	10.005	0.0
26	27	19395.50027	-0.01058	0.005	-2.1
30	31	19385.13203	-0.01921	10.005	0.0
31	32	19382.40614	-0.0008	0.005	-0.2
32	33	19379.61189	0.01101	10.005	0.0
33	34	19376.75337	0.02031	10.005	0.0
34	35	19373.82758	0.02411	10.005	0.0
35	36	19370.81179	-0.00034	10.005	0.0
36	37	19367.80193	0.0429	90.005	0.0
37	38	19364.65553	0.01134	10.005	0.0
38	39	19361.50829	0.04069	90.005	0.0
39	40	19358.25571	0.02642	10.005	0.0
40	41	19354.9536	0.02434	10.005	0.0
41	42	19351.55556	-0.01197	0.005	-2.4
42	43	19348.1453	0.00118	0.005	0.2
43	44	19344.67003	0.01099	10.005	0.0

Table B.2, Electronic Data of ^{184}WO Relative to X1 (*Cont'd*)

J'	J''	Obs	Obs-Calc	Unc	(Obs-Calc)/Unc
44	45	19341.10392	-0.0084	0.005	-1.7
45	46	19337.51256	0.00857	0.005	1.7
46	47	19333.84275	0.00868	0.005	1.7
47	48	19330.10374	0.00114	0.005	0.2
48	49	19326.32588	0.01627	10.005	0.0
49	50	19322.46624	0.01109	0.005	2.2
50	51	19318.55054	0.01129	10.005	0.0
51	52	19314.56311	0.00114	0.005	0.2
52	53	19310.53087	0.00751	0.005	1.5
53	54	19306.43258	0.00911	0.005	1.8
54	55	19302.2603	-0.00206	0.005	-0.4
55	56	19298.03644	-0.00367	0.005	-0.7
56	57	19293.75562	-0.00116	0.005	-0.2
57	58	19289.3967	-0.01575	10.005	0.0
$New(0^+,0)$ Band, Q Branch (p' = e, p'' = f)					
2	2	19439.44034	0.00373	0.005	0.7
3	3	19439.24802	-0.00458	0.005	-0.9
4	4	19439.01049	0.00324	0.005	0.6
5	5	19438.68087	-0.01969	10.005	0.0
6	6	19438.33044	-0.00208	0.005	-0.4
7	7	19437.90162	-0.00152	0.005	-0.3
8	8	19437.41107	-0.00134	0.005	-0.3
9	9	19436.88523	0.02491	10.005	0.0
10	10	19436.24419	-0.00268	0.005	-0.5
11	11	19435.56611	-0.00595	0.005	-1.2
12	12	19434.83648	0.00059	0.005	0.1
13	13	19434.05016	0.01182	0.005	2.4
14	14	19433.16954	-0.00986	0.005	-2.0
15	15	19432.24247	-0.01662	10.005	0.0
16	16	19431.25959	-0.01778	10.005	0.0
17	17	19430.22684	-0.00742	0.005	-1.5
18	18	19429.13063	0.00089	0.005	0.2
19	19	19427.9545	-0.00929	0.005	-1.9
20	20	19426.73776	0.00134	0.005	0.3
21	21	19425.45961	0.01199	0.005	2.4
22	22	19424.09078	-0.00659	0.005	-1.3
23	23	19422.68398	-0.00168	0.005	-0.3
24	24	19421.21396	0.00148	0.005	0.3
25	25	19419.67706	-0.00077	0.005	-0.2
26	26	19418.07911	-0.00257	0.005	-0.5
27	27	19416.42054	-0.0035	0.005	-0.7
28	28	19414.70698	0.0021	0.005	0.4
29	29	19412.92121	-0.00298	0.005	-0.6
30	30	19411.07321	-0.00876	0.005	-1.8
31	31	19409.19121	0.01302	0.005	2.6
32	32	19407.21109	-0.00175	0.005	-0.4
33	33	19405.18678	0.00087	0.005	0.2
34	34	19403.11466	0.01727	10.005	0.0
35	35	19400.94785	0.00059	0.005	0.1
36	36	19398.7334	-0.0021	0.005	-0.4
38	38	19394.12695	-0.00009	0.005	0.0
39	39	19391.73064	0.00033	0.005	0.1
40	40	19389.28019	0.0083	0.005	1.7
41	41	19386.74554	-0.00622	0.005	-1.2
42	42	19384.16855	-0.00135	0.005	-0.3
43	43	19381.52826	0.00195	0.005	0.4
44	44	19378.82311	0.00215	0.005	0.4

Table B.2, Electronic Data of ^{184}WO Relative to X1 (*Cont'd*)

J'	J''	Obs	Obs-Calc	Unc	(Obs-Calc)/Unc
46	46	19373.22617	0.00127	0.005	0.3
47	47	19370.31772	-0.01644	10.005	0.0
48	48	19367.38492	0.00333	0.005	0.7
49	49	19364.37662	0.00945	0.005	1.9
50	50	19361.31433	0.02346	10.005	0.0
51	51	19358.18195	0.02926	10.005	0.0
52	52	19354.9536	0.001	0.005	0.2
53	53	19351.70231	0.01173	0.005	2.3
54	54	19348.35817	-0.00844	0.005	-1.7
55	55	19344.98335	0.00267	0.005	0.5
56	56	19341.52184	-0.01091	0.005	-2.2
57	57	19338.00437	-0.01845	10.005	0.0
58	58	19334.44139	-0.00947	0.005	-1.9
59	59	19330.81144	-0.00541	0.005	-1.1
60	60	19327.12191	0.00114	0.005	0.2
61	61	19323.37163	0.00902	0.005	1.8
62	62	19319.54108	-0.00125	0.005	-0.2
63	63	19315.65526	-0.00466	0.005	-0.9
64	64	19311.71687	0.00151	0.005	0.3
65	65	19307.70652	-0.00211	0.005	-0.4
66	66	19303.64016	0.00046	0.005	0.1
67	67	19299.50681	-0.00175	0.005	-0.4
68	68	19295.32008	0.00489	0.005	1.0
69	69	19291.06367	0.0041	0.005	0.8
70	70	19286.73923	-0.00244	0.005	-0.5
$New(0^+,1)$ Band, R Branch (p' = e, p'' = e)					
16	15	18385.10515	-0.00034	0.003	-0.1
17	16	18384.95636	0.00335	0.003	1.1
18	17	18384.75507	0.01232	90.003	0.0
19	18	18384.48229	0.00761	0.003	2.5
20	19	18384.13255	-0.01624	90.003	0.0
22	21	18383.32643	0.00292	0.003	1.0
23	22	18382.82775	0.00367	0.003	1.2
24	23	18382.27415	0.00737	0.003	2.5
25	24	18381.65894	0.00735	0.003	2.5
26	25	18380.98264	0.00416	0.003	1.4
27	26	18380.25181	0.00436	0.003	1.5
28	27	18379.46827	0.00979	10.003	0.0
29	28	18378.60858	-0.00297	0.003	-1.0
30	29	18377.7104	0.00377	0.003	1.3
31	30	18376.7552	0.01148	10.003	0.0
32	31	18375.71864	-0.00415	0.003	-1.4
33	32	18374.6403	-0.00352	0.003	-1.2
34	33	18373.49998	-0.00682	0.003	-2.3
35	34	18372.32281	0.01112	10.003	0.0
36	35	18371.06223	0.00374	0.003	1.2
37	36	18369.73749	-0.00968	90.003	0.0
38	37	18368.37959	0.00188	0.003	0.6
39	38	18366.9477	-0.00239	0.003	-0.8
40	39	18365.47265	0.00837	0.003	2.8
41	40	18363.92806	0.00779	0.003	2.6
42	41	18362.31693	-0.0011	0.003	-0.4
43	42	18360.64989	-0.00765	0.003	-2.6
44	43	18358.93336	-0.00542	0.003	-1.8
45	44	18357.17199	0.01027	10.003	0.0
46	45	18355.33836	0.01201	10.003	0.0
47	46	18353.44073	0.00809	0.005	1.6

Table B.2, Electronic Data of ^{184}WO Relative to X1 (*Cont'd*)

J'	J''	Obs	Obs-Calc	Unc	(Obs-Calc)/Unc
48	47	18351.47698	-0.00358	0.003	-1.2
49	48	18349.47164	0.00154	0.003	0.5
50	49	18347.40098	-0.00025	0.003	-0.1
51	50	18345.27474	0.00081	0.003	0.3
52	51	18343.08726	-0.00093	0.003	-0.3
53	52	18340.85813	0.01417	10.003	0.0
54	53	18338.54742	0.00618	0.003	2.1
55	54	18336.19284	0.01283	10.003	0.0
56	55	18333.75501	-0.00523	0.003	-1.7
58	57	18328.75146	0.00646	0.003	2.2
59	58	18326.13977	-0.00972	10.003	0.0
60	59	18323.49711	0.00174	0.003	0.6
61	60	18320.78413	0.00152	0.003	0.5
$New(0^+,1)$ Band, P Branch (p' = e, p'' = e)					
1	2	18377.98278	0.00341	0.003	1.1
2	3	18377.02426	-0.01133	0.003	-3.8
3	4	18376.02229	-0.01188	0.003	-4.0
4	5	18374.93753	-0.03759	90.003	0.0
5	6	18373.85701	-0.00142	0.003	-0.5
6	7	18372.67049	-0.01363	10.003	0.0
7	8	18371.45222	0.00004	0.003	0.0
8	9	18370.1707	0.00808	0.003	2.7
9	10	18368.80705	-0.00838	0.003	-2.8
10	11	18367.41619	0.00556	0.003	1.9
12	13	18364.43065	0.00248	0.003	0.8
13	14	18362.86	0.00949	10.003	0.0
14	15	18361.21265	-0.0026	0.003	-0.9
15	16	18359.52257	0.0002	0.003	0.1
16	17	18357.76799	-0.00389	0.003	-1.3
17	18	18355.96424	0.00046	0.003	0.2
18	19	18354.09861	0.00053	0.003	0.2
19	20	18352.17658	0.00181	0.003	0.6
20	21	18350.19839	0.00453	0.003	1.5
21	22	18348.15539	0.00005	0.003	0.0
22	23	18346.06191	0.00268	0.003	0.9
23	24	18343.89452	-0.01101	10.003	0.0
24	25	18341.69792	0.00369	0.003	1.2
25	26	18339.43101	0.00566	0.003	1.9
26	27	18337.10035	0.00147	0.005	0.3
27	28	18334.73029	0.01545	10.003	0.0
28	29	18332.2687	-0.00451	0.003	-1.5
29	30	18329.7724	-0.00163	0.003	-0.5
30	31	18327.21984	0.00256	0.003	0.9
31	32	18324.60714	0.00417	0.003	1.4
32	33	18321.93188	0.00076	0.003	0.3
33	34	18319.20609	0.00435	0.003	1.5
34	35	18316.41441	-0.00042	0.003	-0.1
35	36	18313.57343	0.00303	0.003	1.0
36	37	18310.67304	0.00458	0.003	1.5
37	38	18307.70899	-0.00004	0.003	0.0
38	39	18304.69231	0.00018	0.003	0.1
39	40	18301.61947	0.00171	0.003	0.6
40	41	18298.48056	-0.00539	0.003	-1.8
41	42	18295.29446	-0.00224	0.003	-0.7
42	43	18292.04515	-0.0049	0.003	-1.6
43	44	18288.72675	-0.01926	10.003	0.0
44	45	18285.37985	-0.00475	0.003	-1.6

Table B.2, Electronic Data of ^{184}WO Relative to X1 (*Cont'd*)

J'	J''	Obs	Obs-Calc	Unc	(Obs-Calc)/Unc
45	46	18281.9432	-0.02265	10.003	0.0
$New(0^+,1)$ Band, Q Branch (p' = e, p'' = f)					
1	1	18379.64503	0.00831	0.003	2.8
2	2	18379.52656	0.00444	0.003	1.5
3	3	18379.34858	-0.00165	0.003	-0.6
4	4	18379.11994	-0.0011	0.003	-0.4
5	5	18378.84417	0.00962	10.003	0.0
6	6	18378.48931	-0.00144	0.003	-0.5
7	7	18378.07674	-0.01291	10.003	0.0
8	8	18377.63023	-0.001	0.003	-0.3
9	9	18377.12416	0.00866	0.003	2.9
10	10	18376.54285	0.00041	0.003	0.1
11	11	18375.91088	-0.00117	0.003	-0.4
12	12	18375.22605	0.00172	0.003	0.6
13	13	18374.48106	0.00179	0.003	0.6
14	14	18373.6792	0.00234	0.003	0.8
15	15	18372.81404	-0.00305	0.003	-1.0
16	16	18371.90324	0.00328	0.003	1.1
17	17	18370.92557	0.00011	0.003	0.0
18	18	18369.89239	-0.00118	0.003	-0.4
19	19	18368.80705	0.00276	0.003	0.9
20	20	18367.65685	-0.00076	0.003	-0.3
21	21	18366.45314	-0.00038	0.003	-0.1
22	22	18365.19318	0.00118	0.003	0.4
23	23	18363.87066	-0.00239	0.003	-0.8
24	24	18362.49457	-0.00209	0.003	-0.7
25	25	18361.05726	-0.00555	0.003	-1.8
26	26	18359.57045	-0.00104	0.005	-0.2
27	27	18358.02198	-0.0007	0.003	-0.2
28	28	18356.41622	-0.00017	0.003	-0.1
29	29	18354.75081	-0.00178	0.003	-0.6
30	30	18353.02615	-0.00513	0.003	-1.7
31	31	18351.2507	-0.00173	0.003	-0.6
32	32	18349.41373	-0.00231	0.003	-0.8
33	33	18347.52363	0.00153	0.003	0.5
34	34	18345.56776	-0.00283	0.003	-0.9
35	35	18343.56031	-0.00118	0.003	-0.4
36	36	18341.4983	0.00349	0.003	1.2
37	37	18339.36818	-0.00234	0.003	-0.8
38	38	18337.18709	-0.00153	0.003	-0.5
39	39	18334.94887	-0.00022	0.003	-0.1
40	40	18332.65816	0.00625	0.003	2.1
41	41	18330.29629	-0.0008	0.003	-0.3
42	42	18327.88878	0.00417	0.003	1.4
43	43	18325.41189	-0.00256	0.003	-0.9
44	44	18322.88839	0.00178	0.003	0.6
45	45	18320.30784	0.00675	0.003	2.3
46	46	18317.66251	0.00465	0.003	1.6
47	47	18314.95924	0.00232	0.003	0.8
48	48	18312.19659	-0.00168	0.003	-0.6
49	49	18309.3883	0.0064	0.003	2.1
50	50	18306.51531	0.00751	0.003	2.5
51	51	18303.57998	0.00401	0.003	1.3
52	52	18300.58301	-0.0034	0.003	-1.1
53	53	18297.54188	0.00278	0.003	0.9
54	54	18294.43806	0.00401	0.003	1.3
55	55	18291.2664	-0.00486	0.003	-1.6

Table B.2, Electronic Data of ^{184}WO Relative to X1 (*Cont'd*)

J'	J''	Obs	Obs-Calc	Unc	(Obs-Calc)/Unc
56	56	18288.0531	0.00237	0.003	0.8
57	57	18284.76389	-0.00857	0.003	-2.9
58	58	18281.43552	-0.00093	0.003	-0.3

Appendix C

Energy Origins of BeH Molecule

The 1814 energy origins of the BeH isotopomers calculated using DSParFit[1] are listed in Appendix C

The 765 energy origins of BeH isotopomer are listed in Table C.1.
The 812 energy origins of BeD isotopomer are listed in Table C.2.
The 237 energy origins of BeT isotopomer are listed in Table C.3.

[1]Robert J. Le Roy, Dept. of Chemistry, University of Waterloo, Waterloo, Ontario N2L 3G1

C.1 Energy Origins of BeH Isotopomer

Table C.1: Energy Origins of "Fluorescence Series" of BeH Isotopomer (cm^{-1})

T(v'	j'	p')	Energy Origin	Uncertainty	Sensitivity
T(0	1	+1)	2.005207400000D+04	(+/- 1.7D-02)	3.3D-04
T(0	1	+1)	3.045208000000D+04	(+/- 2.4D-01)	3.3D-04
T(0	2	-1)	2.009224600000D+04	(+/- 2.4D-02)	4.5D-04
T(0	2	+1)	2.009311100000D+04	(+/- 1.7D-02)	3.3D-04
T(0	2	-1)	3.046615000000D+04	(+/- 2.2D-01)	2.7D-04
T(0	2	+1)	3.046615000000D+04	(+/- 2.2D-01)	2.7D-04
T(0	3	-1)	2.015420100000D+04	(+/- 1.7D-02)	3.3D-04
T(0	3	+1)	2.015477000000D+04	(+/- 1.7D-02)	3.3D-04
T(0	3	-1)	3.048736000000D+04	(+/- 1.9D-01)	1.9D-04
T(0	3	+1)	3.048736000000D+04	(+/- 1.9D-01)	1.9D-04
T(0	4	-1)	2.023649600000D+04	(+/- 1.8D-02)	3.2D-04
T(0	4	+1)	2.023692700000D+04	(+/- 1.8D-02)	3.3D-04
T(0	4	-1)	3.051542000000D+04	(+/- 1.9D-01)	1.9D-04
T(0	4	+1)	3.051542000000D+04	(+/- 1.9D-01)	1.9D-04
T(0	5	-1)	2.033912600000D+04	(+/- 1.9D-02)	3.3D-04
T(0	5	+1)	2.046139200000D+04	(+/- 2.7D-02)	4.6D-04
T(0	5	+1)	2.033946500000D+04	(+/- 1.9D-02)	3.3D-04
T(0	5	-1)	3.055062000000D+04	(+/- 1.8D-01)	1.9D-04
T(0	5	+1)	3.055062000000D+04	(+/- 1.8D-01)	1.9D-04
T(0	6	-1)	2.046198100000D+04	(+/- 2.1D-02)	3.3D-04
T(0	6	+1)	2.060413700000D+04	(+/- 2.9D-02)	4.6D-04
T(0	6	+1)	2.046225300000D+04	(+/- 2.1D-02)	3.3D-04
T(0	6	-1)	3.059273000000D+04	(+/- 1.8D-01)	2.1D-04
T(0	6	+1)	3.059273000000D+04	(+/- 1.8D-01)	2.1D-04
T(0	7	-1)	2.060491500000D+04	(+/- 2.5D-02)	4.1D-04
T(0	7	-1)	2.046168500000D+04	(+/- 2.7D-02)	4.6D-04
T(0	7	+1)	2.076677800000D+04	(+/- 5.1D-02)	9.1D-04
T(0	7	+1)	2.060514300000D+04	(+/- 2.5D-02)	4.1D-04
T(0	7	-1)	3.064182000000D+04	(+/- 1.7D-01)	1.9D-04
T(0	7	+1)	3.064182000000D+04	(+/- 1.7D-01)	1.9D-04
T(0	8	-1)	2.076776400000D+04	(+/- 2.7D-02)	4.1D-04
T(0	8	-1)	2.060438600000D+04	(+/- 2.9D-02)	4.6D-04
T(0	8	+1)	2.094910800000D+04	(+/- 5.2D-02)	9.1D-04
T(0	8	+1)	2.076795400000D+04	(+/- 2.7D-02)	4.1D-04
T(0	8	-1)	3.069788000000D+04	(+/- 1.7D-01)	1.9D-04
T(0	8	+1)	3.069788000000D+04	(+/- 1.7D-01)	1.9D-04
T(0	9	-1)	2.095033700000D+04	(+/- 4.8D-02)	8.4D-04
T(0	9	-1)	2.076698400000D+04	(+/- 5.1D-02)	9.1D-04
T(0	9	+1)	2.115095000000D+04	(+/- 1.1D-01)	2.1D-04
T(0	9	+1)	2.095049200000D+04	(+/- 4.8D-02)	8.4D-04
T(0	9	-1)	3.076079000000D+04	(+/- 1.7D-01)	1.9D-04
T(0	9	+1)	3.076079000000D+04	(+/- 1.7D-01)	1.9D-04
T(0	10	-1)	2.115240800000D+04	(+/- 5.0D-02)	8.4D-04
T(0	10	-1)	2.094928600000D+04	(+/- 5.2D-02)	9.1D-04
T(0	10	+1)	2.137200000000D+04	(+/- 1.1D-01)	2.1D-04
T(0	10	+1)	2.115253300000D+04	(+/- 4.9D-02)	8.3D-04
T(0	10	-1)	3.083059000000D+04	(+/- 1.7D-01)	2.0D-04
T(0	10	+1)	3.083059000000D+04	(+/- 1.7D-01)	2.0D-04
T(0	11	-1)	2.137378000000D+04	(+/- 8.2D-02)	1.5D-04
T(0	11	-1)	2.115108000000D+04	(+/- 1.1D-01)	2.1D-04
T(0	11	+1)	2.161199300000D+04	(+/- 9.2D-02)	1.6D-04
T(0	11	+1)	2.137379800000D+04	(+/- 8.5D-02)	1.5D-04
T(0	11	-1)	3.090714000000D+04	(+/- 1.6D-01)	1.9D-04

Table C.1 Energy origins of "fluorescence series" of BeH isotopomer (cm^{-1}) (*Cont'd*)

T(v'	j'	p')	Energy Origin	Uncertainty	Sensitivity
T(0	11	+1)	3.090714000000D+04	(+/- 1.6D-01)	1.9D-04
T(0	12	-1)	2.161411600000D+04	(+/- 5.6D-02)	8.3D-04
T(0	12	-1)	2.137211000000D+04	(+/- 1.1D-01)	2.1D-04
T(0	12	+1)	2.187080200000D+04	(+/- 5.8D-02)	8.6D-04
T(0	12	+1)	2.161411600000D+04	(+/- 5.6D-02)	8.3D-04
T(0	12	-1)	3.099056000000D+04	(+/- 1.6D-01)	1.9D-04
T(0	12	+1)	3.099056000000D+04	(+/- 1.6D-01)	1.9D-04
T(0	13	-1)	2.187317600000D+04	(+/- 5.8D-02)	8.0D-04
T(0	13	-1)	2.161205500000D+04	(+/- 9.2D-02)	1.6D-04
T(0	13	+1)	2.214799300000D+04	(+/- 6.0D-02)	8.6D-04
T(0	13	+1)	2.187317600000D+04	(+/- 5.8D-02)	8.0D-04
T(0	13	-1)	3.108072000000D+04	(+/- 1.7D-01)	2.1D-04
T(0	13	+1)	3.108072000000D+04	(+/- 1.7D-01)	2.1D-04
T(0	14	-1)	2.215063400000D+04	(+/- 4.7D-02)	4.1D-04
T(0	14	-1)	2.187080200000D+04	(+/- 5.8D-02)	8.6D-04
T(0	14	+1)	2.244318400000D+04	(+/- 5.0D-02)	4.6D-04
T(0	14	+1)	2.215063500000D+04	(+/- 4.7D-02)	4.1D-04
T(0	14	-1)	3.117782000000D+04	(+/- 1.7D-01)	2.3D-04
T(0	14	+1)	3.117782000000D+04	(+/- 1.7D-01)	2.3D-04
T(0	15	-1)	2.244619300000D+04	(+/- 4.9D-02)	4.1D-04
T(0	15	-1)	2.214799300000D+04	(+/- 6.0D-02)	8.6D-04
T(0	15	+1)	2.275612700000D+04	(+/- 5.1D-02)	4.5D-04
T(0	15	+1)	2.244619300000D+04	(+/- 4.9D-02)	4.1D-04
T(0	15	-1)	3.128259000000D+04	(+/- 1.8D-01)	2.3D-04
T(0	15	+1)	3.128259000000D+04	(+/- 1.8D-01)	2.3D-04
T(0	16	-1)	2.275951000000D+04	(+/- 4.9D-02)	3.3D-04
T(0	16	-1)	2.244318400000D+04	(+/- 5.0D-02)	4.6D-04
T(0	16	+1)	2.308647300000D+04	(+/- 5.3D-02)	4.5D-04
T(0	16	+1)	2.275951000000D+04	(+/- 4.9D-02)	3.3D-04
T(0	16	-1)	3.138593000000D+04	(+/- 1.7D-01)	2.3D-04
T(0	16	+1)	3.138593000000D+04	(+/- 1.7D-01)	2.3D-04
T(0	17	-1)	2.309021100000D+04	(+/- 5.0D-02)	3.3D-04
T(0	17	-1)	2.275612700000D+04	(+/- 5.1D-02)	4.5D-04
T(0	17	+1)	2.343381300000D+04	(+/- 5.4D-02)	4.5D-04
T(0	17	+1)	2.309021100000D+04	(+/- 5.0D-02)	3.3D-04
T(0	17	-1)	3.150552000000D+04	(+/- 1.9D-01)	2.8D-04
T(0	17	+1)	3.150552000000D+04	(+/- 1.9D-01)	2.8D-04
T(0	18	-1)	2.343794600000D+04	(+/- 5.2D-02)	3.2D-04
T(0	18	-1)	2.308647300000D+04	(+/- 5.3D-02)	4.5D-04
T(0	18	+1)	2.379779300000D+04	(+/- 5.6D-02)	4.5D-04
T(0	18	+1)	2.343794600000D+04	(+/- 5.2D-02)	3.2D-04
T(0	18	-1)	3.162864000000D+04	(+/- 2.0D-01)	2.9D-04
T(0	18	+1)	3.162864000000D+04	(+/- 2.0D-01)	2.9D-04
T(0	19	-1)	2.380230200000D+04	(+/- 5.3D-02)	3.3D-04
T(0	19	-1)	2.343381300000D+04	(+/- 5.4D-02)	4.5D-04
T(0	19	+1)	2.417798700000D+04	(+/- 5.7D-02)	4.5D-04
T(0	19	+1)	2.380230200000D+04	(+/- 5.3D-02)	3.3D-04
T(0	19	-1)	3.175812000000D+04	(+/- 1.8D-01)	2.3D-04
T(0	19	+1)	3.175812000000D+04	(+/- 1.8D-01)	2.3D-04
T(0	20	-1)	2.418287600000D+04	(+/- 5.4D-02)	3.2D-04
T(0	20	-1)	2.379779300000D+04	(+/- 5.6D-02)	4.5D-04
T(0	20	+1)	2.457395900000D+04	(+/- 5.7D-02)	4.5D-04
T(0	20	+1)	2.418287600000D+04	(+/- 5.4D-02)	3.2D-04
T(0	20	-1)	3.189379000000D+04	(+/- 1.8D-01)	2.3D-04
T(0	20	+1)	3.189379000000D+04	(+/- 1.8D-01)	2.3D-04
T(0	21	-1)	2.457924700000D+04	(+/- 5.5D-02)	3.2D-04
T(0	21	-1)	2.417798700000D+04	(+/- 5.7D-02)	4.5D-04

Table C.1 Energy origins of "fluorescence series" of BeH isotopomer (cm^{-1}) (*Cont'd*)

T(v' j' p')	Energy Origin	Uncertainty	Sensitivity
T(0 21 +1)	2.498530400000D+04	(+/- 5.8D-02)	4.6D-04
T(0 21 +1)	2.457924700000D+04	(+/- 5.5D-02)	3.2D-04
T(0 21 -1)	3.203569000000D+04	(+/- 2.0D-01)	2.7D-04
T(0 21 +1)	3.203569000000D+04	(+/- 2.0D-01)	2.7D-04
T(0 22 -1)	2.499097800000D+04	(+/- 5.5D-02)	3.2D-04
T(0 22 -1)	2.457395900000D+04	(+/- 5.7D-02)	4.5D-04
T(0 22 +1)	2.541155200000D+04	(+/- 5.8D-02)	4.5D-04
T(0 22 +1)	2.499097800000D+04	(+/- 5.5D-02)	3.2D-04
T(0 22 -1)	3.218402000000D+04	(+/- 1.8D-01)	2.3D-04
T(0 22 +1)	3.218402000000D+04	(+/- 1.8D-01)	2.3D-04
T(0 23 -1)	2.541761600000D+04	(+/- 5.6D-02)	3.2D-04
T(0 23 -1)	2.498530400000D+04	(+/- 5.8D-02)	4.6D-04
T(0 23 +1)	2.585228600000D+04	(+/- 5.9D-02)	4.6D-04
T(0 23 +1)	2.541761600000D+04	(+/- 5.6D-02)	3.2D-04
T(0 23 -1)	3.233841000000D+04	(+/- 2.0D-01)	2.7D-04
T(0 23 +1)	3.233841000000D+04	(+/- 2.0D-01)	2.7D-04
T(0 24 -1)	2.585870500000D+04	(+/- 5.6D-02)	3.2D-04
T(0 24 -1)	2.541155200000D+04	(+/- 5.8D-02)	4.5D-04
T(0 24 +1)	2.630690800000D+04	(+/- 5.9D-02)	4.6D-04
T(0 24 +1)	2.585870500000D+04	(+/- 5.6D-02)	3.2D-04
T(0 24 -1)	3.249125000000D+04	(+/- 2.1D-01)	2.7D-04
T(0 24 +1)	3.249125000000D+04	(+/- 2.1D-01)	2.7D-04
T(0 25 -1)	2.631376500000D+04	(+/- 5.6D-02)	3.2D-04
T(0 25 -1)	2.585228600000D+04	(+/- 5.9D-02)	4.6D-04
T(0 25 +1)	2.677510700000D+04	(+/- 5.9D-02)	4.6D-04
T(0 25 +1)	2.631376500000D+04	(+/- 5.6D-02)	3.2D-04
T(0 25 -1)	3.266199000000D+04	(+/- 2.1D-01)	2.7D-04
T(0 25 +1)	3.266199000000D+04	(+/- 2.1D-01)	2.7D-04
T(0 26 -1)	2.678231900000D+04	(+/- 5.6D-02)	3.2D-04
T(0 26 -1)	2.630690800000D+04	(+/- 5.9D-02)	4.6D-04
T(0 26 +1)	2.725629900000D+04	(+/- 5.9D-02)	4.6D-04
T(0 26 +1)	2.678231900000D+04	(+/- 5.6D-02)	3.2D-04
T(0 26 -1)	3.283405000000D+04	(+/- 2.2D-01)	2.7D-04
T(0 26 +1)	3.283405000000D+04	(+/- 2.2D-01)	2.7D-04
T(0 27 -1)	2.726386500000D+04	(+/- 5.7D-02)	3.2D-04
T(0 27 -1)	2.677510700000D+04	(+/- 5.9D-02)	4.6D-04
T(0 27 +1)	2.774998600000D+04	(+/- 6.0D-02)	4.6D-04
T(0 27 +1)	2.726386500000D+04	(+/- 5.7D-02)	3.2D-04
T(0 27 -1)	3.301153000000D+04	(+/- 2.9D-01)	4.6D-04
T(0 27 +1)	3.301153000000D+04	(+/- 2.9D-01)	4.6D-04
T(0 28 -1)	2.775790300000D+04	(+/- 5.7D-02)	3.3D-04
T(0 28 -1)	2.725629900000D+04	(+/- 5.9D-02)	4.6D-04
T(0 28 +1)	2.825566300000D+04	(+/- 6.0D-02)	4.6D-04
T(0 28 +1)	2.775790600000D+04	(+/- 5.7D-02)	3.2D-04
T(0 28 -1)	3.319426000000D+04	(+/- 2.7D-01)	3.3D-04
T(0 28 +1)	3.319426000000D+04	(+/- 2.7D-01)	3.3D-04
T(0 29 -1)	2.826391900000D+04	(+/- 5.8D-02)	3.2D-04
T(0 29 -1)	2.775008000000D+04	(+/- 2.4D-01)	4.6D-04
T(0 29 +1)	2.877264000000D+04	(+/- 2.4D-01)	4.6D-04
T(0 29 +1)	2.826391900000D+04	(+/- 5.8D-02)	3.2D-04
T(0 29 -1)	3.339143000000D+04	(+/- 3.8D-01)	4.6D-04
T(0 29 +1)	3.339143000000D+04	(+/- 3.8D-01)	4.6D-04
T(0 30 -1)	2.878139300000D+04	(+/- 5.9D-02)	3.2D-04
T(0 30 -1)	2.825566300000D+04	(+/- 6.0D-02)	4.6D-04
T(0 30 +1)	2.930090700000D+04	(+/- 6.2D-02)	4.6D-04
T(0 30 +1)	2.878139300000D+04	(+/- 5.9D-02)	3.2D-04
T(0 30 -1)	3.356696000000D+04	(+/- 8.9D-01)	1.6D-04

Table C.1 Energy origins of "fluorescence series" of BeH isotopomer (cm^{-1}) (*Cont'd*)

T(v'	j'	p')	Energy Origin	Uncertainty	Sensitivity
T(0	30	+1)	3.356696000000D+04	(+/- 8.9D-01)	1.6D-04
T(0	31	-1)	2.930979200000D+04	(+/- 6.0D-02)	3.3D-04
T(0	31	-1)	2.877281100000D+04	(+/- 6.1D-02)	4.6D-04
T(0	31	+1)	2.930979200000D+04	(+/- 6.0D-02)	3.3D-04
T(0	32	-1)	2.984857500000D+04	(+/- 6.1D-02)	3.3D-04
T(0	32	-1)	2.930090700000D+04	(+/- 6.2D-02)	4.6D-04
T(0	32	+1)	2.984857500000D+04	(+/- 6.1D-02)	3.3D-04
T(0	33	-1)	3.039719900000D+04	(+/- 6.2D-02)	3.3D-04
T(0	33	+1)	3.039719900000D+04	(+/- 6.2D-02)	3.3D-04
T(0	34	-1)	3.095510800000D+04	(+/- 6.4D-02)	3.3D-04
T(0	34	+1)	3.095510800000D+04	(+/- 6.4D-02)	3.3D-04
T(0	35	-1)	3.152173900000D+04	(+/- 6.6D-02)	4.5D-04
T(0	35	+1)	3.152173900000D+04	(+/- 6.6D-02)	4.5D-04
T(0	36	-1)	3.209652800000D+04	(+/- 6.7D-02)	3.3D-04
T(0	36	+1)	3.209652800000D+04	(+/- 6.7D-02)	3.3D-04
T(0	37	-1)	3.267888900000D+04	(+/- 6.8D-02)	3.3D-04
T(0	37	+1)	3.267888900000D+04	(+/- 6.8D-02)	3.3D-04
T(0	38	-1)	3.326823500000D+04	(+/- 7.0D-02)	3.3D-04
T(0	38	+1)	3.326823500000D+04	(+/- 7.0D-02)	3.3D-04
T(0	39	-1)	3.386396900000D+04	(+/- 7.1D-02)	3.3D-04
T(0	39	+1)	3.386396900000D+04	(+/- 7.1D-02)	3.3D-04
T(0	40	-1)	3.446548400000D+04	(+/- 7.2D-02)	3.3D-04
T(0	40	+1)	3.446548400000D+04	(+/- 7.2D-02)	3.3D-04
T(0	41	-1)	3.507216300000D+04	(+/- 7.3D-02)	3.3D-04
T(0	41	+1)	3.507216100000D+04	(+/- 7.3D-02)	3.3D-04
T(0	42	-1)	3.568337800000D+04	(+/- 7.4D-02)	3.3D-04
T(0	42	+1)	3.568337800000D+04	(+/- 7.4D-02)	3.3D-04
T(0	43	-1)	3.629846900000D+04	(+/- 7.6D-02)	4.6D-04
T(0	43	+1)	3.629846900000D+04	(+/- 7.6D-02)	4.6D-04
T(0	44	-1)	3.691682000000D+04	(+/- 1.9D-01)	3.3D-04
T(0	44	+1)	3.691682000000D+04	(+/- 1.9D-01)	3.3D-04
T(0	45	-1)	3.753760000000D+04	(+/- 2.0D-01)	3.3D-04
T(0	45	+1)	3.753760000000D+04	(+/- 2.0D-01)	3.3D-04
T(0	46	-1)	3.815998000000D+04	(+/- 2.2D-01)	3.3D-04
T(0	46	+1)	3.815998000000D+04	(+/- 2.2D-01)	3.3D-04
T(1	1	+1)	2.209708300000D+04	(+/- 4.4D-02)	4.6D-04
T(1	1	+1)	2.205831400000D+04	(+/- 4.1D-02)	3.3D-04
T(1	2	-1)	2.209716700000D+04	(+/- 4.1D-02)	3.3D-04
T(1	2	+1)	2.215693500000D+04	(+/- 4.4D-02)	4.6D-04
T(1	2	+1)	2.209801200000D+04	(+/- 4.4D-02)	4.5D-04
T(1	2	-1)	3.145661000000D+04	(+/- 2.5D-01)	3.1D-04
T(1	2	+1)	3.145661000000D+04	(+/- 2.5D-01)	3.1D-04
T(1	3	-1)	2.215708500000D+04	(+/- 4.1D-02)	3.3D-04
T(1	3	+1)	2.223644300000D+04	(+/- 4.4D-02)	4.6D-04
T(1	3	+1)	2.215765900000D+04	(+/- 4.1D-02)	3.3D-04
T(1	3	-1)	3.147782000000D+04	(+/- 2.4D-01)	2.9D-04
T(1	3	+1)	3.147782000000D+04	(+/- 2.4D-01)	2.9D-04
T(1	4	-1)	2.223671200000D+04	(+/- 4.0D-02)	3.3D-04
T(1	4	-1)	2.215750300000D+04	(+/- 4.4D-02)	4.6D-04
T(1	4	+1)	2.233561100000D+04	(+/- 4.4D-02)	4.6D-04
T(1	4	+1)	2.223715200000D+04	(+/- 4.4D-02)	4.5D-04
T(1	4	-1)	3.150599000000D+04	(+/- 2.4D-01)	2.9D-04
T(1	4	+1)	3.150599000000D+04	(+/- 2.4D-01)	2.9D-04
T(1	5	-1)	2.233601000000D+04	(+/- 4.0D-02)	3.3D-04
T(1	5	-1)	2.223688600000D+04	(+/- 4.4D-02)	4.6D-04
T(1	5	+1)	2.245430300000D+04	(+/- 4.4D-02)	4.6D-04
T(1	5	+1)	2.233635000000D+04	(+/- 4.0D-02)	3.3D-04

Table C.1 Energy origins of "fluorescence series" of BeH isotopomer (cm^{-1}) (*Cont'd*)

T(v'	j'	p')	Energy Origin	Uncertainty	Sensitivity
T(1	5	-1)	3.154123000000D+04	(+/- 2.3D-01)	2.9D-04
T(1	5	+1)	3.154123000000D+04	(+/- 2.3D-01)	2.9D-04
T(1	6	-1)	2.245486300000D+04	(+/- 4.1D-02)	3.3D-04
T(1	6	-1)	2.233596200000D+04	(+/- 4.4D-02)	4.6D-04
T(1	6	+1)	2.259239200000D+04	(+/- 4.4D-02)	4.6D-04
T(1	6	+1)	2.245514000000D+04	(+/- 4.1D-02)	3.3D-04
T(1	6	-1)	3.158348000000D+04	(+/- 2.3D-01)	2.9D-04
T(1	6	+1)	3.158348000000D+04	(+/- 2.3D-01)	2.9D-04
T(1	7	-1)	2.259313500000D+04	(+/- 4.1D-02)	3.3D-04
T(1	7	-1)	2.245459800000D+04	(+/- 4.4D-02)	4.6D-04
T(1	7	+1)	2.274971400000D+04	(+/- 4.5D-02)	4.6D-04
T(1	7	+1)	2.259336300000D+04	(+/- 4.1D-02)	3.3D-04
T(1	7	-1)	3.163276000000D+04	(+/- 2.3D-01)	2.9D-04
T(1	7	+1)	3.163276000000D+04	(+/- 2.3D-01)	2.9D-04
T(1	8	-1)	2.275065900000D+04	(+/- 4.1D-02)	3.3D-04
T(1	8	-1)	2.259266000000D+04	(+/- 1.2D-01)	2.2D-04
T(1	8	+1)	2.292606600000D+04	(+/- 4.5D-02)	4.6D-04
T(1	8	+1)	2.275084900000D+04	(+/- 4.1D-02)	3.3D-04
T(1	8	-1)	3.168918000000D+04	(+/- 2.4D-01)	2.9D-04
T(1	8	+1)	3.168918000000D+04	(+/- 2.4D-01)	2.9D-04
T(1	9	-1)	2.292723000000D+04	(+/- 4.2D-02)	3.3D-04
T(1	9	-1)	2.274991000000D+04	(+/- 1.2D-01)	2.2D-04
T(1	9	+1)	2.312124000000D+04	(+/- 1.2D-01)	2.2D-04
T(1	9	+1)	2.292740400000D+04	(+/- 4.2D-02)	3.3D-04
T(1	9	-1)	3.175205000000D+04	(+/- 3.6D-01)	6.5D-04
T(1	9	+1)	3.175205000000D+04	(+/- 3.6D-01)	6.5D-04
T(1	10	-1)	2.312267400000D+04	(+/- 4.5D-02)	4.4D-04
T(1	10	-1)	2.292625000000D+04	(+/- 1.2D-01)	2.2D-04
T(1	10	+1)	2.333498000000D+04	(+/- 1.1D-01)	2.1D-04
T(1	10	+1)	2.312277300000D+04	(+/- 8.0D-02)	1.3D-04
T(1	10	-1)	3.182234000000D+04	(+/- 3.6D-01)	6.5D-04
T(1	10	+1)	3.182254000000D+04	(+/- 3.6D-01)	6.5D-04
T(1	11	-1)	2.333674900000D+04	(+/- 8.0D-02)	1.3D-04
T(1	11	-1)	2.312140000000D+04	(+/- 1.2D-01)	2.2D-04
T(1	11	+1)	2.356714000000D+04	(+/- 1.1D-01)	2.1D-04
T(1	11	+1)	2.333674900000D+04	(+/- 8.0D-02)	1.3D-04
T(1	11	-1)	3.130390000000D+04	(+/- 3.3D-01)	4.6D-04
T(1	12	-1)	2.356913500000D+04	(+/- 7.9D-02)	1.3D-04
T(1	12	-1)	2.333514000000D+04	(+/- 1.1D-01)	2.1D-04
T(1	12	+1)	2.381728400000D+04	(+/- 9.5D-02)	1.6D-04
T(1	12	+1)	2.356913500000D+04	(+/- 7.9D-02)	1.3D-04
T(1	12	-1)	3.197574000000D+04	(+/- 3.5D-01)	4.6D-04
T(1	12	+1)	3.197577000000D+04	(+/- 3.5D-01)	4.6D-04
T(1	13	-1)	2.381951000000D+04	(+/- 7.4D-02)	1.2D-04
T(1	13	-1)	2.356714000000D+04	(+/- 1.1D-01)	2.1D-04
T(1	13	+1)	2.408516000000D+04	(+/- 9.5D-02)	1.6D-04
T(1	13	+1)	2.381951000000D+04	(+/- 7.4D-02)	1.2D-04
T(1	13	-1)	3.186000000000D+04	(+/- 1.7D+02)	3.3D-01
T(1	13	+1)	3.186000000000D+04	(+/- 1.7D+02)	3.3D-01
T(1	14	-1)	2.408775300000D+04	(+/- 7.5D-02)	1.2D-04
T(1	14	-1)	2.381731600000D+04	(+/- 4.9D-02)	4.5D-04
T(1	14	+1)	2.437047100000D+04	(+/- 5.1D-02)	4.5D-04
T(1	14	+1)	2.408775300000D+04	(+/- 7.5D-02)	1.2D-04
T(1	14	-1)	3.216000000000D+04	(+/- 1.7D+02)	3.2D-01
T(1	14	+1)	3.216000000000D+04	(+/- 1.7D+02)	3.2D-01
T(1	15	-1)	2.437333900000D+04	(+/- 4.8D-02)	3.2D-04
T(1	15	-1)	2.408516700000D+04	(+/- 5.0D-02)	4.5D-04

Table C.1 Energy origins of "fluorescence series" of BeH isotopomer (cm^{-1}) (*Cont'd*)

T(v'	j'	p')	Energy Origin	Uncertainty	Sensitivity
T(1	15	+1)	2.467287000000D+04	(+/- 1.2D-01)	2.2D-04
T(1	15	+1)	2.437333900000D+04	(+/- 4.8D-02)	3.2D-04
T(1	15	-1)	3.226689000000D+04	(+/- 3.6D-01)	6.5D-04
T(1	15	+1)	3.226689000000D+04	(+/- 3.6D-01)	6.5D-04
T(1	16	-1)	2.467606200000D+04	(+/- 4.9D-02)	3.2D-04
T(1	16	-1)	2.437047100000D+04	(+/- 5.1D-02)	4.5D-04
T(1	16	+1)	2.499197000000D+04	(+/- 1.2D-01)	2.2D-04
T(1	16	+1)	2.467606200000D+04	(+/- 4.9D-02)	3.2D-04
T(1	16	-1)	3.238000000000D+04	(+/- 1.7D+02)	3.3D-01
T(1	16	+1)	3.238000000000D+04	(+/- 1.7D+02)	3.3D-01
T(1	17	-1)	2.499552400000D+04	(+/- 5.0D-02)	3.2D-04
T(1	17	-1)	2.467287800000D+04	(+/- 5.2D-02)	4.6D-04
T(1	17	+1)	2.532743000000D+04	(+/- 1.2D-01)	2.1D-04
T(1	17	+1)	2.499552400000D+04	(+/- 5.0D-02)	3.2D-04
T(1	18	-1)	2.533135000000D+04	(+/- 5.1D-02)	3.2D-04
T(1	18	-1)	2.499198600000D+04	(+/- 5.3D-02)	4.6D-04
T(1	18	+1)	2.567889800000D+04	(+/- 5.5D-02)	4.6D-04
T(1	18	+1)	2.533135000000D+04	(+/- 5.1D-02)	3.2D-04
T(1	19	-1)	2.568316100000D+04	(+/- 5.2D-02)	3.2D-04
T(1	19	-1)	2.532743900000D+04	(+/- 5.4D-02)	4.6D-04
T(1	19	+1)	2.604589500000D+04	(+/- 5.5D-02)	4.6D-04
T(1	19	+1)	2.568316100000D+04	(+/- 5.2D-02)	3.2D-04
T(1	20	-1)	2.605049800000D+04	(+/- 5.3D-02)	3.2D-04
T(1	20	-1)	2.567889800000D+04	(+/- 5.5D-02)	4.6D-04
T(1	20	+1)	2.642802300000D+04	(+/- 5.6D-02)	4.6D-04
T(1	20	+1)	2.605049800000D+04	(+/- 5.3D-02)	3.2D-04
T(1	21	-1)	2.643298900000D+04	(+/- 5.3D-02)	3.2D-04
T(1	21	-1)	2.604589500000D+04	(+/- 5.5D-02)	4.6D-04
T(1	21	+1)	2.682486100000D+04	(+/- 5.6D-02)	4.6D-04
T(1	21	+1)	2.643298900000D+04	(+/- 5.3D-02)	3.2D-04
T(1	22	-1)	2.683018200000D+04	(+/- 5.4D-02)	3.2D-04
T(1	22	-1)	2.642802300000D+04	(+/- 5.6D-02)	4.6D-04
T(1	22	+1)	2.723594200000D+04	(+/- 5.7D-02)	4.6D-04
T(1	22	+1)	2.683018200000D+04	(+/- 5.4D-02)	3.2D-04
T(1	23	-1)	2.724161000000D+04	(+/- 5.4D-02)	3.2D-04
T(1	23	-1)	2.682486100000D+04	(+/- 5.6D-02)	4.6D-04
T(1	23	+1)	2.766083000000D+04	(+/- 1.2D-01)	2.1D-04
T(1	23	+1)	2.724161000000D+04	(+/- 5.4D-02)	3.2D-04
T(1	24	-1)	2.766681800000D+04	(+/- 5.5D-02)	3.2D-04
T(1	24	-1)	2.723594200000D+04	(+/- 5.7D-02)	4.6D-04
T(1	24	+1)	2.809897800000D+04	(+/- 5.8D-02)	4.6D-04
T(1	24	+1)	2.766681900000D+04	(+/- 5.4D-02)	3.2D-04
T(1	25	-1)	2.810531800000D+04	(+/- 5.5D-02)	3.2D-04
T(1	25	-1)	2.766083000000D+04	(+/- 1.2D-01)	2.1D-04
T(1	25	+1)	2.810531800000D+04	(+/- 5.5D-02)	3.2D-04
T(1	26	-1)	2.855664700000D+04	(+/- 5.5D-02)	3.2D-04
T(1	26	-1)	2.809897800000D+04	(+/- 5.8D-02)	4.6D-04
T(1	26	+1)	2.855664700000D+04	(+/- 5.5D-02)	3.2D-04
T(1	27	-1)	2.902027300000D+04	(+/- 5.6D-02)	3.2D-04
T(1	27	+1)	2.902027300000D+04	(+/- 5.6D-02)	3.2D-04
T(1	28	-1)	2.949569300000D+04	(+/- 5.6D-02)	3.2D-04
T(1	28	+1)	2.949569300000D+04	(+/- 5.6D-02)	3.2D-04
T(1	29	-1)	2.998238500000D+04	(+/- 5.8D-02)	4.4D-04
T(1	29	+1)	2.998238500000D+04	(+/- 5.8D-02)	4.4D-04
T(1	30	-1)	3.047981100000D+04	(+/- 5.7D-02)	3.2D-04
T(1	30	+1)	3.047981100000D+04	(+/- 5.7D-02)	3.2D-04
T(1	31	-1)	3.098742800000D+04	(+/- 5.8D-02)	3.3D-04

Table C.1 Energy origins of "fluorescence series" of BeH isotopomer (cm^{-1}) (*Cont'd*)

T(v'	j'	p')	Energy Origin	Uncertainty	Sensitivity
T(1	31	+1)	3.098742800000D+04	(+/- 5.8D-02)	3.3D-04
T(1	32	-1)	3.150468600000D+04	(+/- 6.1D-02)	4.5D-04
T(1	32	+1)	3.150468600000D+04	(+/- 6.1D-02)	4.5D-04
T(1	33	-1)	3.203099300000D+04	(+/- 6.1D-02)	3.3D-04
T(1	33	+1)	3.203099300000D+04	(+/- 6.1D-02)	3.3D-04
T(1	34	-1)	3.256580200000D+04	(+/- 6.2D-02)	3.3D-04
T(1	34	+1)	3.256580200000D+04	(+/- 6.2D-02)	3.3D-04
T(1	35	-1)	3.310849800000D+04	(+/- 6.3D-02)	3.3D-04
T(1	35	+1)	3.310849800000D+04	(+/- 6.3D-02)	3.3D-04
T(1	36	-1)	3.365848000000D+04	(+/- 6.5D-02)	3.3D-04
T(1	36	+1)	3.365849400000D+04	(+/- 6.6D-02)	4.6D-04
T(1	37	-1)	3.421515700000D+04	(+/- 6.7D-02)	3.3D-04
T(1	37	+1)	3.421500000000D+04	(+/- 1.7D+01)	3.3D-02
T(1	38	-1)	3.477787000000D+04	(+/- 6.9D-02)	3.3D-04
T(1	38	+1)	3.477786800000D+04	(+/- 7.3D-02)	4.6D-04
T(1	39	-1)	3.534593800000D+04	(+/- 7.1D-02)	3.3D-04
T(1	39	+1)	3.534595400000D+04	(+/- 7.5D-02)	4.6D-04
T(1	40	-1)	3.591880900000D+04	(+/- 7.2D-02)	3.3D-04
T(1	40	+1)	3.591880900000D+04	(+/- 7.2D-02)	3.3D-04
T(1	41	-1)	3.649546000000D+04	(+/- 1.8D-01)	3.3D-04
T(1	41	+1)	3.649546000000D+04	(+/- 1.8D-01)	3.3D-04
T(1	42	-1)	3.707482000000D+04	(+/- 1.9D-01)	3.3D-04
T(1	42	+1)	3.707482000000D+04	(+/- 1.9D-01)	3.3D-04
T(1	43	-1)	3.765850000000D+04	(+/- 2.0D-01)	3.3D-04
T(1	43	+1)	3.765850000000D+04	(+/- 2.0D-01)	3.3D-04
T(2	1	+1)	2.397977300000D+04	(+/- 5.5D-02)	4.5D-04
T(2	2	-1)	2.401726700000D+04	(+/- 5.3D-02)	3.3D-04
T(2	2	+1)	2.401810500000D+04	(+/- 5.5D-02)	4.5D-04
T(2	2	+1)	3.210000000000D+04	(+/- 1.7D+02)	3.3D-01
T(2	3	-1)	2.407515900000D+04	(+/- 5.2D-02)	3.3D-04
T(2	3	+1)	2.415183000000D+04	(+/- 5.5D-02)	4.6D-04
T(2	3	+1)	2.407572900000D+04	(+/- 5.5D-02)	4.5D-04
T(2	3	-1)	3.242160000000D+04	(+/- 2.4D-01)	3.3D-04
T(2	3	+1)	3.242160000000D+04	(+/- 2.4D-01)	3.3D-04
T(2	4	-1)	2.415206800000D+04	(+/- 5.2D-02)	3.2D-04
T(2	4	-1)	2.407558900000D+04	(+/- 6.8D-02)	9.1D-04
T(2	4	+1)	2.424761700000D+04	(+/- 5.4D-02)	4.6D-04
T(2	4	+1)	2.415249400000D+04	(+/- 5.5D-02)	4.5D-04
T(2	4	-1)	3.244965000000D+04	(+/- 2.4D-01)	3.3D-04
T(2	4	+1)	3.244965000000D+04	(+/- 2.4D-01)	3.3D-04
T(2	5	-1)	2.424799800000D+04	(+/- 5.1D-02)	3.3D-04
T(2	5	-1)	2.415227000000D+04	(+/- 1.2D-01)	2.1D-04
T(2	5	+1)	2.436226900000D+04	(+/- 5.4D-02)	4.6D-04
T(2	5	+1)	2.424834100000D+04	(+/- 5.1D-02)	3.3D-04
T(2	5	-1)	3.248476000000D+04	(+/- 2.8D-01)	4.5D-04
T(2	5	+1)	3.248476000000D+04	(+/- 2.8D-01)	4.5D-04
T(2	6	-1)	2.436279400000D+04	(+/- 5.1D-02)	3.3D-04
T(2	6	-1)	2.424796900000D+04	(+/- 5.4D-02)	4.6D-04
T(2	6	+1)	2.449563000000D+04	(+/- 1.2D-01)	2.2D-04
T(2	6	+1)	2.436307300000D+04	(+/- 5.1D-02)	3.3D-04
T(2	6	-1)	3.252745000000D+04	(+/- 2.3D-01)	3.3D-04
T(2	6	+1)	3.252745000000D+04	(+/- 2.3D-01)	3.3D-04
T(2	7	-1)	2.449633000000D+04	(+/- 5.0D-02)	3.3D-04
T(2	7	-1)	2.436255200000D+04	(+/- 5.4D-02)	4.6D-04
T(2	7	+1)	2.464755900000D+04	(+/- 6.7D-02)	9.2D-04
T(2	7	+1)	2.449656100000D+04	(+/- 5.0D-02)	3.3D-04
T(2	7	-1)	3.257472000000D+04	(+/- 2.2D-01)	3.3D-04

Table C.1 Energy origins of "fluorescence series" of BeH isotopomer (cm^{-1}) (*Cont'd*)

T(v'	j'	p')	Energy Origin	Uncertainty	Sensitivity
T(2	7	+1)	3.257472000000D+04	(+/- 2.2D-01)	3.3D-04
T(2	8	-1)	2.464843700000D+04	(+/- 5.0D-02)	3.3D-04
T(2	8	-1)	2.449588000000D+04	(+/- 1.2D-01)	2.2D-04
T(2	8	+1)	2.481787000000D+04	(+/- 1.2D-01)	2.2D-04
T(2	8	+1)	2.464863700000D+04	(+/- 5.0D-02)	3.3D-04
T(2	8	-1)	3.263050000000D+04	(+/- 2.2D-01)	3.3D-04
T(2	8	+1)	3.263050000000D+04	(+/- 2.2D-01)	3.3D-04
T(2	9	-1)	2.481893000000D+04	(+/- 5.0D-02)	3.3D-04
T(2	9	-1)	2.464778000000D+04	(+/- 2.2D-01)	4.1D-04
T(2	9	+1)	2.500624000000D+04	(+/- 1.2D-01)	2.1D-04
T(2	9	+1)	2.481909400000D+04	(+/- 5.0D-02)	3.3D-04
T(2	9	-1)	3.269290000000D+04	(+/- 2.2D-01)	3.3D-04
T(2	9	+1)	3.269290000000D+04	(+/- 2.2D-01)	3.3D-04
T(2	10	-1)	2.500756800000D+04	(+/- 5.3D-02)	4.5D-04
T(2	10	-1)	2.481803000000D+04	(+/- 1.2D-01)	2.2D-04
T(2	10	+1)	2.521259000000D+04	(+/- 1.3D-01)	2.3D-04
T(2	10	+1)	2.500771000000D+04	(+/- 5.2D-02)	4.4D-04
T(2	10	-1)	3.276195000000D+04	(+/- 2.2D-01)	3.3D-04
T(2	10	+1)	3.276195000000D+04	(+/- 2.2D-01)	3.3D-04
T(2	11	-1)	2.521418300000D+04	(+/- 9.2D-02)	1.5D-04
T(2	11	-1)	2.500631000000D+04	(+/- 1.7D-01)	3.3D-04
T(2	11	+1)	2.543654000000D+04	(+/- 1.2D-01)	2.1D-04
T(2	11	+1)	2.521426100000D+04	(+/- 8.9D-02)	1.5D-04
T(2	11	-1)	3.283754000000D+04	(+/- 2.2D-01)	3.3D-04
T(2	11	+1)	3.283754000000D+04	(+/- 2.2D-01)	3.3D-04
T(2	12	-1)	2.543844400000D+04	(+/- 5.3D-02)	4.5D-04
T(2	12	-1)	2.521262300000D+04	(+/- 9.7D-02)	1.6D-04
T(2	12	+1)	2.567794000000D+04	(+/- 6.7D-02)	9.2D-04
T(2	12	+1)	2.543844200000D+04	(+/- 5.3D-02)	4.5D-04
T(2	13	-1)	2.568003500000D+04	(+/- 5.0D-02)	3.2D-04
T(2	13	-1)	2.543662000000D+04	(+/- 1.2D-01)	2.1D-04
T(2	13	+1)	2.593633100000D+04	(+/- 5.3D-02)	4.6D-04
T(2	13	+1)	2.568003500000D+04	(+/- 5.0D-02)	3.2D-04
T(2	14	-1)	2.593872100000D+04	(+/- 5.3D-02)	4.5D-04
T(2	14	-1)	2.567769000000D+04	(+/- 1.3D-01)	2.3D-04
T(2	14	+1)	2.621146900000D+04	(+/- 5.4D-02)	4.6D-04
T(2	14	+1)	2.593871400000D+04	(+/- 5.1D-02)	3.2D-04
T(2	15	-1)	2.621414400000D+04	(+/- 5.1D-02)	3.3D-04
T(2	15	-1)	2.593633200000D+04	(+/- 6.7D-02)	9.2D-04
T(2	15	+1)	2.650301500000D+04	(+/- 5.4D-02)	4.6D-04
T(2	15	+1)	2.621414400000D+04	(+/- 5.1D-02)	3.3D-04
T(2	16	-1)	2.650598800000D+04	(+/- 5.1D-02)	3.2D-04
T(2	16	-1)	2.621147100000D+04	(+/- 6.8D-02)	9.2D-04
T(2	16	+1)	2.681057400000D+04	(+/- 5.4D-02)	4.5D-04
T(2	16	+1)	2.650598600000D+04	(+/- 5.1D-02)	3.3D-04
T(2	17	-1)	2.681387400000D+04	(+/- 5.2D-02)	3.3D-04
T(2	17	-1)	2.650300800000D+04	(+/- 5.4D-02)	4.5D-04
T(2	17	+1)	2.713382300000D+04	(+/- 5.5D-02)	4.6D-04
T(2	17	+1)	2.681387400000D+04	(+/- 5.2D-02)	3.3D-04
T(2	18	-1)	2.713743500000D+04	(+/- 5.2D-02)	3.3D-04
T(2	18	-1)	2.681057700000D+04	(+/- 5.4D-02)	4.6D-04
T(2	18	+1)	2.747233700000D+04	(+/- 5.5D-02)	4.6D-04
T(2	18	+1)	2.713743600000D+04	(+/- 5.2D-02)	3.3D-04
T(2	19	-1)	2.747627200000D+04	(+/- 5.3D-02)	3.2D-04
T(2	19	-1)	2.713382300000D+04	(+/- 5.5D-02)	4.6D-04
T(2	19	+1)	2.782571600000D+04	(+/- 5.6D-02)	4.6D-04
T(2	19	+1)	2.747627200000D+04	(+/- 5.3D-02)	3.2D-04

Table C.1 Energy origins of "fluorescence series" of BeH isotopomer (cm^{-1}) (*Cont'd*)

T(v'	j'	p')	Energy Origin	Uncertainty	Sensitivity
T(2	20	-1)	2.782996500000D+04	(+/- 5.3D-02)	3.2D-04
T(2	20	-1)	2.747233700000D+04	(+/- 5.5D-02)	4.6D-04
T(2	20	+1)	2.819352700000D+04	(+/- 5.6D-02)	4.5D-04
T(2	20	+1)	2.782996500000D+04	(+/- 5.3D-02)	3.2D-04
T(2	21	-1)	2.819809800000D+04	(+/- 5.3D-02)	3.2D-04
T(2	21	-1)	2.782571600000D+04	(+/- 5.6D-02)	4.6D-04
T(2	21	+1)	2.857533700000D+04	(+/- 5.6D-02)	4.5D-04
T(2	21	+1)	2.819809800000D+04	(+/- 5.3D-02)	3.2D-04
T(2	22	-1)	2.858021100000D+04	(+/- 5.4D-02)	3.2D-04
T(2	22	-1)	2.819352700000D+04	(+/- 5.6D-02)	4.5D-04
T(2	22	+1)	2.897068600000D+04	(+/- 5.7D-02)	4.6D-04
T(2	22	+1)	2.858020900000D+04	(+/- 5.4D-02)	3.3D-04
T(2	23	-1)	2.897584800000D+04	(+/- 5.4D-02)	3.2D-04
T(2	23	-1)	2.857533700000D+04	(+/- 5.6D-02)	4.5D-04
T(2	23	+1)	2.937909700000D+04	(+/- 6.8D-02)	8.6D-04
T(2	23	+1)	2.897584800000D+04	(+/- 5.4D-02)	3.2D-04
T(2	24	-1)	2.938456600000D+04	(+/- 5.4D-02)	3.2D-04
T(2	24	-1)	2.897068600000D+04	(+/- 5.7D-02)	4.6D-04
T(2	24	+1)	2.980010700000D+04	(+/- 5.7D-02)	4.5D-04
T(2	24	+1)	2.938458000000D+04	(+/- 5.6D-02)	4.4D-04
T(2	25	-1)	2.980585200000D+04	(+/- 6.1D-02)	6.3D-04
T(2	25	-1)	2.937909700000D+04	(+/- 6.8D-02)	8.6D-04
T(2	25	+1)	3.023320100000D+04	(+/- 5.8D-02)	4.5D-04
T(2	25	+1)	2.980585200000D+04	(+/- 6.1D-02)	6.3D-04
T(2	26	-1)	3.023919900000D+04	(+/- 6.8D-02)	8.5D-04
T(2	26	-1)	2.980010700000D+04	(+/- 5.7D-02)	4.5D-04
T(2	26	+1)	3.067787700000D+04	(+/- 5.8D-02)	4.5D-04
T(2	26	+1)	3.023919800000D+04	(+/- 6.8D-02)	8.5D-04
T(2	27	-1)	3.068409500000D+04	(+/- 5.7D-02)	4.1D-04
T(2	27	-1)	3.023320100000D+04	(+/- 5.8D-02)	4.5D-04
T(2	27	+1)	3.068409500000D+04	(+/- 5.7D-02)	4.1D-04
T(2	28	-1)	3.114001600000D+04	(+/- 5.6D-02)	3.3D-04
T(2	28	-1)	3.067787700000D+04	(+/- 5.8D-02)	4.5D-04
T(2	28	+1)	3.114001600000D+04	(+/- 5.6D-02)	3.3D-04
T(2	29	-1)	3.160643100000D+04	(+/- 5.7D-02)	3.3D-04
T(2	29	+1)	3.160643100000D+04	(+/- 5.7D-02)	3.3D-04
T(2	30	-1)	3.208276900000D+04	(+/- 5.8D-02)	3.3D-04
T(2	30	+1)	3.208276900000D+04	(+/- 5.8D-02)	3.3D-04
T(2	31	-1)	3.256845600000D+04	(+/- 5.9D-02)	3.3D-04
T(2	31	+1)	3.256845600000D+04	(+/- 5.9D-02)	3.3D-04
T(2	32	-1)	3.306287700000D+04	(+/- 6.1D-02)	4.5D-04
T(2	32	+1)	3.306287500000D+04	(+/- 7.2D-02)	8.6D-04
T(2	33	-1)	3.356548500000D+04	(+/- 6.2D-02)	3.3D-04
T(2	33	+1)	3.356549900000D+04	(+/- 6.4D-02)	4.1D-04
T(2	34	-1)	3.407552700000D+04	(+/- 6.4D-02)	4.1D-04
T(2	34	+1)	3.407554500000D+04	(+/- 7.0D-02)	6.5D-04
T(2	35	-1)	3.459138100000D+04	(+/- 6.7D-02)	4.1D-04
T(2	35	+1)	3.459139000000D+04	(+/- 7.4D-02)	6.5D-04
T(2	36	-1)	3.511600000000D+04	(+/- 1.5D+01)	2.9D-02
T(2	36	+1)	3.511600000000D+04	(+/- 1.5D+01)	2.9D-02
T(2	37	-1)	3.564394000000D+04	(+/- 1.9D-01)	3.3D-04
T(2	37	+1)	3.564394000000D+04	(+/- 1.9D-01)	3.3D-04
T(3	1	+1)	2.581448000000D+04	(+/- 1.0D-01)	1.6D-04
T(3	2	-1)	2.585057300000D+04	(+/- 6.3D-02)	4.5D-04
T(3	2	+1)	2.590626000000D+04	(+/- 1.3D-01)	2.2D-04
T(3	2	+1)	2.585142000000D+04	(+/- 6.1D-02)	3.3D-04
T(3	3	-1)	2.590637200000D+04	(+/- 6.3D-02)	4.5D-04

Table C.1 Energy origins of "fluorescence series" of BeH isotopomer (cm^{-1}) (*Cont'd*)

T(v'	j'	p')	Energy Origin	Uncertainty	Sensitivity
T(3	3	+1)	2.598033000000D+04	(+/- 1.3D-01)	2.2D-04
T(3	3	+1)	2.590695600000D+04	(+/- 6.0D-02)	3.3D-04
T(3	4	-1)	2.598053200000D+04	(+/- 6.1D-02)	4.6D-04
T(3	4	-1)	2.590679000000D+04	(+/- 1.3D-01)	2.2D-04
T(3	4	+1)	2.607265000000D+04	(+/- 1.3D-01)	2.2D-04
T(3	4	+1)	2.598096100000D+04	(+/- 6.1D-02)	4.5D-04
T(3	5	-1)	2.607293600000D+04	(+/- 5.8D-02)	3.3D-04
T(3	5	-1)	2.598074000000D+04	(+/- 2.2D-01)	4.1D-04
T(3	5	+1)	2.618305500000D+04	(+/- 6.0D-02)	4.6D-04
T(3	5	+1)	2.607328100000D+04	(+/- 5.8D-02)	3.3D-04
T(3	6	-1)	2.618354000000D+04	(+/- 5.8D-02)	3.3D-04
T(3	6	-1)	2.607293900000D+04	(+/- 7.3D-02)	9.2D-04
T(3	6	+1)	2.631155000000D+04	(+/- 2.2D-01)	4.1D-04
T(3	6	+1)	2.618382200000D+04	(+/- 5.8D-02)	3.3D-04
T(3	7	-1)	2.631218400000D+04	(+/- 5.7D-02)	3.3D-04
T(3	7	-1)	2.618334600000D+04	(+/- 6.0D-02)	4.6D-04
T(3	7	+1)	2.645790000000D+04	(+/- 1.2D-01)	2.2D-04
T(3	7	+1)	2.631241800000D+04	(+/- 5.7D-02)	3.3D-04
T(3	8	-1)	2.645870000000D+04	(+/- 5.6D-02)	3.3D-04
T(3	8	-1)	2.631178900000D+04	(+/- 5.9D-02)	4.6D-04
T(3	8	+1)	2.662187100000D+04	(+/- 5.8D-02)	4.6D-04
T(3	8	+1)	2.645889700000D+04	(+/- 5.6D-02)	3.3D-04
T(3	9	-1)	2.662288300000D+04	(+/- 5.6D-02)	3.3D-04
T(3	9	-1)	2.645808000000D+04	(+/- 2.0D-01)	3.8D-04
T(3	9	+1)	2.680348000000D+04	(+/- 1.8D-01)	3.3D-04
T(3	9	+1)	2.662305500000D+04	(+/- 5.6D-02)	3.3D-04
T(3	10	-1)	2.680452800000D+04	(+/- 6.2D-02)	6.5D-04
T(3	10	-1)	2.662206100000D+04	(+/- 5.8D-02)	4.6D-04
T(3	10	+1)	2.700200000000D+04	(+/- 1.2D-01)	2.1D-04
T(3	10	+1)	2.680467500000D+04	(+/- 6.2D-02)	6.4D-04
T(3	11	-1)	2.700346500000D+04	(+/- 6.7D-02)	8.3D-04
T(3	11	-1)	2.680348000000D+04	(+/- 1.8D-01)	3.3D-04
T(3	11	+1)	2.721752000000D+04	(+/- 1.3D-01)	2.2D-04
T(3	11	+1)	2.700346500000D+04	(+/- 6.7D-02)	8.3D-04
T(3	12	-1)	2.721925600000D+04	(+/- 8.5D-02)	1.3D-04
T(3	12	-1)	2.700205000000D+04	(+/- 1.8D-01)	3.3D-04
T(3	12	+1)	2.744987000000D+04	(+/- 2.4D-01)	4.5D-04
T(3	12	+1)	2.721925600000D+04	(+/- 8.5D-02)	1.3D-04
T(3	13	-1)	2.745172700000D+04	(+/- 6.1D-02)	6.1D-04
T(3	13	-1)	2.721763500000D+04	(+/- 7.0D-02)	9.2D-04
T(3	13	+1)	2.769838000000D+04	(+/- 1.3D-01)	2.3D-04
T(3	13	+1)	2.745172700000D+04	(+/- 6.1D-02)	6.1D-04
T(3	14	-1)	2.770055700000D+04	(+/- 5.6D-02)	4.1D-04
T(3	14	-1)	2.744987000000D+04	(+/- 2.4D-01)	4.5D-04
T(3	14	+1)	2.796300000000D+04	(+/- 1.3D-01)	2.2D-04
T(3	14	+1)	2.770055700000D+04	(+/- 5.6D-02)	4.1D-04
T(3	15	-1)	2.796541800000D+04	(+/- 5.4D-02)	3.2D-04
T(3	15	-1)	2.769838400000D+04	(+/- 7.0D-02)	9.2D-04
T(3	15	+1)	2.824319900000D+04	(+/- 9.9D-02)	1.6D-04
T(3	15	+1)	2.796541700000D+04	(+/- 5.4D-02)	3.2D-04
T(3	16	-1)	2.824597300000D+04	(+/- 5.4D-02)	3.3D-04
T(3	16	-1)	2.796300000000D+04	(+/- 1.3D-01)	2.2D-04
T(3	16	+1)	2.853888200000D+04	(+/- 5.7D-02)	4.5D-04
T(3	16	+1)	2.824597300000D+04	(+/- 5.4D-02)	3.3D-04
T(3	17	-1)	2.854185100000D+04	(+/- 5.7D-02)	4.6D-04
T(3	17	-1)	2.824319900000D+04	(+/- 9.9D-02)	1.6D-04
T(3	17	+1)	2.884942000000D+04	(+/- 1.8D-01)	3.3D-04

Table C.1 Energy origins of "fluorescence series" of BeH isotopomer (cm^{-1}) (*Cont'd*)

T(v'	j'	p')	Energy Origin	Uncertainty	Sensitivity
T(3	17	+1)	2.854185100000D+04	(+/- 5.7D-02)	4.6D-04
T(3	18	-1)	2.885267000000D+04	(+/- 5.5D-02)	3.2D-04
T(3	18	-1)	2.853888200000D+04	(+/- 5.7D-02)	4.5D-04
T(3	18	+1)	2.917451400000D+04	(+/- 6.8D-02)	8.6D-04
T(3	18	+1)	2.885267000000D+04	(+/- 5.5D-02)	3.2D-04
T(3	19	-1)	2.917803000000D+04	(+/- 5.5D-02)	3.3D-04
T(3	19	-1)	2.884942000000D+04	(+/- 1.8D-01)	3.3D-04
T(3	19	+1)	2.951373800000D+04	(+/- 7.0D-02)	9.1D-04
T(3	19	+1)	2.917803000000D+04	(+/- 5.5D-02)	3.3D-04
T(3	20	-1)	2.951750600000D+04	(+/- 5.6D-02)	4.1D-04
T(3	20	-1)	2.917451400000D+04	(+/- 6.8D-02)	8.6D-04
T(3	20	+1)	2.986664800000D+04	(+/- 5.8D-02)	4.5D-04
T(3	20	+1)	2.951750600000D+04	(+/- 5.6D-02)	4.1D-04
T(3	21	-1)	2.987065200000D+04	(+/- 5.5D-02)	3.3D-04
T(3	21	-1)	2.951373800000D+04	(+/- 7.0D-02)	9.1D-04
T(3	21	+1)	3.023280900000D+04	(+/- 1.0D-01)	1.6D-04
T(3	21	+1)	2.987065200000D+04	(+/- 5.5D-02)	3.3D-04
T(3	22	-1)	3.023702700000D+04	(+/- 5.6D-02)	3.3D-04
T(3	22	-1)	2.986664800000D+04	(+/- 5.8D-02)	4.5D-04
T(3	22	+1)	3.061179000000D+04	(+/- 1.2D-01)	2.1D-04
T(3	22	+1)	3.023702700000D+04	(+/- 5.6D-02)	3.3D-04
T(3	23	-1)	3.061615600000D+04	(+/- 5.6D-02)	3.3D-04
T(3	23	-1)	3.023280900000D+04	(+/- 1.0D-01)	1.6D-04
T(3	23	+1)	3.100292200000D+04	(+/- 7.1D-02)	9.2D-04
T(3	23	+1)	3.061615600000D+04	(+/- 5.6D-02)	3.3D-04
T(3	24	-1)	3.100754300000D+04	(+/- 5.6D-02)	3.3D-04
T(3	24	-1)	3.061179000000D+04	(+/- 1.2D-01)	2.1D-04
T(3	24	+1)	3.100754300000D+04	(+/- 5.6D-02)	3.3D-04
T(3	25	-1)	3.141068600000D+04	(+/- 5.6D-02)	3.3D-04
T(3	25	-1)	3.100292200000D+04	(+/- 7.1D-02)	9.2D-04
T(3	25	+1)	3.141068600000D+04	(+/- 5.6D-02)	3.3D-04
T(3	26	-1)	3.182504400000D+04	(+/- 5.7D-02)	3.3D-04
T(3	26	+1)	3.182504400000D+04	(+/- 5.7D-02)	3.3D-04
T(3	27	-1)	3.225004400000D+04	(+/- 5.8D-02)	3.3D-04
T(3	27	+1)	3.225004400000D+04	(+/- 5.8D-02)	3.3D-04
T(3	28	-1)	3.268516300000D+04	(+/- 5.9D-02)	3.3D-04
T(3	28	+1)	3.268516300000D+04	(+/- 5.9D-02)	3.3D-04
T(3	29	-1)	3.312958600000D+04	(+/- 6.0D-02)	3.3D-04
T(3	29	+1)	3.312960000000D+04	(+/- 7.3D-02)	9.2D-04
T(3	30	-1)	3.359238000000D+04	(+/- 3.4D-01)	6.5D-04
T(3	30	+1)	3.359238000000D+04	(+/- 3.4D-01)	6.5D-04
T(3	31	-1)	3.404573000000D+04	(+/- 3.4D-01)	6.5D-04
T(3	31	+1)	3.404573000000D+04	(+/- 3.4D-01)	6.5D-04
T(3	32	-1)	3.451424000000D+04	(+/- 3.4D-01)	6.5D-04
T(3	32	+1)	3.451424000000D+04	(+/- 3.4D-01)	6.5D-04
T(3	33	-1)	3.498664000000D+04	(+/- 3.5D-01)	6.5D-04
T(3	33	+1)	3.498673000000D+04	(+/- 2.2D-01)	4.1D-04
T(3	34	-1)	3.548200000000D+04	(+/- 4.9D-01)	9.2D-04
T(3	34	+1)	3.548249000000D+04	(+/- 4.8D-01)	9.2D-04
T(3	35	-1)	3.596408000000D+04	(+/- 2.1D-01)	3.3D-04
T(3	35	+1)	3.596408000000D+04	(+/- 2.1D-01)	3.3D-04
T(4	1	+1)	2.755959000000D+04	(+/- 1.8D-01)	3.3D-04
T(4	2	-1)	2.759427000000D+04	(+/- 7.0D-02)	4.5D-04
T(4	2	+1)	2.759512000000D+04	(+/- 1.2D-01)	2.1D-04
T(4	3	-1)	2.764786900000D+04	(+/- 6.9D-02)	4.1D-04
T(4	3	+1)	2.764843600000D+04	(+/- 6.9D-02)	4.6D-04
T(4	4	-1)	2.771907100000D+04	(+/- 6.8D-02)	4.6D-04

Table C.1 Energy origins of "fluorescence series" of BeH isotopomer (cm^{-1}) (*Cont'd*)

T(v'	j'	p')	Energy Origin	Uncertainty	Sensitivity
T(4	4	+1)	2.771949900000D+04	(+/- 6.8D-02)	4.6D-04
T(4	5	-1)	2.780790000000D+04	(+/- 1.7D-01)	3.1D-04
T(4	5	+1)	2.791362600000D+04	(+/- 7.8D-02)	9.2D-04
T(4	5	+1)	2.780816900000D+04	(+/- 6.7D-02)	4.5D-04
T(4	6	-1)	2.791404500000D+04	(+/- 6.5D-02)	3.3D-04
T(4	6	-1)	2.780787500000D+04	(+/- 7.9D-02)	9.2D-04
T(4	6	+1)	2.803697000000D+04	(+/- 1.3D-01)	2.2D-04
T(4	6	+1)	2.791433400000D+04	(+/- 6.5D-02)	3.3D-04
T(4	7	-1)	2.803756600000D+04	(+/- 6.3D-02)	3.3D-04
T(4	7	-1)	2.791394000000D+04	(+/- 1.3D-01)	2.3D-04
T(4	7	+1)	2.817750000000D+04	(+/- 1.3D-01)	2.3D-04
T(4	7	+1)	2.803780300000D+04	(+/- 6.3D-02)	3.3D-04
T(4	8	-1)	2.817821500000D+04	(+/- 6.2D-02)	3.3D-04
T(4	8	-1)	2.803727000000D+04	(+/- 1.3D-01)	2.2D-04
T(4	8	+1)	2.817841500000D+04	(+/- 6.2D-02)	3.3D-04
T(4	9	-1)	2.833579000000D+04	(+/- 6.3D-02)	4.5D-04
T(4	9	-1)	2.817770000000D+04	(+/- 1.3D-01)	2.3D-04
T(4	9	+1)	2.833599200000D+04	(+/- 6.3D-02)	4.1D-04
T(4	10	-1)	2.851011400000D+04	(+/- 6.1D-02)	3.3D-04
T(4	10	+1)	2.851027300000D+04	(+/- 6.3D-02)	4.1D-04
T(4	11	-1)	2.870087300000D+04	(+/- 6.7D-02)	6.5D-04
T(4	11	-1)	2.850917000000D+04	(+/- 1.2D-01)	2.1D-04
T(4	11	+1)	2.870100100000D+04	(+/- 6.7D-02)	6.5D-04
T(4	12	-1)	2.890790800000D+04	(+/- 7.3D-02)	8.9D-04
T(4	12	+1)	2.890790800000D+04	(+/- 7.3D-02)	8.9D-04
T(4	13	-1)	2.913081900000D+04	(+/- 6.6D-02)	6.5D-04
T(4	13	+1)	2.913081900000D+04	(+/- 6.6D-02)	6.5D-04
T(4	14	-1)	2.936932100000D+04	(+/- 6.0D-02)	4.1D-04
T(4	14	+1)	2.936932100000D+04	(+/- 6.0D-02)	4.1D-04
T(4	15	-1)	2.962311300000D+04	(+/- 5.9D-02)	3.3D-04
T(4	15	+1)	2.962311300000D+04	(+/- 5.9D-02)	3.3D-04
T(4	16	-1)	2.989181900000D+04	(+/- 5.9D-02)	3.3D-04
T(4	16	+1)	2.989181900000D+04	(+/- 5.9D-02)	3.3D-04
T(4	17	-1)	3.017507800000D+04	(+/- 5.9D-02)	3.3D-04
T(4	17	+1)	3.017507800000D+04	(+/- 5.9D-02)	3.3D-04
T(4	18	-1)	3.047246900000D+04	(+/- 5.9D-02)	3.3D-04
T(4	18	+1)	3.047246900000D+04	(+/- 5.9D-02)	3.3D-04
T(4	19	-1)	3.078359600000D+04	(+/- 5.9D-02)	3.3D-04
T(4	19	+1)	3.078359600000D+04	(+/- 5.9D-02)	3.3D-04
T(4	20	-1)	3.110800400000D+04	(+/- 5.9D-02)	3.3D-04
T(4	20	+1)	3.110800400000D+04	(+/- 5.9D-02)	3.3D-04
T(4	21	-1)	3.144521000000D+04	(+/- 1.8D-01)	3.4D-04
T(4	21	+1)	3.144520800000D+04	(+/- 6.0D-02)	3.3D-04
T(4	22	-1)	3.179466000000D+04	(+/- 1.8D-01)	3.3D-04
T(4	22	+1)	3.179466000000D+04	(+/- 1.8D-01)	3.3D-04
T(4	23	-1)	3.215549000000D+04	(+/- 1.8D-01)	3.3D-04
T(4	23	+1)	3.215549000000D+04	(+/- 1.8D-01)	3.3D-04
T(4	24	-1)	3.253535000000D+04	(+/- 1.8D-01)	3.3D-04
T(4	24	+1)	3.253538200000D+04	(+/- 6.6D-02)	4.6D-04
T(4	25	-1)	3.291373000000D+04	(+/- 1.8D-01)	3.3D-04
T(4	25	+1)	3.291373000000D+04	(+/- 1.8D-01)	3.3D-04
T(4	26	-1)	3.330645000000D+04	(+/- 1.8D-01)	3.3D-04
T(4	26	+1)	3.330645000000D+04	(+/- 1.8D-01)	3.3D-04
T(4	27	-1)	3.370760000000D+04	(+/- 1.7D+00)	3.3D-04
T(4	27	+1)	3.370755000000D+04	(+/- 1.8D-01)	3.3D-04
T(4	28	-1)	3.410110000000D+04	(+/- 1.8D-01)	3.3D-04
T(4	28	+1)	3.410125000000D+04	(+/- 1.8D-01)	3.3D-04

Table C.1 Energy origins of "fluorescence series" of BeH isotopomer (cm^{-1}) (*Cont'd*)

T(v'	j'	p')	Energy Origin	Uncertainty	Sensitivity
T(4	29	-1)	3.455278000000D+04	(+/- 1.9D-01)	3.3D-04
T(4	29	+1)	3.455260000000D+04	(+/- 2.4D+00)	4.6D-04
T(4	30	-1)	3.497613000000D+04	(+/- 2.0D-01)	3.3D-04
T(4	30	+1)	3.497586000000D+04	(+/- 2.6D-01)	4.6D-04
T(4	31	-1)	3.540000000000D+04	(+/- 1.7D+02)	3.2D-01
T(4	31	+1)	3.540000000000D+04	(+/- 1.7D+02)	3.2D-01
T(5	2	-1)	2.924386000000D+04	(+/- 1.2D-01)	1.6D-04
T(5	2	+1)	2.924473000000D+04	(+/- 1.2D-01)	1.6D-04
T(5	3	-1)	2.929519000000D+04	(+/- 1.2D-01)	1.6D-04
T(5	3	+1)	2.929576000000D+04	(+/- 1.2D-01)	1.6D-04
T(5	4	-1)	2.936331000000D+04	(+/- 1.2D-01)	1.6D-04
T(5	4	+1)	2.936374000000D+04	(+/- 1.2D-01)	1.6D-04
T(5	5	-1)	2.944817000000D+04	(+/- 1.2D-01)	1.6D-04
T(5	5	+1)	2.954943000000D+04	(+/- 1.4D-01)	2.3D-04
T(5	5	+1)	2.944856000000D+04	(+/- 1.2D-01)	1.6D-04
T(5	6	-1)	2.954978000000D+04	(+/- 1.2D-01)	1.6D-04
T(5	6	+1)	2.966742000000D+04	(+/- 1.4D-01)	2.3D-04
T(5	6	+1)	2.955007000000D+04	(+/- 1.2D-01)	1.6D-04
T(5	7	-1)	2.966789000000D+04	(+/- 1.1D-01)	1.6D-04
T(5	7	+1)	2.980179000000D+04	(+/- 1.4D-01)	2.3D-04
T(5	7	+1)	2.966812000000D+04	(+/- 1.1D-01)	1.6D-04
T(5	8	-1)	2.980234000000D+04	(+/- 1.1D-01)	1.6D-04
T(5	8	+1)	2.980254000000D+04	(+/- 1.1D-01)	1.6D-04
T(5	9	-1)	2.995294000000D+04	(+/- 1.1D-01)	1.6D-04
T(5	9	+1)	3.011866000000D+04	(+/- 1.4D-01)	2.3D-04
T(5	9	+1)	2.995313000000D+04	(+/- 1.1D-01)	1.6D-04
T(5	10	-1)	3.011951000000D+04	(+/- 1.1D-01)	1.6D-04
T(5	10	+1)	3.030075000000D+04	(+/- 1.4D-01)	2.2D-04
T(5	10	+1)	3.011967000000D+04	(+/- 1.1D-01)	1.6D-04
T(5	11	-1)	3.030170000000D+04	(+/- 1.1D-01)	1.6D-04
T(5	11	+1)	3.049824000000D+04	(+/- 1.4D-01)	2.3D-04
T(5	11	+1)	3.030184000000D+04	(+/- 1.1D-01)	1.6D-04
T(5	12	-1)	3.049934000000D+04	(+/- 1.1D-01)	1.6D-04
T(5	12	+1)	3.071088000000D+04	(+/- 1.4D-01)	2.2D-04
T(5	12	+1)	3.049940000000D+04	(+/- 1.1D-01)	1.6D-04
T(5	13	-1)	3.071196000000D+04	(+/- 1.1D-01)	1.6D-04
T(5	13	+1)	3.093833000000D+04	(+/- 1.4D-01)	2.3D-04
T(5	13	+1)	3.071196000000D+04	(+/- 1.1D-01)	1.6D-04
T(5	14	-1)	3.093920000000D+04	(+/- 1.1D-01)	1.6D-04
T(5	14	-1)	3.071088000000D+04	(+/- 1.4D-01)	2.2D-04
T(5	14	+1)	3.118023000000D+04	(+/- 1.4D-01)	2.3D-04
T(5	14	+1)	3.093922000000D+04	(+/- 1.1D-01)	1.6D-04
T(5	15	-1)	3.117983000000D+04	(+/- 1.1D-01)	1.6D-04
T(5	15	-1)	3.093833000000D+04	(+/- 1.4D-01)	2.3D-04
T(5	15	+1)	3.117989000000D+04	(+/- 1.1D-01)	1.6D-04
T(5	16	-1)	3.144245000000D+04	(+/- 1.1D-01)	1.6D-04
T(5	16	-1)	3.118028000000D+04	(+/- 1.3D-01)	2.1D-04
T(5	16	+1)	3.144245000000D+04	(+/- 1.1D-01)	1.6D-04
T(5	17	-1)	3.170898000000D+04	(+/- 1.1D-01)	1.6D-04
T(5	17	+1)	3.170898000000D+04	(+/- 1.1D-01)	1.6D-04
T(5	18	-1)	3.199132000000D+04	(+/- 1.1D-01)	1.6D-04
T(5	18	+1)	3.199132000000D+04	(+/- 1.1D-01)	1.6D-04
T(5	19	-1)	3.228645000000D+04	(+/- 1.1D-01)	1.6D-04
T(5	19	+1)	3.228645000000D+04	(+/- 1.1D-01)	1.6D-04
T(5	20	-1)	3.259299000000D+04	(+/- 1.1D-01)	1.6D-04
T(5	20	+1)	3.259302000000D+04	(+/- 1.1D-01)	1.6D-04
T(5	21	-1)	3.291000000000D+04	(+/- 1.7D+02)	3.3D-01

Table C.1 Energy origins of "fluorescence series" of BeH isotopomer (cm^{-1}) (*Cont'd*)

T(v'	j'	p')	Energy Origin	Uncertainty	Sensitivity
T(5	21	+1)	3.291000000000D+04	(+/- 1.7D+02)	3.3D-01
T(5	22	-1)	3.326401000000D+04	(+/- 3.5D-01)	6.5D-04
T(5	22	+1)	3.326411000000D+04	(+/- 1.2D-01)	1.6D-04
T(5	23	-1)	3.359732000000D+04	(+/- 1.2D-01)	1.6D-04
T(5	23	+1)	3.359732000000D+04	(+/- 1.2D-01)	1.6D-04
T(5	24	-1)	3.394735000000D+04	(+/- 1.3D-01)	1.6D-04
T(5	24	+1)	3.394735000000D+04	(+/- 1.3D-01)	1.6D-04
T(5	25	-1)	3.430611000000D+04	(+/- 2.0D-01)	3.3D-04
T(5	25	+1)	3.430611000000D+04	(+/- 2.0D-01)	3.3D-04
T(6	2	-1)	3.079391000000D+04	(+/- 1.3D-01)	9.2D-04
T(6	2	+1)	3.079467000000D+04	(+/- 2.6D-01)	4.5D-04
T(6	4	-1)	3.090761000000D+04	(+/- 1.2D-01)	9.2D-04
T(6	4	+1)	3.090791000000D+04	(+/- 2.4D-01)	4.1D-04
T(6	5	-1)	3.098851000000D+04	(+/- 3.3D-01)	6.1D-04
T(6	5	+1)	3.108493000000D+04	(+/- 2.4D-01)	4.1D-04
T(6	5	+1)	3.098893000000D+04	(+/- 1.3D-01)	9.0D-04
T(6	6	-1)	3.108517000000D+04	(+/- 3.4D-01)	6.3D-04
T(6	6	+1)	3.119733000000D+04	(+/- 2.6D-01)	4.5D-04
T(6	6	+1)	3.108556000000D+04	(+/- 1.2D-01)	9.1D-04
T(6	7	-1)	3.119745000000D+04	(+/- 1.1D-01)	4.6D-04
T(6	7	-1)	3.108528000000D+04	(+/- 2.6D-01)	4.6D-04
T(6	7	+1)	3.132516000000D+04	(+/- 2.5D-01)	4.5D-04
T(6	7	+1)	3.119770000000D+04	(+/- 1.9D-01)	3.1D-04
T(6	8	-1)	3.132523000000D+04	(+/- 1.0D-01)	4.6D-04
T(6	8	-1)	3.119760000000D+04	(+/- 2.6D-01)	4.5D-04
T(6	8	+1)	3.146847000000D+04	(+/- 1.1D-01)	9.2D-04
T(6	8	+1)	3.132551000000D+04	(+/- 1.9D-01)	3.2D-04
T(6	9	-1)	3.146816000000D+04	(+/- 1.0D-01)	4.6D-04
T(6	9	-1)	3.132546000000D+04	(+/- 2.5D-01)	4.5D-04
T(6	9	+1)	3.162681000000D+04	(+/- 1.1D-01)	9.2D-04
T(6	9	+1)	3.146841000000D+04	(+/- 1.9D-01)	3.1D-04
T(6	10	-1)	3.162579000000D+04	(+/- 1.9D-01)	3.2D-04
T(6	10	-1)	3.146853000000D+04	(+/- 3.0D-01)	5.5D-04
T(6	10	+1)	3.179976000000D+04	(+/- 3.5D-01)	6.5D-04
T(6	10	+1)	3.162599000000D+04	(+/- 1.9D-01)	3.2D-04
T(6	11	-1)	3.179625000000D+04	(+/- 1.9D-01)	3.3D-04
T(6	11	-1)	3.162697000000D+04	(+/- 1.5D-01)	2.3D-04
T(6	11	+1)	3.198790000000D+04	(+/- 2.0D-01)	3.3D-04
T(6	11	+1)	3.179653000000D+04	(+/- 1.9D-01)	3.3D-04
T(6	12	-1)	3.180015000000D+04	(+/- 1.5D-01)	2.2D-04
T(6	12	+1)	3.218995000000D+04	(+/- 2.0D-01)	3.3D-04
T(6	13	-1)	3.198779000000D+04	(+/- 2.0D-01)	3.3D-04
T(6	13	+1)	3.240593000000D+04	(+/- 2.0D-01)	3.3D-04
T(6	14	-1)	3.241069000000D+04	(+/- 1.9D-01)	3.3D-04
T(6	14	-1)	3.218995000000D+04	(+/- 2.0D-01)	3.3D-04
T(6	14	+1)	3.263547000000D+04	(+/- 2.0D-01)	3.3D-04
T(6	14	+1)	3.241069000000D+04	(+/- 1.9D-01)	3.3D-04
T(6	15	-1)	3.263950000000D+04	(+/- 1.9D-01)	3.3D-04
T(6	15	-1)	3.240593000000D+04	(+/- 2.0D-01)	3.3D-04
T(6	15	+1)	3.287822000000D+04	(+/- 1.5D-01)	2.1D-04
T(6	15	+1)	3.263950000000D+04	(+/- 1.9D-01)	3.3D-04
T(6	16	-1)	3.288175000000D+04	(+/- 2.0D-01)	3.3D-04
T(6	16	-1)	3.263547000000D+04	(+/- 2.0D-01)	3.3D-04
T(6	16	+1)	3.313364000000D+04	(+/- 3.5D-01)	6.5D-04
T(6	16	+1)	3.288175000000D+04	(+/- 2.0D-01)	3.3D-04
T(6	17	-1)	3.313656000000D+04	(+/- 2.5D-01)	4.5D-04
T(6	17	-1)	3.287826000000D+04	(+/- 2.0D-01)	3.3D-04

Table C.1 Energy origins of "fluorescence series" of BeH isotopomer (cm^{-1}) (*Cont'd*)

T(v'	j'	p')	Energy Origin	Uncertainty	Sensitivity
T(6	17	+1)	3.340172000000D+04	(+/- 1.2D-01)	9.2D-04
T(6	17	+1)	3.313662000000D+04	(+/- 2.0D-01)	3.3D-04
T(6	18	-1)	3.340246000000D+04	(+/- 2.0D-01)	3.3D-04
T(6	18	-1)	3.313364000000D+04	(+/- 8.5D-01)	1.6D-04
T(6	18	+1)	3.340246000000D+04	(+/- 2.0D-01)	3.3D-04
T(6	19	-1)	3.340153000000D+04	(+/- 8.5D-01)	1.6D-04
T(6	20	-1)	3.398181000000D+04	(+/- 2.0D-01)	3.3D-04
T(6	20	+1)	3.398181000000D+04	(+/- 2.0D-01)	3.3D-04
T(6	21	-1)	3.428233000000D+04	(+/- 2.1D-01)	3.3D-04
T(6	21	+1)	3.428233000000D+04	(+/- 2.1D-01)	3.3D-04
T(6	22	-1)	3.459429000000D+04	(+/- 2.1D-01)	3.3D-04
T(6	22	+1)	3.459429000000D+04	(+/- 2.1D-01)	3.3D-04
T(6	23	-1)	3.491626000000D+04	(+/- 2.2D-01)	3.3D-04
T(6	23	+1)	3.491626000000D+04	(+/- 2.2D-01)	3.3D-04

C.2 Energy Origins of BeD Isotopomer

Table C.2: Energy Origins of "Fluorescence Series" of BeD Isotopomer (cm^{-1})

T(v'	j'	p')	Energy Origin	Uncertainty	Sensitivity
T(0	1	+1)	1.978818700000D+04	(+/- 3.4D-02)	3.3D-04
T(0	2	-1)	1.980999400000D+04	(+/- 3.4D-02)	3.3D-04
T(0	2	+1)	1.981080100000D+04	(+/- 3.8D-02)	4.5D-04
T(0	3	-1)	1.984430400000D+04	(+/- 3.8D-02)	4.5D-04
T(0	3	+1)	1.984486100000D+04	(+/- 3.4D-02)	3.3D-04
T(0	4	-1)	1.988989300000D+04	(+/- 3.8D-02)	4.5D-04
T(0	4	+1)	1.989032700000D+04	(+/- 3.8D-02)	4.6D-04
T(0	4	-1)	3.035606000000D+04	(+/- 2.9D-01)	3.3D-04
T(0	4	+1)	3.035606000000D+04	(+/- 2.9D-01)	3.3D-04
T(0	5	-1)	1.994676300000D+04	(+/- 3.4D-02)	3.3D-04
T(0	5	+1)	1.994711500000D+04	(+/- 3.7D-02)	4.1D-04
T(0	6	-1)	2.001491000000D+04	(+/- 3.4D-02)	3.3D-04
T(0	6	+1)	2.001520400000D+04	(+/- 3.4D-02)	3.3D-04
T(0	6	-1)	3.039906000000D+04	(+/- 2.5D-01)	2.1D-04
T(0	6	+1)	3.039906000000D+04	(+/- 2.5D-01)	2.1D-04
T(0	7	-1)	2.009427900000D+04	(+/- 3.7D-02)	4.1D-04
T(0	7	+1)	2.018450900000D+04	(+/- 5.6D-02)	9.1D-04
T(0	7	+1)	2.009451400000D+04	(+/- 3.7D-02)	4.1D-04
T(0	7	-1)	3.042611000000D+04	(+/- 2.5D-01)	2.1D-04
T(0	7	+1)	3.042611000000D+04	(+/- 2.5D-01)	2.1D-04
T(0	8	-1)	2.018482600000D+04	(+/- 5.3D-02)	8.3D-04
T(0	8	+1)	2.028610700000D+04	(+/- 5.7D-02)	9.1D-04
T(0	8	+1)	2.018501900000D+04	(+/- 5.3D-02)	8.3D-04
T(0	8	-1)	3.045716000000D+04	(+/- 2.4D-01)	2.0D-04
T(0	8	+1)	3.045716000000D+04	(+/- 2.4D-01)	2.0D-04
T(0	9	-1)	2.028661000000D+04	(+/- 1.2D-01)	2.3D-04
T(0	9	-1)	2.018471800000D+04	(+/- 5.6D-02)	9.1D-04
T(0	9	+1)	2.039882600000D+04	(+/- 5.7D-02)	9.1D-04
T(0	9	+1)	2.028661000000D+04	(+/- 1.2D-01)	2.3D-04
T(0	9	-1)	3.049201000000D+04	(+/- 2.4D-01)	2.0D-04
T(0	9	+1)	3.049201000000D+04	(+/- 2.4D-01)	2.0D-04
T(0	10	-1)	2.039930800000D+04	(+/- 9.6D-02)	1.7D-04
T(0	10	-1)	2.028629900000D+04	(+/- 5.7D-02)	9.1D-04
T(0	10	+1)	2.052243100000D+04	(+/- 5.9D-02)	9.2D-04
T(0	10	+1)	2.039930800000D+04	(+/- 9.6D-02)	1.7D-04
T(0	10	-1)	3.053068000000D+04	(+/- 2.5D-01)	2.3D-04
T(0	10	+1)	3.053068000000D+04	(+/- 2.5D-01)	2.3D-04
T(0	11	-1)	2.052297100000D+04	(+/- 5.6D-02)	8.3D-04
T(0	11	-1)	2.039882600000D+04	(+/- 5.7D-02)	9.1D-04
T(0	11	+1)	2.065692200000D+04	(+/- 5.9D-02)	9.1D-04
T(0	11	+1)	2.052297100000D+04	(+/- 5.6D-02)	8.3D-04
T(0	11	-1)	3.057322000000D+04	(+/- 2.3D-01)	1.9D-04
T(0	11	+1)	3.057322000000D+04	(+/- 2.3D-01)	1.9D-04
T(0	12	-1)	2.065756500000D+04	(+/- 4.4D-02)	4.6D-04
T(0	12	-1)	2.052243100000D+04	(+/- 5.9D-02)	9.2D-04
T(0	12	+1)	2.080222200000D+04	(+/- 6.0D-02)	9.1D-04
T(0	12	+1)	2.065756500000D+04	(+/- 4.4D-02)	4.6D-04
T(0	12	-1)	3.061949000000D+04	(+/- 2.3D-01)	1.9D-04
T(0	12	+1)	3.061949000000D+04	(+/- 2.3D-01)	1.9D-04
T(0	13	-1)	2.080296300000D+04	(+/- 4.1D-02)	3.3D-04
T(0	13	-1)	2.065692200000D+04	(+/- 5.9D-02)	9.1D-04
T(0	13	+1)	2.095822800000D+04	(+/- 4.6D-02)	4.6D-04
T(0	13	+1)	2.080296300000D+04	(+/- 4.1D-02)	3.3D-04

Table C.2 Energy origins of "fluorescence series" of BeD isotopomer (cm^{-1}) (*Cont'd*)

T(v' j' p')	Energy Origin	Uncertainty	Sensitivity
T(0 13 -1)	3.066957000000D+04	(+/- 2.2D-01)	2.0D-04
T(0 13 +1)	3.066957000000D+04	(+/- 2.2D-01)	2.0D-04
T(0 14 -1)	2.095907400000D+04	(+/- 4.3D-02)	3.3D-04
T(0 14 -1)	2.080222200000D+04	(+/- 6.0D-02)	9.1D-04
T(0 14 +1)	2.112484800000D+04	(+/- 4.8D-02)	4.6D-04
T(0 14 +1)	2.095907400000D+04	(+/- 4.3D-02)	3.3D-04
T(0 14 -1)	3.072343000000D+04	(+/- 2.2D-01)	1.9D-04
T(0 14 +1)	3.072343000000D+04	(+/- 2.2D-01)	1.9D-04
T(0 15 -1)	2.112580300000D+04	(+/- 4.5D-02)	3.3D-04
T(0 15 -1)	2.095822800000D+04	(+/- 4.6D-02)	4.6D-04
T(0 15 +1)	2.130195300000D+04	(+/- 5.0D-02)	4.6D-04
T(0 15 +1)	2.112580300000D+04	(+/- 4.5D-02)	3.3D-04
T(0 15 -1)	3.078105000000D+04	(+/- 2.2D-01)	2.1D-04
T(0 15 +1)	3.078105000000D+04	(+/- 2.2D-01)	2.1D-04
T(0 16 -1)	2.130303900000D+04	(+/- 4.7D-02)	3.3D-04
T(0 16 -1)	2.112484800000D+04	(+/- 4.8D-02)	4.6D-04
T(0 16 +1)	2.148947800000D+04	(+/- 6.5D-02)	9.1D-04
T(0 16 +1)	2.130303900000D+04	(+/- 4.7D-02)	3.3D-04
T(0 16 -1)	3.084238000000D+04	(+/- 2.1D-01)	1.9D-04
T(0 16 +1)	3.084238000000D+04	(+/- 2.1D-01)	1.9D-04
T(0 17 -1)	2.149066800000D+04	(+/- 4.9D-02)	3.3D-04
T(0 17 -1)	2.130195300000D+04	(+/- 5.0D-02)	4.6D-04
T(0 17 +1)	2.168721800000D+04	(+/- 6.7D-02)	9.1D-04
T(0 17 +1)	2.149066800000D+04	(+/- 4.9D-02)	3.3D-04
T(0 17 -1)	3.090750000000D+04	(+/- 2.2D-01)	2.2D-04
T(0 17 +1)	3.090750000000D+04	(+/- 2.2D-01)	2.2D-04
T(0 18 -1)	2.168856900000D+04	(+/- 5.0D-02)	3.3D-04
T(0 18 -1)	2.148947800000D+04	(+/- 6.5D-02)	9.1D-04
T(0 18 +1)	2.189515600000D+04	(+/- 6.8D-02)	9.1D-04
T(0 18 +1)	2.168856900000D+04	(+/- 5.0D-02)	3.3D-04
T(0 18 -1)	3.097637000000D+04	(+/- 2.1D-01)	1.9D-04
T(0 18 +1)	3.097637000000D+04	(+/- 2.1D-01)	1.9D-04
T(0 19 -1)	2.189661600000D+04	(+/- 5.6D-02)	4.5D-04
T(0 19 -1)	2.168721800000D+04	(+/- 6.7D-02)	9.1D-04
T(0 19 +1)	2.211305900000D+04	(+/- 5.6D-02)	4.6D-04
T(0 19 +1)	2.189661600000D+04	(+/- 5.6D-02)	4.5D-04
T(0 19 -1)	3.105338000000D+04	(+/- 2.1D-01)	2.1D-04
T(0 19 +1)	3.105338000000D+04	(+/- 2.1D-01)	2.1D-04
T(0 20 -1)	2.211467500000D+04	(+/- 5.4D-02)	3.3D-04
T(0 20 -1)	2.189515600000D+04	(+/- 6.8D-02)	9.1D-04
T(0 20 +1)	2.234086300000D+04	(+/- 5.8D-02)	4.6D-04
T(0 20 +1)	2.211467500000D+04	(+/- 5.4D-02)	3.3D-04
T(0 20 -1)	3.112400000000D+04	(+/- 2.2D-01)	2.3D-04
T(0 20 +1)	3.112400000000D+04	(+/- 2.2D-01)	2.3D-04
T(0 21 -1)	2.234261100000D+04	(+/- 5.5D-02)	3.3D-04
T(0 21 -1)	2.211305900000D+04	(+/- 5.6D-02)	4.6D-04
T(0 21 +1)	2.257838000000D+04	(+/- 7.2D-02)	9.1D-04
T(0 21 +1)	2.234261100000D+04	(+/- 5.5D-02)	3.3D-04
T(0 21 -1)	3.120388000000D+04	(+/- 2.1D-01)	2.2D-04
T(0 21 +1)	3.120388000000D+04	(+/- 2.1D-01)	2.2D-04
T(0 22 -1)	2.258027700000D+04	(+/- 5.7D-02)	3.3D-04
T(0 22 -1)	2.234086300000D+04	(+/- 5.8D-02)	4.6D-04
T(0 22 +1)	2.282546800000D+04	(+/- 6.1D-02)	4.6D-04
T(0 22 +1)	2.258027700000D+04	(+/- 5.7D-02)	3.3D-04
T(0 22 -1)	3.128728000000D+04	(+/- 2.1D-01)	2.1D-04
T(0 22 +1)	3.128728000000D+04	(+/- 2.1D-01)	2.1D-04
T(0 23 -1)	2.282752500000D+04	(+/- 5.8D-02)	3.3D-04

Table C.2 Energy origins of "fluorescence series" of BeD isotopomer (cm^{-1}) (*Cont'd*)

T(v' j' p')	Energy Origin	Uncertainty	Sensitivity
T(0 23 -1)	2.257838000000D+04	(+/- 7.2D-02)	9.1D-04
T(0 23 +1)	2.308199100000D+04	(+/- 7.4D-02)	9.1D-04
T(0 23 +1)	2.282752500000D+04	(+/- 5.8D-02)	3.3D-04
T(0 23 -1)	3.137413000000D+04	(+/- 2.0D-01)	1.9D-04
T(0 23 +1)	3.137413000000D+04	(+/- 2.0D-01)	1.9D-04
T(0 24 -1)	2.308420100000D+04	(+/- 6.0D-02)	3.3D-04
T(0 24 -1)	2.282546800000D+04	(+/- 6.1D-02)	4.6D-04
T(0 24 +1)	2.334777200000D+04	(+/- 7.5D-02)	9.1D-04
T(0 24 +1)	2.308420100000D+04	(+/- 6.0D-02)	3.3D-04
T(0 24 -1)	3.146455000000D+04	(+/- 2.0D-01)	1.9D-04
T(0 24 +1)	3.146455000000D+04	(+/- 2.0D-01)	1.9D-04
T(0 25 -1)	2.335015300000D+04	(+/- 6.2D-02)	4.5D-04
T(0 25 -1)	2.308199100000D+04	(+/- 7.4D-02)	9.1D-04
T(0 25 +1)	2.362267500000D+04	(+/- 7.6D-02)	9.1D-04
T(0 25 +1)	2.335015300000D+04	(+/- 6.2D-02)	4.5D-04
T(0 25 -1)	3.155856000000D+04	(+/- 2.0D-01)	1.9D-04
T(0 25 +1)	3.155855000000D+04	(+/- 2.1D-01)	2.0D-04
T(0 26 -1)	2.362519800000D+04	(+/- 6.2D-02)	3.3D-04
T(0 26 -1)	2.334777200000D+04	(+/- 7.5D-02)	9.1D-04
T(0 26 +1)	2.390653000000D+04	(+/- 7.6D-02)	9.1D-04
T(0 26 +1)	2.362519800000D+04	(+/- 6.2D-02)	3.3D-04
T(0 26 -1)	3.165619000000D+04	(+/- 2.1D-01)	2.2D-04
T(0 26 +1)	3.165619000000D+04	(+/- 2.1D-01)	2.2D-04
T(0 27 -1)	2.390919900000D+04	(+/- 6.3D-02)	3.3D-04
T(0 27 -1)	2.362267500000D+04	(+/- 7.6D-02)	9.1D-04
T(0 27 +1)	2.419909800000D+04	(+/- 6.6D-02)	4.6D-04
T(0 27 +1)	2.390919900000D+04	(+/- 6.3D-02)	3.3D-04
T(0 27 -1)	3.175713000000D+04	(+/- 2.2D-01)	2.2D-04
T(0 27 +1)	3.175713000000D+04	(+/- 2.2D-01)	2.2D-04
T(0 28 -1)	2.420195200000D+04	(+/- 6.4D-02)	3.3D-04
T(0 28 -1)	2.390653000000D+04	(+/- 7.6D-02)	9.1D-04
T(0 28 +1)	2.420195200000D+04	(+/- 6.4D-02)	3.3D-04
T(0 28 -1)	3.186256000000D+04	(+/- 2.0D-01)	1.9D-04
T(0 28 +1)	3.186256000000D+04	(+/- 2.0D-01)	1.9D-04
T(0 29 -1)	2.450329700000D+04	(+/- 6.5D-02)	3.3D-04
T(0 29 -1)	2.419909800000D+04	(+/- 6.6D-02)	4.6D-04
T(0 29 +1)	2.450329700000D+04	(+/- 6.5D-02)	3.3D-04
T(0 29 -1)	3.196858000000D+04	(+/- 2.1D-01)	2.0D-04
T(0 29 +1)	3.196858000000D+04	(+/- 2.1D-01)	2.0D-04
T(0 30 -1)	2.481304500000D+04	(+/- 6.8D-02)	4.5D-04
T(0 30 +1)	2.481304500000D+04	(+/- 6.8D-02)	4.5D-04
T(0 30 -1)	3.208006000000D+04	(+/- 2.2D-01)	2.1D-04
T(0 30 +1)	3.208006000000D+04	(+/- 2.2D-01)	2.1D-04
T(0 31 -1)	2.513102900000D+04	(+/- 6.7D-02)	3.3D-04
T(0 31 +1)	2.513102900000D+04	(+/- 6.7D-02)	3.3D-04
T(0 31 -1)	3.219466000000D+04	(+/- 2.2D-01)	2.3D-04
T(0 31 +1)	3.219466000000D+04	(+/- 2.2D-01)	2.3D-04
T(0 32 -1)	2.545704400000D+04	(+/- 7.9D-02)	8.6D-04
T(0 32 +1)	2.545704400000D+04	(+/- 7.9D-02)	8.6D-04
T(0 32 -1)	3.231252000000D+04	(+/- 2.2D-01)	2.1D-04
T(0 32 +1)	3.231251000000D+04	(+/- 2.2D-01)	2.2D-04
T(0 33 -1)	2.579089700000D+04	(+/- 6.8D-02)	3.3D-04
T(0 33 +1)	2.579089700000D+04	(+/- 6.8D-02)	3.3D-04
T(0 33 -1)	3.243357000000D+04	(+/- 2.3D-01)	2.6D-04
T(0 33 +1)	3.243357000000D+04	(+/- 2.3D-01)	2.6D-04
T(0 34 -1)	2.613240400000D+04	(+/- 6.9D-02)	3.3D-04
T(0 34 +1)	2.613240400000D+04	(+/- 6.9D-02)	3.3D-04

Table C.2 Energy origins of "fluorescence series" of BeD isotopomer (cm^{-1}) (*Cont'd*)

T(v'	j'	p')	Energy Origin	Uncertainty	Sensitivity
T(0	34	-1)	3.255806000000D+04	(+/- 2.5D-01)	3.1D-04
T(0	34	+1)	3.255806000000D+04	(+/- 2.5D-01)	3.1D-04
T(0	35	-1)	2.648136500000D+04	(+/- 7.2D-02)	4.1D-04
T(0	35	+1)	2.648136500000D+04	(+/- 7.2D-02)	4.1D-04
T(0	35	-1)	3.268613000000D+04	(+/- 2.5D-01)	2.7D-04
T(0	35	+1)	3.268613000000D+04	(+/- 2.5D-01)	2.7D-04
T(0	36	-1)	2.683756500000D+04	(+/- 7.1D-02)	3.3D-04
T(0	36	+1)	2.683756500000D+04	(+/- 7.1D-02)	3.3D-04
T(0	36	-1)	3.281582000000D+04	(+/- 2.5D-01)	2.3D-04
T(0	36	+1)	3.281582000000D+04	(+/- 2.5D-01)	2.3D-04
T(0	37	-1)	2.720081900000D+04	(+/- 7.2D-02)	3.3D-04
T(0	37	+1)	2.720081900000D+04	(+/- 7.2D-02)	3.3D-04
T(0	37	-1)	3.294966000000D+04	(+/- 2.8D-01)	3.2D-04
T(0	37	+1)	3.294966000000D+04	(+/- 2.8D-01)	3.2D-04
T(0	38	-1)	2.757090400000D+04	(+/- 7.3D-02)	3.3D-04
T(0	38	+1)	2.757090400000D+04	(+/- 7.3D-02)	3.3D-04
T(0	38	-1)	3.308728000000D+04	(+/- 3.0D-01)	3.2D-04
T(0	38	+1)	3.308728000000D+04	(+/- 3.0D-01)	3.2D-04
T(0	39	-1)	2.794763400000D+04	(+/- 7.4D-02)	3.3D-04
T(0	39	+1)	2.794763400000D+04	(+/- 7.4D-02)	3.3D-04
T(0	39	-1)	3.322635000000D+04	(+/- 3.0D-01)	3.3D-04
T(0	39	+1)	3.322635000000D+04	(+/- 3.0D-01)	3.3D-04
T(0	40	-1)	2.833080000000D+04	(+/- 1.1D-01)	1.6D-04
T(0	40	+1)	2.833080000000D+04	(+/- 1.1D-01)	1.6D-04
T(0	40	-1)	3.337255000000D+04	(+/- 3.7D-01)	4.4D-04
T(0	40	+1)	3.337255000000D+04	(+/- 3.7D-01)	4.4D-04
T(0	41	-1)	2.872013000000D+04	(+/- 1.1D-01)	1.6D-04
T(0	41	+1)	2.872013000000D+04	(+/- 1.1D-01)	1.6D-04
T(0	41	-1)	3.351639000000D+04	(+/- 4.3D-01)	4.6D-04
T(0	41	+1)	3.351639000000D+04	(+/- 4.3D-01)	4.6D-04
T(0	42	-1)	2.911546000000D+04	(+/- 1.1D-01)	1.6D-04
T(0	42	+1)	2.911546000000D+04	(+/- 1.1D-01)	1.6D-04
T(0	43	-1)	2.951657200000D+04	(+/- 9.6D-02)	9.1D-04
T(0	43	+1)	2.951657200000D+04	(+/- 9.6D-02)	9.1D-04
T(0	44	-1)	2.992320800000D+04	(+/- 9.8D-02)	8.6D-04
T(0	44	+1)	2.992320800000D+04	(+/- 9.8D-02)	8.6D-04
T(0	45	-1)	3.033519000000D+04	(+/- 1.4D-01)	2.1D-04
T(0	45	+1)	3.033519000000D+04	(+/- 1.4D-01)	2.1D-04
T(0	46	-1)	3.075222000000D+04	(+/- 1.3D-01)	1.6D-04
T(0	46	+1)	3.075222000000D+04	(+/- 1.3D-01)	1.6D-04
T(0	47	-1)	3.117417000000D+04	(+/- 1.3D-01)	1.6D-04
T(0	47	+1)	3.117417000000D+04	(+/- 1.3D-01)	1.6D-04
T(0	48	-1)	3.160076000000D+04	(+/- 1.4D-01)	1.6D-04
T(0	48	+1)	3.160076000000D+04	(+/- 1.4D-01)	1.6D-04
T(0	49	-1)	3.203167000000D+04	(+/- 1.5D-01)	1.6D-04
T(0	49	+1)	3.203167000000D+04	(+/- 1.5D-01)	1.6D-04
T(1	1	+1)	2.129327000000D+04	(+/- 5.2D-02)	4.5D-04
T(1	2	-1)	2.131450500000D+04	(+/- 6.4D-02)	8.6D-04
T(1	2	+1)	2.131532600000D+04	(+/- 9.6D-02)	1.6D-04
T(1	3	-1)	2.134802100000D+04	(+/- 5.2D-02)	4.5D-04
T(1	3	+1)	2.134856100000D+04	(+/- 9.2D-02)	1.5D-04
T(1	4	-1)	2.139252100000D+04	(+/- 5.2D-02)	4.6D-04
T(1	4	+1)	2.144795000000D+04	(+/- 1.2D-01)	2.1D-04
T(1	4	+1)	2.139295100000D+04	(+/- 4.9D-02)	3.3D-04
T(1	5	-1)	2.144803200000D+04	(+/- 5.1D-02)	4.1D-04
T(1	5	+1)	2.151437300000D+04	(+/- 5.2D-02)	4.6D-04
T(1	5	+1)	2.144838600000D+04	(+/- 4.9D-02)	3.3D-04

Table C.2 Energy origins of "fluorescence series" of BeD isotopomer (cm^{-1}) (*Cont'd*)

T(v'	j'	p')	Energy Origin	Uncertainty	Sensitivity
T(1	6	-1)	2.151454100000D+04	(+/- 4.9D-02)	3.3D-04
T(1	6	-1)	2.144820000000D+04	(+/- 1.8D-01)	3.3D-04
T(1	6	+1)	2.159178000000D+04	(+/- 5.2D-02)	4.6D-04
T(1	6	+1)	2.151482500000D+04	(+/- 5.1D-02)	4.1D-04
T(1	7	-1)	2.159200700000D+04	(+/- 4.9D-02)	3.3D-04
T(1	7	-1)	2.151465900000D+04	(+/- 5.2D-02)	4.6D-04
T(1	7	+1)	2.168013400000D+04	(+/- 5.2D-02)	4.6D-04
T(1	7	+1)	2.159224000000D+04	(+/- 4.9D-02)	3.3D-04
T(1	8	-1)	2.168037200000D+04	(+/- 5.7D-02)	6.5D-04
T(1	8	-1)	2.159201900000D+04	(+/- 5.2D-02)	4.6D-04
T(1	8	+1)	2.177923300000D+04	(+/- 6.6D-02)	9.1D-04
T(1	8	+1)	2.168056900000D+04	(+/- 5.7D-02)	6.5D-04
T(1	9	-1)	2.177962800000D+04	(+/- 6.4D-02)	8.4D-04
T(1	9	-1)	2.168025000000D+04	(+/- 1.8D-01)	3.3D-04
T(1	9	+1)	2.188929000000D+04	(+/- 1.8D-01)	3.3D-04
T(1	9	+1)	2.177977500000D+04	(+/- 6.4D-02)	8.4D-04
T(1	10	-1)	2.188968000000D+04	(+/- 6.4D-02)	8.3D-04
T(1	10	-1)	2.177940800000D+04	(+/- 6.6D-02)	9.1D-04
T(1	10	+1)	2.200986400000D+04	(+/- 6.7D-02)	9.1D-04
T(1	10	+1)	2.188968000000D+04	(+/- 6.4D-02)	8.3D-04
T(1	11	-1)	2.201040000000D+04	(+/- 1.0D-01)	1.7D-04
T(1	11	-1)	2.188929000000D+04	(+/- 1.8D-01)	3.3D-04
T(1	11	+1)	2.214114000000D+04	(+/- 1.8D-01)	3.3D-04
T(1	11	+1)	2.201040000000D+04	(+/- 1.0D-01)	1.7D-04
T(1	12	-1)	2.214172500000D+04	(+/- 6.6D-02)	8.9D-04
T(1	12	-1)	2.200986400000D+04	(+/- 6.7D-02)	9.1D-04
T(1	12	+1)	2.228291100000D+04	(+/- 6.8D-02)	9.1D-04
T(1	12	+1)	2.214172500000D+04	(+/- 6.6D-02)	8.9D-04
T(1	13	-1)	2.228359000000D+04	(+/- 5.4D-02)	4.1D-04
T(1	13	-1)	2.214114000000D+04	(+/- 1.8D-01)	3.3D-04
T(1	13	+1)	2.243512000000D+04	(+/- 1.2D-01)	2.1D-04
T(1	13	+1)	2.228359000000D+04	(+/- 5.4D-02)	4.1D-04
T(1	14	-1)	2.243592300000D+04	(+/- 5.3D-02)	3.3D-04
T(1	14	-1)	2.228291100000D+04	(+/- 6.8D-02)	9.1D-04
T(1	14	+1)	2.259766200000D+04	(+/- 5.6D-02)	4.6D-04
T(1	14	+1)	2.243592300000D+04	(+/- 5.3D-02)	3.3D-04
T(1	15	-1)	2.259859800000D+04	(+/- 5.4D-02)	3.3D-04
T(1	15	-1)	2.243512000000D+04	(+/- 1.2D-01)	2.1D-04
T(1	15	+1)	2.277047000000D+04	(+/- 5.7D-02)	4.6D-04
T(1	15	+1)	2.259859800000D+04	(+/- 5.4D-02)	3.3D-04
T(1	16	-1)	2.277151000000D+04	(+/- 5.5D-02)	3.3D-04
T(1	16	-1)	2.259766200000D+04	(+/- 5.6D-02)	4.6D-04
T(1	16	+1)	2.295340100000D+04	(+/- 7.1D-02)	9.1D-04
T(1	16	+1)	2.277151000000D+04	(+/- 5.5D-02)	3.3D-04
T(1	17	-1)	2.295456000000D+04	(+/- 5.6D-02)	3.3D-04
T(1	17	-1)	2.277047000000D+04	(+/- 5.7D-02)	4.6D-04
T(1	17	+1)	2.314631800000D+04	(+/- 5.9D-02)	4.6D-04
T(1	17	+1)	2.295456000000D+04	(+/- 5.6D-02)	3.3D-04
T(1	18	-1)	2.314760800000D+04	(+/- 5.7D-02)	3.3D-04
T(1	18	-1)	2.295340100000D+04	(+/- 7.1D-02)	9.1D-04
T(1	18	+1)	2.334914400000D+04	(+/- 6.0D-02)	4.6D-04
T(1	18	+1)	2.314760800000D+04	(+/- 5.7D-02)	3.3D-04
T(1	19	-1)	2.335054600000D+04	(+/- 5.8D-02)	3.3D-04
T(1	19	-1)	2.314631800000D+04	(+/- 5.9D-02)	4.6D-04
T(1	19	+1)	2.356164300000D+04	(+/- 6.1D-02)	4.6D-04
T(1	19	+1)	2.335054600000D+04	(+/- 5.8D-02)	3.3D-04
T(1	20	-1)	2.356322200000D+04	(+/- 5.9D-02)	3.3D-04

Table C.2 Energy origins of "fluorescence series" of BeD isotopomer (cm^{-1}) (*Cont'd*)

T(v' j' p')	Energy Origin	Uncertainty	Sensitivity
T(1 20 -1)	2.334914400000D+04	(+/- 6.0D-02)	4.6D-04
T(1 20 +1)	2.378386000000D+04	(+/- 1.2D-01)	2.1D-04
T(1 20 +1)	2.356322200000D+04	(+/- 5.9D-02)	3.3D-04
T(1 21 -1)	2.378551200000D+04	(+/- 6.0D-02)	3.3D-04
T(1 21 -1)	2.356164300000D+04	(+/- 6.1D-02)	4.6D-04
T(1 21 +1)	2.401543400000D+04	(+/- 6.3D-02)	4.6D-04
T(1 21 +1)	2.378551200000D+04	(+/- 6.0D-02)	3.3D-04
T(1 22 -1)	2.401727100000D+04	(+/- 6.1D-02)	3.3D-04
T(1 22 -1)	2.378386000000D+04	(+/- 1.2D-01)	2.1D-04
T(1 22 +1)	2.425636900000D+04	(+/- 6.4D-02)	4.6D-04
T(1 22 +1)	2.401727100000D+04	(+/- 6.1D-02)	3.3D-04
T(1 23 -1)	2.425835300000D+04	(+/- 6.2D-02)	3.3D-04
T(1 23 -1)	2.401543400000D+04	(+/- 6.3D-02)	4.6D-04
T(1 23 +1)	2.450648800000D+04	(+/- 7.6D-02)	9.1D-04
T(1 23 +1)	2.425835300000D+04	(+/- 6.2D-02)	3.3D-04
T(1 24 -1)	2.450859300000D+04	(+/- 6.3D-02)	3.3D-04
T(1 24 -1)	2.425636900000D+04	(+/- 6.4D-02)	4.6D-04
T(1 24 +1)	2.476556400000D+04	(+/- 6.6D-02)	4.6D-04
T(1 24 +1)	2.450859300000D+04	(+/- 6.3D-02)	3.3D-04
T(1 25 -1)	2.476784100000D+04	(+/- 6.3D-02)	3.3D-04
T(1 25 -1)	2.450648800000D+04	(+/- 7.6D-02)	9.1D-04
T(1 25 +1)	2.503350000000D+04	(+/- 6.6D-02)	4.6D-04
T(1 25 +1)	2.476784100000D+04	(+/- 6.3D-02)	3.3D-04
T(1 26 -1)	2.503594900000D+04	(+/- 6.4D-02)	3.3D-04
T(1 26 -1)	2.476556400000D+04	(+/- 6.6D-02)	4.6D-04
T(1 26 +1)	2.531015300000D+04	(+/- 7.8D-02)	9.1D-04
T(1 26 +1)	2.503594900000D+04	(+/- 6.4D-02)	3.3D-04
T(1 27 -1)	2.531269900000D+04	(+/- 6.5D-02)	3.3D-04
T(1 27 -1)	2.503350000000D+04	(+/- 6.6D-02)	4.6D-04
T(1 27 +1)	2.559528000000D+04	(+/- 1.2D-01)	2.1D-04
T(1 27 +1)	2.531269900000D+04	(+/- 6.5D-02)	3.3D-04
T(1 28 -1)	2.559796200000D+04	(+/- 6.7D-02)	4.5D-04
T(1 28 -1)	2.531015300000D+04	(+/- 7.8D-02)	9.1D-04
T(1 28 +1)	2.588867000000D+04	(+/- 1.2D-01)	2.1D-04
T(1 28 +1)	2.559796200000D+04	(+/- 6.7D-02)	4.5D-04
T(1 29 -1)	2.589155800000D+04	(+/- 6.6D-02)	3.3D-04
T(1 29 -1)	2.559528000000D+04	(+/- 1.2D-01)	2.1D-04
T(1 29 +1)	2.619035000000D+04	(+/- 1.8D-01)	3.3D-04
T(1 29 +1)	2.589155800000D+04	(+/- 6.6D-02)	3.3D-04
T(1 30 -1)	2.619330600000D+04	(+/- 6.9D-02)	4.5D-04
T(1 30 -1)	2.588867000000D+04	(+/- 1.2D-01)	2.1D-04
T(1 30 +1)	2.649977000000D+04	(+/- 1.2D-01)	2.1D-04
T(1 30 +1)	2.619330600000D+04	(+/- 6.9D-02)	4.5D-04
T(1 31 -1)	2.650298200000D+04	(+/- 6.7D-02)	3.3D-04
T(1 31 -1)	2.619035000000D+04	(+/- 1.8D-01)	3.3D-04
T(1 31 +1)	2.681712000000D+04	(+/- 1.2D-01)	2.1D-04
T(1 31 +1)	2.650298200000D+04	(+/- 6.7D-02)	3.3D-04
T(1 32 -1)	2.682043800000D+04	(+/- 6.7D-02)	3.3D-04
T(1 32 -1)	2.649977000000D+04	(+/- 1.2D-01)	2.1D-04
T(1 32 +1)	2.682043800000D+04	(+/- 6.7D-02)	3.3D-04
T(1 33 -1)	2.714546500000D+04	(+/- 6.9D-02)	4.1D-04
T(1 33 -1)	2.681712000000D+04	(+/- 1.2D-01)	2.1D-04
T(1 33 +1)	2.714546500000D+04	(+/- 6.9D-02)	4.1D-04
T(1 34 -1)	2.747788600000D+04	(+/- 6.8D-02)	3.3D-04
T(1 34 +1)	2.747788600000D+04	(+/- 6.8D-02)	3.3D-04
T(1 35 -1)	2.781747200000D+04	(+/- 6.9D-02)	3.3D-04
T(1 35 +1)	2.781747200000D+04	(+/- 6.9D-02)	3.3D-04

Table C.2 Energy origins of "fluorescence series" of BeD isotopomer (cm^{-1}) (*Cont'd*)

T(v' j' p')	Energy Origin	Uncertainty	Sensitivity
T(1 36 -1)	2.816403300000D+04	(+/- 6.9D-02)	3.3D-04
T(1 36 +1)	2.816403300000D+04	(+/- 6.9D-02)	3.3D-04
T(1 37 -1)	2.851736300000D+04	(+/- 7.0D-02)	3.3D-04
T(1 37 +1)	2.851736300000D+04	(+/- 7.0D-02)	3.3D-04
T(1 38 -1)	2.887725700000D+04	(+/- 7.0D-02)	3.3D-04
T(1 38 +1)	2.887725700000D+04	(+/- 7.0D-02)	3.3D-04
T(1 39 -1)	2.924348400000D+04	(+/- 7.2D-02)	4.5D-04
T(1 39 +1)	2.924348400000D+04	(+/- 7.2D-02)	4.5D-04
T(1 40 -1)	2.961586000000D+04	(+/- 1.1D-01)	1.6D-04
T(1 40 +1)	2.961586000000D+04	(+/- 1.1D-01)	1.6D-04
T(1 41 -1)	2.999414300000D+04	(+/- 7.3D-02)	3.3D-04
T(1 41 +1)	2.999414300000D+04	(+/- 7.3D-02)	3.3D-04
T(1 42 -1)	3.037810800000D+04	(+/- 8.0D-02)	6.5D-04
T(1 42 +1)	3.037810800000D+04	(+/- 8.0D-02)	6.5D-04
T(1 43 -1)	3.076756000000D+04	(+/- 8.9D-02)	8.6D-04
T(1 43 +1)	3.076756000000D+04	(+/- 8.9D-02)	8.6D-04
T(1 44 -1)	3.116229300000D+04	(+/- 8.7D-02)	8.6D-04
T(1 44 +1)	3.116229300000D+04	(+/- 8.7D-02)	8.6D-04
T(1 45 -1)	3.156199100000D+04	(+/- 9.0D-02)	8.6D-04
T(1 45 +1)	3.156199100000D+04	(+/- 9.0D-02)	8.6D-04
T(1 46 -1)	3.196635000000D+04	(+/- 1.2D-01)	1.6D-04
T(1 46 +1)	3.196635000000D+04	(+/- 1.2D-01)	1.6D-04
T(1 47 -1)	3.237536000000D+04	(+/- 1.9D-01)	3.3D-04
T(1 47 +1)	3.237536000000D+04	(+/- 1.9D-01)	3.3D-04
T(1 48 -1)	3.278867000000D+04	(+/- 1.5D-01)	2.1D-04
T(1 48 +1)	3.278867000000D+04	(+/- 1.5D-01)	2.1D-04
T(2 3 +1)	2.284891000000D+04	(+/- 1.3D-01)	2.3D-04
T(2 4 -1)	2.284893400000D+04	(+/- 6.4D-02)	3.3D-04
T(2 4 +1)	2.290290000000D+04	(+/- 1.3D-01)	2.3D-04
T(2 4 +1)	2.284934300000D+04	(+/- 6.6D-02)	4.5D-04
T(2 5 -1)	2.290308100000D+04	(+/- 6.4D-02)	3.3D-04
T(2 5 -1)	2.284934000000D+04	(+/- 1.3D-01)	2.3D-04
T(2 5 +1)	2.296774000000D+04	(+/- 1.2D-01)	2.1D-04
T(2 5 +1)	2.290341400000D+04	(+/- 6.4D-02)	3.3D-04
T(2 6 -1)	2.296791000000D+04	(+/- 1.5D-01)	2.7D-04
T(2 6 -1)	2.290330700000D+04	(+/- 7.8D-02)	9.2D-04
T(2 6 +1)	2.304355000000D+04	(+/- 8.4D-01)	1.6D-04
T(2 6 +1)	2.296821000000D+04	(+/- 1.2D-01)	2.1D-04
T(2 7 -1)	2.304349400000D+04	(+/- 6.5D-02)	4.1D-04
T(2 7 -1)	2.296786000000D+04	(+/- 1.8D-01)	3.3D-04
T(2 7 +1)	2.312939400000D+04	(+/- 7.7D-02)	9.1D-04
T(2 7 +1)	2.304373600000D+04	(+/- 6.9D-02)	6.5D-04
T(2 8 -1)	2.312965600000D+04	(+/- 6.9D-02)	6.5D-04
T(2 8 -1)	2.304352400000D+04	(+/- 7.7D-02)	9.2D-04
T(2 8 +1)	2.322607500000D+04	(+/- 7.6D-02)	9.1D-04
T(2 8 +1)	2.312985500000D+04	(+/- 6.9D-02)	6.5D-04
T(2 9 -1)	2.322640500000D+04	(+/- 6.9D-02)	6.5D-04
T(2 9 -1)	2.312957900000D+04	(+/- 7.7D-02)	9.1D-04
T(2 9 +1)	2.333334000000D+04	(+/- 1.8D-01)	3.3D-04
T(2 9 +1)	2.322657700000D+04	(+/- 6.9D-02)	6.5D-04
T(2 10 -1)	2.333377400000D+04	(+/- 7.4D-02)	8.3D-04
T(2 10 -1)	2.322621800000D+04	(+/- 7.6D-02)	9.1D-04
T(2 10 +1)	2.345089000000D+04	(+/- 1.8D-01)	3.3D-04
T(2 10 +1)	2.333377400000D+04	(+/- 7.4D-02)	8.3D-04
T(2 11 -1)	2.345145000000D+04	(+/- 1.1D-01)	1.7D-04
T(2 11 -1)	2.333334000000D+04	(+/- 1.8D-01)	3.3D-04
T(2 11 +1)	2.357891700000D+04	(+/- 7.6D-02)	9.1D-04

Table C.2 Energy origins of "fluorescence series" of BeD isotopomer (cm^{-1}) (*Cont'd*)

T(v' j' p')	Energy Origin	Uncertainty	Sensitivity
T(2 11 +1)	2.345145000000D+04	(+/- 1.1D-01)	1.7D-04
T(2 12 -1)	2.357952700000D+04	(+/- 7.4D-02)	8.4D-04
T(2 12 -1)	2.345089000000D+04	(+/- 1.8D-01)	3.3D-04
T(2 12 +1)	2.371715500000D+04	(+/- 7.7D-02)	9.1D-04
T(2 12 +1)	2.357952700000D+04	(+/- 7.4D-02)	8.4D-04
T(2 13 -1)	2.371784200000D+04	(+/- 7.4D-02)	8.3D-04
T(2 13 -1)	2.357891700000D+04	(+/- 7.6D-02)	9.1D-04
T(2 13 +1)	2.386549000000D+04	(+/- 1.8D-01)	3.3D-04
T(2 13 +1)	2.371784200000D+04	(+/- 7.4D-02)	8.3D-04
T(2 14 -1)	2.386634400000D+04	(+/- 6.4D-02)	4.1D-04
T(2 14 -1)	2.371715500000D+04	(+/- 7.7D-02)	9.1D-04
T(2 14 +1)	2.386634400000D+04	(+/- 6.4D-02)	4.1D-04
T(2 15 -1)	2.402491700000D+04	(+/- 6.4D-02)	3.3D-04
T(2 15 -1)	2.386549000000D+04	(+/- 1.8D-01)	3.3D-04
T(2 15 +1)	2.419240400000D+04	(+/- 7.7D-02)	9.1D-04
T(2 15 +1)	2.402491700000D+04	(+/- 6.4D-02)	3.3D-04
T(2 16 -1)	2.419345800000D+04	(+/- 6.4D-02)	3.3D-04
T(2 16 +1)	2.437071000000D+04	(+/- 1.8D-01)	3.3D-04
T(2 16 +1)	2.419345800000D+04	(+/- 6.4D-02)	3.3D-04
T(2 17 -1)	2.437185000000D+04	(+/- 6.6D-02)	4.1D-04
T(2 17 -1)	2.419240400000D+04	(+/- 7.7D-02)	9.1D-04
T(2 17 +1)	2.455874100000D+04	(+/- 6.7D-02)	4.6D-04
T(2 17 +1)	2.437185000000D+04	(+/- 6.6D-02)	4.1D-04
T(2 18 -1)	2.455997300000D+04	(+/- 6.7D-02)	4.6D-04
T(2 18 -1)	2.437071000000D+04	(+/- 1.8D-01)	3.3D-04
T(2 18 +1)	2.475640000000D+04	(+/- 1.8D-01)	3.3D-04
T(2 18 +1)	2.455997300000D+04	(+/- 6.7D-02)	4.6D-04
T(2 19 -1)	2.475771700000D+04	(+/- 6.7D-02)	4.5D-04
T(2 19 -1)	2.455874100000D+04	(+/- 6.7D-02)	4.6D-04
T(2 19 +1)	2.496337600000D+04	(+/- 6.8D-02)	4.6D-04
T(2 19 +1)	2.475771700000D+04	(+/- 6.7D-02)	4.5D-04
T(2 20 -1)	2.496491900000D+04	(+/- 6.6D-02)	3.3D-04
T(2 20 -1)	2.475640000000D+04	(+/- 1.8D-01)	3.3D-04
T(2 20 +1)	2.517983100000D+04	(+/- 6.8D-02)	4.6D-04
T(2 20 +1)	2.496491900000D+04	(+/- 6.6D-02)	3.3D-04
T(2 21 -1)	2.518146100000D+04	(+/- 6.6D-02)	3.3D-04
T(2 21 -1)	2.496337600000D+04	(+/- 6.8D-02)	4.6D-04
T(2 21 +1)	2.540548000000D+04	(+/- 6.8D-02)	4.6D-04
T(2 21 +1)	2.518146100000D+04	(+/- 6.6D-02)	3.3D-04
T(2 22 -1)	2.540720200000D+04	(+/- 6.6D-02)	3.3D-04
T(2 22 -1)	2.517983100000D+04	(+/- 6.8D-02)	4.6D-04
T(2 22 +1)	2.564010700000D+04	(+/- 6.9D-02)	4.6D-04
T(2 22 +1)	2.540720200000D+04	(+/- 6.6D-02)	3.3D-04
T(2 23 -1)	2.564198400000D+04	(+/- 6.8D-02)	4.1D-04
T(2 23 -1)	2.540548000000D+04	(+/- 6.8D-02)	4.6D-04
T(2 23 +1)	2.588363000000D+04	(+/- 1.8D-01)	3.3D-04
T(2 23 +1)	2.564198400000D+04	(+/- 6.8D-02)	4.1D-04
T(2 24 -1)	2.588565900000D+04	(+/- 6.9D-02)	4.5D-04
T(2 24 -1)	2.564010700000D+04	(+/- 6.9D-02)	4.6D-04
T(2 24 +1)	2.613592000000D+04	(+/- 1.8D-01)	3.3D-04
T(2 24 +1)	2.588565900000D+04	(+/- 6.9D-02)	4.5D-04
T(2 25 -1)	2.613806300000D+04	(+/- 6.9D-02)	4.5D-04
T(2 25 -1)	2.588363000000D+04	(+/- 1.8D-01)	3.3D-04
T(2 25 +1)	2.639671300000D+04	(+/- 7.0D-02)	4.6D-04
T(2 25 +1)	2.613806300000D+04	(+/- 6.9D-02)	4.5D-04
T(2 26 -1)	2.639903400000D+04	(+/- 6.8D-02)	3.3D-04
T(2 26 -1)	2.613592000000D+04	(+/- 1.8D-01)	3.3D-04

Table C.2 Energy origins of "fluorescence series" of BeD isotopomer (cm^{-1}) (*Cont'd*)

T(v'	j'	p')	Energy Origin	Uncertainty	Sensitivity
T(2	26	+1)	2.666597400000D+04	(+/- 7.0D-02)	4.6D-04
T(2	26	+1)	2.639903400000D+04	(+/- 6.8D-02)	3.3D-04
T(2	27	-1)	2.666839600000D+04	(+/- 6.8D-02)	3.3D-04
T(2	27	-1)	2.639671300000D+04	(+/- 7.0D-02)	4.6D-04
T(2	27	+1)	2.694340200000D+04	(+/- 7.0D-02)	4.6D-04
T(2	27	+1)	2.666839600000D+04	(+/- 6.8D-02)	3.3D-04
T(2	28	-1)	2.694597700000D+04	(+/- 6.8D-02)	3.3D-04
T(2	28	-1)	2.666597400000D+04	(+/- 7.0D-02)	4.6D-04
T(2	28	+1)	2.694597700000D+04	(+/- 6.8D-02)	3.3D-04
T(2	29	-1)	2.723162700000D+04	(+/- 6.9D-02)	3.3D-04
T(2	29	-1)	2.694340200000D+04	(+/- 7.0D-02)	4.6D-04
T(2	29	+1)	2.723162700000D+04	(+/- 6.9D-02)	3.3D-04
T(2	30	-1)	2.752512000000D+04	(+/- 6.9D-02)	3.3D-04
T(2	30	+1)	2.752512000000D+04	(+/- 6.9D-02)	3.3D-04
T(2	31	-1)	2.782629900000D+04	(+/- 7.1D-02)	4.6D-04
T(2	31	+1)	2.782629900000D+04	(+/- 7.1D-02)	4.6D-04
T(2	32	-1)	2.813500600000D+04	(+/- 7.1D-02)	4.6D-04
T(2	32	+1)	2.813500600000D+04	(+/- 7.1D-02)	4.6D-04
T(2	33	-1)	2.845093100000D+04	(+/- 7.2D-02)	4.5D-04
T(2	33	+1)	2.845093100000D+04	(+/- 7.2D-02)	4.5D-04
T(2	34	-1)	2.877394400000D+04	(+/- 7.0D-02)	3.3D-04
T(2	34	+1)	2.877394400000D+04	(+/- 7.0D-02)	3.3D-04
T(2	35	-1)	2.910389000000D+04	(+/- 7.0D-02)	3.3D-04
T(2	35	+1)	2.910389000000D+04	(+/- 7.0D-02)	3.3D-04
T(2	36	-1)	2.944051200000D+04	(+/- 7.2D-02)	4.5D-04
T(2	36	+1)	2.944051200000D+04	(+/- 7.2D-02)	4.5D-04
T(2	37	-1)	2.978359300000D+04	(+/- 7.3D-02)	4.6D-04
T(2	37	+1)	2.978359300000D+04	(+/- 7.3D-02)	4.6D-04
T(2	38	-1)	3.013295200000D+04	(+/- 7.3D-02)	4.6D-04
T(2	38	+1)	3.013295200000D+04	(+/- 7.3D-02)	4.6D-04
T(2	39	-1)	3.048835400000D+04	(+/- 8.3D-02)	8.6D-04
T(2	39	+1)	3.048835400000D+04	(+/- 8.3D-02)	8.6D-04
T(2	40	-1)	3.084956700000D+04	(+/- 7.6D-02)	4.6D-04
T(2	40	+1)	3.084956700000D+04	(+/- 7.6D-02)	4.6D-04
T(2	41	-1)	3.121641500000D+04	(+/- 7.8D-02)	4.1D-04
T(2	41	+1)	3.121641500000D+04	(+/- 7.8D-02)	4.1D-04
T(2	42	-1)	3.158863500000D+04	(+/- 8.9D-02)	8.6D-04
T(2	42	+1)	3.158863500000D+04	(+/- 8.9D-02)	8.6D-04
T(3	3	-1)	2.421592000000D+04	(+/- 1.8D-01)	3.3D-04
T(3	3	+1)	2.421644000000D+04	(+/- 1.3D-01)	2.1D-04
T(3	4	-1)	2.425817800000D+04	(+/- 7.3D-02)	4.5D-04
T(3	4	+1)	2.425863000000D+04	(+/- 1.3D-01)	2.1D-04
T(3	5	-1)	2.431094000000D+04	(+/- 1.1D-01)	1.6D-04
T(3	5	+1)	2.431127200000D+04	(+/- 7.3D-02)	4.5D-04
T(3	6	-1)	2.437415700000D+04	(+/- 7.2D-02)	4.5D-04
T(3	6	+1)	2.437443100000D+04	(+/- 7.2D-02)	4.5D-04
T(3	7	-1)	2.444774500000D+04	(+/- 7.2D-02)	4.5D-04
T(3	7	+1)	2.453147000000D+04	(+/- 1.8D-01)	3.3D-04
T(3	7	+1)	2.444798300000D+04	(+/- 7.2D-02)	4.5D-04
T(3	8	-1)	2.453173800000D+04	(+/- 8.0D-02)	8.3D-04
T(3	8	+1)	2.462571000000D+04	(+/- 1.8D-01)	3.3D-04
T(3	8	+1)	2.453193000000D+04	(+/- 1.2D-01)	1.9D-04
T(3	9	-1)	2.462597500000D+04	(+/- 8.1D-02)	8.7D-04
T(3	9	-1)	2.453155000000D+04	(+/- 1.8D-01)	3.3D-04
T(3	9	+1)	2.473013000000D+04	(+/- 2.4D-01)	4.5D-04
T(3	9	+1)	2.462614700000D+04	(+/- 8.0D-02)	8.4D-04
T(3	10	-1)	2.473052700000D+04	(+/- 7.5D-02)	6.4D-04

Table C.2 Energy origins of "fluorescence series" of BeD isotopomer (cm^{-1}) (*Cont'd*)

T(v' j' p')	Energy Origin	Uncertainty	Sensitivity
T(3 10 -1)	2.462584000000D+04	(+/- 8.2D-02)	9.1D-04
T(3 10 +1)	2.484469000000D+04	(+/- 1.8D-01)	3.3D-04
T(3 10 +1)	2.473052700000D+04	(+/- 7.5D-02)	6.4D-04
T(3 11 -1)	2.484517500000D+04	(+/- 7.4D-02)	6.4D-04
T(3 11 -1)	2.473013000000D+04	(+/- 2.4D-01)	4.5D-04
T(3 11 +1)	2.496933000000D+04	(+/- 1.8D-01)	3.3D-04
T(3 11 +1)	2.484517500000D+04	(+/- 7.4D-02)	6.4D-04
T(3 12 -1)	2.496988900000D+04	(+/- 8.0D-02)	8.7D-04
T(3 12 -1)	2.484469000000D+04	(+/- 1.8D-01)	3.3D-04
T(3 12 +1)	2.510396000000D+04	(+/- 8.1D-02)	9.2D-04
T(3 12 +1)	2.496988900000D+04	(+/- 8.0D-02)	8.7D-04
T(3 13 -1)	2.510459900000D+04	(+/- 7.9D-02)	8.4D-04
T(3 13 -1)	2.496933000000D+04	(+/- 1.8D-01)	3.3D-04
T(3 13 +1)	2.524841000000D+04	(+/- 1.3D-01)	2.1D-04
T(3 13 +1)	2.510459900000D+04	(+/- 7.9D-02)	8.4D-04
T(3 14 -1)	2.524919600000D+04	(+/- 7.0D-02)	4.6D-04
T(3 14 -1)	2.510396000000D+04	(+/- 8.1D-02)	9.2D-04
T(3 14 +1)	2.540275000000D+04	(+/- 1.2D-01)	2.1D-04
T(3 14 +1)	2.524919600000D+04	(+/- 7.0D-02)	4.6D-04
T(3 15 -1)	2.540360500000D+04	(+/- 7.0D-02)	4.5D-04
T(3 15 -1)	2.524841000000D+04	(+/- 1.3D-01)	2.1D-04
T(3 15 +1)	2.556671000000D+04	(+/- 1.3D-01)	2.2D-04
T(3 15 +1)	2.540360500000D+04	(+/- 7.0D-02)	4.5D-04
T(3 16 -1)	2.556769200000D+04	(+/- 8.0D-02)	8.7D-04
T(3 16 -1)	2.540275000000D+04	(+/- 1.2D-01)	2.1D-04
T(3 16 +1)	2.574026000000D+04	(+/- 1.8D-01)	3.3D-04
T(3 16 +1)	2.556769200000D+04	(+/- 8.0D-02)	8.7D-04
T(3 17 -1)	2.574134200000D+04	(+/- 6.8D-02)	3.3D-04
T(3 17 -1)	2.556671000000D+04	(+/- 1.3D-01)	2.2D-04
T(3 17 +1)	2.592328000000D+04	(+/- 1.8D-01)	3.3D-04
T(3 17 +1)	2.574134200000D+04	(+/- 6.8D-02)	3.3D-04
T(3 18 -1)	2.592445200000D+04	(+/- 6.8D-02)	3.3D-04
T(3 18 -1)	2.574026000000D+04	(+/- 1.8D-01)	3.3D-04
T(3 18 +1)	2.611550000000D+04	(+/- 2.2D-01)	4.1D-04
T(3 18 +1)	2.592445200000D+04	(+/- 6.8D-02)	3.3D-04
T(3 19 -1)	2.611687900000D+04	(+/- 7.0D-02)	4.6D-04
T(3 19 -1)	2.592328000000D+04	(+/- 1.8D-01)	3.3D-04
T(3 19 +1)	2.631711700000D+04	(+/- 7.0D-02)	4.6D-04
T(3 19 +1)	2.611687900000D+04	(+/- 7.0D-02)	4.6D-04
T(3 20 -1)	2.631851200000D+04	(+/- 7.0D-02)	4.5D-04
T(3 20 -1)	2.611550000000D+04	(+/- 2.2D-01)	4.1D-04
T(3 20 +1)	2.652760000000D+04	(+/- 1.8D-01)	3.3D-04
T(3 20 +1)	2.631851200000D+04	(+/- 7.0D-02)	4.5D-04
T(3 21 -1)	2.652919200000D+04	(+/- 6.9D-02)	3.3D-04
T(3 21 -1)	2.631711700000D+04	(+/- 7.0D-02)	4.6D-04
T(3 21 +1)	2.674709300000D+04	(+/- 7.1D-02)	4.6D-04
T(3 21 +1)	2.652919200000D+04	(+/- 6.9D-02)	3.3D-04
T(3 22 -1)	2.674875600000D+04	(+/- 6.9D-02)	3.3D-04
T(3 22 -1)	2.652760000000D+04	(+/- 1.8D-01)	3.3D-04
T(3 22 +1)	2.697535100000D+04	(+/- 7.1D-02)	4.6D-04
T(3 22 +1)	2.674875600000D+04	(+/- 6.9D-02)	3.3D-04
T(3 23 -1)	2.697712300000D+04	(+/- 7.0D-02)	4.1D-04
T(3 23 -1)	2.674709300000D+04	(+/- 7.1D-02)	4.6D-04
T(3 23 +1)	2.721220000000D+04	(+/- 1.3D-01)	2.1D-04
T(3 23 +1)	2.697712300000D+04	(+/- 7.0D-02)	4.1D-04
T(3 24 -1)	2.721408200000D+04	(+/- 7.1D-02)	4.5D-04
T(3 24 -1)	2.697535100000D+04	(+/- 7.1D-02)	4.6D-04

Table C.2 Energy origins of "fluorescence series" of BeD isotopomer (cm^{-1}) (*Cont'd*)

T(v' j' p')	Energy Origin	Uncertainty	Sensitivity
T(3 24 +1)	2.745742000000D+04	(+/- 2.2D-01)	4.1D-04
T(3 24 +1)	2.721408200000D+04	(+/- 7.1D-02)	4.5D-04
T(3 25 -1)	2.745946900000D+04	(+/- 7.1D-02)	4.5D-04
T(3 25 -1)	2.721220000000D+04	(+/- 1.3D-01)	2.1D-04
T(3 25 +1)	2.771094100000D+04	(+/- 7.1D-02)	4.6D-04
T(3 25 +1)	2.745946900000D+04	(+/- 7.1D-02)	4.5D-04
T(3 26 -1)	2.771315100000D+04	(+/- 7.1D-02)	4.5D-04
T(3 26 -1)	2.745742000000D+04	(+/- 2.2D-01)	4.1D-04
T(3 26 +1)	2.797257200000D+04	(+/- 7.1D-02)	4.6D-04
T(3 26 +1)	2.771315100000D+04	(+/- 7.1D-02)	4.5D-04
T(3 27 -1)	2.797489900000D+04	(+/- 8.2D-02)	9.1D-04
T(3 27 -1)	2.771094100000D+04	(+/- 7.1D-02)	4.6D-04
T(3 27 +1)	2.824215000000D+04	(+/- 2.2D-01)	4.1D-04
T(3 27 +1)	2.797489900000D+04	(+/- 8.2D-02)	9.1D-04
T(3 28 -1)	2.824464800000D+04	(+/- 7.1D-02)	4.5D-04
T(3 28 -1)	2.797257200000D+04	(+/- 7.1D-02)	4.6D-04
T(3 28 +1)	2.851957000000D+04	(+/- 1.8D-01)	3.3D-04
T(3 28 +1)	2.824464800000D+04	(+/- 7.1D-02)	4.5D-04
T(3 29 -1)	2.852212500000D+04	(+/- 7.0D-02)	3.3D-04
T(3 29 -1)	2.824215000000D+04	(+/- 2.2D-01)	4.1D-04
T(3 29 +1)	2.880446200000D+04	(+/- 7.2D-02)	4.6D-04
T(3 29 +1)	2.852212500000D+04	(+/- 7.0D-02)	3.3D-04
T(3 30 -1)	2.880715100000D+04	(+/- 7.0D-02)	3.3D-04
T(3 30 -1)	2.851957000000D+04	(+/- 1.8D-01)	3.3D-04
T(3 30 +1)	2.909677000000D+04	(+/- 1.8D-01)	3.3D-04
T(3 30 +1)	2.880715100000D+04	(+/- 7.0D-02)	3.3D-04
T(3 31 -1)	2.909957400000D+04	(+/- 7.0D-02)	3.3D-04
T(3 31 -1)	2.880446200000D+04	(+/- 7.2D-02)	4.6D-04
T(3 31 +1)	2.939625700000D+04	(+/- 8.3D-02)	9.1D-04
T(3 31 +1)	2.909957400000D+04	(+/- 7.0D-02)	3.3D-04
T(3 32 -1)	2.939917700000D+04	(+/- 7.3D-02)	4.5D-04
T(3 32 -1)	2.909677000000D+04	(+/- 1.8D-01)	3.3D-04
T(3 32 +1)	2.939917700000D+04	(+/- 7.3D-02)	4.5D-04
T(3 33 -1)	2.970577000000D+04	(+/- 7.1D-02)	3.3D-04
T(3 33 -1)	2.939625700000D+04	(+/- 8.3D-02)	9.1D-04
T(3 33 +1)	3.001598000000D+04	(+/- 2.2D-01)	4.1D-04
T(3 33 +1)	2.970577000000D+04	(+/- 7.1D-02)	3.3D-04
T(3 34 -1)	3.001916200000D+04	(+/- 7.3D-02)	4.6D-04
T(3 34 +1)	3.033594000000D+04	(+/- 1.8D-01)	3.3D-04
T(3 34 +1)	3.001916200000D+04	(+/- 7.3D-02)	4.6D-04
T(3 35 -1)	3.033911900000D+04	(+/- 7.4D-02)	4.5D-04
T(3 35 -1)	3.001598000000D+04	(+/- 2.2D-01)	4.1D-04
T(3 35 +1)	3.033911900000D+04	(+/- 7.4D-02)	4.5D-04
T(3 36 -1)	3.066549000000D+04	(+/- 1.1D-01)	1.6D-04
T(3 36 -1)	3.033594000000D+04	(+/- 1.8D-01)	3.3D-04
T(3 36 +1)	3.066549000000D+04	(+/- 1.1D-01)	1.6D-04
T(4 6 -1)	2.573235000000D+04	(+/- 7.6D-02)	4.6D-04
T(4 6 +1)	2.573262800000D+04	(+/- 7.6D-02)	4.6D-04
T(4 7 -1)	2.580394300000D+04	(+/- 8.4D-02)	8.6D-04
T(4 7 +1)	2.588553000000D+04	(+/- 2.2D-01)	4.1D-04
T(4 7 +1)	2.580418600000D+04	(+/- 8.4D-02)	8.6D-04
T(4 8 -1)	2.588563200000D+04	(+/- 8.4D-02)	8.6D-04
T(4 8 +1)	2.597707000000D+04	(+/- 2.2D-01)	4.1D-04
T(4 8 +1)	2.588582800000D+04	(+/- 8.4D-02)	8.6D-04
T(4 9 -1)	2.597743100000D+04	(+/- 8.4D-02)	9.0D-04
T(4 9 -1)	2.588553000000D+04	(+/- 2.2D-01)	4.1D-04
T(4 9 +1)	2.607869000000D+04	(+/- 2.2D-01)	4.1D-04

Table C.2 Energy origins of "fluorescence series" of BeD isotopomer (cm^{-1}) (*Cont'd*)

T(v' j' p')	Energy Origin	Uncertainty	Sensitivity
T(4 9 +1)	2.597743100000D+04	(+/- 8.4D-02)	9.0D-04
T(4 10 -1)	2.607906200000D+04	(+/- 8.4D-02)	9.1D-04
T(4 10 -1)	2.597719000000D+04	(+/- 2.2D-01)	4.1D-04
T(4 10 +1)	2.607906200000D+04	(+/- 8.4D-02)	9.1D-04
T(4 11 -1)	2.619054000000D+04	(+/- 7.8D-02)	6.5D-04
T(4 11 -1)	2.607869000000D+04	(+/- 2.2D-01)	4.1D-04
T(4 11 +1)	2.631132000000D+04	(+/- 2.4D-01)	4.5D-04
T(4 11 +1)	2.619054000000D+04	(+/- 7.8D-02)	6.5D-04
T(4 12 -1)	2.631183600000D+04	(+/- 7.3D-02)	4.1D-04
T(4 12 +1)	2.631183600000D+04	(+/- 7.3D-02)	4.1D-04
T(4 13 -1)	2.644284200000D+04	(+/- 7.1D-02)	3.3D-04
T(4 13 -1)	2.631132000000D+04	(+/- 2.4D-01)	4.5D-04
T(4 13 +1)	2.644284200000D+04	(+/- 7.1D-02)	3.3D-04
T(4 14 -1)	2.658344200000D+04	(+/- 7.3D-02)	4.6D-04
T(4 14 +1)	2.673274900000D+04	(+/- 7.3D-02)	4.6D-04
T(4 14 +1)	2.658344200000D+04	(+/- 7.3D-02)	4.6D-04
T(4 15 -1)	2.673357000000D+04	(+/- 1.2D-01)	2.0D-04
T(4 15 +1)	2.689214000000D+04	(+/- 2.4D-01)	4.5D-04
T(4 15 +1)	2.673357000000D+04	(+/- 1.2D-01)	2.0D-04
T(4 16 -1)	2.689310000000D+04	(+/- 1.2D-01)	2.0D-04
T(4 16 -1)	2.673274900000D+04	(+/- 7.3D-02)	4.6D-04
T(4 16 +1)	2.706090000000D+04	(+/- 2.2D-01)	4.1D-04
T(4 16 +1)	2.689310000000D+04	(+/- 1.2D-01)	2.0D-04
T(4 17 -1)	2.706187200000D+04	(+/- 7.0D-02)	3.3D-04
T(4 17 -1)	2.689214000000D+04	(+/- 2.4D-01)	4.5D-04
T(4 17 +1)	2.723869000000D+04	(+/- 2.4D-01)	4.5D-04
T(4 17 +1)	2.706187200000D+04	(+/- 7.0D-02)	3.3D-04
T(4 18 -1)	2.723982400000D+04	(+/- 7.0D-02)	3.3D-04
T(4 18 -1)	2.706090000000D+04	(+/- 2.2D-01)	4.1D-04
T(4 18 +1)	2.742562400000D+04	(+/- 7.2D-02)	4.6D-04
T(4 18 +1)	2.723982400000D+04	(+/- 7.0D-02)	3.3D-04
T(4 19 -1)	2.742680200000D+04	(+/- 7.0D-02)	3.3D-04
T(4 19 -1)	2.723869000000D+04	(+/- 2.4D-01)	4.5D-04
T(4 19 +1)	2.742680200000D+04	(+/- 7.0D-02)	3.3D-04
T(4 20 -1)	2.762271900000D+04	(+/- 7.0D-02)	3.3D-04
T(4 20 -1)	2.742562400000D+04	(+/- 7.2D-02)	4.6D-04
T(4 20 +1)	2.782590000000D+04	(+/- 2.2D-01)	4.1D-04
T(4 20 +1)	2.762271900000D+04	(+/- 7.0D-02)	3.3D-04
T(4 21 -1)	2.782735400000D+04	(+/- 7.0D-02)	3.3D-04
T(4 21 +1)	2.803903000000D+04	(+/- 2.2D-01)	4.1D-04
T(4 21 +1)	2.782735400000D+04	(+/- 7.0D-02)	3.3D-04
T(4 22 -1)	2.804062100000D+04	(+/- 7.0D-02)	3.3D-04
T(4 22 -1)	2.782590000000D+04	(+/- 2.2D-01)	4.1D-04
T(4 22 +1)	2.826065000000D+04	(+/- 2.2D-01)	4.1D-04
T(4 22 +1)	2.804062100000D+04	(+/- 7.0D-02)	3.3D-04
T(4 23 -1)	2.826236000000D+04	(+/- 1.8D-01)	3.2D-04
T(4 23 -1)	2.803903000000D+04	(+/- 2.2D-01)	4.1D-04
T(4 23 +1)	2.849060700000D+04	(+/- 7.3D-02)	4.6D-04
T(4 23 +1)	2.826236000000D+04	(+/- 1.8D-01)	3.2D-04
T(4 24 -1)	2.849238300000D+04	(+/- 7.3D-02)	4.6D-04
T(4 24 -1)	2.826065000000D+04	(+/- 2.2D-01)	4.1D-04
T(4 24 +1)	2.872868000000D+04	(+/- 2.4D-01)	4.5D-04
T(4 24 +1)	2.849238300000D+04	(+/- 7.3D-02)	4.6D-04
T(4 25 -1)	2.873057000000D+04	(+/- 7.1D-02)	3.3D-04
T(4 25 -1)	2.849060700000D+04	(+/- 7.3D-02)	4.6D-04
T(4 25 +1)	2.897477000000D+04	(+/- 2.2D-01)	4.1D-04
T(4 25 +1)	2.873057000000D+04	(+/- 7.1D-02)	3.3D-04

Table C.2 Energy origins of "fluorescence series" of BeD isotopomer (cm^{-1}) (*Cont'd*)

T(v' j' p')	Energy Origin	Uncertainty	Sensitivity
T(4 26 -1)	2.897667400000D+04	(+/- 7.3D-02)	4.6D-04
T(4 26 -1)	2.872868000000D+04	(+/- 2.4D-01)	4.5D-04
T(4 26 +1)	2.922860000000D+04	(+/- 1.3D-01)	2.2D-04
T(4 26 +1)	2.897667400000D+04	(+/- 7.3D-02)	4.6D-04
T(4 27 -1)	2.923068600000D+04	(+/- 7.3D-02)	4.6D-04
T(4 27 -1)	2.897477000000D+04	(+/- 2.2D-01)	4.1D-04
T(4 27 +1)	2.949008000000D+04	(+/- 2.4D-01)	4.5D-04
T(4 27 +1)	2.923068600000D+04	(+/- 7.3D-02)	4.6D-04
T(4 28 -1)	2.949229000000D+04	(+/- 1.7D-01)	3.1D-04
T(4 28 -1)	2.922860000000D+04	(+/- 1.3D-01)	2.2D-04
T(4 28 +1)	2.949229000000D+04	(+/- 1.7D-01)	3.1D-04
T(4 29 -1)	2.976132900000D+04	(+/- 7.2D-02)	3.3D-04
T(4 29 -1)	2.949008000000D+04	(+/- 2.4D-01)	4.5D-04
T(4 29 +1)	2.976132900000D+04	(+/- 7.2D-02)	3.3D-04
T(4 30 -1)	3.003761500000D+04	(+/- 7.3D-02)	4.5D-04
T(4 30 +1)	3.003761500000D+04	(+/- 7.3D-02)	4.5D-04
T(4 31 -1)	3.032100500000D+04	(+/- 7.5D-02)	4.6D-04
T(4 31 +1)	3.032100500000D+04	(+/- 7.5D-02)	4.6D-04
T(4 32 -1)	3.061124300000D+04	(+/- 7.5D-02)	4.6D-04
T(4 32 +1)	3.061124300000D+04	(+/- 7.5D-02)	4.6D-04
T(4 33 -1)	3.090816000000D+04	(+/- 1.7D-01)	3.1D-04
T(4 33 +1)	3.090816000000D+04	(+/- 1.7D-01)	3.1D-04
T(4 34 -1)	3.121149700000D+04	(+/- 7.6D-02)	3.3D-04
T(4 34 +1)	3.121149700000D+04	(+/- 7.6D-02)	3.3D-04
T(4 35 -1)	3.152108600000D+04	(+/- 8.8D-02)	9.1D-04
T(4 35 +1)	3.152108600000D+04	(+/- 8.8D-02)	9.1D-04
T(4 36 -1)	3.183676400000D+04	(+/- 8.6D-02)	4.6D-04
T(4 36 +1)	3.183676400000D+04	(+/- 8.6D-02)	4.6D-04
T(5 6 -1)	2.704128000000D+04	(+/- 2.5D-01)	4.5D-04
T(5 6 +1)	2.704162700000D+04	(+/- 8.3D-02)	4.6D-04
T(5 7 -1)	2.711088700000D+04	(+/- 8.2D-02)	4.5D-04
T(5 7 +1)	2.711114100000D+04	(+/- 8.2D-02)	4.5D-04
T(5 8 -1)	2.719021600000D+04	(+/- 9.0D-02)	8.6D-04
T(5 8 +1)	2.719040500000D+04	(+/- 9.0D-02)	8.6D-04
T(5 9 -1)	2.727935500000D+04	(+/- 8.9D-02)	8.6D-04
T(5 9 +1)	2.727937900000D+04	(+/- 8.9D-02)	8.6D-04
T(5 10 -1)	2.737807300000D+04	(+/- 9.0D-02)	9.0D-04
T(5 10 +1)	2.737807300000D+04	(+/- 9.0D-02)	9.0D-04
T(5 11 -1)	2.748632800000D+04	(+/- 9.0D-02)	9.0D-04
T(5 11 +1)	2.748632800000D+04	(+/- 9.0D-02)	9.0D-04
T(5 12 -1)	2.760408200000D+04	(+/- 8.4D-02)	6.5D-04
T(5 12 +1)	2.760408200000D+04	(+/- 8.4D-02)	6.5D-04
T(5 13 -1)	2.773123600000D+04	(+/- 7.8D-02)	3.3D-04
T(5 13 +1)	2.773123600000D+04	(+/- 7.8D-02)	3.3D-04
T(5 14 -1)	2.786770300000D+04	(+/- 7.9D-02)	4.6D-04
T(5 14 +1)	2.786770300000D+04	(+/- 7.9D-02)	4.6D-04
T(5 15 -1)	2.801340500000D+04	(+/- 7.8D-02)	3.3D-04
T(5 15 +1)	2.801340500000D+04	(+/- 7.8D-02)	3.3D-04
T(5 16 -1)	2.816816000000D+04	(+/- 1.8D-01)	3.1D-04
T(5 16 +1)	2.816816000000D+04	(+/- 1.8D-01)	3.1D-04
T(5 17 -1)	2.833196400000D+04	(+/- 7.7D-02)	3.3D-04
T(5 17 +1)	2.833196400000D+04	(+/- 7.7D-02)	3.3D-04
T(5 18 -1)	2.850457500000D+04	(+/- 7.7D-02)	3.3D-04
T(5 18 +1)	2.850457500000D+04	(+/- 7.7D-02)	3.3D-04
T(5 19 -1)	2.868593800000D+04	(+/- 7.9D-02)	4.5D-04
T(5 19 +1)	2.868593800000D+04	(+/- 7.9D-02)	4.5D-04
T(5 20 -1)	2.887589300000D+04	(+/- 7.9D-02)	4.5D-04

Table C.2 Energy origins of "fluorescence series" of BeD isotopomer (cm^{-1}) (*Cont'd*)

T(v' j' p')	Energy Origin	Uncertainty	Sensitivity
T(5 20 +1)	2.887589300000D+04	(+/- 7.9D-02)	4.5D-04
T(5 21 -1)	2.907432600000D+04	(+/- 7.9D-02)	4.5D-04
T(5 21 +1)	2.907432600000D+04	(+/- 7.9D-02)	4.5D-04
T(5 22 -1)	2.928104100000D+04	(+/- 7.9D-02)	4.5D-04
T(5 22 +1)	2.928104100000D+04	(+/- 7.9D-02)	4.5D-04
T(5 23 -1)	2.949587500000D+04	(+/- 8.9D-02)	9.0D-04
T(5 23 +1)	2.949587500000D+04	(+/- 8.9D-02)	9.0D-04
T(5 24 -1)	2.971880000000D+04	(+/- 7.9D-02)	4.6D-04
T(5 24 +1)	2.971880000000D+04	(+/- 7.9D-02)	4.6D-04
T(5 25 -1)	2.994949000000D+04	(+/- 1.8D-01)	3.2D-04
T(5 25 +1)	2.994949000000D+04	(+/- 1.8D-01)	3.2D-04
T(5 26 -1)	3.018788000000D+04	(+/- 1.8D-01)	3.2D-04
T(5 26 +1)	3.018788000000D+04	(+/- 1.8D-01)	3.2D-04
T(5 27 -1)	3.043378000000D+04	(+/- 1.3D-01)	2.0D-04
T(5 27 +1)	3.043378000000D+04	(+/- 1.3D-01)	2.0D-04
T(5 28 -1)	3.068688200000D+04	(+/- 7.9D-02)	4.1D-04
T(5 28 +1)	3.068688200000D+04	(+/- 7.9D-02)	4.1D-04
T(5 29 -1)	3.094713700000D+04	(+/- 7.9D-02)	3.3D-04
T(5 29 +1)	3.094713700000D+04	(+/- 7.9D-02)	3.3D-04
T(5 30 -1)	3.121434000000D+04	(+/- 1.3D-01)	2.1D-04
T(5 30 +1)	3.121434000000D+04	(+/- 1.3D-01)	2.1D-04
T(5 31 -1)	3.148822600000D+04	(+/- 8.2D-02)	4.6D-04
T(5 31 +1)	3.148822600000D+04	(+/- 8.2D-02)	4.6D-04
T(6 7 -1)	2.836696200000D+04	(+/- 1.0D-01)	4.1D-04
T(6 7 +1)	2.836717300000D+04	(+/- 1.0D-01)	4.1D-04
T(6 8 -1)	2.844385000000D+04	(+/- 1.0D-01)	6.5D-04
T(6 8 +1)	2.844405000000D+04	(+/- 1.1D-01)	9.1D-04
T(6 9 -1)	2.853016600000D+04	(+/- 9.9D-02)	4.6D-04
T(6 9 +1)	2.853028000000D+04	(+/- 1.1D-01)	9.1D-04
T(6 10 -1)	2.862581000000D+04	(+/- 1.0D-01)	6.5D-04
T(6 10 +1)	2.862590600000D+04	(+/- 9.8D-02)	4.5D-04
T(6 11 -1)	2.873071000000D+04	(+/- 1.0D-01)	8.6D-04
T(6 11 +1)	2.873078200000D+04	(+/- 9.6D-02)	4.1D-04
T(6 12 -1)	2.884480900000D+04	(+/- 9.5D-02)	4.5D-04
T(6 12 +1)	2.884485400000D+04	(+/- 9.9D-02)	6.5D-04
T(6 13 -1)	2.896796000000D+04	(+/- 1.0D-01)	9.1D-04
T(6 13 +1)	2.896797000000D+04	(+/- 1.4D-01)	2.1D-04
T(6 14 -1)	2.910018900000D+04	(+/- 9.4D-02)	4.1D-04
T(6 14 +1)	2.910018900000D+04	(+/- 9.4D-02)	4.1D-04
T(6 15 -1)	2.924128800000D+04	(+/- 9.4D-02)	4.1D-04
T(6 15 +1)	2.924128800000D+04	(+/- 9.4D-02)	4.1D-04
T(6 16 -1)	2.939117900000D+04	(+/- 9.3D-02)	3.3D-04
T(6 16 +1)	2.939117900000D+04	(+/- 9.3D-02)	3.3D-04
T(6 17 -1)	2.954972300000D+04	(+/- 9.2D-02)	3.3D-04
T(6 17 +1)	2.954972300000D+04	(+/- 9.2D-02)	3.3D-04
T(6 18 -1)	2.971677000000D+04	(+/- 1.5D-01)	2.3D-04
T(6 18 +1)	2.971677000000D+04	(+/- 9.3D-02)	4.6D-04
T(6 19 -1)	2.989235600000D+04	(+/- 9.4D-02)	4.6D-04
T(6 19 +1)	2.989234000000D+04	(+/- 1.0D-01)	8.6D-04
T(6 20 -1)	3.007613700000D+04	(+/- 9.3D-02)	4.1D-04
T(6 20 +1)	3.007613600000D+04	(+/- 9.3D-02)	4.5D-04
T(6 21 -1)	3.026804000000D+04	(+/- 1.0D-01)	9.1D-04
T(6 21 +1)	3.026805000000D+04	(+/- 1.4D-01)	2.1D-04
T(6 22 -1)	3.046796700000D+04	(+/- 9.6D-02)	6.5D-04
T(6 22 +1)	3.046796700000D+04	(+/- 9.6D-02)	6.5D-04
T(6 23 -1)	3.067568400000D+04	(+/- 9.3D-02)	4.1D-04
T(6 23 +1)	3.067568500000D+04	(+/- 9.6D-02)	6.5D-04

Table C.2 Energy origins of "fluorescence series" of BeD isotopomer (cm^{-1}) (*Cont'd*)

T(v' j' p')	Energy Origin	Uncertainty	Sensitivity
T(6 24 -1)	3.089110200000D+04	(+/- 9.4D-02)	4.5D-04
T(6 24 +1)	3.089115800000D+04	(+/- 9.9D-02)	7.7D-04

C.3 Energy Origins of BeT Isotopomer

Table C.3: Energy Origins of "Fluorescence Series" of BeT Isotopomer (cm^{-1})

T(v'	j'	p')	Energy Origin	Uncertainty	Sensitivity
T(0	3	-1)	1.971762000000D+04	(+/- 1.7D-01)	3.3D-04
T(0	3	+1)	1.971762000000D+04	(+/- 1.7D-01)	3.3D-04
T(0	4	-1)	1.975084000000D+04	(+/- 1.7D-01)	3.3D-04
T(0	4	+1)	1.975084000000D+04	(+/- 1.7D-01)	3.3D-04
T(0	5	-1)	1.979262000000D+04	(+/- 1.7D-01)	3.3D-04
T(0	5	+1)	1.979262000000D+04	(+/- 1.7D-01)	3.3D-04
T(0	6	-1)	1.984198000000D+04	(+/- 1.7D-01)	3.3D-04
T(0	6	+1)	1.984198000000D+04	(+/- 1.7D-01)	3.3D-04
T(0	7	-1)	1.990002000000D+04	(+/- 1.7D-01)	3.3D-04
T(0	7	+1)	1.990002000000D+04	(+/- 1.7D-01)	3.3D-04
T(0	8	-1)	1.997000000000D+04	(+/- 1.7D+02)	3.3D-01
T(0	8	+1)	1.997000000000D+04	(+/- 1.7D+02)	3.3D-01
T(0	9	-1)	2.004060000000D+04	(+/- 1.7D-01)	3.3D-04
T(0	9	+1)	2.004060000000D+04	(+/- 1.7D-01)	3.3D-04
T(0	10	-1)	2.012303000000D+04	(+/- 1.7D-01)	3.3D-04
T(0	10	+1)	2.012303000000D+04	(+/- 1.7D-01)	3.3D-04
T(0	11	-1)	2.021375000000D+04	(+/- 1.7D-01)	3.3D-04
T(0	11	+1)	2.021375000000D+04	(+/- 1.7D-01)	3.3D-04
T(0	12	-1)	2.031224000000D+04	(+/- 1.7D-01)	3.3D-04
T(0	12	+1)	2.031224000000D+04	(+/- 1.7D-01)	3.3D-04
T(0	13	-1)	2.041888000000D+04	(+/- 1.7D-01)	3.3D-04
T(0	13	+1)	2.041888000000D+04	(+/- 1.7D-01)	3.3D-04
T(0	14	-1)	2.053336000000D+04	(+/- 1.7D-01)	3.3D-04
T(0	14	+1)	2.053336000000D+04	(+/- 1.7D-01)	3.3D-04
T(0	15	-1)	2.065593000000D+04	(+/- 1.7D-01)	3.3D-04
T(0	15	+1)	2.065593000000D+04	(+/- 1.7D-01)	3.3D-04
T(0	16	-1)	2.078623000000D+04	(+/- 1.7D-01)	3.3D-04
T(0	16	+1)	2.078623000000D+04	(+/- 1.7D-01)	3.3D-04
T(0	17	-1)	2.092429000000D+04	(+/- 1.8D-01)	3.3D-04
T(0	17	+1)	2.092429000000D+04	(+/- 1.8D-01)	3.3D-04
T(0	18	-1)	2.107013000000D+04	(+/- 1.8D-01)	3.3D-04
T(0	18	+1)	2.107013000000D+04	(+/- 1.8D-01)	3.3D-04
T(0	19	-1)	2.122357000000D+04	(+/- 8.4D-01)	1.6D-04
T(0	19	+1)	2.122357000000D+04	(+/- 8.4D-01)	1.6D-04
T(0	20	-1)	2.138489000000D+04	(+/- 8.4D-01)	1.6D-04
T(0	20	+1)	2.138489000000D+04	(+/- 8.4D-01)	1.6D-04
T(0	21	-1)	2.155308000000D+04	(+/- 1.8D-01)	3.3D-04
T(0	21	+1)	2.155308000000D+04	(+/- 1.8D-01)	3.3D-04
T(0	22	-1)	2.172910000000D+04	(+/- 1.8D-01)	3.3D-04
T(0	22	+1)	2.172910000000D+04	(+/- 1.8D-01)	3.3D-04
T(0	23	-1)	2.191237000000D+04	(+/- 1.8D-01)	3.3D-04
T(0	23	+1)	2.191237000000D+04	(+/- 1.8D-01)	3.3D-04
T(0	24	-1)	2.210280000000D+04	(+/- 1.8D-01)	3.3D-04
T(0	24	+1)	2.210280000000D+04	(+/- 1.8D-01)	3.3D-04
T(0	25	-1)	2.230077000000D+04	(+/- 1.8D-01)	3.3D-04
T(0	25	+1)	2.230077000000D+04	(+/- 1.8D-01)	3.3D-04
T(0	26	-1)	2.250539000000D+04	(+/- 1.8D-01)	3.3D-04
T(0	26	+1)	2.250539000000D+04	(+/- 1.8D-01)	3.3D-04
T(0	27	-1)	2.271707000000D+04	(+/- 1.8D-01)	3.3D-04
T(0	27	+1)	2.271707000000D+04	(+/- 1.8D-01)	3.3D-04
T(0	28	-1)	2.293581000000D+04	(+/- 1.8D-01)	3.3D-04
T(0	28	+1)	2.293581000000D+04	(+/- 1.8D-01)	3.3D-04
T(0	29	-1)	2.316098000000D+04	(+/- 1.9D-01)	3.3D-04

Table C.3 Energy origins of "fluorescence series" of BeT isotopomer (cm^{-1}) (*Cont'd*)

T(v' j' p')	Energy Origin	Uncertainty	Sensitivity
T(0 29 +1)	2.316098000000D+04	(+/- 1.9D-01)	3.3D-04
T(0 30 -1)	2.339331000000D+04	(+/- 1.9D-01)	3.3D-04
T(0 30 +1)	2.339331000000D+04	(+/- 1.9D-01)	3.3D-04
T(0 31 -1)	2.363199000000D+04	(+/- 1.9D-01)	3.3D-04
T(0 31 +1)	2.363199000000D+04	(+/- 1.9D-01)	3.3D-04
T(0 32 -1)	2.387728000000D+04	(+/- 1.9D-01)	3.3D-04
T(0 32 +1)	2.387728000000D+04	(+/- 1.9D-01)	3.3D-04
T(0 33 -1)	2.412877000000D+04	(+/- 1.9D-01)	3.3D-04
T(0 33 +1)	2.412877000000D+04	(+/- 1.9D-01)	3.3D-04
T(0 34 -1)	2.438657000000D+04	(+/- 1.9D-01)	3.3D-04
T(0 34 +1)	2.438657000000D+04	(+/- 1.9D-01)	3.3D-04
T(0 35 -1)	2.465039000000D+04	(+/- 1.9D-01)	3.3D-04
T(0 35 +1)	2.465039000000D+04	(+/- 1.9D-01)	3.3D-04
T(0 36 -1)	2.492041000000D+04	(+/- 1.9D-01)	3.3D-04
T(0 36 +1)	2.492041000000D+04	(+/- 1.9D-01)	3.3D-04
T(0 37 -1)	2.519637000000D+04	(+/- 1.9D-01)	3.3D-04
T(0 37 +1)	2.519637000000D+04	(+/- 1.9D-01)	3.3D-04
T(0 38 -1)	2.547784000000D+04	(+/- 1.9D-01)	3.3D-04
T(0 38 +1)	2.547784000000D+04	(+/- 1.9D-01)	3.3D-04
T(0 39 -1)	2.576546000000D+04	(+/- 1.9D-01)	3.3D-04
T(0 39 +1)	2.576546000000D+04	(+/- 1.9D-01)	3.3D-04
T(1 2 -1)	2.098249000000D+04	(+/- 1.8D-01)	3.3D-04
T(1 2 +1)	2.098249000000D+04	(+/- 1.8D-01)	3.3D-04
T(1 3 -1)	2.100738000000D+04	(+/- 8.4D-01)	1.6D-04
T(1 3 +1)	2.100738000000D+04	(+/- 8.4D-01)	1.6D-04
T(1 4 -1)	2.103960000000D+04	(+/- 1.8D-01)	3.3D-04
T(1 4 +1)	2.103960000000D+04	(+/- 1.8D-01)	3.3D-04
T(1 5 -1)	2.108052000000D+04	(+/- 1.8D-01)	3.3D-04
T(1 5 +1)	2.108052000000D+04	(+/- 1.8D-01)	3.3D-04
T(1 6 -1)	2.112889000000D+04	(+/- 1.8D-01)	3.3D-04
T(1 6 +1)	2.112889000000D+04	(+/- 1.8D-01)	3.3D-04
T(1 7 -1)	2.118574000000D+04	(+/- 1.8D-01)	3.3D-04
T(1 7 +1)	2.118574000000D+04	(+/- 1.8D-01)	3.3D-04
T(1 8 -1)	2.125080000000D+04	(+/- 1.8D-01)	3.3D-04
T(1 8 +1)	2.125080000000D+04	(+/- 1.8D-01)	3.3D-04
T(1 9 -1)	2.132362000000D+04	(+/- 1.8D-01)	3.3D-04
T(1 9 +1)	2.132362000000D+04	(+/- 1.8D-01)	3.3D-04
T(1 10 -1)	2.140440000000D+04	(+/- 1.8D-01)	3.3D-04
T(1 10 +1)	2.140440000000D+04	(+/- 1.8D-01)	3.3D-04
T(1 11 -1)	2.149312000000D+04	(+/- 1.8D-01)	3.3D-04
T(1 11 +1)	2.149312000000D+04	(+/- 1.8D-01)	3.3D-04
T(1 12 -1)	2.158957000000D+04	(+/- 1.8D-01)	3.3D-04
T(1 12 +1)	2.158957000000D+04	(+/- 1.8D-01)	3.3D-04
T(1 13 -1)	2.169391000000D+04	(+/- 1.8D-01)	3.3D-04
T(1 13 +1)	2.169391000000D+04	(+/- 1.8D-01)	3.3D-04
T(1 14 -1)	2.180619000000D+04	(+/- 1.8D-01)	3.3D-04
T(1 14 +1)	2.180619000000D+04	(+/- 1.8D-01)	3.3D-04
T(1 15 -1)	2.192628000000D+04	(+/- 1.8D-01)	3.3D-04
T(1 15 +1)	2.192628000000D+04	(+/- 1.8D-01)	3.3D-04
T(1 17 -1)	2.219000000000D+04	(+/- 1.7D+02)	3.3D-01
T(1 17 +1)	2.219000000000D+04	(+/- 1.7D+02)	3.3D-01
T(1 18 -1)	2.233000000000D+04	(+/- 1.7D+02)	3.3D-01
T(1 18 +1)	2.233000000000D+04	(+/- 1.7D+02)	3.3D-01
T(1 19 -1)	2.248000000000D+04	(+/- 1.7D+02)	3.3D-01
T(1 19 +1)	2.248000000000D+04	(+/- 1.7D+02)	3.3D-01
T(1 20 -1)	2.264000000000D+04	(+/- 1.7D+02)	3.3D-01
T(1 20 +1)	2.264000000000D+04	(+/- 1.7D+02)	3.3D-01

Table C.3 Energy origins of "fluorescence series" of BeT isotopomer (cm^{-1}) (*Cont'd*)

T(v' j' p')	Energy Origin	Uncertainty	Sensitivity
T(1 21 -1)	2.281000000000D+04	(+/- 1.7D+02)	3.3D-01
T(1 21 +1)	2.281000000000D+04	(+/- 1.7D+02)	3.3D-01
T(1 22 -1)	2.298000000000D+04	(+/- 1.7D+02)	3.3D-01
T(1 22 +1)	2.298000000000D+04	(+/- 1.7D+02)	3.3D-01
T(1 23 -1)	2.316000000000D+04	(+/- 1.7D+02)	3.3D-01
T(1 23 +1)	2.316000000000D+04	(+/- 1.7D+02)	3.3D-01
T(1 24 -1)	2.334411000000D+04	(+/- 8.4D-01)	1.6D-04
T(1 24 +1)	2.334411000000D+04	(+/- 8.4D-01)	1.6D-04
T(1 25 -1)	2.354000000000D+04	(+/- 1.7D+02)	3.3D-01
T(1 25 +1)	2.354000000000D+04	(+/- 1.7D+02)	3.3D-01
T(1 26 -1)	2.374000000000D+04	(+/- 1.7D+02)	3.3D-01
T(1 26 +1)	2.374000000000D+04	(+/- 1.7D+02)	3.3D-01
T(1 27 -1)	2.395000000000D+04	(+/- 1.7D+02)	3.3D-01
T(1 27 +1)	2.395000000000D+04	(+/- 1.7D+02)	3.3D-01
T(1 28 -1)	2.415938000000D+04	(+/- 8.4D-01)	1.6D-04
T(1 28 +1)	2.415938000000D+04	(+/- 8.4D-01)	1.6D-04
T(1 30 -1)	2.461000000000D+04	(+/- 2.4D+02)	4.6D-01
T(1 30 +1)	2.461000000000D+04	(+/- 1.7D+02)	3.3D-01
T(1 31 -1)	2.484000000000D+04	(+/- 1.7D+02)	3.3D-01
T(1 31 +1)	2.484000000000D+04	(+/- 1.7D+02)	3.3D-01
T(1 32 -1)	2.508000000000D+04	(+/- 1.7D+02)	3.3D-01
T(1 32 +1)	2.508000000000D+04	(+/- 1.7D+02)	3.3D-01
T(1 33 -1)	2.533000000000D+04	(+/- 1.7D+02)	3.3D-01
T(1 33 +1)	2.533000000000D+04	(+/- 1.7D+02)	3.3D-01
T(2 5 -1)	2.233496000000D+04	(+/- 1.8D-01)	3.3D-04
T(2 5 +1)	2.233496000000D+04	(+/- 1.8D-01)	3.3D-04
T(2 6 -1)	2.238295000000D+04	(+/- 1.8D-01)	3.3D-04
T(2 6 +1)	2.238295000000D+04	(+/- 1.8D-01)	3.3D-04
T(2 7 -1)	2.243813000000D+04	(+/- 1.8D-01)	3.3D-04
T(2 7 +1)	2.243813000000D+04	(+/- 1.8D-01)	3.3D-04
T(2 8 -1)	2.250148000000D+04	(+/- 8.4D-01)	1.6D-04
T(2 8 +1)	2.250148000000D+04	(+/- 8.4D-01)	1.6D-04
T(2 9 -1)	2.257303000000D+04	(+/- 8.4D-01)	1.6D-04
T(2 9 +1)	2.257303000000D+04	(+/- 8.4D-01)	1.6D-04
T(2 10 -1)	2.265209000000D+04	(+/- 1.8D-01)	3.3D-04
T(2 10 +1)	2.265209000000D+04	(+/- 1.8D-01)	3.3D-04
T(2 11 -1)	2.273904000000D+04	(+/- 1.8D-01)	3.3D-04
T(2 11 +1)	2.273904000000D+04	(+/- 1.8D-01)	3.3D-04
T(2 12 -1)	2.283358000000D+04	(+/- 8.4D-01)	1.6D-04
T(2 12 +1)	2.283358000000D+04	(+/- 8.4D-01)	1.6D-04
T(2 13 -1)	2.293575000000D+04	(+/- 1.8D-01)	3.3D-04
T(2 13 +1)	2.293575000000D+04	(+/- 1.8D-01)	3.3D-04
T(2 14 -1)	2.304547000000D+04	(+/- 1.8D-01)	3.3D-04
T(2 14 +1)	2.304547000000D+04	(+/- 1.8D-01)	3.3D-04
T(2 15 -1)	2.316341000000D+04	(+/- 1.8D-01)	3.3D-04
T(2 15 +1)	2.316341000000D+04	(+/- 1.8D-01)	3.3D-04
T(2 16 -1)	2.328797000000D+04	(+/- 1.9D-01)	3.3D-04
T(2 16 +1)	2.328797000000D+04	(+/- 1.9D-01)	3.3D-04
T(2 17 -1)	2.342022000000D+04	(+/- 1.9D-01)	3.3D-04
T(2 17 +1)	2.342022000000D+04	(+/- 1.9D-01)	3.3D-04
T(2 19 -1)	2.370698000000D+04	(+/- 1.9D-01)	3.3D-04
T(2 19 +1)	2.370698000000D+04	(+/- 1.9D-01)	3.3D-04
T(2 20 -1)	2.386138000000D+04	(+/- 8.4D-01)	1.6D-04
T(2 20 +1)	2.386138000000D+04	(+/- 8.4D-01)	1.6D-04
T(2 21 -1)	2.402000000000D+04	(+/- 1.7D+02)	3.3D-01
T(2 21 +1)	2.402000000000D+04	(+/- 1.7D+02)	3.3D-01
T(2 22 -1)	2.419149000000D+04	(+/- 8.4D-01)	1.6D-04

Table C.3 Energy origins of "fluorescence series" of BeT isotopomer (cm^{-1}) (*Cont'd*)

T(v'	j'	p')	Energy Origin	Uncertainty	Sensitivity
T(2	22	+1)	2.419149000000D+04	(+/- 8.4D-01)	1.6D-04
T(2	23	-1)	2.436772000000D+04	(+/- 8.4D-01)	1.6D-04
T(2	23	+1)	2.436772000000D+04	(+/- 8.4D-01)	1.6D-04
T(2	24	-1)	2.455000000000D+04	(+/- 1.7D+02)	3.3D-01
T(2	24	+1)	2.455000000000D+04	(+/- 1.7D+02)	3.3D-01
T(2	26	-1)	2.494000000000D+04	(+/- 1.7D+02)	3.3D-01
T(2	26	+1)	2.494000000000D+04	(+/- 1.7D+02)	3.3D-01
T(2	27	-1)	2.514000000000D+04	(+/- 1.7D+02)	3.3D-01
T(2	27	+1)	2.514000000000D+04	(+/- 1.7D+02)	3.3D-01
T(2	28	-1)	2.535000000000D+04	(+/- 1.7D+02)	3.3D-01
T(2	28	+1)	2.535000000000D+04	(+/- 1.7D+02)	3.3D-01
T(3	2	-1)	2.346000000000D+04	(+/- 1.7D+02)	3.3D-01
T(3	2	+1)	2.346000000000D+04	(+/- 1.7D+02)	3.3D-01
T(3	3	-1)	2.348000000000D+04	(+/- 1.7D+02)	3.3D-01
T(3	3	+1)	2.348000000000D+04	(+/- 1.7D+02)	3.3D-01
T(3	4	-1)	2.351592000000D+04	(+/- 1.9D-01)	3.3D-04
T(3	4	+1)	2.351592000000D+04	(+/- 1.9D-01)	3.3D-04
T(3	5	-1)	2.355539000000D+04	(+/- 1.9D-01)	3.3D-04
T(3	5	+1)	2.355539000000D+04	(+/- 1.9D-01)	3.3D-04
T(3	7	-1)	2.365625000000D+04	(+/- 1.9D-01)	3.3D-04
T(3	7	+1)	2.365625000000D+04	(+/- 1.9D-01)	3.3D-04
T(3	8	-1)	2.371855000000D+04	(+/- 1.9D-01)	3.3D-04
T(3	8	+1)	2.371855000000D+04	(+/- 1.9D-01)	3.3D-04
T(3	9	-1)	2.379000000000D+04	(+/- 1.7D+02)	3.3D-01
T(3	9	+1)	2.379000000000D+04	(+/- 1.7D+02)	3.3D-01
T(3	10	-1)	2.386548000000D+04	(+/- 1.9D-01)	3.3D-04
T(3	10	+1)	2.386548000000D+04	(+/- 1.9D-01)	3.3D-04
T(3	11	-1)	2.395059000000D+04	(+/- 1.9D-01)	3.3D-04
T(3	11	+1)	2.395059000000D+04	(+/- 1.9D-01)	3.3D-04
T(3	12	-1)	2.404319000000D+04	(+/- 1.9D-01)	3.3D-04
T(3	12	+1)	2.404319000000D+04	(+/- 1.9D-01)	3.3D-04
T(3	13	-1)	2.414317000000D+04	(+/- 1.9D-01)	3.3D-04
T(3	13	+1)	2.414317000000D+04	(+/- 1.9D-01)	3.3D-04
T(3	14	-1)	2.425078000000D+04	(+/- 8.4D-01)	1.6D-04
T(3	14	+1)	2.425078000000D+04	(+/- 8.4D-01)	1.6D-04
T(3	15	-1)	2.436530000000D+04	(+/- 1.9D-01)	3.3D-04
T(3	15	+1)	2.436530000000D+04	(+/- 1.9D-01)	3.3D-04
T(3	16	-1)	2.448751000000D+04	(+/- 1.9D-01)	3.3D-04
T(3	16	+1)	2.448751000000D+04	(+/- 1.9D-01)	3.3D-04
T(3	17	-1)	2.461664000000D+04	(+/- 8.4D-01)	1.6D-04
T(3	17	+1)	2.461664000000D+04	(+/- 8.4D-01)	1.6D-04
T(3	18	-1)	2.475376000000D+04	(+/- 1.9D-01)	3.3D-04
T(3	18	+1)	2.475376000000D+04	(+/- 1.9D-01)	3.3D-04

Appendix D

Energy Origins of MgH Molecule

The 713 energy origins of the MgH isotopomers calculated using DSParFit[1] are listed in Appendix D

The 270 energy origins of ^{24}MgH isotopomer are listed in Table D.1.
The 59 energy origins of ^{25}MgH isotopomer are listed in Table D.2.
The 59 energy origins of ^{26}MgH isotopomer are listed in Table D.3.
The 202 energy origins of ^{24}MgD isotopomer are listed in Table D.4.
The 63 energy origins of ^{25}MgD isotopomer are listed in Table D.5.
The 60 energy origins of ^{26}MgD isotopomer are listed in Table D.6.

[1]Robert J. Le Roy, Dept. of Chemistry, University of Waterloo, Waterloo, Ontario N2L 3G1

D.1 Energy Origins of ^{24}MgH Isotopomer

Table D.1: Energy Origins of "Fluorescence Series" of ^{24}MgH Isotopomer (cm^{-1})

T(v'	j'	p')	Energy Origin	Uncertainty	Sensitivity
T(0	0	+1)	2.208236800000D+04	(+/- 7.5D-02)	3.4D-04
T(0	1	+1)	2.208754330000D+04	(+/- 9.3D-03)	2.4D-05
T(0	2	+1)	2.209793300000D+04	(+/- 1.2D-02)	4.1D-05
T(0	3	+1)	2.211348850000D+04	(+/- 8.3D-03)	1.7D-05
T(0	4	+1)	2.213423010000D+04	(+/- 8.8D-03)	2.2D-05
T(0	5	+1)	2.216013700000D+04	(+/- 1.1D-02)	3.9D-05
T(0	6	+1)	2.219119600000D+04	(+/- 1.1D-02)	3.9D-05
T(0	7	+1)	2.222738360000D+04	(+/- 8.2D-03)	2.3D-05
T(0	8	+1)	2.226871820000D+04	(+/- 6.4D-03)	1.7D-05
T(0	9	+1)	2.231513610000D+04	(+/- 6.4D-03)	1.7D-05
T(0	10	+1)	2.236663770000D+04	(+/- 8.0D-03)	2.2D-05
T(0	11	+1)	2.242320480000D+04	(+/- 8.0D-03)	2.0D-05
T(0	12	+1)	2.248478380000D+04	(+/- 6.9D-03)	1.7D-05
T(0	13	+1)	2.255135300000D+04	(+/- 2.2D-02)	9.4D-05
T(0	14	+1)	2.262293330000D+04	(+/- 8.7D-03)	2.0D-05
T(0	15	+1)	2.269940830000D+04	(+/- 9.3D-03)	2.9D-05
T(0	16	+1)	2.278077850000D+04	(+/- 8.0D-03)	2.2D-05
T(0	17	+1)	2.286703600000D+04	(+/- 1.0D-02)	2.9D-05
T(0	18	+1)	2.295810000000D+04	(+/- 1.0D-02)	1.7D-05
T(0	19	+1)	2.305395000000D+04	(+/- 1.1D-02)	2.2D-05
T(0	20	+1)	2.315449100000D+04	(+/- 1.2D-02)	1.6D-05
T(0	21	+1)	2.325975900000D+04	(+/- 1.2D-02)	2.2D-05
T(0	22	+1)	2.336969400000D+04	(+/- 1.3D-02)	2.3D-05
T(0	23	+1)	2.348420700000D+04	(+/- 1.7D-02)	5.4D-05
T(0	24	+1)	2.360329100000D+04	(+/- 1.5D-02)	2.4D-05
T(0	25	+1)	2.372686500000D+04	(+/- 1.6D-02)	2.4D-05
T(0	26	+1)	2.385487900000D+04	(+/- 1.7D-02)	2.4D-05
T(0	27	+1)	2.398731300000D+04	(+/- 1.9D-02)	2.4D-05
T(0	28	+1)	2.412409600000D+04	(+/- 3.9D-02)	1.6D-04
T(0	29	+1)	2.426517600000D+04	(+/- 3.8D-02)	1.5D-04
T(0	30	+1)	2.441050700000D+04	(+/- 4.1D-02)	1.5D-04
T(0	31	+1)	2.456001900000D+04	(+/- 4.5D-02)	1.4D-04
T(0	32	+1)	2.471368600000D+04	(+/- 6.4D-02)	2.3D-04
T(0	33	+1)	2.487137700000D+04	(+/- 7.4D-02)	2.7D-04
T(0	34	+1)	2.503309400000D+04	(+/- 8.4D-02)	3.0D-04
T(0	35	+1)	2.519870000000D+04	(+/- 1.1D-01)	3.4D-04
T(0	36	+1)	2.536821000000D+04	(+/- 1.2D-01)	3.4D-04
T(0	37	+1)	2.554150000000D+04	(+/- 1.2D-01)	3.0D-04
T(0	38	+1)	2.571882000000D+04	(+/- 1.5D-01)	1.6D-04
T(0	39	+1)	2.589941000000D+04	(+/- 1.5D-01)	3.4D-04
T(0	40	+1)	2.608401000000D+04	(+/- 1.7D-01)	3.4D-04
T(0	41	+1)	2.627424000000D+04	(+/- 2.3D-01)	6.0D-04
T(0	42	+1)	2.646367000000D+04	(+/- 2.1D-01)	4.2D-04
T(1	0	+1)	2.288747400000D+04	(+/- 4.9D-02)	2.2D-04
T(1	1	+1)	2.289265840000D+04	(+/- 8.7D-03)	1.7D-05
T(1	2	+1)	2.290307110000D+04	(+/- 8.3D-03)	1.2D-05
T(1	3	+1)	2.291867660000D+04	(+/- 8.4D-03)	1.7D-05
T(1	4	+1)	2.293947830000D+04	(+/- 8.6D-03)	1.9D-05
T(1	5	+1)	2.296545650000D+04	(+/- 7.3D-03)	1.2D-05
T(1	6	+1)	2.299660280000D+04	(+/- 7.3D-03)	1.3D-05
T(1	7	+1)	2.303289230000D+04	(+/- 7.0D-03)	1.3D-05
T(1	8	+1)	2.307431440000D+04	(+/- 7.1D-03)	1.4D-05

Table D.1 Energy origins of "fluorescence series" of ^{24}MgH isotopomer (cm^{-1}) (*Cont'd*)

T(v'	j'	p')	Energy Origin	Uncertainty	Sensitivity
T(1	9	+1)	2.312085720000D+04	(+/- 7.0D-03)	1.3D-05
T(1	10	+1)	2.317248120000D+04	(+/- 8.0D-03)	2.1D-05
T(1	11	+1)	2.322916300000D+04	(+/- 1.0D-02)	3.6D-05
T(1	12	+1)	2.329090130000D+04	(+/- 8.5D-03)	2.3D-05
T(1	13	+1)	2.335795020000D+04	(+/- 7.4D-03)	1.2D-05
T(1	14	+1)	2.342842400000D+04	(+/- 3.7D-02)	1.7D-04
T(1	15	+1)	2.350542390000D+04	(+/- 9.9D-03)	2.3D-05
T(1	16	+1)	2.358682500000D+04	(+/- 2.7D-02)	1.2D-04
T(1	17	+1)	2.367314670000D+04	(+/- 9.9D-03)	2.3D-05
T(1	18	+1)	2.376422000000D+04	(+/- 1.0D-02)	1.7D-05
T(1	19	+1)	2.386002600000D+04	(+/- 1.1D-02)	1.7D-05
T(1	20	+1)	2.396052500000D+04	(+/- 1.1D-02)	2.2D-05
T(1	21	+1)	2.406564400000D+04	(+/- 1.2D-02)	1.7D-05
T(1	22	+1)	2.417535600000D+04	(+/- 1.3D-02)	2.2D-05
T(1	23	+1)	2.428990900000D+04	(+/- 3.2D-02)	2.4D-05
T(1	24	+1)	2.440841200000D+04	(+/- 1.4D-02)	1.7D-05
T(1	25	+1)	2.453189400000D+04	(+/- 1.5D-02)	1.7D-05
T(1	26	+1)	2.465900700000D+04	(+/- 1.8D-02)	2.3D-05
T(1	27	+1)	2.479083400000D+04	(+/- 1.6D-02)	2.4D-05
T(1	28	+1)	2.492711400000D+04	(+/- 1.8D-02)	2.4D-05
T(1	29	+1)	2.506753900000D+04	(+/- 2.0D-02)	2.4D-05
T(1	30	+1)	2.521205400000D+04	(+/- 2.3D-02)	2.4D-05
T(1	31	+1)	2.536063200000D+04	(+/- 4.0D-02)	1.3D-04
T(1	32	+1)	2.551322800000D+04	(+/- 5.3D-02)	1.6D-04
T(1	33	+1)	2.567058000000D+04	(+/- 1.0D-01)	4.2D-04
T(1	34	+1)	2.583027000000D+04	(+/- 1.1D-01)	4.2D-04
T(1	35	+1)	2.599452000000D+04	(+/- 1.2D-01)	4.2D-04
T(1	36	+1)	2.616252000000D+04	(+/- 1.3D-01)	4.2D-04
T(1	37	+1)	2.633418000000D+04	(+/- 1.4D-01)	4.2D-04
T(1	38	+1)	2.650944000000D+04	(+/- 1.5D-01)	4.2D-04
T(1	39	+1)	2.668819000000D+04	(+/- 1.7D-01)	4.2D-04
T(1	40	+1)	2.687042000000D+04	(+/- 1.8D-01)	4.2D-04
T(1	41	+1)	2.705609000000D+04	(+/- 1.9D-01)	4.2D-04
T(2	1	+1)	2.367408200000D+04	(+/- 9.6D-02)	4.2D-04
T(2	2	+1)	2.368476800000D+04	(+/- 9.5D-02)	4.2D-04
T(2	3	+1)	2.370040900000D+04	(+/- 9.5D-02)	4.2D-04
T(2	4	+1)	2.372006200000D+04	(+/- 9.4D-02)	4.2D-04
T(2	5	+1)	2.374671600000D+04	(+/- 6.5D-02)	3.0D-04
T(2	6	+1)	2.377794300000D+04	(+/- 5.8D-02)	2.7D-04
T(2	7	+1)	2.381431800000D+04	(+/- 2.3D-02)	9.7D-05
T(2	8	+1)	2.385571200000D+04	(+/- 9.3D-02)	4.2D-04
T(2	9	+1)	2.390226300000D+04	(+/- 2.9D-02)	1.2D-04
T(2	10	+1)	2.395382400000D+04	(+/- 4.3D-02)	2.0D-04
T(2	11	+1)	2.401046700000D+04	(+/- 3.5D-02)	1.5D-04
T(2	12	+1)	2.407214200000D+04	(+/- 4.9D-02)	2.3D-04
T(2	13	+1)	2.413866000000D+04	(+/- 3.5D-02)	1.6D-04
T(2	14	+1)	2.421019000000D+04	(+/- 2.9D-02)	1.3D-04
T(2	15	+1)	2.428661600000D+04	(+/- 3.4D-02)	1.5D-04
T(2	16	+1)	2.436791800000D+04	(+/- 3.5D-02)	1.6D-04
T(2	17	+1)	2.445398700000D+04	(+/- 3.0D-02)	1.3D-04
T(2	18	+1)	2.454487400000D+04	(+/- 3.1D-02)	1.4D-04
T(2	19	+1)	2.464065100000D+04	(+/- 3.2D-02)	1.4D-04
T(2	20	+1)	2.474154200000D+04	(+/- 3.3D-02)	1.5D-04
T(2	21	+1)	2.484827200000D+04	(+/- 3.6D-02)	1.6D-04
T(2	22	+1)	2.495580700000D+04	(+/- 4.6D-02)	2.0D-04
T(3	1	+1)	2.443331000000D+04	(+/- 1.3D-01)	6.0D-04
T(3	2	+1)	2.444365000000D+04	(+/- 6.5D-02)	3.0D-04

Table D.1 Energy origins of "fluorescence series" of ^{24}MgH isotopomer (cm^{-1}) (*Cont'd*)

T(v'	j'	p')	Energy Origin	Uncertainty	Sensitivity
T(3	3	+1)	2.445925600000D+04	(+/- 6.5D-02)	3.0D-04
T(3	4	+1)	2.447999000000D+04	(+/- 4.9D-02)	2.3D-04
T(3	5	+1)	2.450593000000D+04	(+/- 5.3D-02)	2.4D-04
T(3	6	+1)	2.453700900000D+04	(+/- 4.9D-02)	2.3D-04
T(3	7	+1)	2.457319000000D+04	(+/- 5.3D-02)	2.4D-04
T(3	8	+1)	2.461455500000D+04	(+/- 4.9D-02)	2.3D-04
T(3	9	+1)	2.466100400000D+04	(+/- 4.9D-02)	2.3D-04
T(3	10	+1)	2.471245100000D+04	(+/- 5.3D-02)	2.4D-04
T(3	11	+1)	2.476905700000D+04	(+/- 6.5D-02)	3.0D-04
T(3	12	+1)	2.483073700000D+04	(+/- 5.3D-02)	2.4D-04
T(3	13	+1)	2.489749000000D+04	(+/- 4.3D-02)	2.0D-04
T(3	14	+1)	2.496961900000D+04	(+/- 6.5D-02)	3.0D-04
T(3	15	+1)	2.504642300000D+04	(+/- 4.3D-02)	2.0D-04
T(3	17	+1)	2.520694600000D+04	(+/- 9.2D-02)	4.2D-04
T(3	18	+1)	2.529835500000D+04	(+/- 6.5D-02)	3.0D-04
T(3	19	+1)	2.539368600000D+04	(+/- 6.6D-02)	3.0D-04
T(3	20	+1)	2.549340900000D+04	(+/- 7.6D-02)	3.4D-04
T(3	21	+1)	2.559761100000D+04	(+/- 6.6D-02)	3.0D-04
T(3	22	+1)	2.570633300000D+04	(+/- 7.6D-02)	3.4D-04
T(3	23	+1)	2.581954500000D+04	(+/- 6.7D-02)	3.0D-04
T(3	24	+1)	2.593727000000D+04	(+/- 7.7D-02)	3.4D-04
T(4	0	+1)	2.516383200000D+04	(+/- 9.1D-02)	4.2D-04
T(4	1	+1)	2.516880700000D+04	(+/- 6.4D-02)	3.0D-04
T(4	2	+1)	2.517923400000D+04	(+/- 6.5D-02)	3.0D-04
T(4	3	+1)	2.519467000000D+04	(+/- 7.4D-02)	3.4D-04
T(4	4	+1)	2.521538600000D+04	(+/- 5.8D-02)	2.7D-04
T(4	5	+1)	2.524118200000D+04	(+/- 4.9D-02)	2.3D-04
T(4	6	+1)	2.527209500000D+04	(+/- 6.4D-02)	3.0D-04
T(4	7	+1)	2.530814200000D+04	(+/- 7.4D-02)	3.4D-04
T(4	8	+1)	2.534876200000D+04	(+/- 4.9D-02)	2.3D-04
T(4	9	+1)	2.539507500000D+04	(+/- 4.9D-02)	2.3D-04
T(4	10	+1)	2.544614000000D+04	(+/- 4.9D-02)	2.3D-04
T(4	11	+1)	2.550226700000D+04	(+/- 4.9D-02)	2.3D-04
T(4	12	+1)	2.556329500000D+04	(+/- 5.3D-02)	2.4D-04
T(4	13	+1)	2.562918200000D+04	(+/- 5.3D-02)	2.4D-04
T(4	14	+1)	2.569986700000D+04	(+/- 6.5D-02)	3.0D-04
T(4	15	+1)	2.577537700000D+04	(+/- 6.3D-02)	2.9D-04
T(4	16	+1)	2.585570500000D+04	(+/- 6.5D-02)	3.0D-04
T(4	17	+1)	2.594098500000D+04	(+/- 5.8D-02)	2.7D-04
T(4	18	+1)	2.603067500000D+04	(+/- 5.4D-02)	2.4D-04
T(4	19	+1)	2.612499400000D+04	(+/- 6.6D-02)	3.0D-04
T(4	20	+1)	2.622419300000D+04	(+/- 6.6D-02)	3.0D-04
T(4	21	+1)	2.632846100000D+04	(+/- 5.5D-02)	2.4D-04
T(5	0	+1)	2.587610000000D+04	(+/- 9.1D-02)	4.2D-04
T(5	1	+1)	2.588109700000D+04	(+/- 6.4D-02)	3.0D-04
T(5	2	+1)	2.589138700000D+04	(+/- 6.4D-02)	3.0D-04
T(5	3	+1)	2.590675000000D+04	(+/- 6.4D-02)	3.0D-04
T(5	4	+1)	2.592721000000D+04	(+/- 6.4D-02)	3.0D-04
T(5	5	+1)	2.595277200000D+04	(+/- 6.4D-02)	3.0D-04
T(5	6	+1)	2.598335800000D+04	(+/- 6.4D-02)	3.0D-04
T(5	7	+1)	2.601903900000D+04	(+/- 5.8D-02)	2.7D-04
T(5	8	+1)	2.605974700000D+04	(+/- 5.8D-02)	2.7D-04
T(5	9	+1)	2.610538500000D+04	(+/- 5.8D-02)	2.7D-04
T(5	10	+1)	2.615601100000D+04	(+/- 5.8D-02)	2.7D-04
T(5	11	+1)	2.621154600000D+04	(+/- 5.3D-02)	2.4D-04
T(5	12	+1)	2.627195000000D+04	(+/- 6.5D-02)	3.0D-04
T(5	13	+1)	2.633714500000D+04	(+/- 6.5D-02)	3.0D-04

Table D.1 Energy origins of "fluorescence series" of ^{24}MgH isotopomer (cm^{-1}) (*Cont'd*)

T(v' j' p')	Energy Origin	Uncertainty	Sensitivity
T(5 14 +1)	2.640713300000D+04	(+/- 6.5D-02)	3.0D-04
T(5 15 +1)	2.648185000000D+04	(+/- 5.8D-02)	2.7D-04
T(5 16 +1)	2.656122900000D+04	(+/- 5.3D-02)	2.4D-04
T(5 17 +1)	2.664537400000D+04	(+/- 5.3D-02)	2.4D-04
T(5 18 +1)	2.673239300000D+04	(+/- 5.9D-02)	2.7D-04
T(5 19 +1)	2.682640700000D+04	(+/- 5.4D-02)	2.4D-04
T(5 20 +1)	2.692392200000D+04	(+/- 5.5D-02)	2.4D-04
T(5 21 +1)	2.702579700000D+04	(+/- 6.0D-02)	2.7D-04
T(5 22 +1)	2.713190700000D+04	(+/- 5.6D-02)	2.4D-04
T(5 23 +1)	2.724219800000D+04	(+/- 6.7D-02)	3.0D-04
T(5 24 +1)	2.735664400000D+04	(+/- 6.2D-02)	2.7D-04
T(5 25 +1)	2.747515900000D+04	(+/- 7.0D-02)	3.0D-04
T(5 26 +1)	2.759753700000D+04	(+/- 7.3D-02)	3.0D-04
T(5 27 +1)	2.772520700000D+04	(+/- 8.7D-02)	3.4D-04
T(6 0 +1)	2.656474000000D+04	(+/- 9.1D-02)	4.2D-04
T(6 1 +1)	2.656967200000D+04	(+/- 7.4D-02)	3.4D-04
T(6 2 +1)	2.657984300000D+04	(+/- 9.1D-02)	4.2D-04
T(6 3 +1)	2.659510000000D+04	(+/- 6.4D-02)	3.0D-04
T(6 4 +1)	2.661529800000D+04	(+/- 6.4D-02)	3.0D-04
T(6 5 +1)	2.664060000000D+04	(+/- 6.4D-02)	3.0D-04
T(6 6 +1)	2.667098000000D+04	(+/- 6.4D-02)	3.0D-04
T(6 7 +1)	2.670624800000D+04	(+/- 6.4D-02)	3.0D-04
T(6 8 +1)	2.674661200000D+04	(+/- 5.8D-02)	2.7D-04
T(6 9 +1)	2.679210500000D+04	(+/- 5.8D-02)	2.7D-04
T(6 10 +1)	2.684268500000D+04	(+/- 6.4D-02)	3.0D-04
T(6 11 +1)	2.690000900000D+04	(+/- 6.4D-02)	3.0D-04
T(6 12 +1)	2.695493200000D+04	(+/- 6.5D-02)	3.0D-04
T(6 13 +1)	2.701995600000D+04	(+/- 5.8D-02)	2.7D-04
T(6 14 +1)	2.708906300000D+04	(+/- 6.5D-02)	3.0D-04
T(6 15 +1)	2.716288900000D+04	(+/- 5.8D-02)	2.7D-04
T(6 16 +1)	2.724123500000D+04	(+/- 6.5D-02)	3.0D-04
T(6 17 +1)	2.732413100000D+04	(+/- 5.8D-02)	2.7D-04
T(6 18 +1)	2.741145100000D+04	(+/- 5.3D-02)	2.4D-04
T(6 19 +1)	2.750314700000D+04	(+/- 5.9D-02)	2.7D-04
T(6 20 +1)	2.759924100000D+04	(+/- 5.0D-02)	2.3D-04
T(6 21 +1)	2.769959800000D+04	(+/- 5.9D-02)	2.7D-04
T(6 22 +1)	2.780451900000D+04	(+/- 5.5D-02)	2.4D-04
T(6 23 +1)	2.791334900000D+04	(+/- 6.1D-02)	2.7D-04
T(6 24 +1)	2.802520400000D+04	(+/- 9.4D-02)	4.2D-04
T(7 2 +1)	2.724355100000D+04	(+/- 9.1D-02)	4.2D-04
T(7 3 +1)	2.725878500000D+04	(+/- 9.1D-02)	4.2D-04
T(7 4 +1)	2.727871800000D+04	(+/- 6.5D-02)	3.0D-04
T(7 6 +1)	2.733346400000D+04	(+/- 7.4D-02)	3.4D-04
T(7 7 +1)	2.736832100000D+04	(+/- 6.4D-02)	3.0D-04
T(7 8 +1)	2.740788300000D+04	(+/- 7.4D-02)	3.4D-04
T(7 9 +1)	2.745232700000D+04	(+/- 6.4D-02)	3.0D-04
T(7 10 +1)	2.750166200000D+04	(+/- 7.4D-02)	3.4D-04
T(7 11 +1)	2.755566200000D+04	(+/- 7.4D-02)	3.4D-04
T(7 12 +1)	2.761442500000D+04	(+/- 9.1D-02)	4.2D-04
T(7 13 +1)	2.767782100000D+04	(+/- 7.5D-02)	3.4D-04
T(7 14 +1)	2.774567300000D+04	(+/- 9.1D-02)	4.2D-04
T(7 15 +1)	2.781817600000D+04	(+/- 7.5D-02)	3.4D-04
T(7 16 +1)	2.789521700000D+04	(+/- 7.5D-02)	3.4D-04
T(7 17 +1)	2.797666800000D+04	(+/- 7.5D-02)	3.4D-04
T(7 18 +1)	2.806241700000D+04	(+/- 5.8D-02)	2.7D-04
T(7 19 +1)	2.815247800000D+04	(+/- 9.2D-02)	4.2D-04
T(7 20 +1)	2.824635900000D+04	(+/- 6.6D-02)	3.0D-04

Table D.1 Energy origins of "fluorescence series" of ^{24}MgH isotopomer (cm^{-1}) (*Cont'd*)

T(v'	j'	p')	Energy Origin	Uncertainty	Sensitivity
T(7	21	+1)	2.834493200000D+04	(+/- 5.9D-02)	2.7D-04
T(7	22	+1)	2.844733600000D+04	(+/- 6.6D-02)	3.0D-04
T(7	23	+1)	2.855358600000D+04	(+/- 6.8D-02)	3.0D-04
T(7	24	+1)	2.866387400000D+04	(+/- 6.8D-02)	3.0D-04
T(7	25	+1)	2.877801000000D+04	(+/- 8.0D-02)	3.4D-04
T(7	26	+1)	2.889581800000D+04	(+/- 7.6D-02)	3.0D-04
T(7	27	+1)	2.901787600000D+04	(+/- 8.5D-02)	3.0D-04
T(7	28	+1)	2.914032900000D+04	(+/- 9.6D-02)	4.2D-04
T(7	29	+1)	2.926866400000D+04	(+/- 9.5D-02)	4.2D-04
T(8	8	+1)	2.804255700000D+04	(+/- 9.1D-02)	4.2D-04
T(8	9	+1)	2.808626600000D+04	(+/- 9.1D-02)	4.2D-04
T(8	10	+1)	2.813560800000D+04	(+/- 9.1D-02)	4.2D-04
T(8	11	+1)	2.818879100000D+04	(+/- 9.1D-02)	4.2D-04
T(8	12	+1)	2.824737900000D+04	(+/- 9.1D-02)	4.2D-04
T(8	13	+1)	2.830530600000D+04	(+/- 9.1D-02)	4.2D-04
T(8	17	+1)	2.860082300000D+04	(+/- 9.2D-02)	4.2D-04
T(8	18	+1)	2.868488800000D+04	(+/- 7.5D-02)	3.4D-04
T(8	19	+1)	2.877307300000D+04	(+/- 9.2D-02)	4.2D-04
T(8	20	+1)	2.886513100000D+04	(+/- 7.5D-02)	3.4D-04
T(8	21	+1)	2.896138100000D+04	(+/- 7.6D-02)	3.4D-04
T(8	22	+1)	2.906140600000D+04	(+/- 6.6D-02)	3.0D-04
T(8	23	+1)	2.916523600000D+04	(+/- 7.6D-02)	3.4D-04
T(8	24	+1)	2.927290900000D+04	(+/- 7.7D-02)	3.4D-04
T(8	25	+1)	2.938475300000D+04	(+/- 9.5D-02)	4.2D-04
T(9	2	+1)	2.849289900000D+04	(+/- 9.1D-02)	4.2D-04
T(9	4	+1)	2.852662700000D+04	(+/- 9.1D-02)	4.2D-04
T(9	5	+1)	2.855102800000D+04	(+/- 9.1D-02)	4.2D-04
T(9	6	+1)	2.857965400000D+04	(+/- 7.4D-02)	3.4D-04
T(9	8	+1)	2.865127900000D+04	(+/- 6.4D-02)	3.0D-04
T(9	9	+1)	2.869408000000D+04	(+/- 7.4D-02)	3.4D-04
T(9	10	+1)	2.874146600000D+04	(+/- 6.5D-02)	3.0D-04
T(9	11	+1)	2.879333900000D+04	(+/- 7.5D-02)	3.4D-04
T(9	12	+1)	2.884970700000D+04	(+/- 7.5D-02)	3.4D-04
T(9	13	+1)	2.891053400000D+04	(+/- 7.5D-02)	3.4D-04
T(9	14	+1)	2.897570400000D+04	(+/- 9.1D-02)	4.2D-04
T(9	15	+1)	2.904512900000D+04	(+/- 9.1D-02)	4.2D-04
T(9	16	+1)	2.911870000000D+04	(+/- 9.1D-02)	4.2D-04
T(9	17	+1)	2.919652300000D+04	(+/- 9.1D-02)	4.2D-04
T(9	18	+1)	2.927844300000D+04	(+/- 9.2D-02)	4.2D-04
T(9	19	+1)	2.936432800000D+04	(+/- 9.2D-02)	4.2D-04
T(10	18	+1)	2.984186300000D+04	(+/- 9.2D-02)	4.2D-04
T(10	19	+1)	2.992685800000D+04	(+/- 9.2D-02)	4.2D-04

D.2 Energy Origins of ^{25}MgH Isotopomer

Table D.2: Energy Origins of "Fluorescence Series" of ^{25}MgH Isotopomer (cm^{-1})

T(v'	j'	p')	Energy Origin	Uncertainty	Sensitivity
T(0	2	+1)	2.209768500000D+04	(+/- 9.2D-02)	4.2D-04
T(0	3	+1)	2.211314300000D+04	(+/- 7.5D-02)	3.4D-04
T(0	4	+1)	2.213385900000D+04	(+/- 7.5D-02)	3.4D-04
T(0	5	+1)	2.215972000000D+04	(+/- 5.8D-02)	2.7D-04
T(0	6	+1)	2.219070700000D+04	(+/- 5.8D-02)	2.7D-04
T(0	7	+1)	2.222682800000D+04	(+/- 5.3D-02)	2.4D-04
T(0	8	+1)	2.226809800000D+04	(+/- 5.3D-02)	2.4D-04
T(0	9	+1)	2.231444500000D+04	(+/- 5.3D-02)	2.4D-04
T(0	10	+1)	2.236587100000D+04	(+/- 5.3D-02)	2.4D-04
T(0	11	+1)	2.242233000000D+04	(+/- 5.3D-02)	2.4D-04
T(0	12	+1)	2.248379400000D+04	(+/- 5.3D-02)	2.4D-04
T(0	13	+1)	2.255027100000D+04	(+/- 5.3D-02)	2.4D-04
T(0	14	+1)	2.262172500000D+04	(+/- 5.3D-02)	2.4D-04
T(0	15	+1)	2.269808200000D+04	(+/- 5.3D-02)	2.4D-04
T(0	16	+1)	2.277932700000D+04	(+/- 5.4D-02)	2.4D-04
T(0	17	+1)	2.286541500000D+04	(+/- 5.4D-02)	2.4D-04
T(0	18	+1)	2.295631900000D+04	(+/- 5.4D-02)	2.4D-04
T(0	19	+1)	2.305201000000D+04	(+/- 5.9D-02)	2.7D-04
T(0	20	+1)	2.315245000000D+04	(+/- 5.9D-02)	2.7D-04
T(0	21	+1)	2.325755100000D+04	(+/- 5.5D-02)	2.4D-04
T(0	22	+1)	2.336732600000D+04	(+/- 6.0D-02)	2.7D-04
T(0	23	+1)	2.348165100000D+04	(+/- 6.0D-02)	2.7D-04
T(0	24	+1)	2.360060000000D+04	(+/- 7.6D-02)	3.4D-04
T(0	25	+1)	2.372399100000D+04	(+/- 7.7D-02)	3.4D-04
T(0	26	+1)	2.385184100000D+04	(+/- 7.7D-02)	3.4D-04
T(0	27	+1)	2.398418400000D+04	(+/- 9.3D-02)	4.2D-04
T(0	28	+1)	2.412082000000D+04	(+/- 1.3D-01)	6.0D-04
T(0	29	+1)	2.426169100000D+04	(+/- 9.5D-02)	4.2D-04
T(0	30	+1)	2.440669900000D+04	(+/- 9.6D-02)	4.2D-04
T(0	31	+1)	2.455600000000D+04	(+/- 1.8D+01)	8.5D-02
T(1	2	+1)	2.290207800000D+04	(+/- 9.1D-02)	4.2D-04
T(1	3	+1)	2.291766900000D+04	(+/- 9.1D-02)	4.2D-04
T(1	4	+1)	2.293847100000D+04	(+/- 9.1D-02)	4.2D-04
T(1	5	+1)	2.296435800000D+04	(+/- 6.5D-02)	3.0D-04
T(1	6	+1)	2.299550500000D+04	(+/- 5.8D-02)	2.7D-04
T(1	7	+1)	2.303171800000D+04	(+/- 4.9D-02)	2.3D-04
T(1	8	+1)	2.307307000000D+04	(+/- 5.3D-02)	2.4D-04
T(1	9	+1)	2.311949300000D+04	(+/- 4.9D-02)	2.3D-04
T(1	10	+1)	2.317105600000D+04	(+/- 4.9D-02)	2.3D-04
T(1	11	+1)	2.322762500000D+04	(+/- 4.9D-02)	2.3D-04
T(1	12	+1)	2.328921400000D+04	(+/- 5.8D-02)	2.7D-04
T(1	13	+1)	2.335607200000D+04	(+/- 6.5D-02)	3.0D-04
T(1	14	+1)	2.342636300000D+04	(+/- 6.5D-02)	3.0D-04
T(1	15	+1)	2.350338800000D+04	(+/- 5.4D-02)	2.4D-04
T(1	16	+1)	2.358474400000D+04	(+/- 5.9D-02)	2.7D-04
T(1	17	+1)	2.367094300000D+04	(+/- 5.9D-02)	2.7D-04
T(1	18	+1)	2.376181800000D+04	(+/- 7.6D-02)	3.4D-04
T(1	19	+1)	2.385747700000D+04	(+/- 6.5D-02)	3.0D-04
T(1	20	+1)	2.395782300000D+04	(+/- 5.9D-02)	2.7D-04
T(1	21	+1)	2.406277900000D+04	(+/- 6.6D-02)	3.0D-04
T(1	22	+1)	2.417232800000D+04	(+/- 5.9D-02)	2.7D-04
T(1	23	+1)	2.428643500000D+04	(+/- 7.6D-02)	3.4D-04

Table D.2 Energy origins of "fluorescence series" of ^{25}MgH isotopomer (cm^{-1}) (*Cont'd*)

T(v' j' p')	Energy Origin	Uncertainty	Sensitivity
T(1 24 +1)	2.440505400000D+04	(+/- 6.6D-02)	3.0D-04
T(1 25 +1)	2.452833000000D+04	(+/- 7.6D-02)	3.4D-04
T(1 26 +1)	2.465530700000D+04	(+/- 9.3D-02)	4.2D-04
T(1 27 +1)	2.478700000000D+04	(+/- 9.3D-02)	4.2D-04
T(1 28 +1)	2.492296400000D+04	(+/- 9.4D-02)	4.2D-04
T(1 29 +1)	2.506317500000D+04	(+/- 9.5D-02)	4.2D-04

D.3 Energy Origins of ^{26}MgH Isotopomer

Table D.3: Energy Origins of "Fluorescence Series" of ^{26}MgH Isotopomer (cm^{-1})

T(v'	j'	p')	Energy Origin	Uncertainty	Sensitivity
T(0	2	+1)	2.209725500000D+04	(+/- 6.5D-02)	3.0D-04
T(0	3	+1)	2.211277500000D+04	(+/- 5.8D-02)	2.7D-04
T(0	4	+1)	2.213343100000D+04	(+/- 5.3D-02)	2.4D-04
T(0	5	+1)	2.215929300000D+04	(+/- 4.9D-02)	2.3D-04
T(0	6	+1)	2.219023300000D+04	(+/- 4.9D-02)	2.3D-04
T(0	7	+1)	2.222631900000D+04	(+/- 4.6D-02)	2.1D-04
T(0	8	+1)	2.226749900000D+04	(+/- 4.6D-02)	2.1D-04
T(0	9	+1)	2.231378800000D+04	(+/- 4.3D-02)	2.0D-04
T(0	10	+1)	2.236512500000D+04	(+/- 4.6D-02)	2.1D-04
T(0	11	+1)	2.242150100000D+04	(+/- 4.3D-02)	2.0D-04
T(0	12	+1)	2.248292000000D+04	(+/- 4.3D-02)	2.0D-04
T(0	13	+1)	2.254927900000D+04	(+/- 4.9D-02)	2.3D-04
T(0	14	+1)	2.262062300000D+04	(+/- 4.1D-02)	1.9D-04
T(0	15	+1)	2.269686400000D+04	(+/- 4.6D-02)	2.1D-04
T(0	16	+1)	2.277801700000D+04	(+/- 4.2D-02)	1.9D-04
T(0	17	+1)	2.286397200000D+04	(+/- 4.4D-02)	2.0D-04
T(0	18	+1)	2.295478500000D+04	(+/- 4.4D-02)	2.0D-04
T(0	19	+1)	2.305033200000D+04	(+/- 4.7D-02)	2.1D-04
T(0	20	+1)	2.315059300000D+04	(+/- 4.7D-02)	2.1D-04
T(0	21	+1)	2.325554000000D+04	(+/- 4.3D-02)	1.9D-04
T(0	22	+1)	2.336512700000D+04	(+/- 4.3D-02)	1.9D-04
T(0	23	+1)	2.347932100000D+04	(+/- 5.1D-02)	2.3D-04
T(0	24	+1)	2.359804300000D+04	(+/- 5.5D-02)	2.4D-04
T(0	25	+1)	2.372125400000D+04	(+/- 6.6D-02)	3.0D-04
T(0	26	+1)	2.384890300000D+04	(+/- 5.2D-02)	2.3D-04
T(0	27	+1)	2.398098100000D+04	(+/- 6.0D-02)	2.7D-04
T(0	28	+1)	2.411736800000D+04	(+/- 6.8D-02)	3.0D-04
T(0	29	+1)	2.425801800000D+04	(+/- 6.2D-02)	2.7D-04
T(0	30	+1)	2.440298900000D+04	(+/- 6.3D-02)	2.7D-04
T(0	31	+1)	2.455227900000D+04	(+/- 8.0D-02)	3.4D-04
T(0	32	+1)	2.470503600000D+04	(+/- 9.7D-02)	4.2D-04
T(1	3	+1)	2.291666000000D+04	(+/- 7.5D-02)	3.4D-04
T(1	4	+1)	2.293750000000D+04	(+/- 7.5D-02)	3.4D-04
T(1	5	+1)	2.296338000000D+04	(+/- 6.5D-02)	3.0D-04
T(1	6	+1)	2.299439900000D+04	(+/- 5.8D-02)	2.7D-04
T(1	7	+1)	2.303058500000D+04	(+/- 5.8D-02)	2.7D-04
T(1	8	+1)	2.307188200000D+04	(+/- 5.3D-02)	2.4D-04
T(1	9	+1)	2.311828000000D+04	(+/- 6.5D-02)	3.0D-04
T(1	10	+1)	2.316975000000D+04	(+/- 5.3D-02)	2.4D-04
T(1	11	+1)	2.322626400000D+04	(+/- 5.8D-02)	2.7D-04
T(1	12	+1)	2.328772700000D+04	(+/- 5.3D-02)	2.4D-04
T(1	13	+1)	2.335444800000D+04	(+/- 5.8D-02)	2.7D-04
T(1	14	+1)	2.342465300000D+04	(+/- 5.8D-02)	2.7D-04
T(1	15	+1)	2.350156700000D+04	(+/- 6.5D-02)	3.0D-04
T(1	16	+1)	2.358283900000D+04	(+/- 5.4D-02)	2.4D-04
T(1	17	+1)	2.366893500000D+04	(+/- 7.5D-02)	3.4D-04
T(1	18	+1)	2.375967500000D+04	(+/- 5.4D-02)	2.4D-04
T(1	19	+1)	2.385512900000D+04	(+/- 6.5D-02)	3.0D-04
T(1	20	+1)	2.395533900000D+04	(+/- 6.6D-02)	3.0D-04
T(1	21	+1)	2.406016300000D+04	(+/- 7.5D-02)	3.4D-04
T(1	22	+1)	2.416960800000D+04	(+/- 5.9D-02)	2.7D-04
T(1	23	+1)	2.428351500000D+04	(+/- 6.6D-02)	3.0D-04

Table D.3 Energy origins of "fluorescence series" of ^{26}MgH isotopomer (cm^{-1}) (*Cont'd*)

T(v' j' p')	Energy Origin	Uncertainty	Sensitivity
T(1 24 +1)	2.440193500000D+04	(+/- 6.6D-02)	3.0D-04
T(1 25 +1)	2.452506700000D+04	(+/- 9.3D-02)	4.2D-04
T(1 26 +1)	2.465200000000D+04	(+/- 1.5D+01)	6.9D-02
T(1 27 +1)	2.478346200000D+04	(+/- 9.3D-02)	4.2D-04
T(1 28 +1)	2.491914700000D+04	(+/- 9.4D-02)	4.2D-04
T(1 29 +1)	2.505913000000D+04	(+/- 9.5D-02)	4.2D-04

D.4 Energy Origins of ^{24}MgD Isotopomer

Table D.4: Energy Origins of "Fluorescence Series" of ^{24}MgD Isotopomer (cm^{-1})

T(v'	j'	p')	Energy Origin	Uncertainty	Sensitivity
T(0	0	+1)	2.196886200000D+04	(+/- 6.2D-02)	2.7D-04
T(0	1	+1)	2.197154600000D+04	(+/- 5.8D-02)	2.4D-04
T(0	2	+1)	2.197695200000D+04	(+/- 4.4D-02)	1.8D-04
T(0	3	+1)	2.198506700000D+04	(+/- 4.3D-02)	1.7D-04
T(0	4	+1)	2.199587900000D+04	(+/- 4.3D-02)	1.7D-04
T(0	5	+1)	2.200937000000D+04	(+/- 4.1D-02)	1.7D-04
T(0	6	+1)	2.202556900000D+04	(+/- 4.0D-02)	1.7D-04
T(0	7	+1)	2.204445300000D+04	(+/- 4.0D-02)	1.7D-04
T(0	8	+1)	2.206601400000D+04	(+/- 4.0D-02)	1.7D-04
T(0	9	+1)	2.209025300000D+04	(+/- 3.9D-02)	1.6D-04
T(0	10	+1)	2.211717300000D+04	(+/- 3.7D-02)	1.5D-04
T(0	11	+1)	2.214675400000D+04	(+/- 3.9D-02)	1.6D-04
T(0	12	+1)	2.217899600000D+04	(+/- 4.0D-02)	1.7D-04
T(0	13	+1)	2.221389500000D+04	(+/- 3.9D-02)	1.6D-04
T(0	14	+1)	2.225141800000D+04	(+/- 3.9D-02)	1.6D-04
T(0	15	+1)	2.229159400000D+04	(+/- 3.9D-02)	1.6D-04
T(0	16	+1)	2.233437400000D+04	(+/- 4.0D-02)	1.7D-04
T(0	17	+1)	2.237979600000D+04	(+/- 3.9D-02)	1.6D-04
T(0	18	+1)	2.242778500000D+04	(+/- 3.9D-02)	1.6D-04
T(0	19	+1)	2.247836800000D+04	(+/- 4.0D-02)	1.6D-04
T(0	20	+1)	2.253151300000D+04	(+/- 4.2D-02)	1.7D-04
T(0	21	+1)	2.258729700000D+04	(+/- 4.2D-02)	1.7D-04
T(0	22	+1)	2.264559900000D+04	(+/- 4.4D-02)	1.7D-04
T(0	23	+1)	2.270642000000D+04	(+/- 4.5D-02)	1.7D-04
T(0	24	+1)	2.276976100000D+04	(+/- 4.6D-02)	1.7D-04
T(0	25	+1)	2.283562700000D+04	(+/- 4.7D-02)	1.7D-04
T(0	26	+1)	2.290397200000D+04	(+/- 4.8D-02)	1.7D-04
T(0	27	+1)	2.297481300000D+04	(+/- 5.0D-02)	1.7D-04
T(0	28	+1)	2.304811400000D+04	(+/- 5.1D-02)	1.7D-04
T(0	29	+1)	2.312384800000D+04	(+/- 5.6D-02)	1.9D-04
T(0	30	+1)	2.320202900000D+04	(+/- 6.1D-02)	2.1D-04
T(0	31	+1)	2.328262500000D+04	(+/- 6.6D-02)	2.3D-04
T(0	32	+1)	2.336559900000D+04	(+/- 6.9D-02)	2.3D-04
T(0	33	+1)	2.345097000000D+04	(+/- 7.1D-02)	2.3D-04
T(0	34	+1)	2.353866000000D+04	(+/- 7.5D-02)	2.4D-04
T(0	35	+1)	2.362876600000D+04	(+/- 8.0D-02)	2.7D-04
T(0	36	+1)	2.372115200000D+04	(+/- 8.2D-02)	2.7D-04
T(0	37	+1)	2.381580400000D+04	(+/- 9.9D-02)	3.4D-04
T(0	38	+1)	2.391279800000D+04	(+/- 9.3D-02)	3.0D-04
T(0	39	+1)	2.401202300000D+04	(+/- 9.6D-02)	3.0D-04
T(0	40	+1)	2.411351000000D+04	(+/- 1.0D-01)	3.4D-04
T(0	41	+1)	2.421721900000D+04	(+/- 1.0D-01)	3.0D-04
T(0	42	+1)	2.432317000000D+04	(+/- 1.2D-01)	4.2D-04
T(0	43	+1)	2.443121000000D+04	(+/- 1.1D-01)	3.4D-04
T(0	44	+1)	2.454100000000D+04	(+/- 1.2D+01)	5.4D-02
T(0	45	+1)	2.465374000000D+04	(+/- 1.3D-01)	4.2D-04
T(0	46	+1)	2.476823000000D+04	(+/- 1.3D-01)	3.4D-04
T(0	47	+1)	2.488471000000D+04	(+/- 1.5D-01)	4.2D-04
T(0	48	+1)	2.500300000000D+04	(+/- 1.5D+01)	6.9D-02
T(0	49	+1)	2.512408000000D+04	(+/- 1.5D-01)	4.2D-04
T(0	50	+1)	2.524700000000D+04	(+/- 1.8D+01)	8.5D-02
T(1	1	+1)	2.255715800000D+04	(+/- 6.0D-02)	2.7D-04

Table D.4 Energy origins of fluorescence series of ^{24}MgD isotopomer (cm^{-1}) (*Cont'd*)

T(v'	j'	p')	Energy Origin	Uncertainty	Sensitivity
T(1	2	+1)	2.256252200000D+04	(+/- 4.3D-02)	1.8D-04
T(1	3	+1)	2.257064600000D+04	(+/- 4.3D-02)	1.8D-04
T(1	4	+1)	2.258150300000D+04	(+/- 4.2D-02)	1.7D-04
T(1	5	+1)	2.259504400000D+04	(+/- 4.0D-02)	1.7D-04
T(1	6	+1)	2.261127500000D+04	(+/- 3.8D-02)	1.5D-04
T(1	7	+1)	2.263021000000D+04	(+/- 3.9D-02)	1.6D-04
T(1	8	+1)	2.265183700000D+04	(+/- 3.7D-02)	1.5D-04
T(1	9	+1)	2.267615700000D+04	(+/- 3.7D-02)	1.5D-04
T(1	10	+1)	2.270311400000D+04	(+/- 4.1D-02)	1.7D-04
T(1	11	+1)	2.273281400000D+04	(+/- 3.8D-02)	1.6D-04
T(1	12	+1)	2.276506300000D+04	(+/- 3.7D-02)	1.5D-04
T(1	13	+1)	2.280004500000D+04	(+/- 3.7D-02)	1.5D-04
T(1	14	+1)	2.283766600000D+04	(+/- 3.8D-02)	1.6D-04
T(1	15	+1)	2.287790800000D+04	(+/- 4.0D-02)	1.7D-04
T(1	16	+1)	2.292079200000D+04	(+/- 3.8D-02)	1.6D-04
T(1	17	+1)	2.296626100000D+04	(+/- 4.1D-02)	1.7D-04
T(1	18	+1)	2.301435500000D+04	(+/- 3.9D-02)	1.6D-04
T(1	19	+1)	2.306501900000D+04	(+/- 4.1D-02)	1.7D-04
T(1	20	+1)	2.311825900000D+04	(+/- 4.3D-02)	1.7D-04
T(1	21	+1)	2.317407000000D+04	(+/- 4.2D-02)	1.7D-04
T(1	22	+1)	2.323240600000D+04	(+/- 4.2D-02)	1.7D-04
T(1	23	+1)	2.329330500000D+04	(+/- 4.3D-02)	1.7D-04
T(1	24	+1)	2.335667900000D+04	(+/- 4.4D-02)	1.7D-04
T(1	25	+1)	2.342259400000D+04	(+/- 4.8D-02)	1.8D-04
T(1	26	+1)	2.349097300000D+04	(+/- 4.9D-02)	1.8D-04
T(1	27	+1)	2.356181000000D+04	(+/- 5.0D-02)	1.8D-04
T(1	28	+1)	2.363508200000D+04	(+/- 5.3D-02)	1.9D-04
T(1	29	+1)	2.371081900000D+04	(+/- 5.7D-02)	2.0D-04
T(1	30	+1)	2.378892200000D+04	(+/- 6.0D-02)	2.1D-04
T(1	31	+1)	2.386942200000D+04	(+/- 6.6D-02)	2.4D-04
T(1	32	+1)	2.395232500000D+04	(+/- 6.8D-02)	2.4D-04
T(1	33	+1)	2.403762900000D+04	(+/- 7.1D-02)	2.4D-04
T(1	34	+1)	2.412516800000D+04	(+/- 8.0D-02)	3.0D-04
T(1	35	+1)	2.421514000000D+04	(+/- 8.2D-02)	3.0D-04
T(1	36	+1)	2.430717200000D+04	(+/- 8.4D-02)	3.0D-04
T(1	37	+1)	2.440164600000D+04	(+/- 9.5D-02)	3.4D-04
T(1	38	+1)	2.449835300000D+04	(+/- 9.5D-02)	3.4D-04
T(1	39	+1)	2.459732600000D+04	(+/- 9.7D-02)	3.4D-04
T(1	40	+1)	2.469859800000D+04	(+/- 1.0D-01)	3.4D-04
T(1	41	+1)	2.480203000000D+04	(+/- 1.1D-01)	4.2D-04
T(1	42	+1)	2.490900000000D+04	(+/- 1.8D+01)	8.5D-02
T(2	1	+1)	2.313047200000D+04	(+/- 9.5D-02)	4.2D-04
T(2	2	+1)	2.313590700000D+04	(+/- 7.9D-02)	3.4D-04
T(2	3	+1)	2.314405400000D+04	(+/- 7.9D-02)	3.4D-04
T(2	4	+1)	2.315488700000D+04	(+/- 6.9D-02)	3.0D-04
T(2	5	+1)	2.316845500000D+04	(+/- 6.8D-02)	3.0D-04
T(2	6	+1)	2.318468100000D+04	(+/- 6.8D-02)	3.0D-04
T(2	7	+1)	2.320366800000D+04	(+/- 6.8D-02)	3.0D-04
T(2	8	+1)	2.322528500000D+04	(+/- 6.8D-02)	3.0D-04
T(2	9	+1)	2.324963500000D+04	(+/- 6.8D-02)	3.0D-04
T(2	10	+1)	2.327662600000D+04	(+/- 6.7D-02)	3.0D-04
T(2	11	+1)	2.330628600000D+04	(+/- 6.7D-02)	3.0D-04
T(2	12	+1)	2.333865900000D+04	(+/- 6.7D-02)	3.0D-04
T(2	13	+1)	2.337360400000D+04	(+/- 6.7D-02)	3.0D-04
T(2	14	+1)	2.341124400000D+04	(+/- 6.7D-02)	3.0D-04
T(2	15	+1)	2.345156900000D+04	(+/- 7.7D-02)	3.4D-04
T(2	16	+1)	2.349444200000D+04	(+/- 7.7D-02)	3.4D-04

Table D.4 Energy origins of fluorescence series of ^{24}MgD isotopomer (cm^{-1}) (*Cont'd*)

T(v' j' p')	Energy Origin	Uncertainty	Sensitivity
T(2 17 +1)	2.353992100000D+04	(+/- 7.7D-02)	3.4D-04
T(2 18 +1)	2.358800600000D+04	(+/- 7.8D-02)	3.4D-04
T(2 19 +1)	2.363869500000D+04	(+/- 7.8D-02)	3.4D-04
T(2 20 +1)	2.369196900000D+04	(+/- 9.4D-02)	4.2D-04
T(2 21 +1)	2.374778300000D+04	(+/- 9.4D-02)	4.2D-04
T(2 24 +1)	2.393002000000D+04	(+/- 9.6D-02)	4.2D-04
T(2 25 +1)	2.399587200000D+04	(+/- 7.1D-02)	3.0D-04
T(2 26 +1)	2.406419700000D+04	(+/- 7.2D-02)	3.0D-04
T(2 27 +1)	2.413500100000D+04	(+/- 9.8D-02)	4.2D-04
T(2 28 +1)	2.420814300000D+04	(+/- 8.3D-02)	3.4D-04
T(2 29 +1)	2.428361800000D+04	(+/- 9.9D-02)	4.2D-04
T(2 30 +1)	2.436151000000D+04	(+/- 1.0D-01)	4.2D-04
T(2 31 +1)	2.444180000000D+04	(+/- 1.0D-01)	4.2D-04
T(2 32 +1)	2.452461000000D+04	(+/- 1.0D-01)	4.2D-04
T(2 33 +1)	2.460997000000D+04	(+/- 9.1D-01)	4.2D-03
T(3 2 +1)	2.369709800000D+04	(+/- 9.5D-02)	4.2D-04
T(3 3 +1)	2.370533800000D+04	(+/- 9.5D-02)	4.2D-04
T(3 4 +1)	2.371619000000D+04	(+/- 6.9D-02)	3.0D-04
T(3 5 +1)	2.372975200000D+04	(+/- 6.9D-02)	3.0D-04
T(3 6 +1)	2.374601000000D+04	(+/- 6.8D-02)	3.0D-04
T(3 7 +1)	2.376499500000D+04	(+/- 6.8D-02)	3.0D-04
T(3 8 +1)	2.378665300000D+04	(+/- 6.8D-02)	3.0D-04
T(3 9 +1)	2.381100200000D+04	(+/- 6.8D-02)	3.0D-04
T(3 10 +1)	2.383807000000D+04	(+/- 9.4D-02)	4.2D-04
T(3 11 +1)	2.386779600000D+04	(+/- 9.4D-02)	4.2D-04
T(3 12 +1)	2.390005000000D+04	(+/- 9.1D-01)	4.2D-03
T(4 1 +1)	2.424091300000D+04	(+/- 9.3D-02)	4.2D-04
T(4 2 +1)	2.424647400000D+04	(+/- 6.5D-02)	3.0D-04
T(4 3 +1)	2.425461500000D+04	(+/- 6.7D-02)	3.0D-04
T(4 4 +1)	2.426543800000D+04	(+/- 5.9D-02)	2.7D-04
T(4 5 +1)	2.427894000000D+04	(+/- 6.7D-02)	3.0D-04
T(4 6 +1)	2.429515400000D+04	(+/- 6.6D-02)	3.0D-04
T(4 7 +1)	2.431410500000D+04	(+/- 6.6D-02)	3.0D-04
T(4 8 +1)	2.433572200000D+04	(+/- 5.4D-02)	2.4D-04
T(4 9 +1)	2.436002800000D+04	(+/- 5.9D-02)	2.7D-04
T(4 10 +1)	2.438694900000D+04	(+/- 5.0D-02)	2.3D-04
T(4 11 +1)	2.441659200000D+04	(+/- 5.8D-02)	2.7D-04
T(4 12 +1)	2.444881300000D+04	(+/- 5.8D-02)	2.7D-04
T(4 13 +1)	2.448379500000D+04	(+/- 5.3D-02)	2.4D-04
T(4 14 +1)	2.452133900000D+04	(+/- 5.3D-02)	2.4D-04
T(4 15 +1)	2.456147800000D+04	(+/- 5.8D-02)	2.7D-04
T(4 16 +1)	2.460423500000D+04	(+/- 5.3D-02)	2.4D-04
T(4 17 +1)	2.464957700000D+04	(+/- 5.3D-02)	2.4D-04
T(4 18 +1)	2.469751100000D+04	(+/- 5.8D-02)	2.7D-04
T(4 19 +1)	2.474800400000D+04	(+/- 5.9D-02)	2.7D-04
T(4 20 +1)	2.480119300000D+04	(+/- 5.9D-02)	2.7D-04
T(4 21 +1)	2.485707300000D+04	(+/- 5.9D-02)	2.7D-04
T(4 23 +1)	2.497635500000D+04	(+/- 9.2D-02)	4.2D-04
T(5 1 +1)	2.477840600000D+04	(+/- 9.1D-02)	4.2D-04
T(5 2 +1)	2.478400000000D+04	(+/- 1.8D+01)	8.5D-02
T(5 3 +1)	2.479205500000D+04	(+/- 7.5D-02)	3.4D-04
T(5 4 +1)	2.480285200000D+04	(+/- 6.5D-02)	3.0D-04
T(5 5 +1)	2.481634200000D+04	(+/- 6.5D-02)	3.0D-04
T(5 6 +1)	2.483253800000D+04	(+/- 6.5D-02)	3.0D-04
T(5 7 +1)	2.485137400000D+04	(+/- 6.5D-02)	3.0D-04
T(5 8 +1)	2.487293000000D+04	(+/- 6.5D-02)	3.0D-04
T(5 9 +1)	2.489713500000D+04	(+/- 6.5D-02)	3.0D-04

Table D.4 Energy origins of fluorescence series of ^{24}MgD isotopomer (cm^{-1}) (*Cont'd*)

T(v' j' p')	Energy Origin	Uncertainty	Sensitivity
T(5 10 +1)	2.492405700000D+04	(+/- 6.5D-02)	3.0D-04
T(5 11 +1)	2.495350200000D+04	(+/- 6.5D-02)	3.0D-04
T(5 12 +1)	2.498572500000D+04	(+/- 7.5D-02)	3.4D-04
T(5 13 +1)	2.502041700000D+04	(+/- 7.5D-02)	3.4D-04
T(5 14 +1)	2.505789400000D+04	(+/- 6.5D-02)	3.0D-04
T(5 15 +1)	2.509800800000D+04	(+/- 9.1D-02)	4.2D-04
T(5 16 +1)	2.514057400000D+04	(+/- 9.1D-02)	4.2D-04
T(5 17 +1)	2.518597500000D+04	(+/- 9.2D-02)	4.2D-04
T(5 19 +1)	2.528299900000D+04	(+/- 7.5D-02)	3.4D-04
T(5 20 +1)	2.533578600000D+04	(+/- 5.9D-02)	2.7D-04
T(5 21 +1)	2.539120900000D+04	(+/- 6.6D-02)	3.0D-04
T(5 22 +1)	2.544901100000D+04	(+/- 6.7D-02)	3.0D-04
T(5 23 +1)	2.550931300000D+04	(+/- 5.5D-02)	2.4D-04
T(5 24 +1)	2.557190000000D+04	(+/- 6.1D-02)	2.7D-04
T(5 25 +1)	2.563726300000D+04	(+/- 5.7D-02)	2.4D-04
T(5 26 +1)	2.570502300000D+04	(+/- 9.3D-02)	4.2D-04
T(5 27 +1)	2.577498300000D+04	(+/- 6.9D-02)	3.0D-04
T(5 28 +1)	2.584765400000D+04	(+/- 7.9D-02)	3.4D-04
T(5 29 +1)	2.592268500000D+04	(+/- 7.9D-02)	3.4D-04
T(5 30 +1)	2.600040100000D+04	(+/- 8.1D-02)	3.4D-04
T(5 31 +1)	2.608041000000D+04	(+/- 9.1D-01)	4.2D-03
T(6 9 +1)	2.542123000000D+04	(+/- 9.1D-02)	4.2D-04
T(6 11 +1)	2.547774900000D+04	(+/- 9.1D-02)	4.2D-04
T(6 12 +1)	2.550976300000D+04	(+/- 9.1D-02)	4.2D-04
T(6 13 +1)	2.554431500000D+04	(+/- 7.5D-02)	3.4D-04
T(6 14 +1)	2.558150100000D+04	(+/- 6.5D-02)	3.0D-04
T(6 15 +1)	2.562131900000D+04	(+/- 6.5D-02)	3.0D-04
T(6 16 +1)	2.566366000000D+04	(+/- 6.5D-02)	3.0D-04
T(6 17 +1)	2.570855300000D+04	(+/- 6.5D-02)	3.0D-04
T(6 18 +1)	2.575593400000D+04	(+/- 6.5D-02)	3.0D-04
T(6 19 +1)	2.580585800000D+04	(+/- 6.5D-02)	3.0D-04
T(6 20 +1)	2.585831900000D+04	(+/- 6.6D-02)	3.0D-04
T(6 21 +1)	2.591321100000D+04	(+/- 7.6D-02)	3.4D-04
T(6 22 +1)	2.597063300000D+04	(+/- 6.6D-02)	3.0D-04
T(6 23 +1)	2.603043100000D+04	(+/- 6.7D-02)	3.0D-04
T(6 24 +1)	2.609271900000D+04	(+/- 7.7D-02)	3.4D-04
T(6 25 +1)	2.615730900000D+04	(+/- 6.8D-02)	3.0D-04
T(6 26 +1)	2.622432600000D+04	(+/- 7.8D-02)	3.4D-04
T(6 27 +1)	2.629362800000D+04	(+/- 7.0D-02)	3.0D-04
T(6 28 +1)	2.636528500000D+04	(+/- 9.6D-02)	4.2D-04
T(6 29 +1)	2.643915500000D+04	(+/- 9.7D-02)	4.2D-04

D.5 Energy Origins of ^{25}MgD Isotopomer

Table D.5: Energy Origins of "Fluorescence Series" of ^{25}MgD Isotopomer (cm^{-1})

T(v'	j'	p')	Energy Origin	Uncertainty	Sensitivity
T(0	8	+1)	2.206523500000D+04	(+/- 9.4D-02)	4.2D-04
T(0	9	+1)	2.208943900000D+04	(+/- 9.4D-02)	4.2D-04
T(0	10	+1)	2.211622800000D+04	(+/- 7.7D-02)	3.4D-04
T(0	11	+1)	2.214576300000D+04	(+/- 6.8D-02)	3.0D-04
T(0	12	+1)	2.217789600000D+04	(+/- 6.8D-02)	3.0D-04
T(0	13	+1)	2.221271300000D+04	(+/- 7.7D-02)	3.4D-04
T(0	14	+1)	2.225008900000D+04	(+/- 6.8D-02)	3.0D-04
T(0	15	+1)	2.229014000000D+04	(+/- 6.8D-02)	3.0D-04
T(0	16	+1)	2.233281400000D+04	(+/- 6.1D-02)	2.7D-04
T(0	17	+1)	2.237806400000D+04	(+/- 5.7D-02)	2.4D-04
T(0	18	+1)	2.242591100000D+04	(+/- 5.3D-02)	2.3D-04
T(0	19	+1)	2.247639200000D+04	(+/- 5.4D-02)	2.3D-04
T(0	20	+1)	2.252939200000D+04	(+/- 5.4D-02)	2.3D-04
T(0	21	+1)	2.258492300000D+04	(+/- 5.1D-02)	2.1D-04
T(0	22	+1)	2.264306800000D+04	(+/- 5.2D-02)	2.1D-04
T(0	23	+1)	2.270371700000D+04	(+/- 5.3D-02)	2.1D-04
T(0	24	+1)	2.276686600000D+04	(+/- 6.0D-02)	2.4D-04
T(0	25	+1)	2.283254800000D+04	(+/- 5.5D-02)	2.1D-04
T(0	26	+1)	2.290063300000D+04	(+/- 5.9D-02)	2.3D-04
T(0	27	+1)	2.297131700000D+04	(+/- 6.8D-02)	2.7D-04
T(0	28	+1)	2.304439600000D+04	(+/- 6.1D-02)	2.3D-04
T(0	29	+1)	2.311992100000D+04	(+/- 6.3D-02)	2.3D-04
T(0	30	+1)	2.319785800000D+04	(+/- 6.8D-02)	2.4D-04
T(0	31	+1)	2.327817800000D+04	(+/- 8.8D-02)	3.4D-04
T(0	32	+1)	2.336092300000D+04	(+/- 7.2D-02)	2.4D-04
T(0	33	+1)	2.344603200000D+04	(+/- 8.2D-02)	3.0D-04
T(0	34	+1)	2.353346200000D+04	(+/- 7.9D-02)	2.7D-04
T(0	35	+1)	2.362318000000D+04	(+/- 1.4D-01)	6.0D-04
T(0	36	+1)	2.371511000000D+04	(+/- 1.1D-01)	4.2D-04
T(0	37	+1)	2.380983000000D+04	(+/- 1.1D-01)	4.2D-04
T(0	38	+1)	2.390633000000D+04	(+/- 1.1D-01)	4.2D-04
T(0	39	+1)	2.400522000000D+04	(+/- 1.2D-01)	4.2D-04
T(1	10	+1)	2.270126600000D+04	(+/- 6.7D-02)	3.0D-04
T(1	11	+1)	2.273086800000D+04	(+/- 7.7D-02)	3.4D-04
T(1	12	+1)	2.276302000000D+04	(+/- 6.7D-02)	3.0D-04
T(1	13	+1)	2.279797300000D+04	(+/- 6.0D-02)	2.7D-04
T(1	14	+1)	2.283541300000D+04	(+/- 5.6D-02)	2.4D-04
T(1	15	+1)	2.287555100000D+04	(+/- 5.6D-02)	2.4D-04
T(1	16	+1)	2.291830800000D+04	(+/- 5.6D-02)	2.4D-04
T(1	17	+1)	2.296365000000D+04	(+/- 5.6D-02)	2.4D-04
T(1	18	+1)	2.301159500000D+04	(+/- 5.6D-02)	2.4D-04
T(1	19	+1)	2.306216100000D+04	(+/- 5.6D-02)	2.4D-04
T(1	20	+1)	2.311518200000D+04	(+/- 6.2D-02)	2.7D-04
T(1	21	+1)	2.317081400000D+04	(+/- 6.2D-02)	2.7D-04
T(1	22	+1)	2.322899300000D+04	(+/- 6.9D-02)	3.0D-04
T(1	23	+1)	2.328972800000D+04	(+/- 6.9D-02)	3.0D-04
T(1	24	+1)	2.335295800000D+04	(+/- 7.9D-02)	3.4D-04
T(1	25	+1)	2.341863700000D+04	(+/- 9.6D-02)	4.2D-04
T(1	26	+1)	2.348675700000D+04	(+/- 8.1D-02)	3.4D-04
T(1	27	+1)	2.355741600000D+04	(+/- 8.2D-02)	3.4D-04
T(1	28	+1)	2.363038900000D+04	(+/- 8.3D-02)	3.4D-04
T(1	29	+1)	2.370587800000D+04	(+/- 8.2D-02)	3.4D-04

Table D.5 Energy origins of "fluorescence series" of ^{25}MgD isotopomer (cm^{-1}) (*Cont'd*)

T(v' j' p')	Energy Origin	Uncertainty	Sensitivity
T(1 30 +1)	2.378375600000D+04	(+/- 7.5D-02)	3.0D-04
T(1 31 +1)	2.386406700000D+04	(+/- 8.5D-02)	3.4D-04
T(1 32 +1)	2.394668200000D+04	(+/- 7.8D-02)	3.0D-04
T(1 33 +1)	2.403164000000D+04	(+/- 1.0D-01)	4.2D-04
T(2 19 +1)	2.363487100000D+04	(+/- 9.4D-02)	4.2D-04
T(2 20 +1)	2.368797100000D+04	(+/- 9.4D-02)	4.2D-04
T(2 24 +1)	2.392536800000D+04	(+/- 9.6D-02)	4.2D-04
T(2 25 +1)	2.399089500000D+04	(+/- 9.7D-02)	4.2D-04
T(2 26 +1)	2.405910400000D+04	(+/- 9.8D-02)	4.2D-04
T(2 27 +1)	2.413000000000D+04	(+/- 1.8D+01)	8.5D-02
T(2 28 +1)	2.420300000000D+04	(+/- 1.8D+01)	8.5D-02

D.6 Energy Origins of ^{26}MgD Isotopomer

Table D.6: Energy Origins of "Fluorescence Series" of ^{26}MgD Isotopomer (cm^{-1})

T(v'	j'	p')	Energy Origin	Uncertainty	Sensitivity
T(0	8	+1)	2.206452700000D+04	(+/- 9.4D-02)	4.2D-04
T(0	9	+1)	2.208865100000D+04	(+/- 9.4D-02)	4.2D-04
T(0	10	+1)	2.211543700000D+04	(+/- 6.8D-02)	3.0D-04
T(0	11	+1)	2.214481400000D+04	(+/- 6.8D-02)	3.0D-04
T(0	12	+1)	2.217686800000D+04	(+/- 9.3D-02)	4.2D-04
T(0	13	+1)	2.221155100000D+04	(+/- 6.8D-02)	3.0D-04
T(0	14	+1)	2.224886400000D+04	(+/- 6.1D-02)	2.7D-04
T(0	15	+1)	2.228879300000D+04	(+/- 5.7D-02)	2.4D-04
T(0	16	+1)	2.233134900000D+04	(+/- 5.7D-02)	2.4D-04
T(0	17	+1)	2.237645600000D+04	(+/- 5.7D-02)	2.4D-04
T(0	18	+1)	2.242420200000D+04	(+/- 5.3D-02)	2.3D-04
T(0	19	+1)	2.247450000000D+04	(+/- 5.4D-02)	2.3D-04
T(0	20	+1)	2.252732600000D+04	(+/- 5.7D-02)	2.4D-04
T(0	21	+1)	2.258279800000D+04	(+/- 5.4D-02)	2.3D-04
T(0	22	+1)	2.264074200000D+04	(+/- 5.2D-02)	2.1D-04
T(0	23	+1)	2.270121300000D+04	(+/- 5.3D-02)	2.1D-04
T(0	24	+1)	2.276418500000D+04	(+/- 6.0D-02)	2.4D-04
T(0	25	+1)	2.282966700000D+04	(+/- 5.5D-02)	2.1D-04
T(0	26	+1)	2.289762800000D+04	(+/- 5.8D-02)	2.3D-04
T(0	27	+1)	2.296806600000D+04	(+/- 6.0D-02)	2.3D-04
T(0	28	+1)	2.304096400000D+04	(+/- 6.1D-02)	2.3D-04
T(0	29	+1)	2.311623200000D+04	(+/- 6.6D-02)	2.4D-04
T(0	30	+1)	2.319396900000D+04	(+/- 7.2D-02)	2.7D-04
T(0	31	+1)	2.327408500000D+04	(+/- 7.4D-02)	2.7D-04
T(0	32	+1)	2.335660800000D+04	(+/- 7.6D-02)	2.7D-04
T(0	33	+1)	2.344143600000D+04	(+/- 7.8D-02)	2.7D-04
T(0	34	+1)	2.352867100000D+04	(+/- 7.6D-02)	2.4D-04
T(0	35	+1)	2.361820700000D+04	(+/- 8.7D-02)	3.0D-04
T(0	36	+1)	2.371000500000D+04	(+/- 9.6D-02)	3.4D-04
T(0	37	+1)	2.380432500000D+04	(+/- 9.2D-02)	3.0D-04
T(0	38	+1)	2.390079000000D+04	(+/- 1.0D-01)	3.4D-04
T(0	39	+1)	2.399937000000D+04	(+/- 1.0D-01)	3.4D-04
T(0	40	+1)	2.410038000000D+04	(+/- 1.2D-01)	4.2D-04
T(0	41	+1)	2.420352000000D+04	(+/- 1.2D-01)	4.2D-04
T(1	12	+1)	2.276121800000D+04	(+/- 9.3D-02)	4.2D-04
T(1	13	+1)	2.279598900000D+04	(+/- 6.0D-02)	2.7D-04
T(1	14	+1)	2.283334400000D+04	(+/- 6.0D-02)	2.7D-04
T(1	15	+1)	2.287340000000D+04	(+/- 6.0D-02)	2.7D-04
T(1	16	+1)	2.291603900000D+04	(+/- 5.6D-02)	2.4D-04
T(1	17	+1)	2.296124700000D+04	(+/- 5.6D-02)	2.4D-04
T(1	18	+1)	2.300905300000D+04	(+/- 6.1D-02)	2.7D-04
T(1	19	+1)	2.305940700000D+04	(+/- 5.6D-02)	2.4D-04
T(1	20	+1)	2.311236900000D+04	(+/- 6.2D-02)	2.7D-04
T(1	21	+1)	2.316781100000D+04	(+/- 6.2D-02)	2.7D-04
T(1	22	+1)	2.322588200000D+04	(+/- 6.9D-02)	3.0D-04
T(1	23	+1)	2.328636200000D+04	(+/- 6.9D-02)	3.0D-04
T(1	24	+1)	2.335000000000D+04	(+/- 1.5D+01)	6.9D-02
T(1	25	+1)	2.341499500000D+04	(+/- 9.6D-02)	4.2D-04
T(1	26	+1)	2.348289900000D+04	(+/- 8.1D-02)	3.4D-04
T(1	27	+1)	2.355329700000D+04	(+/- 8.2D-02)	3.4D-04
T(1	28	+1)	2.362603500000D+04	(+/- 9.8D-02)	4.2D-04
T(1	29	+1)	2.370140100000D+04	(+/- 7.4D-02)	3.0D-04

Table D.6 Energy origins of "fluorescence series" of ^{26}MgD isotopomer (cm^{-1}) (*Cont'd*)

T(v' j' p')	Energy Origin	Uncertainty	Sensitivity
T(1 30 +1)	2.377907400000D+04	(+/- 8.3D-02)	3.4D-04
T(1 31 +1)	2.385893000000D+04	(+/- 1.4D-01)	6.0D-04
T(1 32 +1)	2.394160100000D+04	(+/- 8.7D-02)	3.4D-04
T(1 33 +1)	2.402630000000D+04	(+/- 1.4D-01)	6.0D-04
T(2 20 +1)	2.368443300000D+04	(+/- 9.4D-02)	4.2D-04
T(2 21 +1)	2.373988800000D+04	(+/- 9.4D-02)	4.2D-04
T(2 24 +1)	2.392102600000D+04	(+/- 9.6D-02)	4.2D-04
T(2 25 +1)	2.398646200000D+04	(+/- 9.7D-02)	4.2D-04
T(2 27 +1)	2.412500000000D+04	(+/- 1.8D+01)	8.5D-02
T(2 28 +1)	2.419800000000D+04	(+/- 1.8D+01)	8.5D-02